Numerically efficient modelling of turbulent non-premixed flames

Baburić, Mario

SVEUČILIŠTE U ZAGREBU

FAKULTET STROJARSTVA I BRODOGRADNJE

NUMERIČKI EFIKASNO MODELIRANJE TURBULENTNIH NEPREDMIJEŠANIH PLAMENOVA

DOKTORSKI RAD

NUMERICALLY EFFICIENT MODELLING OF TURBULENT NON-PREMIXED FLAMES

PHD THESIS

MARIO BABURIĆ

ZAGREB, 2005

SVEUČILIŠTE U ZAGREBU

FAKULTET STROJARSTVA I BRODOGRADNJE

NUMERIČKI EFIKASNO MODELIRANJE TURBULENTNIH NEPREDMIJEŠANIH PLAMENOVA

DOKTORSKI RAD

NUMERICALLY EFFICIENT MODELLING OF TURBULENT NON-PREMIXED FLAMES

PHD THESIS

Mentor:

Doc.dr.sc. NEVEN DUIĆ

MARIO BABURIĆ

ZAGREB, 2005

BIBLIOGRAPHY DATA:

UDC:	662.61:519.876.5
Keywords:	Non-premixed combustion, stationary laminar flamelet model, reaction progress variable, presumed conditional moments, chemistry pre-tabulation, diffusion flames, discrete transfer radiation method, hybrid turbulence model
Scientific area:	Technical sciences
Scientific field:	Mechanical engineering
Institution:	Faculty of Mechanical Engineering and Naval Architecture (FMENA), University of Zagreb
Principal supervisor:	Dr.sc. Neven Duić, Assistant Professor
Number of pages:	176
Number of figures:	76
Number of tables:	1
Number of references:	149
Date of oral examination:	14.10.2005

Jury members:

Dr.sc. Željko Bogdan (FMENA, Zagreb), Full Professor

Dr.sc. Neven Duić (FMENA, Zagreb), Assistant Professor

Dr.sc. Antun Galović (FMENA, Zagreb), Full Professor

Dr. Pedro Coelho (Instituto Superior Técnico, Lisbon), Associate Professor

Dr. Reinhard Tatschl (AVL AST, Graz)

ISBN 953-6313-76-6

Acknowledgments

This work has taken place at the Power Engineering Department of the Faculty of Mechanical Engineering and Naval Architecture, University of Zagreb.

My sincere thanks go to Assistant Professor Neven Duić, my mentor and supervisor, a person who introduced me to an engaging field of the computational fluid dynamics and who made this work possible. His constant support, valuable comments and patience helped me a lot while preparing this thesis.

This thesis considerably benefited also from many discussions I have had with my colleagues and collaborators at the Power Engineering Department – Assistant Professor Daniel Rolph Schneider, Milan Vujanović and Marko Ban. Their support and constant availability are greatly acknowledged.

I learned a lot on CFD matters in many discussions and collaboration with AVL AST people – Dr. Peter Priesching, Dr. Reinhard Tatschl, Dr. Branislav Basara, and others. AVL AST Zagreb is acknowledged for the financial support for this work. Special thanks in this respect go to AVL AST Zagreb director, Mr. Goran Mirković.

I am very thankful for valuable suggestions on a draft of this thesis that I received from other jury members, Professors Željko Bogdan, Antun Galović and Pedro Coelho. Their insightful observations and comments made this work of better quality.

My family is acknowledged for a steady support and patience.

Zagreb, September 2005

Mario Baburić

It is the mark of an educated mind to rest satisfied with the degree of precision which the nature of the subject admits and not to seek exactness where only an approximation is possible.

Aristotle

Contents

Preface VII
Abstract VIII
Keywords X
Nomenclature XI
List of Figures XX
List of Tables XXIV
1 Introduction 1
1.1 Motivation and general overview 1
1.2 State-of-the-art research – a survey 3
1.3 Work hypothesis and outline 11
1.4 Thesis contribution 13
2 Mathematical modelling 15
2.1 Conservation equations 15
2.1.1 Conservation of mass 15
2.1.2 Conservation of momentum 15
2.1.3 Conservation of angular momentum 16
2.1.4 Conservation of energy 17
2.1.5 Scalar transport 17
2.2 Thermo-chemical relations 18
2.3 Combustion modelling 21
2.3.1 Phenomenological perspective 21
2.3.2 Conserved scalar approach 24
2.3.3 Stationary laminar flamelet concept 25
2.3.4 Reaction progress variable 30
2.3.5 Low-dimensional manifolds in composition space 31
2.3.6 A new tabulation procedure 34
2.3.6.1 Premixed flamelets 34
2.3.6.2 Non-premixed flamelets 36

2.3.6.3 Mixed formulation 38
2.4 Thermal radiation modelling 39
2.4.1 Radiation transfer equation 39
2.4.2 Discrete transfer method 40
2.4.3 Radiative properties 44
2.5 Statistical description 45
2.5.1 Turbulent and chemical scales 45
2.5.2 Reynolds and Favre averaging 48
2.5.3 Averaged equations: continuity, momentum and energy 49
2.5.4 Turbulence closures 50
2.5.5 The statistical moments of tracking scalars 53
2.5.6 Turbulence/chemistry interaction 54
2.5.7 Mean scalar dissipation rate 57
2.5.8 The presumed conditional moments of the reaction progress variable 57
3 Numerical procedure 61
3.1 Chemistry pre-processor 62
3.1.1 Infinitely fast chemistry models 62
3.1.2 Numerical solution of the flamelet equations 64
3.1.2.1 Finite differences discretisation 64
3.1.2.2 Differential/algebraic system solution 68
3.1.2.3 PDF integrations 68
3.1.3 CSC solver implementation 71
3.1.3.1 Solver structure 71
3.1.3.2 Chemistry solver 72
3.1.3.3 PDF creator 74
3.2 Fluid flow solver 76
3.2.1 Integral form of the transport equation 76
3.2.2 Control volume discretisation 77
3.2.3 Solution procedure 80
3.2.4 Combustion module implementation 83
3.3 DTRM implementation 85

4 Hydrogen jet flame 89
4.1 Experimental configuration 89
4.2 Numerical set-up 90
4.3 Results 92
4.3.1 Pre-tabulated chemistry profiles 92
4.3.1.1 SLFM database 92
4.3.1.2 FPI database 94
4.3.1.3 SLFM database (reaction progress variable) 96
4.3.2 Jet spreading 98
4.3.3 Adiabatic vs. non-adiabatic profiles 99
4.3.4 Combustion models comparison 102
5 Methane jet flame 109
5.1 Experimental configuration 109
5.2 Numerical set-up 110
5.3 Results 112
5.3.1 Pre-tabulated chemistry profiles 112
5.3.2 Adiabatic vs. non-adiabatic profiles 118
5.3.3 Combustion models comparison 120
6 TECFLAM combustion chamber 129
6.1 Experimental configuration 129
6.2 Numerical set-up 131
6.3 Results 133
6.3.1 Pre-tabulated chemistry profiles 133
6.3.2 Simulation results 137
7 Conclusions 145
Appendix A – A step-by-step derivation of flamelet equations 149
Appendix B – A flamelet model with differential diffusion 155
Appendix C – The stationary laminar 1D premixed flame 159
Bibliography 161
Curriculum vitae 175

Preface

Computational fluid dynamics (CFD) has become a widely used methodology in science, technology and industrial design applications, whenever complicated physical processes involving fluids are considered. This includes turbulent fluid flow, combustion processes, thermal radiation, heat and mass transfer, etc. As such, CFD has become a powerful tool in hands of an engineer who is trying to improve the equipment efficiency or to speed-up the overall design cycle.

An increased application of the CFD methods in power engineering sector gained its momentum because of many reasons. Fossil fuels are expected to remain a primary source of energy in the 21st century and the appropriate combustion modelling is very important in this respect. CFD inevitably emerges here as a tool of choice when trying to accurately predict the subtle combustion phenomena of interest, like pollutant emissions, combustion efficiency, etc. A need for an appropriate thermal radiation modelling often comes in the same package with combustion and must be simultaneously treated.

The scientific research in combustion and radiation has significantly advanced during the last few decades and reliable models were developed for both. However, high computational demands often prevent many of those models to be efficiently applied in the industrial and other applications of practical interest. In this respect, a compromise still has to be found in order to satisfy a need for sufficiently accurate, but still computationally affordable solutions.

A pre-tabulated chemistry approach in combustion modelling seems a good candidate to satisfy the mentioned criteria. A procedure where the demanding chemistry calculations are decoupled from the fluid flow solver often results in an efficient overall methodology when compared to a joint calculation of the both. This makes it possible to apply the detailed chemistry representation in deliberately complex configurations, with an acceptable surplus in computational demand when compared to non-reactive flow calculations. The modelling of thermal radiation, on the other hand, is a problem *per se* and often it is even more demanding than combustion modelling. The simplified radiation models are usually retained in the industrial applications.

Abstract

A pre-tabulated chemistry approach, based on the premixed and non-premixed laminar flamelets, was developed and implemented in this work. A devoted software application was developed in order to perform the chemistry calculations and tabulations in the pre-processor step. The combustion modelling within the CFD procedure consisted of calculating the field distribution for a set of tracking scalars – mixture fraction and reaction progress variable – while the chemistry composition space was functionally related to these two scalars, depending on a model. The developed models were applied in the combustion simulations of three different configurations of varying complexity. The results were compared to experimental data and to the stationary laminar flamelet model predictions. The simulated configurations were the following – a diluted hydrogen jet flame (H_2/He-air flame B), a piloted methane jet flame (Sandia flame D) and a confined natural gas bluff-body stabilised flame (TECFLAM). The detailed chemical mechanisms were used in all cases. The discrete transfer radiation method was implemented into the CFD code (FIRE) in order to account for thermal radiation. The impact of radiation inclusion was investigated. A hybrid turbulence model was applied and its predictions were compared to those obtained with the standard k-ε model.

A new tabulation procedure based on the normalised reaction progress variable has shown as a possible alternative to the standard stationary laminar flamelets methodology. In the case of premixed flamelets a complete range from the cold-mixing up to the chemical equilibrium can be covered, making this approach promising if searching towards more universal combustion models. NO was reasonably well predicted when using premixed flamelets, while non-premixed flamelets have shown as inappropriate in this particular situation. The reaction progress variable based models, as implemented in this work, have shown deficient in the fuel-rich regions in the methane jet configuration (Sandia flame D), making a space for possible improvements in this respect. The inclusion of radiation modelling has shown important for accurate temperature predictions. In general, the hybrid turbulence model has shown as superior to the standard k-ε turbulence model.

Pristup tabeliranja kemijskih vrsta u pretprocesoru, baziran na izračunima predmiješanih ili nepredmiješanih plamenova, je razvijen i implementiran u ovome radu. U tu svrhu je razvijen računalni program u kojem se vrše proračuni kemijskih vrsta u pretprocesoru. Modeliranje izgaranja tijekom same CFD procedure se sastoji u izračunu prostorne raspodijeljenosti različitih skalara – udjela smjese goriva i varijable napretka reakcije – dok su udjeli pojedinih kemijskih vrsta funkcionalno povezani sa ta dva skalara ovisno o modelu. Razvijeni modeli su primijenjeni u proračunima izgaranja na tri konfiguracije s različitim stupnjem složenosti. Rezultati simulacije su uspoređeni s eksperimentalno dobivenim vrijednostima te s rezultatima simulacije dobivenih upotrebom standardnog stacionarnog laminarnog flamelet modela. Simulirane konfiguracije su bile sljedeće – prorijeđeni vodikov slobodni mlazni plamen (H_2/He-zrak plamen B), pilotirani metanov slobodni mlazni plamen (Sandia plamen D) te zatvoreni plamen prirodnog plina u TECFLAM ložištu. U sva tri slučaja su upotrijebljeni detaljni kemijski mehanizmi. Metoda diskretnog prijenosa topline zračenjem je implementirana u CFD program (FIRE), a da bi se prilikom modeliranja obuhvatio proces prijenosa topline zračenjem. Također, upotrebljen je hibridni model turbulencije prilikom modeliranja protoka fluida te su njegovi rezultati uspoređeni s rezultatima dobivenim upotrebom standardnog k-ε modela turbulencije.

Nova procedura tabeliranja kemijskih vrsta se pokazala kao mogućom alternativom standardnom laminarnom *flamelet* modelu. U slučaju predmiješanih plamenova moguće je obuhvatiti cjelokupno područje od hladnog miješanja reaktanata do ravnotežnog izgaranja, što dopridonosi povećanoj univerzalnosti ovog modela. NO je dobro predviđen modelom baziranom na predmiješanim plamenovima, dok se je upotreba nepredmiješanih plamenova pokazala lošim izborom u ovome slučaju. Modeli bazirani na varijabli napretka reakcije su se pokazali manjkavima u područjima s bogatom smjesom goriva u slučaju Sandia plamena D te je potrebno ostvariti daljnji napredak u ovome pogledu. Uključivanje modeliranja prijenosa topline zračenjem se pokazalo bitnim za točni izračun temperaturnih polja. U općem slučaju, hibridni model turbulencije se pokazao boljim od standardnog k-ε modela.

Keywords

Non-premixed combustion, stationary laminar flamelet model, reaction progress variable, presumed conditional moments, chemistry pre-tabulation, diffusion flames, discrete transfer radiation method, hybrid turbulence model

Nepredmiješano izgaranje, stacionarni laminarni *flamelet* model, varijabla napretka reakcije, pretpostavljeni kondicionalni momenti, tabeliranje kemijskih vrsta, difuzijski plamenovi, metoda diskretnog prijenosa topline zračenjem, hibridni model turbulencije

Nomenclature

Roman	Description	Unit
a	Absorption coefficient	1/m
$a_1 \dots a_5$	Stoichiometric factors	kmol
a_P, a_k	Coefficients in matrix $\mathbf{A}_\phi$	Variable
A	Area;	m^2
	Coefficient in expression for the scalar dissipation rate	1/s
$A_1^{(i)}, \dots, A_4^{(i)}$	Factors in the flamelet equations	Variable
$\boldsymbol{A}_l$	Coefficient in the Arrhenius expression for the reaction l	Variable
$\mathbf{A}_\phi$	Coefficient matrix of the linearised equation system	Variable
b	Boundary face	
b_ε	Polynomial fit in WSGGM	Variable
c	Normalised reaction progress variable	
c_p	Specific heat	J/(kgK)
c_{pk}	Specific heat of the species k	J/(kgK)
$C_1^{(k)}, \dots, C_8^{(k)}$	Discretisation coefficients	Variable
C_R	Conservation correction factor	
$C_{\varepsilon 1}, C_{\varepsilon 1}, C_s$	Constants in turbulence model	
C_μ	Structure parameter	
C_χ	Constant	
d	Diameter	m
D	Thermal diffusivity	m^2/s
Da	Damköhler number	
D_{ij}	Strain rate tensor component	1/s
D_c	Molecular diffusivity of the reaction progress variable	m^2/s
D_k	Molecular diffusivity of the species k	m^2/s

D_Z	Molecular diffusivity of mixture fraction	m^2/s
E_l	Activation energy of the reaction l	J/kmol
f_i	Cartesian component of the volume force vector	$kg/(m^2s^2)$
$f_{k,i}$	f_i for the species k	$kg/(m^2s^2)$
F	Cumulative distribution function	
h	Specific enthalpy	J/kg
h_k	Specific enthalpy of the species k	J/kg
$\Delta h^0_{f,k}$	Specific enthalpy of formation of the species k	J/kg
i'	Radiant intensity	W/m^2
I	Number of gray gases	
I_∞	Relative free-stream turbulence intensity	
J	Number of polynomial constituents in WSGGM	
k	Turbulent kinetic energy;	m^2/s^2
	Discrete point index	
$k_{f,b}$	Backward rate coefficient of the reaction l	Variable
$k_{f,l}$	Forward rate coefficient of the reaction l	Variable
$K_{C,l}$	Equilibrium constant of the reaction l	
l	Distance;	m
	Length scale	m
L	Cylinder radius	m
Le_k	Lewis number of the species k	
$\dot{m}$	Mass flow	kg/s
M	Molecular weight of mixture	kg/kmol
M_k	Molecular weight of the species k	kg/kmol
$\vec{n}$	Unit normal vector	
n_j	Cartesian component of the unit normal vector	
n_Z	Number of discrete point in mixture fraction space	
N	Number	

p	Pressure	Pa
P	Sum of partial pressures of absorbing species;	atm
	Production term in equation for the turbulent kinetic energy;	kg/(ms^3)
	Probability density function;	
	Computational node in control volume formulation	
q	Volumetric source	Variable
q_j	Cartesian component of the heat diffusion vector	W/m^2
Q	Non-dimensional heat flux	
r	Radius	m
$\vec{r}_P$	Computational node position vector	
$\vec{r}_{Pb}$	Vector connecting the computational node with the boundary face b	
$\vec{r}_{Pj}$	Vector connecting two neighbouring computational nodes over common face j	
R	Gas constant of the mixture;	J/(kgK)
	Radius	m
$\boldsymbol{R}$	Universal gas constant ($\boldsymbol{R}$ = 8314.4)	J/(kmolK)
Re	Reynolds number	
$\vec{s}, \vec{s}', \vec{s}_{kk}$	Unit direction vectors	
S	Distance;	m
	Surface	
Sc	Schmidt number	
$\overline{S}_k$	Radiative source term in control volume k	W
S_L	Laminar flame speed	m/s
t	Time	s
t_i	Cartesian component of the surface force vector	N/m
T	Temperature	K
u	Velocity;	m/s
	Normal velocity	m/s

u_j	Cartesian velocity component	m/s
$\widetilde{u_i"u_j"}$	Reynolds stress tensor component	m^2/s^2
V	Volume	m^3
V_j	Cartesian differential velocity component	m/s
$V_{k,j}$	Cartesian differential velocity component of the species k	m/s
w	Tangential velocity	m/s
x	Co-ordinate direction	
x_j	Cartesian co-ordinate	m
X_k	Species mole fraction	kmol/kmol
$[X_k]$	Species mole concentration	$kmol/m^3$
$[X_{k,e}]$	Species mole concentration at equilibrium	$kmol/m^3$
Y	Mass fraction	
Y_c	Reaction progress variable mass fraction	
Y_k	Species mass fraction	
Z	Mixture fraction	
Z_m	Local flame co-ordinate	

Greek	**Description**	**Unit**
α, β	Arguments in beta function	
α_ε	Weighting factor in WSGGM	
α_ϕ	Under-relaxation factor of an unknown ϕ	
β_l	Coefficient in Arrhenius expression for the reaction l	Variable
Γ	Diffusion coefficient	Variable
$\Delta^-_{(k)}, \Delta^+_{(k)}$	Backward and forward grid difference	
ε	Emissivity;	
	Dissipation rate of the turbulent kinetic energy	m^2/s^3
η	Kolmogorov length scale	m
Θ	Polar angle	rad

λ	Thermal conductivity	W/(mK)
μ	Dynamic viscosity (molecular)	Pas
μ_t	Turbulent viscosity	kg/(ms)
ν	Kinematic viscosity (molecular)	m^2/s
$\nu'_{k,l}$	Reactant species stoichiometric coefficient	kmol
$\nu''_{k,l}$	Product species stoichiometric coefficient	kmol
ξ	$\xi \equiv \chi_{st}$ or $\xi \equiv c$	1/s or –
ρ	Density	kg/m^3
σ	Prandtl number;	
	Stefan-Boltzmann constant ($\sigma = 5.6696 \cdot 10^{-8}$)	$W/(m^2K^4)$
σ_{ij}	Stress tensor component	N/m^2
σ_s	Scattering coefficient	1/m
τ	Time	s
τ_{ij}	Tangential stress tensor component	N/m^2
Υ_k	Species k	
ϕ	Fuel-to-oxidiser equivalence ratio;	
	Reactive scalar variable;	
	Vector with unknowns	Variable
φ	Intensive (scalar) property	Variable
Φ	Scattering phase function	1/sr
Φ_{ij}	Pressure-strain tensor component	m^2/s^3
χ	Scalar dissipation rate	1/s
$\dot{\omega}_c$	Production rate of reaction progress variable	$kg/(m^3s)$
$\dot{\omega}_k$	Production rate of the species k	$kg/(m^3s)$
Ω	Solid angle	sr
Ω_l	Rate of the single reaction l	$1/(m^3s)$

Subscripts	**Description**
0	Referent;
	Beginning of incremental path;
	Integral scale
b	Black body;
	Boundary
c	Chemical;
	Centre
CV	Control volume
DI	Dissipation-inertial
e	Extinction
eq	Equation(s)
EI	Energy-inertial
Ext	Extinction
faces	Faces
F	Fuel
h	Specific enthalpy
ii	Gray gases index
in	Incoming
j	Control volume surface index
k	Turbulent kinetic energy
(k)	Discrete point index
kk	Ray index
max	Maximum
min	Minimum
n	Position where a ray enters the control volume
$n+1$	Position where a ray leaves the control volume
net	Net
out	Outgoing
O	Oxidiser

p	Pilot
rays	Rays
reac	Reaction
R	Radiation
s	Scaled
spec	Species
st	Stoichiometric
S	Source
t	Turbulent
thresh	Threshold
vis	Visible
w	Wall
ε	Dissipation rate of the turbulent kinetic energy
η	Kolmogorov scale
λ	Wavelength
ϕ	Unknown scalar property
φ	Intensive (scalar) property

Superscripts	**Description**
'	Reynolds fluctuation
"	Favre fluctuation
‾	Reynolds average
~	Favre average
$\overline{\vert Z}$	Conditional average (average conditioned on Z)
Eq	Equilibrium
Ext	Extinction
(i)	Solution in the current iteration step
$(i-1)$	Solution from the previous iteration step
(k)	Discrete point index
Mix	Mixing

(*new*)	Solution of the linear equation system
n_Z	Last discrete point in mixture fraction space index

Mathematical symbols	**Description**
$e = 2.718281828\ldots$	
erfc^{-1}	Inverse complementary error function
exp	Exponential function ($\exp(x) \equiv e^x$)
sign	Sign ($+$ or $-$)
B	Beta function
Γ	Gamma function
$\prod$	Product
$\sum$	Summation
δ_{ij}	Kronecker tensor component
$\pi = 3.141592654\ldots$	

Abbreviations	**Description**
1D, 2D, 3D	One-, two-, three-dimensional
ASCII	American standard code for information interchange
AMG	Algebraic multi-grid
CDS	Central differencing scheme
CFD	Computational fluid dynamics
CGS	Conjugate gradients squared solver
CGSTAB	CGS stabilised
CK	k -distribution method
CMC	Conditional moment closure
CSC	Chemistry pre-processor (abbr. conserved scalar chemistry)
DNS	Direct numerical simulation
DOM	Discrete ordinates method
DTRM	Discrete transfer radiation method
EMST	Euclidean minimum spanning tree
FGM	Flamelet generated manifold

FPI	Flame prolongation of ILDM
FVM	Finite volume method
GUI	Graphical user interface
HTM	Hybrid turbulence model
IEM	Interaction by exchange with the mean
ILDM	Intrinsic low-dimensional manifolds
ISAT	*In situ* adaptive tabulation
JPDF	Joint probability density function
LDV	Laser Doppler velocimetry
LES	Large-eddy simulation
LFM	Laminar flamelet model
LIF	Laser-induced fluorescence
LU	Lower-upper
MC	Curl mixing
MIX	Mixing
ODE	Ordinary differential equation
OTM	Optically thin model
PCM	Presumed conditional moment
PDF	Probability density function
RANS	Reynolds averaged Navier-Stokes
RMS	Root-mean-square
RPV	Reaction progress variable
SIMPLE	Semi-implicit method for pressure-linked equations
SLFM	Stationary laminar flamelet model
SNB	Statistical narrow-band
TNF	Turbulent non-premixed flame
TRI	Turbulence/radiation interaction
WSGGM	Weighted sum of gray gases model

List of Figures

Figure 1 – Laminar flame speed for H_2/He-air premixed flame (fuel: H_2 80% vol., He 20% vol., 295 K; oxidiser: air, 294 K) 22
Figure 2 – Two-feed jet diffusion flame configuration 23
Figure 3 – Temperature flamelet (steady) profiles for H_2/He-air flame (fuel: H_2 80% vol., He 20% vol., 295 K; air: 294 K) 28
Figure 4 – Adiabatic temperature profiles from the premixed flamelet database (diluted methane (25% CH_4, 75% air – by volume)/air): a) T-x plots; b) T_{burnt}-Φ plot 32
Figure 5 – Adiabatic temperature profiles from the premixed flamelet database (diluted methane (25% CH_4, 75% air – by volume)/air): a) T-Y_{CO2} plots; b) T-Y_{CO2}+Y_{CO}+Y_{H2O} plots 33
Figure 6 – Reaction progress variable (premixed flamelets) 34
Figure 7 – O_2 profiles (premixed flamelets) for H_2/He-air flame (fuel: H_2 80% vol., He 20% vol., 295 K; air: 294 K) 35
Figure 8 – Reaction progress variable (non-premixed flamelets) 36
Figure 9 – O_2 profiles (non-premixed flamelets) for H_2/He-air flame (fuel: H_2 80% vol., He 20% vol., 295 K; air: 294 K) 37
Figure 10 – Maximum NO mass fractions, diluted methane (25% CH_4, 75% air – by volume)/air flame: mixed formulation vs. premixed flamelets 38
Figure 11 – Absorbing, scattering and emitting medium [115] 40
Figure 12 – Ray tracing (2D) 41
Figure 13 – Hemisphere discretisation around a boundary cell face 43
Figure 14 – Turbulent energy cascade (Kolmogorov cascade) 45
Figure 15 – Averaged profile 48
Figure 16 – Shapes of β-PDF for different values of parameters $\tilde{\boldsymbol{Z}}$ and $\widetilde{\boldsymbol{Z''^2}}$ 56
Figure 17 – H_2O profiles (H_2-air system; zoom near the stoichiometry): 1-step irreversible reaction and equilibrium models 64
Figure 18 – Finite differences (1D) grid 64

Figure 19 – Integrated (presumed β-PDF) temperature profile (adiabatic, $\chi_{st} = \mathbf{0.01}$ s^{-1}) for H_2/He-air flame (fuel: H_2 80% vol., He 20% vol., 295 K; air: 294 K) – see Fig. 3 70
Figure 20 – CSC solver structure 71
Figure 21 – CSC solver structure: chemistry solver 73
Figure 22 – CSC solver structure: PDF creator 75
Figure 23 – Domain discretisation into control volumes (2D) 77
Figure 24 – Control volume (arbitrary polyhedron) 78
Figure 25 – Combustion module implementation (schematics) 84
Figure 26 – Finite cylinder 85
Figure 27 – Non-dimensional heat flux vs. non-dimensional wall distance for different numbers of rays (optical thickness $\mathbf{aL = 1.0}$) 86
Figure 28 – Non-dimensional heat flux vs. non-dimensional wall distance for different optical thicknesses $\mathbf{aL}$ (48(4x12) rays) 87
Figure 29 – Hydrogen flame configuration 89
Figure 30 – Computational mesh (hydrogen flame; vertical axial cut; centreline) 90
Figure 31 – SLFM (standard) database (hydrogen flame) 93
Figure 32 – FPI database (hydrogen flame) 95
Figure 33 – SLFM (RPV) database (hydrogen flame) 97
Figure 34 – Radial profiles of mean axial velocity at $x/l_{vis}=1/8$ and $x/l_{vis}=3/8$ (hydrogen flame; k-ε; adiabatic) 98
Figure 35 – Axial profiles at centreline position (hydrogen flame; adiabatic vs. DTRM; k-ε vs. HTM): a) Mean temperature; b) Mean H_2O mass fraction 99
Figure 36 – Axial profiles at centreline position (hydrogen flame; non-adiabatic; k-ε vs. HTM): a) Mean mixture fraction; b) Mixture fraction RMS 100
Figure 37 – Radial profiles at $x/l_{vis}=3/8$ (hydrogen flame; adiabatic vs. non-adiabatic; k-ε vs. HTM): a) Mean temperature; b) Mean H_2O mass fraction 100
Figure 38 – Radial profiles of mean axial velocity at $x/l_{vis}=1/8$ and $x/l_{vis}=3/8$ (hydrogen flame; k-ε vs. HTM; non-adiabatic) 101
Figure 39 – Radial profiles at $x/l_{vis}=3/8$ (hydrogen flame; non-adiabatic; k-ε vs. HTM): a) Mean mixture fraction; b) Mixture fraction RMS 101

Figure 40 – Radial profiles of mixture fraction moments (mean and RMS) at various axial positions (hydrogen flame; non-adiabatic; HTM) 103
Figure 41 – Axial profiles of the mean temperature and species mass fractions (hydrogen flame; centreline position; non-adiabatic; HTM)..... 105
Figure 42 – Tabulation parameters (hydrogen flame): a) $\widetilde{\chi}_{st}$ (Eq. (91)), SLFM database; b) $\widetilde{c}$ (Eq. (100)), FPI database..... 106
Figure 43 – Radial profiles of the mean temperature and species mass fractions at x/l_{vis}=1/4 (hydrogen flame; non-adiabatic; HTM) 107
Figure 44 – Radial profiles of the mean temperature and species mass fractions at x/l_{vis}=3/4 (hydrogen flame; non-adiabatic; HTM) 108
Figure 45 – Methane flame configuration 109
Figure 46 – Computational mesh (methane flame; vertical axial cut; centreline)..... 110
Figure 47 – Inlet velocity profiles (methane flame) 111
Figure 48 – Premixed diluted methane (25% CH_4, 75% air – by volume)/air flames: a) Laminar flame speed; b) Burnt gas temperature..... 113
Figure 49 – SLFM (standard) database (methane flame) 114
Figure 50 – FPI database (methane flame) 115
Figure 51 – SLFM (RPV) database (methane flame) 116
Figure 52 – Mixed database (methane flame)..... 117
Figure 53 – Mean temperature axial profile at centreline position (methane flame; adiabatic vs. DTRM; k-ε vs. HTM) 118
Figure 54 – Axial profiles at centreline position (methane flame; adiabatic vs. DTRM; k-ε vs. HTM): a) Mean CO_2 mass fraction; b) Mean H_2O mass fraction 119
Figure 55 – Radial profiles of mean axial velocity (methane flame; DTRM; k-ε vs. HTM) at various axial locations (methane flame) 120
Figure 56 – Axial profiles (centreline) of mixture fraction moments (mean and RMS) (methane flame) 121
Figure 57 – Radial profiles of mixture fraction moments (mean and RMS) at various axial locations (methane flame)..... 122
Figure 58 – Radial profiles of mean temperature at various axial locations (methane flame) 123

Figure 59 – Axial profiles (centreline) of mean species mass fractions (methane flame) 124
Figure 60 – Radial profiles of mean species mass fractions at x/d=30 (methane flame) 126
Figure 61 – Radial profiles of mean species mass fractions at x/d=60 (methane flame) 127
Figure 62 – Combustion chamber (TECFLAM) 130
Figure 63 – Burner configuration (TECFLAM) 130
Figure 64 – Computational mesh (TECFLAM; vertical axial cut; centreline) 131
Figure 65 – Mean velocity profiles of air at the burner exit (TECFLAM) 132
Figure 66 – SLFM (standard) database (TECFLAM) 134
Figure 67 – FPI database (TECFLAM) 135
Figure 68 – SLFM (RPV) database (TECFLAM) 136
Figure 69 – Radial profiles of mean axial (u) and tangential (w) velocities at various axial positions (TECFLAM) 137
Figure 70 – Radial profiles of mixture fraction moments at axial positions x=20 mm and x=90 mm (TECFLAM) 138
Figure 71 – Axial profiles (centreline) of mean mixture fraction (TECFLAM) 139
Figure 72 – Radial profiles of mean temperature at axial positions x=20 mm and x=90 mm (TECFLAM) 139
Figure 73 – Radial profile of $\overline{c}$ (Eq. (100); FPI) at axial position x=20 mm (TECFLAM) 140
Figure 74 – Radial profiles of mean species mass fractions at axial position x=20 mm (TECFLAM) 141
Figure 75 – Radial profiles of mean species mass fractions at axial position x=60 mm (TECFLAM) 142
Figure 76 – Radial profiles of mean species mass fractions at axial position x=120 mm (TECFLAM) 143

List of Tables

Table 1 – Radiative heat balance (methane flame)..... 119

1 Introduction

1.1 Motivation and general overview

The turbulent combustion science has been attracting the attention of many researchers for the last few decades [1] and it still seems to be an evolving field of the overall community interest. Environmental issues, pollutant formation, competitiveness on the energy equipment market, the new ways of sustainable energy reasoning, etc., are only a few major reasons for this tendency. Moreover, the usage of fossil fuels throughout the 21st century is expected to play an almost equally important role as it does at the moment [2, 3], additionally justifying the need for further research and development in the field of combustion. In particular, the increased need for the control of the pollutant emissions (NO_x, SO_x) in the power generation sector, as well as the CO_2 emission reduction urge due to a recent international greenhouse gas debate, have contributed considerably to ever growing combustion research since the 1970s [4]. Some other important sectors benefiting from a good understanding of combustion processes are transportation, heating, automobile industry, aeronautics, etc.

While relying almost completely on experimental methods in the early days of practical combustion engineering, the application of the computational fluid dynamics (CFD) methods [5, 6] in today's solving of combustion related problems has become a widely accepted practice [7-12]. However, as there are many different physical phenomena simultaneously involved, the task of a complete mathematical description of such problems is rather challenging [13-16].

Turbulence, which itself is a difficult to solve non-linear physical problem [17-19], is ordinarily encountered in practical combustion devices. The inclusion of combustion modelling into the overall solution procedure raises the difficulty level substantially. As a complete range of temporal and spatial scales due to turbulence and combustion spreads over multiple orders of magnitude, an increased difficulty arises when one attempts to solve all these scales directly (direct numerical simulation – DNS) [3, 15, 20]. Due to extreme and prohibitive computational costs DNS is still an intractable way of solving most of practically relevant fluid problems today [18, 21]. If solving averaged quantities

instead, the prohibitive computational cost is overcome and a tractable method is obtained. It is Reynolds [22] who was the first to average the leading Navier-Stokes equations, and accordingly, this methodology is nowadays referred to as the Reynolds averaged Navier-Stokes (RANS) approach. Due to its effectiveness and tractability this is the favourable methodology in industrial applications today [23], although due to a limited range of information it provides and due to the problematic modelling issues its drawbacks are becoming increasingly evident [24]. It must be mentioned, though, that the constantly growing computational resources open up new horizons for generically better and more descriptive modelling approaches, like large eddy simulation (LES). However, in spite of the known deficiencies, RANS is still expected to be a common framework for the fluid flow and combustion modelling for some time to come, at least as a component of a likely hybrid modelling procedure [25].

In addition to the problems associated with the closure of the Reynolds stresses and turbulent fluxes in the modelling of non-reactive flows, a major new difficulty in the reactive flow situations appears when averaging the highly nonlinear source terms in the transport equations for mean species mass fractions. A direct attempt to average the reaction rate expressions results in numerous new unclosed correlations, solely in the simplest case of the 1-step irreversible reaction ([20]), making this approach arduous if complex chemistry is considered. Thus, due to the unacceptable limitations of this classical approach alternative ways had to be found. Different combustion models with a various degree of complexity have been proposed in the last two decades, the most famous among them being the laminar flamelet model (LFM) [15, 26] and its variations, the conditional moment closure (CMC) model [27], the model based on the solution of the joint probability density function (JPDF) [18, 28], etc. Because of a different physical reasoning behind their derivation, and because of different starting modelling points, these models differ with respect to description complexity, applicability, efficiency, etc. Therefore, a compromise is usually needed when deciding upon which to use in a particular situation.

At last but not least, a goal of an accurate turbulent diffusion flame prediction, especially in the industrial applications, usually presumes the accurate heat transfer modelling as well. Thermal radiation is very important in this respect. Not solely

motivated by a need to accurately account for heat fluxes at the walls of practical devices, the radiation mode of heat transfer has also been recognised within the combustion community as a very important ingredient of the overall modelling procedure [29]. This especially holds when the accurate modelling of NO_x is required – a pollutant whose formation strongly depends on temperature. Unfortunately, at the moment it seems that a full account of the accomplished radiation modelling is too much of a burden for an efficient overall modelling procedure and the simplified radiation models are usually retained in the industrial applications. Nonetheless, the importance of radiation details, like the spectral dependence of radiative properties [30], is recognised.

1.2 State-of-the-art research – a survey

As mentioned earlier, DNS rapidly becomes intractable if the problems of practical relevance (moderate or high Reynolds numbers) are attempted to be solved. However, apart from that, DNS has always been of great importance to researchers when trying to understand some basic physical phenomena in simple academic examples. A significant research effort using DNS in the multi-component reactive flows was devoted to the problem of differential diffusion between the species [31, 32]. As this phenomenon occurs at the molecular level, DNS is needed for an accurate solution. Differential diffusion in isotropic, decaying turbulence was investigated by DNS in [32], and the conditional fluctuations in the species compositions were found to be important in this respect. This information is quite valuable to the CMC modellers. The influence of differential diffusion on the maximum flame temperature in turbulent hydrogen/air flames was investigated by 2D DNS in [33]. It is shown there that differential diffusion can change the reaction zone structure by shifting the lighter species, like H_2 and H, towards the lean side, while peaks are not located at the stoichiometry anymore. The exact flamelet formulation that takes into account the effects of differential diffusion in non-premixed combustion was derived in [34]. Together with an unsteady flamelet model, it was subsequently applied in a turbulent jet diffusion flame simulation in [35].

Although the advantages of the LES application in reactive flows were not that obvious from the beginning [14], when compared to RANS, many recent developments in the combustion modelling are based on the LES methodology. The larger scales are

directly resolved by LES and these are responsible for bringing the fuel and oxidiser to mixing in non-premixed combustion. However, as combustion occurs at the smallest scales that are not directly resolved by LES, the appropriate sub-grid modelling of combustion is still necessary, similarly as in RANS [13]. Thus, the problems associated with the closure of non-linear reaction rates are inherited in LES as well. However, as LES needs much coarser numerical grids when compared to DNS, it can be already applied in the simulations of some practically relevant combustion systems (moderate Reynolds numbers), e.g. [36-39]. It must be noted, however, that LES, as an unsteady method, is still computationally much more demanding than the adequate RANS methodology. This is particularly emphasised in the simulations of stationary operating devices, where sufficiently long calculations are necessary to accumulate enough results to get a valid time statistics. On the other hand, the arguments speak more in favour of LES in the simulations of inherently time-dependent configurations, like internal combustion engines, or while simulating the important transients during combustion, like auto-ignition, flame oscillations, etc. [13]. The LES of a piloted methane/air diffusion flame (Sandia flame D [40]), together with the extended flamelet model [41], are shown in [42-44]. The same flame was simulated by using LES and CMC modelling in [45]. Some other interesting LESs of turbulent diffusion flames with partial premixing can be found in [46, 47]. The LES of premixed flames can be found, e.g., in [48, 49].

From the modelling point of view, the application of the probability density function (PDF) methods in turbulent reactive flows [28] is suitable because the reaction and convection terms appear in a closed form. Additionally, because PDF is solved and not presumed, unlike in the CMC model or in the stationary laminar flamelet model (SLFM), a much weaker hypothesis on PDF's shape is involved. Two major problems in the PDF approach, however, are the modelling of molecular mixing and the development of an accurate Monte Carlo solution scheme [14, 16, 28]. Some older models for molecular mixing, like the interaction by exchange with the mean model (IEM), or the modified Curl mixing model (MC), have proven deficient in some situations due to the non-localness in composition space. Accordingly, the model based on the Euclidean minimum spanning tree (EMST) was recently proposed [50] as an alternative. The performances of these mixing models are compared in [51, 52]. Interesting differences were found,

especially in situations with extinction, showing superiority of the EMST model. A series of piloted methane/air flames [40] was successfully simulated using the PDF/EMST model in [53], showing the capability of this approach to represent the local extinction and re-ignition phenomena encountered in some of these flames (especially in flame F). Methane/air flames in a simple piloted jet configuration, as well as a more complex bounded flow configuration of the TECFLAM burner [54], were numerically simulated using the transported PDF method in [55]. In this work IEM and MC were used. Since many particles per computational cell (nominally 100 in [53], e.g.) are needed to represent the PDF evolution satisfactorily, the PDF based methods are computationally still expensive, especially if complex chemistry is involved. In order to reduce the computational cost a storage/retrieval methodology based on the *in situ* adaptive tabulation (ISAT) was proposed in [56]. Its increased efficiency, when compared to the standard direct integration approach, was demonstrated recently in [57] in a simple reaction-diffusion example, showing speed-up factors up to five. Even greater speed-up factors were achieved in another example with detailed chemistry [58]. The PDF calculations of the bluff-body stabilised flames with detailed chemistry can be found in [59]. An interesting new partial PDF approach was recently introduced in [60], but validation in real test cases is still needed before judging its performance.

The conditional moment closure (CMC) method was independently derived by Bilger and Klimenko in the early 1990s, and its thorough description and recent review can be found in their common paper [27]. The basic presumption in the CMC modelling is that the fluctuations of scalar quantities (species mass fractions, temperature) are associated with the fluctuations of only one key quantity – this quantity usually being mixture fraction in non-premixed combustion. The fluctuations of the conditionally averaged scalars were found to be much lesser in magnitude than unconditional fluctuations, leading, thus, to an easier closure of the non-linear reaction terms in the former case. This closure is usually performed at the level of first moments (first-order closure), e.g. [61-63], although the importance of the second-order closure is more and more emphasised, especially when substantial conditional fluctuations are expected [63]. In [63] the turbulent jet methane/air diffusion flame (Sandia flame D [40]) was simulated using the first-order CMC closure. Three chemical schemes of different complexity were applied.

Good agreements with experimental data were obtained, especially if considering the conditional statistics. The predictions of NO have shown to be highly sensitive to the reaction scheme complexity, while the second-order CMC closure is suggested if more accurate NO predictions are required. Subsequent applications of the first-order CMC in hydrogen and methane jet diffusion flame configurations can be found in [61, 62, 64]. As expected, the second-order turbulence modelling is reported to be superior to the simple eddy-viscosity modelling concept [61, 62]. The second-order CMC closure is suggested for the flames with the higher possibility of the local extinction [62]. The lift-off height was accurately predicted in a hydrogen flame simulation in [64]. However, the moderate computational costs associated with the method still represent a major difficulty in an effective CMC application in practical problems. If, for instance, the sample space variable (mixture fraction in non-premixed combustion) is subdivided into N points, while a chemical mechanism consisting of M species is applied, the total number of conditionally averaged species transport equations that have to be solved is $N \times M$. Thus, in the case of the GRI-Mech 3.0 chemical mechanism [65] (53 species), and, say, 50 grid points in the sample variable space (68 used in [63], e.g.), the total number of 2650 species transport equations should be solved. It is obvious that such an approach becomes very demanding computationally if a joint calculation of the turbulent flow field and the CMC chemistry is performed with detailed chemistry. In practice, the CMC calculations are usually separated from the flow field solution in order to reduce the computational costs, and if possible, the CMC equations are additionally averaged in spatial directions with small conditional fluctuations (in cross-stream directions in axisymmetric jets in [61-63], e.g.). The inclusion of the second-order CMC modelling additionally increases the overall computational cost. In [66] it is shown that 14 additional transport equations for variances and covariances arise if only two reactions steps from the chemical mechanism are subjected to the second-order closure. Nonetheless, it is shown that improved predictions are obtained with the second-order CMC closure as well.

The flamelet concept assumes a turbulent diffusion flame to be composed of an ensemble of the stretched laminar flamelets attached to the instantaneous position of the flame surface, which itself is impacted by the flow field [15, 67]. As long as these thin flamelet structures (flamelets) are small, when compared in size to the Kolmogorov

eddies, the flamelet concept is fully justified [16]. Once the position of the flame surface is determined, all reactive scalars normal to the surface can be obtained by solving the flamelet equations [15]. In the case that turbulence becomes very intensive (lower Damköhler numbers), where small eddies become comparable in size with the flamelets, the flamelets are not embedded within the quasy-laminar flow layers of an eddy anymore and they are corrugated by the flow field. The application of the flamelet concept in such situations was disputed, for instance, in [68], leading to an interesting debate afterwards [69, 70].

If flamelet equations are solved to their stationary solutions and if the obtained profiles are used in the combustion calculations, the stationary laminar flamelet model (SLFM) is obtained [15]. The main advantage of SLFM, when compared to the classical moment methods, is that the transport equations for species mass fractions do not have to be solved. The first two moments (mean and variance) of mixture fraction are solved in the standard CFD procedure only, while mean species mass fractions are recovered from the stationary laminar flamelet profiles, assuming their statistical distribution as a β-PDF of the mixture fraction moments. The stationary laminar flamelets can be solved apart from the CFD calculation in the pre-processor step and the results can be stored in the, so called, PDF tables. These PDF tables can then be used in as many subsequent CFD calculations as necessary. An alternative, but a less stringent way when considering the turbulent flame structure, would be to use only the species source terms from the stationary laminar flamelet library and to calculate the species transport equations in the CFD procedure [20].

Unlike CMC and transported PDF, the flamelet concept is suitable for the inclusion of differential diffusion effects. In [34] a consistent flamelet formulation with differential diffusion was derived in the case of non-premixed combustion. Also, in order to relax the original hypothesis of the SLFM concept, which implies that the temporal scales in flamelet equations are much smaller than the temporal scales found in the turbulent flow field, a flamelet formulation that takes into account the temporal evolution of the scalar dissipation rate was proposed in [35]. It was applied in the simulation of the $CH_4/H_2/N_2$-air diffusion flame, together with the differential diffusion modelling, showing good agreements with the experiments. The unsteady flamelet modelling of the piloted jet

diffusion flame (Sandia flame D [40]) was performed in [71], while the same modelling strategy was successfully applied in the simulation of a mild combustor in [72].

The historical development in combustion modelling followed the lines of natural distinction of combustion processes into the non-premixed and premixed processes. In this respect, well established models were developed that are sufficiently accurate and reliable if applied within the ranges of their definition. However, the application of these models in situations with partial premixing is rather questionable [16]. In diffusion flames, for instance, the partial premixing occurs in the regions of local extinction and re-ignition (edge flames), or at the lift-off height of the jet stabilisation (triple flames). As these subtle phenomena strongly depend on the details of flame dynamics, local heat fluxes, etc., it is hard to expect that a combustion model within the RANS concept would capture these effects accurately. However, efforts are made to capture major behaviour like global extinction. While some models are not limited by the classification into premixed or non-premixed, like the PDF or CMC models, and can be used in both cases, some other models, like SLFM, are limited. Although SLFM can partly account for non-equilibrium effects via scalar dissipation rate [15], it was observed in some configurations that there exist regions below the quenching limit predicted by SLFM where the flame is still burning. These parts correspond to partial premixing and are not accessible by the classical SLFM.

A chemistry tabulation procedure based on the combined usage of the premixed and non-premixed laminar flamelets in the RANS simulation of a methane/air flame was recently proposed in [47]. As it uses the conditional moments of a suitably chosen reaction progress variable to enter the pre-tabulated chemistry, while at the same time the turbulence/chemistry coupling is done via the presumed β-PDF, the methodology is referred to as the presumed conditional moment (PCM) concept. As, both, premixed and non-premixed flamelets are used, all possible realisations from the pure fuel/oxidiser mixing until the equilibrium burning limit are covered with this approach nominally, making it promising while modelling turbulent diffusion flames with various degree of partial premixing. Premixed flamelets can be obtained either from the FPI (flame prolongation of ILDM; ILDM – intrinsic low-dimensional manifold) [73] or FGM (flamelet generated manifolds) [74] method, while for non-premixed flamelets the

classical SLFM database can be used [15]. The application of the FPI pre-tabulation methodology in the simulations of laminar and turbulent flames can be found in [75-78]. The re-parameterisation of the classical non-premixed SLFM database using the reaction progress variable is proposed in [79].

The modelling of thermal radiation within the overall CFD procedure is not that straightforward because of the non-continuous character of radiation. Some early methods, like the Hottel's zone method [80] or the Monte Carlo technique applied on the radiative heat transfer problems [81], although accurate, have not found wide usage, mostly due to their poor computational economy. Three methods of choice, which are sufficiently economical and suitable for the implementation into the CFD codes, are the discrete ordinates method (DOM) [82, 83], the finite volume method (FVM) [84] and the discrete transfer radiation method (DTRM) [85]. The inclusion of radiation is especially important in the problems where the heat fluxes at the domain boundaries (e.g. furnace walls) are substantial, while an accurate radiation prediction is often of crucial importance for the proper functionality of the device in consideration. Some interesting applications of the former methods in configurations with complex geometry can be found in [86-90]. However, the importance of radiation even in the simple configurations, like jet diffusion flames, is recognised by the combustion community interested in the accurate predictions of minor species [29]. Also, if following the conclusions from a series of international workshops on measurement and computation of turbulent nonpremixed flames (TNF) [29], the numerical simulations of targeted test flames proposed there should include radiation whenever possible.

Because of the simplicity, computational efficiency and ease of implementation, the first radiation model to be used in the simulations of TNF flames was the optically thin model (OTM). Some results can be found in the proceedings at [29], while the detailed model description together with the curve fits for the Planck mean absorption coefficients from RADCAL [91] can be found in [92]. In [92] OTM was applied together with CMC in the simulations of diluted hydrogen jet flames and has proven appropriate. However, in the subsequent simulations with hydrocarbon fuels it is reported to over-predict the radiation heat losses substantially, and, generally, it is considered as an insufficiently accurate model. In [63] the RADCAL [91] radiation sub-model was used in the CMC

simulation of the methane/air flame (Sandia flame D [40]), with radiant heat losses being over-predicted by factor 2.45. This has shown to have a considerable effect on the chemical pathways of NO and its prediction accuracy. The medium was considered grey. In [30] the OTM and DOM radiation models were compared for the same flame configuration (Sandia flame D [40]). Similar results were obtained in both cases, with radiant losses being over-predicted. However, if taking into account the spectral radiative effects and turbulence/radiation interaction (TRI), better predictions can be expected, as shown in [93]. In that paper the DOM and ray-tracing method capabilities of predicting the radiation heat loss in the Sandia flame D configuration [40] are compared, while the spectral gas properties are accounted for by using the statistical narrow-band (SNB) and k-distribution (CK) models. The DOM and ray-tracing methods have shown similar results, while the appropriate TRI modelling has proven very important (the fraction of radiation losses due to turbulent fluctuations amounted to around 50%). It is mentioned, however, that large computational costs are associated with such calculations when the details, like spectral effects, are taken into account. Very recently comprehensive CFD calculations of the oxygen-enriched turbulent diffusion flames were performed by incorporating the state-of-the-art modelling of chemistry, soot formation and oxidation, and thermal radiation in [94]. It is confirmed there that the inclusion of spectral dependence in the evaluation of gaseous radiative properties is important if accurate NO predictions and the correct radiative heat flux distribution are desired. The interaction between radiation and chemistry was recently investigated in [95]. Significant over-predictions in the soot and NO concentrations were obtained if neglecting radiation.

1.3 Work hypothesis and outline

It is presumed that the pre-tabulated chemistry approach can be applied with sufficient accuracy in numerical simulations of turbulent diffusion flames with various degree of complexity. As only two or three additional transport equations have to be solved during the CFD calculation as a part of combustion modelling, while the chemical composition space is extracted from the pre-calculated tables, it can be stated that such an approach is numerically efficient when compared to the classical turbulent combustion modelling approach, where numerous, non-linear and hard-to-close transport equations for mean species mass fractions have to be solved. As such, the pre-tabulated chemistry approach can be readily applied in the combustion simulations of practically relevant problems, without restrictions regarding the chemistry complexity and CPU power.

Two different RANS combustion closures, based on the pre-tabulated chemistry approach, have been implemented in this work – the stationary laminar flamelet model (SLFM) [15] and the presumed conditional moment (PCM) closure [47]. While SLFM is nominally restricted to pure diffusion flames, PCM can be used (by definition) in situations with the deliberate degree of partial premixing. The chemistry related calculations and tabulations were performed in the pre-processor step by using a specially developed software application – the CSC solver [96]. Although not an issue in this work, the laminar flamelet formulation taking into account differential diffusion, according to [34], was additionally implemented into the CSC solver. The premixed 1D laminar flames computations, as a part of the overall PCM modelling procedure, were performed by using the adapted PREMIX solver [97], while the CHEMKIN II libraries [98] were used for the chemical kinetics and species properties evaluations. A new tabulation procedure, based on the suitably defined normalised reaction progress variable, has been proposed for premixed, non-premixed and combined flamelet formulations. The turbulence/chemistry interaction was accomplished via the presumed β-PDF, parameterised with the first two moments of mixture fraction, while mean species mass fractions, obtained by weighting the instantaneous steady profiles with such presumed β-PDF, were tabulated in the pre-processor step. The CFD solver FIRE [99] was used throughout this work for the variable density flow calculations. In order to account for

radiative heat transfer the conservative formulation of the discrete transfer radiation method (DTRM) [85, 100], together with the weighted sum of grey gases model (WSGGM) [101], was implemented into the FIRE code additionally [102].

Three different diffusion flame configurations of increasing complexity (in order) have been simulated in this work – the diluted hydrogen/air jet flame [103, 104], the piloted methane/air jet flame [40] (Sandia flame D), and the confined, swirled, natural gas flame, as the one in the TECFLAM combustion chamber [54]. In the case of the hydrogen flame, the chemistry is relatively simple and well known, and the detailed chemical mechanism for hydrogen chemistry consisting of 37 reactions, including NO pathways, was used. For the more complex methane chemistry, in the case of the methane/air jet flame and the TECFLAM flame, the detailed GRI-Mech 3.0 [65] chemical mechanism, consisting of 53 species and 325 reactions, was used. While the first two flames are geometrically relatively simple (jet configurations), the TECFLAM flame is geometrically complex because of the swirled fuel inlet and the bluff-body stabilisation. Additionally, this flame is confined and the radiation heat transfer modelling is especially necessary in this case. The numerical results have been compared to experimental data for all three cases.

The outline of this work is as follows. After the introduction, the main components of the mathematical model, as used in this work, are presented first. Among others, this includes the description of the basic conservation principles, the description of the combustion and radiation modelling, as well as the statistical description. Next, the numerical procedure is described. In this part the details of the numerical implementation of the CSC solver are outlined first, while the DTRM implementation with a verification test is described subsequently. The components of the fluid flow solver are briefly described as well. Finally, the experimental and simulation set-up for the flame configurations simulated in this work are presented, while the simulation results are compared to the available experimental data. The conclusions are made at the end.

1.4 Thesis contribution

This work is expected to contribute to recent developments in the combustion science that search for means of the inclusion of as detailed as possible combustion representation in the simulations of practically relevant combustion systems and at affordable computational cost. It is recognised, however, that more advanced and rigorous combustion modelling procedures exist, but the emphasis here is put on a compromised solution between accuracy and affordability. The tools developed in this work are use-ready for the application in the real industrial problems, while at the same time they can easily serve as a solid basis for further research and development of the combustion models based on the pre-tabulated chemistry approach.

The contributions can be summarised as:

- The development of the CSC pre-processor:
  - Chemistry calculations – Burke-Schumann model/equilibrium model/stationary laminar flamelet model (SLFM)/stationary laminar flamelet model with differential diffusion
  - PDF integrations – structured tables ready for use in CFD calculations
- A new chemistry pre-tabulation procedure based on the normalised reaction progress variable:
  - Premixed flamelets
  - Non-premixed flamelets
  - Premixed/non-premixed flamelets
- The implementation of the discrete transfer radiation method (DTRM), and its application, together with a hybrid turbulence model, in the computational simulations of non-premixed flames with a various degree of complexity
- A turbulent combustion closure based on the presumed conditional moments of the reaction progress variable

2 Mathematical modelling

2.1 Conservation equations

A basic set of equations governing the fluid flow can be deduced by applying the conservation laws to the fluid passing through an infinitesimal control volume. These equations are briefly summarised here, while for deeper insight and derivation details one is referred to the standard literature on this topic, e.g. [5, 17, 105-108]. As usual in the fluid mechanics, the Eulerian frame of reference is adopted. Whenever encountered, and if not stated otherwise, the Einstein's summation convention over the repeated indices of the Cartesian components is presumed [105, 109].

2.1.1 Conservation of mass

The fluid mass that enters the control volume through its boundaries cannot be destroyed and any net flux on the control volume boundaries is followed by the changes in density only. After balancing, and if presuming an infinitesimal control volume, the differential form[1] of the continuity equation is obtained as:

$$\frac{\partial \rho}{\partial t} + \frac{\partial \left(\rho u_j \right)}{\partial x_j} = 0 \tag{1}$$

The equation of continuity, as given in Eq. (1), is valid, both, in single- and multi-component systems. The exact derivation for multi-component systems is given in [108].

2.1.2 Conservation of momentum

According to the Newton's second law of motion[2], the rate of the momentum change of a moving fluid particle is balanced by the net force (sum of surface and volume forces) acting on that particle. Within the Eulerian framework, and for the *i*-th Cartesian component of the velocity vector, this can be expressed as:

[1] Density ρ is presumed to be continuous and derivable everywhere within the contol volume V_k

[2] Formal statement of the Newton's second law of motion: *'The acceleration of an object as produced by a net force is directly proportional to the magnitude of the net force, in the same direction as the net force, and inversely proportional to the mass of the object.'*

$$\frac{\partial(\rho u_i)}{\partial t}+\frac{\partial(\rho u_i u_j)}{\partial x_j}=f_i+\frac{\partial \sigma_{ij}}{\partial x_j} \tag{2}$$

Terms on the right hand-side in Eq. (2) represent the volume and surface forces acting on the fluid. The surface force vector components t_i are usually expressed in terms of the stress tensor components σ_{ij} as $t_i=\sigma_{ij}n_j$. The overall stress tensor can be decomposed into the normal and tangential components as:

$$\sigma_{ij}=-p\delta_{ij}+\tau_{ij} \tag{3}$$

If the fluid is isotropic and Newtonian, the tangential stress components are related to the rate-of-strain tensor $D_{ij}=\frac{1}{2}\left(\frac{\partial u_i}{\partial x_j}+\frac{\partial u_j}{\partial x_i}\right)$ as:

$$\tau_{ij}=2\mu\left(D_{ij}-\frac{D_{kk}}{3}\delta_{ij}\right) \tag{4}$$

In Eq. (4) it is presumed that the bulk viscosity coefficient is zero [108].

2.1.3 Conservation of angular momentum

The angular momentum conservation law, when applied to the fluid particle, states that the total rate of change of the angular momentum is balanced by a net angular momentum of all the forces acting on that fluid element, resulting in an important statement that the stress tensor is symmetric, i.e.:

$$\sigma_{ij}=\sigma_{ji} \tag{5}$$

A direct mathematical consequence of this is that the stress tensor can be decomposed into its spherical and deviatoric part, as in Eq. (3).

2.1.4 Conservation of energy

In multi-component systems the specific enthalpy (chemical + sensible) is usually used as an energy representative. The specific enthalpy equation for the multi-component mixture, as derived in [20], is written:

$$\frac{\partial(\rho h)}{\partial t}+\frac{\partial(\rho h u_j)}{\partial x_j}=\frac{\partial p}{\partial t}+u_j\frac{\partial p}{\partial x_j}-\frac{\partial q_j}{\partial x_j}+\tau_{ij}\frac{\partial u_i}{\partial x_j}+\rho\sum_{k=1}^{N_{spec}}Y_k f_{k,j}V_{k,j}+q_h \tag{6}$$

The first two terms on the right hand-side represent the contribution to the specific enthalpy change due to temporal and spatial pressure gradients. The fourth term is due to the viscous heating, while the last (sixth) term represents the specific enthalpy contribution due to external sources, e.g. radiation. The summation term on the right hand side in Eq. (6) accounts for the power generated by volume forces acting on species that move with diffusion velocities $\vec{V}_k$. The third term is a divergence of the heat flux vector $\vec{q}$ and accounts for all the diffusive heat transport. The heat flux vector is calculated as:

$$q_j=-\lambda\frac{\partial T}{\partial x_j}+\rho\sum_{k=1}^{N_{spec}}Y_k h_k V_{k,j} \tag{7}$$

2.1.5 Scalar transport

A generic conservation equation for any specific (intensive) scalar property φ [5], e.g. species mass fraction or mixture fraction, can be written as:

$$\frac{\partial(\rho\varphi)}{\partial t}+\frac{\partial(\rho\varphi u_j)}{\partial x_j}=\frac{\partial}{\partial x_j}\left(\Gamma_\varphi\frac{\partial\varphi}{\partial x_j}\right)+q_\varphi \tag{8}$$

The modelling of the diffusion coefficient Γ_φ and the source term q_φ is required in order to close Eq. (8). If the source term q_φ is zero, the scalar is conserved. If the scalar, on the other hand, has no direct impact on the flow field (via density e.g.), it is called the passive scalar.

2.2 Thermo-chemical relations

The specific enthalpy (chemical + sensible) of the species k in a multi-component system with N_{spec} species, where $k = 1, 2, \ldots, N_{spec}$, is defined as:

$$h_k = \Delta h^0_{f,k} + \int_{T_0}^{T} c_{pk}(T)\, dT \tag{9}$$

The first term on the right hand-side represents the specific enthalpy of formation of the species k at referent temperature T_0 (usually $T_0 = 298.15\ K$), and it contains the chemically bond energy. The values of the specific formation enthalpies for the specified referent temperature are tabulated and are available in the literature, e.g. [20, 108], or in the computational databases, e.g. [98]. The second term on the right hand-side in Eq. (9) stands for the sensible specific enthalpy of the species k. Once the specific enthalpies of individual species are known, the specific enthalpy of a mixture is obtained as a mass-weighted sum:

$$h = \sum_{k=1}^{N_{spec}} Y_k h_k \tag{10}$$

Similarly, whenever necessary, the specific heat of the mixture is obtained as:

$$c_p = \sum_{k=1}^{N_{spec}} Y_k c_{pk} \tag{11}$$

Presuming an ideal gas, density and pressure are related as:

$$\rho = \frac{p}{RT} \tag{12}$$

In Eq. (12) R stands for the mixture gas constant. It is calculated from the universal gas constant $\boldsymbol{R}$ and the mixture molecular weight M as:

$$R = \frac{\boldsymbol{R}}{M} \tag{13}$$

The mixture molecular weight is obtained from the molecular weights of individual species M_k and mixture composition Y_k as:

$$M = \frac{1}{\sum_{k=1}^{N_{spec}} \frac{Y_k}{M_k}} \tag{14}$$

When it is necessary to represent the gas mixture in terms of species mole fractions, the conversion formula is:

$$X_k = Y_k \frac{M}{M_k} \tag{15}$$

In the chemical kinetics problems one usually deals with molar concentrations:

$$[X_k] = \rho \frac{Y_k}{M_k} \tag{16}$$

No summation convention is applied in Eqs. (15) and (16).

The species source terms ω_k appear in the balance equations for species mass fractions (e.g. in flamelet equations – as will be shown later). It is the chemical kinetics science that tries to give the answers on the rates of chemical reactions and to make a closure of these terms. The already available data, as collected from different sources, is usually given in terms of chemical mechanisms, which consist of many elementary reactions and prescribed reaction rate data, mostly in the format as that used by the CHEMKIN II package [98].

A general set of elementary chemical reactions can be mathematically represented as:

$$\sum_{k=1}^{N_{spec}} \nu'_{k,l} \Upsilon_k \underset{k_{b,l}}{\overset{k_{f,l}}{\rightleftarrows}} \sum_{k=1}^{N_{spec}} \nu''_{k,l} \Upsilon_k \tag{17}$$

The symbol Υ_k represents the species involved in an elementary chemical reaction step l, e.g. $\Upsilon_k \equiv CO_2$, while $\nu'_{k,l}$ and $\nu''_{k,l}$ represent the stoichiometric coefficients for the same reaction. The total number of elementary reactions is N_{reac} ($l = 1,...,N_{reac}$). Symbols $k_{f,l}$ and $k_{b,l}$ stand for the forward and backward rate coefficients of the reaction l, respectively.

The rate of the single elementary reaction l is calculated as:

$$\Omega_l = k_{f,l} \prod_{k=1}^{N_{spec}} \left[X_k\right]^{\nu'_{k,l}} - k_{b,l} \prod_{k=1}^{N_{spec}} \left[X_k\right]^{\nu''_{k,l}} \tag{18}$$

Once the reaction rates are known for all the elementary reactions from the chemical mechanism, the chemical source terms for each of the species are calculated as:

$$\dot{\omega}_k = M_k \sum_{l=1}^{N_{reac}} \left(\boldsymbol{\nu}''_{k,l} - \boldsymbol{\nu}'_{k,l}\right) \Omega_l \tag{19}$$

Because of the mass conservation, the sum of chemical source terms for all species must vanish, i.e. $\sum_{k=1}^{N_{spec}} \dot{\omega}_k = 0$.

The forward rate coefficients $k_{f,l}$ are obtained from the Arrhenius expressions as:

$$k_{f,l} = \boldsymbol{A}_l T^{\beta_l} \exp\left(-\frac{E_l}{\boldsymbol{R}T}\right) \tag{20}$$

The coefficients $\boldsymbol{A}_l$, β_l and E_l are prescribed for each of the elementary reactions and come as an input in the chemical mechanism. The backward rate coefficients $k_{b,l}$ are related to the forward coefficients $k_{f,l}$ through the equilibrium constants $K_{C,l} = \frac{k_{f,l}}{k_{b,l}}$, which are obtained as:

$$K_{C,l} = \prod_{k=1}^{N_{spec}} \left[X_{k,e}\right]^{\left(\boldsymbol{\nu}''_{k,l} - \boldsymbol{\nu}'_{k,l}\right)} = \frac{k_{f,l}}{k_{b,l}} \tag{21}$$

In Eq. (21) $\left[X_{k,e}\right]$ stands for the molar concentration of the species k at equilibrium [98, 108].

2.3 Combustion modelling

2.3.1 Phenomenological perspective

Two different combustion regimes, depending on the fuel/oxidiser pre-mixing, can be identified – premixed and non-premixed combustion.

In the premixed case the reactants (fuel and oxidiser) are mixed to a molecular level before entering the combustion chamber, and, during combustion, a unique transition from the reactants to products is established. As such, premixed flames are able to propagate. The flame front is identified as a thin transition layer (0.1-1 mm, [16]) between the reactants and products, with steep gradients in temperature and species concentrations. As the reactants are consumed, the flame propagates towards the reactant side with a laminar flame speed S_L [20]. The flame speed, structure and the thickness of the flame front depend on the initial state of the reactant mixture, which is characterised by its composition and temperature. A very important parameter in premixed combustion is the equivalence ratio ϕ, defined as:

$$\phi = \left(\frac{Y_F}{Y_O} \right) \Bigg/ \left(\frac{Y_F}{Y_O} \right)_{st} \tag{22}$$

In the case of a stoichiometric mixture $\phi = 1$, if $\phi < 1$ the mixture is called lean (excess air) and if $\phi > 1$ the mixture is called rich (excess fuel). If there is too much fuel or too much oxidiser in the reactant mixture, the flame will not be able to propagate, and, thus, it will not burn. There is a range in the equivalence ratio space, $\phi_{\min} \le \phi \le \phi_{\max}$, where the flame propagation is possible, and the limits of this range, $\phi_{\min}$ and $\phi_{\max}$, respectively, are denoted as the flammability limits. Fig. 1 shows a variation of the laminar flame speed of the H_2/He-air flame for different values of the equivalence ratio within the flammability range – as obtained with the PREMIX software [97].

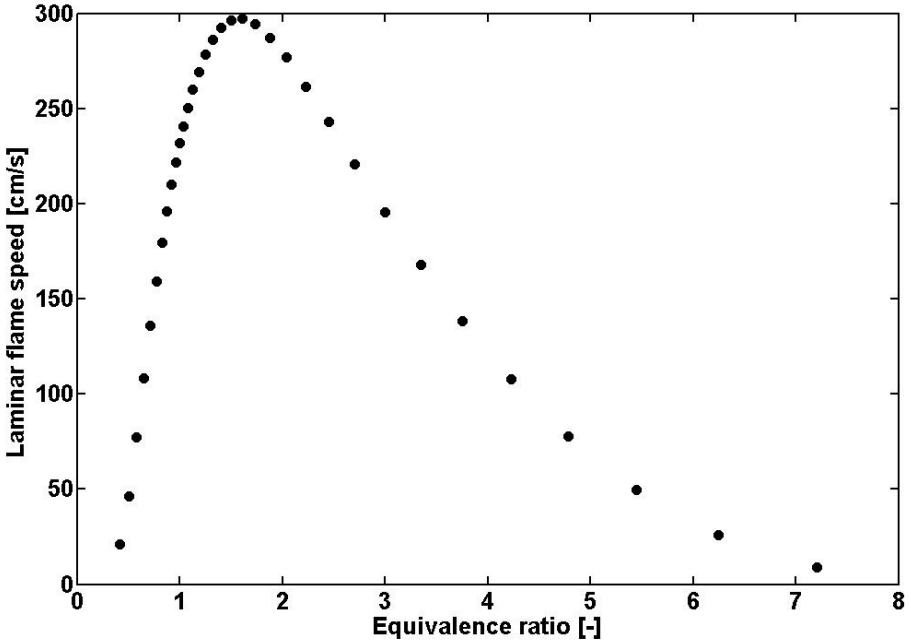

Figure 1 – Laminar flame speed for H_2/He-air premixed flame (fuel: H_2 80% vol., He 20% vol., 295 K; oxidiser: air, 294 K)

In non-premixed combustion, on the other hand, the fuel and oxidiser are not premixed to a molecular level before entering the combustion chamber, but rather enter the combustion chamber in separate streams. Mixing and combustion, subsequently, appear simultaneously as two competitive processes. The flame front is established around the stoichiometric fuel/oxidiser mixing surface ($\phi = 1$). As the reactants (fuel and oxidiser) are located on the both sides of the flame front, they have to diffuse to the flame front location in order to sustain combustion, and, in this respect, the flames that burn in the non-premixed combustion regime are also called the diffusion flames.

An important variable in diffusion flames is mixture fraction Z. It represents the mass fraction of all elements that stem from the fuel stream. In a two-feed system[3] mixture fraction could be defined as:

$$Z = \frac{\dot{m}_F}{\dot{m}_F + \dot{m}_O} \tag{23}$$

[3] Two feed: 1 fuel composition + 1oxidiser composition.

In the fuel stream it has value $Z = 1$, while in the oxidiser stream it has value $Z = 0$. The flame is located around the mixture fraction iso-surface $Z = Z_{st}$ (Fig. 2).

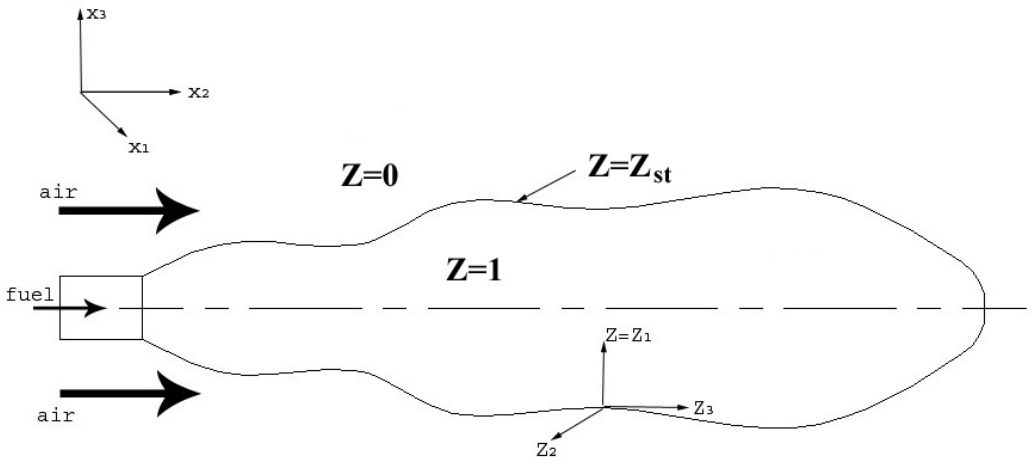

Figure 2 – Two-feed jet diffusion flame configuration

Mixture fraction and equivalence ratio are uniquely related as [15]:

$$\phi = \frac{Z\left(1 - Z_{st}\right)}{\left(1 - Z\right)Z_{st}} \tag{24}$$

In the non-premixed combustion systems equivalence ratio ϕ should be considered locally, because of the non-homogenous fuel/oxidiser mixing. Accordingly, stoichiometric iso-surface $Z = Z_{st}$ is located at positions where the local equivalence ratio is $\phi = 1$. Definitions of the mixture fraction variable other than Eq. (23) are listed in [15].

Unlike in premixed flames, there is no flame front propagation in diffusion flames. The reaction zone thickness depends strongly on the local mixing conditions. Thus, it is difficult to uniquely determine the relevant time and spatial scales in diffusion flames, which makes them harder to model within the statistical framework.

2.3.2 Conserved scalar approach

The classical approach in combustion modelling would be to solve the transport equations for all the species ($k = 1, 2, \ldots, N_{spec}$) that are encountered in a considered combustion problem:

$$\frac{\partial(\rho Y_k)}{\partial t} + \frac{\partial(\rho Y_k u_j)}{\partial x_j} = \frac{\partial}{\partial x_j}\left(\rho D_k \frac{\partial Y_k}{\partial x_j}\right) + \dot{\omega}_k \tag{25}$$

Fick's law is usually used while modelling the molecular species diffusion, where the molecular species diffusivities D_k are simply prescribed for each of the species.

However, as the total number of species involved in chemical reactions, while burning even simple fuels like hydrogen or methane, is quite high and tends to dramatically increase with the complexity of the fuel, this direct approach of solving for each of the species rapidly becomes intractable. Not solely the large number of species, but also associated numerical problems (stiffness) and problematic closure in the turbulent case make this approach further inaccessible. Thus, lowering the dimensionality of the problem and the chemistry pre-processing seems to be necessary if an effective numerical tool is searched for.

In non-premixed combustion the conserved scalar of choice is mixture fraction. Its transport equation can be written as:

$$\frac{\partial(\rho Z)}{\partial t} + \frac{\partial(\rho Z u_j)}{\partial x_j} = \frac{\partial}{\partial x_j}\left(\rho D_Z \frac{\partial Z}{\partial x_j}\right) \tag{26}$$

Originally it was applied by Burke and Schumann [110].

The first attempts to relate the chemical state to mixture fraction were under the presumption of the infinitely fast chemistry [15, 110]. In this respect, the Burke-Schumann and equilibrium profiles can be written in the form:

$$T = T(Z) \qquad Y_k = Y_k(Z) \tag{27}$$

Because in the infinitely fast chemistry limit any flow field impact onto the local chemical composition is excluded, while species are presumed to be in the local chemical equilibrium everywhere, the more complex combustion phenomena, like extinction, jet

flame stabilisation, etc., are inaccessible with this modelling approach. In order to cover these and similar non-equilibrium effects, more advanced models are necessary.

2.3.3 Stationary laminar flamelet concept

The stationary laminar flamelet model (SLFM) is due to Peters [15, 26, 67]. Peters shows two different approaches to derive the flamelet equations – a two scale asymptotic analysis and the local coordinate transformation in the species and temperature balance equations and application of the boundary layer argumentation. In this work the second approach will be shortly presented (more details on the derivation in Appendix A).

Beside the equation for species mass fractions (Eq. (25)), the starting point in the derivation of flamelet equations is the energy equation in terms of temperature [15]:

$$\frac{\partial(\rho T)}{\partial t}+\frac{\partial(\rho T u_j)}{\partial x_j}=\frac{1}{c_p}\frac{\partial}{\partial x_j}\left(\rho c_p D\frac{\partial T}{\partial x_j}\right)+ \\ \frac{1}{c_p}\sum_{k=1}^{N_{spec}}\rho c_{pk} D_k\frac{\partial Y_k}{\partial x_j}\frac{\partial T}{\partial x_j}-\frac{1}{c_p}\sum_{k=1}^{N_{spec}}h_k\dot{\omega}_k+\frac{q_R}{c_p} \tag{28}$$

In Eq. (28) D stands for the thermal diffusivity, defined as $D=\frac{\lambda}{\rho c_p}$, while q_R is the radiation source/sink term.

The Lewis number of the species k is defined as the ratio of thermal and mass diffusivities:

$$\mathrm{Le}_k=\frac{D}{D_k} \tag{29}$$

A common assumption in the flamelet modelling is that species and heat diffuse equally, i.e. that the Lewis numbers for all the species are equal and $\mathrm{Le}_k=1$. This assumption is justified in turbulent flows, because the turbulent diffusion exceeds the molecular diffusion by orders of magnitude, making differential diffusion negligible. When the flow, on the other hand, is laminar, or there are laminarised regions within the turbulent flow field, the differential diffusion effects become more pronounced and their appropriate modelling should be considered [34, 35].

If taking into account the fact that in non-premixed combustion the chemical reactions take place in thin layers at stoichiometric conditions and if presuming that the gradients of reactive scalars are negligible in tangential directions to the mixture fraction iso-surfaces, the flamelet equations in terms of the mixture fraction variable can be derived. This is done by introducing locally a new coordinate system, as shown in Fig. 2, and by transforming Eqs. (25) and (28) to this coordinate system:

$$\begin{aligned} &Y_k\left(t, x_j\right) \rightarrow Y_k\left(\tau, Z_m\right) \\ &T\left(t, x_j\right) \rightarrow T\left(\tau, Z_m\right) \qquad\qquad m = 1, 2, 3 \end{aligned} \tag{30}$$

For convenience reasons, a new local coordinate Z_1 is simply denoted as $Z \equiv Z_1$ because it coincides with the direction of the mixture fraction gradient. In other two local directions, Z_2 and Z_3, respectively, the reactive scalar variations are presumed negligible.

Transformation rules applied to Eqs. (25) and (28) are:

$$\frac{\partial}{\partial t} = \frac{\partial}{\partial \tau} + \frac{\partial Z}{\partial t}\frac{\partial}{\partial Z} \qquad\qquad \frac{\partial}{\partial x_j} = \frac{\partial Z}{\partial x_j}\frac{\partial}{\partial Z} \tag{31}$$

Under the presumption of unity Lewis numbers, and by virtue of Eqs. (1) and (26), the equation for the species mass fraction in the mixture fraction space is obtained as:

$$\rho\frac{\partial Y_k}{\partial \tau} - \rho\frac{\chi}{2}\frac{\partial^2 Y_k}{\partial Z^2} - \dot{\omega}_k = 0 \tag{32}$$

A new quantity appearing in Eq. (32) is the scalar dissipation rate χ, defined as:

$$\chi = 2D\left(\frac{\partial Z}{\partial x_j}\right)^2 \tag{33}$$

The scalar dissipation rate $\chi = \chi\left(Z\right)$ plays an important role in flamelet equations. It can be characterised as the inverse of the diffusion time and, as such, it measures how fast the reactive scalars diffuse from the stoichiometric regions. By increasing its value the diffusive transport increases as well. By definition (Eq. (33)), it represents the link between the flow field and the chemistry in the mixture fraction space. In order to be able

to solve Eq. (32), the functional dependence $\chi = \chi(Z)$ must be given. In [15] Peters has shown how this functional dependence can be derived for two rather different mixing cases – a counter-flow diffusion flame and a 1-dimensional unsteady laminar mixing layer. In both cases the following functional form was obtained:

$$\chi(Z) = A \exp\left\{-2\left[\operatorname{erfc}^{-1}(2Z)\right]^2\right\} \tag{34}$$

In order to circumvent the modelling of the coefficient A, which is configuration dependent, the following parameterised scalar dissipation rate equation is usually used in the flamelet pre-processing:

$$\chi(Z) = \chi_{st} \frac{\exp\left\{-2\left[\operatorname{erfc}^{-1}(2Z)\right]^2\right\}}{\exp\left\{-2\left[\operatorname{erfc}^{-1}(2Z_{st})\right]^2\right\}} \tag{35}$$

The value of the stoichiometric scalar dissipation rate parameter χ_{st} must be imposed in advance[4] while creating the flamelet libraries.

In a similar way and under the same assumptions as used during the derivation of Eq. (32), the temperature equation in the mixture fraction space is obtained as:

$$\rho\frac{\partial T}{\partial \tau} - \rho\frac{\chi}{2}\frac{\partial^2 T}{\partial Z^2} - \rho\frac{\chi}{2c_p}\frac{\partial T}{\partial Z}\frac{\partial c_p}{\partial Z} - \sum_{k=1}^{N_{spec}} \rho\frac{\chi}{2}\frac{c_{pk}}{c_p}\frac{\partial Y_k}{\partial Z}\frac{\partial T}{\partial Z} + \frac{1}{c_p}\sum_{k=1}^{N_{spec}} h_k\dot{\omega}_k - \frac{q_R}{c_p} = 0 \tag{36}$$

In the SLFM concept the stationary forms of Eqs. (32) and (36) are retained, obtained by cancelling out the temporal (leftmost) terms, or, alternatively, unsteady flamelet equations – Eqs. (32) and (36) – are integrated in time until stationary state. These two approaches are equivalent, and the second approach is adopted in this work. As a result, the stationary laminar flamelet profiles, in the dependence of mixture fraction and the stoichiometric scalar dissipation rate parameter, are obtained as:

$$T = T(Z, \chi_{st}) \qquad Y_k = Y_k(Z, \chi_{st}) \tag{37}$$

[4] Usually χ_{st} should cover the range from $\chi_{st} \to 0$ (near equilibrium) to $\chi_{st} = \chi_{st,e}$ (extinction).

Unlike the infinitely fast chemistry models, here an additional parameter – the stoichiometric scalar dissipation rate χ_{st} – measures the impact of the flow field onto the thermo-chemical profiles and allows for slight departures from the equilibrium.

If letting $\chi \to 0$ the equilibrium limit is being approached. If, in contrary, increasing the scalar dissipation rate, the diffusion of the reactive scalars from the reaction zone increases as well and at a certain point, when the scalar dissipation rate is sufficiently high, reactions cannot be sustained anymore and the flamelet extinction occurs. Fig. 3 shows three stationary laminar flamelet temperature profiles for different values of the stoichiometric scalar dissipation rate parameter χ_{st} (H_2/He-air diffusion flame configuration from Chapter 4):

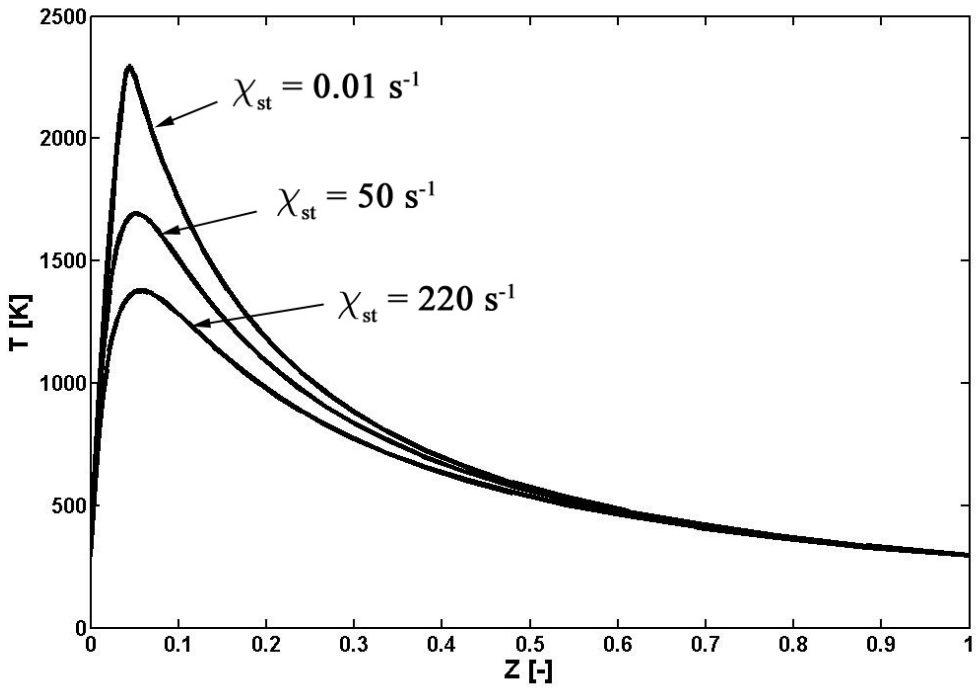

Figure 3 – Temperature flamelet (steady) profiles for H_2/He-air flame (fuel: H_2 80% vol., He 20% vol., 295 K; air: 294 K)

An issue with the stationary flamelet modelling is its poor prediction capability of the transient effects, like extinction and ignition. Some general agreement is that, when applied in the standard form, it is not capable of capturing such transients well. The prediction of minor species, like NO, is also reported to be unsatisfactory [3, 71].

Accordingly, improvements were proposed in order to remedy the mentioned drawbacks. The unsteady flamelet modelling is one of such attempts, and improvements in minor species predictions were achieved by using this model in [71, 111]. An extension taking into account differential diffusion was proposed in [34] (Appendix B). The choice of the stoichiometric scalar dissipation rate, which is solely a flow field variable, to parameterise the chemical database in the original SLFM concept, is probably a reason for relatively poor performance of the standard SLFM in the mentioned situations. In this respect, some recent combustion model developments making use of an additional tracking scalar, the reaction progress variable, seem promising while trying to circumvent the mentioned difficulties [47, 73, 79].

2.3.4 Reaction progress variable

Pierce [79] introduces the reaction progress variable to re-parameterise the stationary laminar flamelet database. The transport equation for the reaction progress variable can be written as:

$$\frac{\partial\left(\rho Y_c\right)}{\partial t}+\frac{\partial\left(\rho Y_c u_j\right)}{\partial x_j}=\frac{\partial}{\partial x_j}\left(\rho D_c \frac{\partial Y_c}{\partial x_j}\right)+\dot{\omega}_c \tag{38}$$

Eq. (38) is formally the same as Eq. (25). Usually, one or a linear combination of more representative species is chosen as the reaction progress variable. The source term $\dot{\omega}_c$ is calculated according to Eq. (19) for one or a linear combination of more species, depending on the choice of the reaction progress variable, respectively.

Furthermore, provided the stationary laminar flamelet library of the form in Eq. (37), and choosing the reaction progress variable so that it monotonically varies with the stoichiometric scalar dissipation rate parameter χ_{st}, Pierce suggests to re-parameterise the flamelet database by a new parameter $\chi_{st}^{*}=\chi_{st}^{*}\left(Z,Y_c\right)$, which is obtained from the standard flamelet database, leading to a new relationship:

$$T=T\left(Z,Y_c\right) \qquad Y_k=Y_k\left(Z,Y_c\right) \tag{39}$$

This way, actually, the flow field parameter χ_{st} is replaced by a chemical parameter Y_c. For the same stationary laminar flamelet solutions, and due to different parameterisation, a new flow field/chemistry relationship is established. Because, in general, $\chi_{st}\neq\chi_{st}^{*}$, and when formally appropriately expressed [79], this new parameterisation procedure resembles the dynamic response of the thermo-chemical state to the changes of the scalar dissipation, just like in unsteady flamelet models.

A thing that is yet not foreseeable is the question whether this new parameterisation procedure will be able to cover the extinction/ignition phenomena, or, will it, for instance, be able to predict the burning in regions with high straining, as in the configuration in [112], and where the standard flamelets fail?

2.3.5 Low-dimensional manifolds in composition space

The interesting new developments based on the reaction progress variable tracking and chemistry pre-tabulation are the flamelet generated manifolds (FGM) method [74] and the flame prolongation of ILDM (FPI) method [73]. Both these methods reside on the ideas of the original intrinsic low-dimensional manifold (ILDM) method [113], but trying even more to reduce the computational costs. ILDM was introduced in [113] as a chemistry reduction technique, basically exploiting an idea that reaction rates of some species are much faster than those of the others, allowing for their separation and different treatment. Practically, a small sub-set of 'slow' representative species is searched for such that all other species and thermodynamic properties can be appropriately tabulated in the dependence only of these. The species from this small sub-set are, thus, the co-ordinates of a low-dimensional space, spanning the hyper-surfaces (manifolds) along which all the other reactive scalars move. The question that naturally arises is: What is the smallest number of independent co-ordinates that is necessary to appropriately parameterise the whole composition space? If the number or such co-ordinates is too high, computational costs of such a tabulation/retrieval system rapidly become prohibitive. Also, there is a problem of the ILDM representation with a small number of co-ordinates in the low temperature regions with stiff chemical kinetics.

In the FPI and FGM methods the low-dimensional manifolds are constructed from the 1-dimensional premixed flamelets. By this approach even the low-temperature regions are efficiently covered [73], making this approach very promising while attempting to model extinction/ignition in turbulent combustion. Additionally, not solely thermo-chemistry is being resolved, as in ILDM, but also transport processes are taken into account by solving the 1D premixed flamelets, which allows for the incorporation of the differential diffusion effects into this tabulation approach [73].

The 1-dimensional premixed flamelets can be obtained by calculating the freely propagating adiabatic premixed flames, as in the PREMIX software [97] (Appendix C), and for different values of equivalence ratios within the flammability range. This approach is applied in this work. Fig. 4 shows, for example, the adiabatic temperature profiles of a freely propagating flame of diluted methane (25% CH_4, 75% air – by

volume) and air (Sandia, [40]). It can be seen that the maximum temperatures are obtained for the near stoichiometric ($\phi \approx 1$) mixtures, as expected.

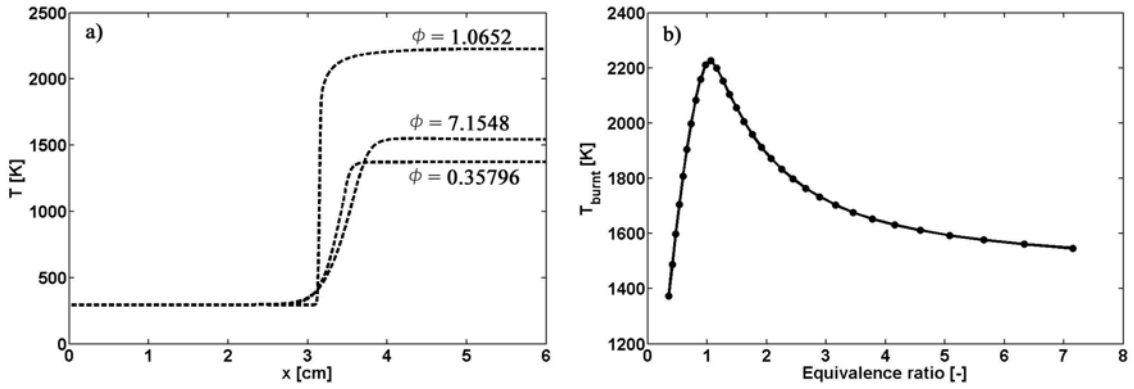

Figure 4 – Adiabatic temperature profiles from the premixed flamelet database (diluted methane (25% CH_4, 75% air – by volume)/air): a) T-x plots; b) T_{burnt}-Φ plot

However, when trying to apply premixed flamelets in the modelling of diffusion flames, with mixture fraction as one of tracking variables, it is necessary to extend the 1-dimensional premixed flamelet databases outside the flammability limits. This is usually approximated by a linear interpolation between the lean/rich flammability limit and the pure oxidiser/fuel side [47, 75]. Furthermore, in the FPI methodology [73] the low-dimensional manifolds are obtained for two independent variables – the reaction progress variable and mixture fraction (equivalence ratio). However, the choice of the reaction progress variable is not arbitrary, but must be rather suitably selected [75, 79] such that it uniquely varies between the reactants and products, serving as a measure of how far the reaction has progressed. As a chemistry tabulation parameter, on the other hand, it should also provide the unique mapping of other reactive scalars. Usually the final product species, like H_2O and CO_2, or their linear combination, are used as the reaction progress variable. Fiorina et al. [75], for instance, recommend a linear combination of mass fractions of CO_2 and CO, i.e. $Y_c \equiv Y_{CO_2} + Y_{CO}$, as the reaction progress variable in their simulation of a laminar methane/air flame.

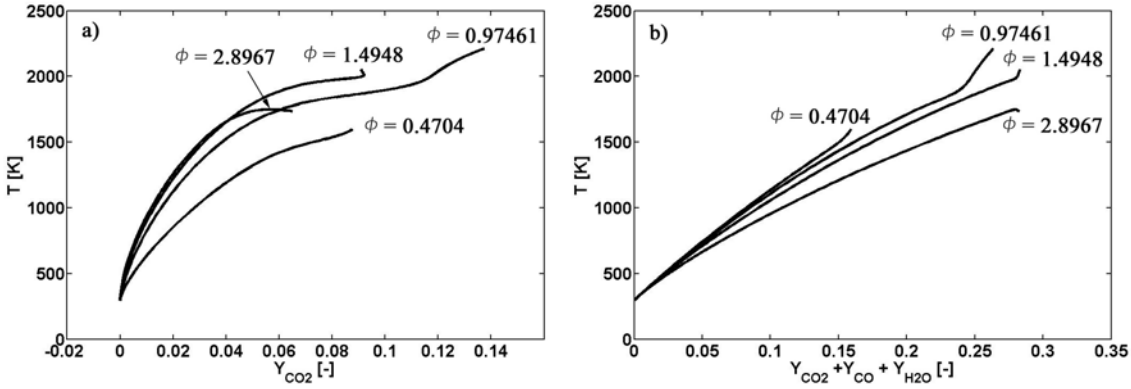

Figure 5 – Adiabatic temperature profiles from the premixed flamelet database (diluted methane (25% CH_4, 75% air – by volume)/air): a) T-Y_{CO2} plots; b) T-Y_{CO2}+Y_{CO}+Y_{H2O} plots

As mentioned in [75], it is important that reactive scalars evolve uniformly with the reaction progress variable, so that there is no ambiguous mapping. Fig. 5 shows the temperature profiles as functions of the reaction progress variable in the CH_4/air flame (Sandia, [40]) from Chapter 5: a) The mass fraction of CO_2 is used as the reaction progress variable, i.e. $Y_c \equiv Y_{CO_2}$; b) A linear combination of mass fractions of CO_2, CO and H_2O is used as the reaction progress variable, i.e. $Y_c \equiv Y_{CO_2} + Y_{CO} + Y_{H_2O}$. In Fig. 5a it can be noticed that there is an ambiguous profile $\phi = 1.4948$ which has a turning point[5], and where the temperature mapping is not unique. The nearby profiles (not shown here) behave similarly. If choosing a linear combination of mass fractions of CO_2 and CO, i.e. $Y_c \equiv Y_{CO_2} + Y_{CO}$, as the reaction progress variable (not shown here), somewhat improved (less backward bending) profiles were obtained, but still there were turning points in the temperature profiles for a range of rich mixtures. However, for $Y_c \equiv Y_{CO_2} + Y_{CO} + Y_{H_2O}$, as shown in Fig. 5b, an unambiguous mapping was obtained, and, because of that, a linear combination of mass fractions of CO_2, CO and H_2O was adopted as the reaction progress variable in the mentioned case (Chapter 5). Accordingly, similar unambiguous mappings should be ensured for all other reactive scalars in the premixed laminar flamelet database.

[5] This is due to chemical decomposition of CO_2 into CO for rich methane/air mixtures at near-equilibrium temperatures.

2.3.6 A new tabulation procedure

The normalised reaction progress variable is chosen as a controlling parameter to enter the pre-tabulated chemistry database in order to extract the species composition. As an input one can use either premixed [73] (FPI) or non-premixed [15, 79] (SLFM) flamelets, or a suitable combination of them, as in [47].

2.3.6.1 Premixed flamelets

For a given mixture fraction iso-surface, the reaction progress variable can vary from its cold mixing values $Y_c^{Mix}(Z)$ up to the equilibrium values $Y_c^{Eq}(Z)$, Fig. 6. The normalised reaction progress variable in the case of premixed flamelets, thus, can be defined as:

$$c(Z) = \frac{Y_c(Z) - Y_c^{Mix}(Z)}{Y_c^{Eq}(Z) - Y_c^{Mix}(Z)} \tag{40}$$

As such, the normalised reaction progress variable varies between zero (cold mixture, $Y_c(Z) = Y_c^{Mix}(Z)$) and unity (burnt equilibrium mixture, $Y_c(Z) = Y_c^{Eq}(Z)$) – $0 \le c(Z) \le 1$, Fig. 6.

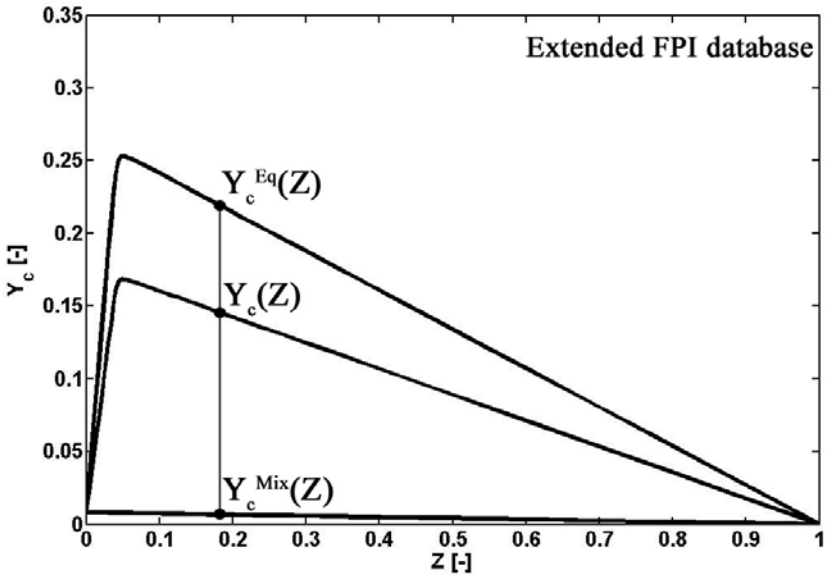

Figure 6 – Reaction progress variable (premixed flamelets)

The premixed flamelets databases were created in this work by using the PREMIX software [97]. Outside the flammability limits the reactive scalars were linearly interpolated between the lean/rich flammability limit and the pure oxidiser/fuel side. Thus, a unique structured mapping of the reactive scalars in terms of two independent co-ordinates – the normalized reaction progress variable, $0 \le c \le 1$; and mixture fraction, $0 \le Z \le 1$ – was obtained in the form:

$$T = T(Z,c) \qquad Y_k = Y_k(Z,c) \tag{41}$$

A complete range between the pure mixing until the burning equilibrium limit is covered this way – Fig. 7.

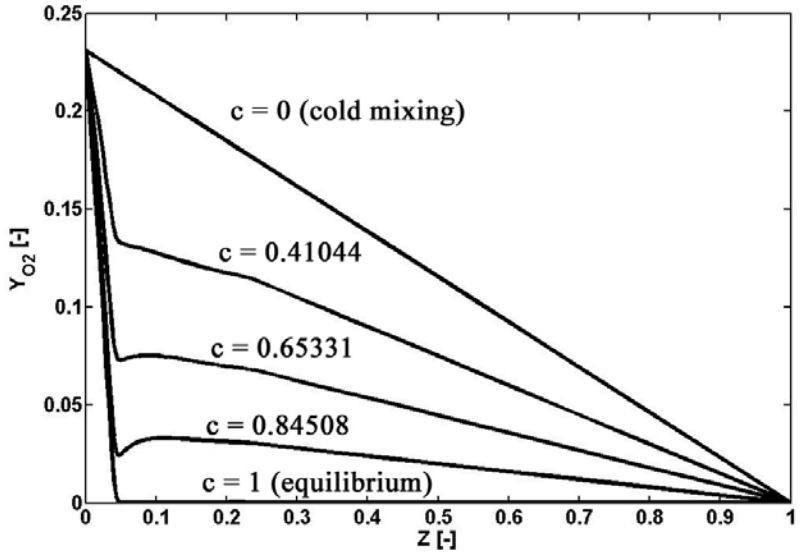

Figure 7 – O_2 profiles (premixed flamelets) for H_2/He-air flame (fuel: H_2 80% vol., He 20% vol., 295 K; air: 294 K)

A question that remains to be answered is whether premixed flamelets are good representatives for the application in the diffusion flame configurations? In [47] it is argued that premixed flamelets, basically, are not able to accurately reproduce the diffusion flame structure at higher equivalence ratios and if intermediates are considered.

2.3.6.2 Non-premixed flamelets

If trying to re-parameterise the stationary laminar diffusion flamelet library, similarly as proposed in [79], but by using the normalised reaction progress variable, a somewhat different situation arises when compared to premixed flamelets. In the standard diffusion flamelet database (Eq. (37)) the reaction progress variable varies, for a given mixture fraction iso-surface, between the lower limit that is determined with the near extinction flamelet in the database ($\chi_{st} = \chi_{st,\max}$), and the upper equilibrium limit ($\chi_{st} \to 0$), just like in the premixed flamelet database. Thus, because of different ranges covered by premixed and non-premixed flamelets, a different definition of the normalised reaction progress variable has to be used in the non-premixed flamelet case. In order to retain the same database structure in both, premixed and non-premixed flamelets, according to Eq. (41), the normalised reaction progress variable in the non-premixed case (Fig. 8) is defined as:

$$c(Z) = \frac{Y_c(Z) - Y_c^{Ext}(Z)}{Y_c^{Eq}(Z) - Y_c^{Ext}(Z)} \tag{42}$$

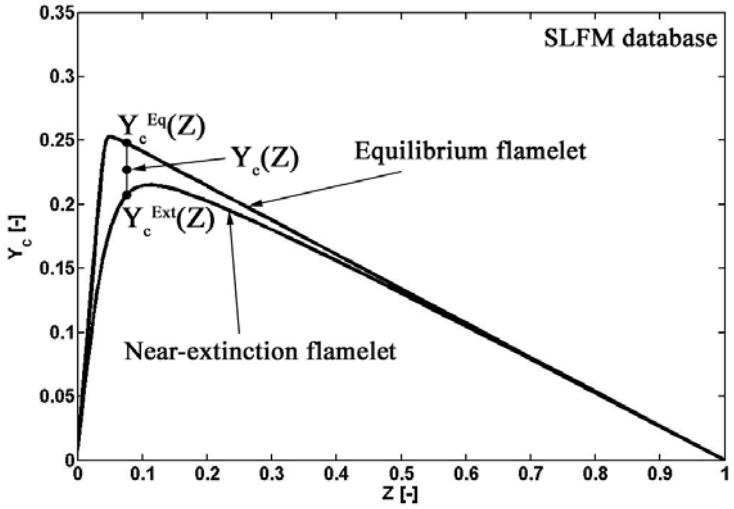

Figure 8 – Reaction progress variable (non-premixed flamelets)

Thus, the normalised reaction progress variables defined in Eqs. (40) and (42) both vary in the range $0 \le c(Z) \le 1$, but the lower limits in terms of the reaction progress variable Y_c differ between the cases.

By design, a new tabulation procedure according to Eq. (41) covers exactly the same range as the original SLFM according to Eq. (37), with $c = 0$ corresponding to $\chi_{st} = \chi_{st,\max}$ and $c = 1$ corresponding to $\chi_{st} \to 0$.

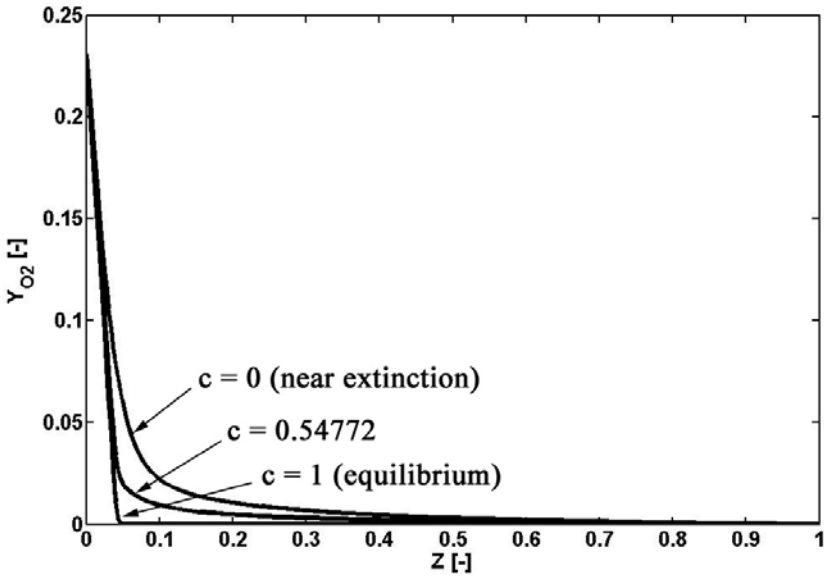

Figure 9 – O_2 profiles (non-premixed flamelets) for H_2/He-air flame (fuel: H_2 80% vol., He 20% vol., 295 K; air: 294 K)

In the case of non-premixed flamelets the reaction progress variable does not span all the realisable range from the cold mixing up to the equilibrium limit. In [79] it is mentioned, however, that the non-premixed flamelet equations actually do provide a complete set of solutions ranging from equilibrium to extinction, but the stoichiometric scalar dissipation rates is blamed as a badly chosen parameterisation variable in the classical SLFM approach. The application of the reaction progress variable as a tabulation parameter is expected to bring an improvement in this respect.

2.3.6.3 Mixed formulation

In order to cover the possible realisations of the reaction progress variable below the extinction limit in the non-premixed flamelet libraries, similarly as in [47], a hybrid procedure is proposed where premixed flamelets are used in the regions below extinction. Thus, a complete range from the cold mixing up to the equilibrium burning is covered this way, but with an important difference that non-premixed flamelets are used whenever possible. It is expected that such a procedure should better reproduce the flame structure in the non-premixed configurations, especially when considering intermediate species at fuel-rich conditions [47]. The normalized reaction progress variable is, thus, defined according to Eq. (40), as in the premixed flamelets case, with the same mapping according to Eq. (41). Additionally, for each point in the mixture fraction space a threshold value of the normalised reaction progress variable is defined as:

$$c_{thresh}\left(Z\right)=\frac{Y_c^{Ext}\left(Z\right)-Y_c^{Mix}\left(Z\right)}{Y_c^{Eq}\left(Z\right)-Y_c^{Mix}\left(Z\right)} \tag{43}$$

For $c\left(Z\right)\geq c_{thresh}\left(Z\right)$ non-premixed flamelets are used, while for $c\left(Z\right)<c_{thresh}\left(Z\right)$ premixed flamelets are used for tabulation purposes. Figure 10, for instance, compares the peak NO mass fractions in the case of a methane/air flame for different tabulations.

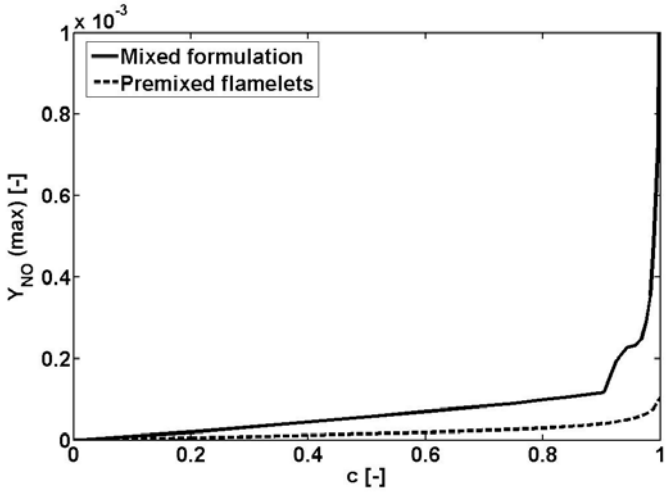

Figure 10 – Maximum NO mass fractions, diluted methane (25% CH_4, 75% air – by volume)/air flame: mixed formulation vs. premixed flamelets

2.4 Thermal radiation modelling

The modelling of thermal radiation is a complex area by itself and its inclusion into a solution procedure within the common CFD framework is not trivial. Various radiation modelling strategies were proposed in the past while trying to meet three major aspects – a good computational economy, a relatively simple mathematical description and the applicability in arbitrary complex geometries. These are obviously contradictory tasks put in front of a radiation modeller and compromised solutions must be often searched for.

In the following sections only the basic concepts relevant to the radiation model implemented in this work are outlined, while for more information on the radiation fundamentals and terminology one is referred to the standard literature [114, 115]. Some examples with radiation modelling in practical configurations can be found in [30, 81, 83-88, 93, 100, 116, 117].

2.4.1 Radiation transfer equation

In combustion problems, in general, the medium participates in the radiative heat transfer. Depending on its radiative properties, the medium can absorb, emit and scatter the radiant energy [115]. The scattering occurs when radiation interacts with particles of any size and when part of the radiant energy is redirected. In this work scattering is neglected. Also, when present, soot substantially contributes to the radiant energy exchange [118].

It is customary to introduce the spectral radiation intensity i_λ as a measure of the radiation energy passing through the area per unit time, per unit of the projected area, per unit small wavelength interval around a wavelength λ, and per unit solid angle [115]. Along the path S (Fig. 11), while passing through the participating medium, the radiant intensity is partly attenuated by absorption and scattering, while at the same time the medium contributes to the radiant intensity by emission and scattering in the direction S.

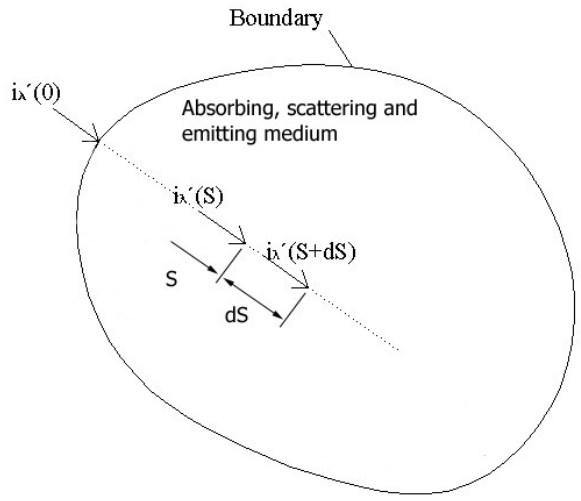

Figure 11 – Absorbing, scattering and emitting medium [115]

For the radiant intensity leaving a boundary surface and travelling through the participating medium along the path S the net change is given through the radiation transfer equation (RTE) [115] as:

$$\frac{di_\lambda^{'}(S)}{dS} = -\left(a_\lambda + \sigma_{s\lambda}\right) i_\lambda^{'}(S) + a_\lambda i_{\lambda b}^{'}(S) + \frac{\sigma_{s\lambda}}{4\pi}\int_{4\pi} i_\lambda^{'}(S,\vec{s}\,')\Phi(\lambda,\vec{s}\,',\vec{s})\,d\Omega' \qquad (44)$$

The first term on the right hand side is the attenuation due to absorption and scattering, while the second and third term represent the gain due to gas emission, and scattering in the direction S, respectively.

2.4.2 Discrete transfer method

If presuming non-scattering and gray medium, RTE can be written as:

$$\frac{di^{'}(S)}{dS} = -ai^{'}(S) + ai_b^{'}(S) \qquad (45)$$

Because the medium is presumed gray, no spectral dependence is sustained in RTE anymore. Black body emissivity is obtained as $i_b^{'} = \frac{\sigma T^4}{\pi}$, while σ is the Stefan-Boltzmann constant.

The discrete transfer radiation method (DTRM) [85] considers a domain discretised into a finite number of control volumes and the irradiation of each boundary face is

obtained by collecting irradiations through a finite number of rays fired from that boundary face – Fig. 12.

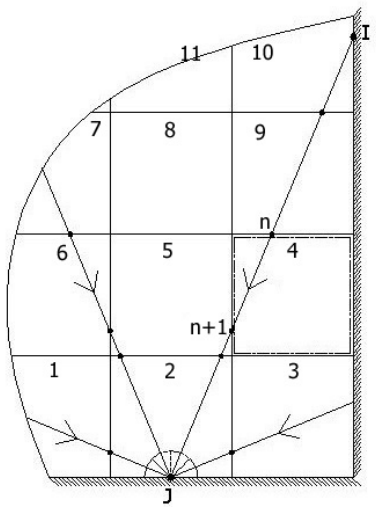

Figure 12 – Ray tracing (2D)

Rays are fired from the boundary cells into a finite number of solid angles that cover the radiating hemisphere about each cell. The main assumption in DTRM is that the radiant intensity flux through a solid angle can be approximated by the radiant intensity along a single ray passing through the centroid of this solid angle. Thus, with finer hemisphere discretisation (more rays per boundary cell) a better prediction accuracy is expected.

Within a single control volume the temperature and radiative properties are presumed homogeneous, which allows for an analytical solution of Eq. (45) on the single control volume basis. For the control volume number 4 from Fig. 12, for example, and if considering the ray $\overrightarrow{IJ}$ that intersects that control volume, Eq. (45) could be integrated as:

$$i_{n+1}^{\cdot} = i_n^{\cdot}(1-\varepsilon) + \varepsilon\frac{\sigma T^4}{\pi} \tag{46}$$

Eq. (46) is valid for any control volume in the domain intersected by a ray. The total emissivity, defined as $\varepsilon = 1 - e^{-al}$, is a property that depends on the absorption coefficient a and distance l that a ray makes in a given control volume.

Within the CFD framework, the solution procedure for radiative transfer consists of performing the ray-tracing calculations first. In this part, the rays are fired from all the boundary faces that participate in the radiant exchange and each ray is tracked, together

with its intersection with the control volumes that it passes through, until the opposite boundary. This part is done only once in the pre-processor step, while all geometrical information is saved to a file. When all ray paths are known, as well as their intersections with the control volumes, the radiation exchange can be calculated by using Eq. (46). However, in order to start the calculation from the opposite boundary, the value of the radiant intensity at the beginning of the incremental path $i_0^{\prime}$ (point I in Fig. 12) is needed. This value is obtained from the appropriate boundary treatment. It is customary to assume that radiant surfaces are gray and obey the Lambert cosine law [115], leading to the following boundary relation:

$$i_0^{\prime} = \frac{q_{out}}{\pi} = \frac{q_{in}}{\pi}(1-\varepsilon_w) + \varepsilon_w \frac{\sigma T_w^4}{\pi} \tag{47}$$

According to Eq. (47), the total radiant intensity leaving a boundary face consists of the reflected part (the first term on the right-hand-side) and the directly emitted part (the second term on the right-hand side). In this equation q_{in} represents the total radiant power per unit area that impinges the boundary face, while ε_w stands for the wall emissivity of the same face. The symbol T_w represents the cell face temperature.

The total hemispherical irradiation of the boundary cell face is obtained by collecting the incoming radiant intensities for all the rays fired from that face:

$$q_{in} = \int_{\vec{s}\cdot\vec{n}<0} i^{\prime}\vec{s}\cdot\vec{n}d\Omega \approx \sum_{kk=1}^{N_{rays}} i_{kk}^{\prime}\cos\Theta_{kk}\Delta\Omega_{kk} \tag{48}$$

In Eq. (48) Θ_{kk} is the angle between the unit direction vector $\vec{s}_{kk}$ of the *kk*-th ray and the boundary face unit normal vector $\vec{n}$, while $\Delta\Omega_{kk}$ represents the solid angle around the ray [85] – Fig. 13.

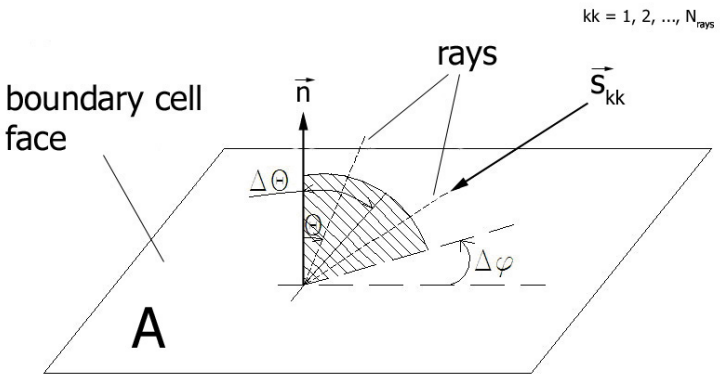

Figure 13 – Hemisphere discretisation around a boundary cell face

As each radiosity ray propagates through the domain it exchanges the radiative energy with the participating medium, yielding a contribution to the source term in the energy equation for the medium (fluid). For a control volume that is intersected by a ray, the energy source due to the radiant intensity change along one ray is calculated as:

$$\overline{S}_{k_j} = (i_{n+1} - i_n) A_j \cos\Theta_j \Delta\Omega_j \tag{49}$$

A_j is the area of the boundary face from which the ray is emitted. The total energy source within the control volume is obtained by collecting the source terms due to all rays that intersect that control volume, i.e.:

$$\overline{S}_k = \sum_{intersecting\_rays\_j} \overline{S}_{k_j} \tag{50}$$

In [100] it has be noticed that the standard DTRM, as described by Eqs. (46)–(50), does not satisfy the conservation of energy exactly. Starting from this observation, it is found that, when thermal radiation is the only heat transfer mechanism, the overall net radiative flux at boundaries is not equal to the radiative power generated within the enclosure, i.e.:

$$\sum_{boundary\_faces\_j} A_j \left(q_{in,j} - q_{out,j} \right) \neq \sum_{\substack{internal \\ cells\_k}} \overline{S}_k \tag{51}$$

Because of that, the conservative formulation of DTRM has been proposed in [100], where the conservation correction factor C_R is defined as:

$$C_R = \frac{\sum_{boundary\_faces\_j} A_j q_{out,j}}{\sum_{\substack{starting \\ points\_j}} \left(q_{out,j} \left(\sum_{\substack{i=ending\_points \\ of\_ray\_j}} \cos\Theta_{i,j} \Delta\Omega_{i,j} A_i / \pi \right) \right)} \tag{52}$$

Then the intensity leaving the boundary face (Eq. (47)) is corrected as:

$$i_0^{,} = C_R . \frac{q_{out}}{\pi} \tag{53}$$

Apart from that, the standard DTRM algorithm remains the same.

2.4.3 Radiative properties

According to WSGGM [101], the total emissivity ε is obtained as a weighted sum of gray gases emissivities:

$$\varepsilon = \sum_{ii=1}^{I+1} \alpha_{\varepsilon,ii}(T)(1 - e^{-a_{ii} Pl}) \tag{54}$$

In Eq. (54) $\alpha_{\varepsilon,ii}(T)$ denotes the emissivity weighting factor for the *ii*-th gray gas and it depends on temperature only. The absorption coefficient a_{ii} of the *ii*-th gray gas, on the other hand, is temperature independent, while P represents the sum of partial pressures of absorbing species (CO_2, H_2O). Symbol l denotes the path length and in the DTRM implementation in this work this is the distance that a ray makes in an intersecting control volume. The weighting factors are calculated as:

$$\alpha_{\varepsilon,I+1}(T) = 1 - \sum_{ii=1}^{I} \sum_{jj=1}^{J} b_{\varepsilon,ii,jj} T^{jj-1} \tag{55}$$

For the total number of gray gases $I = 3$, and using the third order polynomials ($J = 4$), the polynomial coefficients $b_{\varepsilon,ii,jj}$ are given in [101].

2.5 Statistical description

2.5.1 Turbulent and chemical scales

Turbulent flows are characterised by temporal and spatial scales of various magnitude and if one attempted to directly simulate all of them (DNS), the computational domain should have been large enough to cover the largest length scales of the turbulent motion (eddies comparable in size to the apparatus that is simulated, e.g. the pipe diameter in a pipe flow), but at the same time it should be discretised fine enough in order to capture the smallest eddies (the Kolmogorov eddies). As the largest and smallest length scales can differ for multiple orders of magnitude, the task of DNS becomes arduous if the high Reynolds number flows are considered. The situation becomes even more complicated if combustion is considered, because the computational mesh should be additionally refined in order to capture the flame structure as well.

As summarised in [18], it is due to Richardson [119] and Kolmogorov [120] that one is able to conceptually and quantitatively describe a phenomenon of energy transfer between the length scales of various size. In this concept the turbulent flow field is considered to be composed of eddies of different sizes. The turbulent energy is produced and mainly contained in the largest eddies of size l_0 and it is successively transferred to ever smaller eddies until it is finally dissipated at the smallest length scales η due to viscous forces. This process is often referred to as the Kolmogorov energy cascade while the smallest scales in the turbulent flow field are also called the Kolmogorov scales. Fig. 14 (following the notion from [18]) schematically describes the turbulent energy cascade from the largest to the smallest length scales.

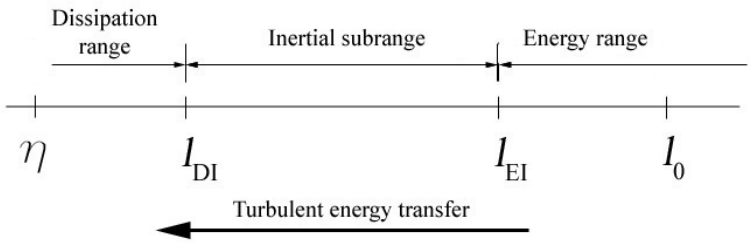

Figure 14 – Turbulent energy cascade (Kolmogorov cascade)

According to Fig. 14, there are three different ranges in the turbulent energy cascade that can be recognised. The largest, energy containing eddies can be grouped into the energy range ($l > l_{EI} \approx \frac{1}{6} l_0$ [18]) and motions from this range can be characterised as anisotropic, depending on the geometrical characteristics of the computational domain and on the boundary conditions. The Reynolds number of these eddies is $\mathrm{Re}_0 = \frac{l_0 u_0}{\nu}$ and it is comparable in magnitude to the standard Reynolds number of the flow in consideration (e.g. $\mathrm{Re}_0 \approx \mathrm{Re} = \frac{du}{\nu}$ in the case of the pipe flow, where d is the pipe diameter). Below the energy range ($l < l_{EI}$) turbulent motions are more universal and isotropic [18] and they do not depend on the geometrical characteristics of the computational domain nor on the boundary conditions. The statistics of these universal motions depends only on the viscosity ν and the energy transfer rate from the larger scales ε. Within the inertial sub-range ($60\eta \approx l_{DI} \ll l \ll l_{EI}$ [18], Fig. 14) eddies are still large enough, so that viscous effects can be neglected and dependence solely on ε is exhibited.

The smallest turbulent scales (the Kolmogorov scales) are defined as [15, 17, 18]:

$$\eta = \left(\frac{\nu^3}{\varepsilon} \right)^{\frac{1}{4}} \quad u_\eta = (\varepsilon \nu)^{\frac{1}{4}} \quad t_\eta = \left(\frac{\nu}{\varepsilon} \right)^{\frac{1}{2}} \tag{56}$$

From Eq. (56) and from the $\varepsilon \sim u^3 / l$ scaling law [18] it is easy to show that the energy containing eddies and the Kolmogorov eddies scale as $l_0 / \eta \sim \mathrm{Re}^{3/4}$, implying that, with the increased turbulence, the smallest length scales of turbulence become smaller and smaller, while the complete length scale range broadens. Additionally, if N represents a number of mesh points in one spatial direction, the required mesh resolution should be $N > \mathrm{Re}^{3/4}$ if the Kolmogorov length scales are to be captured [20]. In the case of moderate Reynolds numbers, let say $\mathrm{Re} = 2000$, this would mean that more than 27 millions grid cells ($N \approx 300$, $N \times N \times N = 2.7 \cdot 10^7$) in three dimensions would be necessary. In practical configurations the Reynolds numbers are usually much higher [38], putting the DNS approach out of reach for some time to come.

The temporal and length scales in combustion, on the other hand, are usually much smaller than adequate turbulence scales. The Damköhler number is defined as the ratio of turbulent and chemical time scales [16] as:

$$Da = \frac{\tau_t}{\tau_c} \tag{57}$$

In the limit of sufficiently high Damköhler numbers ($Da \gg 1$) the chemical reactions occur very fast, while turbulence is not able to effect the internal flame structure substantially [20]. This regime ($Da \gg 1$) was usually presumed while developing the non-premixed combustion models based on mixture fraction, like SLFM [15]. There are situations, on the other hand, where chemical reactions occur slowly ($Da \approx 1$ or less), like by the NO chemistry, and the application of the combustion models developed in a high Da limit is conceptually inappropriate for such species. This is witnessed by a poor performance of these models in the predictions of slowly varying species (see TNF proceedings at [29], e.g.). Thus, one has to keep in mind the presumptions under which combustion models were developed and, accordingly, one should apply these models only in the situations when underlying presumptions are satisfied, if possible.

As can be concluded from previous analysis, there is a wide range of temporal and length scales that occur in configurations where turbulence and combustion come together, and an attempt to simulate these two phenomena by DNS in practically relevant situations is still far out of reach when considering available computational power [16, 20]. The statistical approach, thus, is still a preferred choice at the moment.

2.5.2 Reynolds and Favre averaging

Because DNS is computationally still too expensive, the averaged equations are solved instead. Some instantaneous quantity is decomposed into its mean and fluctuating part as (Fig. 15):

$$\varphi = \overline{\varphi} + \varphi' \tag{58}$$

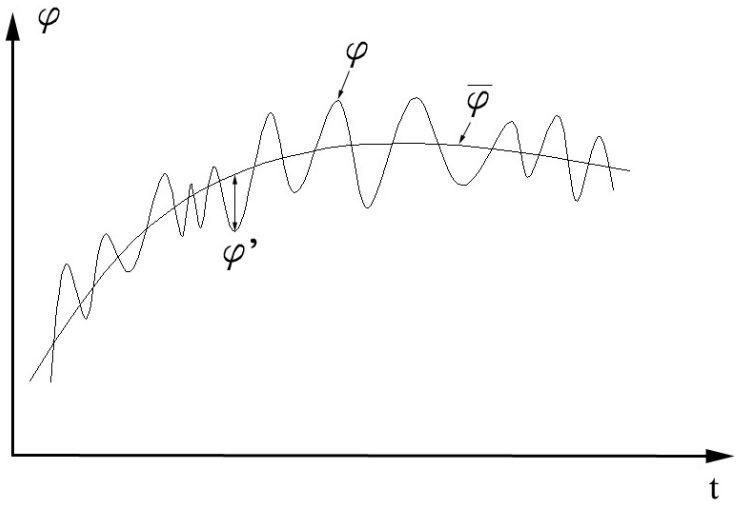

Figure 15 – Averaged profile

As can be seen from Fig. 15, the averaged profile $\overline{\varphi}$ smoothly varies in time when compared to the instantaneous profile φ, and, consequently, it is much easier to solve. By definition, the averaged fluctuation is zero, i.e. $\overline{\varphi'} = 0$. In the classical RANS concept the averaged equations are obtained by inserting Eq. (58) for dependent variables into the leading instantaneous equations and by closing the correlations that emerge because of averaging [17, 18, 23].

In configurations with strong density variations, on the other hand, a more appropriate averaging procedure is that based on the Favre averaging [16, 121]. The Favre mean is defined as:

$$\tilde{\varphi} = \frac{\overline{\rho\varphi}}{\overline{\rho}} \tag{59}$$

Similarly as in Eq. (58), the Favre fluctuation is defined as $\varphi" = \varphi - \widetilde{\varphi}$, where $\widetilde{\varphi"} = 0$. The advantage of the Favre averaging over the Reynolds averaging is in a lesser number of unclosed correlation terms that appear as a consequence of the averaging procedure in the case with variable density [16]. Also, as the Favre averaged equations are formally identical with the Reynolds averaged equations in the case of constant density, the low Mach number RANS solvers, originally developed for non-reactive flows, can be used in reactive cases as well [16].

2.5.3 Averaged equations: continuity, momentum and energy

The equations governing the fluid flow – Eqs. (1), (2) and (6) – are averaged, where the instantaneous quantities are decomposed into their mean and fluctuating parts as:

$$\begin{aligned} \rho &= \overline{\rho} + \rho' \\ p &= \overline{p} + p' \\ u_i &= \tilde{u}_i + u_i" \\ h &= \tilde{h} + h" \end{aligned} \tag{60}$$

The instantaneous variables in the governing equations, where appropriate, are replaced with Eq. (60), and after some algebraic manipulations and application of the basic averaging rules [16, 17], the equations in terms of mean quantities are obtained. By following this procedure the averaged continuity equation becomes:

$$\frac{\partial \overline{\rho}}{\partial t} + \frac{\partial \left(\overline{\rho} \tilde{u}_j \right)}{\partial x_j} = 0 \tag{61}$$

When applying the same procedure to the momentum equations (Eq. (2)) the following averaged equations (for $i = 1, 2, 3$) are obtained:

$$\frac{\partial \left(\overline{\rho} \tilde{u}_i \right)}{\partial t} + \frac{\partial \left(\overline{\rho} \tilde{u}_i \tilde{u}_j \right)}{\partial x_j} = \overline{f}_i - \frac{\partial \overline{p}}{\partial x_i} + \frac{\partial \overline{\tau}_{ij}}{\partial x_j} - \frac{\partial \left(\overline{\rho} \widetilde{u_i" u_j"} \right)}{\partial x_j} \tag{62}$$

The mean tangential stress tensor components $\overline{\tau}_{ij}$ in Eq. (62) are given through Eq. (4), but in terms of the mean rate-of-strain tensor $\overline{D}_{ij} = \frac{1}{2}\left(\frac{\partial \tilde{u}_i}{\partial x_j} + \frac{\partial \tilde{u}_j}{\partial x_i} \right)$. The last term on the

right-hand side in Eq. (62) is a consequence of averaging and it needs to be modelled, as will be shown later.

In the turbulent flows the molecular fluxes are often by orders of magnitude smaller than turbulent fluxes, and, thus, it is customary to neglect the molecular effects when solving the averaged equations [15]. If doing so in the case of enthalpy equation (Eq. (6)), the mean enthalpy equation becomes:

$$\frac{\partial\left(\bar{\rho}\tilde{h}\right)}{\partial t}+\frac{\partial\left(\bar{\rho}\tilde{h}\tilde{u}_j\right)}{\partial x_j}=\frac{\partial\bar{p}}{\partial t}+\tilde{u}_j\frac{\partial\bar{p}}{\partial x_j}+\bar{q}_h+\overline{u_j"\frac{\partial p}{\partial x_j}}-\frac{\partial\left(\bar{\rho}\widetilde{h"u_j"}\right)}{\partial x_j} \tag{63}$$

The last two terms on the right-hand side in Eq. (63) emerge additionally as a consequence of averaging. While the correlation of the pressure gradient and the velocity fluctuation is usually presumed negligible, as done in this work, the last term in Eq. (63) is modelled.

2.5.4 Turbulence closures

The main issue in turbulent modelling is how to close or model the newly appearing terms in the averaged equations that take into account the fluctuations. Over the last few decades the closure of the, so called, turbulent Reynolds stresses $\bar{\rho}\widetilde{u_i"u_j"}$ (Eq. (62)) has been attracting attention of many researchers, but still no general solution was found that could be successfully applicable in all possible configurations [18, 23-25]. Also, most of the turbulence modelling in the past was performed in the association with the non-reactive flow configurations, and the effects of the Favre averaging and heat release on the turbulent Reynolds stresses were usually not taken into account while developing [16]. However, in spite of this, in the reactive flows one usually relies on such developed turbulence models simply rewritten in terms of the Favre averaging [20].

In this work two turbulence models – the $k-\varepsilon$ model [122] and the hybrid turbulence model (HTM) [123] – as in the FIRE CFD solver [99], are used. Both models rely on the Boussinesq's hypothesis while closing the turbulent Reynolds stresses [17-19, 23]:

$$-\bar{\rho}\widetilde{u_i"u_j"}=2\mu_t\bar{D}_{ij}-\frac{2}{3}\bar{\rho}k\delta_{ij} \tag{64}$$

There are two new variables that appear in Eq. (64) – the turbulent dynamic viscosity μ_t and the turbulent kinetic energy k. These are not fluid properties but rather turbulent quantities and they need modelling. The turbulent dynamic viscosity is modelled as:

$$\mu_t = \overline{\rho} C_\mu \frac{k^2}{\varepsilon} \tag{65}$$

In the standard $k-\varepsilon$ model the structure parameter C_μ has the constant value $C_\mu = 0.09$, while the dissipation rate of the turbulent kinetic energy ε is modelled via transport equation.

According to the turbulent-viscosity concept (Eqs. (64) and (65)), thus, the two unknown turbulence parameters are the turbulent kinetic energy k and its dissipation rate ε. In the standard $k-\varepsilon$ model these are modelled as [18, 122]:

$$\frac{\partial\left(\overline{\rho}k\right)}{\partial t} + \frac{\partial\left(\overline{\rho}k\tilde{u}_j\right)}{\partial x_j} = \frac{\partial}{\partial x_j}\left(\frac{\mu_t}{\sigma_k}\frac{\partial k}{\partial x_j}\right) + P - \overline{\rho}\varepsilon \tag{66}$$

$$\frac{\partial\left(\overline{\rho}\varepsilon\right)}{\partial t} + \frac{\partial\left(\overline{\rho}\varepsilon\tilde{u}_j\right)}{\partial x_j} = \frac{\partial}{\partial x_j}\left(\frac{\mu_t}{\sigma_\varepsilon}\frac{\partial \varepsilon}{\partial x_j}\right) + C_{\varepsilon 1}\frac{\varepsilon}{k}P - C_{\varepsilon 2}\overline{\rho}\frac{\varepsilon^2}{k} \tag{67}$$

The production term P in Eqs. (66) and (67) is calculated as:

$$P = 2\mu_t \overline{D}_{ij}\overline{D}_{ij} - \frac{2}{3}\overline{D}_{ii}\left(\overline{\rho}k + \mu_t \overline{D}_{ii}\right) \tag{68}$$

The standard values for constants in the equations for k and ε are:

$$\begin{aligned} C_{\varepsilon 1} &= 1.44 \quad C_{\varepsilon 2} = 1.92 \\ \sigma_k &= 1.0 \qquad \sigma_\varepsilon = 1.3 \end{aligned} \tag{69}$$

In HTM concept [123] the transport equation for the turbulent kinetic energy is not solved, but it is rather obtained from the resolved Reynolds stresses as:

$$k = \frac{1}{2}\widetilde{u_i" u_i"} \tag{70}$$

Thus, in order to make a closure, the modelled transport equations for the Reynolds stresses have to be solved as:

$$\frac{d\left(\widetilde{u_i"u_j"}\right)}{dt}+\frac{\partial\left(\widetilde{u_i"u_j"}\tilde{u}_k\right)}{\partial x_k}=-\left(\widetilde{u_i"u_k"}\frac{\partial\tilde{u}_j}{\partial x_k}+\widetilde{u_j"u_k"}\frac{\partial\tilde{u}_i}{\partial x_k}\right)+$$
$$\frac{\partial}{\partial x_k}\left[\nu\frac{\partial\left(\widetilde{u_i"u_j"}\right)}{\partial x_k}+C_s\frac{k}{\varepsilon}\widetilde{u_k"u_l"}\frac{\partial\left(\widetilde{u_i"u_j"}\right)}{\partial x_l}\right]-\frac{2}{3}\varepsilon\delta_{ij}+\Phi_{ij} \tag{71}$$

In Eq. (71) ν is the kinematic viscosity. A simple gradient transport hypothesis ($C_s=0.22$) was used while modelling the diffusion by turbulence fluctuations, while viscous dissipation is taken to be isotropic. A wall-distance dependent pressure-reflection term from the original model of Gibson and Launder [124] was partially replaced by inclusion of some non-linear terms into modelled pressure-strain term Φ_{ij} according to [125]. For more details on the modelling of Φ_{ij} one is encouraged to refer to [123]. Also, because the turbulent Reynolds stresses are available, the transport equation for the dissipation rate of the turbulent kinetic energy ε has a common form as encountered in the second moment turbulent closures [123]. Additionally, in HTM the structure parameter C_μ is not taken as constant ($C_\mu=0.09$), but it is rather modelled as [123]:

$$C_\mu=\left(-\widetilde{u_i"u_j"}\frac{\partial\tilde{u}_i}{\partial x_j}\right)\Bigg/\left(2\bar{D}_{ij}\bar{D}_{ij}\frac{k^2}{\varepsilon}\right) \tag{72}$$

For the closure of the turbulent fluxes in scalar equations, like $\bar{\rho}\widetilde{h"u_j"}$ in Eq. (63), the classical gradient hypothesis is usually adopted:

$$\bar{\rho}\widetilde{h"u_j"}=-\frac{\mu_t}{\mathrm{Sc}_t}\frac{\partial\tilde{h}}{\partial x_j} \tag{73}$$

Similarly is done also in other mean scalar equations that appear in this work, like the mean mixture fraction, the mixture fraction variance and the mean reaction progress variable. It must be noted, however, that the presumption that scalar turbulent fluxes are aligned with their mean gradients is rather questionable, as shown in [18], and it cannot account for counter-gradient turbulent transport, as observed in some situations [16].

2.5.5 The statistical moments of tracking scalars

As a part of the combustion solution in this work, three additional averaged transport equations must be solved – the mean mixture fraction, the mixture fraction variance and the mean reaction progress variable. Turbulent fluxes in all three equations are closed by using the gradient hypothesis, while molecular effects are neglected.

Mixture fraction has no source term in its transport equation (Eq. (26)) and the only additional term that appears in the equation for the mean mixture fraction is the one due to turbulent fluxes. Mean mixture fraction equation is written, thus, as [15, 20]:

$$\frac{\partial\left(\bar{\rho}\tilde{Z}\right)}{\partial t}+\frac{\partial\left(\bar{\rho}\tilde{Z}\tilde{u}_j\right)}{\partial x_j}=\frac{\partial}{\partial x_j}\left(\overline{\rho D_Z\frac{\partial Z}{\partial x_j}}\right)+\frac{\partial}{\partial x_j}\left(\frac{\mu_t}{\mathrm{Sc}_{t1}}\frac{\partial\tilde{Z}}{\partial x_j}\right) \tag{74}$$

The first term on the right-hand side is due to molecular diffusion and it is usually negligible when compared to other terms. However, for completeness and for further reference in the case of the extended flamelet model [34] (Appendix B) it is written here. The second term on the right-hand side represents the turbulent fluxes.

Transport equation for the mixture fraction variance is [20]:

$$\frac{\partial\left(\bar{\rho}\widetilde{Z''^2}\right)}{\partial t}+\frac{\partial\left(\bar{\rho}\widetilde{Z''^2}\tilde{u}_j\right)}{\partial x_j}=\frac{\partial}{\partial x_j}\left(\frac{\mu_t}{\mathrm{Sc}_{t1}}\frac{\partial\widetilde{Z''^2}}{\partial x_j}\right)+2\frac{\mu_t}{\mathrm{Sc}_{t2}}\frac{\partial\tilde{Z}}{\partial x_j}\frac{\partial\tilde{Z}}{\partial x_j}-\overline{\rho\chi} \tag{75}$$

The first term on the right-hand side in Eq. (75) is the turbulent transport, while the second term represents the production due to mean mixture fraction gradients. The last term represents the sink and its modelling will be shown later.

The reaction progress variable is used to parameterise the pre-tabulated chemistry in this work, and according to Eq. (38), the transport equation for the mean reaction progress variable can be written as [47]:

$$\frac{\partial\left(\bar{\rho}\tilde{Y}_c\right)}{\partial t}+\frac{\partial\left(\bar{\rho}\tilde{Y}_c\tilde{u}_j\right)}{\partial x_j}=\frac{\partial}{\partial x_j}\left(\frac{\mu_t}{\mathrm{Sc}_{t1}}\frac{\partial\tilde{Y}_c}{\partial x_j}\right)+\widetilde{\dot{\omega}_c} \tag{76}$$

Turbulent Schmidt numbers in Eqs. (74)-(76) are chosen $\mathrm{Sc}_{t1} = \mathrm{Sc}_{t2} = 0.7$, while the mean source term $\widetilde{\dot{\omega}_c}$ in Eq. (76) can be presumed from the premixed or non-premixed flamelets library, depending on the combustion model.

2.5.6 Turbulence/chemistry interaction

There is a two-way interaction between the turbulent flow field and combustion [20]. Combustion affects the turbulence via heat release by changing the molecular viscosity and density. In this respect combustion can either enhance turbulence or suppress it (re-laminarisation due to increased viscosity). Turbulence, on the other hand, enhances combustion by increasing the reactions rates and it is often the prerequisite for an efficient combustion to occur. As already mentioned, most of the practical combustion configurations operate in turbulent mode. However, turbulent vortices can affect the internal flame structure in the limit of low Damköhler numbers, and, in the extreme situations, the increased turbulence levels could even lead to blow-off and flame extinction [16].

The application of the probability density function (PDF) in the non-premixed RANS combustion modelling is appropriate because one often deals with the statistical moments of various variables. In terms of mixture fraction as a sample space variable the probability density function is defined as:

$$P(Z) = \frac{dF(Z)}{dZ} \tag{77}$$

In Eq. (77) variable $F(Z)$ represents the probability of finding a value z in the subspace $z < Z$. Accordingly, the product $P(Z)dZ$ represents the possibility of finding the value of z in some differential interval $Z \le z < Z + dZ$ [15, 18, 108].

Because the probability of finding a value of z (or any other sample space variable) in the interval $-\infty \le z \le +\infty$ is certain, the integral of PDF in this interval is:

$$\int_{-\infty}^{+\infty} P(Z)dZ = 1 \tag{78}$$

This is a common property of all PDF functions. In our case, a complete range of possible realisations of z by definition lies within the interval $0 \le z \le 1$, and Eq. (78) becomes:

$$\int_0^1 P(Z)\,dZ = 1 \tag{79}$$

A mean value (expectation) of some function $\varphi = \varphi(Z)$ is calculated as:

$$\overline{\varphi} = \int_0^1 \varphi(Z) P(Z)\,dZ \tag{80}$$

This feature is later used to calculate the mean values of reactive scalars. The variance (the 2nd central moment) is defined as:

$$\overline{\varphi'^2} = \int_0^1 \left(\varphi(Z) - \overline{\varphi}\right)^2 P(Z)\,dZ \tag{81}$$

The conditional mean of some variable ψ for a fixed value of Z is defined as:

$$\overline{\psi|Z} = \int_0^1 \psi P(\psi|Z)\,d\psi \tag{82}$$

$P(\psi|Z)$ is the conditional PDF of ψ for a fixed value of Z.

From experimental observations it was found that the presumed β-PDF shape is often a good statistical representative for reactive scalars [108], and, thus, it is applied in this work also. Accordingly, the statistical moments of reactive scalars are uniquely related to the statistical moments of mixture fraction through the presumed β-PDF as:

$$P(Z) = \frac{Z^{\alpha-1}\left(1-Z^{\beta-1}\right)}{B(\alpha,\beta)} \tag{83}$$

In Eq. (83) $B(\alpha,\beta)$ stands for the beta function of coefficients α and β. These coefficients must always take nonnegative values and they are calculated as:

$$\alpha = \tilde{Z}\left[\frac{\tilde{Z}\left(1-\tilde{Z}\right)}{\widetilde{Z''^2}} - 1\right] \qquad \beta = \left(1-\tilde{Z}\right)\left[\frac{\tilde{Z}\left(1-\tilde{Z}\right)}{\widetilde{Z''^2}} - 1\right] \tag{84}$$

The beta function is usually written in terms of the gamma function Γ as:

$$B(\alpha,\beta)=\frac{\Gamma(\alpha)\Gamma(\beta)}{\Gamma(\alpha+\beta)} \tag{85}$$

The gamma function is defined as:

$$\Gamma(x)=\int_0^\infty e^{-t}t^{x-1}dt \tag{86}$$

Some shapes of the β-PDF, and for different values of parameters $\tilde{Z}$ and $\widetilde{Z''^2}$, are shown in Fig. 16.

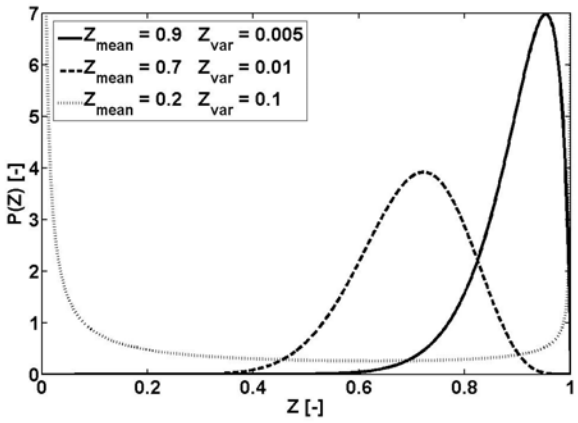

Figure 16 – Shapes of β-PDF for different values of parameters $\tilde{Z}$ and $\widetilde{Z''^2}$

The averaged values of species mass fractions and temperature can be obtained as [15]:

$$\tilde{Y}_i(\xi)=\int_0^1 Y_i(Z,\xi)P(Z)dZ \tag{87}$$

$$\tilde{T}(\xi)=\int_0^1 T(Z,\xi)P(Z)dZ \tag{88}$$

In Eqs. (87) and (88) $Y_i(Z,\xi)$ and $T(Z,\xi)$ are the instantaneous values of the species mass fractions and temperature and they are obtained in the pre-processor either according to the classical SLFM concept (Eq. (37)) with parameter $\xi \equiv \chi_{st}$, or from the normalised reaction progress variable based tabulation (Eq. (41)) with $\xi \equiv c$.

2.5.7 Mean scalar dissipation rate

Although there are proposals to solve an additional transport equation for the mean scalar dissipation rate $\overline{\chi}$ [126], in most of cases it is simply modelled by using a simple linear relaxation model:

$$\overline{\chi} = C_\chi \frac{\varepsilon}{k} \widetilde{Z''^2} \tag{89}$$

As suggested in [15], the constant C_χ is chosen to have a value $C_\chi = 2$. If taking the average of Eq. (35), one gets:

$$\overline{\chi} = \overline{\chi}_{st} \frac{\int_0^1 \exp\left\{-2\left[\operatorname{erfc}^{-1}(2Z)\right]^2\right\} P(Z)\, dZ}{\exp\left\{-2\left[\operatorname{erfc}^{-1}(2Z_{st})\right]^2\right\}} \tag{90}$$

From Eqs. (89) and (90) the mean scalar dissipation rate at stoichiometry $\overline{\chi}_{st}$ can be obtained as:

$$\overline{\chi}_{st} = \frac{C_\chi \frac{\varepsilon}{k} \widetilde{Z''^2} \exp\left\{-2\left[\operatorname{erfc}^{-1}(2Z_{st})\right]^2\right\}}{\int_0^1 \exp\left\{-2\left[\operatorname{erfc}^{-1}(2Z)\right]^2\right\} P(Z)\, dZ} \tag{91}$$

Under the presumption of the inertial sub-range (Fig. 14) invariance of the scalar dissipation rates [15, 71, 72], the mean scalar dissipation rate at stoichiometry can be used as the parameter in Eq. (35), i.e. $\chi_{st} \equiv \overline{\chi}_{st}$. This closure is adopted in this work.

2.5.8 The presumed conditional moments of the reaction progress variable

In order to extract the species concentrations and temperature from the chemistry pre-tabulations according to Eq. (41), it is necessary to approximate the normalised reaction progress variable c (Eq. (40) or Eq. (42)) in the turbulent case. In this work the basic idea of the presumed conditional moments, as described in [47], is followed while making a closure.

The first conditional moment of the reaction progress variable Y_c, according to the definition in Eq. (82), is:

$$\overline{Y_c(Z)|Z} = \int_0^1 Y_c(Z) P(Y_c|Z) dY_c \tag{92}$$

$P(Y_c|Z)$ is the conditional PDF of Y_c for a fixed value of Z. The Favre averaged value of the reaction progress variable can be obtained as:

$$\tilde{Y}_c = \int_0^1 \overline{Y_c(Z)|Z}\, P(Z) dZ \tag{93}$$

The first conditional moment of the reaction progress variable Y_c can be also obtained by taking the conditional average of Eq. (40):

$$\overline{Y_c(Z)|Z} = \overline{c(Z)|Z}\left(Y_c^{Eq}(Z) - Y_c^{Mix}(Z)\right) + Y_c^{Mix}(Z) \tag{94}$$

$Y_c^{Eq}(Z)$ and $Y_c^{Mix}(Z)$ are constant over the mixture fraction surfaces, i.e. $\overline{Y_c^{Eq}(Z)|Z} \equiv Y_c^{Eq}(Z)$ and $\overline{Y_c^{Mix}(Z)|Z} \equiv Y_c^{Mix}(Z)$. The conditionally averaged normalised reaction progress variable $\overline{c(Z)|Z}$ is used as the parameter to access the reactive scalar concentrations from the pre-tabulated chemistry (Eq. (40)).

In [47] it is argued that there exist conditions at which the conditional PDF $P(c|Z)$ weakly depends on mixture fraction if the normalised reaction progress variable is suitably chosen. For this case $P(c|Z) \approx P(c)$ and Eq. (94) could be approximately rewritten as:

$$\overline{Y_c(Z)|Z} = \overline{c}\left(Y_c^{Eq}(Z) - Y_c^{Mix}(Z)\right) + Y_c^{Mix}(Z) \tag{95}$$

If integrating Eq. (95) over the mixture fraction surfaces according to Eq. (93) the Favre averaged reaction progress variable is obtained as:

$$\tilde{Y}_c = \overline{c}\left(\tilde{Y}_c^{Eq} - \tilde{Y}_c^{Mix}\right) + \tilde{Y}_c^{Mix} \tag{96}$$

In Eq. (96) the Favre averaged equilibrium and mixing values of the reaction progress variable are obtained (by using the presumed β-PDF) as:

$$\tilde{Y}_c^{Eq} = \int_0^1 Y_c^{Eq}(Z) P(Z) dZ \tag{97}$$

$$\tilde{Y}_c^{Mix} = \int_0^1 Y_c^{Mix}(Z) P(Z) dZ \tag{98}$$

Similarly, and for the case of non-premixed flamelets, it is:

$$\tilde{Y}_c^{Ext} = \int_0^1 Y_c^{Ext}(Z) P(Z) dZ \tag{99}$$

From Eq. (96) and from the presumption that $P(c|Z) \approx P(c)$, the conditionally averaged normalised reaction progress variable $\overline{c(Z)|Z}$ is approximated as:

$$\overline{c(Z)|Z} \approx \overline{c} = \frac{\tilde{Y}_c - \tilde{Y}_c^{Mix}}{\tilde{Y}_c^{Eq} - \tilde{Y}_c^{Mix}} \tag{100}$$

Values of $\tilde{Y}_c^{Eq}$ and $\tilde{Y}_c^{Mix}$ can be pre-tabulated, together with other chemistry, while the mean reaction progress variable $\tilde{Y}_c$ is obtained from the transport equation – Eq. (76). In the case of non-premixed flamelets (Section 2.3.6.2) $\tilde{Y}_c^{Mix}$ in Eq. (100) is replaced by $\tilde{Y}_c^{Ext}$ according to Eq. (99).

With Eq. (100) the parameter for entering the pre-tabulated chemistry database according to Eq. (40) (or Eq. (42) in the case of non-premixed flamelets) is approximately determined from the resolved turbulent quantities. The closure is still needed for the mean reaction progress variable source term $\widetilde{\dot{\omega}_c}$ in Eq. (76). It can be either presumed from the FPI database [47] or from the SLFM database, depending on the tabulation procedure (Section 2.3.6):

$$\widetilde{\dot{\omega}_c} = \int_0^1 \dot{\omega}_c \left(Z, \overline{c(Z)|Z}\right) P(Z) dZ \tag{101}$$

Finally, the Favre averaged values of species mass fractions and temperature, according to Eqs. (87) and (88), are extracted from the pre-tabulated chemistry as:

$$\tilde{Y}_i = \int_0^1 Y_i\left(Z, \overline{c(Z)|Z}\right) P(Z)\, dZ \tag{102}$$

$$\tilde{T} = \int_0^1 T\left(Z, \overline{c(Z)|Z}\right) P(Z)\, dZ \tag{103}$$

The closure according to Eqs. (101)-(103) does not take into account the fluctuations of the normalised reaction progress variable for given mixture fraction iso-levels, and accordingly, it is referred to as the first-order approximation [47]. The principles of the extension that takes into account the fluctuations, referred to as the second-order approximation, can be found in [47].

3 Numerical procedure

The turbulent flow field, radiative heat transfer and non-premixed combustion modelling were simultaneously included into the overall calculation procedure. However, in order to reduce the computational cost some steps were done in the pre-processor. The stationary laminar flamelet profiles, and subsequently the PDF integrations, were performed by using the CSC solver [96] before the CFD calculation. These were created by assuming adiabatic conditions, i.e. by setting $q_R = 0$ in Eq. (36). Adiabatic conditions were also presumed in the pre-tabulations based on the normalised reaction progress variable. However, during the CFD calculation the temperature field was not extracted from these adiabatic pre-tabulated profiles, but it was rather obtained iteratively from the resolved enthalpy equation (which takes into account the radiation losses) and from the pre-tabulated species concentrations. This way the impact of radiation losses on the species profiles is not directly taken into account and the inclusion of an additional co-ordinate (specific enthalpy) in the chemistry pre-tabulations would be necessary to accommodate for that, as proposed in some recent works [75]. In DTRM, on the other hand, all ray tracing calculations were performed only once in the pre-processor step, where all the geometrical information (ray directions, their intersections with the control volumes, etc.) was stored to a file and used later by the DTRM solver [102]. The turbulence/radiation interaction (TRI) was not taken into account and the mean quantities (temperatures and species mass fractions), as encountered in the control volumes, were applied in the radiation calculations (Eq. (46) and WSGGM [101]).

3.1 Chemistry pre-processor

In order to perform the chemistry pre-tabulations in the pre-processor step the software application – the CSC solver [96] – was developed. Its functionality is twofold. First, it is used to obtain the stationary solutions of the flamelet equations (Eqs. (32) and (36)), and second, it is used to perform the PDF integrations according to Eqs. (87) and (88), independently of the chemistry model used. As an output of the second step is a binary file with the, so called, PDF tables, which is later used by the CFD solver in order to extract the species concentrations, depending on a resolved statistical field of the tracking scalars (mixture fraction and reaction progress variable). The chemistry pre-tabulations using the normalised reaction progress variable (premixed flamelets and mixed formulation) are partly based on the application of the PREMIX software [97]. The CHEMKIN II libraries were used to evaluate the species thermodynamic properties and to accommodate the chemical kinetics [98]. Hereafter only the specific information as relevant to the CSC solver implementation is outlined.

3.1.1 Infinitely fast chemistry models

Because of completeness and necessary initialisation in the solution procedure of the flamelet equations, the models based on the infinitely fast chemistry presumption – the 1-step irreversible reaction model and the equilibrium model [20] – were built into the CSC solver as well. However, because of their relative simplicity and impossibility to account for non-equilibrium effects they were not used in combustion simulations in this work.

According to the 1-step irreversible reaction model the fuel and oxidiser cannot co-exist at the same location and a full conversion from reactants to products is assumed. The general one-step irreversible reaction can be written as:

$$C_{a_1}H_{a_2}S_{a_3}O_{a_4}N_{a_5} + \left(a_1 + \frac{a_2}{4} + a_3 - \frac{a_4}{2}\right)O_2 \rightarrow a_1 CO_2 + \frac{a_2}{2}H_2O + a_3 SO_2 + \frac{a_5}{2}N_2 \qquad (104)$$

The fuel is represented in a general form as $C_{a_1}H_{a_2}S_{a_3}O_{a_4}N_{a_5}$ and any fuel composition given in terms of the fractions of individual species can be recast into this form. Because Burke and Schumann were presumably the first ones who used this approach in the non-premixed combustion modelling back in the 1928 [110] this model is also often referred

to as the Burke-Schumann model. The mass fractions of chemically reacting species are uniquely related to mixture fracture Z according to:

$$Y_j = Y_{j,O}\frac{Z_{st}-Z}{Z_{st}}; \quad Z < Z_{st}$$
$$Y_j = Y_{j,F}\frac{Z-Z_{st}}{1-Z_{st}}; \quad Z \geq Z_{st} \tag{105}$$

Eqs. (105) describe the linear or piecewise linear distribution of the reactant species in the mixture fraction space. The distribution of product species is obtained by subtracting from unity the reactant composition. The composition of individual species among the products is subsequently obtained from the stoichiometric ratios according to Eq. (104). The intermediate species are not calculated because the complete and irreversible reaction is presumed.

The equilibrium composition of chemically reacting species, on the other hand, can be calculated either with the use of equilibrium constants, or by the minimisation of free energy – see [108]. These are, thus, the two equivalent approaches. In this work no additional effort was devoted to the development of an own equilibrium program, and, instead, the already available equilibrium routines accompanying the CHEMKIN II package were used [98, 127].

Figure 17 shows the H_2O mass fraction profiles (near stoichiometry) obtained with the 1-step irreversible reaction model and the equilibrium model for the hydrogen/air system simulated in Chapter 4. The maximum H_2O value of the equilibrium profile is lower because of the dissociation of H_2O at high temperatures.

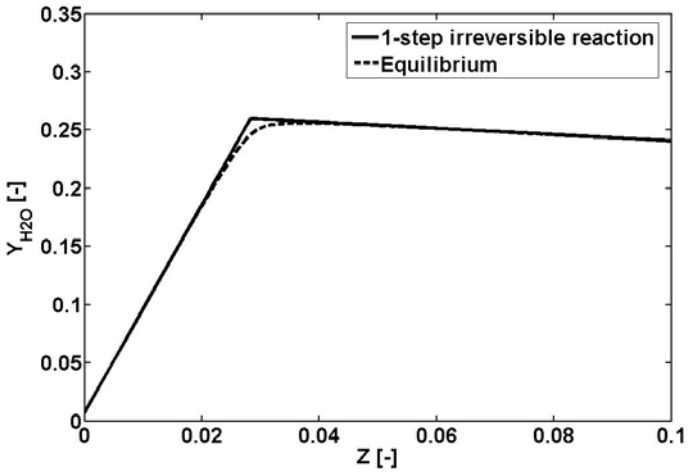

Figure 17 – H_2O profiles (H_2-air system; zoom near the stoichiometry): 1-step irreversible reaction and equilibrium models

The stoichiometric mixture fraction Z_{st} is readily obtained from the known stoichiometric coefficients in Eq. (104), as described in [15].

3.1.2 Numerical solution of the flamelet equations

3.1.2.1 Finite differences discretisation

The finite differences [5, 106, 107, 128] were applied during the numerical solution of the flamelet equations (Eqs. (32) and (36)). The spatial co-ordinate (mixture fraction Z) is discretised into a finite number of points n_Z and the stationary solutions on such a discretised computational grid are searched for. The mixture fraction points, accordingly, are denoted as $Z^{(k)}$, where $k = 1, 2, \ldots, n_Z$, with boundary co-ordinates always being $Z^{(1)} = 0$ and $Z^{(n_Z)} = 1$ (Fig. 18).

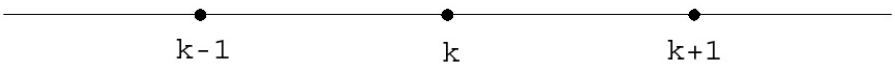

Figure 18 – Finite differences (1D) grid

The discretised stationary laminar flamelet solutions are denoted as $T^{(k)} = T^{(k)}\left(Z^{(k)}, \chi_{st}\right)$ and $Y_i^{(k)} = Y_i^{(k)}\left(Z^{(k)}, \chi_{st}\right)$, with $i = 1, 2, \ldots, N_{spec}$.

In order to get an algebraic system the derivates in Eqs. (32) and (36) are replaced by appropriate algebraic expressions. In this work the central differencing scheme (CDS) [5]

was used for both, the 1st and the 2nd derivatives. Accordingly, the derivatives of some dependent variable ϕ at position k (Fig. 18) on a computational grid with the non-uniform grid distribution can be approximated as:

$$\left(\frac{\partial \phi}{\partial Z}\right)_{(k)} = \frac{\phi^{(k+1)}\left(\Delta^{-}_{(k)}\right)^2 - \phi^{(k-1)}\left(\Delta^{+}_{(k)}\right)^2 + \phi^{(k)}\left[\left(\Delta^{+}_{(k)}\right)^2 - \left(\Delta^{-}_{(k)}\right)^2\right]}{\left(\Delta^{+}_{(k)} + \Delta^{-}_{(k)}\right)\Delta^{-}_{(k)}\Delta^{+}_{(k)}} \tag{106}$$

$$\left(\frac{\partial^2 \phi}{\partial Z^2}\right)_{(k)} = \frac{\phi^{(k+1)}\Delta^{-}_{(k)} + \phi^{(k-1)}\Delta^{+}_{(k)} - \phi^{(k)}\left(\Delta^{-}_{(k)} + \Delta^{+}_{(k)}\right)}{0.5\left(\Delta^{-}_{(k)} + \Delta^{+}_{(k)}\right)\Delta^{-}_{(k)}\Delta^{+}_{(k)}} \tag{107}$$

In above equations the distances between the neighbouring grid points are shortly denoted as:

$$\Delta^{-}_{(k)} = Z^{(k)} - Z^{(k-1)} \qquad \Delta^{+}_{(k)} = Z^{(k+1)} - Z^{(k)} \tag{108}$$

Beside the derivatives in the mixture fraction space, the temporal derivatives also appear in the flamelet equations. However, these are not resolved in a standard fashion [5], where the stationary solutions are searched by simply marching in time with the prescribed time steps until the time derivatives disappear. Instead, a method based on the backward differentiation formulas (Gear's method) had to be employed in order to manage the numerical *stiffness* associated with the flamelet equations. This is done here by employing the DDASSL solver [129].

After applying the discretisation rules (Eqs. (106) and (107)) in the flamelet equations, in the first step one gets the following equations:

$$\left(\frac{\partial Y_i}{\partial \tau}\right)_{(k)} - \left(\frac{\chi}{2}\right)_{(k)} \frac{Y_i^{(k+1)}\Delta^{-}_{(k)} + Y_i^{(k-1)}\Delta^{+}_{(k)} - Y_i^{(k)}\left(\Delta^{-}_{(k)} + \Delta^{+}_{(k)}\right)}{0.5\left(\Delta^{-}_{(k)} + \Delta^{+}_{(k)}\right)\Delta^{-}_{(k)}\Delta^{+}_{(k)}} - \left(\frac{\dot{\omega}_i}{\rho}\right)_{(k)} = 0 \tag{109}$$

$$\left(\frac{\partial T}{\partial \tau}\right)_{(k)} - \left(\frac{\chi}{2}\right)_{(k)} \frac{T^{(k+1)}\Delta^{-}_{(k)} + T^{(k-1)}\Delta^{+}_{(k)} - T^{(k)}\left(\Delta^{-}_{(k)} + \Delta^{+}_{(k)}\right)}{0.5\left(\Delta^{-}_{(k)} + \Delta^{+}_{(k)}\right)\Delta^{-}_{(k)}\Delta^{+}_{(k)}} -$$

$$\left(\frac{\chi}{2c_p}\frac{\partial c_p}{\partial Z}\right)_{(k)} \frac{T^{(k+1)}\left(\Delta^{-}_{(k)}\right)^2 - T^{(k-1)}\left(\Delta^{+}_{(k)}\right)^2 + T^{(k)}\left[\left(\Delta^{+}_{(k)}\right)^2 - \left(\Delta^{-}_{(k)}\right)^2\right]}{\left(\Delta^{+}_{(k)} + \Delta^{-}_{(k)}\right)\Delta^{-}_{(k)}\Delta^{+}_{(k)}} -$$

$$\left(\frac{\chi}{2c_p}\right)_{(k)} \sum_{i=1}^{N_{spec}} \left\{\left(c_{pi}\frac{\partial Y_i}{\partial Z}\right)_{(k)} \frac{T^{(k+1)}\left(\Delta^{-}_{(k)}\right)^2 - T^{(k-1)}\left(\Delta^{+}_{(k)}\right)^2 + T^{(k)}\left[\left(\Delta^{+}_{(k)}\right)^2 - \left(\Delta^{-}_{(k)}\right)^2\right]}{\left(\Delta^{+}_{(k)} + \Delta^{-}_{(k)}\right)\Delta^{-}_{(k)}\Delta^{+}_{(k)}}\right\} +$$

$$\left[\frac{1}{\rho c_p}\left(\sum_{i=1}^{N_{spec}} h_i\dot{\omega}_i - q_R\right)\right]_{(k)} = 0 \tag{110}$$

After rearranging Eqs. (109) and (110) and expressing the temporal terms explicitly, the resulting set of differential/algebraic equations can be written as:

$$\left(\frac{\partial Y_i}{\partial \tau}\right)_{(k)} = C_1^{(k)}Y_i^{(k-1)} + C_2^{(k)}Y_i^{(k)} + C_3^{(k)}Y_i^{(k+1)} + C_4^{(k)} \tag{111}$$

$$\left(\frac{\partial T}{\partial \tau}\right)_{(k)} = C_5^{(k)}T^{(k-1)} + C_6^{(k)}T^{(k)} + C_7^{(k)}T^{(k+1)} + C_8^{(k)} \tag{112}$$

The coefficients $C_1^{(k)} \ldots C_8^{(k)}$ are:

$$\begin{aligned}
C_1^{(k)} &= \frac{\chi^{(k)}}{\left(\Delta^{-}_{(k)} + \Delta^{+}_{(k)}\right)\Delta^{-}_{(k)}} \\
C_2^{(k)} &= -\frac{\chi^{(k)}}{\Delta^{-}_{(k)}\Delta^{+}_{(k)}} \\
C_3^{(k)} &= \frac{\chi^{(k)}}{\left(\Delta^{-}_{(k)} + \Delta^{+}_{(k)}\right)\Delta^{+}_{(k)}} \\
C_4^{(k)} &= \left(\frac{\dot{\omega}_i}{\rho}\right)_{(k)}
\end{aligned} \tag{113}$$

$$
\begin{aligned}
C_5^{(k)} &= C_1^{(k)} - \left(\frac{\chi}{2c_p}\right)_{(k)} \left[\left(\frac{\partial c_p}{\partial Z}\right)_{(k)} + \sum_{i=1}^{N_{spec}} \left(c_{pi}\frac{\partial Y_i}{\partial Z}\right)_{(k)}\right] \frac{\Delta_{(k)}^{+}}{\left(\Delta_{(k)}^{-} + \Delta_{(k)}^{+}\right)\Delta_{(k)}^{-}} \\
C_6^{(k)} &= C_2^{(k)} + \left(\frac{\chi}{2c_p}\right)_{(k)} \left[\left(\frac{\partial c_p}{\partial Z}\right)_{(k)} + \sum_{i=1}^{N_{spec}} \left(c_{pi}\frac{\partial Y_i}{\partial Z}\right)_{(k)}\right] \\
C_7^{(k)} &= C_3^{(k)} + \left(\frac{\chi}{2c_p}\right)_{(k)} \left[\left(\frac{\partial c_p}{\partial Z}\right)_{(k)} + \sum_{i=1}^{N_{spec}} \left(c_{pi}\frac{\partial Y_i}{\partial Z}\right)_{(k)}\right] \frac{\Delta_{(k)}^{-}}{\left(\Delta_{(k)}^{-} + \Delta_{(k)}^{+}\right)\Delta_{(k)}^{+}} \\
C_8^{(k)} &= \left[\frac{1}{\rho c_p}\left(q_R - \sum_{i=1}^{N_{spec}} h_i \dot{\omega}_i\right)\right]_{(k)}
\end{aligned}
\tag{114}
$$

The first derivatives in square brackets in Eq. (114) are evaluated as:

$$
\left(\frac{\partial c_p}{\partial Z}\right)_{(k)} = \frac{c_p^{(k+1)}\left(\Delta_{(k)}^{-}\right)^2 - c_p^{(k-1)}\left(\Delta_{(k)}^{+}\right)^2 + c_p^{(k)}\left[\left(\Delta_{(k)}^{+}\right)^2 - \left(\Delta_{(k)}^{-}\right)^2\right]}{\left(\Delta_{(k)}^{+} + \Delta_{(k)}^{-}\right)\Delta_{(k)}^{-}\Delta_{(k)}^{+}} \tag{115}
$$

$$
\sum_{i=1}^{N_{spec}} \left(c_{pi}\frac{\partial Y_i}{\partial Z}\right)_{(k)} = \sum_{i=1}^{N_{spec}} \left\{ c_{pi}^{(k)} \frac{Y_i^{(k+1)}\left(\Delta_{(k)}^{-}\right)^2 - Y_i^{(k-1)}\left(\Delta_{(k)}^{+}\right)^2 + Y_i^{(k)}\left[\left(\Delta_{(k)}^{+}\right)^2 - \left(\Delta_{(k)}^{-}\right)^2\right]}{\left(\Delta_{(k)}^{+} + \Delta_{(k)}^{-}\right)\Delta_{(k)}^{-}\Delta_{(k)}^{+}} \right\} \tag{116}
$$

Because the values of species mass fractions and temperature are prescribed at the boundaries, the discretised flamelet equations are solved for the inner points only, i.e. for $k = 2,...,n_Z - 1$. For given initial profiles (1-step irreversible reaction or equilibrium solutions) the discretised flamelet equations (Eqs. (111) and (112)) are solved by using the DDASSL solver [129] until the time derivatives in Eqs. (111) and (112) disappear.

3.1.2.2 Differential/algebraic system solution

In general, a complete set of reactions describing some chemical system is often complex and many elementary reactions are involved. The production/destruction rates of various species differ for orders of magnitude, leading to an unsteady system with a wide range of time constants. Systems with such a wide range of different time scales are denoted as numerically stiff and they are hard to solve by using the standard numerical methods. The terms responsible for stiffness in the flamelet equations are the chemical source terms. In the discretised flamelet equations these terms are embodied within the coefficients $C_4^{(k)}$ and $C_8^{(k)}$ (see Eqs. (113) and (114)). However, the problem of solving the stiff ODE systems is rather of mathematical nature and efficient solutions are already available. The Gear's method that uses the backward differentiation formulas, as implemented in the DDASSL solver [129], is applied in this work to perform the time-marching procedure while searching for the stationary solutions of the discretised set of the flamelet equations in the form $G\left(t,\phi,\frac{d\phi}{dt}\right)=0$. The discretised flamelet equations are solved for each of the inner points ($k=2,...,n_Z-1$) in the mixture fraction space. As there are N_{spec} different species equations (Eq. (32)) and one temperature equation (Eq. (36)) the complete differential/algebraic set totals in $\left(N_{spec}+1\right)\left(n_Z-2\right)$ equations that have to be solved.

3.1.2.3 PDF integrations

As described in Section 2.5.6, in turbulent case the stationary instantaneous profiles of reactive scalars are linked to the statistical moments of mixture fraction through Eqs. (87) and (88). However, instead of performing the integrations in Eqs. (87) and (88) repeatedly during the CFD calculation, which could become time consuming if too many species are involved, it is possible to make these calculations only once in the pre-processor step and to store the results. It is first necessary to identify the bounding values of the mixture fraction moments (mean and variance), which are used as parameters in the β-PDF construction, and to discretise the space spanned with these two variables. Finally, the integrations then can be performed for each of the discrete points in this space.

The mean mixture fraction variable $\tilde{Z}$ is uniquely bounded, having value $\tilde{Z}=1$ at the fuel inlet and $\tilde{Z}=0$ at the oxidiser inlet. As fuel and oxidiser mix any value between these two limits can occur, i.e.:

$$0 \le \tilde{Z} \le 1 \tag{117}$$

The mixture fraction variance $\widetilde{Z''^2}$, on the other hand, does not have clearly identified boundaries. As it is by definition a positive scalar, and from the requirement that the coefficients α and β in Eq. (84) be non-negative, the following inequality can be obtained:

$$0 \le \widetilde{Z''^2} \le \tilde{Z}\left(1-\tilde{Z}\right) \tag{118}$$

From Eq. (118) it is clear that its upper limit depends on the mean mixture fraction $\tilde{Z}$. However, it is easy to find that the mean mixture fraction realisation at which the mixture fraction variance has its peak ($\widetilde{Z''^2_{\max}}=0.25$) is $\tilde{Z}=0.5$. In this respect it is customary to introduce the scaled mixture fraction variance variable $\widetilde{Z''^2_s}$, defined as:

$$\widetilde{Z''^2_s} = \widetilde{Z''^2_{\max}} \frac{\widetilde{Z''^2}}{\tilde{Z}\left(1-\tilde{Z}\right)} \tag{119}$$

The short inspection shows that this variable has fixed boundary limits, independent of the mean mixture fraction $\tilde{Z}$, i.e.:

$$0 \le \widetilde{Z''^2_s} \le 0.25 \tag{120}$$

Thus, if using the mean mixture fraction and the scaled mixture fraction variance as two co-ordinates, the space they span can be uniquely discretised in advance and PDF integrations can be performed for each of the discretised points. The mixture fraction variance is easily recovered from Eq. (119). The calculated mean values of reactive scalars (Eqs. (87) and (88)) are, subsequently, collected into the, so called, PDF tables, and are stored into a file for later use by the CFD solver. During the CFD calculation only the moments of mixture fraction are calculated, while the mean species mass fractions are

obtained from the PDF tables by means of interpolation. An example of a PDF table for temperature (adiabatic) is shown in Fig. 19.

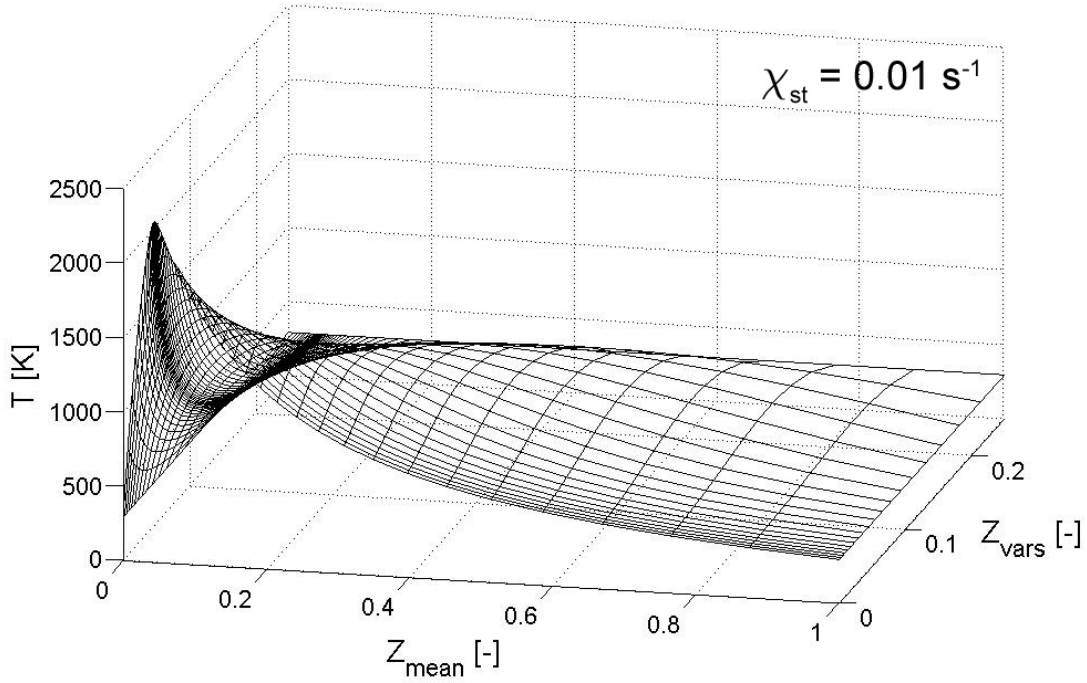

Figure 19 – Integrated (presumed β-PDF) temperature profile (adiabatic, $\chi_{st} = 0.01$ s^{-1}) for H_2/He-air flame (fuel: H_2 80% vol., He 20% vol., 295 K; air: 294 K) – see Fig. 3

Integrations in Eqs. (87) and (88) were performed numerically by using the trapezoidal rule [130] for inner discrete sub-intervals in the mixture fraction space. For the boundary sub-intervals, i.e. $Z \in \left[Z^{(1)}, Z^{(2)} \right]$ and $Z \in \left[Z^{(n_Z-1)}, Z^{(n_Z)} \right]$, the open integration formulas, like the Gaussian integration formulas [130, 131], or similar, had to be used in order to manage the singularities that the β-PDF can have for certain values of the mixture fraction parameters (e.g. $\tilde{Z} = 0.2$ and $\widetilde{Z''^2} = 0.1$, Fig. 16). For more information on the numerical integration methods one is referred to the standard mathematical textbooks, like [130, 132, 133].

3.1.3 CSC solver implementation

The CSC solver [96] was developed in order to perform the chemistry calculations (1-step irreversible reaction/equilibrium/stationary laminar flamelet profiles) and PDF integrations in the pre-processor step. The overall pre-processor application consists of two main parts – the CSC solver itself and the MATLAB [134] generated graphical user interface (GUI). The solver is written in the standard FORTRAN 90 programming language [135]. Its structure will be described next. The MATLAB based GUI, on the other hand, was used only for facilitating the CSC solver input file (formatted ASCII) management and for the results post-processing, and as such, it is not essential for the pre-processor functionality. Thus, its thorough description is not given here and for more information one is referred to [96].

3.1.3.1 Solver structure

All necessary input to the CSC solver is given through a formatted ASCII file. Accordingly, solver either performs the chemistry calculations (1-step irreversible reaction/equilibrium/stationary laminar flamelet) or it creates the PDF tables from the known chemistry profiles. The results are stored subsequently into the files. Fig. 20 shows schematically the functional structure of the CSC solver.

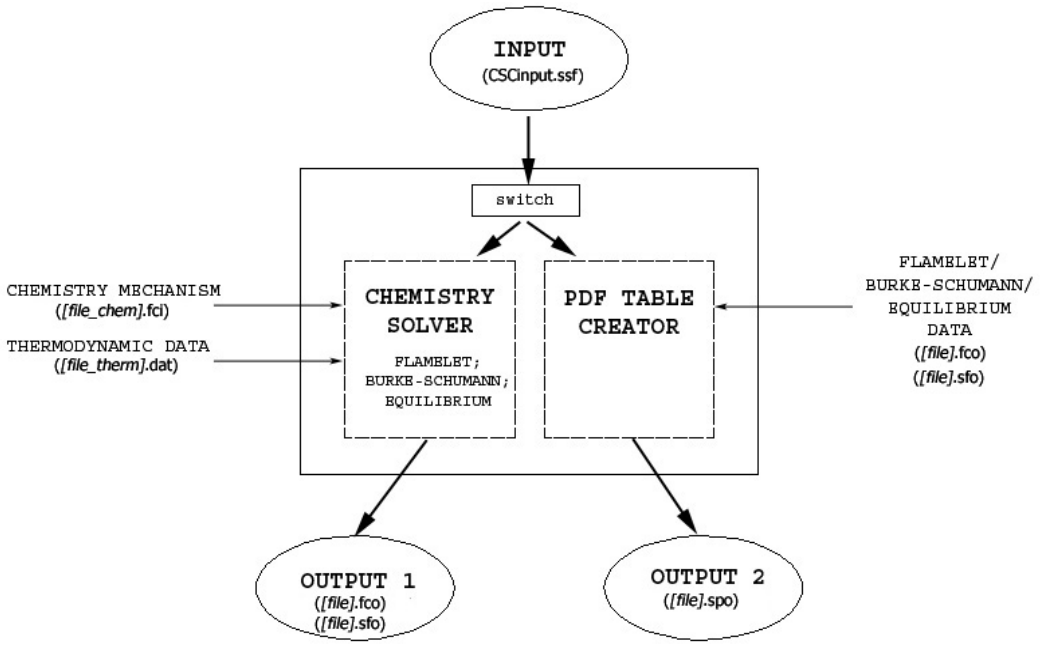

Figure 20 – CSC solver structure

3.1.3.2 Chemistry solver

The chemistry solver is a sequence in which the thermo-chemical profiles are calculated according to different models – 1-step irreversible reaction (Burke-Schumann), equilibrium or stationary laminar flamelet. Temperature and species mass fractions are calculated in the dependence of the discretised instantaneous mixture fraction variable and solutions are stored into the files (OUTPUT 1 in Fig. 20).

Shortly, after all the necessary initialisations, boundary prescriptions and stoichiometry calculations, the 1-dimensional computational grid is calculated. It can be either equidistant or non-equidistant. In the latter case the rule of denser point distribution in the vicinity of the stoichiometric mixture fraction value, where the thermo-chemical profiles are expected to have the steepest gradients, is allowed as a possibility. Afterwards, the computations are performed according to the chemistry model chosen in the input file and for the prescribed pressure levels[6]. In the case that the stationary laminar flamelets are calculated, the initial profiles are obtained either from the 1-step irreversible reaction model or from the equilibrium model. For updating the thermodynamic properties and for the chemical source terms evaluations the CHEMKIN II libraries [98] are employed. Figure 21 gives schematically an overview of the chemistry solver structure.

[6] Burke-Schumann species profiles do not depend on pressure.

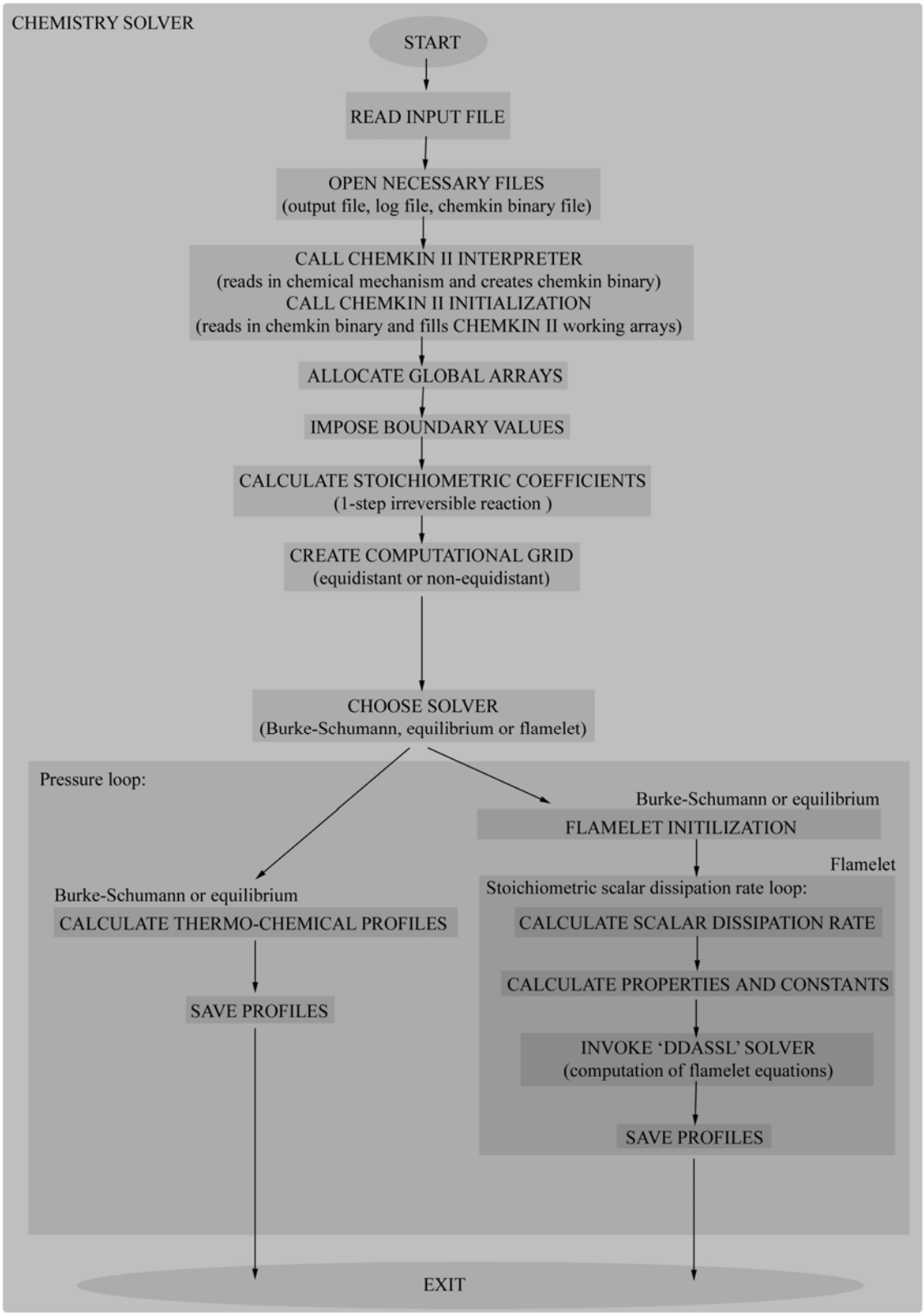

Figure 21 – CSC solver structure: chemistry solver

3.1.3.3 PDF creator

According to the imported instantaneous thermo-chemical profiles and in the dependence of the mixture fraction statistical moments the appropriate mean thermo-chemical profiles are computed in the PDF creator sequence of the CSC solver (Fig. 20). The thermo-chemical profiles can either be those obtained with the chemistry solver, as just described before, or those profiles based on the normalised reaction progress variable (Eq. (41)). For purposes of the numerical integration the imported profiles are mapped onto a special mixture fraction grid used for integrations only. A grid spanned by the mean mixture fraction and the scaled mixture fraction variance is created next. In the input file one defines the total number of discrete grid points for each of these two co-ordinates. Due to steeper gradients expected in the near-stoichiometry regions it is recommended here as well to use the non-equidistant point distribution (see Fig. 19) near the stoichiometry. Finally, the numerical integrations for each combination of the mixture fraction moments are performed next – see Section 3.1.2.3. Depending on the thermo-chemical profiles imported, the appropriate mean thermo-chemical values are obtained for various pressure levels and for various stoichiometric scalar dissipation rate or the normalised reaction progress variable parameters. The PDF creator structure is schematically given in Fig. 22. Integrated PDF profiles are stored into a file (OUTPUT 2 in Fig. 20) that is later used by the CFD solver.

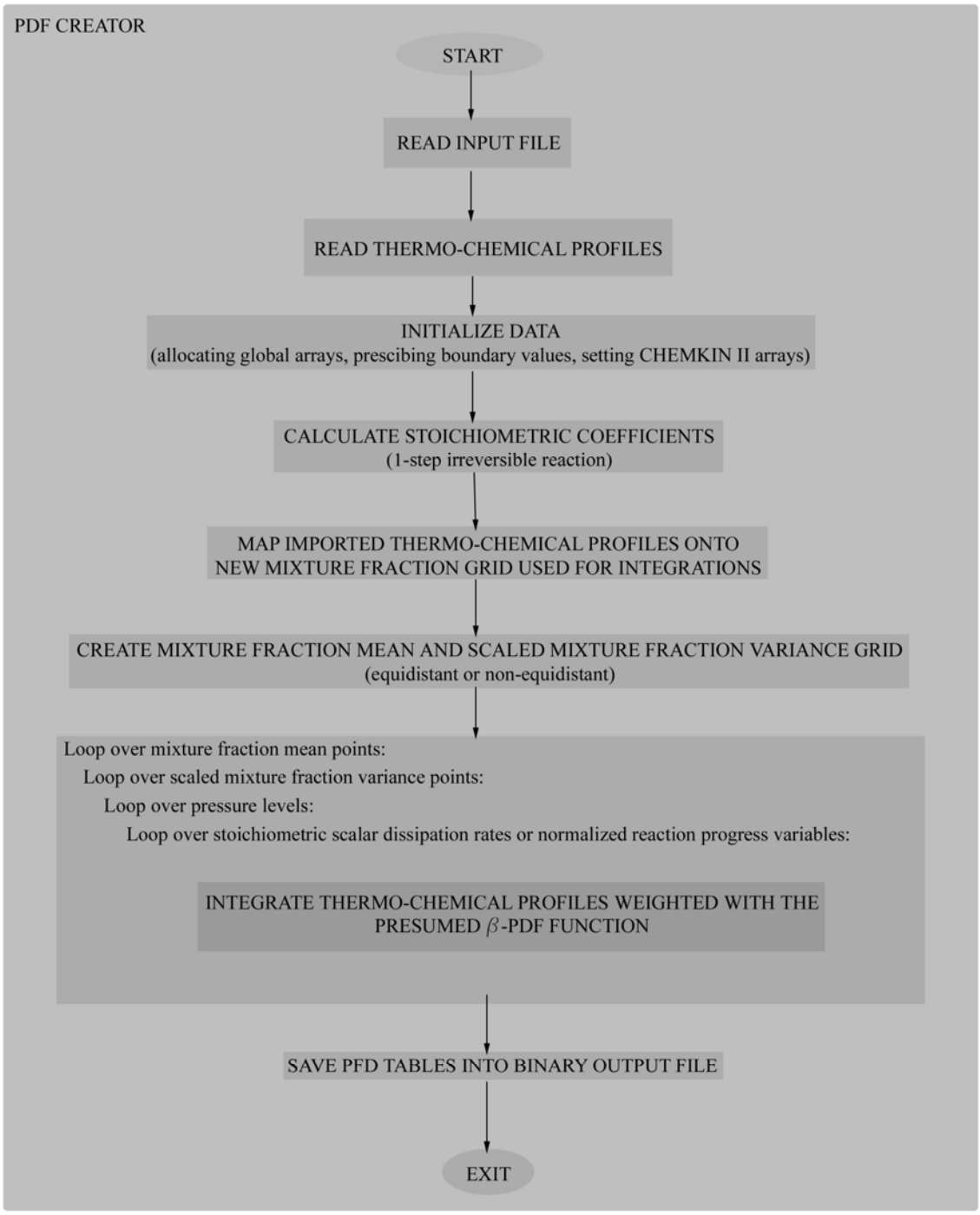

Figure 22 – CSC solver structure: PDF creator

3.2 Fluid flow solver

The averaged equations governing the fluid flow, as presented in Section 2.5.3, together with their closures, have to be solved in order to obtain the spatial and temporal distributions of the mean quantities that they describe. However, the mentioned set of partial differential equations is non-linear and analytical solutions, in general, are not possible. In order to establish a general solution procedure that is applicable in arbitrary complex configurations, the spatial and temporal domain are discretised, and, after applying adequate numerical methods, the set of differential equations is transformed into a set of approximate algebraic equations which can be solved [5].

In this work the CFD solver FIRE [99] was used for the fluid flow computations. It is based on a fully implicit method that allows the use of unstructured grids composed of arbitrary polyhedrons [99]. The transport equations relevant to combustion modelling in this work were additionally implemented into the FIRE code via user-defined functions.

Hereafter, only the basic information about the solution procedure and discretisation practices employed in FIRE will be outlined, while the detailed information about the solver can be found in [99]. Implementation of the combustion module will be described as well.

3.2.1 Integral form of the transport equation

The governing transport equations in the integral form are the starting point and basis for the control volume discretisation method. Thus, the transport equations given in the differential form, as in Chapter 2, have to be stated in the integral form in order to be applicable in the control volume method. Here only the generic transport equation, as defined in Eq. (8), is transformed into its integral form. The procedure applied to Eq. (8) holds also for all other equations that need to be solved – be it for instantaneous or averaged quantities, or for the scalars, vector or tensor components [5, 99].

If integrating Eq. (8) over the control volume V_{CV} that is encompassed by a surface S_{CV}, the following integral form of Eq. (8) is obtained:

$$\frac{\partial}{\partial t}\int_{V_{CV}} \rho\varphi dV + \int_{S_{CV}} \rho\varphi\, u_j n_j dS = \int_{S_{CV}} \Gamma_\varphi \frac{\partial \varphi}{\partial x_j} n_j dS + \int_{V_{CV}} q_\varphi dV \tag{121}$$

It is presumed that the control volume does not move[7], as is the case in the flame configurations simulated in this work. The first term on the left hand-side represents the rate of change of the property φ in the control volume. The net flux of this property through the control volume boundaries, due to a relative fluid motion to the control volume boundaries, is represented with the second term on the left hand-side. The first term on the right hand-side is due to net diffusive flux through the control volume boundaries, while the last term represents the volumetric source/sink of the intensive property φ. In the derivation of Eq. (121) the Gauss' divergence theorem [105] was applied for the transformation of volume into surface integrals in the convection and diffusion terms:

$$\int_{V_{CV}} \frac{\partial\left(\rho\varphi u_j\right)}{\partial x_j} dV = \int_{S_{CV}} \rho\varphi\, u_j n_j dS \tag{122}$$

$$\int_{V_{CV}} \frac{\partial}{\partial x_j}\left(\Gamma_\varphi \frac{\partial\varphi}{\partial x_j}\right) dV = \int_{S_{CV}} \Gamma_\varphi \frac{\partial\varphi}{\partial x_j} n_j dS \tag{123}$$

3.2.2 Control volume discretisation

The spatial domain is discretised into a finite number of control volumes. The computational nodes are located in the geometrical centres of these control volumes – Fig. 23.

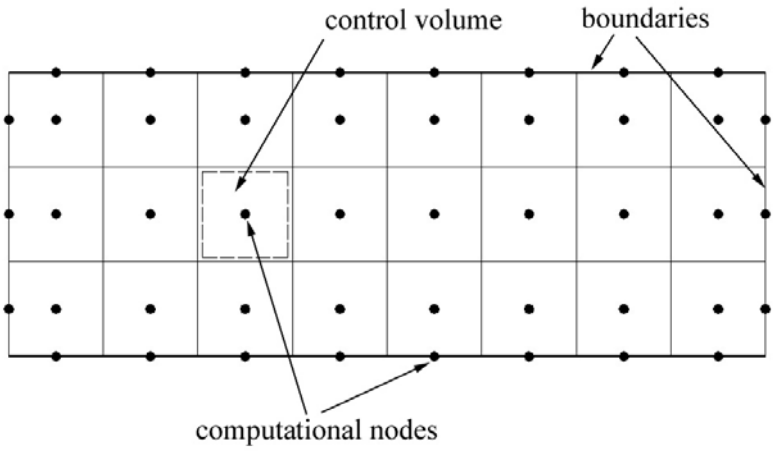

Figure 23 – Domain discretisation into control volumes (2D)

[7] FIRE supports moving meshes, though.

In general, control volumes can be polyhedrons of any type, with a finite number of planar surfaces that encompass them. Control volumes must not overlap. A complete set of control volumes that covers the spatial domain constitutes a numerical mesh. The control volumes on the domain boundaries can be regarded as infinitely thin and coinciding with the connecting faces to the neighbouring internal control volumes. The boundary control volumes, thus, are often denoted as boundary faces, while boundary conditions are imposed in their computational nodes (Fig. 23), when necessary. Figure 24 shows some arbitrary control volume.

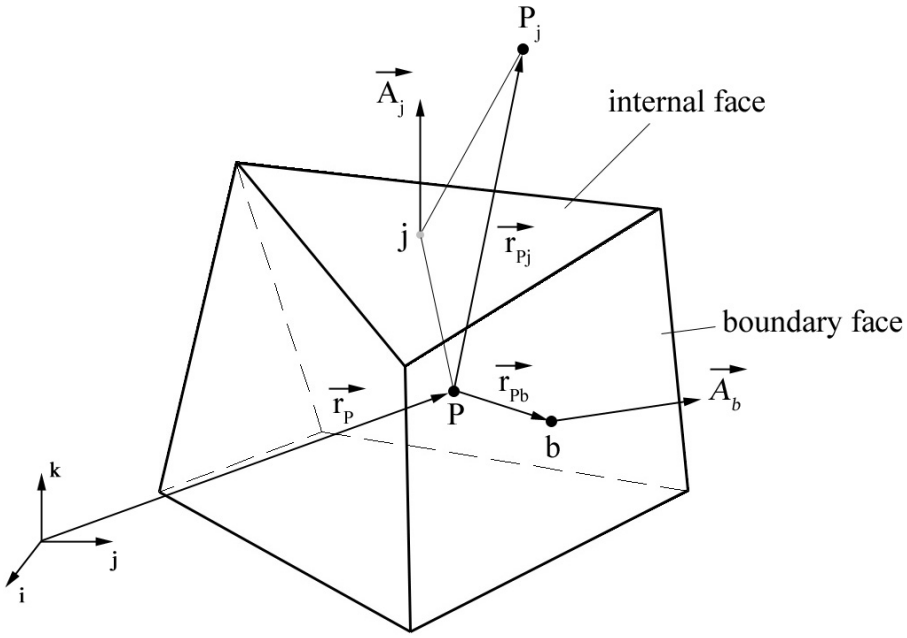

Figure 24 – Control volume (arbitrary polyhedron)

Any dependent variable (velocity component, enthalpy, density, pressure, etc.) is presumed to be homogeneous within the control volume and to have a value as obtained in the computational node (point P in Fig. 24). This is the, so called, collocated variable arrangement [5]. When the values of dependent variables or their gradients are needed at other locations than computational nodes, like in the surface integrals in Eqs. (122) and (123), depending on the differencing scheme and the gradient approximation method, these are obtained by interpolation from the neighbouring computational nodes. An appropriate choice of a discretisation scheme is often of the crucial importance for different important numerical aspects, like accuracy, convergence, stability, boundedness,

conservation, etc. [5, 6]. Depending on the calculated quantity, different differencing schemes can be applied [5]. For more information on the differencing schemes, gradient approximation method, and interpolation practices, as used in the FIRE code, one is referred to [99].

The volume and surface integrals in Eq. (121) are calculated on the control volume basis. As the control volume boundary consists of a finite number of (planar) surfaces, i.e. $S_{CV} = \sum_{k=1}^{N_{faces}} S_k$, the surface integrals in Eq. (121) can be decomposed as:

$$\int_{S_{CV}} \rho\varphi\, u_j n_j dS = \sum_{k=1}^{N_{faces}} \int_{S_k} \rho\varphi\, u_j n_j dS \tag{124}$$

$$\int_{S_{CV}} \Gamma_\varphi \frac{\partial\varphi}{\partial x_j} n_j dS = \sum_{k=1}^{N_{faces}} \int_{S_k} \Gamma_\varphi \frac{\partial\varphi}{\partial x_j} n_j dS \tag{125}$$

Eq. (121) can now be written as:

$$\frac{\partial}{\partial t}\int_{V_{CV}} \rho\varphi dV + \sum_{k=1}^{N_{faces}} \int_{S_k} \rho\varphi\, u_j n_j dS = \sum_{k=1}^{N_{faces}} \int_{S_k} \Gamma_\varphi \frac{\partial\varphi}{\partial x_j} n_j dS + \int_{V_{CV}} q_\varphi dV \tag{126}$$

The approximation to the exact solution is introduced by approximating the surface and volume integrals in Eq. (126). As already mentioned, the dependent variables are presumed homogeneous within a single control volume and so are the integrands in the volume integrals as well. With this presumption, the volume integrals in Eq. (126) can be evaluated as:

$$\frac{\partial}{\partial t}\int_{V_{CV}} \rho\varphi dV = \frac{\partial}{\partial t}\left[\left(\rho\varphi\right)_c V_{CV}\right] \tag{127}$$

$$\int_{V_{CV}} q_\varphi dV = \left(q_\varphi\right)_c V_{CV} \tag{128}$$

The integrand values in the computational node are $\left(\rho\varphi\right)_c$ and $\left(q_\varphi\right)_c$.

For the approximation of the surface integrals the midpoint rule is adopted [5]. The integrand value at the geometrical centre of a single face is presumed to prevail over the whole face and the surface integrals are approximated as:

$$\int_{S_k} \rho\varphi\, u_j n_j dS = \left(\rho\varphi\, u_j n_j\right)_c S_k \tag{129}$$

$$\int_{S_k} \Gamma_\varphi \frac{\partial\varphi}{\partial x_j} n_j dS = \left(\Gamma_\varphi \frac{\partial\varphi}{\partial x_j} n_j\right)_c S_k \tag{130}$$

The integrand values at the geometrical centre of a face are $\left(\rho\varphi\, u_j n_j\right)_c$ and $\left(\Gamma_\varphi \frac{\partial\varphi}{\partial x_j} n_j\right)_c$. In order to ensure the conservation of the surface fluxes it is important that the surface integrals over the common faces between the neighbouring control volumes are calculated in the same way [6].

3.2.3 Solution procedure

Beside the spatial discretisation based on the control volumes, as just described before, in the unsteady fluid flow problems Eq. (126) is discretised in time as well. However, as the flame configurations simulated in this work are stationary, the steady flow solver in FIRE was used, and the temporal discretisation practices are not outlined here.

The result of the discretisation procedure performed on the basis of a one internal control volume (Fig. 24) is an algebraic equation of type:

$$a_P\varphi_P = \sum_{k=1}^{N_{faces}} a_k\varphi_{Pk} + S_\varphi \tag{131}$$

The summation is performed over the control volume faces (including boundary faces). The value in the computational node P depends on values in the neighbouring computational nodes and on the source/sink within that control volume. A total number of algebraic expressions according to Eq. (131) for one dependent variable equals to the total number of internal control volumes (N_{CV}) used in the domain discretisation. Thus, the overall total number of algebraic equations equals the number of transport equations (N_{eq}) multiplied with the number of internal control volumes ($N_{CV} \times N_{eq}$). The values of the dependent variable in the boundary computational nodes, on the other hand, are either prescribed according to the boundary conditions (Dirichlet or von Neumann [5]) or they are estimated from the neighbouring internal control volumes.

After performing the discretisation of some transport equation over the whole domain (i.e. in all internal control volumes) the system of algebraic equations is obtained:

$$A_\phi \phi = S_\phi \tag{132}$$

The coefficient matrix A_ϕ is sparse and asymmetric, and efficient solvers are required to obtain the unknown vectors ϕ. Also, the diagonal dominance ($a_P \geq \sum_{k=1}^{N_{faces}} a_k$, with $sign(a_P) \equiv sign(a_k)$ [6]) must be ensured. In general, the system in Eq. (132) is non-linear and it is solved iteratively by guessing the solutions first and then by solving such a linearised system to get improved solutions. The process is repeated until convergence [5]. Additionally, because of high numerical costs, the direct linear solvers (Gauss elimination, LU decomposition, etc. [130, 132]) are usually not used, and, instead, the iterative methods are applied. Among many iterative methods [5, 130] available, those based on the conjugate gradients (CGS, CGSTAB, etc.) or multi-grid methods (AMG) are usually used in the CFD solvers [5].

The basic problem while solving the momentum equations in incompressible flows (low Mach numbers) is the determination of the pressure such that the continuity equation is satisfied. The SIMPLE algorithm [6, 136] is used for the velocity-pressure coupling. The pressure-correction equation is solved in order to update the pressure and velocity fields such that the mass conservation is satisfied [99]. Also, because the dependent variables that are represented by their own transport equations also appear in the transport equations for other dependent variables, the equation systems that appear in the fluid flow problems are coupled and they need a special treatment. There are basically two different approaches when accounting for these interconnections between various equations – the coupled and the segregated approach. In the coupled approach all the equations are considered part of a single system and they are simultaneously resolved. However, the resulting non-linear systems are large and expensive to compute, and, thus, this approach is usually not applied in the CFD solvers. The alternative is the segregated approach, as retained in FIRE, where each transport equation is solved for its dependent variable solely, while other non-linear terms are kept as constant during this solution. By

iterating through the equations (outer iterations) and by updating the non-linear terms the converged coupled solutions are searched for [5].

Finally, two important numerical techniques that are often used to increase the diagonal dominance in the coefficients matrix A_ϕ are briefly explained. These are the under-relaxation and the source term linearization. These techniques were introduced in [6] in order to improve the calculation stability and convergence.

If $\phi^{(new)}$ is a solution of the equation system according to Eq. (132), and if $\phi^{(i-1)}$ represents the known solution vector from the previous iteration cycle, the solution in a new iteration cycle is under-relaxed as:

$$\phi^{(i)} = \phi^{(i-1)} + \alpha_\phi \left(\phi^{(new)} - \phi^{(i-1)} \right) \tag{133}$$

The under-relaxation factors α_ϕ can have values between 0 and 1 and their appropriate choice depends on the equation that is being solved and on the configuration that is being simulated [5, 6]. In general, the lower values of under-relaxation factors ($\alpha_\phi \to 0$) improve the calculation stability and convergence, but at the same time more iterative cycles are required in order to obtain convergence. Thus, the under-relaxation factors should be carefully chosen in the way that a stable, but computationally still an efficient calculation procedure is ensured.

The source term S_φ in Eq. (131) is linearly decomposed as:

$$S_\varphi = S_{\varphi,S} - S_{\varphi,P}\varphi_P \qquad with \quad S_{\varphi,S} \geq 0,\ S_{\varphi,P} \geq 0 \tag{134}$$

The negative source contribution (the second term on the right-hand side) is implicitly treated by adding $S_{\varphi,P}$ part to the diagonal coefficient a_P, and thus, increasing the diagonal dominance of the coefficient matrix A_ϕ.

3.2.4 Combustion module implementation

The combustion module has been coupled to the FIRE solver by means of user-defined functions. In the initialisation part the input file with the pre-tabulated PDF profiles is read in and the boundary conditions for additional transported quantities are imposed. In each iteration cycle the transport equations for the mean enthalpy (Eq. (63)), the mixture fraction moments (Eqs. (74) and (75)) and the mean reaction progress variable (Eq. (76)) are solved, and accordingly, the species composition is extracted from the pre-tabulated PDF profiles. The mean temperature is obtained iteratively from the known mean species mass fractions and the mean enthalpy according to:

$$\tilde{h} = \sum_{k=1}^{N_{spec}} \tilde{Y}_k h_k \left(\tilde{T} \right) \tag{135}$$

The mean density field and other fluid properties are updated after each outer iteration cycle. The implementation sequence is schematically shown in Fig. 25.

There are four different combustion models depending on the pre-tabulation parameterisation and for further reference they are summarised here:

- Standard stationary laminar flamelet model – SLFM. The mean scalar dissipation rate at stoichiometry $\overline{\chi}_{st}$ (Eq. (91)) is used as a parameter entering the pre-tabulated chemistry. The transport equation for the mean reaction progress variable (Eq. (76)) is not calculated.
- Parameterisation with the normalised mean reaction progress variable $\overline{c}$; based on the premixed flamelets library (Section 2.3.6.1) – RPV (FPI).
- Parameterisation with the normalised mean reaction progress variable $\overline{c}$; based on the non-premixed flamelets library (Section 2.3.6.2) – RPV (SLFM).
- Parameterisation with the normalised mean reaction progress variable $\overline{c}$; based on the mixed flamelet formulation (Section 2.3.6.3) – RPV (MIX).

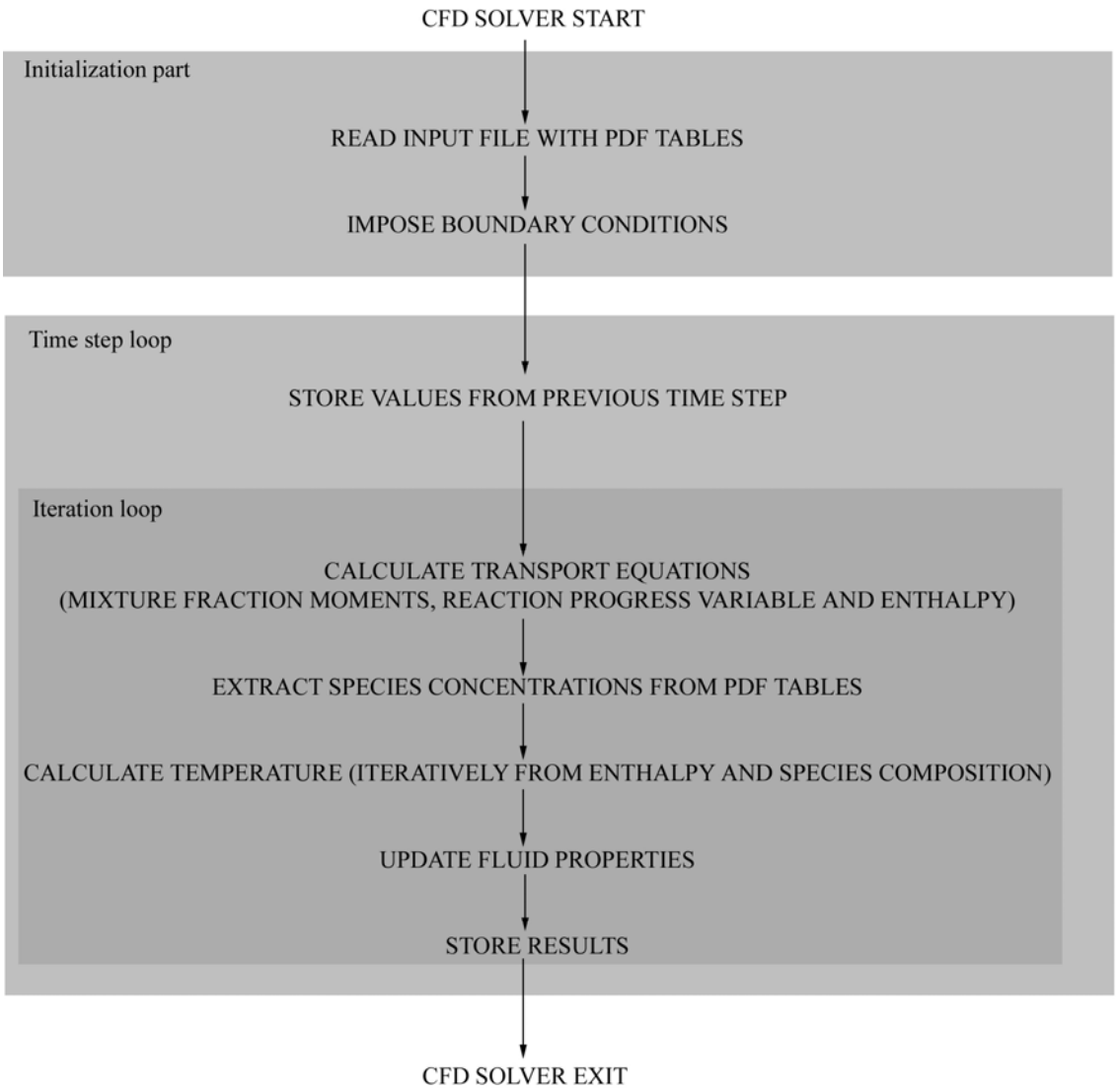

Figure 25 – Combustion module implementation (schematics)

3.3 DTRM implementation

The discrete transfer radiation method was implemented into the FIRE code by means of user-defined functions [102, 137].

In the initialisation step the ray tracing calculations are performed first, where the rays are emitted from the boundary faces and they are tracked until they reach the opposite boundary. The geometrical information about the ray intersections with the control volumes on their path to the opposite boundary is stored. During the main iteration cycle the DTRM solver is invoked within each iteration and the enthalpy source term $\overline{q}_h$ (Eq. (63)) is being updated with the radiation contribution according to Eq. (50). The turbulence/radiation interaction is not taken into account and the mean quantities (temperatures and species mass fractions), as encountered in control volumes, are directly applied in the radiative calculations (Eq. (46), WSGGM [101]).

As a part of the DTRM implementation verification the finite cylinder example [138] was simulated and predictions were compared to exact solutions. The finite cylinder geometry is shown in Fig. 26.

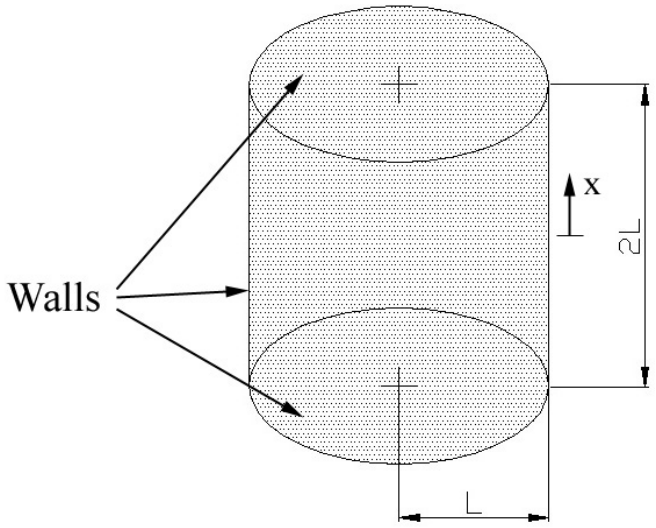

Figure 26 – Finite cylinder

This is a hypothetical test case where the cylinder walls are held at constant temperature $T_w = 0$ K and they are presumed black ($\varepsilon_w = 1$). The medium within the cylinder is held at constant temperature $T = 500$ K. Also, solely DTRM calculations are performed and

there is no energy exchange between the medium and walls. The number of rays and the medium absorption coefficient were varied in order to investigate their impact on the prediction accuracy.

Figure 27 shows the non-dimensional heat flux $Q = \frac{q_{net}}{\sigma T^4}$ against the non-dimensional cylinder height x/L, with the medium optical thickness $aL = 1.0$. The DTRM calculations were preformed for 4, 16 and 48 rays per boundary face on a structured computational mesh with 6000 control volumes. As expected, with increased number of rays better predictions were obtained. The DTRM predictions with 16 and 48 rays per boundary face show satisfactory agreement with the exact solution, while 4 rays per boundary face provide inaccurate predictions.

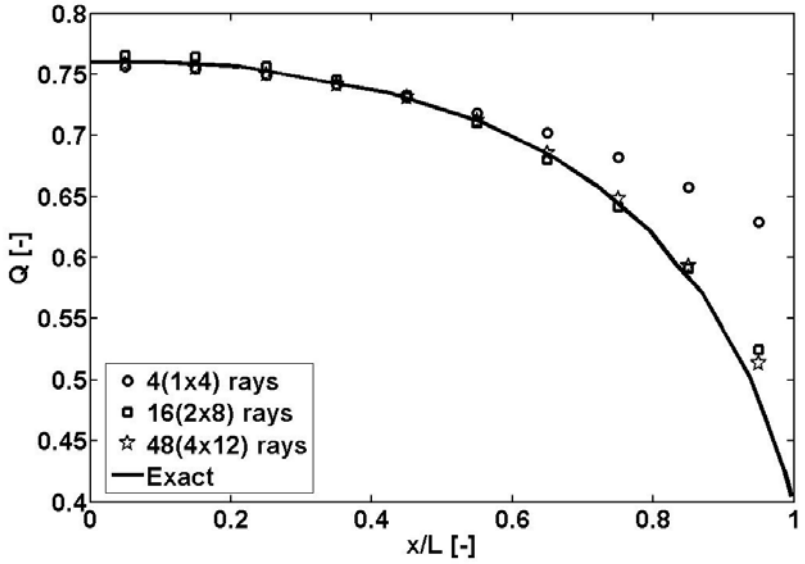

Figure 27 – Non-dimensional heat flux vs. non-dimensional wall distance for different numbers of rays (optical thickness $aL = 1.0$)

Figure 28 shows the non-dimensional fluxes for different optical thicknesses – $aL = 0.1$, $aL = 1.0$ and $aL = 5.0$, while 48 rays per boundary face were used in all calculations. Predictions agree very well with exact solutions in all simulated cases.

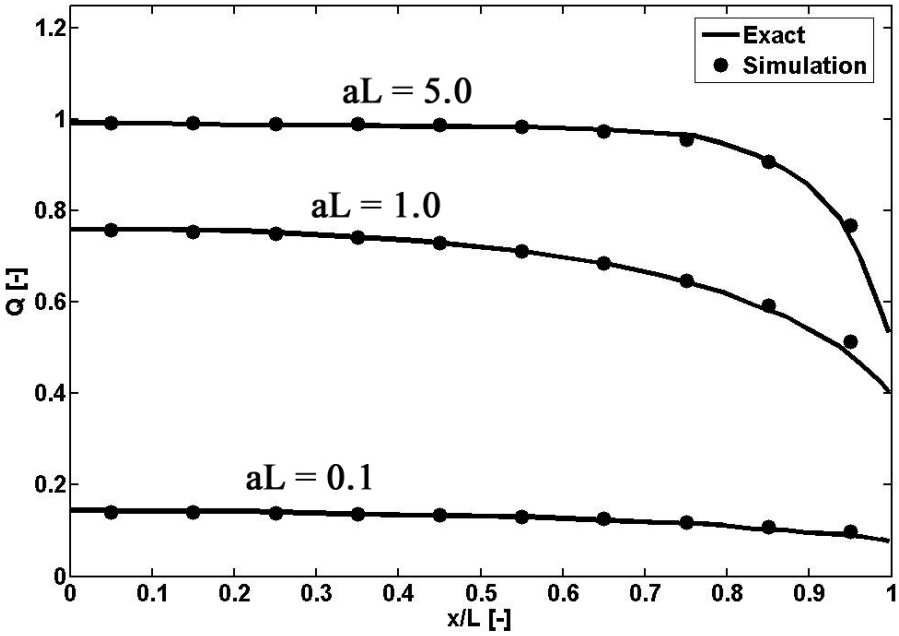

Figure 28 – Non-dimensional heat flux vs. non-dimensional wall distance for different optical thicknesses aL (48(4x12) rays)

The simulations of the finite cylinder test case verify the proper DTRM implementation into the FIRE code. Successful applications of the DTRM module in more complex configurations can be found in [87, 139].

4 Hydrogen jet flame

4.1 Experimental configuration

A series of laboratory hydrogen flames was experimentally investigated and described in [103, 104, 140, 141]. The experimental data can be obtained at [29].

The burner was a straight tube with an inner diameter $d = 3.75$ mm (outer diameter $d_o = 4.84$ mm) centred in a vertical wind tunnel (30 cm by 30 cm). The co-flow air velocity was around 1.0 m/s (± 0.06 m/s), with temperature 294 K (± 2 K). The configuration, as chosen for simulation in this work, had a fuel composition of 80 % H_2 (hydrogen) and 20 % He (helium) by volume. The pure hydrogen was diluted in order to reduce the radiation influence on thermal NO production [103]. The fuel exit velocity was 294 m/s ($\mathrm{Re} = 9800$ [103]) and the fuel temperature was 295 K (± 2 K). The co-flow air was humid with an average H_2O mole fraction 0.013. The flame was unconfined. The visible flame length was around $l_{vis} / d = 150$, while the stoichiometric axial length was $l_{st} = 375$ mm. Figure 29 shows the burner configuration.

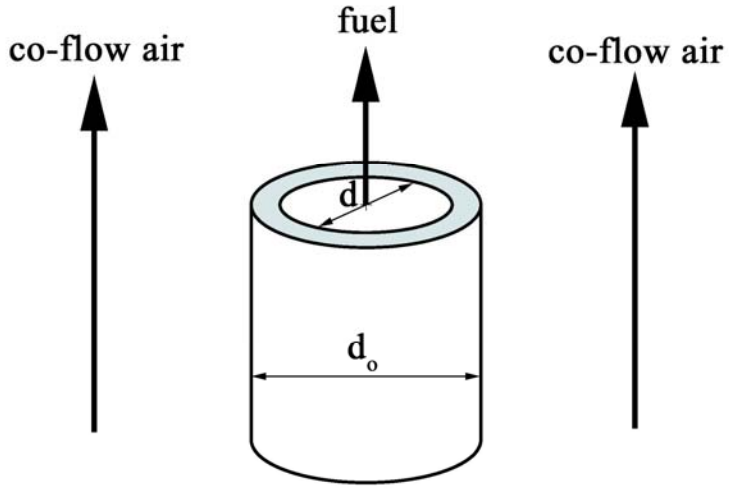

Figure 29 – Hydrogen flame configuration

The scalar and velocity measurements are available as axial centreline profiles and as radial profiles at axial positions $\frac{x}{l_{vis}} = \frac{1}{8}, \frac{1}{4}, \frac{3}{8}, \frac{1}{2}, \frac{5}{8}, \frac{3}{4}, \frac{1}{1}$. The measurements are given in terms of ensemble (Reynolds), Favre and conditional averages, but also single-shot measurements at various positions are available. The laser Doppler velocimetry (LDV) was used for the velocity measurements [141], while major species mass fractions and temperature measurements were obtained by combining the Raman scattering, Rayleigh scattering and laser-induced fluorescence (LIF) [103]. For more information on the experimental set-up and measurement techniques employed, one is referred to the original publications [103, 104, 140, 141].

4.2 Numerical set-up

A simulation was performed on a structured computational mesh consisting of 339000 control volumes covering a cylindrical domain spanning from $x/d = 0$ to $x/d = 400$ in axial direction, and from $r/d = 0$ to $r/d = 75$ in radial direction. The mesh distribution was denser towards the axis and inlets (Fig. 30). The mesh density in axial and radial directions was similar to those from the simulations reported in TNF proceedings [29], and no thorough mesh sensitivity analysis was performed in this work.

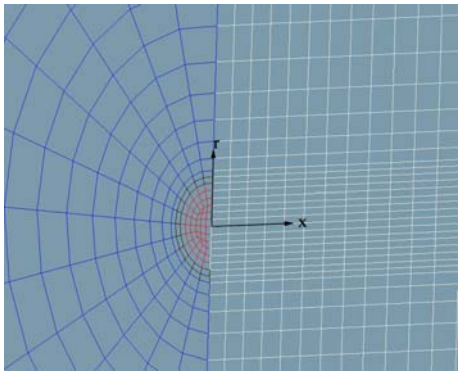

Figure 30 – Computational mesh (hydrogen flame; vertical axial cut; centreline)

The fuel inlet normal velocity was calculated according to the following expression obtained by fitting experimental data:

$$u(r)_{x=0} = -4 \cdot 10^{10} r^3 + 6 \cdot 10^7 r^2 - 37109 r + 306.39 \qquad 0 \le r \le 0.001875\ m \qquad (136)$$

The co-flow air inlet normal velocity was set as uniform, with its bulk value 1.0 m/s. The values of the turbulent kinetic energy and its dissipation rate at inlet boundaries were estimated from empirical relations as implemented in FIRE [99]:

$$k_b = \frac{3}{2}\left(I_\infty u_b\right)^2 \qquad \varepsilon_b = \frac{C_\mu^{3/4} k_b^{3/2}}{l} \tag{137}$$

The relative free-stream turbulence intensity was chosen $I_\infty = 7\,\%$.

Adiabatic and non-adiabatic calculations were performed, depending whether radiation modelling was included or not. In the non-adiabatic case the number of rays used in DTRM calculations was 48 (4x12), while the domain boundaries (inlets, outlets) were considered as black surfaces ($\varepsilon_b = 1$). In all cases the adiabatic species mass fractions, as available in pre-tabulated profiles, were used. WSGGM [101] was used for radiative properties evaluations.

Turbulence was modelled by standard k-ε model and by HTM [123]. As suggested in TNF proceedings (available at [29]), the constant $C_{\varepsilon 2}$ (Eq. (67)) was set to 1.83.

Combustion was modelled according to standard SLFM and models based on the reaction progress variable (Section 3.2.4). A stationary laminar flamelet library was generated in the pre-processor step by using the CSC solver [96] for 10 different values of the stoichiometric scalar dissipation rate parameters. A detailed hydrogen mechanism consisting of 13 species and 37 reactions (including NO chemistry) was used. In all cases the turbulence/chemistry coupling was accomplished via the presumed β-PDF (see Section 3.1.2.3).

A stationary low Mach number (incompressible) solver was used. At the outlet boundaries the constant static pressure was imposed. Iterative procedure was repeated until the normalised residuals for all equations have fallen below 10^{-6}. The convection term in the continuity equation was discretised using the central differencing scheme (2nd order), while the same terms in the momentum equations were discretised using a hybrid between the central differences and the upwind scheme (blending factor 0.5). The convection terms in the scalar equations were discretised using the upwind scheme (1st order). As usually, diffusion terms in all equations were discretised using the central differences. Other numerical set-up was as default in the FIRE solver [99].

4.3 Results

4.3.1 Pre-tabulated chemistry profiles

4.3.1.1 SLFM database

The stationary laminar flamelet profiles, according to standard SLFM (Section 2.3.3), were calculated in the CSC pre-processor [96] for the following values of the stoichiometric scalar dissipation rate parameters:

$$\chi_{st} = 0.01, 0.1, 1, 5, 10, 20, 50, 100, 150, 220\ s^{-1} \quad (138)$$

The first flamelet ($\chi_{st} = 0.01\ s^{-1}$) has a near-equilibrium composition, while the last one ($\chi_{st} = 220\ s^{-1}$) is nearly the last burning flamelet before extinction. The boundary species compositions and temperatures were imposed according to experimental data. The mixture fraction space was discretised into 50 non-equally distributed points, with denser point distribution near the stoichiometry ($Z_{st} \approx 0.042$).

Figure 31 shows the SLFM profiles for temperature (adiabatic) and various species mass fractions. While temperature and major species vary 'regularly' over the stoichiometric scalar dissipation rate parameters, the minor species NO and OH exhibit stronger gradients near the equilibrium. This is especially true in the case of NO where the first few profiles in the database (near equilibrium) differ substantially from the rest of the NO database. The same, but to a lesser extent, holds for the OH profiles as well.

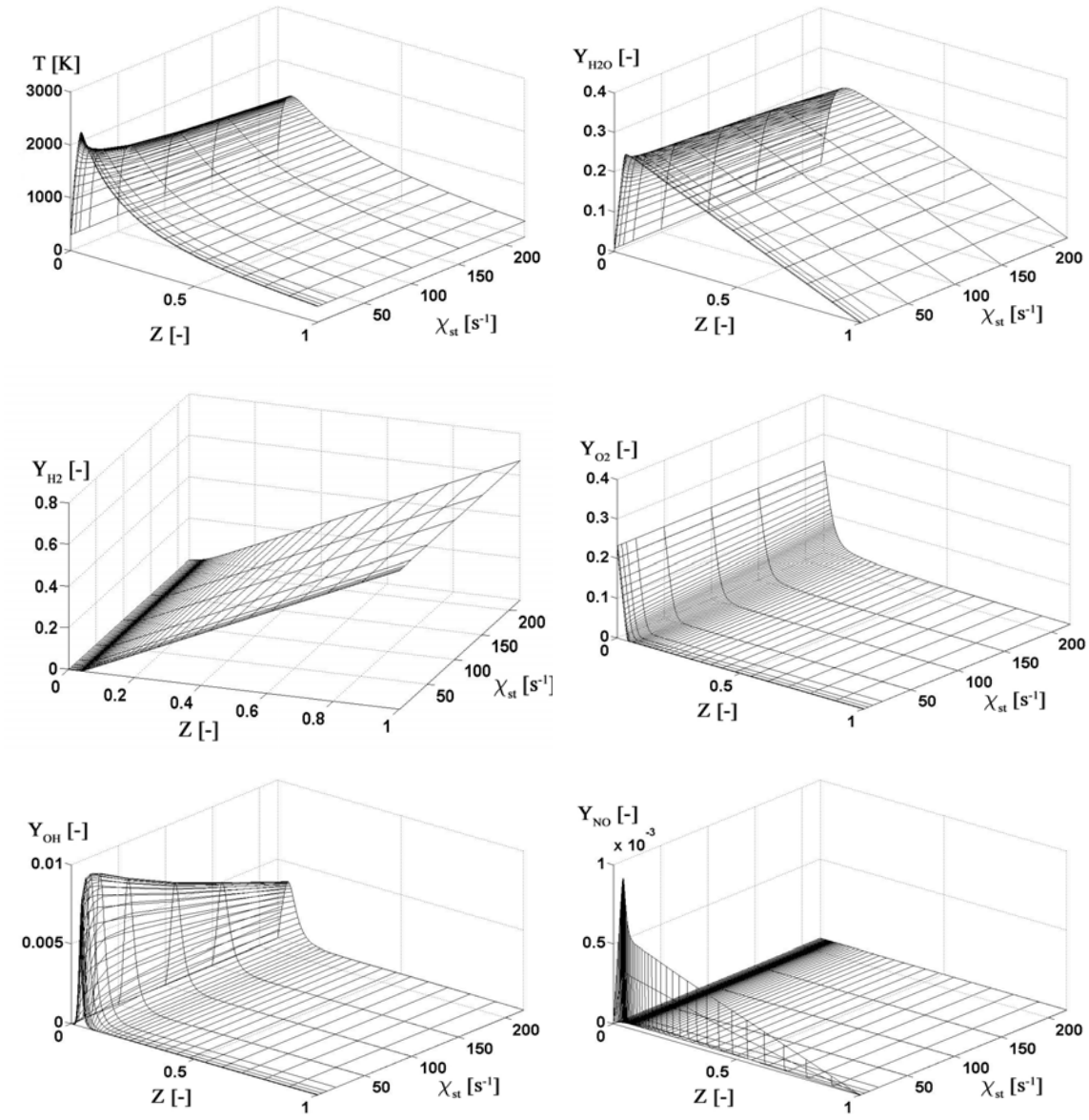

Figure 31 – SLFM (standard) database (hydrogen flame)

4.3.1.2 FPI database

The FPI database was created by using the PREMIX solver [97]. By following the same point discretisation in *Z*-space as in the SLFM database, the adiabatic one-dimensional freely propagating premixed laminar flames were calculated within the flammability range. Outside the flammability limits the profiles were obtained by interpolation with the boundary compositions. The flammability limits were approximately determined by approaching the fuel-rich and the fuel-lean side until the premixed flames were not able to propagate anymore (Fig. 1, e.g.). There were overall 34 premixed flamelet sets in the flammability range ($0.42 \le \phi \le 7.208$[8]), while the remaining 16 sets were obtained by interpolation. Given the mixture fraction (or equivalence ratio), the reactant composition was determined from the cold-mixing profiles.

Figure 32 shows the FPI database. The same species are shown as in Fig. 31, while instead of temperature the instantaneous reaction progress variable source term profiles are presented. As described in Section 2.3.6.1, the normalised reaction progress variable c was used as the second independent co-ordinate. In this case H_2O mass fraction was chosen, i.e. $Y_c \equiv Y_{H_2O}$. Unlike in the SLFM database, here the whole range from the cold-mixing ($c = 0$) up to the equilibrium ($c = 1$) is represented. There were 21 different sets of profiles in c direction, with denser distribution towards unity. Species compare similarly in magnitude in two databases (FPI and SLFM), except for NO, which is substantially different.

[8] Or, equivalently, $0.01796 \le Z \le 0.23894$ – see Eq. (24).

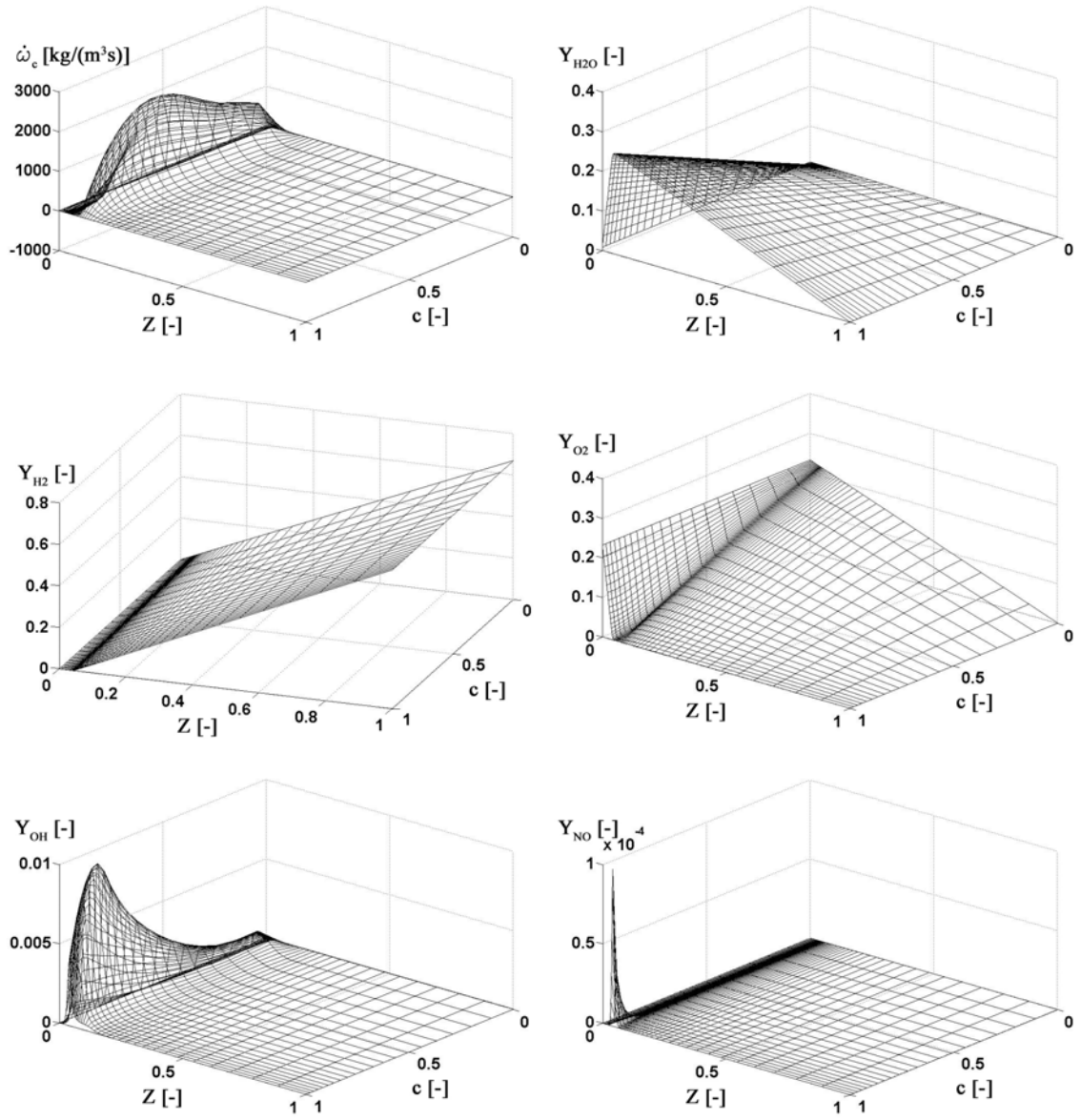

Figure 32 – FPI database (hydrogen flame)

4.3.1.3 SLFM database (reaction progress variable)

By following the procedure described in Section 2.3.6.2, the SLFM database was re-parameterised with the normalised reaction progress variable according to Eq. (42). However, due to partially non-monotonic variation of the reaction progress variable in the SLFM database for certain mixture fraction points, and if going along the stoichiometric scalar dissipation rate parameters – $\chi_{st} \in [0.01, 220]$ (in order), the unique mapping $Y_c(Z, \chi_{st}) \rightarrow Y_c(Z, c)$ was not possible if using all the flamelets from the database. This was simply remedied here by using only those flamelets from the SLFM database ($\chi_{st} = 0.01, 150$ and $220\ s^{-1}$) for which the unique mapping was ensured. It becomes clear, thus, that such an approximation is very crude in this particular case and leads, actually, to a linear weighting between the near-equilibrium ($\chi_{st} = 0.01\ s^{-1}$) and the $\chi_{st} = 150\ s^{-1}$ flamelet. The inspection of other species mass fractions in the SLFM database, or their linear combinations, revealed no appropriate reaction progress variable alternative to H_2O in this respect.

Figure 33 shows the re-parameterised SLFM database obtained with the previously described approximations. Shown are the profiles for the same species as in the FPI database (Fig. 32). However, it must be beard in mind that the normalised reaction progress variable in this case is defined according to Eq. (42) and that the covered range is much narrower (flamelet burning). While major species (H_2, O_2 and H_2O) seem to be little influenced by mentioned approximations, the repercussions on NO and OH profiles are obvious. The maximum values of OH are not reproduced correctly, while the near-equilibrium NO profile ($\chi_{st} = 0.01\ s^{-1}$) is artificially expanded in the re-parameterised database over a much wider range than in the original SLFM database. It could be stated, thus, the re-parameterised SLFM database, as shown in Fig. 33, is a very crude approximation of the original one, and, moreover, that it is qualitatively wrong if considering OH and NO. The simulation results to be presented later in this chapter, thus, should be viewed with a necessary criticism and caution, especially that being the case for OH and NO predictions.

A database composed of premixed and non-premixed flamelets, as described in Section 2.3.6.3, is not shown here nor was it used in the simulations. This is because of the same reasons with the choice of the reaction progress variables.

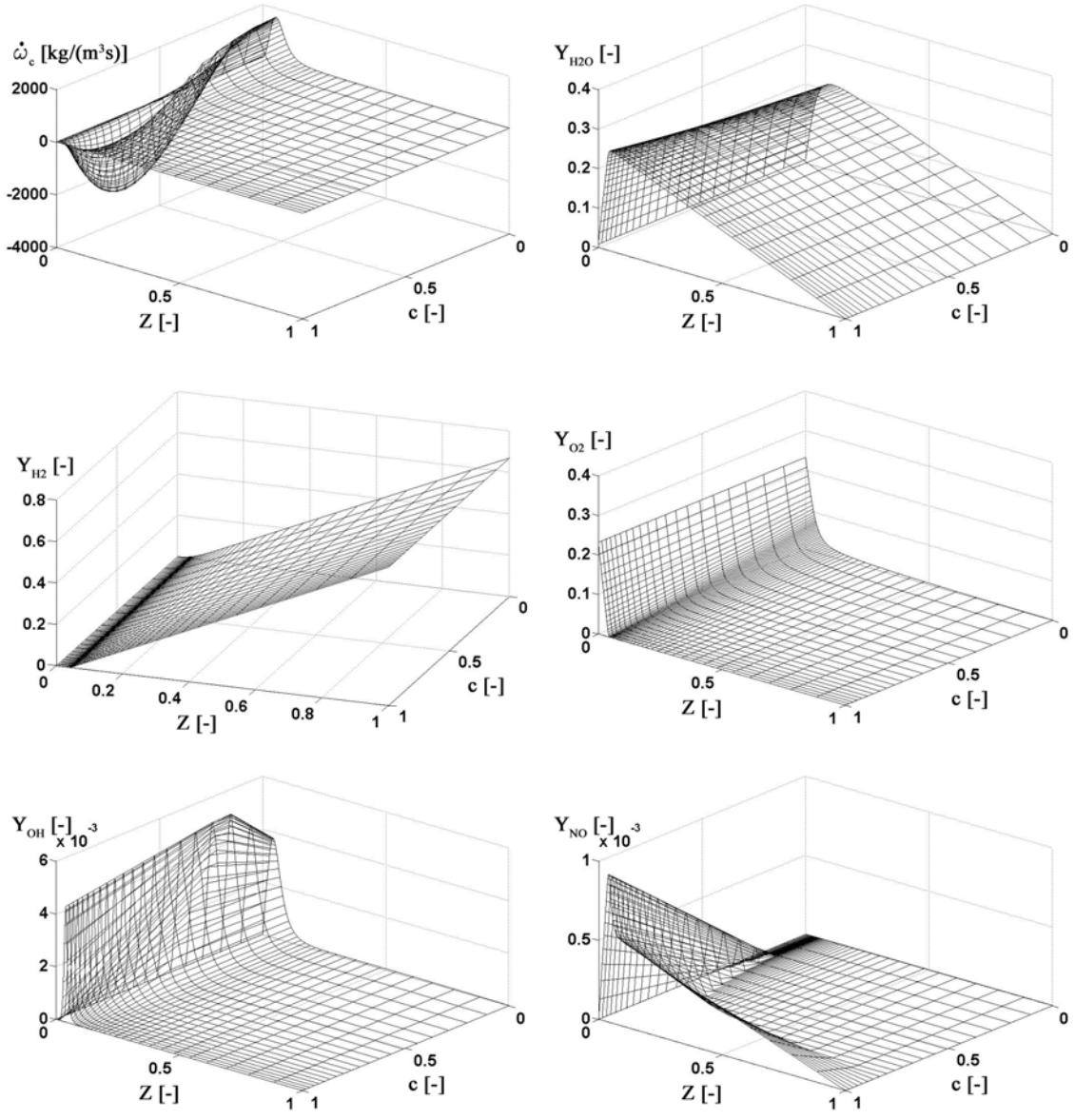

Figure 33 – SLFM (RPV) database (hydrogen flame)

4.3.2 Jet spreading

Figure 34 shows the radial profiles of mean axial velocities at axial positions $x/l_{vis}=1/8$ and $x/l_{vis}=3/8$. The standard k-ε model with different values of $C_{\varepsilon 2}$ constant (Eq. (67)) was used. The adiabatic conditions were presumed and the standard SLFM combustion model was used. Improved jet spreading predictions were achieved with $C_{\varepsilon 2}=1.83$. The predictions at the axial position closer to the nozzle ($x/l_{vis}=1/8$) are less favourable if compared to experimental data than is the case with the radial profiles at $x/l_{vis}=3/8$. Similar trends were observed at other axial locations as well. Because of proven better performance in the predictions of other flow field variables (not shown here), the tuned $C_{\varepsilon 2}=1.83$ value was retained in all subsequent hydrogen flame simulations.

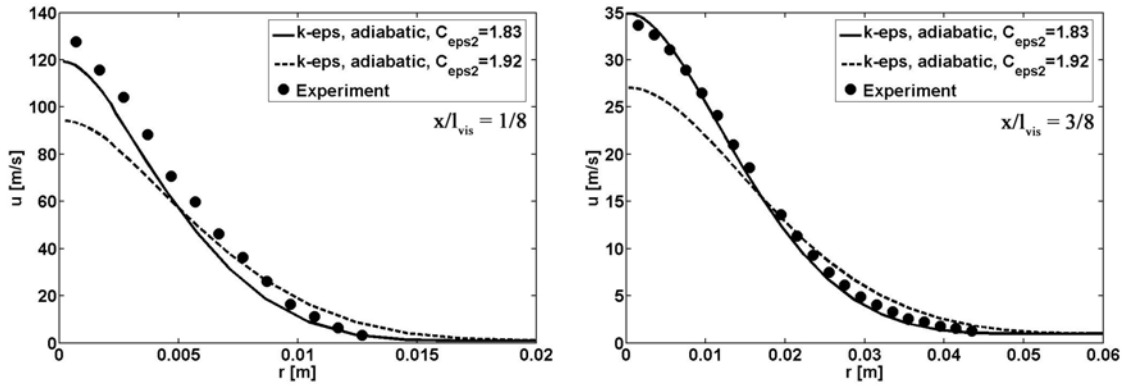

Figure 34 – Radial profiles of mean axial velocity at $x/l_{vis}=1/8$ and $x/l_{vis}=3/8$ (hydrogen flame; k-ε; adiabatic)

4.3.3 Adiabatic vs. non-adiabatic profiles

The impact of radiation inclusion into the overall modelling procedure was investigated. The standard SLFM was used for combustion modelling while the predictions obtained with two different turbulence models – k-ε and HTM – were compared. Figure 35 shows the axial (centreline) profiles of mean temperatures and H_2O[9] mass fractions.

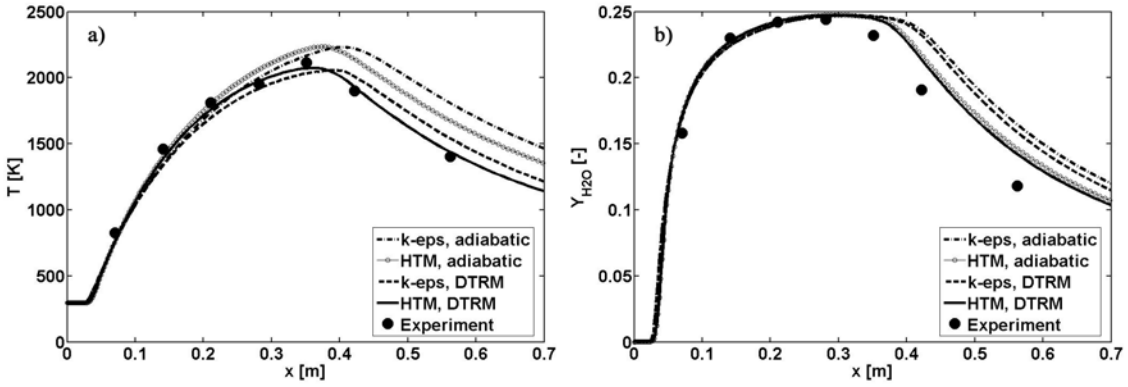

Figure 35 – Axial profiles at centreline position (hydrogen flame; adiabatic vs. DTRM; k-ε vs. HTM): a) Mean temperature; b) Mean H_2O mass fraction

The non-adiabatic (DTRM) axial profiles agree much better with experimental data than those obtained if neglecting the radiative heat transfer. Thus, even in such a simple configuration as simulated here, the inclusion of radiative heat transfer modelling is important if accurate temperature profiles are needed. Figure 35a also reveals that HTM predictions agree better with experimental data than those of k-ε model. The peak temperature magnitude and position are very well predicted in the former case.

Figure 36 shows the non-adiabatic axial predictions of mixture fraction moments – mean and root-mean-square[10] (RMS). The predictions compare well with the measurements. This is important because the mixture fraction moments are used as the co-ordinates in chemistry pre-tabulations (see Fig. 19, e.g.) and their accurate solution is pre-requisite for the accurate predictions of other reactive scalars as well. The profiles obtained with HTM and k-ε are very similar.

[9] The only species participating in the gaseous radiative heat exchange in this case (WSGGM).

[10] $Z_{RMS} \equiv \sqrt{\widetilde{Z''^2}}$

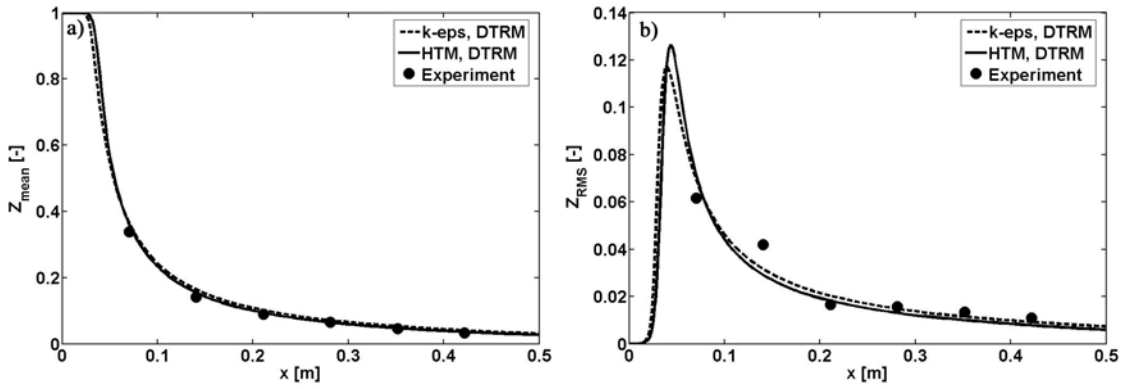

Figure 36 – Axial profiles at centreline position (hydrogen flame; non-adiabatic; k-ε vs. HTM): a) Mean mixture fraction; b) Mixture fraction RMS

The radial profiles of mean temperature and H_2O mass fraction at axial position $x/l_{vis} = 3/8$ are shown in Fig. 37. The impact of radiation is more emphasised near the centreline axis where the predictions compare well with experimental data, while farther from the axis the inclusion of radiation does not seem to bring substantial improvements. If comparing different turbulence models it can be concluded that HTM is better in predicting the reactive scalars near the axis, while away from it the k-ε predictions slightly better match with experimental data. Similar observations hold also for other species and for radial profiles at other axial positions.

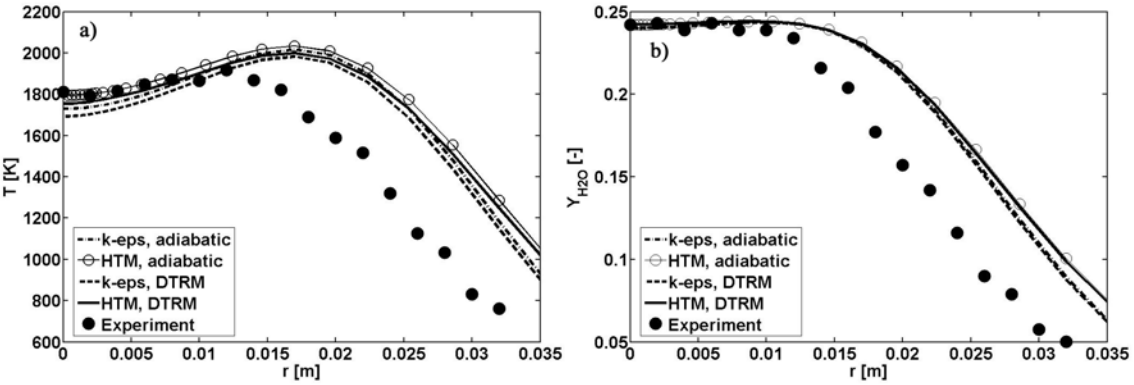

Figure 37 – Radial profiles at x/l_{vis}=3/8 (hydrogen flame; adiabatic vs. non-adiabatic; k-ε vs. HTM): a) Mean temperature; b) Mean H_2O mass fraction

The non-adiabatic radial profiles of mean axial velocity at axial positions $x/l_{vis} = 1/8$ and $x/l_{vis} = 3/8$ are shown in Fig. 38.

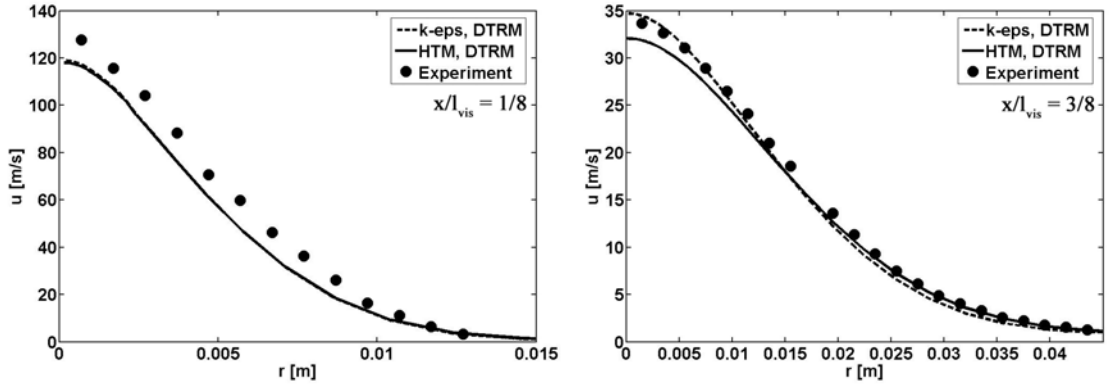

Figure 38 – Radial profiles of mean axial velocity at x/l_{vis}=1/8 and x/l_{vis}=3/8 (hydrogen flame; k-ε vs. HTM; non-adiabatic)

Similarly as in the adiabatic case (Fig. 34), the predictions are better at downstream locations than close to the nozzle. The k-ε model performs better than HTM if comparing the predictions with experimental data at axial position $x/l_{vis} = 3/8$ and close to the centreline axis, while away from the axis HTM performs better.

In order to further investigate the reasons for the departures of the radial predictions at axial position $x/l_{vis} = 3/8$ (Fig. 37), in Fig. 39 are shown the radial profiles of mixture fraction moments for the same axial position. The relative disagreement of these scalars in the regions away from the centreline axis ($r > 0.015$ m) explains the departures of other reactive scalars in these regions as well. The probable reason for such behaviour lies in a simple gradient transport hypothesis adopted for turbulent fluxes modelling in the transport equations for mixture fraction moments.

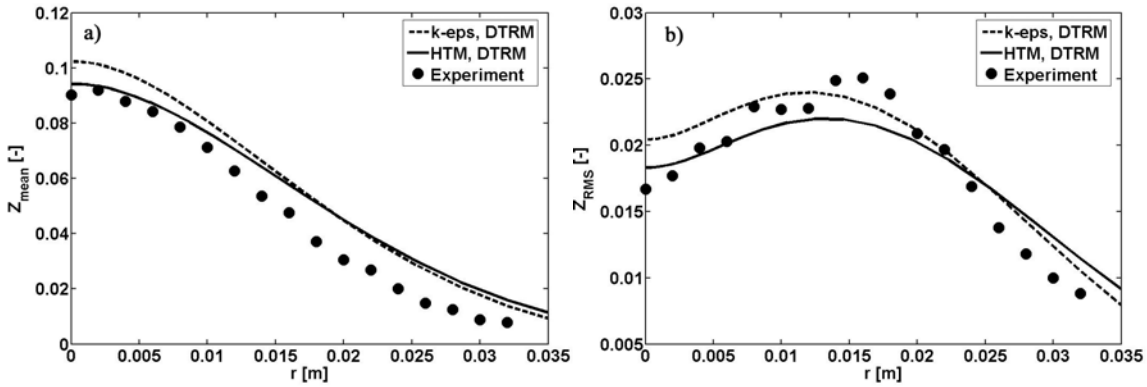

Figure 39 – Radial profiles at x/l_{vis}=3/8 (hydrogen flame; non-adiabatic; k-ε vs. HTM): a) Mean mixture fraction; b) Mixture fraction RMS

4.3.4 Combustion models comparison

In order to compare different combustion models – SLFM, RPV (FPI), and RPV (SLFM) (Section 3.2.4) – the calculation procedure was as follows. The referent converged stationary solutions were first obtained by using HTM in a combined calculation procedure together with DTRM (48 rays) and the standard SLFM. Mean species mass fractions according to RPV models were subsequently extracted from adequate chemistry pre-tabulations in the post-processor step. This way the combustion modelling was to a great extent decoupled from other flow field calculations (mean velocities, mixture fraction moments and enthalpy) and their mutual interaction was eliminated. Thus, the co-ordinates entering the chemistry pre-tabulations (mixture fraction moments) were the same in all cases, while the transport equation for the mean reaction progress variable (Eq. (76)) was additionally solved in order to obtain the mean normalised reaction progress variable (Section 2.5.8). Based on the resolved enthalpy field and extracted species composition, the temperature field was iteratively obtained in the same manner as described in Section 3.2.4.

The radial profiles of mixture fraction moments at various axial locations are shown in Fig. 40. The mean mixture fraction profiles at axial locations $x/l_{vis} = 1/4$ and $x/l_{vis} = 3/4$ are somewhat over-predicted for all radial points, while the predictions of mixture fraction RMS are less good close to the axis. In general, the referent solutions for mixture fraction moments fairly agree with experimental data.

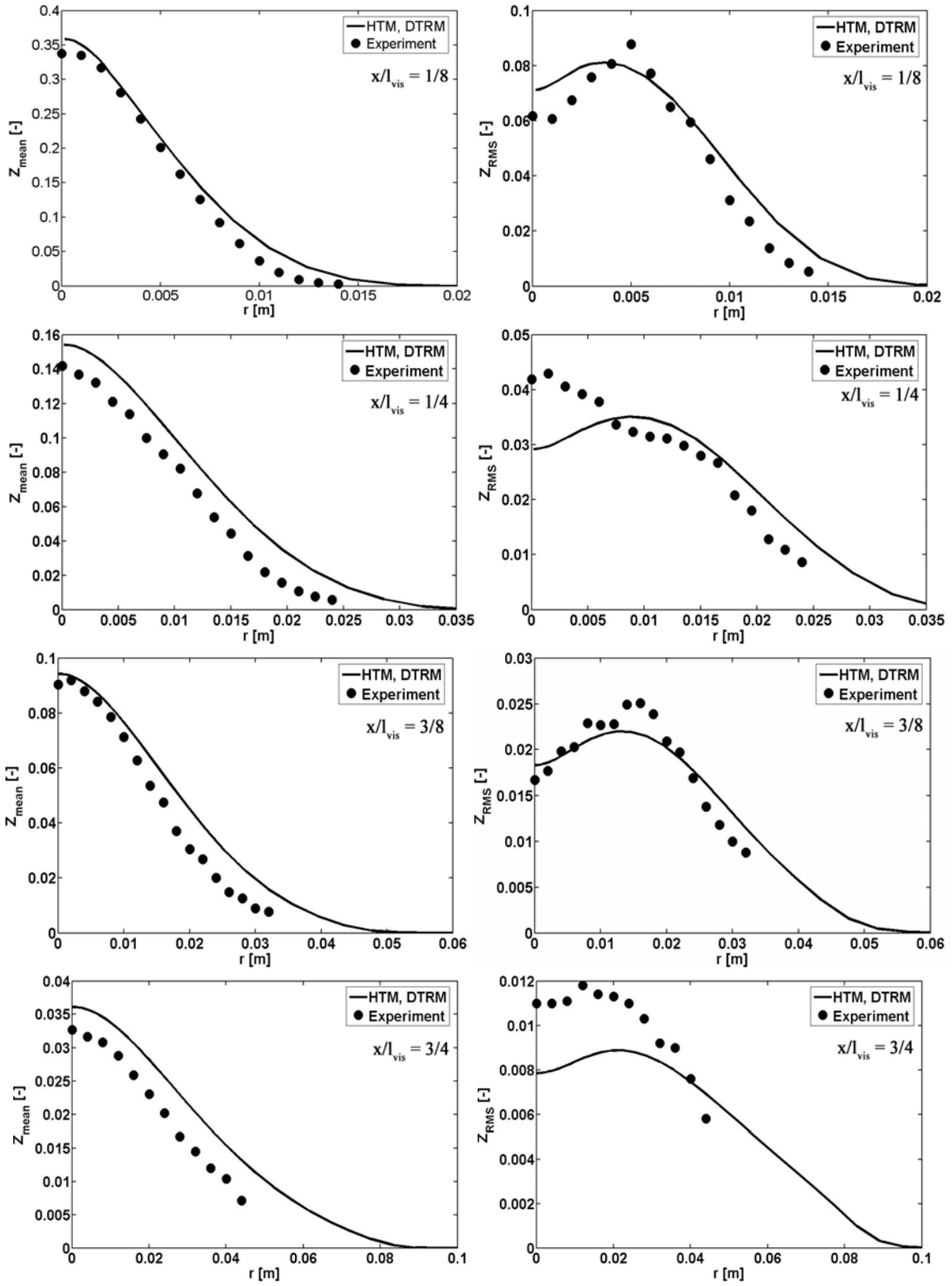

Figure 40 – Radial profiles of mixture fraction moments (mean and RMS) at various axial positions (hydrogen flame; non-adiabatic; HTM)

The mean temperature and species mass fractions (H_2O, H_2, O_2, OH and NO) at centreline axis are shown in Fig. 41. The temperature predictions agree very well with the experiments for all combustion models. RPV (FPI) slightly under-predicts the temperature in axial regions $0.1 \le x \le 0.2$ m, while it provides the best agreement with experimental data at further downstream locations. The predictions of major species (H_2O, H_2 and O_2) compare very similarly and are barely distinguishable between the models. In the post-flame regions ($x > l_{st} = 375$ mm), however, the H_2O profiles are over-predicted, indicating an excessive combustion there. O_2 is relatively poorly predicted in the regions near the fuel nozzle. The minor species OH and NO are also presented, and while OH is fairly well predicted by both, RPV (FPI) and SLFM, the NO predictions compare less favourably with experimental data. SLFM gives lower OH peak values, and presumably, agrees better with the experiments in this respect. RPV (FPI), on the other hand, gives better OH predictions near the fuel nozzle. The NO profiles are greatly over-predicted by models based on the non-premixed flamelet pre-tabulations (SLFM and RPV (SLFM)). As the simulated configuration operated at relatively low Reynolds number ($\mathrm{Re} \approx 10000$), the turbulence impact on the chemistry is relatively low (Fig. 42), and accordingly, the extracted chemistry profiles do not depart substantially from the equilibrium ones. If inspecting the SLFM database (Fig. 31) it can be seen that equilibrium NO profiles ($\chi_{st} \to 0$) are very large in magnitude when compared to the rest of the database, and thus, these are responsible for over-predictions in simulations. The FPI database (Fig. 32), on the other hand, provides substantially lower NO values near the equilibrium ($c \to 1$). As mentioned previously, the RPV (SLFM) results for NO and OH should be considered with a special precaution because of the artificially introduced impurities in the pre-tabulated database (Section 4.3.1.3).

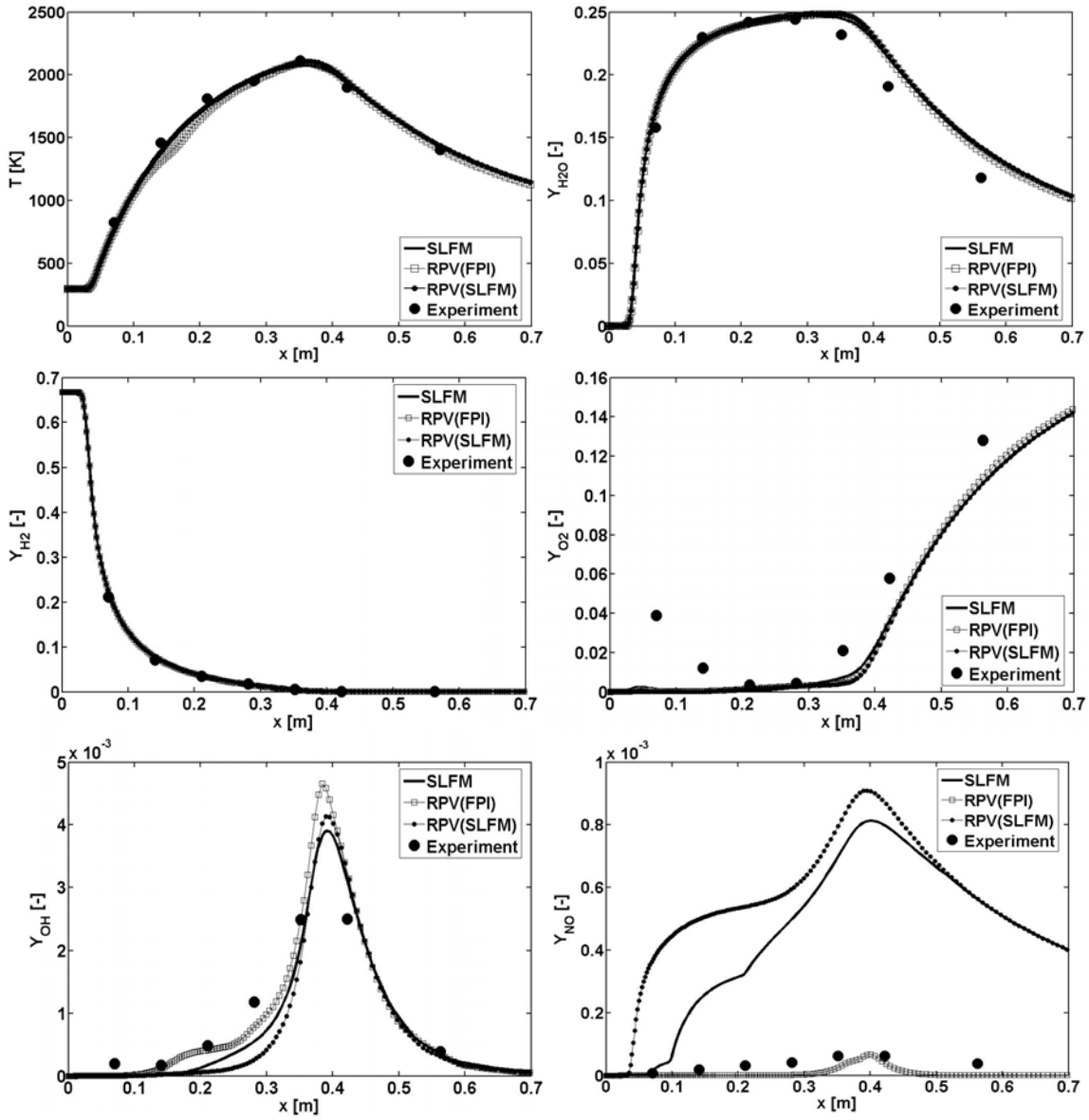

Figure 41 – Axial profiles of the mean temperature and species mass fractions (hydrogen flame; centreline position; non-adiabatic; HTM)

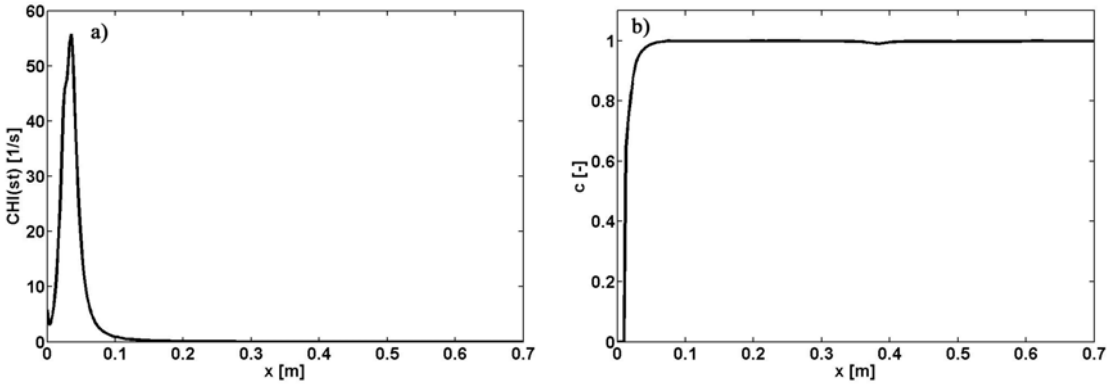

Figure 42 – Tabulation parameters (hydrogen flame): a) $\overline{\chi}_{st}$ (Eq. (91)), SLFM database; b) $\overline{c}$ (Eq. (100)), FPI database

The radial profiles of the mean temperature and species mass fractions (H_2O, H_2, O_2, OH and NO) at axial positions $x/l_{vis} = 1/4$ and $x/l_{vis} = 3/4$ are shown in Figs. 43 and 44. The predictions of temperature and major species are close among the models, except the H_2 profile at $x/l_{vis} = 3/4$ which is badly predicted by RPV models. The radial predictions of temperature worsen away from the centreline axis. The largest differences between the combustion models are evident if comparing the OH and NO predictions. While SLFM is slightly better in the OH predictions, the radial profiles of NO are better predicted with RPV (FPI) at all axial locations. In this respect, RPV (FPI) seems to be the model of choice (among those models used in this work) if more accurate NO predictions are wanted. SLFM fails by an order of magnitude if considering the NO predictions. Due to the same reasons as before, the RPV (SLFM) profiles of OH and NO should be taken with a reserve.

The radial profiles at other axial locations (not shown) behave similarly.

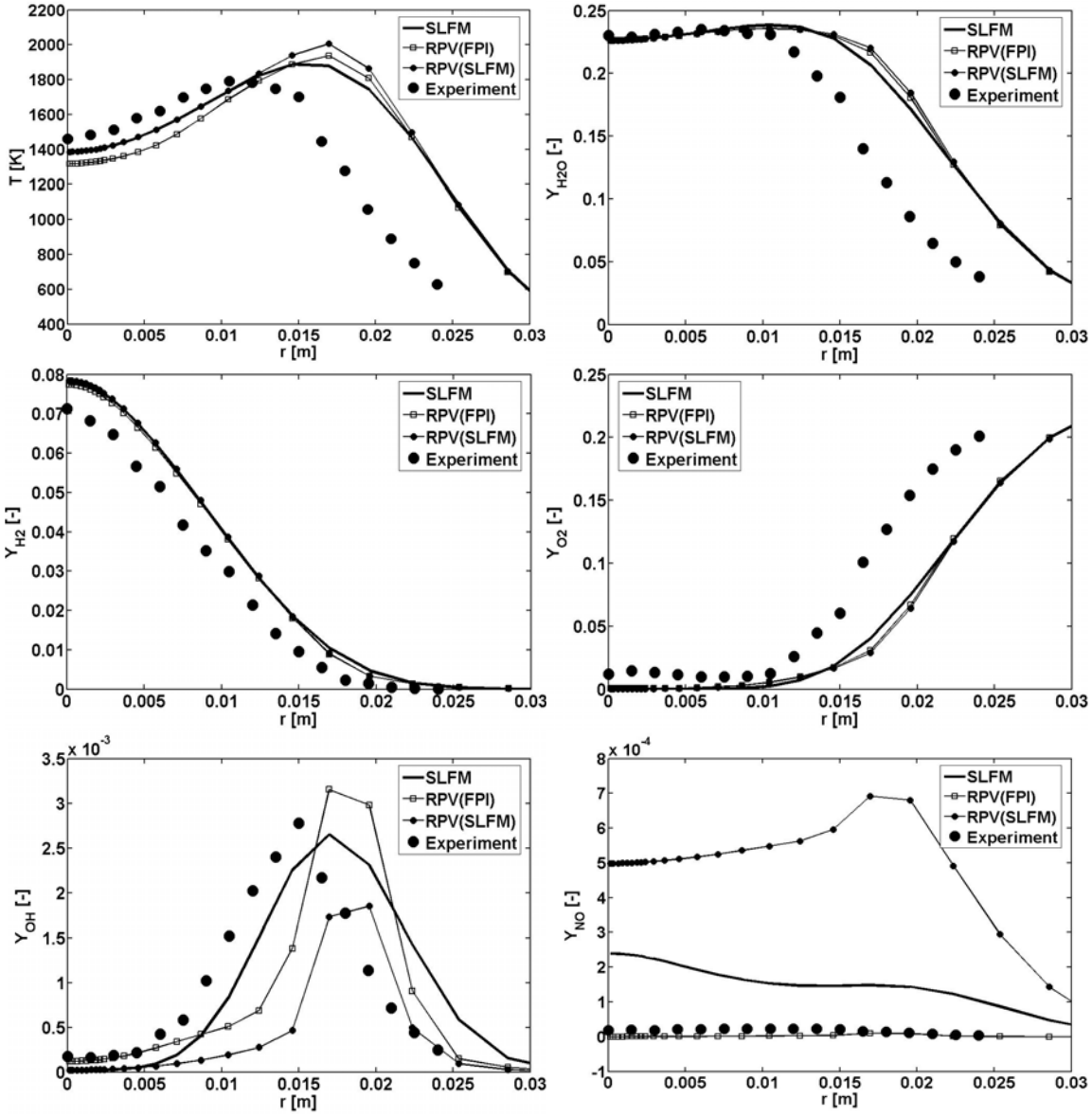

Figure 43 – Radial profiles of the mean temperature and species mass fractions at x/l_{vis}=1/4 (hydrogen flame; non-adiabatic; HTM)

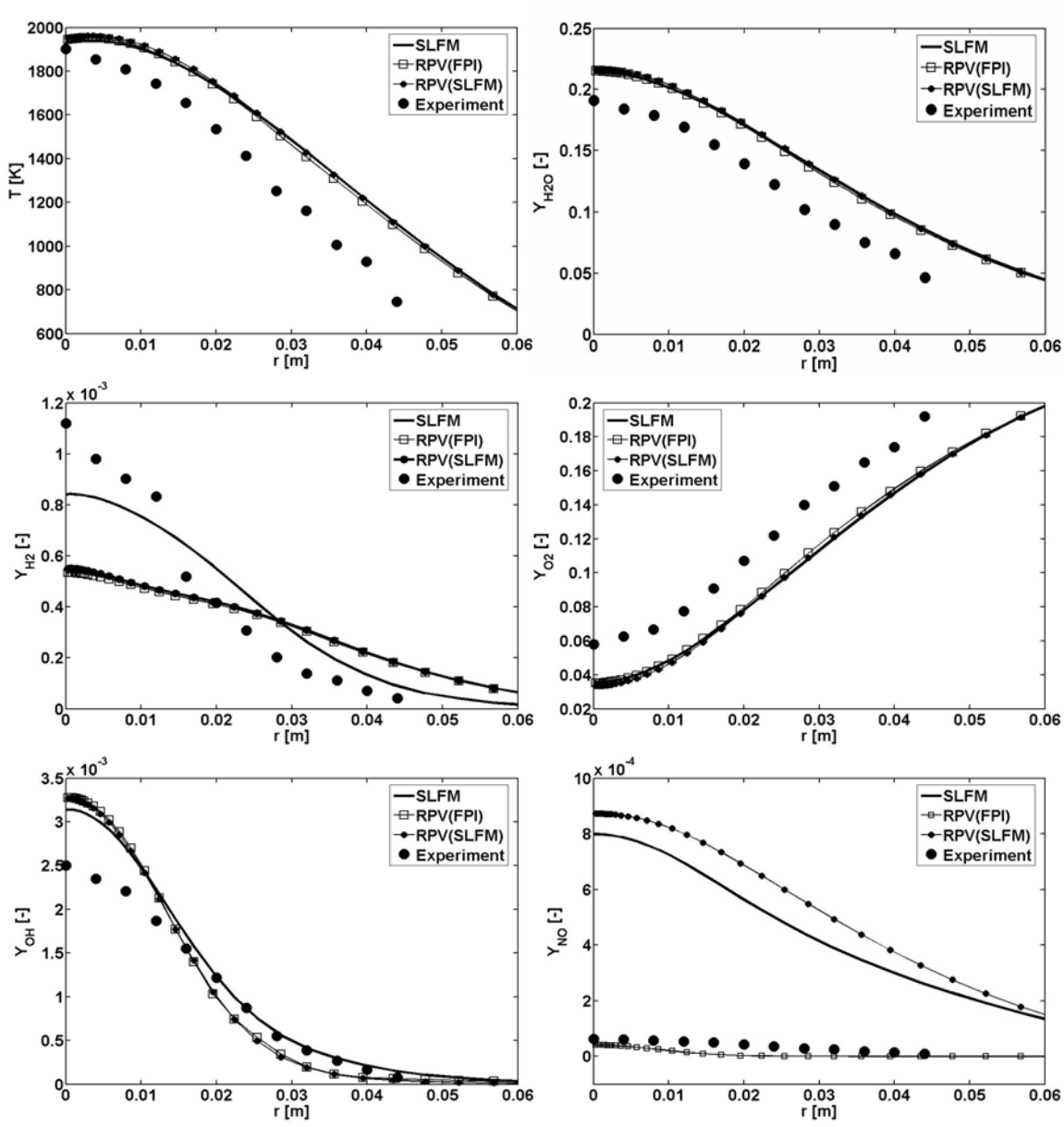

Figure 44 – Radial profiles of the mean temperature and species mass fractions at $x/l_{vis}=3/4$ (hydrogen flame; non-adiabatic; HTM)

5 Methane jet flame

5.1 Experimental configuration

The burner had a central fuel jet, a pilot jet and a co-flow air jet in a concentric annular arrangement (Fig. 45) [29, 40, 142]. The fuel was composed of 25% methane (CH_4) and 75% air by volume and had a temperature 294 K. The surrounding pilot had an equivalent equilibrium composition to methane/air at $Z = 0.27$, with the temperature 1880 K. The co-flowing air was held at 291 K. The flame operated at $\mathrm{Re} = 22400$ with a small degree of local extinction (Sandia flame D). The bulk velocities were 49.6 m/s for the fuel, 11.4 m/s for the pilot and 0.9 m/s for the air. The flame was unconfined.

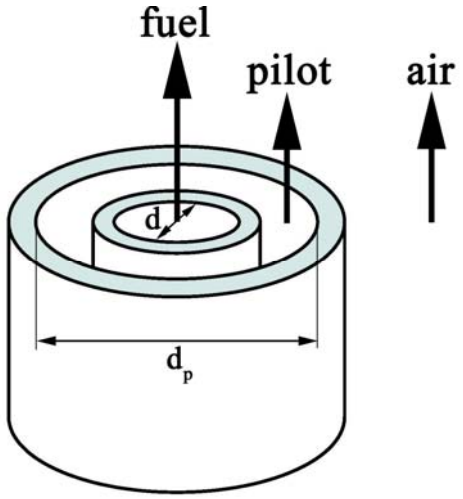

Figure 45 – Methane flame configuration

The burner dimensions were as follows (Fig. 45):

Main jet inner diameter:	$d = 7.2$ mm
Pilot annulus inner diameter:	7.7 mm (tube thickness 0.25 mm)
Pilot annulus outer diameter:	$d_p = 18.2$ mm
Co-flow annulus inner diameter:	18.9 mm (tube thickness 0.35 mm)
Co-flow annulus outer diameter:	300 mm

The flame documentation and experimental measurements are available at [29].

5.2 Numerical set-up

A computational mesh consisted of 338400 control volumes covering a cylindrical domain from $x/d = 0$ to $x/d = 150$ in axial direction and from $r/d = 0$ to $r/d = 40$ in radial direction. Similarly as in the hydrogen flame example, the mesh was denser towards the central axis and inlets (Fig. 46). The mesh density in axial and radial directions was similar to those from the simulations reported in TNF proceedings [29], and no thorough mesh sensitivity analysis was performed.

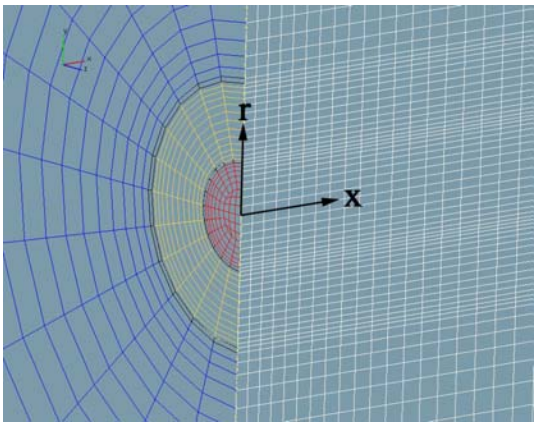

Figure 46 – Computational mesh (methane flame; vertical axial cut; centreline)

The GRI Mech 3.0 [65] chemical mechanism, consisting of 53 species and 325 reactions, was used for chemistry pre-tabulations. Similarly as in the hydrogen flame example, combustion was modelled by the standard SLFM and by models based on the reaction progress variable (Section 3.2.4). The turbulence/chemistry coupling was done via the presumed β-PDF.

The DTRM calculations were performed using 48 (4x12), 16 (2x8) and 4 (1x4) rays per boundary face in order to investigate the impact of the ray number on prediction accuracy. WSGGM [101] was used for the radiative properties evaluations. As the flame was unconfined, the domain boundaries (inlets, outlets) were considered as black surfaces ($\varepsilon_b = 1$).

The constant $C_{\varepsilon 2}$ in the transport equation for the dissipation rate of the turbulent kinetic energy was set to $C_{\varepsilon 2} = 1.8$, as suggested in the TNF proceedings (available at [29]). HTM and k-ε were used for turbulence modelling.

The inlet velocities were imposed according to experimental measurements (Fig. 47) [143].

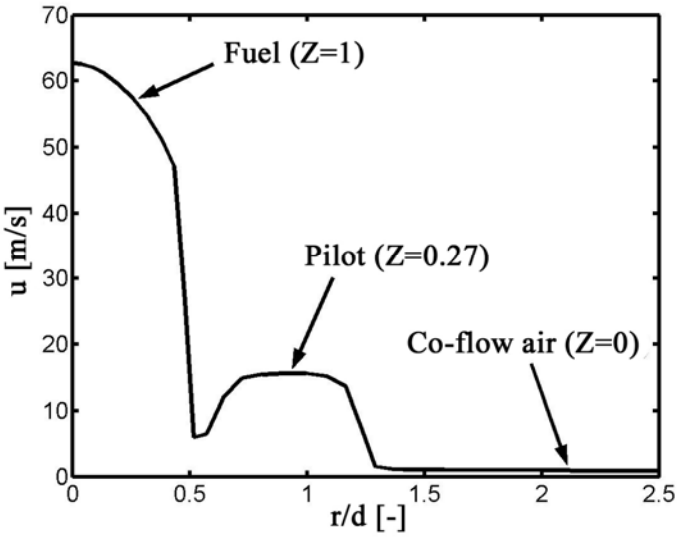

Figure 47 – Inlet velocity profiles (methane flame)

The turbulent kinetic energy at inlet boundaries was estimated from the experimental measurements of the Reynolds stresses. The dissipation rate of the turbulent kinetic energy was prescribed, similarly as in [55], as:

$$\varepsilon = \sqrt{C_\mu} k \left| \frac{\partial u}{\partial r} \right| \tag{139}$$

Similarly as in the hydrogen flame example, the constant ambient pressure conditions were imposed at all outlet boundary selections. The low Mach number (incompressible) solver was used. The calculation was stationary. The iterative procedure was repeated until the normalised residuals for all equations have fallen below 10^{-6} (whenever possible). The convection term in the continuity equation was discretised using the central differencing scheme (2nd order), while the same terms in the momentum equations were discretised using a hybrid between the central differences and the upwind scheme (blending factor 0.5). The convection terms in the scalar equations were discretised using the upwind scheme (1st order). As usually, diffusion terms in all equations were discretised using the central differences. Other numerical set-up was as default in the FIRE solver [99].

5.3 Results

5.3.1 Pre-tabulated chemistry profiles

Figures 49-52 show the chemistry pre-tabulations used in the simulations of the methane flame. The original SLFM database (Fig. 49) was created for a range of the stoichiometric scalar dissipation rate parameters (14 profiles):

$$\chi_{st} = 0.01, 0.1, 1, 2, 5, 10, 20, 50, 100, 150, 200, 300, 450, 575\ s^{-1} \quad (140)$$

The first flamelet ($\chi_{st} = 0.01\ s^{-1}$) has a near-equilibrium composition, while the last one ($\chi_{st} = 575\ s^{-1}$) is nearly the last burning flamelet before extinction. The boundary species compositions and temperatures were imposed according to experimental data. The mixture fraction space was discretised into 50 non-equally distributed points, with a denser point distribution near the stoichiometry ($Z_{st} \approx 0.353$).

A linear combination of CO_2, CO and H_2O mass fractions was used as the reaction progress variable, i.e. $Y_c \equiv Y_{CO_2} + Y_{CO} + Y_{H_2O}$. The flammable range was approximately $0.369 \le \phi \le 7.193$ [11] (Fig. 48). There were 29 premixed flames sets obtained with the adapted PREMIX solver [97] within the flammability limits, while the remaining 21 sets were obtained by linear interpolation with boundary values. The mixture fraction discretisation from the original SLFM database was retained. The FPI database is shown in Fig. 50. Similarly as in the hydrogen flame example, the FPI profiles for NO considerably differ from those based on non-premixed flamelets. Other species have similar maximum values as in the SLFM (Fig. 49) or re-parameterised SLFM (Fig. 51) databases. The interpolated profiles between the rich flammability limit and the fuel boundary can be identified in the FPI database in the regions $Z > 0.8$, especially if considering the CO_2, CO, H_2O and H_2 profiles.

There were no such problems with the re-parameterisation of the SLFM database as was the case in the hydrogen flame example. The re-parameterised SLFM database (Fig. 51) clearly reflects all important features of the original SLFM database (Fig. 49) – the

[11] Or, equivalently, $0.16729 \le Z \le 0.79678$ – see Eq. (24)

maximum values and the starting/ending profiles ($\chi_{st} = 0.01/575$ s^{-1} and $c = 1/0$) are equal in both cases. It can be noticed, though, that the species profiles vary more uniquely in the re-parameterised SLFM database than in the original one, this being especially the case if considering major species.

The database composed of premixed and non-premixed flamelets, according to definition in Section 2.3.6.3, is shown in Fig. 52. It retains the major features of both – the premixed (FPI) and non-premixed (SLFM) database. It must be remembered, however, that the normalised reaction progress variables in the re-parameterised SLFM database (Fig. 51) and in the mixed/FPI databases cover different ranges, as explained in Section 2.3.6. The transition between premixed (lower values of the normalised reaction variable) and non-premixed flamelets (higher values of the normalised reaction variable) can be identified at threshold points c_{thresh} (Eq. (43)).

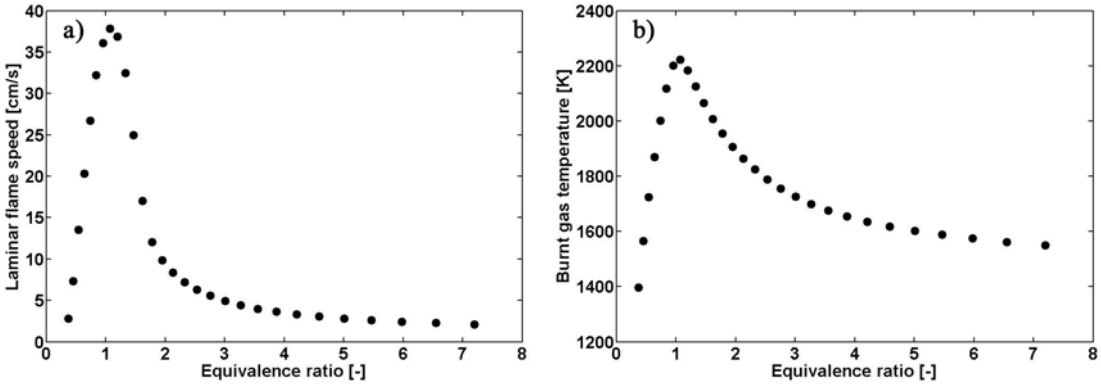

Figure 48 – Premixed diluted methane (25% CH_4, 75% air – by volume)/air flames: a) Laminar flame speed; b) Burnt gas temperature

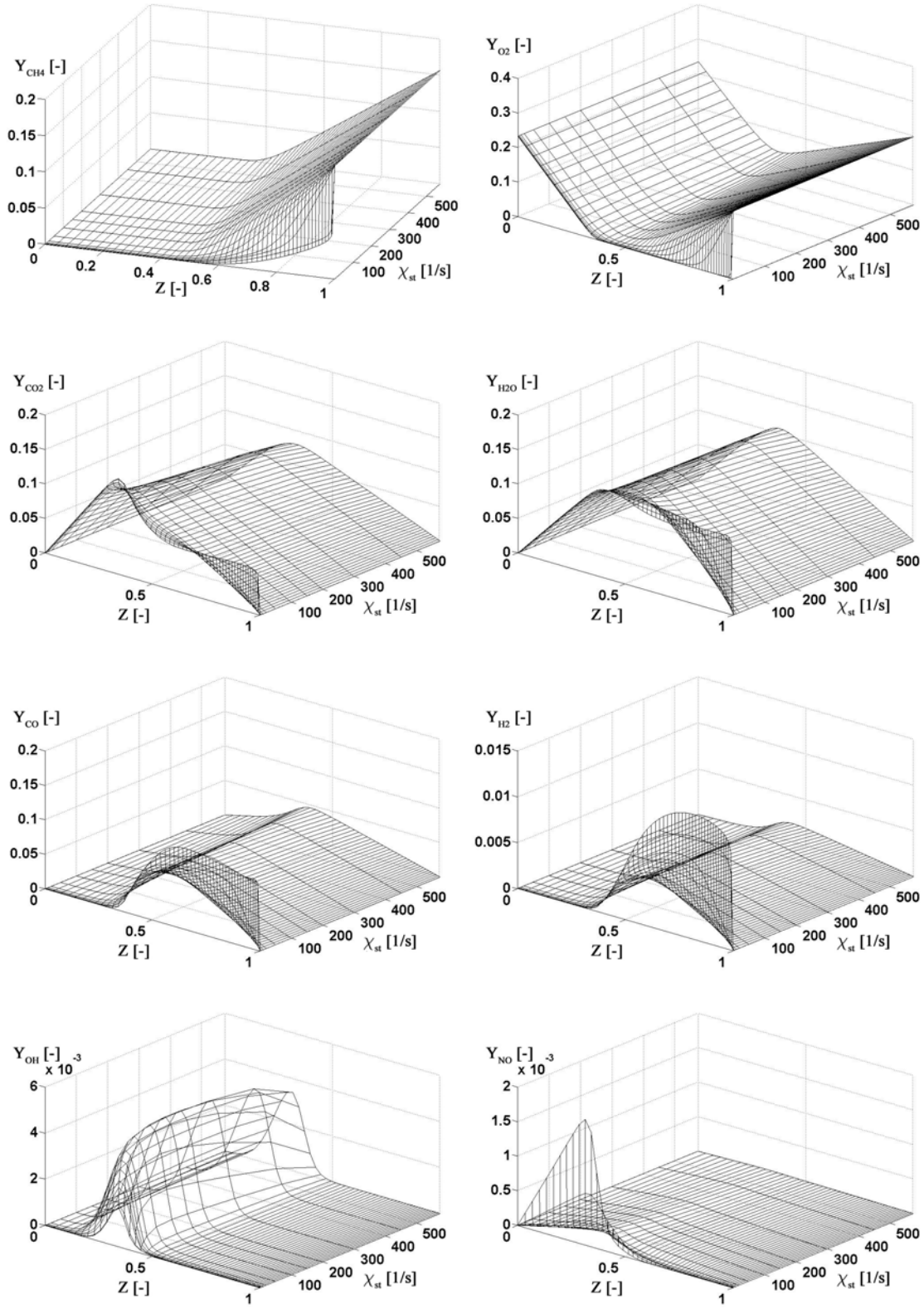

Figure 49 – SLFM (standard) database (methane flame)

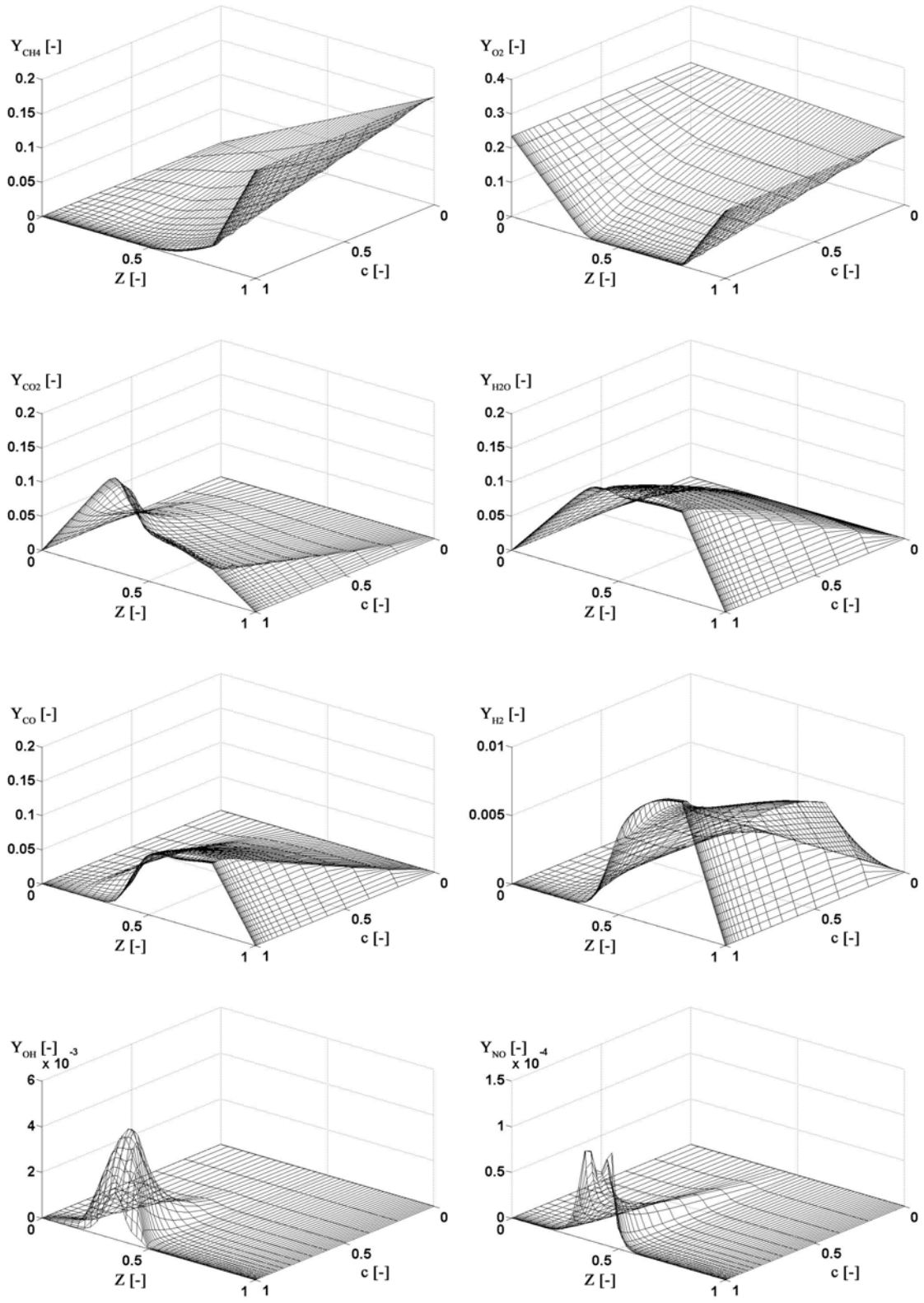

Figure 50 – FPI database (methane flame)

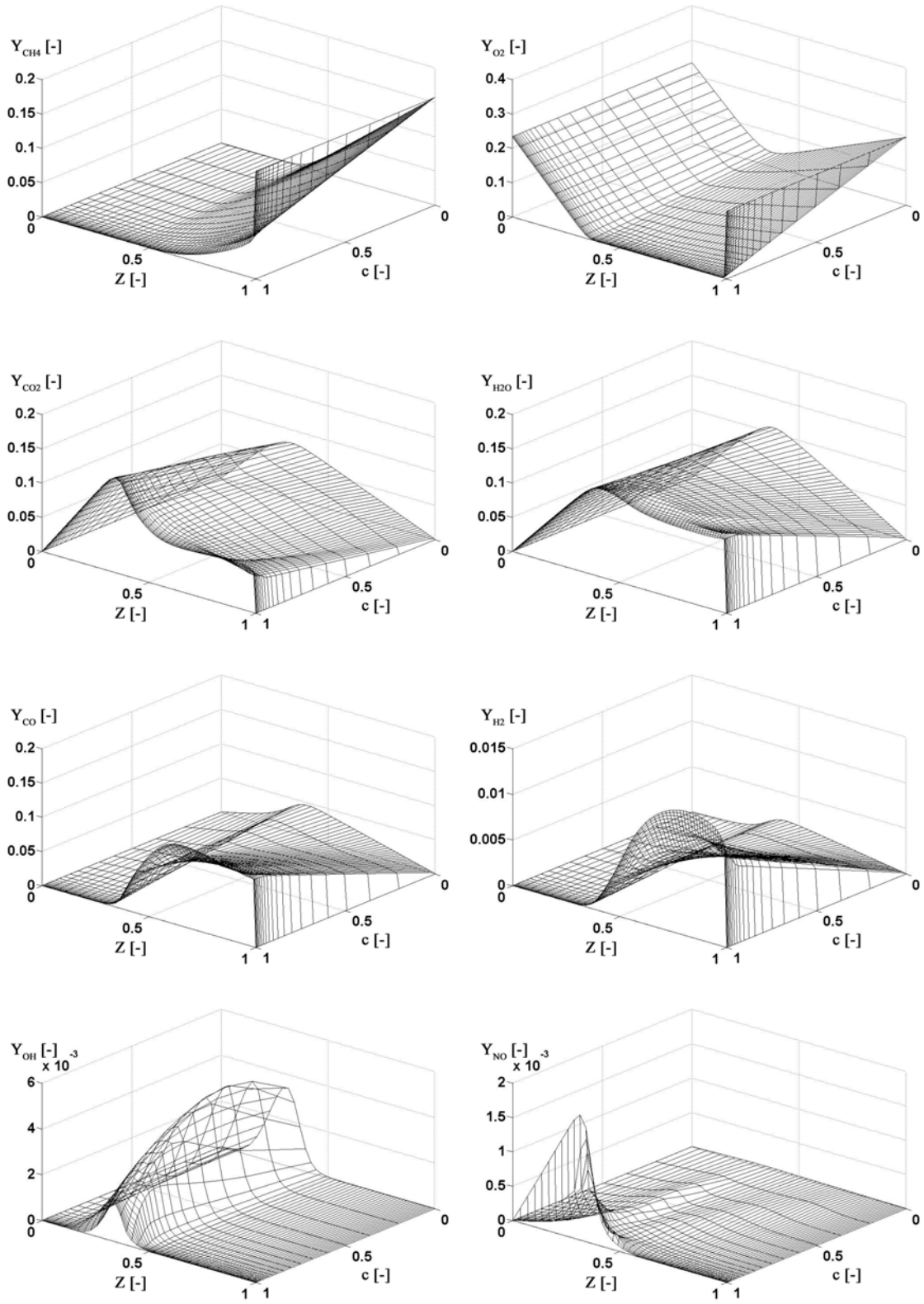

Figure 51 – SLFM (RPV) database (methane flame)

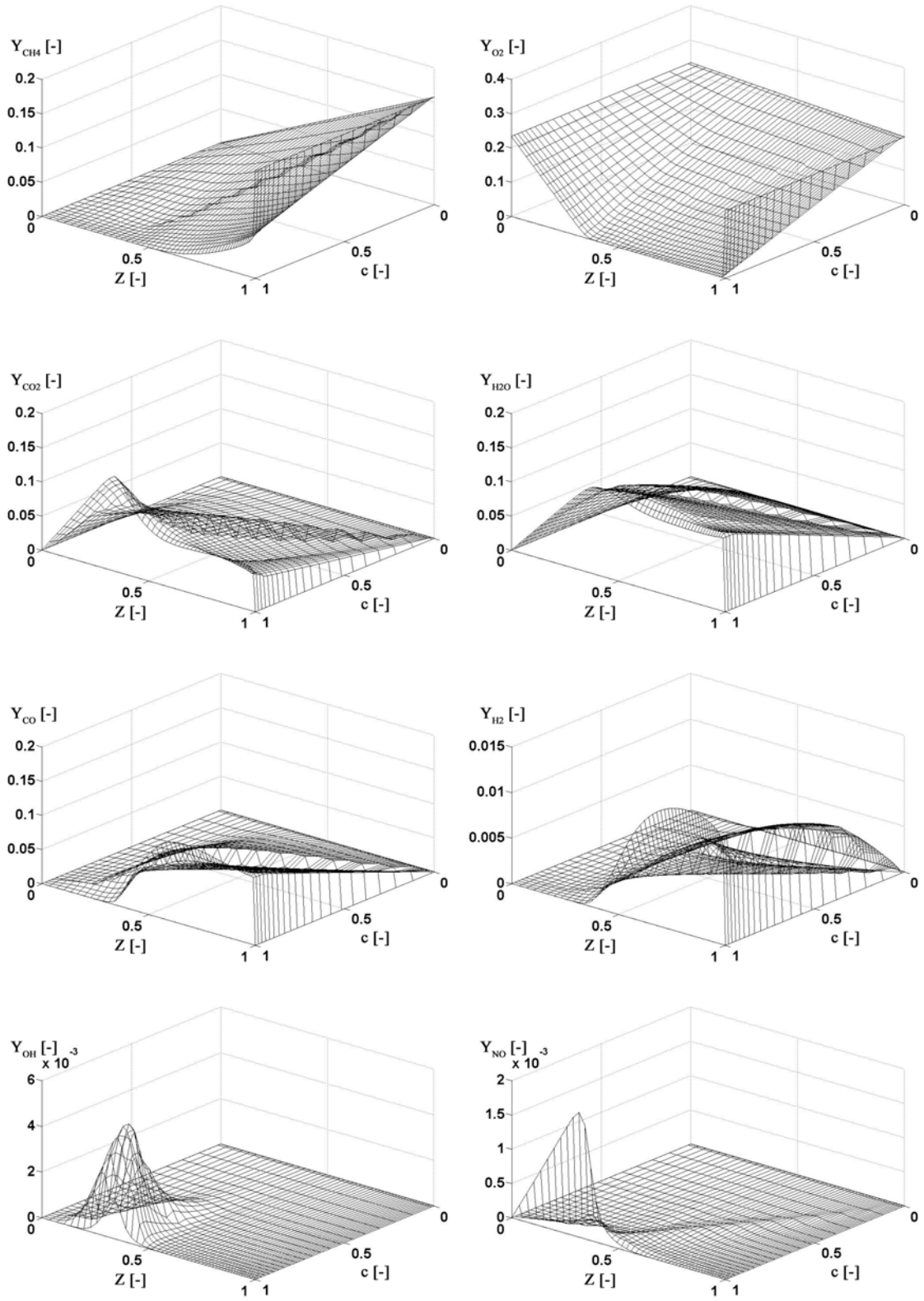

Figure 52 – Mixed database (methane flame)

5.3.2 Adiabatic vs. non-adiabatic profiles

The axial centreline profiles of mean temperature obtained with and without radiation modelling are shown in Fig. 53. The standard k-ε and HTM were used for turbulence modelling, while DTRM (48 rays per boundary face) and WSGGM were used when modelling radiation. Improved temperatures were obtained if including radiation, as expected. While there is a little difference between the adiabatic and non-adiabatic profiles close to the nozzle ($x/d < 0.25$), substantial differences emerge at further downstream locations with larger concentrations of CO_2 and H_2O (radiative species in WSGGM [101]; Fig. 54). The k-ε and HTM perform similarly in the regions close to the nozzle, while differences are evident in the regions $x/d > 0.2$. Both models over-predict temperature in the range $0.15 < x/d < 0.3$. The k-ε model better predicts the peak temperature location and gives higher temperatures when compared to HTM at further downstream locations ($x/d > 0.325$). The adiabatic temperature profile is over-predicted substantially at all axial positions.

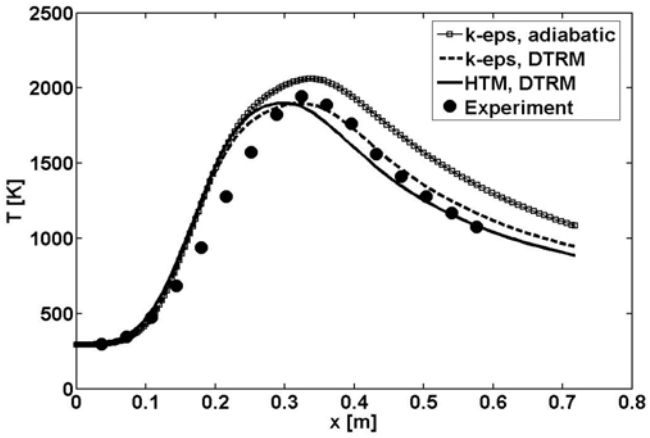

Figure 53 – Mean temperature axial profile at centreline position (methane flame; adiabatic vs. DTRM; k-ε vs. HTM)

The mean mass fractions of CO_2 and H_2O are shown in Fig. 54. The differences between the turbulence models are more emphasised than differences because of the adiabatic, i.e. non-adiabatic modelling. This can be partly explained by a fact that the direct impact of radiation inclusion on species production was eliminated by using the adiabatic pre-tabulated chemistry profiles. In this respect, the radiation impact on species predictions via change in the density field is relatively small when compared to different

turbulence modelling. Similarly as in the case with temperatures, HTM provides the CO_2 and H_2O predictions that are shifted towards the left when compared to the k-ε model. The HTM predictions of CO_2 and H_2O are better at downstream locations ($x/d > 0.35$), while k-ε provides better CO_2 predictions at locations closer to the nozzle.

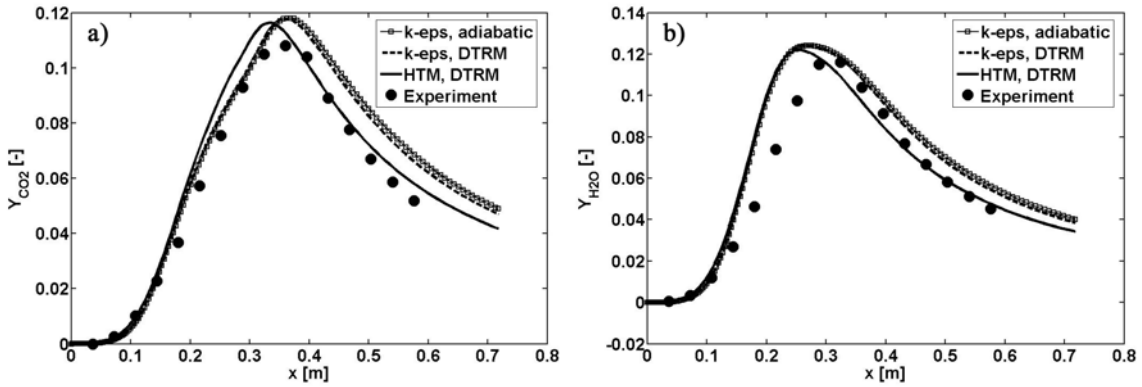

Figure 54 – Axial profiles at centreline position (methane flame; adiabatic vs. DTRM; k-ε vs. HTM): a) Mean CO_2 mass fraction; b) Mean H_2O mass fraction

The number of rays in DTRM calculations was varied in order to evaluate their impact on the prediction accuracy. Table 1 shows the net radiation losses for different numbers of rays used – 48, 16 and 4. As expected, with the increased number of rays better predictions were obtained. In all simulated cases, however, the radiation losses were substantially over-predicted when compared to the measured value. Similar results were already reported in [63] when using the optically thin radiation model. WSGGM [101] can partly be blamed for inaccurate radiative fluxes predictions in this case as it does not take into account any spectral dependence of radiative properties. Spectral effects have shown important in a simulation of the same methane flame configuration in [30].

Table 1 – Radiative heat balance (methane flame)

	Radiative heat balance [kW]
Measured	-0.8870
Predicted, DTRM (48 rays)	-2.1727
Predicted, DTRM (16 rays)	-3.1528
Predicted, DTRM (4 rays)	-6.8973

5.3.3 Combustion models comparison

Similarly as in Section 4.3.4, different combustion models – SLFM, RPV (FPI), RPV (MIX) and RPV (SLFM) (Section 3.2.4) – were used in the post-processor (given a referent solution) to extract the species composition from chemistry pre-tabulations. The referent solution was obtained by using the standard SLFM for combustion modelling, combined with DTRM (48 rays) and WSGGM for radiation modelling.

HTM was used for turbulence modelling due to better velocity predictions when compared to k-ε model, see Fig. 55. The jet spreading predictions compare reasonably well with the measurements (Fig. 55) at all axial locations, while the differences between the turbulence models become more obvious, in favour of HTM, at farther downstream locations.

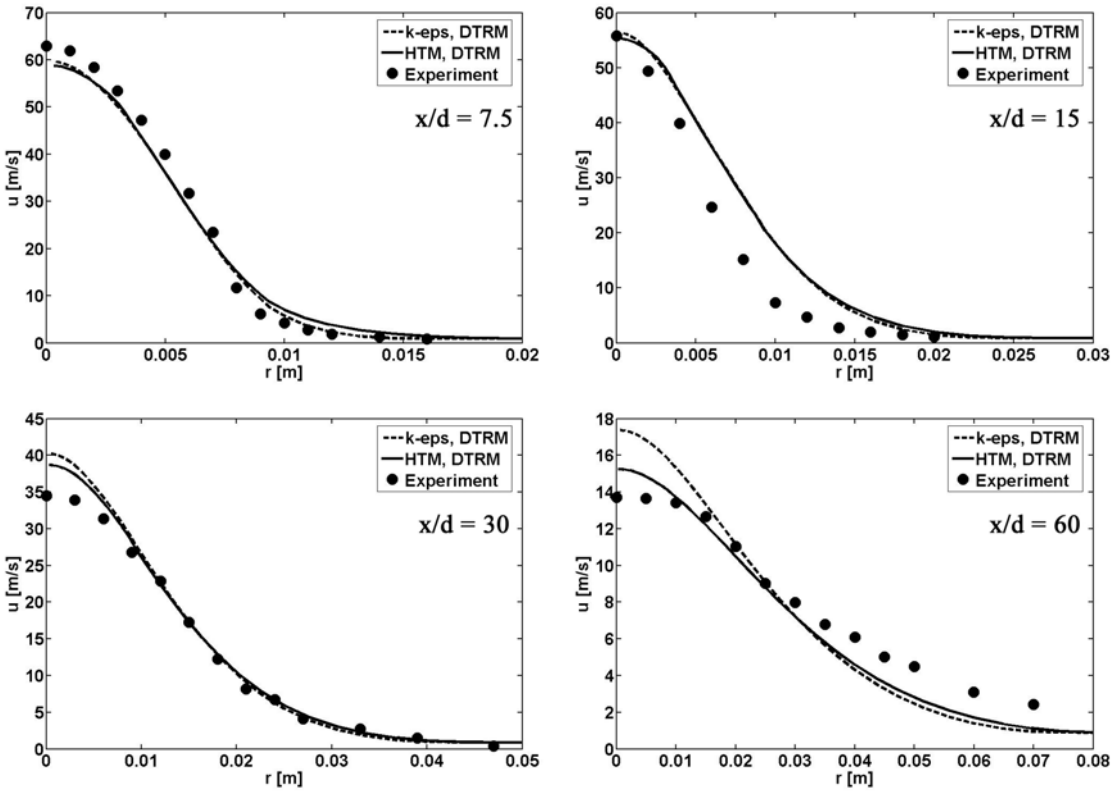

Figure 55 – Radial profiles of mean axial velocity (methane flame; DTRM; k-ε vs. HTM) at various axial locations (methane flame)

The referent axial profiles of mixture fraction moments are shown in Fig. 56. The radial profiles at various axial positions are shown in Fig. 57. In general, the mean

mixture fraction is in a better agreement with experimental data than the mixture fraction RMS. A simple modelling of turbulent fluxes and of the mean scalar dissipation rate is a possible reason for the relative discrepancies of the mixture fraction RMS profiles. Overall, the agreements are satisfactory and in the line with other publications (TNF proceedings [29]).

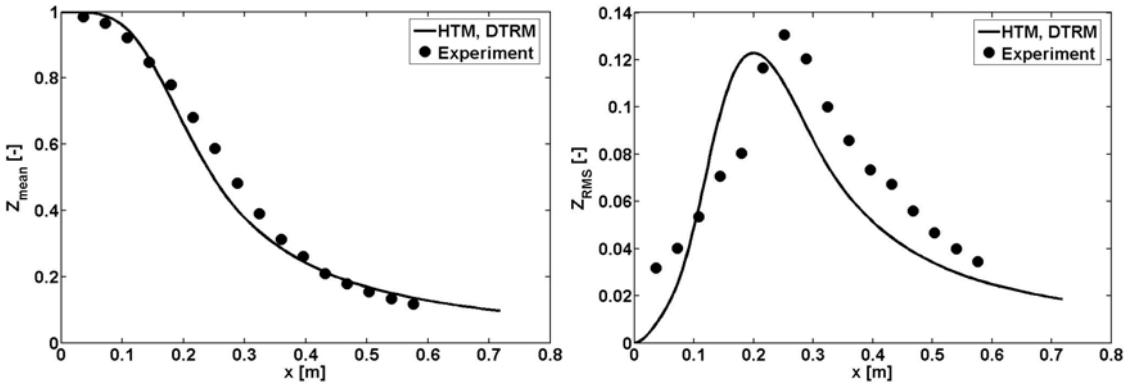

Figure 56 – Axial profiles (centreline) of mixture fraction moments (mean and RMS) (methane flame)

The radial profiles of the mean temperature at various axial locations, as obtained using different combustion models, are shown in Fig. 58. Some differences between the combustion models are present in the fuel-rich regions close to the nozzle ($x/d = 7.5$ and $x/d = 15$), while far away from the centreline axis these differences vanish. In general, the predictions agree less favourably with experimental data away from the axis.

The axial centreline profiles of various mean species mass fractions are shown in Fig. 59. All combustion models based on the reaction progress variable show larger departures form experimental data than SLFM in the fuel-rich regions ($x < 0.325$ m). The axial profiles are shifted towards the left when compared to the measurements. Differences are larger for H_2 and CO than for the major combustion products CO_2 and H_2O. The lower fuel (CH_4) and oxidiser (O_2) values in the fuel-rich regions indicate an excessive reaction predicted by the RPV models there. Combustion models perform similarly at other downstream locations. The OH profiles are predicted similarly, with best performance of RPV (SLFM) in the post-flame regions ($x > 0.4$ m).

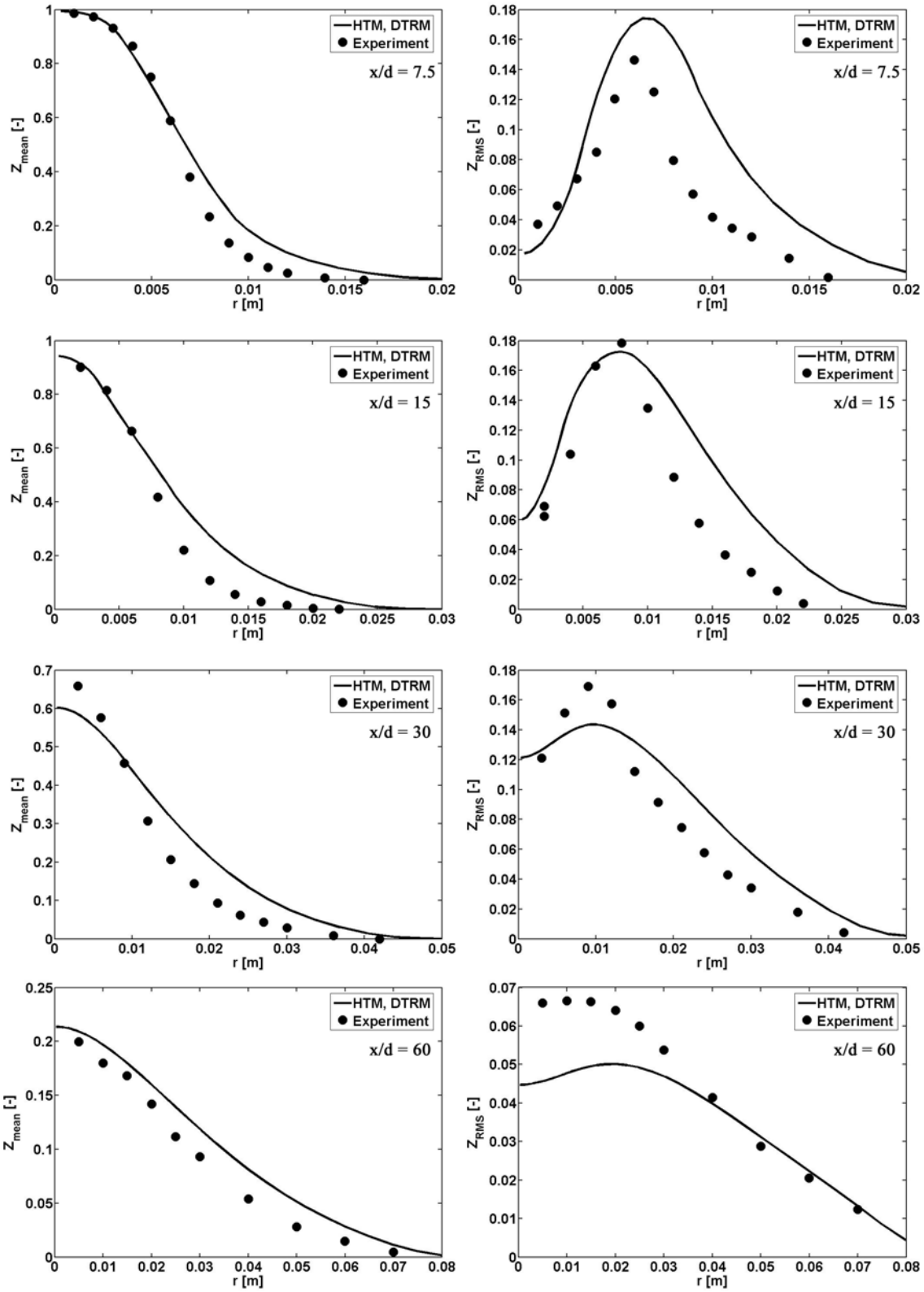

Figure 57 – Radial profiles of mixture fraction moments (mean and RMS) at various axial locations (methane flame)

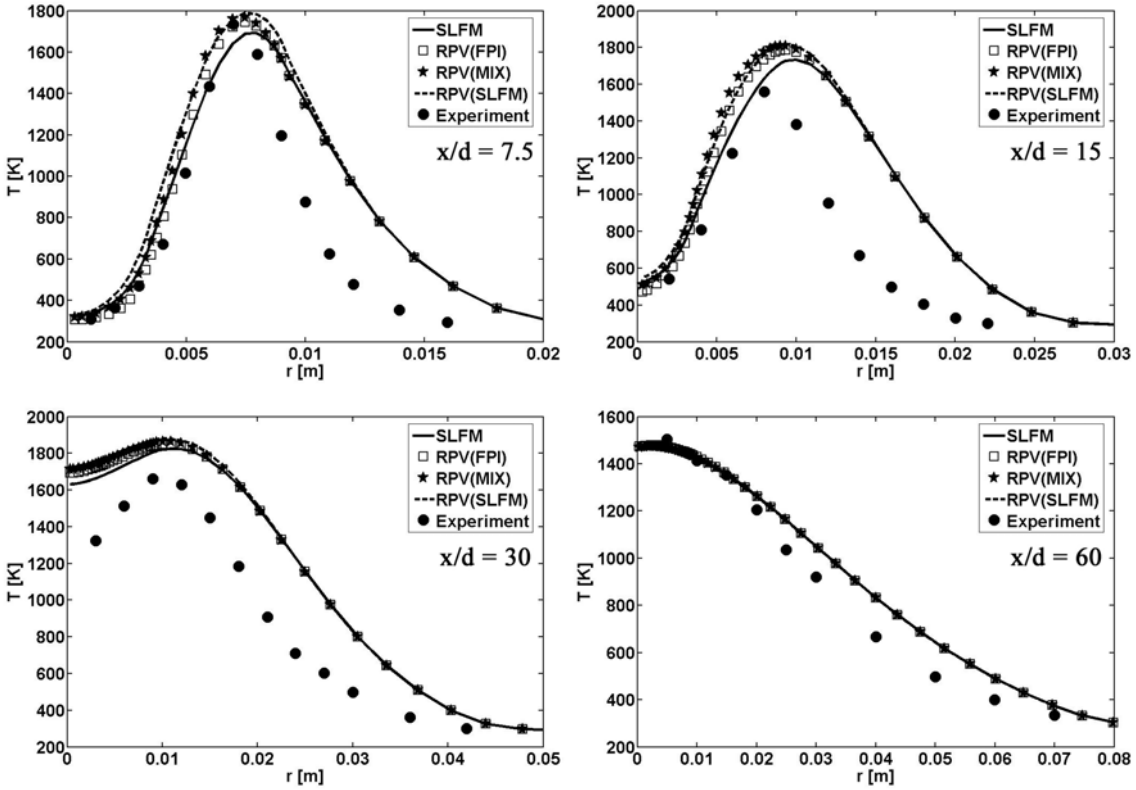

Figure 58 – Radial profiles of mean temperature at various axial locations (methane flame)

The major difference between the models, however, is again visible in the predictions of NO. Here as well the models based on non-premixed flamelets substantially over-predict NO at all axial locations, while remarkably best agreements with experimental data are achieved by RPV (FPI). Improved NO predictions are achieved by the re-parameterised SLFM database (RPV (SLFM)) when compared to original SLFM as well. The mixed formulation (RPV (MIX)) provides the worst NO predictions especially in the post-flame regions.

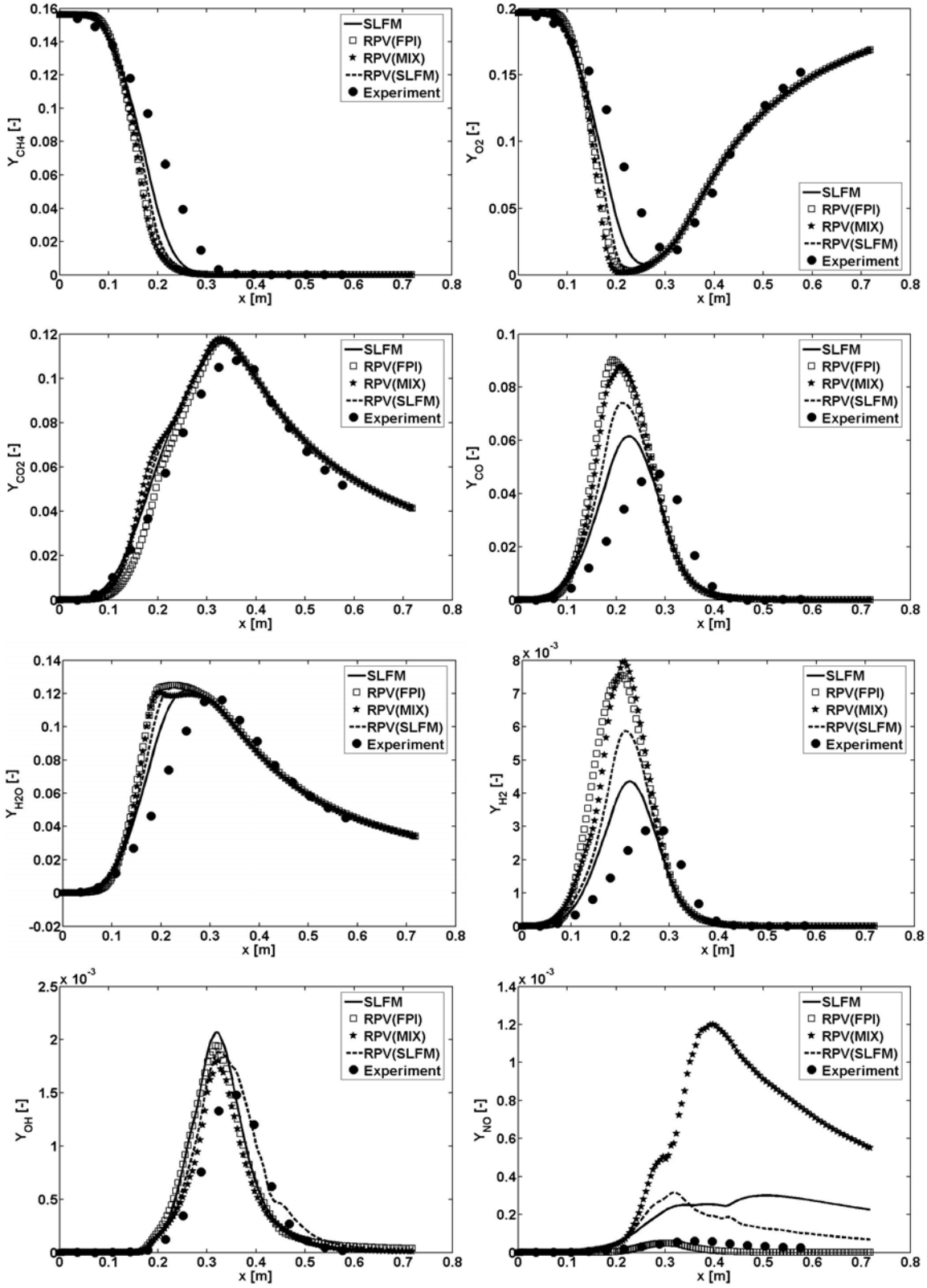

Figure 59 – Axial profiles (centreline) of mean species mass fractions (methane flame)

The radial species profiles at two axial positions – $x/d = 30$ and $x/d = 60$ – are shown in Figs. 60 and 61.

At the first axial position ($x/d = 30$) fuel-rich conditions prevail around the centreline axis and a relative imprecision of RPV models can be observed there as well. SLFM provides better predictions than RPV models near the axis for most of the major species (CH_4, O_2, H_2O, etc.). However, the same does not hold for CO_2 and minor species (OH and NO). CO_2 is best predicted by RPV (FPI) near the axis, while away from the axis the predictions are similar between the models and compare less well with experimental data. The OH peak values are well predicted by RPV (SLFM), while other models predict higher OH values than measured. Yet again, the NO profiles are by far over-predicted by non-premixed flamelets, while RPV (FPI) provides satisfactory NO predictions. The irregular behaviour of RPV (MIX) NO profile can be observed away from the axis, probably caused by a transition between premixed and non-premixed flamelets in the RPV (MIX) database (Fig. 52). CH_4 and O_2 are strongly under-predicted near the axis with all combustion models, as already noticed in axial profiles (Fig. 59).

The radial profiles at $x/d = 60$ show better overall performance of RPV models when compared to the profiles at $x/d = 30$. The major combustion products (CO_2 and H_2O) are well predicted, with marginal differences between the models. RPV (FPI) and SLFM similarly predict CO and are closer to the measurements than other two models. The same is with H_2, although in this case the departures from experimental data are larger. RPV (SLFM) again gives the best OH predictions, while RPV (FPI) is the best model at NO predictions. RPV (MIX) substantially over-predicts NO and seems as a bad choice if NO is considered.

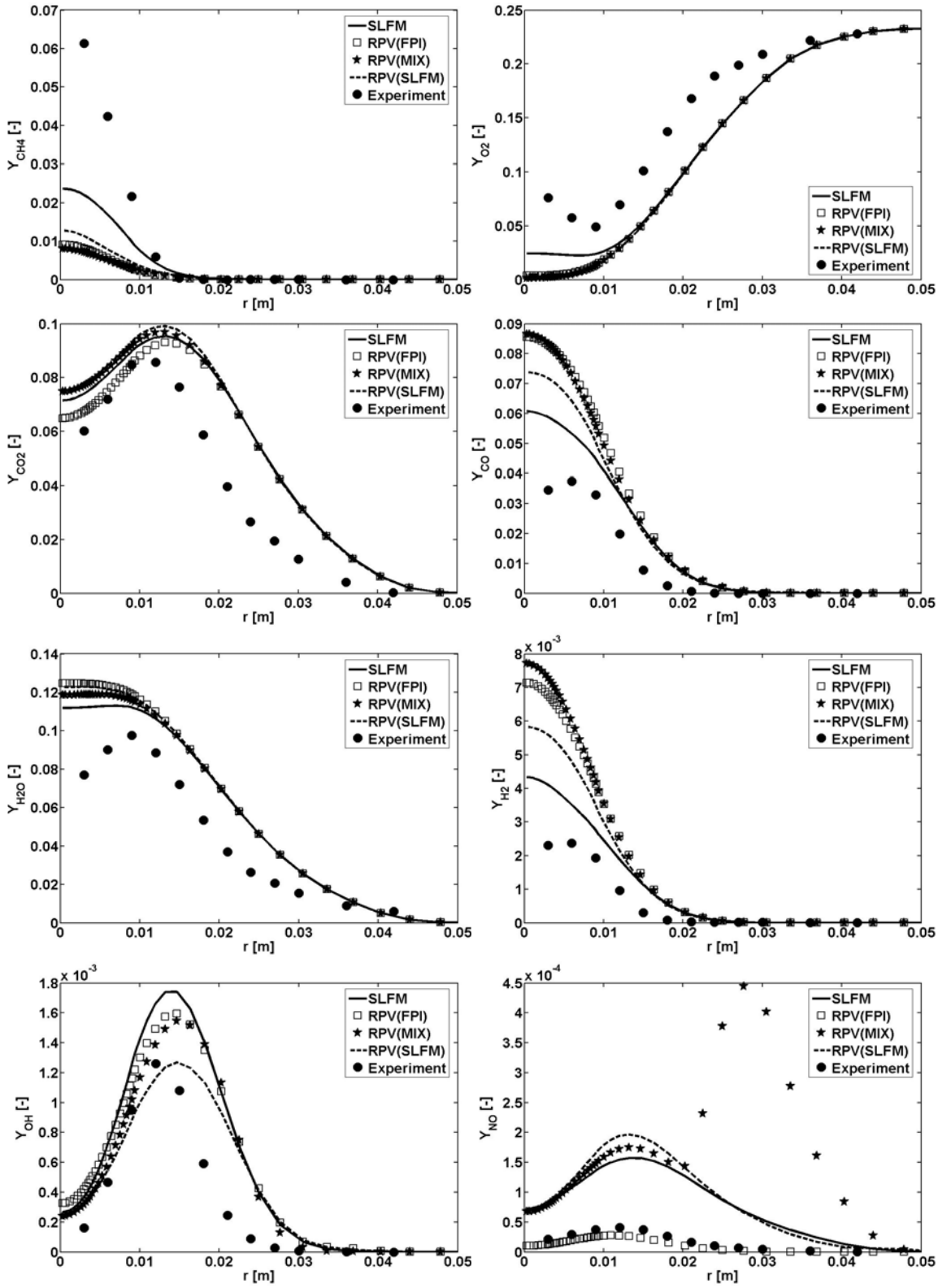

Figure 60 – Radial profiles of mean species mass fractions at x/d=30 (methane flame)

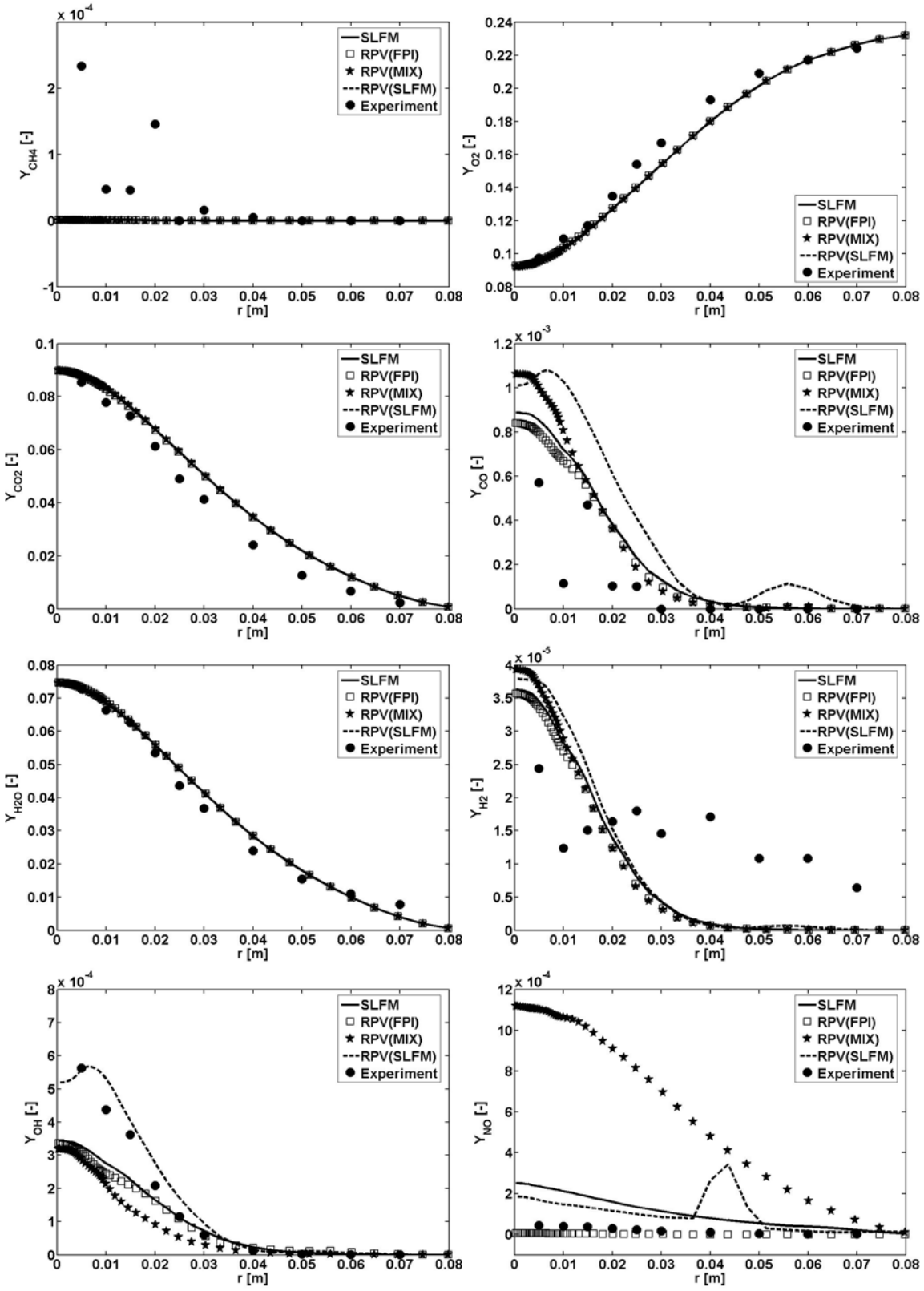

Figure 61 – Radial profiles of mean species mass fractions at x/d=60 (methane flame)

6 TECFLAM combustion chamber

6.1 Experimental configuration

The TECFLAM combustion chamber was experimentally investigated by various groups. An exhaustive documentation can be found at [54]. The S09c configuration was chosen for the simulation in this work.

The TECFLAM combustion chamber was fired with natural gas. The chamber itself was a vertically positioned cylinder, with a burner centred at the bottom. The exhaust gases exited the chamber through an annulus at the opposite side to the burner. The combustion chamber layout and dimensions are schematically given in Fig. 62.

The swirl burner consisted of a central bluff body, an annulus for the fuel and an annulus for the swirled air. Figure 63 schematically shows the TECFLAM burner configuration with given dimensions. The air was swirled by a moveable block positioned before the burner exit. The theoretical swirl number was $S = 0.9$. The thermal load was around 150 kW, while approximately 80 kW power was removed from the chamber through the water cooled walls [55]. The chamber operated at an ambient pressure, with the overall fuel-to-air equivalence ratio 0.83. The exit bulk velocity of the air was 23 m/s ($\mathrm{Re} = 42900$), while that of the fuel (natural gas) was 21 m/s ($\mathrm{Re} = 7900$).

The spontaneous Raman scattering was used to simultaneously measure the temperature, mixture fraction, and species mass fractions (CH_4, N_2, O_2, H_2, CO, H_2O, CO_2) [144]. All states of the reaction progress, from the cold non-reacted mixing up to the chemical equilibrium, were observed in the fuel/air mixing regions. Two re-circulations zones (inner and outer) were observed also. The LDV measurements of the velocity field are summarised in [145].

Additional information and simulation results provided by various groups, can be found in the TNF proceedings at [29].

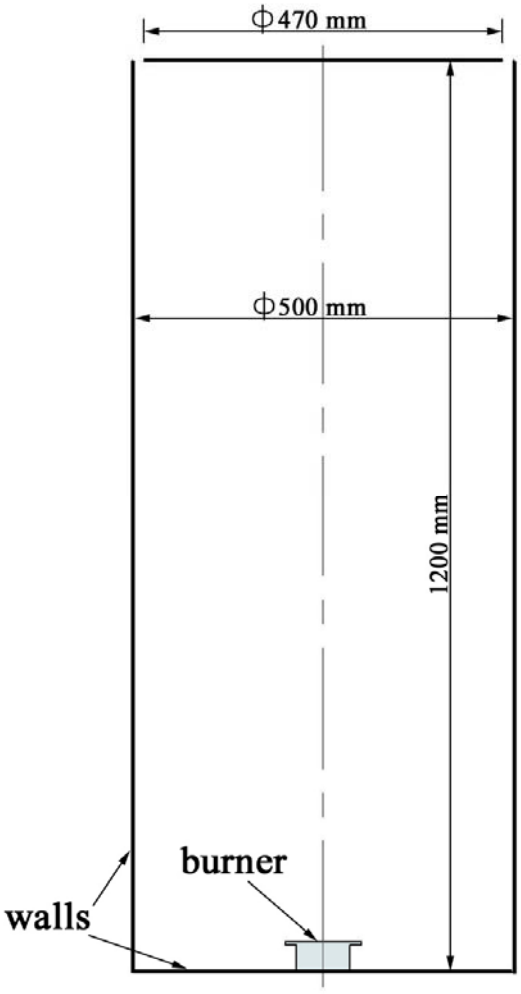

Figure 62 – Combustion chamber (TECFLAM)

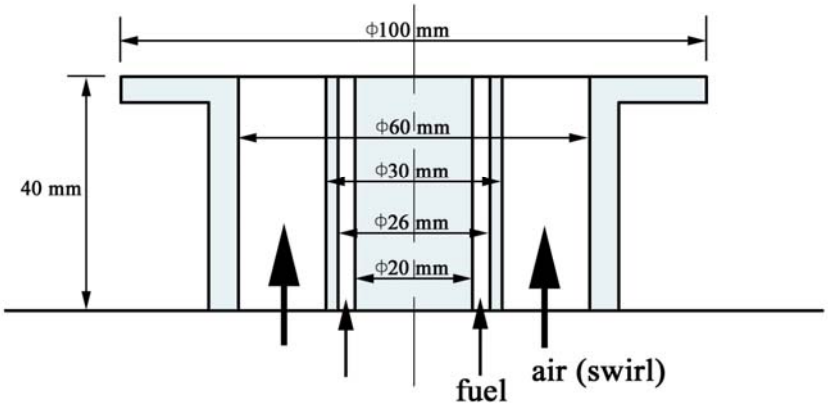

Figure 63 – Burner configuration (TECFLAM)

6.2 Numerical set-up

A structured mesh, consisting of 267864 control volumes (hexahedrons), was used for the computational domain discretisation. The mesh distribution was denser towards the inlets and in the radial positions of the fuel and air annulus (Fig. 64). The computational domain dimensions fitted those presented in Fig. 62. The outlet annulus was additionally extended in order to avoid the possibility of a reversed flow at the exit boundary. The domain around the burner can be seen in Fig. 64.

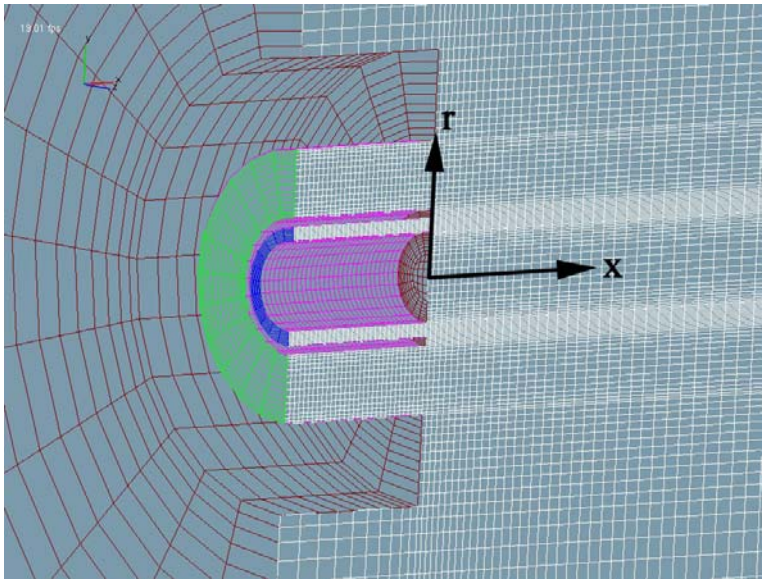

Figure 64 – Computational mesh (TECFLAM; vertical axial cut; centreline)

The appropriate prescription of the inlet boundary conditions was not that straightforward, as was the case in the hydrogen and methane jet flame examples. The fuel and the air annulus were extended (40 mm) in order to obtain the developed velocity profiles at the burner exit position ($x = 0$ mm; Fig. 64). The air was given additionally a tangential velocity component (green selection in Fig. 64) such that the nominal swirl intensity ($S = 0.9$) at the burner exit was approximately achieved. According to the swirl definition from Eq. (141) (as used e.g. in [146-148]), and if taking the velocity and density radial profiles at the axial position $x = 1$ mm, with $R = 0.03$ m, the calculated swirl number was 0.9019. Figure 65 shows the air velocity profiles just before the burner exit ($x = -1$ mm).

$$S = \frac{\int_0^R \bar{\rho}\tilde{u}\tilde{w}r^2 dr}{R\int_0^R \bar{\rho}\tilde{u}^2 r dr} \tag{141}$$

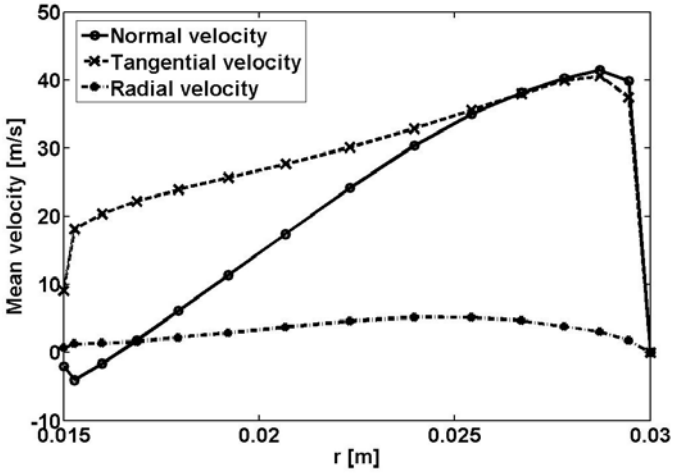

Figure 65 – Mean velocity profiles of air at the burner exit (TECFLAM)

The values of the turbulent kinetic energy and its dissipation rate at inlet boundaries were prescribed according to relations in Eq. (137). The relative free-stream turbulence intensity was chosen $I_\infty = 10\,\%$.

The non-adiabatic calculations were performed using DTRM with 48 ray per boundary face and WSGGM [101]. The emissivity for the domain walls was set $\varepsilon_w = 0.7$, while the wall temperatures were chosen such that the radiative heat losses approximately amounted to 80 kW, as measured during the experiment [55]. Inlets and outlet were considered as black surfaces.

Turbulence was modelled by the standard k-ε model and by HTM [123]. The default values for the turbulence modelling constants were retained in this case (Eq. (69)).

The GRI Mech 3.0 [65] chemical mechanism was used for chemistry pre-tabulations. Combustion was modelled by the standard SLFM, and by RPV (FPI) and RPV (SLFM) models. The turbulence/chemistry coupling was done via the presumed β-PDF.

Other numerical set-up was similar as in the hydrogen and methane jet flame examples.

6.3 Results

6.3.1 Pre-tabulated chemistry profiles

The standard SLFM database, the FPI database and the re-parameterised SLFM database are shown in Figs. 66-68. The original SLFM database (Fig. 66) was created for a range of the stoichiometric scalar dissipation rate parameters (10 profiles):

$$\chi_{st} = 0.01, 0.05, 0.1, 0.5, 1, 2, 5, 10, 20, 30\ s^{-1} \tag{142}$$

The first flamelet ($\chi_{st} = 0.01\ s^{-1}$) has a near-equilibrium composition, while the last one ($\chi_{st} = 30\ s^{-1}$) is nearly the last burning flamelet before extinction. The following natural gas molar composition was taken for the simulation purposes: 95 % CH_4, 2.5 % C_2H_6, 1.5 % N_2 and 1 % CO_2. The fuel and air temperatures were set to 294 K. The mixture fraction space was discretised into 50 non-equally distributed points, with denser point distribution near the stoichiometry ($Z_{st} \approx 0.0581$).

A linear combination of CO_2 and CO mass fractions was used as the reaction progress variable, i.e. $Y_c \equiv Y_{CO_2} + Y_{CO}$. The flammable range was approximately $0.385 \le \phi \le 2.949$ [12]. There were 30 premixed flames sets obtained with the adapted PREMIX solver [97] within the flammability limits, while the remaining 20 sets were obtained by linear interpolation with boundary values. The mixture fraction discretisation from the original SLFM database was retained.

The peak values of species mass fractions are similar among the databases. The re-parameterised SLFM database (Fig. 68) is consistent with the original one (Fig. 66). Shown are only those species that were experimentally measured.

[12] Or, equivalently, $0.02319 \le Z \le 0.15398$ – see Eq. (24)

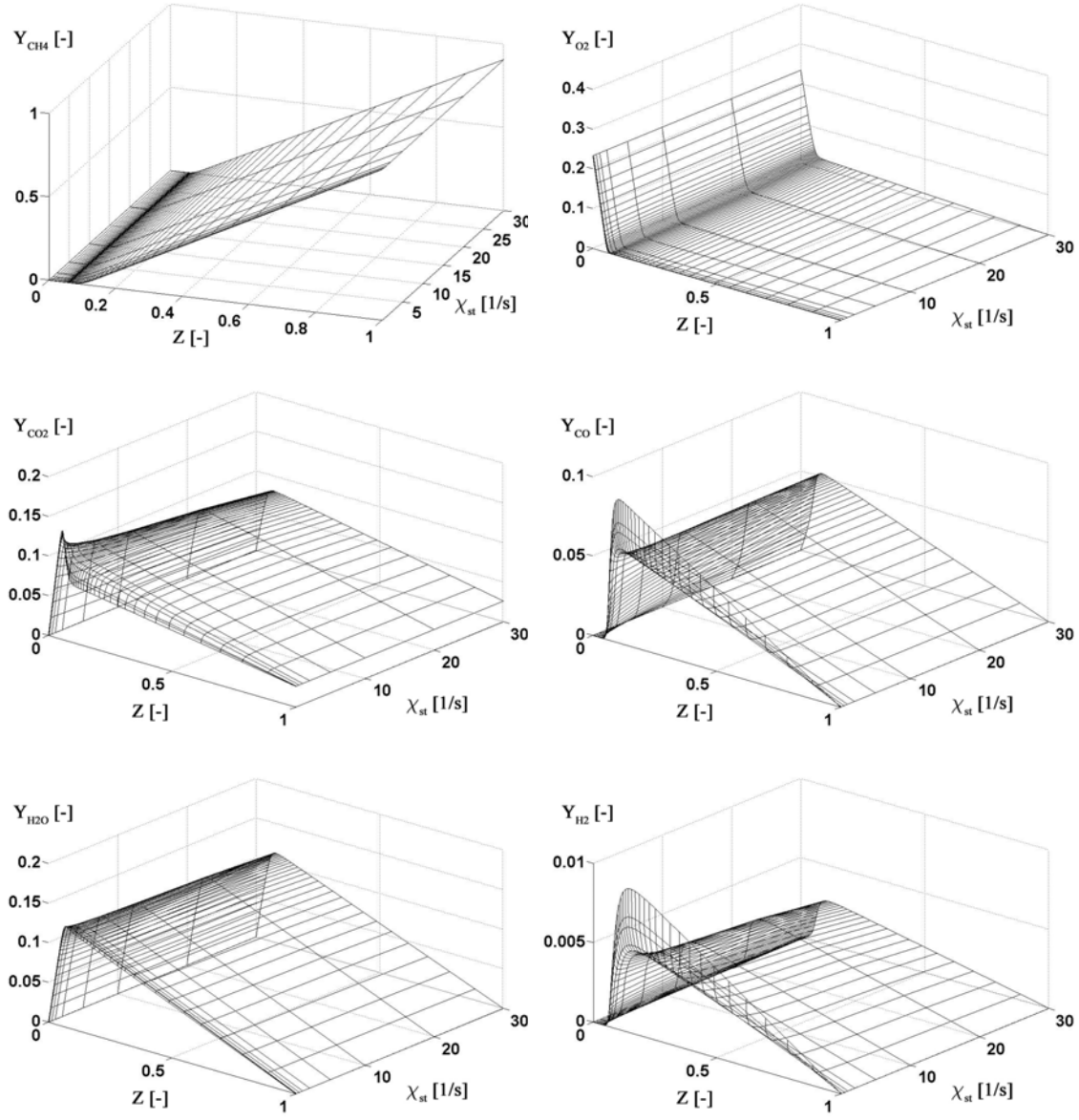

Figure 66 – SLFM (standard) database (TECFLAM)

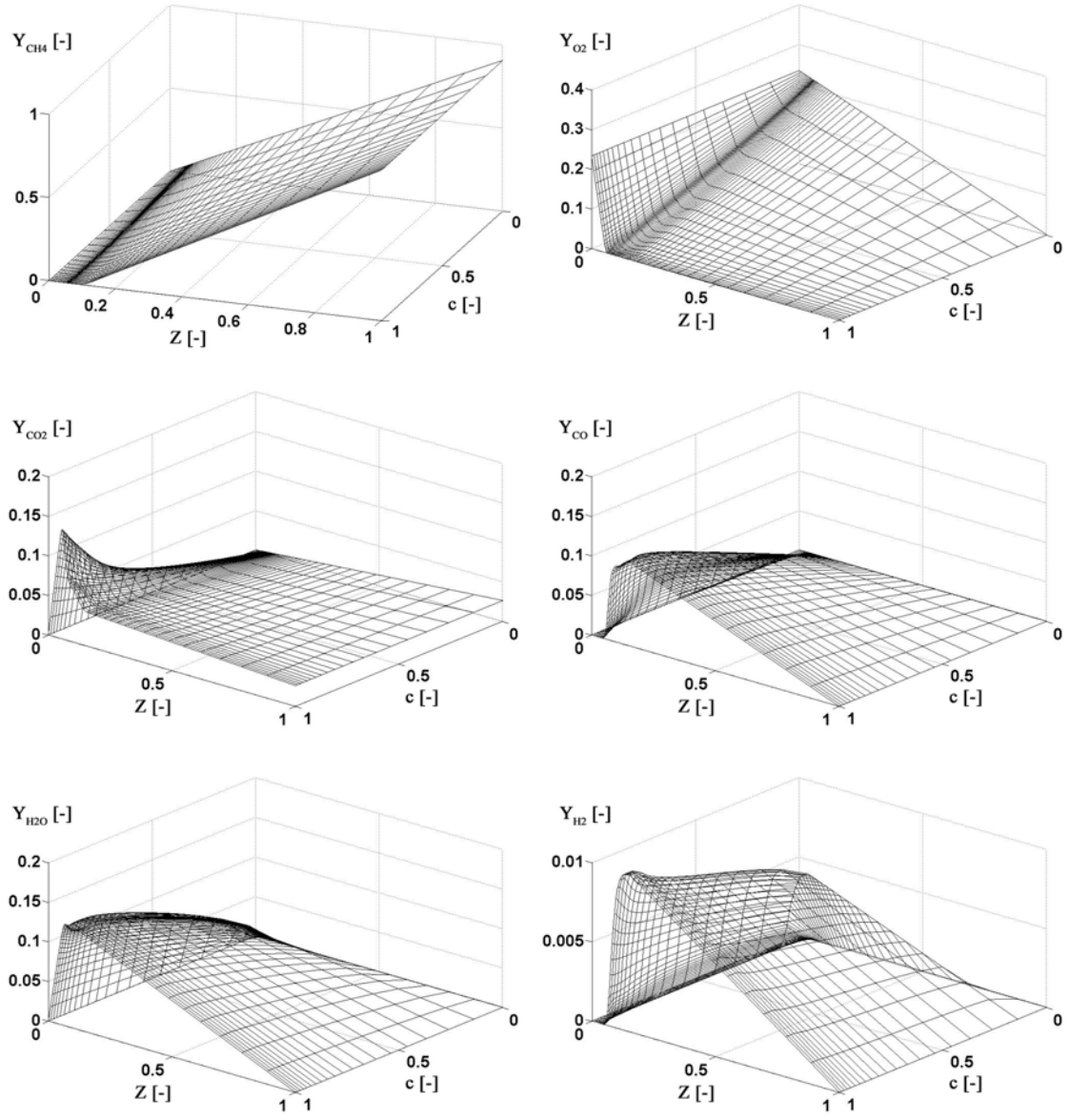

Figure 67 – FPI database (TECFLAM)

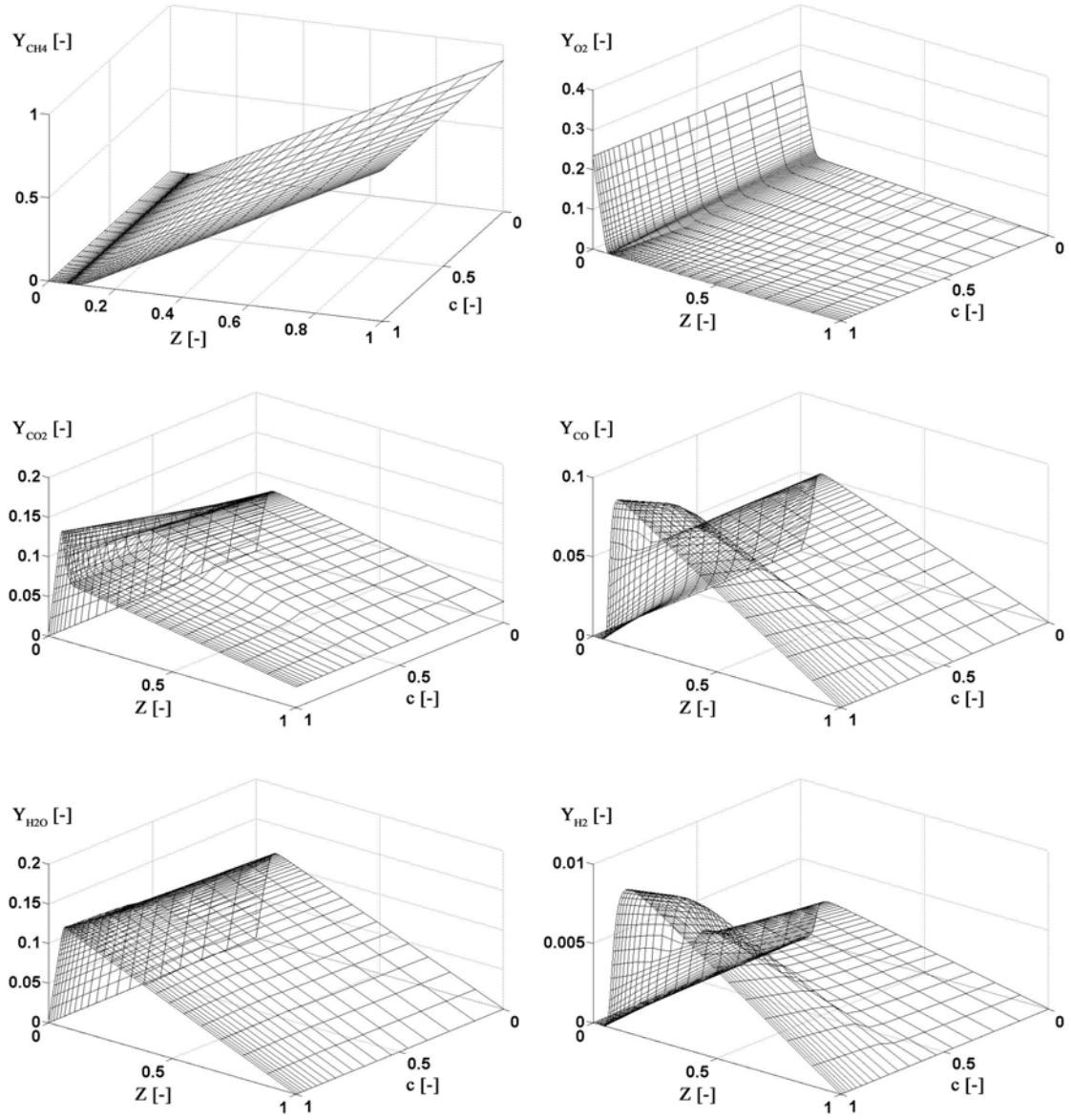

Figure 68 – SLFM (RPV) database (TECFLAM)

6.3.2 Simulation results

The radial profiles of the mean axial and tangential velocities at various axial positions are shown in Fig. 69. The standard k-ε model and HTM predictions are shown and compared to the measurements. The predictions were obtained by using the standard SLFM, while DTRM with 48 rays per boundary face and WSGGM were used for the thermal radiation modelling.

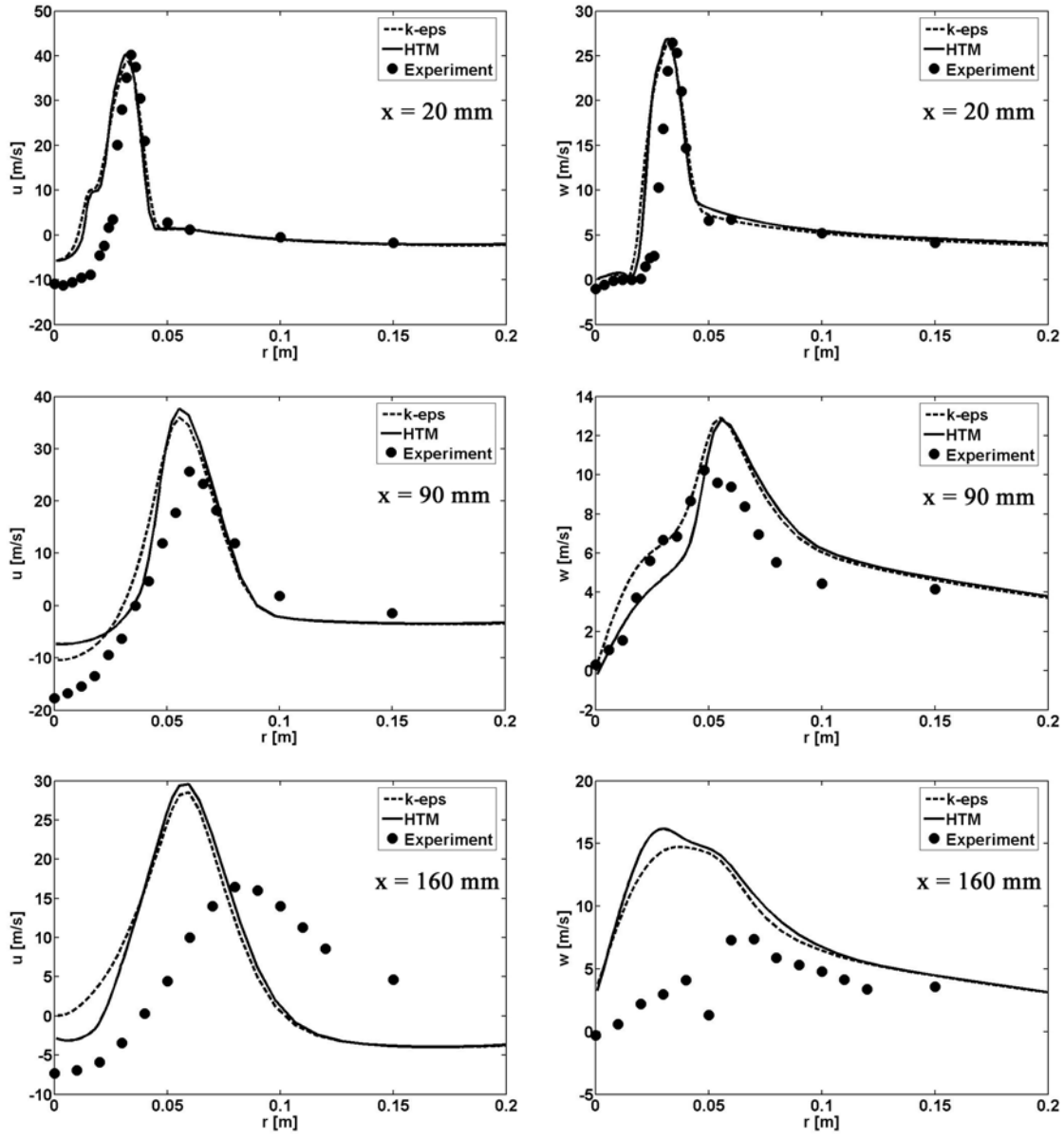

Figure 69 – Radial profiles of mean axial (u) and tangential (w) velocities at various axial positions (TECFLAM)

The velocities agree reasonably well with experimental data, especially near the burner ($x = 20$ mm), while further downstream the predictions deteriorate. The differences between the turbulence models are small at the axial position $x = 20$ mm, while at other two positions, $x = 90$ mm and $x = 160$ mm, the differences are larger, with no clear evidence which one of the two turbulence models performs better. The velocity predictions are in the line with other similar predictions obtained by other groups for the same TECFLAM configuration, as reported in the TNF proceedings at [29].

The radial profiles of mixture fraction moments (mean and RMS) at axial positions $x = 20$ mm and $x = 90$ mm are shown in Fig. 70. While the predictions reasonably well agree with experimental data away from the centreline axis, the relatively large departures form the measurements are observed at the radial positions near the centreline axis. HTM provides slightly better predictions at $x = 20$ mm, while k-ε is in closer agreement with the measurements at the farther location ($x = 90$ mm). Similar trends are observed in the axial mixture fraction mean profiles, as shown in Fig. 71. The relative discrepancies between the predictions and measurements diminish away from the burner.

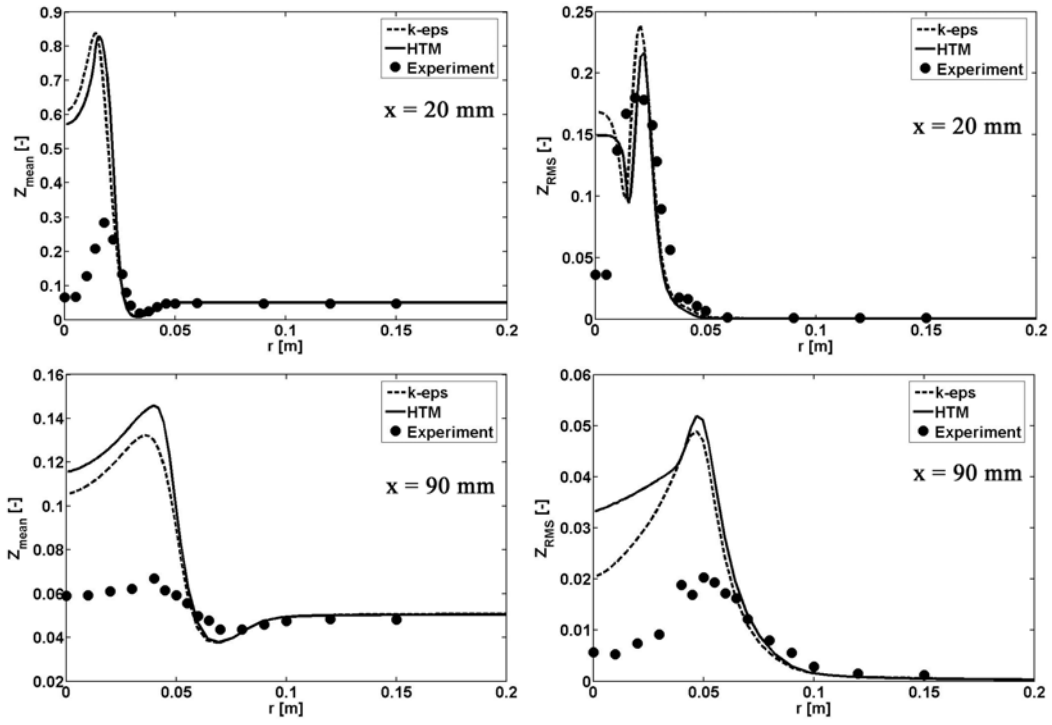

Figure 70 – Radial profiles of mixture fraction moments at axial positions x=20 mm and x=90 mm (TECFLAM)

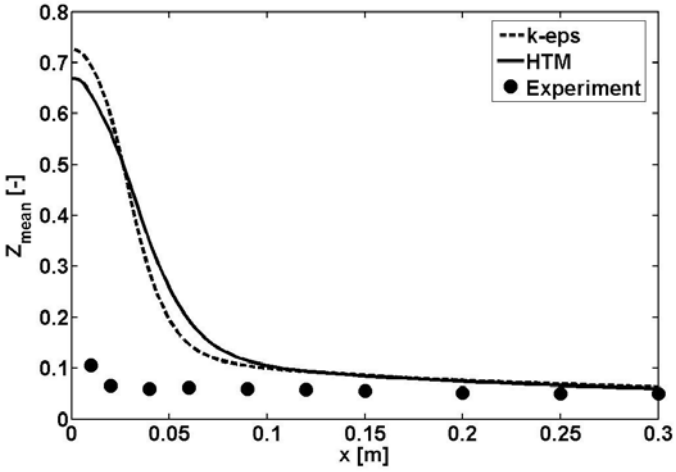

Figure 71 – Axial profiles (centreline) of mean mixture fraction (TECFLAM)

The radial profiles of mean temperature at axial positions $x = 20$ mm and $x = 90$ mm are shown in Fig. 72. Similarly as with mixture fraction, the predictions near the centreline axis largely depart from the measurements, while away from it the predictions are better. Temperature is better predicted near the burner ($x = 20$ mm). HTM and k-ε provide similar temperature profiles.

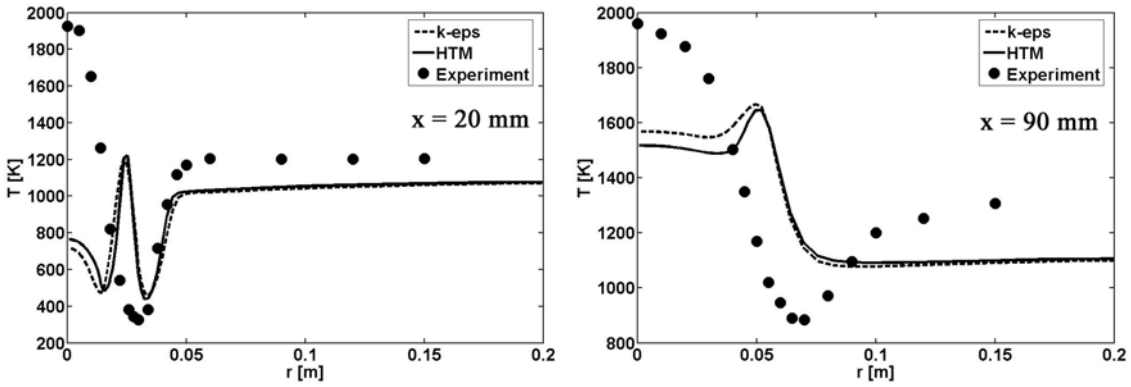

Figure 72 – Radial profiles of mean temperature at axial positions x=20 mm and x=90 mm (TECFLAM)

Based on a referent solution (k-ε, SLFM, DTRM, WSGGM), the species mass fractions according to the RPV (FPI) and RPV (SLFM) models (Section 3.2.4) were post-processed. The transport equation for the reaction progress variable (Eq. (76)) was additionally solved. Figure 73 shows the radial profile of the normalised reaction variable according to the RPV (FPI) model (Eq. (100)). The fuel/oxidiser mixture is partially

reacted in the inner recirculation zone ($0 \le r \le 0.02$ m) where the lack of oxygen prevents a complete reaction. In the region of intensified fuel/air mixing ($0.02 \le r \le 0.04$ m) reaction occurs at very small levels, while further away from the centreline axis ($r > 0.05$ m) the mixture is fully reacted.

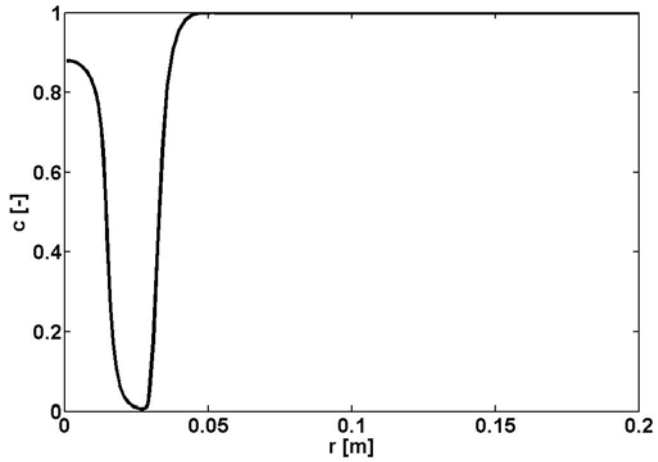

Figure 73 – Radial profile of $\overline{c}$ (Eq. (100); FPI) at axial position x=20 mm (TECFLAM)

Figures 74-76 show the radial profiles of the mean species mass fractions at axial locations $x = 20$ mm, $x = 60$ mm and $x = 120$ mm. The fuel (CH_4) is largely over-predicted at the axial location $x = 20$ mm near the centreline axis with all combustion models, while the oxidiser (O_2) is well predicted, especially with RPV (FPI). However, lower levels of reaction are predicted near the centreline axis, as evidenced by lower CO_2 and H_2O mass fractions, than it is experimentally observed. Higher levels of CO and H_2 are predicted in these regions instead. Similar behaviour, although to a lesser extent, can be observed at other axial locations – $x = 60$ mm and $x = 120$ mm. While O_2 remains relatively well predicted at all radial positions, CH_4, H_2 and CO are over-predicted near the axis.

In general, predictions do not compare that well to experimental data, as was the case in the hydrogen and methane flame configurations. This is because of a much more complex flow pattern introduced by the swirled air motion at the inlet in this case. Also, because of higher turbulence levels, the need for appropriate turbulent fluxes modelling becomes more emphasised. This is evidenced by poor mixture fraction radial predictions at $x = 20$ mm (Fig. 70), while the velocities are well predicted there (Fig. 69). Thus, a relatively bad prediction of the fuel/oxidiser mixing, especially near the centreline axis, is

responsible for deviations of other species mass fractions from experimental data. Also, RPV (FPI) seems to qualitatively better reproduce the evolution of radial profiles in the fuel-rich regions (near the centreline axis) when compared to the SLFM and RPV (SLFM) models. This is probably due to the RPV (FPI) database parameterisation with a normalised reaction progress variable that covers a complete range from the pure mixing until the equilibrium, unlike with the non-premixed flamelets in the SLFM and RPV (SLFM) models.

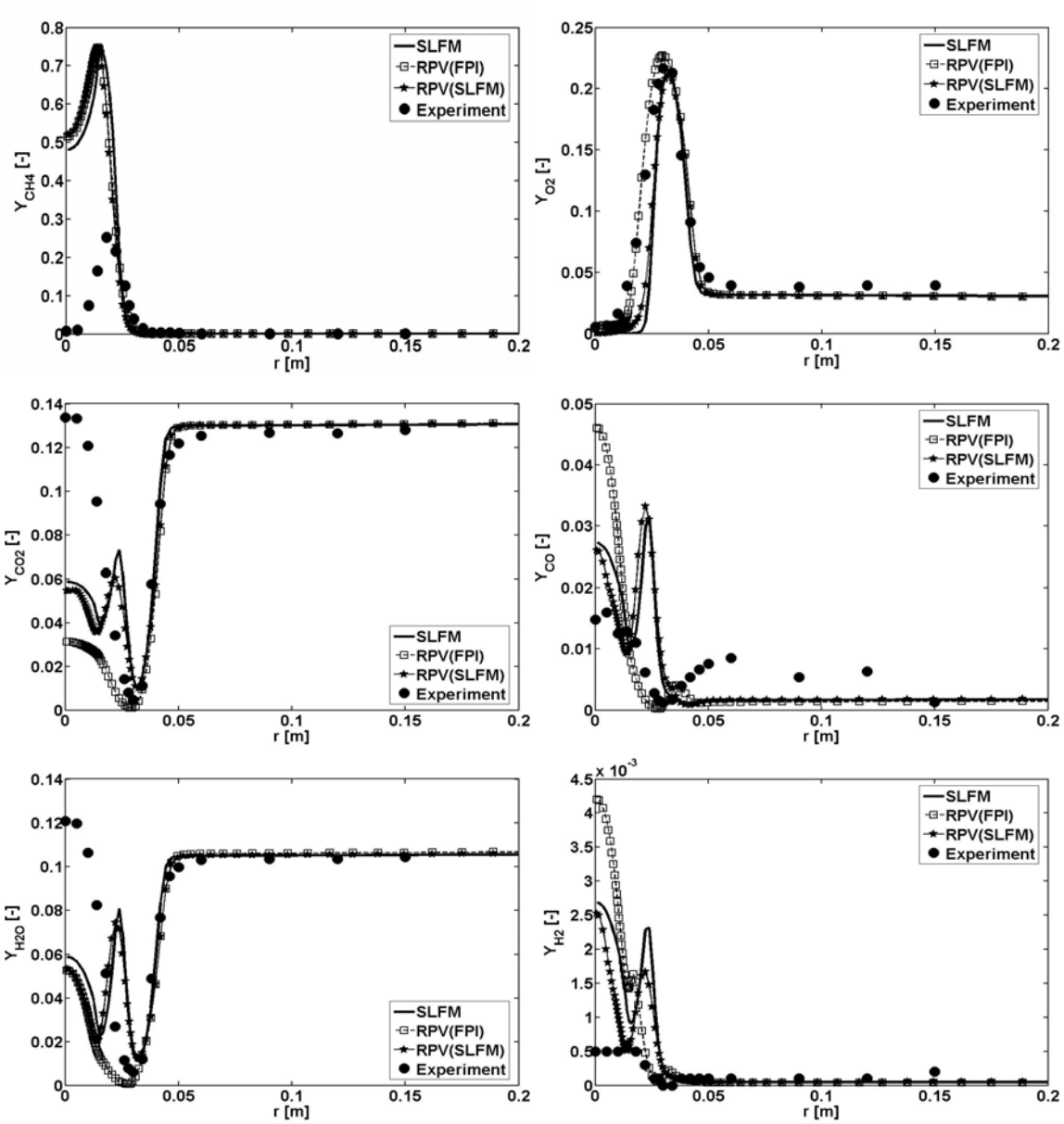

Figure 74 – Radial profiles of mean species mass fractions at axial position x=20 mm (TECFLAM)

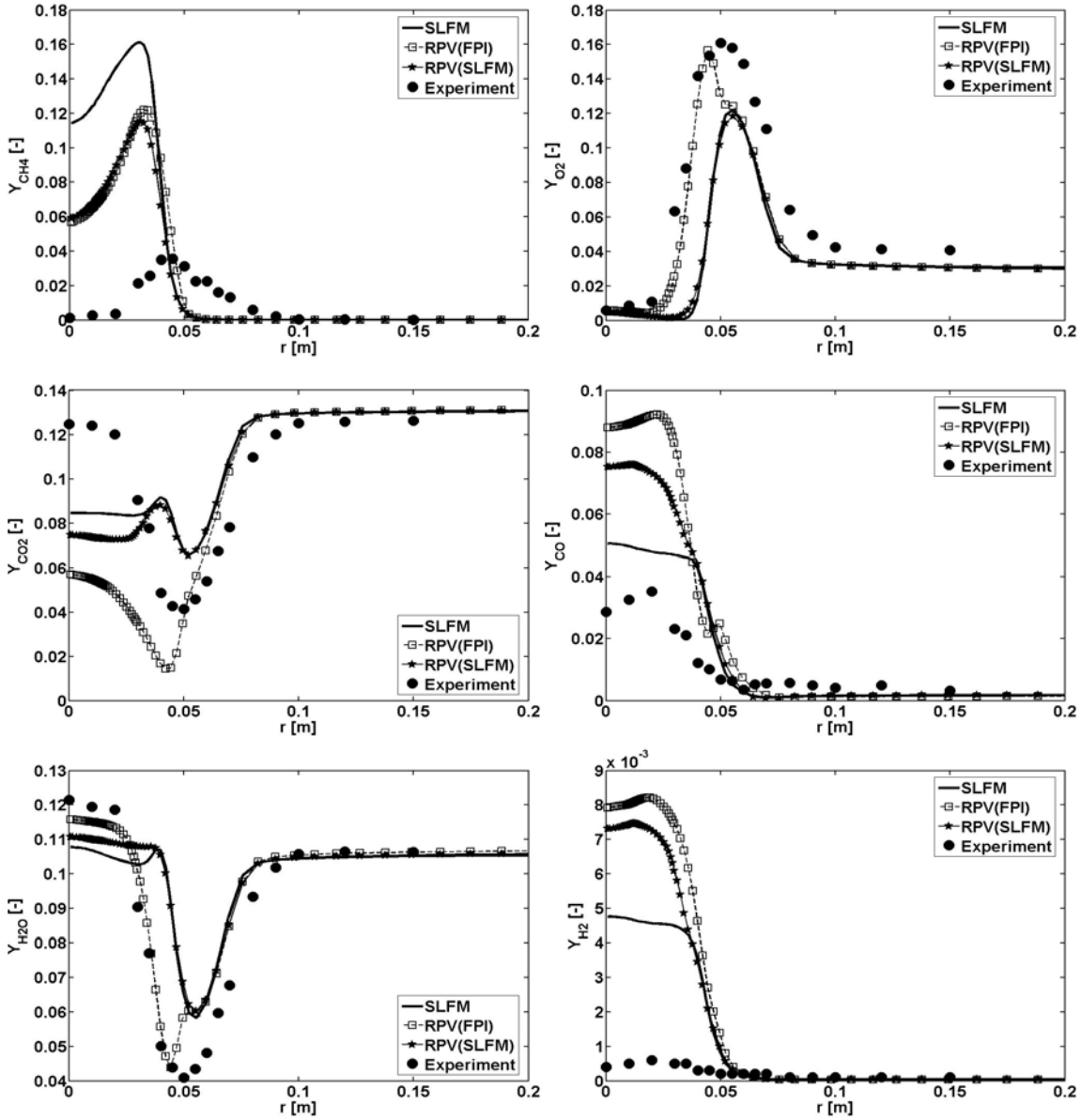

Figure 75 – Radial profiles of mean species mass fractions at axial position x=60 mm (TECFLAM)

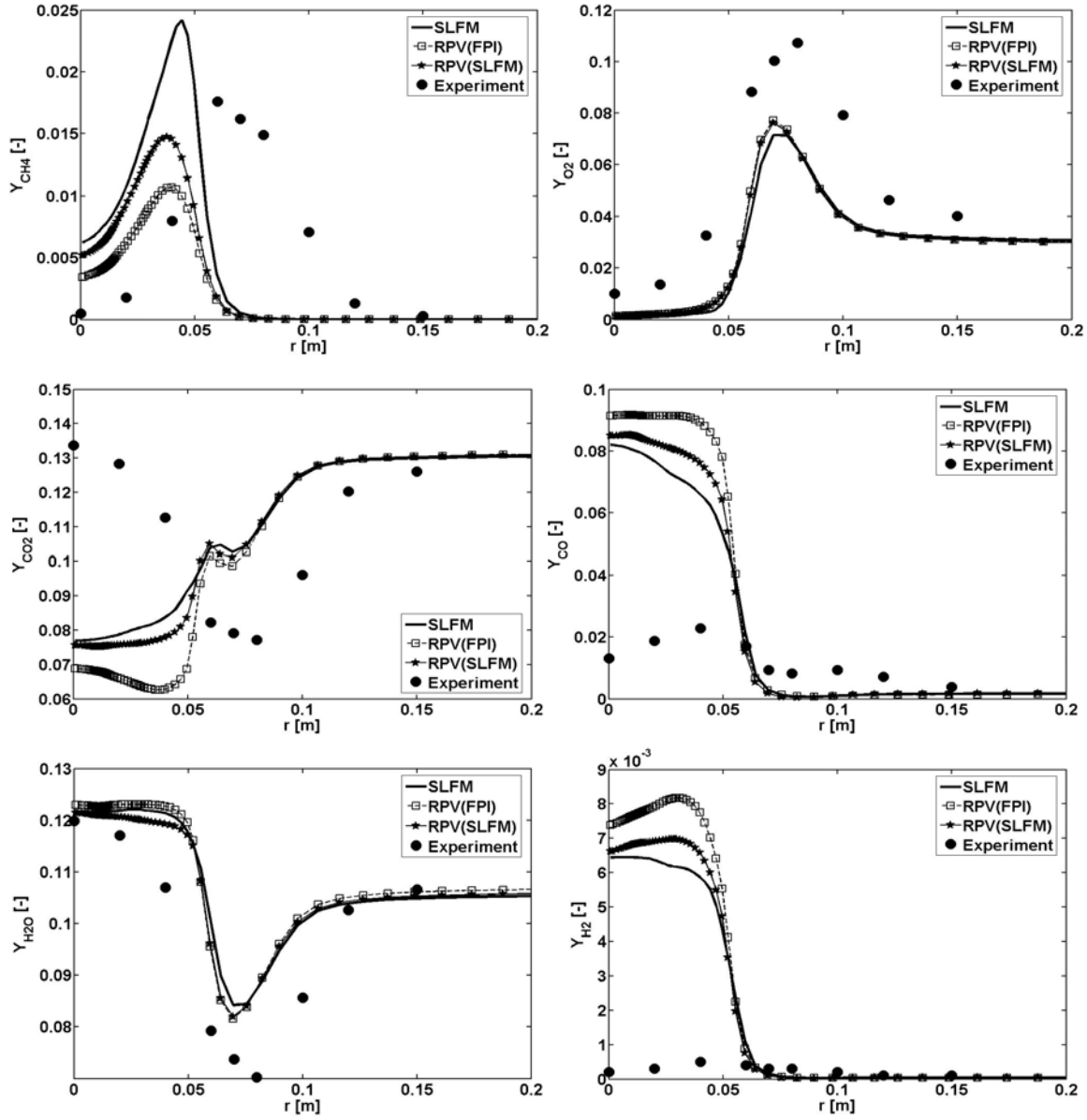

Figure 76 – Radial profiles of mean species mass fractions at axial position x=120 mm (TECFLAM)

7 Conclusions

The pre-tabulated chemistry approach, based on premixed and non-premixed laminar flamelets, was developed and implemented in this work. A devoted software application (CSC solver) was developed in order to perform the chemistry calculations and tabulations in the pre-processor step. The combustion modelling in the CFD procedure consisted of calculating the field distribution for a set of tracking scalars – mixture fraction and the reaction progress variable – while the chemistry composition space was functionally related to these two scalars, depending on a model. The developed models were applied in the combustion simulations of three different configurations of varying complexity. The results were compared to experimental data and to the stationary laminar flamelet model predictions. The simulated configurations were the following – a diluted hydrogen jet flame (H_2/He-air flame B), a piloted methane jet flame (Sandia flame D) and a confined natural gas bluff-body stabilised flame (TECFLAM). Detailed chemical mechanisms were used in all cases. The discrete transfer radiation method was implemented into the CFD code (FIRE) in order to account for thermal radiation. The impact of radiation inclusion was investigated. A hybrid turbulence model (HTM) was applied and its predictions were compared to those obtained with the standard k-ε model.

The hydrogen/air diffusion flame was successfully simulated by using different combustion models that are based on the pre-tabulated chemistry approach. The predictions of mean temperatures and major species mass fractions agree similarly among the models and compare reasonably well to experimental data. Substantial differences among the combustion models, however, appear in the predictions of minor species. In this respect a newly proposed model – RPV (FPI) – gives the NO predictions that are much closer to experimental data than are the predictions based on non-premixed flamelets. Due to the problems with the re-parameterisation of the original SLFM database the predictions obtained with the RPV (SLFM) model should be appraised with a special care in this particular case. The inclusion of radiation modelling showed to be important for accurate temperature predictions. The improvements due to radiation inclusion are especially emphasised near the centreline axis. However, the direct impact of radiation on the species mass fractions predictions was eliminated by using the pre-

tabulated chemistry obtained under adiabatic conditions. In this respect, the inclusion of the enthalpy loss as an additional co-ordinate in chemistry pre-tabulations seems to be necessary. HTM has shown as superior to the standard k-ε model in this case. Although both models reside on a simple eddy-viscosity hypothesis, the functional prescription of the structure parameter C_μ and the evaluation of the turbulent kinetic energy from the resolved Reynolds stresses seem to bring improvements in the predictions of turbulent mixing.

The conclusions for the methane jet flame configuration (Sandia flame D) are similar to those for the hydrogen flame. No difficulties with the choice of the reaction progress variable were encountered in this case and consistent chemistry pre-tabulations were possible with respect to the original SLFM database. The inclusion of radiation modelling brought improvements in the temperature predictions in this case as well. When increasing the number of rays per boundary face in the DTRM calculations better predictions of radiative losses were achieved, as expected. In order to improve the prediction accuracy, the inclusion of spectral radiative effects seems to be necessary, as already suggested in some other works. HTM was better in the jet spreading predictions than k-ε model, and accordingly, the HTM predictions were chosen as a referent solution for the evaluation of different combustion models. The mixture fraction moments were reasonably well predicted in this configuration, although less well than was the case in the hydrogen flame configurations. The increased chemistry complexity and higher turbulence levels in the methane flame configuration are most likely reasons for this. Due to increased turbulent levels the modelling of turbulent fluxes becomes more pronounced and has a relatively bigger impact on the overall prediction accuracy. Different combustion models – SLFM, RPV (FPI), RPV (SLFM) and RPV (MIX) – perform similarly when considering major species, like CO_2 and H_2O. However, larger differences occur at the predictions of minor species, like CO and H_2, and in the fuel-rich regions, as evidenced in both, axial and radial profiles. The models based on the reaction progress variable over-predict these species in the fuel-rich regions and compare less favourably with experimental data than the standard SLFM. Improvements in this respect remain as a possible target for the future work. While the OH predictions are similar between the models, and actually best predicted with RPV (SLFM) (re-parameterised SLFM), the NO

predictions are by far best predicted with RPV (FPI), as was the case in the hydrogen flame example. In this respect, RPV (FPI) seems to be the model of choice if more accurate NO predictions are wanted. Poor near-equilibrium NO profiles obtained by using non-premixed flamelets are partly responsible for a relative RPV (FPI) success in this case.

The TECFLAM combustion chamber configuration was simulated the last. This was the most complex configuration among those simulated in this work, and accordingly, the prediction results are in the least agreement with experimental data. The complex methane chemistry (GRI Mech 3.0), the swirled air motion with the high Reynolds number at the inlet, and the complex bluff-body burner geometry, are the reasons for the overall complexity of this simulated case. The simulated flow velocities compare reasonably well with experimental data in the vicinity of the burner, while on the further downstream locations the predictions deteriorate. HTM and k-ε perform similarly in this case, with no clear advantage of one of the models. Both turbulence models reside on a simple eddy-viscosity hypothesis that is known to be insufficiently accurate in the flow simulations with complex features, like swirl, streamline curvature, etc. The application of second-order turbulence closures would probably bring improvements in this respect. The mixture fraction moments prediction are relatively poor near the centreline axis, even in the regions where the velocity field is reasonably well predicted. This suggests that a simple gradient hypothesis used for the turbulent fluxes modelling is insufficiently accurate, especially when higher Reynolds numbers are encountered, as in this case. The inaccurate predictions of mixture fraction near the centreline axis are clearly reflected in the predictions of others species mass fractions as well. A possible application of LES in this configuration, thus, seems to have a great potential because the larger scales responsible for fuel/oxidiser mixing would be directly resolved, while the modelling of turbulence/chemistry interaction only at a sub-grid level would additionally relax a stringent β-PDF hypothesis. Combustion models perform similarly, although RPV (FPI) seems to provide a qualitatively more accurate behaviour, at least when considering the major combustion products near the burner.

In general, a new tabulation procedure based on the normalised reaction progress variable has shown as a possible alternative to the standard stationary laminar flamelets

methodology. In the case of premixed flamelets a complete range from the cold-mixing up to the chemical equilibrium can be covered, making this approach promising if searching towards more universal combustion models. NO was reasonably well predicted when using premixed flamelets, while non-premixed flamelets have shown as a bad choice in this particular situation. The models based on tracking the reaction progress variable, as implemented in this work, have shown a somewhat lesser accuracy in the fuel-rich regions of the methane jet configuration (Sandia flame D), making the space for possible improvements in the future. The inclusion of radiation modelling was important for accurate temperature predictions, even in the simple jet flame configurations. The inclusion of enthalpy as an additional co-ordinate in the chemistry pre-tabulations is recommended in this respect. HTM, in general, has shown as superior to the standard k-ε turbulence model.

Appendix A – A step-by-step derivation of flamelet equations

The starting point in the derivation of flamelet equations are the transport equations for species mass fractions and temperature in a weak conservative form:

$$\rho\frac{\partial Y_k}{\partial t}+\rho u_j\frac{\partial Y_k}{\partial x_j}=\frac{\partial}{\partial x_j}\left(\rho D_k\frac{\partial Y_k}{\partial x_j}\right)+\dot{\omega}_k \tag{A.1}$$

$$\rho\frac{\partial T}{\partial t}+\rho u_j\frac{\partial T}{\partial x_j}=\frac{1}{c_p}\frac{\partial}{\partial x_j}\left(\rho c_p D\frac{\partial T}{\partial x_j}\right)+\frac{1}{c_p}\sum_{k=1}^{N_{spec}}\rho c_{pk}D_k\frac{\partial Y_k}{\partial x_j}\frac{\partial T}{\partial x_j}-\frac{1}{c_p}\sum_{k=1}^{N_{spec}}h_k\dot{\omega}_k+\frac{q_R}{c_p} \tag{A.2}$$

A weak conservative form of the transport equation for mixture fraction is:

$$\rho\frac{\partial Z}{\partial t}+\rho u_j\frac{\partial Z}{\partial x_j}=\frac{\partial}{\partial x_j}\left(\rho D_Z\frac{\partial Z}{\partial x_j}\right) \tag{A.3}$$

Under the presumption of unity Lewis numbers, species and heat diffuse equally, i.e. $D_k = D_Z = D$. If neglecting the gradients of reactive scalars (species mass fractions and temperature) in tangential directions to mixture fraction iso-surfaces, the transformation rules applied to Eqs. (A.1) and (A.2) are:

$$\frac{\partial}{\partial t}=\frac{\partial}{\partial \tau}+\frac{\partial Z}{\partial t}\frac{\partial}{\partial Z} \qquad \frac{\partial}{\partial x_j}=\frac{\partial Z}{\partial x_j}\frac{\partial}{\partial Z} \tag{A.4}$$

Z is the local co-ordinate attached to the flame surface pointing in a direction of the mixture fraction gradient (Fig. 2).

Species mass fractions

After applying the transformation rules (Eq. (A.4)) to Eq. (A.1), in a first step one gets:

$$\rho\left(\frac{\partial Y_k}{\partial \tau}+\frac{\partial Z}{\partial t}\frac{\partial Y_k}{\partial Z}\right)+\rho u_j\frac{\partial Z}{\partial x_j}\frac{\partial Y_k}{\partial Z}=\underbrace{\frac{\partial}{\partial x_j}\left(\rho D\frac{\partial Z}{\partial x_j}\frac{\partial Y_k}{\partial Z}\right)}_{\{1\}}+\dot{\omega}_k \tag{A.5}$$

$\{1\}$ develops as:

$$\begin{aligned}\frac{\partial}{\partial x_j}\left(\rho D\frac{\partial Z}{\partial x_j}\frac{\partial Y_k}{\partial Z}\right)&=\frac{\partial(\rho D)}{\partial x_j}\frac{\partial Z}{\partial x_j}\frac{\partial Y_k}{\partial Z}+\rho D\frac{\partial}{\partial x_j}\left(\frac{\partial Z}{\partial x_j}\frac{\partial Y_k}{\partial Z}\right)\\&=\frac{\partial(\rho D)}{\partial x_j}\frac{\partial Z}{\partial x_j}\frac{\partial Y_k}{\partial Z}+\rho D\left[\frac{\partial Y_k}{\partial Z}\frac{\partial^2 Z}{\partial {x_j}^2}+\frac{\partial Z}{\partial x_j}\frac{\partial^2 Y_k}{\partial Z^2}\frac{\partial Z}{\partial x_j}\right]\\&=\frac{\partial(\rho D)}{\partial x_j}\frac{\partial Z}{\partial x_j}\frac{\partial Y_k}{\partial Z}+\underbrace{\rho D\frac{\partial Y_k}{\partial Z}\frac{\partial^2 Z}{\partial {x_j}^2}}_{\{1'\}}+\rho D\left(\frac{\partial Z}{\partial x_j}\right)^2\frac{\partial^2 Y_k}{\partial Z^2}\end{aligned} \tag{A.6}$$

$\{1'\}$ can be rewritten as:

$$\rho D\frac{\partial Y_k}{\partial Z}\frac{\partial^2 Z}{\partial {x_j}^2}=\frac{\partial Y_k}{\partial Z}\frac{\partial}{\partial x_j}\left(\rho D\frac{\partial Z}{\partial x_j}\right)-\frac{\partial Y_k}{\partial Z}\frac{\partial Z}{\partial x_j}\frac{\partial(\rho D)}{\partial x_j} \tag{A.7}$$

After inserting Eq. (A.7) back into Eq. (A.6) one gets:

$$\frac{\partial}{\partial x_j}\left(\rho D\frac{\partial Z}{\partial x_j}\frac{\partial Y_k}{\partial Z}\right)=\frac{\partial Y_k}{\partial Z}\frac{\partial}{\partial x_j}\left(\rho D\frac{\partial Z}{\partial x_j}\right)+\rho D\left(\frac{\partial Z}{\partial x_j}\right)^2\frac{\partial^2 Y_k}{\partial Z^2} \tag{A.8}$$

After inserting Eq. (A.8) back into Eq. (A.5) and after some rearrangement, one obtains:

$$\rho\frac{\partial Y_k}{\partial \tau}+\frac{\partial Y_k}{\partial Z}\underbrace{\left[\rho\frac{\partial Z}{\partial t}+\rho u_j\frac{\partial Z}{\partial x_j}-\frac{\partial}{\partial x_j}\left(\rho D\frac{\partial Z}{\partial x_j}\right)\right]}_{\{2\}}=\rho D\left(\frac{\partial Z}{\partial x_j}\right)^2\frac{\partial^2 Y_k}{\partial Z^2}+\dot{\omega}_k \tag{A.9}$$

$\{2\}$ vanishes by means of Eq. (A.3). The first term on the right hand-side in Eq. (A.9) can be rewritten by using Eq. (33). The final form of the flamelet equations for species mass fractions ($k=1,\ldots,N_{spec}$) then becomes:

$$\rho \frac{\partial Y_k}{\partial \tau} = \rho \frac{\chi}{2} \frac{\partial^2 Y_k}{\partial Z^2} + \dot{\omega}_k \tag{A.10}$$

Temperature

If starting from Eq. (A.2), and if applying the transformation rules according to Eq. (A.4), one first gets:

$$\begin{aligned}&\rho\left(\frac{\partial T}{\partial \tau}+\frac{\partial T}{\partial Z}\frac{\partial Z}{\partial t}\right)+\rho u_j\frac{\partial T}{\partial Z}\frac{\partial Z}{\partial x_j}\\&=\underbrace{\frac{1}{c_p}\frac{\partial}{\partial x_j}\left(\rho c_p D\frac{\partial T}{\partial Z}\frac{\partial Z}{\partial x_j}\right)}_{\{1\}}+\underbrace{\frac{1}{c_p}\sum_{i=1}^{N_{spec}}\rho c_{pi}D\frac{\partial Y_i}{\partial Z}\frac{\partial Z}{\partial x_j}\frac{\partial T}{\partial Z}\frac{\partial Z}{\partial x_j}}_{\{2\}}-\frac{1}{c_p}\sum_{i=1}^{N_{spec}}h_i\dot{\omega}_i+\frac{q_R}{c_p}\end{aligned}\tag{A.11}$$

After inserting Eq. (33) where appropriate, $\{1\}$ develops as:

$$\begin{aligned}&\frac{1}{c_p}\frac{\partial}{\partial x_j}\left(\rho c_p D\frac{\partial T}{\partial Z}\frac{\partial Z}{\partial x_j}\right)=\frac{1}{c_p}\frac{\partial T}{\partial Z}\frac{\partial Z}{\partial x_j}\frac{\partial\left(\rho c_p D\right)}{\partial x_j}+\rho D\frac{\partial}{\partial x_j}\left(\frac{\partial T}{\partial Z}\frac{\partial Z}{\partial x_j}\right)\\&=\frac{\partial T}{\partial Z}\frac{\partial Z}{\partial x_j}\frac{\partial\left(\rho D\right)}{\partial x_j}+\frac{\rho D}{c_p}\frac{\partial T}{\partial Z}\frac{\partial Z}{\partial x_j}\frac{\partial c_p}{\partial Z}\frac{\partial Z}{\partial x_j}+\rho D\frac{\partial T}{\partial Z}\frac{\partial^2 Z}{\partial x_j^{\,2}}+\rho D\frac{\partial Z}{\partial x_j}\frac{\partial^2 T}{\partial Z^2}\frac{\partial Z}{\partial x_j}\\&=\frac{\partial T}{\partial Z}\frac{\partial Z}{\partial x_j}\frac{\partial\left(\rho D\right)}{\partial x_j}+\frac{\rho D}{c_p}\frac{\partial T}{\partial Z}\left(\frac{\partial Z}{\partial x_j}\right)^2\frac{\partial c_p}{\partial Z}+\rho D\frac{\partial T}{\partial Z}\frac{\partial^2 Z}{\partial x_j^{\,2}}+\rho D\left(\frac{\partial Z}{\partial x_j}\right)^2\frac{\partial^2 T}{\partial Z^2}\\&=\frac{\partial T}{\partial Z}\frac{\partial Z}{\partial x_j}\frac{\partial\left(\rho D\right)}{\partial x_j}+\frac{\rho\chi}{2c_p}\frac{\partial T}{\partial Z}\frac{\partial c_p}{\partial Z}+\underbrace{\rho D\frac{\partial T}{\partial Z}\frac{\partial^2 Z}{\partial x_j^{\,2}}}_{\{1'\}}+\rho\frac{\chi}{2}\frac{\partial^2 T}{\partial Z^2}\end{aligned}\tag{A.12}$$

$\{1'\}$ can be rewritten:

$$\rho D\frac{\partial T}{\partial Z}\frac{\partial^2 Z}{\partial x_j^{\,2}}=\frac{\partial T}{\partial Z}\frac{\partial}{\partial x_j}\left(\rho D\frac{\partial Z}{\partial x_j}\right)-\frac{\partial T}{\partial Z}\frac{\partial Z}{\partial x_j}\frac{\partial\left(\rho D\right)}{\partial x_j}\tag{A.13}$$

$\{1\}$ finally looks like (after cancellation of two terms):

$$\frac{1}{c_p}\frac{\partial}{\partial x_j}\left(\rho c_p D\frac{\partial T}{\partial Z}\frac{\partial Z}{\partial x_j}\right)=\frac{\rho\chi}{2c_p}\frac{\partial T}{\partial Z}\frac{\partial c_p}{\partial Z}+\frac{\partial T}{\partial Z}\frac{\partial}{\partial x_j}\left(\rho D\frac{\partial Z}{\partial x_j}\right)+\rho\frac{\chi}{2}\frac{\partial^2 T}{\partial Z^2}\tag{A.14}$$

After inserting Eq. (33), $\{2\}$ becomes:

$$\frac{1}{c_p}\sum_{i=1}^{N_{spec}}\rho c_{pi}D\frac{\partial Y_i}{\partial Z}\frac{\partial Z}{\partial x_j}\frac{\partial T}{\partial Z}\frac{\partial Z}{\partial x_j}=\sum_{i=1}^{N_{spec}}\rho\frac{\chi}{2}\frac{c_{pi}}{c_p}\frac{\partial Y_i}{\partial Z}\frac{\partial T}{\partial Z}\tag{A.15}$$

By inserting Eq. (A.14) and Eq. (A.15) back into Eq. (A.11), and after some rearrangement, one gets:

$$\rho\frac{\partial T}{\partial \tau}+\frac{\partial T}{\partial Z}\underbrace{\left[\rho\frac{\partial Z}{\partial t}+\rho u_j\frac{\partial Z}{\partial x_j}-\frac{\partial}{\partial x_j}\left(\rho D\frac{\partial Z}{\partial x_j}\right)\right]}_{\{3\}} = \frac{\rho\chi}{2c_p}\frac{\partial T}{\partial Z}\frac{\partial c_p}{\partial Z}+\rho\frac{\chi}{2}\frac{\partial^2 T}{\partial Z^2}+\sum_{i=1}^{N_{spec}}\rho\frac{\chi}{2}\frac{c_{pi}}{c_p}\frac{\partial Y_i}{\partial Z}\frac{\partial T}{\partial Z}-\frac{1}{c_p}\sum_{i=1}^{N_{spec}}h_i\dot{\omega}_i+\frac{q_R}{c_p} \tag{A.16}$$

Term $\{3\}$ disappears by virtue of Eq. (A.3). The final form of the flamelet equation for temperature is then obtained as:

$$\rho\frac{\partial T}{\partial \tau}=\frac{\rho\chi}{2c_p}\frac{\partial T}{\partial Z}\frac{\partial c_p}{\partial Z}+\rho\frac{\chi}{2}\frac{\partial^2 T}{\partial Z^2}+\sum_{i=1}^{N_{spec}}\rho\frac{\chi}{2}\frac{c_{pi}}{c_p}\frac{\partial Y_i}{\partial Z}\frac{\partial T}{\partial Z}-\frac{1}{c_p}\sum_{i=1}^{N_{spec}}h_i\dot{\omega}_i+\frac{q_R}{c_p} \tag{A.17}$$

Appendix B – A flamelet model with differential diffusion

The laminar flamelet formulation that takes into account differential diffusion, according to [34], has been implemented as an additional option into the CSC solver [96]. The Lewis numbers are presumed constant, but they can be deliberately set for each of the species. Accordingly, the original formulation from [34] has been recast into a form suitable for the implementation into the CSC solver, as will be described next. More details about the model itself and its derivation can be found in the original reference [34].

In abbreviated form the flamelet model can be formally written as:

$$\frac{\partial \phi_i}{\partial \tau} + A_1^{(i)} \frac{\partial^2 \phi_i}{\partial Z^2} + A_2^{(i)} \frac{\partial \phi_i}{\partial Z} + A_3^{(i)} \phi_i + A_4^{(i)} = 0 \qquad i = 1, 2, \ldots, N_{spec} + 1 \tag{B.1}$$

In Eq. (B.1) $\phi_i \equiv Y_i$ if $i \le N_{spec}$ and $\phi_i \equiv T$ if $i = N_{spec} + 1$. The coefficients $A_1^{(i)} \ldots A_4^{(i)}$ in the case of species mass fractions (i.e. $i \le N_{spec}$) are:

$$A_1^{(i)} = -\frac{\chi}{2} \frac{\mathrm{Le}_Z}{\mathrm{Le}_i} \tag{B.2}$$

$$A_2^{(i)} = \frac{\mathrm{Le}_Z \chi}{2} \sum_{k=1}^{N_{spec}} \left[\frac{1}{\mathrm{Le}_k} \left(\frac{Y_k}{M} \frac{\partial M}{\partial Z} + \frac{\partial Y_k}{\partial Z} \right) \right] - \frac{1}{2} \frac{\mathrm{Le}_Z}{\mathrm{Le}_i} \frac{\partial M}{\partial Z} \frac{\chi}{M} - \frac{1}{4\rho} \left\{ \left(\frac{\mathrm{Le}_Z}{\mathrm{Le}_i} - 1 \right) \left[\frac{\partial (\rho \chi)}{\partial Z} + \frac{\rho \chi c_p}{\lambda} \frac{\partial}{\partial Z} \left(\frac{\lambda}{c_p} \right) \right] \right\} \tag{B.3}$$

$$A_3^{(i)} = \frac{\mathrm{Le}_Z \chi}{2} \sum_{k=1}^{N_{spec}} \left[\frac{1}{\mathrm{Le}_k} \left(\frac{\partial^2 Y_k}{\partial Z^2} + \frac{Y_k}{M} \frac{\partial^2 M}{\partial Z^2} \right) \right] - \frac{\mathrm{Le}_Z}{\mathrm{Le}_i} \left\{ \frac{\chi}{2M} \frac{\partial^2 M}{\partial Z^2} + \frac{1}{4\rho} \frac{\partial M}{\partial Z} \left[\frac{\partial}{\partial Z} \left(\frac{\rho\chi}{M} \right) + \frac{\rho\chi c_p}{\lambda} \frac{\partial}{\partial Z} \left(\frac{\lambda}{c_p M} \right) \right] \right\} + \frac{\mathrm{Le}_Z}{4\rho} \sum_{k=1}^{N_{spec}} \left\{ \frac{1}{\mathrm{Le}_k} \left[\begin{array}{l} \frac{\partial Y_k}{\partial Z} \left(\frac{\partial(\rho\chi)}{\partial Z} + \frac{\rho\chi c_p}{\lambda} \frac{\partial}{\partial Z} \left(\frac{\lambda}{c_p} \right) \right) + \\ \frac{\partial M}{\partial Z} \left(\frac{\partial}{\partial Z} \left(\frac{\rho\chi Y_k}{M} \right) + \frac{\rho\chi c_p}{\lambda} \frac{\partial}{\partial Z} \left(\frac{\lambda}{c_p} \frac{Y_k}{M} \right) \right) \end{array} \right] \right\} \tag{B.4}$$

$$A_4^{(i)} = -\frac{\dot{\omega}_i}{\rho} \tag{B.5}$$

The coefficients $A_1^{(i)} \ldots A_4^{(i)}$ in the case of temperature (i.e. $i = N_{spec} + 1$) are:

$$A_1^{(i)} = -\frac{\mathrm{Le}_Z \chi}{2} \tag{B.6}$$

$$A_2^{(i)} = \frac{\mathrm{Le}_Z \chi}{2} \sum_{k=1}^{N_{spec}} \left[\frac{1}{\mathrm{Le}_k} \left(\frac{Y_k}{M} \frac{\partial M}{\partial Z} + \frac{\partial Y_k}{\partial Z} \right) \left(1 - \frac{c_{pk}}{c_p} \right) \right] - \frac{1}{4\rho} \left\{ \left(\mathrm{Le}_Z - 1 \right) \left[\frac{\partial(\rho\chi)}{\partial Z} + \frac{\rho\chi c_p}{\lambda} \frac{\partial}{\partial Z} \left(\frac{\lambda}{c_p} \right) \right] \right\} - \frac{\mathrm{Le}_Z \chi}{2c_p} \frac{\partial c_p}{\partial Z} \tag{B.7}$$

$$A_3^{(i)} = 0 \tag{B.8}$$

$$A_4^{(i)} = \frac{1}{\rho c_p} \left(\sum_{k=1}^{N_{spec}} h_k \dot{\omega}_k - q_R \right) \tag{B.9}$$

The Lewis number for mixture fraction Le_Z, according to Eq. (29), is defined as:

$$\mathrm{Le}_Z = \frac{\lambda}{\rho c_p D_Z} \tag{B.10}$$

The thermal conductivity λ is calculated by using the gas phase libraries from [149].

Similarly as in Section 3.1.2.1, the finite difference rules according to Eqs. (106) and (107), and a grid notation according to Eq. (108), are applied in Eq. (B.1). The following differential/algebraic equation set is obtained:

$$\left(\frac{\partial \phi_i}{\partial \tau}\right)_{(k)} = C_1^{(k)}(i)\,\phi_i^{(k-1)} + C_2^{(k)}(i)\,\phi_i^{(k)} + C_3^{(k)}(i)\,\phi_i^{(k+1)} + C_4^{(k)}(i) \tag{B.11}$$

The coefficients $C_1^{(k)} \ldots C_4^{(k)}$ are:

$$C_1^{(k)}(i) = \frac{A_2^{(i)}(k)\,\Delta_{(k)}^{+}}{\left(\Delta_{(k)}^{-} + \Delta_{(k)}^{+}\right)\Delta_{(k)}^{-}} - \frac{A_1^{(i)}(k)}{0.5\left(\Delta_{(k)}^{-} + \Delta_{(k)}^{+}\right)\Delta_{(k)}^{-}} \tag{B.12}$$

$$C_2^{(k)}(i) = \frac{A_1^{(i)}(k)}{0.5\Delta_{(k)}^{-}\Delta_{(k)}^{+}} - \frac{A_2^{(i)}(k)\left(\Delta_{(k)}^{+} - \Delta_{(k)}^{-}\right)}{\Delta_{(k)}^{-}\Delta_{(k)}^{+}} - A_3^{(i)}(k) \tag{B.13}$$

$$C_3^{(k)}(i) = -\frac{A_1^{(i)}(k)}{0.5\left(\Delta_{(k)}^{-} + \Delta_{(k)}^{+}\right)\Delta_{(k)}^{+}} - \frac{A_2^{(i)}(k)\,\Delta_{(k)}^{-}}{\left(\Delta_{(k)}^{-} + \Delta_{(k)}^{+}\right)\Delta_{(k)}^{+}} \tag{B.14}$$

$$C_4^{(k)}(i) = -A_4^{(i)}(k) \tag{B.15}$$

The discretised equation set according to Eq. (B.11) is directly applicable in the DDASSL solver [129]. The 1st and 2nd derivatives that appear in the coefficients $A_1^{(i)} \ldots A_4^{(i)}$ are approximated with the central differences, similarly like in Eqs. (115) and (116).

Appendix C – The stationary laminar 1D premixed flame

The PREMIX solver [97] has been used for computations of the freely propagating premixed flames (Section 2.3.6.1). It is based on a numerical solution (finite differences) of the following set of equations:

$$\dot{m} = \rho u A \tag{C.1}$$

$$\dot{m}\frac{dY_k}{dx} + \frac{d}{dx}\left(\rho A Y_k V_k\right) - A\dot{\omega}_k = 0 \tag{C.2}$$

$$\dot{m}\frac{dT}{dx} - \frac{1}{c_p}\frac{d}{dx}\left(\lambda A\frac{dT}{dx}\right) + \frac{A}{c_p}\sum_{k=1}^{N_{spec}}\rho Y_k V_k c_{pk}\frac{dT}{dx} + \frac{A}{c_p}\sum_{k=1}^{N_{spec}} h_k\dot{\omega}_k = 0 \tag{C.3}$$

The CHEMKIN II library [98] is used for the evaluations of the thermo-chemical properties, while the transport properties (thermal conductivity) are obtained from [149]. Thus, given the boundary conditions, the predicted stationary profiles describe the species and temperature evolutions from the unburnt until the fully burnt state in the functional dependence of a spatial co-ordinate x and a given reactant composition ϕ as:

$$\begin{aligned} Y_k &= Y_k\left(x,\phi\right) \\ T &= T\left(x,\phi\right) \end{aligned} \tag{C.4}$$

For more information on the numerical techniques, solution algorithm, and other issues relevant to the PREMIX solver, one is referred to the original reference [97].

Bibliography

[1] L. D. Smoot, *A Decade of Combustion Research*, Prog. Energy Combust. Sci., 23 (1997), pp. 203-232.

[2] R. W. Bilger, *The future for energy from the combustion of fossil fuels*, Proc. 5th Intl. Conference on Technologies and Combustion for a Clean Environment, Lisbon, 1999.

[3] R. W. Bilger, *Future progress in turbulent combustion research*, Prog. Energy Combust. Sci., 26 (2000), pp. 367-380.

[4] J. M. Beér, *Combustion technology developments in power generation in response to environmental challenges*, Prog. Energy Combust. Sci., 26 (2000), pp. 301-327.

[5] J. Ferziger and M. Perić, *Computational Methods for Fluid Dynamics*, Springer Verlag, 1999.

[6] S. V. Patankar, *Numerical Heat Transfer and Fluid Flow*, Hemisphere Publishing Corporation, Washington, 1980.

[7] A. D. Gosman, *Development and current status of industrial thermofluids CFD analysis*, ICHMT International Symposium on Advances in Computational Heat Transfer, CHT-04-K2, 2004.

[8] N. Duić, *Contribution to the Mathematical Modelling of Gaseous Fuel Combustion in a Steam Generator Furnace*, PhD thesis (in Croatian), Power Engineering Department, University of Zagreb, Zagreb, 1998.

[9] N. Duić, *Trodimenzionalni matematički model procesa u ložištu generatora pare*, Master thesis (in Croatian), Power Engineering Department, University of Zagreb, Zagreb, 1993.

[10] Ž. Bogdan and N. Duić, *The mathematical model of the steam generator combustion chamber*, Proc. 24th Symposium KoREMA, Zagreb, 1992.

[11] Ž. Bogdan and N. Duić, *Three-dimensional simulation of the combustion process in an oil-fired furnace*, Proc. of the 15th International Conference Information Technology Interfaces '93, Pula, 1993.

[12] Ž. Bogdan, N. Duić and D. R. Schneider, *Three-dimensional simulation of the performance of an oil-fired combustion chamber*, Proc. 2nd European Thermal Sciences & 14th UIT National Heat Transfer Conference, Rome, 1996.

[13] K. N. C. Bray, *The challenge of turbulent combustion*, Proc. 26th Symposium (International) on Combustion, The Combustion Institute, 1996.

[14] S. B. Pope, *Computations of turbulent combustion: progress and challenges*, Proc. 23rd Symposium (International) on Combustion, The Combustion Institute, 1990.

[15] N. Peters, *Turbulent Combustion*, Cambridge University Press, Cambridge, 2000.

[16] D. Veynante and L. Vervisch, *Turbulent combustion modeling*, Prog. Energy Combust. Sci., 28 (2002), pp. 193-266.

[17] J. O. Hinze, *Turbulence*, McGraw-Hill, New York, 1975.

[18] S. B. Pope, *Turbulent Flows*, Cambridge University Press, Cambridge, 2000.

[19] H. Tennekes and J. L. Lumley, *A First Course in Turbulence*, MIT Press, Cambridge, MA, 1972.

[20] T. Poinsot and D. Veynante, *Theoretical and Numerical Combustion*, R.T. Edwards, Inc., Philadelphia, 2001.

[21] P. Givi, *Model free simulations of turbulent reactive flows*, Prog. Energy Combust. Sci., 15 (1989), pp. 1-107.

[22] O. Reynolds, *On the dynamical theory of incompressible viscous flows and the determination of the criterion*, Philos. Trans. R. Soc. London Ser. A, 186 (1894), pp. 123-161.

[23] D. C. Wilcox, *Turbulence modeling for CFD*, DCW Industries, Inc., La Cañada, California, 1993.

[24] P. Bradshaw, *Understanding and prediction of turbulent flow - 1996*, Int. J. Heat and Fluid Flow, 18 (1997), pp. 45-54.

[25] P. R. Spalart, *Strategies for turbulence modelling and simulations*, Int. J. Heat and Fluid Flow, 21 (2000), pp. 252-263.

[26] N. Peters, *Laminar diffusion flamelet models in non-premixed turbulent combustion*, Prog. Energy Combust. Sci., 10 (1984), pp. 319-339.

[27] A. Y. Klimenko and R. W. Bilger, *Conditional moment closure for turbulent combustion*, Prog. Energy Combust. Sci., 25 (1999), pp. 595-687.

[28] S. B. Pope, *Pdf method for turbulent reactive flows*, Prog. Energy Combust. Sci., 11 (1985), pp. 119-195.

[29] http://www.ca.sandia.gov/TNF/abstract.html.

[30] P. J. Coelho, O. J. Teerling and D. Roekaerts, *Spectral radiative effects and turbulence/radiation interaction in a non-luminous turbulent jet diffusion flame*, Combust. Flame, 133 (2003), pp. 75-91.

[31] R. Hilbert, F. Tap, H. El-Rabii and D. Thévenin, *Impact of detailed chemistry and transport models on turbulent combustion simulations*, Prog. Energy Combust. Sci., 30 (2004), pp. 61-117.

[32] V. Nilsen and G. Kosály, *Differential Diffusion in Turbulent Reacting Flows*, Combust. Flame, 117 (1999), pp. 493-513.

[33] R. Hilbert and D. Thévenin, *Influence of differential diffusion on maximum flame temperature in turbulent nonpremixed hydrogen/air flames*, Combust. Flame, 138 (2004), pp. 175-187.

[34] H. Pitsch and N. Peters, *A Consistent Flamelet Formulation for Non-Premixed Combustion Considering Differential Diffusion Effects*, Combust. Flame, 114 (1998), pp. 26-40.

[35] H. Pitsch, *Unsteady Flamelet Modeling of Differential Diffusion in Turbulent Jet Diffusion Flames*, Combust. Flame, 123 (2000), pp. 358-374.

[36] B. Wegner, A. Sadiki and J. Janicka, *Prediction of Flow and Combustion in Generic Gas Turbine Combustor Using Large Eddy Simulation*, Proc. 2nd International Workshop on TRENDS IN NUMERICAL AND PHYSICAL MODELLING OF TURBULENT PROCESSES IN GAS TURBINE COMBUSTORS (AND AUTOMOTIVE ENGINES), Heidelberg, Germany, 2004.

[37] L. Davidson and S. Dahlström, *Hybrid LES-RANS: An approach to make LES applicable at high Reynolds number*, ICHMT International Symposium on Advances in Computational Heat Transfer, CHT-04-K1, 2004.

[38] S. Menon, Modeling and Computational Constraints for LES of Turbulent Reacting Flows, CCL Report 2004-017, Computational Combustion Laboratory, School of Aerospace Engineering, Georgia Institute of Technology, 2004.

[39] A. Sadiki and J. Janicka, *Unsteady methods (URANS and LES) for simulation of combustion systems*, ICHMT International Symposium on Advances in Computational Heat Transfer, CHT-04-K3, 2004.

[40] R. S. Barlow and J. H. Frank, *Effects of turbulence on species mass fractions in methane/air jet flames*, Proc. 27th Symposium (International) on Combustion, The Combustion Institute, 1998.

[41] H. Pitsch, Extended flamelet model for LES of non-premixed combustion, Annual Research Briefs 2000, Center for Turbulence Research, 2000.

[42] H. Pitsch and H. Steiner, *Large-eddy simulation of a turbulent piloted methane/air diffusion flame (Sandia flame D)*, Phys. Fluids, 12 (2000), pp. 2541-2554.

[43] H. Pitsch and H. Steiner, Large-eddy simulation of a turbulent piloted methane/air flame (Sandia flame D), Annual Research Briefs 1999, Center for Turbulence Research, 1999.

[44] H. Pitsch and H. Steiner, *Scalar mixing and dissipation rate in large-eddy simulations of non-premixed turbulent combustion*, Proc. 28th Symposium (International) on Combustion, The Combustion Institute, 2000.

[45] S. Navarro-Martinez and A. Kronenburg, *Conditional Moment Closure Modelling in Large Eddy Simulation*, Proc. 2nd International Workshop on TRENDS IN NUMERICAL AND PHYSICAL MODELLING OF TURBULENT PROCESSES IN GAS TURBINE COMBUSTORS (AND AUTOMOTIVE ENGINES), Heidelberg, Germany, 2004.

[46] P. Domingo, L. Vervisch and K. N. C. Bray, *Partially premixed flamelets in LES of nonpremixed turbulent combustion*, Combust. Theory Modelling, 6 (2002), pp. 529-551.

[47] L. Vervisch, R. Hauguel, P. Domingo and M. Rullaud, *Three facets of turbulent combustion modelling: DNS of premixed V-flame, LES of lifted nonpremixed flame and RANS of jet-flame*, J. of Turbulence, 5 (2004), pp. 1-36.

[48] O. Colin, F. Ducros, D. Veynante and T. Poinsot, *A thickened flame model for large eddy simulations of turbulent premixed combustion*, Phys. Fluids, 12 (2000), pp. 1843-1863.

[49] R. Knikker, D. Veynante and C. Meneveau, *A priori testing of a similarity model for large eddy simulations of turbulent premixed combustion*, Proc. 29th Symposium (International) on Combustion, 2002.

[50] S. Subramaniam and S. B. Pope, *A Mixing Model for Turbulent Reactive Flows based on Euclidean Minimum Spanning Trees*, Combust. Flame, 115 (1998), pp. 487-514.

[51] Z. Ren and S. B. Pope, *An investigation of the performance of turbulent mixing models*, Combust. Flame, 136 (2004), pp. 208-216.

[52] S. Subramaniam and S. B. Pope, *Comparison of Mixing Model Performance for Nonpremixed Turbulent Reactive Flow*, Combust. Flame, 117 (1999), pp. 732-754.

[53] J. Xu and S. B. Pope, *PDF Calculations of Turbulent Nonpremixed Flames with Local Extinction*, Combust. Flame, 123 (2000), pp. 281-307.

[54] http://www.tu-darmstadt.de/fb/mb/ekt/tecflam/.

[55] A. Hinz, *Numerische Simulation turbulenter Methandiffusionsflammen mittels Monte Carlo PDF Methoden*, PhD thesis, Technische Universität Darmstadt, Darmstadt, 2000.

[56] S. B. Pope, *Computationally efficient implementation of combustion chemistry using in situ adaptive tabulation*, Combust. Theory Modelling, 1 (1997), pp. 41-63.

[57] M. A. Singer and S. B. Pope, *Exploiting ISAT to solve the reaction-diffusion equation*, Combust. Theory Modelling, 8 (2004), pp. 361-383.

[58] V. Saxena and S. B. Pope, *PDF Simulations of Turbulent Combustion Incorporating Detailed Chemistry*, Combust. Flame, 117 (1999), pp. 340-350.

[59] K. Liu, S. B. Pope and D. A. Caughey, *Calculations of bluff-body stabilized flames using a joint probability density function model with detailed chemistry*, Combust. Flame, Article in press (2005), pp. 1-29.

[60] A. Mura and R. Borghi, *Introducing a new partial PDF approach for turbulent combustion modeling*, Combust. Flame, 136 (2004), pp. 377-382.

[61] M. Fairweather and R. M. Woolley, *First-order conditional moment closure modeling of turbulent, nonpremixed hydrogen flames*, Combust. Flame, 133 (2003), pp. 393-405.

[62] M. Fairweather and R. M. Woolley, *First-order conditional moment closure modeling of turbulent, nonpremixed methane flames*, Combust. Flame, 138 (2004), pp. 3-19.

[63] M. R. Roomina and R. W. Bilger, *Conditional Moment Closure (CMC) Predictions of a Turbulent Methane-Air Jet Flame*, Combust. Flame, 125 (2001), pp. 1176-1195.

[64] C. B. Devaud and K. N. C. Bray, *Assessment of the applicability of conditional moment closure to a lifted turbulent flame: first order model*, Combust. Flame, 132 (2003), pp. 102-114.

[65] http://www.me.berkeley.edu/gri_mech/.

[66] S. H. Kim and K. Y. Huh, *Second-order conditional moment closure modeling of turbulent piloted jet diffusion flames*, Combust. Flame, 138 (2004), pp. 336-352.

[67] N. Peters, *Laminar flamelet concepts in turbulent combustion*, Proc. 21st Symposium (International) on Combustion, The Combustion Institute, Pittsburgh, 1986.

[68] N. Swaminathan and R. W. Bilger, *Assessment of Combustion Submodels for Turbulent Nonpremixed Hydrocarbon Flames*, Combust. Flame, 116 (1998), pp. 519-545.

[69] N. Peters, *Comment and Reply on the "Assessment of Combustion Submodels for Turbulent Nonpremixed Hydrocarbon Flames"*, Combust. Flame, 116 (1999), pp. 675-676.

[70] N. Swaminathan, *Flamelet Regime in Non-premixed Combustion*, Combust. Flame, 129 (2002), pp. 217-219.

[71] P. J. Coelho and N. Peters, *Unsteady Modelling of a Piloted Methane/Air Jet Flame Based on the Eulerian Particle Flamelet Model*, Combust. Flame, 124 (2001), pp. 444-465.

[72] P. J. Coelho and N. Peters, *Numerical Simulation of a Mild Combustion Burner*, Combust. Flame, 124 (2001), pp. 503-518.

[73] O. Gicquel, N. Darabiha and D. Thévenin, *Laminar premixed hydrogen/air counterflow flame simulations using flame prolongation of ILDM with differential diffusion*, Proc. 28th Symposium (International) on Combustion, The Combustion Institute, 2000.

[74] J. A. van Oijen, F. A. Lammers and L. P. H. de Goey, *Modeling of Complex Premixed Burner Systems by Using Flamelet-Generated Manifolds*, Combust. Flame, 127 (2001), pp. 2124-2134.

[75] B. Fiorina, R. Baron, O. Gicquel, D. Thévenin, S. Carpentier and N. Darabiha, *Modelling non-adiabatic partially premixed flames using flame-prolongation ILDM*, Combust. Theory Modelling, 7 (2003), pp. 449-470.

[76] B. Fiorina, O. Gicquel, L. Vervisch, S. Carpentier and N. Darabiha, *Approximating the chemical structure of partially premixed and diffusion counterflow flames using FPI flamelet tabulation*, Combust. Flame, 140 (2005), pp. 147-160.

[77] G. Ribert, M. Champion, O. Gicquel, N. Darabiha and D. Veynante, *Modeling nonadiabatic turbulent premixed reactive flows including tabulated chemistry*, Combust. Flame, Article in press (2005), pp. 1-10.

[78] G. Ribert, O. Gicquel and N. Darabiha, *Flame Prolongation of ILDM kinetics reduction technique applied to kerosene reaction mechanism*, Proc. European Combustion Meeting, 2003.

[79] C. D. Pierce, *Progress-variable approach for large-eddy simulation of turbulent combustion*, PhD thesis, Department of Mechanical Engineering, Stanford University, 2001.

[80] H. C. Hottel and A. F. Sarofim, *Radiative Transfer*, McGraw-Hill, New York, 1967.

[81] J. R. Howell, *Application of Monte Carlo to Heat Transfer Problems*, Advances in Heat Transfer, 5 (1968).

[82] B. G. Carlson and K. D. Lathrop, *Transport Theory - The Method of Discrete Ordinates*, Computing Methods in Reactor Physics (1968).

[83] W. A. Fiveland, *Discrete-Ordinates Solutions of the Radiative Transport Equation for Rectangular Enclosures*, J. Heat Transfer, 106 (1984), pp. 699-706.

[84] G. D. Raithby and E. H. Chui, *A Finite Volume Method for Predicting Radiant Heat Transfer in Enclosures with Participating Media*, J. Heat Transfer, 112 (1990), pp. 415-423.

[85] F. C. Lockwood and N. G. Shah, *A New Radiation Solution for Incorporation in General Combustion Prediction Procedures*, Proc. 18th Symposium (International) on Combustion, The Combustion Institute, 1981.

[86] B. R. Adams and P. J. Smith, *Three-dimensional Discrete-ordinates Modeling of Radiative Transfer in a Geometrically Complex Furnace*, Combust. Sci. and Tech., 88 (1993), pp. 293-308.

[87] M. Baburić, A. Raulot, P. J. Coelho and N. Duić, *Application of the Conservative Discrete Transfer Radiation Method to a Furnace With Complex Geometry*, ICHMT International Symposium on Advances in Computational Heat Transfer, CHT-04-168, 2004.

[88] M. Y. Kim, S. W. Baek and J. H. Park, *Unstructured Finite-Volume Method for Radiative Heat Transfer in a Complex Two-Dimensional Geometry with Obstacles*, Numerical Heat Transfer, Part B, 39 (2001), pp. 617-635.

[89] Ž. Bogdan, D. R. Schneider and N. Duić, *Prediction of the thermal radiation heat transfer in a furnace by Monte Carlo zone method*, Proc. of the 16th International Conference Information Technology Interfaces '94, Pula, 1994.

[90] D. R. Schneider, *Modeliranje prijenosa topline zračenjem u ložištu primjenom Monte Carlo metode*, Master thesis (in Croatian), Power Engineering Department, University of Zagreb, Zagreb, 1997.

[91] W. L. Grosshandler, RADCAL: A Narrow-Band Model for Radiation Calculations in a Combustion Environment, 1993.

[92] R. S. Barlow, A. N. Karpetis, J. H. Frank and J.-Y. Chen, *Scalar Profiles of NO Formation in Laminar Opposed-Flow Partially Premixed Methane/Air Flames*, Combust. Flame, 127 (2001), pp. 2102-2118.

[93] P. J. Coelho, *Detailed numerical simulation of radiative transfer in a nonluminous turbulent jet diffusion flame*, Combust. Flame, 136 (2004), pp. 481-492.

[94] L. Wang, D. C. Haworth, S. R. Turns and M. F. Modest, *Interactions among soot, thermal radiation, and NOx emissions in oxygen-enriched turbulent nonpremixed flames: a computational fluid dynamics modeling study*, Combust. Flame, Article in press (2005), pp. 1-10.

[95] X. L. Zhu and J. P. Gore, *Radiation effects on combustion and pollutant emissions of high-pressure opposed flow methane/air diffusion flames*, Combust. Flame, Article in press (2005), pp. 1-13.

[96] http://powerlab.fsb.hr/mbaburic/CSC.htm.

[97] R. J. Kee, J. F. Grcar, M. Smooke and J. A. Miller, PREMIX: A Fortran program for modelling steady laminar one-dimensional flames, SAND85-8240, Sandia National Laboratories, 1985.

[98] R. J. Kee, F. M. Rupley and J. A. Miller, Chemkin-II: A Fortran Chemical Kinetics Package for the Analysis of Gas-Phase Chemical Kinetics, SAND89-8009, Sandia National Laboratories, 1989.

[99] AVL AST, FIRE manual v8.1.1, AVL List GmbH, 2003.

[100] P. J. Coelho and M. G. Carvalho, *A Conservative Formulation of Discrete Transfer Method*, ASME Journal of Heat Transfer, 119 (1997), pp. 118-128.

[101] P. J. Smith, Z. F. Shen and J. N. Friedman, *Evaluation of Coefficients for the Weighted Sum of Gray Gases Model*, J. Heat Transfer, 104 (1982).

[102] M. Baburić, A. Raulot and N. Duić, *Implementation of discrete transfer radiation method into SWIFT computational fluid dynamics code*, Thermal Science, 8 (2004), pp. 19-28.

[103] R. S. Barlow, *Sandia H2/He Flame Data - Release 2.0, http://www.ca.sandia.gov/TNF*, Sandia National Laboratories, 2003.

[104] R. S. Barlow and C. D. Carter, *Raman/Rayleigh/LIF measurements of nitric oxide formation in turbulent hydrogen jet flames*, Combust. Flame, 97 (1994), pp. 261-280.

[105] I. Alfirević, *Uvod u tenzore i mehaniku kontinuuma*, Golden marketing, Zagreb, 2003.

[106] D. A. Anderson, J. C. Tannehill and R. H. Pletcher, *Computational Fluid Mechanics and Heat Transfer*, Hemisphere Publishing Corporation, 1984.

[107] C. Hirsch, *Numerical Computation of Internal and External Flows*, Volume 1: Fundamentals of Numerical Discretization, John Wiley & Sons, 1988.

[108] K. K. Kuo, *Principles of Combustion*, John Wiley & Sons, Inc., 1986.

[109] J. H. Heinbockel, Introduction to Tensor Calculus and Continuum Mechanics, Department of Mathematics and Statistics, Old Dominion University, 1996.

[110] S. P. Burke and T. E. W. Schumann, *Diffusion flames*, Proc. 1st Symposium (International) on Combustion, The Combustion Institute, Pittsburgh, 1928.

[111] H. Pitsch, M. Chen and N. Peters, *Unsteady Flamelet Modeling of Turbulent Hydrogen-Air Diffusion Flames*, Proc. 27th Symposium (International) on Combustion, The Combustion Institute, 1998.

[112] D. Bradley, P. H. Gaskell and X. J. Gu, *The Mathematical Modelling of Liftoff and Blowoff of Turbulent Non-Premixed Methane Jet Flames at High Strain Rates*, Proc. 27th Symposium (International) on Combustion, The Combustion Institute, 1998.

[113] U. Maas and S. B. Pope, *Simplifying chemical kinetics: Intrinsic low-dimensional manifolds in composition space*, Combust. Flame, 88 (1992), pp. 239-264.

[114] M. F. Modest, *Radiative Heat Transfer*, McGraw-Hill, Inc., 1993.

[115] R. Siegel and J. R. Howell, *Thermal Radiation Heat Transfer*, Hemisphere Publishing Corporation, McGraw-Hill Book Company, 1981.

[116] M. G. Carvalho, T. Farias and P. Fontes, *Predicting Radiative Heat Transfer In Absorbing, Emitting And Scattering Media Using Discrete Transfer Method*, Fundamentals of Radiation Heat Transfer, 160 (1991), pp. 17-26.

[117] T. R. Johnson, *Application of the Zone Method of Analysis to the Calculation of Heat Transfer from Luminous Flames*, PhD thesis, Department of Chemical Engineering and Fuel Technology, University of Sheffield, Sheffield, 1971.

[118] J. S. Truelove, A Mixed Grey Gas Model for Flame Radiation, AERE-R-8494, United Kingdom Atomic Energy Authority, 1976.

[119] L. F. Richardson, *Weather Prediction by Numerical Process*, Cambridge University Press, Cambridge, 1922.

[120] A. N. Kolmogorov, *The local structure of turbulence in incompressible viscous fluid for very large Reynolds numbers*, Dokl. Akad. Nauk SSSR 30 (1941), pp. 299-303.

[121] A. Favre, *Statistical equations of turbulent gases*, In: SIAM, editor. Problems of hydrodynamics and continuum mechanics. Philadelphia: SIAM (1969), pp. 231-266.

[122] W. P. Jones and B. E. Launder, *The prediction of laminarization with a two-equation model of turbulence*, Int. J. Heat Mass Transfer, 15 (1972), pp. 301-314.

[123] B. Basara and S. Jakirlic, *A new hybrid turbulence modelling strategy for industrial CFD*, Int. J. Numer. Meth. Fluids, 42 (2003), pp. 89-116.

[124] M. M. Gibson and B. E. Launder, *Ground Effects on Pressure Fluctuations in the Atmospheric Boundary Layer*, J. Fluid Mech., 86 (1978), pp. 491-511.

[125] C. G. Speziale, S. Sarkar and T. B. Gatski, *Modeling of Pressure-Strain Correlation of Turbulence: An Invariant Dynamical System Approach*, J. Fluid Mech., 227 (1991), pp. 245-272.

[126] W. P. Jones and P. Musonge, *Closure of the Reynolds stress and scalar flux equations*, Phys. Fluids, 31 (1988), pp. 3589-3604.

[127] MAE 504, Fluid Dynamics of Combustion I, Running EQUIL, 2002.

[128] J. D. Anderson, Jr., *Computational fluid dynamics: the basics with applications*, McGraw-Hill, Inc., 1995.

[129] http://www.kachinatech.com/~hjjou/slatec-doc/code/DDASSL.html.

[130] E. Kreyszig, *Advanced Engineering Mathematics*, John Wiley & Sons, Inc., 1993.

[131] M. Rogina, S. Singer and S. Singer, Numerička analiza, Prirodoslovno-matematički fakultet, Sveučilište u Zagrebu, 2002.

[132] J. W. Harris and H. Stocker, *Handbook of Mathematics and Computational Science*, Springer-Verlag, New York, Inc., New York, 1998.

[133] S. C. Chapra and R. P. Canale, *Numerical methods for engineers: with software and programming applications*, McGraw-Hill, New York, 2002.

[134] http://www.mathworks.com/.

[135] Intel, Intel® Fortran Programmer's Reference, FWL-710-02, Intel Corporation, 2003.

[136] S. V. Patankar and D. B. Spalding, *A calculation procedure for heat, mass and momentum transfer in three-dimensional parabolic flows*, Int. J. Heat Mass Transfer, 15 (1972).

[137] M. Baburić, D. R. Schneider, Ž. Bogdan and N. Duić, *User function approach in combustion and radiation modelling in commercial CFD environment*, Transactions of FAMENA, 26 (2002), pp. 1-12.

[138] S. S. Dua and P. Cheng, *Multi-dimensional Radiative Transfer in Non-isothermal Cylindrical Media with Non-isothermal Bounding Walls*, Int. J. Heat Mass Transfer, 18 (1975), pp. 246-259.

[139] M. Baburić, N. Duić, A. Raulot, R. Tatschl and B. Wiesler, *Accurate Discrete Transfer Radiation Modelling in Industrial Furnaces - a Validation Study*, Proc. Conference on MODELLING FLUID FLOW, Department of Fluid Mechanics, Budapest University of Technology and Economics, Budapest, 2003.

[140] R. S. Barlow and C. D. Carter, *Relationships among Nitric Oxide, Temperature, and Mixture Fraction in Hydrogen Jet Flames*, Combust. Flame, 104 (1996), pp. 288-299.

[141] M. Flury and M. Schlatter, *Laser Doppler Velocimetry Measurements in Turbulent Non Premixed Hydrogen/Helium Flames,* http://www.ca.sandia.gov/TNF, Institute of Energy Technology, ETH, Zuerich.

[142] R. S. Barlow and J. H. Frank, *Piloted CH4/Air Flames C, D, E, and F - Release 2.0,* http://www.ca.sandia.gov/TNF, Sandia National Laboratories, 2003.

[143] C. Schneider, A. Dreizler, J. Janicka and E. P. Hassel, *Flow field measurements of stable and locally extinguishing hydrocarbon-fuelled jet flames*, Combust. Flame, 135 (2003), pp. 185-190.

[144] W. Meier, O. Keck, V. Jörres and W. Stricker, Raman Measurements of Temperature and Major Species Concentrations in Confined Swirling Natural Gas Flames, http://www.tu-darmstadt.de/fb/mb/ekt/tecflam/Web-TECFLAM.html, EKT Data Archive, DLR Stuttgart.

[145] C. Schneider, A. Dreizler and J. Janicka, Velocity Measurements in Unconfined and Confined Strongly Swirling Natural Gas Flames, http://www.tu-darmstadt.de/fb/mb/ekt/tecflam/ekt.html, EKT Data Archive, Technische Universität Darmstadt.

[146] M. Garcia-Villalba, J. Fröhlich and W. Rodi, Large Eddy Simulation of oscillating flow in combustion chambers, SFB 606, Project A6, status report, University of Karlsruhe, 2003.

[147] J. U. Schlüter and H. Pitsch, Consistent boundary conditions for integrated LES/RANS simulations: LES outflow conditions, Annual Research Briefs 2001, Center for Turbulence Research, 2001.

[148] P. R. van Slooten and S. B. Pope, *Application of PDF Modeling to Swirling and Nonswirling Turbulent Jets*, Flow, Turbulence and Combustion, 62 (1999), pp. 295-333.

[149] R. J. Kee, J. Warnatz and J. A. Miller, A Fortran computer code package for the evaluation of gas phase viscosities, conductivities, and diffusion coefficients, SAND83-8209, Sandia National Laboratories, 1983.

Curriculum vitae

Personal:

Name:	Mario
Family name:	Baburić
Date of birth:	05.11.1977
Place of birth:	Karlovac
Citizenship:	Croatian
E-mail:	Mario.Baburic@fsb.hr
URL:	http://powerlab.fsb.hr/mbaburic

Education:

1983-1995	Elementary and high school in Karlovac
1995-2000	Faculty of Mechanical Engineering and Naval Architecture (FMENA), University of Zagreb
2001-2005	PhD study at FMENA, University of Zagreb

Professional:

2001-…	Research assistant at the Power Engineering Department, FMENA; Teaching assistance in under-graduate courses 'Numerical Methods in Engineering' and 'Numerical Methods in Aerodynamics II' at FMENA

Foreign languages:

English, German – fluent (written and spoken)

Spanish, French – communication level

Osobni podaci:

Ime:	Mario
Prezime:	Baburić
Datum rođenja:	05.11.1977
Mjesto rođenja:	Karlovac
Državljanstvo:	Hrvatsko
E-mail:	Mario.Baburic@fsb.hr
URL:	http://powerlab.fsb.hr/mbaburic

Obrazovanje:

1983-1995	Osnovna škola 'Braća Ribar' u Skakavcu. Opća gimnazija u Karlovcu.
1995-2000	Fakultet strojarstva i brodogradnje (FSB), Sveučilište u Zagrebu
2001-2005	Doktorski poslijediplomski studij na FSB, Sveučilište u Zagrebu

Profesionalne aktivnosti:

2001-…	Stručni suradnik na Katedri za energetska postrojenja, FSB; Asistent u nastavi na dodiplomskom predmetu 'Numeričke metode u inženjerstvu' te 'Numeričke metode u zrakoplovstvu II' na FSB-u

Strani jezici:

Engleski, njemački – vrlo dobro (pisanje i govor)

Španjolski, francuski – komunikacijski nivo

BIBLIOGRAFSKA KARTICA:

UDK:	662.61:519.876.5
Ključne riječi:	Nepredmiješano izgaranje, stacionarni laminarni flamelet model, varijabla napretka reakcije, pretpostavljeni kondicionalni momenti, tabeliranje kemije, difuzijski plamenovi, metoda diskretnog prijenosa topline zračenjem, hibridni model turbulencije
Znanstveno područje:	Tehničke znanosti
Znanstveno polje:	Strojarstvo
Institucija:	Fakultet strojarstva i brodogradnje (FSB), Sveučilište u Zagrebu
Mentor:	Doc.dr.sc. Neven Duić
Broj stranica:	174
Broj slika:	76
Broj tablica:	1
Broj referenci:	149
Datum usmene obrane:	14.10.2005
Članovi povjerenstva:	Prof.dr.sc. Željko Bogdan (FSB, Zagreb) Doc.dr.sc. Neven Duić (FSB, Zagreb) Prof.dr.sc. Antun Galović (FSB, Zagreb) Prof.dr.sc. Pedro Coelho (Instituto Superior Técnico, Lisbon) Dr.sc. Reinhard Tatschl (AVL AST, Graz)

ISBN 953-6313-75-8

Zahvale

Ovaj rad je nastao na Katedri za energetska postrojenja, Fakulteta strojarstva i brodogradnje, Sveučilišta u Zagrebu.

Iskreno se zahvaljujem doc.dr.sc. Nevenu Duiću, mom mentoru i supervizoru, čovjeku koji me je uveo u zanimljivi svijet računalne dinamike fluida i koji je omogućio ovaj rad. Njegova konstantna podrška, vrijedni komentari i strpljivost su mi značajno pomogli prilikom izrade ove disertacije.

Kvaliteti ovog rada su značajno doprinijele brojne diskusije koje sam imao s kolegama i suradnicima na Katedri za energetska postrojenja – doc.dr.sc. Danielom Rolph Schneiderom, Milanom Vujanovićom i Markom Banom. Zahvaljujem se na njihovoj potpori i stalnoj dostupnosti.

Mnogo sam naučio o računalnoj dinamici fluida kroz diskusije i suradnju s kolegama iz AVL AST-a – dr.sc. Peterom Prieschingom, dr.sc. Reinhardom Tatschlom, dr.sc. Branislavom Basarom, i drugima – kojima se također zahvaljujem. Zahvaljujem se AVL AST Zagreb na financijskoj potpori projekta u sklopu kojeg je nastao ovaj rad. Posebne zahvale u tom pogledu idu direktoru AVL AST-a Zagreb mr.sc. Goranu Mirkoviću.

Zahvaljujem se i ostalim članovima povjerenstva, prof.dr.sc. Željku Bogdanu, prof.dr.sc. Antunu Galoviću i prof.dr.sc. Pedru Coelhu, na vrijednim sugestijama prilikom čitanja prve verzije ove disertacije. Njihovi primjedbe i komentari značajno su doprinijeli boljoj kvaliteti ovog rada.

Zahvaljujem se mojoj obitelji na stalnoj podršci i strpljivosti.

Zagreb, rujan 2005

Mario Baburić

Obilježje obrazovanog uma je da ostaje zadovoljan stupnjem preciznosti koje priroda problema dopušta te da ne traži egzaktnost u situacijama u kojima je samo aproksimacija moguća.

Aristotel

Sadržaj

Predgovor VII
Sažetak VIII
Ključne riječi X
Popis oznaka XI
Popis slika XX
Popis tablica XXV
1 Uvod 1
1.1 Motivacija i generalni pregled 1
1.2 Pregled trenutnih istraživanja 3
1.3 Hipoteza i izgled rada 11
1.4 Doprinos rada 13
2 Matematičko modeliranje 15
2.1 Jednadžbe očuvanja 15
2.1.1 Očuvanje mase 15
2.1.2 Očuvanje količine gibanja 15
2.1.3 Očuvanje momenta količine gibanja 16
2.1.4 Očuvanje energije 17
2.1.5 Transport skalarne veličine 17
2.2 Termo-kemijske relacije 18
2.3 Modeliranje izgaranja 21
2.3.1 Fenomenološka perspektiva 21
2.3.2 Pristup očuvanja skalara 24
2.3.3 Stacionarni laminarni *flamelet* model 25
2.3.4 Varijabla napretka reakcije 29
2.3.5 Nisko-dimenzijski prostori 30
2.3.6 Nova procedura tabeliranja kemijskih vrsta 33
2.3.6.1 Predmiješani plamenovi 33
2.3.6.2 Nepredmiješani plamenovi 35

2.3.6.3 Mješovita formulacija 37
2.4 Modeliranje prijenosa topline zračenjem 38
2.4.1 Jednadžba prijenosa topline zračenjem 38
2.4.2 Metoda diskretnog prijenosa topline zračenjem 39
2.4.3 Svojstva participirajućeg medija 43
2.5 Statistički opis 44
2.5.1 Turbulentne i kemijske skale 44
2.5.2 Reynoldsovo i Favreovo usrednjavanje 47
2.5.3 Usrednjene jednadžbe: održanje mase, momenta i energije 48
2.5.4 Modeliranje turbulencije 49
2.5.5 Statistički momenti praćenih skalara 52
2.5.6 Interakcija turbulencije i izgaranja 53
2.5.7 Usrednjena vrijednost brzine skalarne disipacije 56
2.5.8 Pretpostavljeni kondicionalni momenti varijable napretka reakcije 57
3 Numerička procedura 61
3.1 Kemijski pretprocesor 62
3.1.1 Modeli s pretpostavkom beskonačno brzih kemijskih reakcija 62
3.1.2 Numeričko rješenje *flamelet* jednadžbi 64
3.1.2.1 Diskretizacija konačnim razlikama 64
3.1.2.2 Rješenje sustava diferencijalno-algebarskih jednadžbi 67
3.1.2.3 PDF integracije 67
3.1.3 Implementacija CSC rješavača 70
3.1.3.1 Struktura rješavača 70
3.1.3.2 Kemijski rješavač 71
3.1.3.3 PDF rješavač 73
3.2 Rješavač toka fluida 75
3.2.1 Integralna forma transportnih jednadžbi 75
3.2.2 Diskretizacija kontrolnim volumenima 76
3.2.3 Procedura rješavanja 79
3.2.4 Implementacija modela izgaranja 82
3.3 Implementacija DTRM-a 84

4 Vodikov mlazni plamen ... 87
4.1 Eksperimentalna konfiguracija ... 87
4.2 Numerička konfiguracija ... 88
4.3 Rezultati ... 90
4.3.1 Pretabulirani kemijski profili ... 90
4.3.1.1 SLFM baza ... 90
4.3.1.2 FPI baza ... 92
4.3.1.3 SLFM baza (varijabla napretka reakcije) ... 94
4.3.2 Širenje mlaza ... 96
4.3.3 Adijabatski vs. neadijabatski profili ... 97
4.3.4 Usporedba modela izgaranja ... 100
5 Metanov mlazni plamen ... 107
5.1 Eksperimentalna konfiguracija ... 107
5.2 Numerička konfiguracija ... 108
5.3 Rezultati ... 110
5.3.1 Pretabulirani kemijski profili ... 110
5.3.2 Adijabatski vs. neadijabatski profili ... 116
5.3.3 Usporedba modela izgaranja ... 118
6 TECFLAM ložište ... 127
6.1 Eksperimentalna konfiguracija ... 127
6.2 Numerička konfiguracija ... 129
6.3 Rezultati ... 131
6.3.1 Pretabulirani kemijski profili ... 131
6.3.2 Rezultati simulacije ... 135
7 Zaključak ... 143
Prilog A – Korak-po-korak izvod *flamelet* jednadžbi ... 147
Prilog B – *Flamelet* model s diferencijalnom difuzijom ... 153
Prilog C – Stacionarni laminarni 1D predmiješani plamen ... 157
Popis literature ... 159
Curriculum vitae ... 173

Predgovor

Računalna dinamika fluida (eng. *computational fluid dynamics* – CFD) je postala široko upotrebljavana metodologija u znanosti, tehnologiji i u industrijskom dizajnu, kao i u svim drugim prilikama u kojima se susreću složeni fizikalni procesi s fluidima. To uključuje turbulentni tok fluida, procese izgaranja, procese prijenosa topline zračenjem, prijenos topline i mase, i dr. Kao takav CFD je postao snažan alat u rukama inženjera koji pokušava poboljšati efikasnost opreme ili ubrzati cjelokupni ciklus dizajna nekog proizvoda.

Povećana upotreba CFD metoda u energetskom sektoru dobila je na snazi zbog više razloga. Očekuje se da će fosilna goriva ostati glavni izvor energije u 21. stoljeću te je zbog toga bitno na odgovarajući način modelirati procese izgaranja. CFD se javlja kao nezaobilazno sredstvo dok se pokušavaju točno predvidjeti važni fenomeni vezani za izgaranje, kao što su emisija polutanata, efikasnost procesa izgaranja, i sl. Često se u istom paketu javlja i potreba za točnim predviđanjem prijenosa topline zračenjem te se i to mora uzeti u obzir.

Znanstvena istraživanja u polju izgaranja i prijenosa topline zračenjem su značajno uznapredovala tijekom posljednjih nekoliko desetljeća te su razvijeni pouzdani matematički modeli. Međutim, preveliki zahtjevi za računalnom snagom često sprečavaju efikasnu primjenu mnogih tih modela u praktičnim industrijskim primjerima. Zbog toga je često potrebno postići kompromis između točnosti simulacije i dostupnosti računalne snage.

Pristup tabeliranja kemijskih vrsta u pretprocesoru prilikom modeliranja izgaranja nameće se kao legitiman kandidat za postizanje gore navedenih kompromisa. Procedura u kojoj se proračun kemijskih vrsta odvaja od proračuna toka fluida vrlo često rezultira u efikasnoj metodologiji u usporedbi sa slučajem u kojem se oba proračuna simultano odvijaju. To omogućava primjenu detaljnih kemijskih mehanizama u simulacijama izgaranja, uz prihvatljive zahtjeve za računalnom snagom. Modeliranje prijenosa topline zračenjem je problem *per se* te je često zahtjevnije od modeliranja izgaranja. Pojednostavljeni modeli prijenosa topline zračenjem se najčešće koriste u industrijskim aplikacijama.

Sažetak

Pristup tabeliranja kemijskih vrsta u pretprocesoru, baziran na izračunima predmiješanih ili nepredmiješanih plamenova, je razvijen i implementiran u ovome radu. U tu svrhu je razvijen računalni program u kojem se vrše proračuni kemijskih vrsta u pretprocesoru. Modeliranje izgaranja tijekom same CFD procedure se sastoji u izračunu prostorne raspodijeljenosti različitih skalara – udjela smjese goriva i varijable napretka reakcije – dok su udjeli pojedinih kemijskih vrsta funkcijski povezani sa ta dva skalara ovisno o modelu. Razvijeni modeli su primijenjeni u proračunima izgaranja na tri konfiguracije s različitim stupnjem složenosti. Rezultati simulacije su uspoređeni s eksperimentalno dobivenim vrijednostima te s rezultatima simulacije dobivenih upotrebom standardnog stacionarnog laminarnog flamelet modela. Simulirane konfiguracije su bile sljedeće – prorijeđeni vodikov slobodni mlazni plamen (H_2/He-zrak plamen B), pilotirani metanov slobodni mlazni plamen (Sandia plamen D) te zatvoreni plamen prirodnog plina u TECFLAM ložištu. U sva tri slučaja su upotrijebljeni detaljni kemijski mehanizmi. Metoda diskretnog prijenosa topline zračenjem je implementirana u CFD program (FIRE), a da bi se prilikom modeliranja obuhvatio proces prijenosa topline zračenjem. Također, upotrebljen je hibridni model turbulencije prilikom modeliranja protoka fluida te su njegovi rezultati uspoređeni s rezultatima dobivenim upotrebom standardnog k-ε modela turbulencije.

Nova procedura tabeliranja kemijskih vrsta se pokazala kao mogućom alternativom standardnom laminarnom *flamelet* modelu. U slučaju predmiješanih plamenova moguće je obuhvatiti cjelokupno područje od hladnog miješanja reaktanata do ravnotežnog izgaranja, što dopridonosi povećanoj univerzalnosti ovog modela. NO je dobro predviđen modelom baziranom na predmiješanim plamenovima, dok se upotreba nepredmiješanih plamenova pokazala lošim izborom u ovome slučaju. Modeli bazirani na varijabli napretka reakcije pokazali su se manjkavima u područjima s bogatom smjesom goriva u slučaju Sandia plamena D te je potrebno ostvariti daljnji napredak u ovome pogledu. Uključivanje modeliranja prijenosa topline zračenjem pokazalo se bitnim za točni izračun temperaturnih polja. U općem slučaju, hibridni model turbulencije pokazao se boljim od standardnog k-ε modela.

A pre-tabulated chemistry approach, based on premixed and non-premixed laminar flamelets, was developed and implemented in this work. A devoted software application was developed in order to perform the chemistry calculations and tabulations in the pre-processor step. The combustion modelling in CFD procedure consisted of calculating the field distribution for a set of tracking scalars – mixture fraction and reaction progress variable – while the chemistry composition space was functionally related to these two scalars, depending on a model. The developed models were applied in the combustion simulations of three different configurations of varying complexity. The results were compared to experimental data and to the stationary laminar flamelet model predictions. The simulated configurations were following – a diluted hydrogen jet flame (H_2/He-air flame B), a piloted methane jet flame (Sandia flame D) and a confined natural gas bluff-body stabilised flame (TECFLAM). Detailed chemical mechanisms were used in all cases. The discrete transfer radiation method was implemented into the CFD code (FIRE) in order to account for thermal radiation. The impact of radiation inclusion was investigated. A hybrid turbulence model was applied and its predictions were compared to those obtained with a standard k-ε model.

A new tabulation procedure based on the normalised reaction progress variable has shown as a possible alternative to the standard stationary laminar flamelets methodology. In the case of premixed flamelets a complete range from the cold-mixing up to the chemical equilibrium can be covered, making this approach promising if searching towards more universal combustion models. NO was reasonably well predicted when using premixed flamelets, while non-premixed flamelets have shown as inappropriate in this particular situation. The reaction progress variable based models, as implemented in this work, have shown deficient in the fuel-rich regions in the methane jet configuration (Sandia flame D), making a space for possible improvements in this respect. The inclusion of radiation modelling has shown important for accurate temperature predictions. In general, the hybrid turbulence model has shown as superior to the standard k-ε turbulence model.

Ključne riječi

Nepredmiješano izgaranje, stacionarni laminarni *flamelet* model, varijabla napretka reakcije, pretpostavljeni kondicionalni momenti, tabeliranje kemijskih vrsta, difuzijski plamenovi, metoda diskretnog prijenosa topline zračenjem, hibridni model turbulencije

Non-premixed combustion, stationary laminar flamelet model, reaction progress variable, presumed conditional moments, chemistry pre-tabulation, diffusion flames, discrete transfer radiation method, hybrid turbulence model

Popis oznaka

Rimske oznake	Opis	Jedinica
a	Faktor apsorpcije	1/m
$a_1 \ldots a_5$	Stehiometrijski faktori	kmol
a_P, a_k	Koeficijenti matrice $\mathbf{A}_\phi$	Promjenjiva
A	Površina;	m^2
	Koeficijenti u izrazu za brzinu skalarne disipacije	1/s
$A_1^{(i)}, \ldots, A_4^{(i)}$	Faktori u flamelet jednadžbama	Promjenjiva
$\boldsymbol{A}_l$	Koeficijent u Arrheniusovom izrazu za reakciju l	Promjenjiva
$\mathbf{A}_\phi$	Matrica koeficijenata linearnog sustava jednadžbi	Promjenjiva
b	Rubna ploha	
b_ε	Polinomski faktor u WSGGM	Promjenjiva
c	Normalizirana varijabla napretka reakcije	
c_p	Specifični toplinski kapacitet pri konstantnom tlaku	J/(kgK)
c_{pk}	Specifični toplinski kapacitet kemijske vrste k	J/(kgK)
$C_1^{(k)}, \ldots, C_8^{(k)}$	Diskretizacijski koeficijenti	Promjenjiva
C_R	Konzervacijski korektivni faktor	
$C_{\varepsilon 1}, C_{\varepsilon 1}, C_s$	Konstante modela turbulencije	
C_μ	Strukturni parametar	
C_χ	Konstanta	
d	Promjer	m
D	Toplinska difuzivnost	m^2/s
Da	Damköhlerov broj	
D_{ij}	Komponenta tenzora brzine posmičnog naprezanja	1/s
D_c	Molekularna difuzivnost varijable napretka reakcije	m^2/s
D_k	Molekularna difuzivnost kemijske vrste k	m^2/s

D_Z	Molekularna difuzivnost udjela smjese goriva	m^2/s
E_l	Aktivacijska energija reakcije l	J/kmol
f_i	Kartezijeva komponenta vektora volumnih sila	$kg/(m^2s^2)$
$f_{k,i}$	f_i kemijske vrste k	$kg/(m^2s^2)$
F	Kumulativna distribucijska funkcija	
h	Specifična entalpija	J/kg
h_k	Specifična entalpija kemijske vrste k	J/kg
$\Delta h^0_{f,k}$	Specifična entalpija formacije kemijske vrste k	J/kg
i'	Intenzitet zračenja	W/m^2
I	Broj sivih plinova	
I_∞	Relativni intenzitet slobodne turbulencije	
J	Stupanj polinoma u WSGGM	
k	Kinetička energija turbulencije;	m^2/s^2
	Indeks diskretne točke	
$k_{f,b}$	Povratni koeficijent brzine kemijske reakcije l	Promjenjiva
$k_{f,l}$	Koeficijent brzine kemijske reakcije l	Promjenjiva
$K_{C,l}$	Konstanta ravnoteže kemijske reakcije l	
l	Duljina;	m
	Dužinska mjera	m
L	Radijus cilindra	m
Le_k	Lewisov broj kemijske vrste k	
$\dot{m}$	Maseni tok	kg/s
M	Molarna masa smjese plinova	kg/kmol
M_k	Molarna masa kemijske vrste k	kg/kmol
$\vec{n}$	Jedinični normalni vektor	
n_j	Kartezijeva komponenta jediničnog normalnog vektora	
n_Z	Broj diskretnih točaka u prostoru udjela smjese goriva	
N	Broj	

p	Tlak	Pa
P	Suma parcijalnih tlakova apsorbirajućih kemijskih vrsta;	Pa
	Izvorni član u jednadžbi za turbulentnu kinetičku energiju;	kg/(ms^3)
	Funkcija gustoće vjerojatnosti;	
	Računalna točka u formulaciji kontrolnih volumena	
q	Volumni izvorski član	Promjenjiva
q_j	Kartezijeva komponenta vektora provođenja topline	W/m^2
Q	Bezdimenzijski toplinski tok	
r	Radijus	m
$\vec{r}_P$	Pozicijski vektor računalne točke	
$\vec{r}_{Pb}$	Vektor što spaja računalnu točku sa rubnom plohom b	
$\vec{r}_{Pj}$	Vektor što spaja dvije susjedne računalne točke preko plohe j	
R	Plinska konstanta smjese plinova;	J/(kgK)
	Radijus	m
$\boldsymbol{R}$	Univerzalna (molarna) plinska konstanta ($\boldsymbol{R}$ = 8314.4)	J/(kmolK)
Re	Reynoldsov broj	
$\vec{s}$, $\vec{s}$ ', $\vec{s}_{kk}$	Jedinični vektori smjera	
S	Udaljenost;	m
	Površina	
Sc	Schmidtov broj	
$\overline{S}_k$	Izvorni član zračenja u kontrolnom volumenu k	W
S_L	Brzina laminarnog plamena	m/s
t	Vrijeme	s
t_i	Kartezijeva komponenta vektora površinskih sila	N/m
T	Temperatura	K
u	Brzina;	m/s
	Normalna brzina	m/s
u_j	Kartezijeva komponenta vektora brzine	m/s

$\widetilde{u_i"u_j"}$	Komponenta tenzora Reynoldsovih naprezanja	m^2/s^2
V	Volumen	m^3
V_j	Kartezijeva komponenta vektora diferencijalne brzine	m/s
$V_{k,j}$	Kartezijeva komponenta vektora diferencijalne brzine kemijske vrste k	m/s
w	Tangencijalna brzina	m/s
x	Koordinata	
x_j	Kartezijeva koordinata	m
X_k	Molni udio kemijske vrste k	kmol/kmol
$[X_k]$	Koncentracija kemijske vrste k	$kmol/m^3$
$[X_{k,e}]$	Ravnotežna koncentracija kemijske vrste k	$kmol/m^3$
Y	Maseni udio	
Y_c	Maseni udio varijable napretka reakcije	
Y_k	Maseni udio kemijske vrste k	
Z	Udio smjese goriva	
Z_m	Lokalna koordinata na fronti plamena	

Grčke oznake	**Opis**	**Jedinica**
α, β	Argumenti beta funkcije	
α_ε	Težinski faktori u WSGGM	
α_ϕ	Podrelaksacijski faktor nepoznanice ϕ	
β_l	koeficijent u Arrheniusovom izrazu za kemijsku reakciju l	Promjenjiva
Γ	Difuzijski koeficijent	Promjenjiva
$\Delta^-_{(k)}, \Delta^+_{(k)}$	Razlika prema unatrag i unaprijed na prostornoj mreži	
ε	Emisijski faktor; Brzina disipacije turbulentne kinetičke energije	m^2/s^3
η	Kolmogorovljeva dužinska mjera	m

Θ	Polarni kut	rad
λ	Koeficijent toplinske provodnosti	W/(mK)
μ	Molekularna dinamička viskoznost	Pas
μ_t	Turbulentna viskoznost	kg/(ms)
ν	Molekularna kinematička viskoznost	m^2/s
$\nu'_{k,l}$	Stehiometrijski koeficijent reaktanta	kmol
$\nu''_{k,l}$	Stehiometrijski koeficijent produkta	kmol
ξ	$\xi \equiv \chi_{st}$ ili $\xi \equiv c$	1/s or –
ρ	Gustoća	kg/m^3
σ	Prandtlov broj;	
	Stefan-Boltzmann-ova konstanta ($\sigma = 5.6696 \cdot 10^{-8}$)	$W/(m^2K^4)$
σ_{ij}	Komponenta tenzora naprezanja	N/m^2
σ_s	Koeficijent raspršivanja	1/m
τ	Vrijeme	s
τ_{ij}	Tangencijalna komponenta tenzora naprezanja	N/m^2
Υ_k	Kemijska vrsta k	
ϕ	Ekvivalentni omjer;	
	Reaktivni skalar;	
	Vektor nepoznanica	Promjenjiva
φ	Specifični skalar	Promjenjiva
Φ	Fazna funkcija raspršivanja	1/sr
Φ_{ij}	Komponenta tenzora naprezanja uslijed gradijenta tlaka	m^2/s^3
χ	Brzina skalarne disipacije	1/s
$\dot{\omega}_c$	Izvorni član varijable napretka reakcije	$kg/(m^3s)$
$\dot{\omega}_k$	Izvorni član kemijske vrste k	$kg/(m^3s)$
Ω	Prostorni kut	sr
Ω_l	Brzina kemijske reakcije l	$1/(m^3s)$

Donji znakovi	**Opis**
0	Referentno stanje;
	Početak inkrementalnog puta;
	Integralna mjera
b	Crno tijelo;
	Rub
c	Kemijski;
	Centar
CV	Kontrolni volumen
DI	Disipacijski-inercijalni
e	Gašenje
eq	Jednadžba
EI	Energijski-inercijalni
Ext	Gašenje
faces	Plohe
F	Gorivo
h	Specifična entalpija
ii	Indeks sivog plina
in	Dolazni
j	Indeks plohe kontrolnog volumena
k	Kinetička energija turbulencije
(k)	Indeks diskretne točke
kk	Indeks zrake
max	Maksimum
min	Minimum
n	Pozicija ulaza zrake u kontrolni volumen
$n+1$	Pozicija izlaza zrake iz kontrolnog volumena
net	Neto
out	Izlazni
O	Oksidant

p	Pilot
rays	Zrake
reac	Reakcija
R	Zračenje
s	Skalirani
spec	Kemijska vrsta
st	Stehiometrijski
S	Izvorski član
t	Turbulentan
thresh	Granična vrijednost
vis	Vidljivi
w	Zid
ε	Brzina disipacije turbulentne kinetičke energije
η	Kolmogorovljeva mjera
λ	Valna duljina
ϕ	Nepoznanica (skalar)
φ	Specifična skalarna vrijednost

Gornji znakovi	**Opis**
'	Reynoldsovo odstupanje od srednje vrijednosti
"	Favreovo odstupanje od srednje vrijednosti
$^-$	Reynoldsova srednja vrijednost
$^\sim$	Favreova srednja vrijednost
$\overline{\vert Z}$	Kondicionalna srednja vrijednost
Eq	Ravnoteža
Ext	Gašenje
(i)	Rješenje u trenutnoj iteraciji
$(i-1)$	Rješenje iz prethodne iteracije
(k)	Indeks diskretne točke
Mix	Miješanje

(*new*)	Rješenje linearnog sustava jednadžbi
n_Z	Broj diskretnih točaka u polju udjela smjese goriva

Matematički znakovi	**Opis**
$e = 2.718281828\ldots$	
erfc^{-1}	Inverzna komplementarna funkcija greške
exp	Eksponencijalna funkcija ($\exp(x) \equiv e^x$)
sign	Predznak ($+$ ili $-$)
B	Beta funkcija
Γ	Gama funkcija
$\prod$	Produkt
$\sum$	Suma
δ_{ij}	Kroneckerov tenzor
$\pi = 3.141592654\ldots$	

Skraćenice	**Opis**
1D, 2D, 3D	Jedan-, dva-, tri-dimenzijski
ASCII	Standardni američki kod za izmjenu informacija
AMG	Algebarski multi-grid
CDS	Shema središnje derivacije
CFD	Računalna dinamika fluida
CGS	Rješavač linearnog sustava baziran na kvadratima konjugiranih gradijenata
CGSTAB	Stabilizirani CGS
CK	Metoda k -distribucije
CMC	Metoda kondicionalnih momenata
CSC	Kemijski pretprocesor
DNS	Direktna numerička simulacija
DOM	Metoda diskretnih ordinata
DTRM	Metoda diskretnog prijenosa topline zračenjem
EMST	Metoda minimalnog Euklidovog naprezanja

FGM	Metoda *flamelet*-a
FPI	Metoda produženja ILDM -a
FVM	Metoda konačnih volumena
GUI	Grafičko sučelje
HTM	Hibridni model turbulencije
IEM	Interakcija izmjenom sa srednjom vrijednosti
ILDM	Intrinzični nisko-dimenzijski prostori
ISAT	*In situ* adaptivno tabeliranje
JPDF	Zajednička funkcija gustoće vjerojatnosti
LDV	Laser-Dopplerova metoda mjerenja brzine
LES	Large-eddy simulacija
LFM	Laminarni flamelet model
LIF	Laserski inducirana fluorescencija
LU	Gornji donji
MC	Curlovo miješanje
MIX	Miješanje
ODE	Obična diferencijalna jednadžba
OTM	Model zračenja u optički slabo apsorbirajućem mediju
PCM	Pretpostavljeni kondicionalni momenti
PDF	Funkcija gustoće vjerojatnosti
RANS	Usrednjene Navier-Stokesove jednadžbe po Reynoldsu
RMS	Korijen kvadrata srednje vrijednosti
RPV	Varijabla napretka reakcije
SIMPLE	Poluimplicitna metoda povezivanja jednadžbi brzine i tlaka
SLFM	Stacionarni laminarni flamelet model
SNB	Statistička uskopojasna metoda
TNF	Turbulentni nepredmiješani plamen
TRI	Interakcija turbulencije i zračenja
WSGGM	Model težinske sume sivih plinova

Popis slika

Slika 1 – Brzina propagacije laminarnog plamena H_2/He-zrak (gorivo: H_2 80%, He 20% – molni udjeli, 295 K; oksidant: zrak, 294 K) 22
Slika 2 – Slobodni mlazni nepredmiješani plamen sa po jednim ulazom goriva i zraka.. 23
Slika 3 – Temperaturni flamelet profili plamena H_2/He-zrak (gorivo: H_2 80%, He 20% – molni udjeli, 295 K; zrak: 294 K)..... 28
Slika 4 – Adijabatski temperaturni profili iz baze predmiješanih plamenova (razrijeđeni metan (25% CH_4, 75% zrak – molni udjeli)/zrak): a) T-x graf; b) T_{burnt}-Φ graf31
Slika 5 – Adijabatski temperaturni profili iz baze predmiješanih plamenova (razrijeđeni metan (25% CH_4, 75% zrak – molni udjeli)/zrak): a) T-Y_{CO2} graf; b) T-Y_{CO2}+Y_{CO}+Y_{H2O} graf..... 32
Slika 6 – Varijabla napretka reakcije (baza predmiješanih plamenova)..... 33
Slika 7 – O_2 profili (baza predmiješanih plamenova) za sustav H_2/He-zrak (gorivo: H_2 80%, He 20% – molni udjeli, 295 K; zrak: 294 K) 34
Slika 8 – Varijabla napretka reakcije (baza nepredmiješanih plamenova)..... 35
Slika 9 – O_2 profili (baza nepredmiješanih plamenova) za sustav H_2/He-zrak (gorivo: H_2 80%, He 20% – molni udjeli, 295 K; zrak: 294 K) 36
Slika 10 – Maksimalni maseni udjeli NO, razrijeđeni metan (25% CH_4, 75% zrak – molni udjeli)/zrak plamen: mješovita formulacija i predmiješani plamenovi 37
Slika 11 – Apsorbirajući, raspršivajući i emitirajući medij [115]..... 39
Slika 12 – Praćenje zraka (2D) 40
Slika 13 – Diskretizacija hemisfere oko rubne plohe 42
Slika 14 – Kaskada turbulentne energije (Kolmogorovljeva kaskada)..... 44
Slika 15 – Usrednjeni profil..... 47
Slika 16 – Oblici β-PDF funkcije za različite vrijednosti parametara $\tilde{\boldsymbol{Z}}$ i $\widetilde{\boldsymbol{Z''^2}}$ 55
Slika 17 – H_2O profili (sustav H_2-zrak; povećano u blizini stehiometrije): Model 1-stupanjske ireverzibilne reakcije i ravnotežni model..... 63
Slika 18 – Mreža za metodu konačnih razlika (1D) 64

Slika 19 – Integrirani (pretpostavljeni β-PDF) adijabatski temperaturni profili (χ_{st} **= 0.01** s^{-1}) za plamen H_2/He-zrak (gorivo: H_2 80%, He 20% – molni udjeli, 295 K; zrak: 294 K) – vidi Sl. 3 69
Slika 20 – Struktura CSC rješavača 70
Slika 21 – Struktura CSC rješavača: kemijski rješavač 72
Slika 22 – Struktura CSC rješavača: PDF rješavač 74
Slika 23 – Diskretizacija prostorne domene u kontrolne volumene (2D) 76
Slika 24 – Kontrolni volumen (proizvoljni polihedron) 77
Slika 25 – Implementacija modela izgaranja (shema) 83
Slika 26 – Konačni cilindar 84
Slika 27 – Bezdimenzijski toplinski tok vs. bezdimenzijska pozicija na zidu za različiti broj zraka (optička debljina **aL = 1.0**) 85
Slika 28 – Bezdimenzijski toplinski tok vs. bezdimenzijska pozicija na zidu za različite optičke debljine **aL** (48(4x12) zraka) 86
Slika 29 – Konfiguracija vodikovog plamena 87
Slika 30 – Računalna mreža (vodikov plamen; vertikalni aksijalni presjek uzduž osi) ... 88
Slika 31 – SLFM (standardni) baza (vodikov plamen) 91
Slika 32 – FPI baza (vodikov plamen) 93
Slika 33 – SLFM (RPV) baza (vodikov plamen) 95
Slika 34 – Radijalni profili usrednjene aksijalne brzine na poziciji x/l_{vis}=1/8 i x/l_{vis}=3/8 (vodikov plamen; k-ε; adijabatski) 96
Slika 35 – Aksijalni profili uzduž osi (vodikov plamen; adijabatski vs. DTRM; k-ε vs. HTM): a) Usrednjena temperatura; b) Usrednjeni maseni udio H_2O 97
Slika 36 – Aksijalni profili uzduž osi (vodikov plamen; adijabatski vs. DTRM; k-ε vs. HTM): a) Usrednjeni maseni udio smjese goriva; b) RMS masenog udjela smjese goriva 98
Slika 37 – Radijalni profili na poziciji x/l_{vis}=3/8 (vodikov plamen; adijabatski vs. DTRM; k-ε vs. HTM): a) Usrednjena temperatura; b) Usrednjeni maseni udio H_2O 98
Slika 38 – Radijalni profili usrednjene aksijalne brzine na poziciji x/l_{vis}=1/8 i x/l_{vis}=3/8 (vodikov plamen; k-ε vs. HTM; neadijabatski) 99

Slika 39 – Radijalni profili na poziciji x/l_{vis}=3/8 (vodikov plamen; neadijabatski; k-ε vs. HTM): a) Usrednjeni maseni udio smjese goriva; b) RMS masenog udjela smjese goriva 99
Slika 40 – Radijalni profili momenata masenog udjela smjese goriva (usrednjena vrijednost i RMS) na različitim aksijalnim pozicijama (vodikov plamen; neadijabatski; HTM) 101
Slika 41 – Aksijalni profili usrednjenih vrijednosti temperature i masenih udjela različitih kemijskih vrsta (vodikov plamen; uzduž osi; neadijabatski; HTM) 103
Slika 42 – Parametri tabulacije (vodikov plamen): a) $\overline{\chi}_{st}$ (jed. 91), SLFM baza; b) $\overline{c}$ (jed. 100), FPI baza 104
Slika 43 – Radijalni profili usrednjenih vrijednosti temperature i masenih udjela različitih kemijskih vrsta na poziciji x/l_{vis}=1/4 (vodikov plamen; neadijabatski; HTM) 105
Slika 44 – Radijalni profili usrednjenih vrijednosti temperature i masenih udjela različitih kemijskih vrsta na poziciji x/l_{vis}=3/4 (vodikov plamen; neadijabatski; HTM) 106
Slika 45 – Konfiguracija metanovog plamena 107
Slika 46 – Računalna mreža (metanov plamen; vertikalni aksijalni presjek uzduž osi). 108
Slika 47 – Profili brzine na ulazu (metanov plamen) 109
Slika 48 – Predmiješani plamen razrijeđenog metana (25% CH_4, 75% zrak – molni udjeli)/zraka: a) Brzina propagacije laminarnog plamena; b) Temperatura produkata izgaranja 111
Slika 49 – SLFM (standardni) baza (metanov plamen) 112
Slika 50 – FPI baza (metanov plamen) 113
Slika 51 – SLFM (RPV) baza (metanov pamen) 114
Slika 52 – Mješovita baza (metanov plamen) 115
Slika 53 – Aksijalni profili usrednjene temperature uzduž osi (metanov plamen; adijabatski vs. DTRM; k-ε vs. HTM) 116
Slika 54 – Aksijalni profili uzduž osi (metanov plamen; adijabatski vs. DTRM; k-ε vs. HTM): a) Usrednjeni maseni udio CO_2; b) Usrednjeni maseni udio H_2O 117
Slika 55 – Radijalni profili usrednjene aksijalne brzine (metanov plamen; DTRM; k-ε vs. HTM) na različitim aksijalnim pozicijama (metanov plamen) 118

Slika 56 – Aksijalni profili (uzduž osi) momenata masenog udjela smjese goriva (usrednjena vrijednost i RMS) (metanov plamen)..... 119
Slika 57 – Radijalni profili momenata masenog udjela smjese goriva (usrednjena vrijednost i RMS) na različitim aksijalnim pozicijama (metanov plamen)..... 120
Slika 58 – Radijalni profili usrednjene temperature na različitim aksijalnim pozicijama (metanov plamen) 121
Slika 59 – Aksijalni profili (uzduž osi) usrednjenih vrijednosti masenih udjela različitih kemijskih vrsta (metanov plamen)..... 122
Slika 60 – Radijalni profili usrednjenih vrijednosti masenih udjela različitih kemijskih vrsta na poziciji x/d=30 (metanov plamen) 124
Slika 61 – Radijalni profili usrednjenih vrijednosti masenih udjela različitih kemijskih vrsta na poziciji x/d=60 (metanov plamen) 125
Slika 62 – Ložište (TECFLAM) 128
Slika 63 – Konfiguracija gorionika (TECFLAM) 128
Slika 64 – Računalna mreža (TECFLAM; vertikalni aksijalni presjek uzduž osi)..... 129
Slika 65 – Profili usrednjene brzine zraka na izlazu iz gorionika (TECFLAM) 130
Slika 66 – SLFM (standardni) baza (TECFLAM)..... 132
Slika 67 – FPI baza (TECFLAM)..... 133
Slika 68 – SLFM (RPV) baza (TECFLAM)..... 134
Slika 69 – Radijalni profili usrednjenih aksijalnih (u) i tangencijalnih (w) brzina na različitim aksijalnim pozicijama (TECFLAM)..... 135
Slika 70 – Radijalni profili momenata masenog udjela smjese goriva na aksijalnim pozicijama x=20 mm i x=90 mm (TECFLAM) 136
Slika 71 – Aksijalni profili (uzduž osi) usrednjenog masenog udjela goriva (TECFLAM) 137
Slika 72 – Radijalni profili usrednjene temperature na aksijalnim pozicijama x=20 mm i x=90 mm (TECFLAM)..... 137
Slika 73 – Radijalni profil $\overline{c}$ (jed. (100); FPI) na aksijalnoj poziciji x=20 mm (TECFLAM)..... 138
Slika 74 – Radijalni profili masenih udjela različitih kemijskih vrsta na aksijalnoj poziciji x=20 mm (TECFLAM)..... 139

Slika 75 – Radijalni profili masenih udjela različitih kemijskih vrsta na aksijalnoj poziciji x=60 mm (TECFLAM)..... 140
Slika 76 – Radijalni profili masenih udjela različitih kemijskih vrsta na aksijalnoj poziciji x=120 mm (TECFLAM)..... 141

Popis tablica

Tablica 1 – Bilanca toplinskog toka zbog zračenja (metanov plamen) 117

1 Uvod

1.1 Motivacija i generalni pregled

Znanost turbulentnog izgaranja privlači pozornost brojnih istraživača u posljednjih nekoliko desetljeća [1]. Problemi očuvanja okoliša, stvaranje polutanata, kompetitivnost na tržištu energetskom opremom, novi koncepti energetske održivosti, i dr., samo se neki od razloga te pojačane pozornosti. Nadalje, očekuje se da će upotreba fosilnih goriva kroz 21. stoljeće igrati i dalje jednako važnu ulogu kao i danas [2, 3], što dodatno opravdava napore koji se ulažu u pojačano razumijevanje procesa izgaranja. Posebice se to odnosi na pojačanu potrebu za kontrolom emisija polutanata (NO_x, SO_x) u sektoru proizvodnje energije, te problem redukcije CO_2, a kako je naglašavano tijekom internacionalne debate o stakleničkim plinovima nakon 1970-ih [4]. Neki ostali sektori koji imaju koristi od boljeg razumijevanja procesa izgaranja su prijevoz, grijanje, automobilska industrija, zrakoplovstvo, i dr.

Dok se je u počecima istraživanja izgaranja uglavnom oslanjalo na eksperimentalne metode, upotreba računalne dinamike fluida (eng. *computational fluid dynamics* – CFD) [5, 6] u današnjim rješavanjima problema izgaranja se nametnula kao neizostavna praksa [7-12]. Međutim, kako se uz izgaranje simultano javljaju i drugi fizikalni problemi, cjelokupan problem matematičkog modeliranja postaje izrazito složen [13-16].

Turbulencija, koja je sama po sebi jedan složen nelinearni problem [17-19] čije modeliranje još uvijek nije u potpunosti riješeno, vrlo često se pojavljuje tijekom izgaranja u praktičnim ložištima. Uključivanje modeliranja izgaranja značajno otežava cjelokupnu proceduru rješavanja. Kompletno se područje prostornih i vremenskih skala uslijed izgaranja i turbulencije prostire preko više redova veličine te je njihovo direktno rješavanje (direktna numerička simulacija – DNS) [3, 15, 20] još uvijek nedostupno u praktičnim slučajevima zbog prevelikih zahtijeva za računalnom snagom [18, 21]. Međutim, ukoliko se računaju jednadžbe samo za usrednjene vrijednosti, dobiva se metoda kojom je moguće rješavati složene praktične probleme uz postojeće računalne resurse. Kako je Reynolds [22] bio prvi koji je izveo usrednjene Navier-Stokesove jednadžbe, ta metodologija rješavanja usrednjenih jednadžbi toka fluida se još naziva i

Reynolds averaged Navier-Stokes (RANS) metodologija. Zbog njene efikasnosti ona se najčešće upotrebljava u industrijskim aplikacijama danas [23], premda se sve više naglašavaju i problemi uslijed malog broja informacija koje ova metodologija pruža [24] u usporedbi s DNS metodom. Potrebno je i spomenuti da se s porastom dostupne računalne snage otvaraju i novi horizonti u modeliranju izgaranja, pri čemu se otvara prostor za primjenu naprednijih metoda simulacije tok fluida poput *large eddy simulation* (LES). Međutim, očekuju se da će upotreba RANS metoda u modeliranju toka fluida i izgaranja prevladavati još neko buduće vrijeme, barem kao dio neke nove hibridne procedure [25].

Uz probleme povezane s modeliranjem Reynoldsovih naprezanja i turubulentnih fluktuacija kod simulacija nereaktivnih tokova, glavna se nova poteškoća kod modeliranja izgaranja javlja prilikom usrednjavanja izvorskih članova u transportnim jednadžbama za usrednjene kemijske vrste. Izravni pristup usrednjavanja tih članova rezultira u brojnim novim korelacijama koje je potrebno modelirati u najjednostavnijem slučaju 1-stupanjske ireverzibilne reakcije ([20]), što se dodatno komplicira ako se primjene modeli izgaranja sa složenom kemijom. Dakle, zbog nepremostivih praktičkih poteškoća koje se javljaju u tom klasičnom pristupu, bilo je potrebno potražiti alternativne pravce modeliranja. Različiti modeli izgaranja različitog stupnja složenosti razvijeni su u posljednja dva desetljeća, od kojih su najpoznatiji laminarni flamelet model (eng. *laminar flamelet model* – LFM) [15, 26] i njegove varijacije, model kondicionalnih momenata (eng. *conditional moment closure* – CMC) [27], model baziran na rješavanju zajedničke funkcije vjerojatnosti (eng. *joint probability density function* – JPDF) [18, 28], i dr. Zbog različitog pristupa i polaznih točaka od kojih se krenulo prilikom razvijanja tih modela, oni se međusobno razlikuju u pogledu složenosti, točnosti, primjenjivosti, isl. Dakle, potreban je kompromis prilikom odlučivanja koji od postojećih model upotrijebiti u nekoj praktičnoj situaciji.

I na kraju, premda ne najmanje značajno, uključivanje modeliranja prijenosa topline zračenjem u cjelokupnu proceduru rješavanja nekog problema izgaranja je vrlo bitno, posebice u problemima od industrijskog značaja i u velikim ložištima [29]. To je naročito naglašeno u slučaju potrebe za točnim predviđanjem formacije polutanata poput NO_x-a, a koja jako ovisi o temperaturi. Međutim, zbog složenosti modeliranja procesa zračenja i

velikih zahtjeva za računalnim resursima, u industrijskoj primjeni su zaživjele samo najjednostavnije metode prijenosa topline zračenjem, premda se sve više i više naglašava potreba za uključivanjem i detaljnijeg prikaza zračenja, poput spektralne ovisnosti radijacijskih svojstava medija [30].

1.2 Pregled trenutnih istraživanja

Kao što je spomenuto prije, DNS brzo postaje neprihvatljiva metoda ako se pokušavaju rješavati praktični problemi (umjereno visoki do visoki Reynoldsovi bojevi). No, važnost DNS-a je uvijek bila naglašena prilikom rješavanja akademskih primjera (niski Reynoldsovi brojevi) gdje su se pokušavali razumjeti osnovni fenomeni vezani za tok fluida. Značajan dio istraživanja vezan uz korištenje DNS-a u reaktivnim tokovima odnosi se na fenomen diferencijalne difuzije između kemijskih vrsta [31, 32]. Kako se taj fenomen odvija na molekularnom nivou, DNS ostaje kao jedina metoda za dobivanje točnih rezultata simulacijom. Diferencijalna difuzija u izotropnoj, slabećoj turbulenciji istraživana je upotrebom DNS-a u [32], gdje je ustanovljeno da kondicionalne fluktuacije masenih udjela kemijskih vrsta imaju značajan utjecaj na diferencijalnu difuziju. Ta informacija je nadasve važna istraživačima koji se bave razvojem CMC modela izgaranja. Utjecaj diferencijalne difuzije na maksimalne vrijednosti temperature turbulentnog plamena vodik-zrak je istraživan uz pomoć 2D DNS-a u [33]. Tamo je pokazano da diferencijalna difuzija može promijeniti strukturu fronte plamena na način da su lakše kemijske vrste, poput H_2 i H, pomaknute prema područjima siromašnijim gorivom u usporedbi s rezultatima kad je diferencijalna difuzija zanemarena, dok se točka maksimalne temperature ne nalazi točno više u području stehiometrijskog omjera goriva i oksidanta. Egzaktna formulacija *flamelet* modela za nepredmiješano izgaranje koja uključuje u obzir efekte diferencijalne difuzije predstavljena je u [34]. Zajedno s nestacionarnim *flamelet* modelom, taj je model upotrebljen u simulaciji turbulentnog mlaznog nepredmiješanog plamena u [35].

Premda prednosti upotrebe LES metoda u reaktivnim tokovima nisu bile očite od samog početka [14], a kad se usporedi s RANS metodama, mnoga trenutna istraživanja se baziraju upravo na LES metodologiji. Veći se vrtlozi u turbulentnom strujanju fluida direktno rješavaju LES-om te su ti vrtlozi najznačajniji prilikom miješanja goriva i

oksidanta u primjerima nepredmiješanog izgaranja. Međutim, kako se samo izgaranje odvija na nivou najmanjih vrtloga, problem modeliranja i usrednjavanja izvorskih članova u transportnim jednadžbama za kemijske vrste ostaje i kod LES-a, slično kao i kod RANS-a [13]. Međutim, kako LES zahtijeva puno manje računalnih resursa od DNS-a te se može primijeniti i na grubljim mrežama u usporedbi s DNS-om, ta metodologija se već sada može primijeniti u simulacijama praktički relevantnih primjera izgaranja (umjereni Reynoldsovi brojevi), npr. [36-39]. Mora se spomenuti, međutim, da LES kao nestacionarna metoda je još uvijek značajno zahtjevnija za računalnim resursa od adekvatne RANS metode. To je posebice naglašeno prilikom simulacija ložišta koja rade u stacionarnom modu, a gdje je potrebno dovoljno dugo provesti nestacionarnu LES simulaciju da bi se dobili stacionarni rezultati simulacije i pravilna statistika u vremenu. S druge strane, upotreba LES-a u simulacijama nestacionarnih problema, poput motora s unutrašnjim izgaranjem, ili kad se proučavaju tranzijenti izgaranja poput samozapaljenja ili oscilacije plamena, nameće se kao metoda odabira [13]. LES simulacija pilotiranog nepredmiješanog plamena metana i zraka (Sandia plamen D [40]), zajedno s proširenim *flamelet* modelom [41], je opisana u [42-44]. Isti plamen je simuliran uz upotrebu CMC modela u [45]. Neke se druge zanimljive simulacije nepredmiješanog izgaranja upotrebom LES-a mogu naći u [46, 47]. Aplikacije u simulacijama predmiješanih plamenova mogu se pronaći, npr., u [48, 49].

Upotreba metoda baziranih na funkciji gustoće vjerojatnosti (eng. *probability density function* – PDF) u reaktivnim tokovima [28] pogodna je zato što se ne trebaju modelirati izvorski i konvektivni članovi u transportnim jednadžbama za kemijske vrste. Također, kako se PDF izravno računa te se ne pretpostavlja, kako je to slučaj kod CMC-a ili stacionarnog laminarnog *flamelet* modela (eng. *stationary laminar flamelet model* – SLFM), puno je manja je aproksimacija kada je u pitanju oblik PDF-a. Dva glavna problema u PFD formulaciji, međutim, su modeliranje člana molekularnog miješanja te razvoj precizne Monte Carlo procedure rješavanja [14, 16, 28]. Neki stariji modeli molekularnog miješanja, kao model interakcije s usrednjenom vrijednosti (eng. *interaction by exchange with the mean model* – IEM) ili modificirani Curlov model miješanja (eng. *the modified Curl mixing model* – MC), su se pokazali manjkavim u nekim situacijama zbog nelokalnosti u sastavu kemijskih vrsta. Da bi se uklonio taj

nedostatak razvijen je model minimalnog Euklidovog naprezanja (eng. *Euclidean minimum spanning tree* – EMST) [50]. Modeli miješanja su uspoređeni u [51, 52]. Pronađene su zanimljive razlike, posebice u slučajevima s lokalnim gašenjima plamena, a EMST se pokazao kao najbolji izbor. Serija pilotiranih plamena metana i zraka [40] je uspješno simulirana uz primjenu PDF/EMST modela u [53], pokazujući sposobnost ovog pristupa da obuhvati fenomene poput lokalnog gašenja i ponovnog zapaljenja plamena (posebice to vrijedi za plamen F iz spomenute serije). Plameni metana i zraka te složena konfiguracija TECFLAM ložišta [54] numerički su simulirani uz upotrebu transportne PDF metode u [55]. Modeli IEM i MC su korišteni za molekularno miješanje. No, kako je potrebno mnogo računalnih čestica (nominalno 100 u [53], npr.) da bi se na pravilan način prikazala statistika razvoja PDF-a, metode bazirane na PDF-u su računalno još uvijek jako zahtjevne, posebice u slučajevima s kompleksnim prikazom kemije. Da bi se smanjili zahtjevi PDF metoda za računalnim resursima razvijena je posebna metodologija tabeliranja podataka nazvana *in situ* adaptivna tabulacija (eng. *in situ adaptive tabulation* – ISAT) [56]. Prednost ovog pristupa u odnosu na klasični pristup izravnog integriranja tijekom simulacije je prikazan nedavno na slučaju jednostavne reakcijsko-difuzijske jednadžbe u [57], gdje su dobiveni faktori ubrzanja čak do pet puta. Čak još bolji faktori ubrzanja su dobiveni na jednom drugom primjeru s kompleksnim prikazom kemije [58]. Neke PDF simulacije stabiliziranih plamenova s detaljnom kemijom se mogu pronaći u [59]. Još valja spomenuti i najnoviji princip baziran na parcijalnom PDF-u, a kako je objavljeno u [60]. No, još je prerano govoriti o učinkovitosti ovog modela dok se ne isproba na dovoljnom broju konfiguracija te dok se ne usporedi s drugim modelima.

Metoda kondicionalnih momenata (eng. *conditional moment closure* – CMC) je neovisno razvijena od Bilgera i Klimenka početkom 1990-ih, te se njen detaljan opis i trenutni pregled mogu pronaći u [27]. Osnovna pretpostavka CMC-a je da su fluktuacije reaktivnih skalara (masenih udjela kemijskih vrsta i temperature) povezane samo s fluktuacijama jedne ključne veličine – a to je najčešće maseni udio smjese goriva u slučaju nepredmiješanog izgaranja. Fluktuacije kondicionalno usrednjenih vrijednosti skalara su se pokazale znatno manjima od fluktuacija nekondicionalno usrednjenih vrijednosti, a što je dovelo do manje izraženog problema modeliranja nelinearnih izvorskih članova u daljem slučaju. CMC modeliranje se obično provodi na nivou prvih

momenata (modeliranje prvog reda), kao, npr., u [61-63], premda se sve više i više naglašava potreba za modeliranjem na nivou drugih momenata (modeliranje drugog reda), posebice u slučajevima s većim kondicionalnim fluktuacijama [63]. U [63] je prikazana simulacija turbulentnog plamena metana i zraka (Sandia plamen D [40]) uz upotrebu CMC modela prvog reda. Tamo su korištena tri kemijska mehanizma različitog stupnja složenosti. Rezultati simulacije se dobro poklapaju s mjerenjima, a što se posebno odnosi na kondicionalnu statistiku. Rezultati simulacije NO-a su se pokazali izrazito osjetljivim na odabir kemijskog mehanizma te se CMC modeliranje drugog reda pokazalo izrazito značajnim u tom pogledu. Simulacije vodikovih i metanovih mlaznih plamena uz upotrebu CMC-a prvog reda mogu se pronaći u [61, 62, 64]. Modeliranje turbulencije na razini drugih momenata pokazalo se boljim od modeliranja na razini prvih momenata [61, 62], kao što se i očekivalo. CMC model drugog reda se preporuča za simulaciju plamenova s mogućnošću lokalnog gašenja [62]. Visina odvajanja plamena je uspješno simulirana u kod vodikovog plamena u [64]. Međutim, umjereno veliki računalni resursi koje zahtijeva CMC metoda su glavni razlozi zašto ta metoda nije našla široku primjenu u praktičnim primjerima. Ako se, npr., kondicionalna varijabla (maseni udio smjese goriva u nepredmiješanom izgaranju) diskretizira u N točaka, te ako se upotrebljeni kemijski mehanizam, npr., sastoji od M različitih kemijskih vrsta, ukupni broj kondicionalnih transportnih jednadžbi koji se treba riješiti je $N \times M$. Dakle, u slučaju da se koristi GRI-Mech 3.0 kemijski mehanizam [65] (53 kemijske vrste) i, recimo, 50 točaka u diskretizaciji kondicionalne varijable (68 korišteno u [63], npr.), ukupno bi trebalo računati 2650 transportnih jednadžbi za tijekom simulacije u sklopu CMC modela. Očito je da ovaj pristup postaje računalno preskup ukoliko se jednadžbe tok fluida simultano rješavaju sa spomenutim jednadžbama CMC-a. U praksi se to često rješava na način da se rješavanje spomenutih jednadžbi odvoji, te se također vrlo često CMC jednadžbe dodatno usrednjavaju u prostornim pravcima s malim kondicionalnim fluktuacijama (u poprečnim pravcima osno-simetričnih mlaznih plamenova u [61-63], npr.). Uključivanje CMM modeliranja drugog reda dodatno povećava računalne troškove. U [66] je pokazano da se javljaju dodatne 14 jednadžbe za varijance i kovarijance ako se samo dvije reakcije iz kemijskog mehanizma podvrgnu CMC modeliranju drugog reda.

No, mora se naglasiti da su dobiveni i precizniji rezultati s tom metodom u odnosu na CMC prvog reda.

Flamelet koncept pretpostavlja da se turbulentni nepredmiješani plamen sastoji od mnoštva malih izduženih laminarnih plamenova (*flamelet*-a) koji se nalaze na trenutnoj fronti plamena, a koja je sama određena tokom fluida i te stupnjem miješanja goriva i oksidanta [15, 67]. Tako dugo dok su ti plamenovi (*flamelet*-i) mali u usporedbi s najmanjim vrtlozima (Kolmogorovljevi vrtlozi) u turbulentnom polju tuka fluida, *flamelet* koncept je opravdan i u području definicije [16]. Jednom kada se odredi pozicija trenutne fronte plamena, svi se reaktivni skalari (maseni udjeli kemijskih vrsta i temperatura) u normalnom smjeru na frontu plamena mogu odrediti rješavajući *flamelet* jednadžbe [15]. U slučaju vrlo intenzivne turbulencije (niski Damköhlerovi brojevi), gdje su najmanji vrtlozi dovoljno mali i usporedivi s veličinom *flamelet*-a, dolazi do mogućnosti da *flamelet*-i nisu više samo nošeni tokom fluida, već tok fluida preko najmanjih vrtloga može promijeniti i njihovu strukturu. Primjena *flamelet* u tom slučaju je osporena, npr. u [68], što je dovelo do zanimljive polemike u akademskim krugovima nakon toga [69, 70].

Ako se *flamelet* jednadžbe rješavaju do stacionarnih rezultata te ako se ti profili koriste u simulacijama izgaranja, dobiva se stacionarni laminarni flamelet model (eng. *stationary laminar flamelet model* – SLFM) [15]. Glavna prednost SLFM-a u usporedbi klasičnih metoda gdje se modeliraju izvorski članovi kemijskih vrsta je u tome da se transportne jednadžbe za kemijske vrste uopće ne moraju rješavati tijekom same CFD simulacije. Prva dva momenta (usrednjena vrijednost i varijanca) masenog udjela smjese goriva se računa tijekom CFD procedure, dok se usrednjene vrijednosti masenih udjela pojedinih kemijskih vrsta dobivaju iz stacionarnih *flamelet* profila uz pomoć pretpostavljenog β-PDF oblika. Stacionarni *flamelet* profili se mogu dobiti odvojeno u pretprocesoru te se rezultati spremaju u tzv. PDF tablice. Tako stvorene PDF tablice se mogu koristiti u proizvoljnom broju naknadnih CFD proračuna. Mogući alternativni, ali računalno skuplji, pristup bi bio da se računaju transportne jednadžbe za kemijske vrste, a samo da se usrednjeni izvorski članovi u tim jednadžbama aproksimiraju iz PDF tablica [20].

Za razliku od CMC i transportnih PDF metoda, *flamelet* koncept je pogodan za uključivanje efekta diferencijalne difuzije između kemijskih vrsta. U [34] je izvedena

flamelet formulacija koja uključuje diferencijalnu difuziju za slučaj nepredmiješanog izgaranja. Također, da bi se ublažila originalna hipoteza SLFM-a, a gdje se pretpostavlja da su vremenske skale u *flamelet* jednadžbama puno manje od istih u turbulentnom polju, razvijena je formulacija koja uzima u obzir efekte nestacionarnosti na razvoj brzine skalarne disipacije, a kako je pokazano u [35]. Taj model je primijenjen u simulaciji nepredmiješanog plamena $CH_4/H_2/N_2$ i zraka, zajedno s modelom diferencijalne difuzije, pokazavši dobre rezultate kada se usporede s eksperimentalnim vrijednostima. Nestacionarni *flamelet* model je primijenjen u simulaciji pilotiranog nepredmiješanog plamena metana i zraka (Sandia plamen D [40]) u [71], te prilikom simulacije nisko-temperaturnog ložišta u [72].

Povijesni razvoj modela izgaranja išao je u pravcu glavne podjele procesa izgaranja na premiješane i nepredmiješane procese. U tom pogledu su razvijeni pouzdani modeli u svakoj od tih potkategorija. Međutim, u slučajevima gdje se javlja djelomično predmiješanje goriva i oksidanta prije izgaranja primjena gore spomenutih modela je upitna [16]. U nepredmiješanim plamenovima, npr., parcijalno predmiješanje se događa u područjima s lokalnim gašenjima i ponovnim zapaljenjima (rubni plamenovi), ili na visini odvajanja plamena (trostruki plamenovi). Kako ti fenomeni jako ovise o dinamici plamena, toplinskim tokovima, i dr., teško je očekivati od modela izgaranja unutar RANS koncepta da simulira te fenomene s dovoljnom točnošću. Međutim, napori se ulažu na poboljšanje modela tako da obuhvate neke glavne efekte kao što su globalno gašenje, i sl. Dok neki razvijeni modeli ne ovise o klasifikaciji plamenova u premiješane ili nepredmiješane, poput CMC ili PDF modela, neki drugi modeli, poput SLFM-a, ovise o toj klasifikaciji. Premda SLFM može djelomično obuhvatiti odstupanja od kemijske ravnoteže preko varijable brzine skalarne disipacije [15], ustanovljeno je da taj model ne može obuhvatiti efekte predmiješanja u područjima s lokalnim gašenjima, a koja su primijećena u nekim konfiguracijama plamenova.

Procedura tabeliranja kemijskih vrsta bazirana na kombiniranoj upotrebi predmiješanih i nepredmiješanih laminarnih plamenova u RANS simulaciji plamena metana i zraka je opisana u [47]. Kako se tamo koristi momenti podobno odabrane varijable napretka reakcije kao parametri tabeliranja, dok je istovremeno interakcija kemije i turbulencije obuhvaćena preko pretpostavljenog β-PDF-a, ova metodologija se

još naziva kao koncept pretpostavljenih kondicionalnih momenata (eng. *presumed conditional moments* – PCM). Kako se koriste i predmiješani i nepredmiješani plamenovi prilikom tabeliranja, moguće je ovim pristupom obuhvatiti cjelokupno područje mogućih realizacija miješanja reaktanata – od hladnog miješanja do ravnotežnog izgaranja, što čini ovaj pristup obećavajućim u pokušaju modeliranja turbulentnih nepredmiješanih plamenova sa različitim stupnjem parcijalnog predmiješanja reaktanata. Predmiješani laminarni plamenovi mogu se dobiti bilo upotrebom metode proširenja ILDM-a (eng. *intrinsic low-dimensional manifold*) (eng. *flame prolongation of ILDM* – FPI) [73] ili metodom *flamelet*-a (eng. *flamelet generated manifolds* – FGM) [74], dok se klasična SLFM baza može koristiti za nepredmiješane laminarne plamenove [15]. Upotreba metode tabeliranja pomoću FPI metode prilikom simulacije laminarnih i turbulentnih plamenova može se pronaći u [75-78]. Re-parametrizacija klasične SLFM baze uz pomoć varijable napretka reakcije je prikazana u [79].

Modeliranje prijenosa topline zračenjem u sklopu cjelokupne procedure modeliranja u CFD-u nije jednostavno zbog toga što medij nije nužno potreban za proces zračenja, dok je klasično CFD modeliranje bazirano na simulaciji toka medija po zakonima mehanike kontinuuma. Neke najranije metode prijenosa topline zračenjem, poput Hottelove zonalne metode [80] ili metode Monte Carlo [81], premda točne, nisu našle svoje mjesto u široj svakodnevnoj upotrebi zbog prevelikih računalnih resursa koje zahtijevaju. U tom pogledu su se izdvojile tri metode, a koje predstavljaju zadovoljavajući kompromis između točnosti i ekonomičnosti – metoda diskretnih ordinata (eng. *discrete ordinates method* – DOM) [82, 83], metoda konačnih volumena (eng. *finite volume method* – FVM) [84] te metoda diskretnog prijenosa topline zračenjem (eng. *discrete transfer radiation method* – DTRM) [85]. Uključivanje modeliranje zračenja je naročito važno u problemima sa značajnim toplinskim tokovima na rubovima (npr. zidovi ložišta), a gdje je točno modeliranje zračenja od vrlo velike važnosti za pravilno funkcioniranje cijelog aparata. Neke zanimljive primjene gore navedenih metoda zračenja u konfiguracijama sa složenom geometrijom mogu se pronaći, npr., u [86-90]. Međutim, važnost uključivanja modeliranja zračenja i u geometrijski jednostavnim konfiguracijama je naglašena, pogotovo ako se žele postići točni rezultati simulacije polutanata i drugih sporednih vrsta [29]. Također, ako se prate zaključci sa serije internacionalnih radionica o

nepredmiješanim plamenovima (eng. *international workshops on measurement and computation of turbulent nonpremixed flames* – TNF) [29] potrebno je uključiti modeliranje prijenosa topline zračenjem prilikom simulacija TNF plamenova kad god je to moguće.

Zbog jednostavnosti, računalne efikasnosti i lakoće implementacije u računalne programe, prvi model zračenja koji je korišten u simulacijama TNF plamenova je bio model zračenja u optički slabo apsorbirajućem mediju (eng. *optically thin model* – OTM). Neke rezultate simulacija s tim modelom je moguće pronaći u zbornicima na [29], dok se detaljni prikaz tog modela, zajedno s koeficijentima za izračune usrednjenih Planckovih apsorpcijskih faktora iz programa RADCAL-a [91] mogu pronaći u [92]. U [92] je OTM primijenjen zajedno s CMC modelom izgaranja u simulaciji razrijeđenih vodikovih mlaznih plamenova te se pokazao kao pogodan. Međutim, lošiji su rezultati dobiveni u naknadnim simulacijama plamenova s ugljikovodičnim gorivima te se pokazalo da OTM predviđa gubitke topline uslijed zračenja značajno većima nego što je to eksperimentalno izmjereno. U generalnom slučaju OTM se smatra jednostavnim, ali i nedovoljno točnim modelom prijenosa topline zračenjem. U [63] je korišten pod-model iz RADCAL-a [91] te CMC model izgaranja u simulaciji plamena metana i zraka (Sandia plamen D [40]), gdje se pokazalo da su gubitci topline zračenjem dobiveni simulacijom 2.45 puta veći od izmjerenih. To se pokazalo značajnim na rezultate formacije NO-a. Pretpostavljeno je da je medij optički siv, tj. da njegova apsorpcijska svojstva ne ovise o valnoj duljini. U [30] su uspoređeni modeli OTM i DOM na istoj konfiguraciji plamena (Sandia plamen D [40]) te su dobiveni slični rezultati, gdje su dobiveni toplinski tokovi veći od eksperimentalno izmjerenih. Međutim, u slučaju kad su uzete u obzir spektralne ovisnosti apsorpcijskih svojstava participirajućeg medija te interakcija turbulencije i zračenja (eng. *turbulence/radiation interaction* – TRI), dobiveni su puno bolji rezultati simulacije, kao što je pokazano u [93]. U tom članku su uspoređene mogućnosti DOM-a i DTRM-a kod simulacije toplinskih gubitaka na plamenu Sandia D [40], dok su spektralne ovisnosti apsorpcijskih svojstava medija uzete u obzir preko statistički uskopojasnog modela (eng. *statistical narrow-band* – SNB) te k-distribucijskog modela (eng. *k-distribution* –CK). DOM i DTRM su pokazali sličnu razinu točnosti, dok se prikladno TRI modeliranje pokazalo vrlo značajnim (utjecaj od oko 50% na toplinske gubitke dobivene

simulacijom). Međutim, također je naglašeno da su veliki zahtjevi za računalnom snagom povezani sa tim tipom proračuna gdje se uzimaju u obzir spektralne ovisnosti. U [94] su prikazane CFD simulacije kisikom obogaćenih turbulentnih nepredmiješanih plamenova, gdje su korišteni s*tate-of-the-art* modeli izgaranja, formacije i oksidacije čađe te prijenosa topline zračenjem. Još jednom je potvrđena važnost uključenja spektralne ovisnosti apsorpcijskih svojstava medija za dobivanje točnijih NO rezultata te raspodjele toplinskih tokova na rubovima. Interakcija zračenja i izgaranja je istraživana u [95]. Značajno veće vrijednosti čađe i NO-a su dobivene u slučaju kad je zanemareno zračenje.

1.3 Hipoteza i izgled rada

Pretpostavlja se da je metodom tabeliranja kemijskih vrsta u pretprocesoru moguće numerički simulirati slučajeve turbulentnog nepredmiješanog izgaranja različitih stupnjeva složenosti s dovoljnom točnošću. Kako se samo dvije ili tri dodatne transportne jednadžbe moraju rješavati tijekom CFD procedure kao dio modeliranja izgaranja, dok se kemijske vrste dobivaju interpolacijom iz izračunatih tablica u pretprocesoru, može se reći da je ovakav način numeričkog rješavanja efikasan ako ga usporedimo s klasičnim načinom modeliranja turbulentnog izgaranja u kojem se moraju rješavati brojne transportne jednadžbe pojedinih kemijskih vrsta. Kao takav, predloženi pristup računanja masenih udjela kemijskih vrsta u pretprocesoru već sada se može primijeniti u numeričkim simulacijama praktički relevantnih problema, bez ograničenja što se tiče složenosti kemije ili dostupnih računalnih resursa.

Dvije različite metode izgaranja, bazirane na RANS jednadžbama i tabeliranju kemijskih vrsta u pretprocesoru, implementirane su u ovome radu – klasični stacionarni laminarni *flamelet* model (SLFM) [15], te model baziran na modeliranju pretpostavljenih kondicionalnih momenata (eng. *presumed conditional moment* – PCM) [47]. Dok je primjena SLFM-a nominalno ograničena na slučajeve čistog nepredmiješanog izgaranja, PCM se po definiciji može koristiti u svim situacijama, neovisno o stupnju predmiješanosti goriva i oksidanta. Za proračun kemijskih vrsta u pretprocesoru razvijen je posebni računalni program – CSC rješavač [96]. Premda nije direktni predmet istraživanja u ovome radu, *flamelet* model koji uzima u obzir diferencijalnu difuziju među pojedinim kemijskim vrstama, a prema [34], također je implementiran u CSC

rješavač. Za proračun predmiješanih 1D plamenova, a kao dio PCM procedure, upotrebljen je prerađeni PREMIX program [97], dok su datoteke iz CHEMKIN II [98] programske baze korištene za izračune vezane uz kemijsku kinetiku te dobivanje termodinamičkih svojstava kemijskih vrsta i njihovih mješavina. Razvijena je nova procedura tabeliranja kemijskih vrsta u pretprocesoru bazirana na upotrebi normalizirane varijable napretka reakcije za premiješane, nepredmiješane te kombinaciju premiješanih i nepredmiješanih plamenova. U sklopu CSC programa također je implementiran modul za numeričku integraciju laminarnih profila izgaranja, a da bi se, uz pretpostavku β-PDF funkcije, dobile usrednjene vrijednosti masenih udjela kemijskih vrsta u funkcijskoj zavisnosti od statističkih momenata masenog udjela smjese. Za potrebe same računalne simulacije nepredmiješanih plamenova u ovom radu korišten je CFD rješavač FIRE [99]. Za proračun prijenosa topline zračenjem dodatno je implementirana metoda diskretnog prijenosa zračenjem (eng. *discrete transfer radiation method* – DTRM) [85, 100], zajedno s metodom sivih plinova (eng. *weighted sum of grey gases model* – WSGGM) [101], a kako je više opisano u [102].

Tri različite konfiguracije nepredmiješanih plamenova, s različitim stupnjevima složenosti (po redu), simulirane su u ovome radu – slobodni mlazni plamen vodika i zraka [103, 104], pilotirani slobodni mlazni plamen metana i zraka [40] (Sandia plamen D), te zatvoreni vrtložni plamen prirodnog plina i zraka u TECFLAM ložištu [54]. U slučaju vodikovog plamena kemijske reakcije su relativno jednostavne te je korišten detaljni kemijski mehanizam koji se sastoji od 37 kemijskih reakcija, uključujući kemijske reakcije nastajanja za NO. Za složenije slučajeve izgaranja s metanom i prirodnim plinom korišten je detaljni GRI-Mech 3.0 [65] kemijski mehanizam koji se sastoji od 325 kemijskih reakcija te obuhvaća 53 kemijske vrste. Dok su prve dvije konfiguracije relativno jednostavne što se tiče geometrije, TECFLAM plamen je dosta složeniji zbog vrtložnog strujanja zraka na ulazu. Budući da se taj plamen odvija unutar ložišta, modeliranje prijenosa topline zračenjem na zidove ložišta posebno je važno u ovom slučaju. Numerički rezultati su uspoređeni s dostupnim eksperimentalnim mjerenjima.

Izgled ovog rada je kako slijedi. Nakon uvoda su prikazane osnovne komponente matematičkog modela. U tom dijelu su, između ostalog, opisani osnovni zakoni očuvanja,

opis modela izgaranja i zračenja, te statistički opis. Numerička procedura je opisana nakon toga. U tom dijelu su opisani detalji implementacije CSC rješavača i DTRM modela zračenja. Komponente rješavača toka fluida su također ukratko opisane. Konačno su prikazani rezultati simulacija prethodno navedenih plamenova te njihova usporedba s eksperimentalnim podacima. Zaključci su navedeni na samom kraju.

1.4 Doprinos rada

Doprinos ovog rada se očekuje u unapređenju i nadopuni modernih trendova u modeliranju izgaranja koji se bave razvojem računalno efikasnih metoda primjenjivih u praktični relevantnim problemima te uz prihvatljive računalne troškove. Istovremeno se uvažava činjenica da postoje napredniji modeli izgaranja, no naglasak je na kompromisu između točnosti i računalne dostupnosti. Numerički alati razvijeni u ovom radu mogu pronaći direktnu primjenu u praktički relevantnim problemima izgaranja te istovremeno mogu poslužiti i kao solidna baza za daljnji znanstveno-istraživači rad u modeliranju procesa izgaranja. Očekivani doprinosi:

- Razvoj CSC rješavača:
    - Kemijski proračuni – Burke-Schumann model/ravnotežni model/stacionarni laminarni *flamelet* model (SLFM)/stacionarni laminarni *flamelet* model s diferencijalnom difuzijom
    - PDF integracije – strukturirane tablice spremne za upotrebu u CFD kalkulacijama
- Razvoj nove procedure tabeliranja kemijskih vrsta u pretprocesoru bazirane na normaliziranoj varijabli napretka reakcije:
    - Predmiješani plamenovi
    - Nepredmiješani plamenovi
    - Predmiješani/nepredmiješani plamenovi
- Implementacija modela diskretnog prijenosa topline zračenjem (DTRM) te njegova primjena, zajedno s hibridnim modelom turbulencije, u računalnim simulacijama nepredmiješanih plamenova različitog stupnja složenosti
- Modeliranje turbulentnog izgaranja primjenom pretpostavljenih kondicionalnih momenata varijable napretka reakcije

2 Matematičko modeliranje

2.1 Jednadžbe očuvanja

Osnovni sustav jednadžbi toka fluida može se dobiti primjenom zakona očuvanja na fluid koji prolazi kroz infinitezimalno maleni kontrolni volumen. Te jednadžbe će ukratko biti opisane u narednim poglavljima, dok je za dublji uvid i detalje izvoda tih jednadžbi potrebno konzultirati standardnu literaturu o tom području, npr. [5, 17, 105-108]. Kao što je to i uobičajeno u mehanici fluida, prihvaćen je Eulerov okvir zapisa jednadžbi. Kod indeksnog zapisivanja jednadžbi, osim ako nije rečeno drukčije, prihvaćena je Einsteinova konvencija o sumaciji po ponovljenim indeksima Kartezijevih komponenti [105, 109].

2.1.1 Očuvanje mase

Fluid što ulazi u kontrolni volumen kroz njegove granice ne može se uništiti te svaka promjena ukupnog protoka kroz granice kontrolnog volumena je praćena promjenom u gustoći fluida unutar kontrolnog volumena. Nakon bilanciranja, te pod pretpostavkom infinitezimalno malenog kontrolnog volumena, dobiva se diferencijalna forma[1] jednadžbe kontinuiteta:

$$\frac{\partial \rho}{\partial t} + \frac{\partial \left(\rho u_j \right)}{\partial x_j} = 0 \tag{1}$$

Jednadžba kontinuiteta vrijedi i za jednokomponentne i za višekomponentne sustave. Egzaktni izvod u slučaju višekomponentnog sustava je dan u [108].

2.1.2 Očuvanje količine gibanja

Prema drugom Newtonovom zakonu gibanja[2], brzina promjene količine gibanja čestice fluida koja se giba je jednaka ukupnoj sili (suma površinskih i volumnih sila) koje djeluju

[1] Pretpostavlja se da je gustoća ρ kontinuirano derivabilno polje bilo gdje unutar kontrolnog volumena V_k

[2] Newtonov drugi zakon formalno glasi: '*Ubrzanje objekta uslijed djelovanja neke sile je proporcionalno jačini sile, u istom smjeru kao i sila, te obrnuto proporcionalno masi objekta.*'

na tu česticu. U Eulerovom okviru zapisa, *i*-ta Kartezijeva komponenta vektora brzine se može izraziti kao:

$$\frac{\partial\left(\rho u_i\right)}{\partial t}+\frac{\partial\left(\rho u_i u_j\right)}{\partial x_j}=f_i+\frac{\partial \sigma_{ij}}{\partial x_j} \tag{2}$$

Članovi na desnoj strani jed. (2) predstavljaju volumne, odnosno površinske sile koje djeluju na fluid. Komponente vektora površinskih sila t_i se obično izražavaju preko komponenti tenzora naprezanja σ_{ij} kao $t_i=\sigma_{ij}n_j$. Ukupni tenzor naprezanja može se rastaviti na normalne i tangencijalne komponente:

$$\sigma_{ij}=-p\delta_{ij}+\tau_{ij} \tag{3}$$

Ukoliko je fluid izotropan i Newtonovski, komponente tenzora tangencijalnog naprezanja su povezane s tenzorom brzine deformacije $D_{ij}=\frac{1}{2}\left(\frac{\partial u_i}{\partial x_j}+\frac{\partial u_j}{\partial x_i}\right)$ kao:

$$\tau_{ij}=2\mu\left(D_{ij}-\frac{D_{kk}}{3}\delta_{ij}\right) \tag{4}$$

U jed. (4) se pretpostavlja da je koeficijent druge viskoznosti jednak nuli [108].

2.1.3 Očuvanje momenta količine gibanja

Zakon očuvanja momenta količine gibanja primijenjen na česticu fluida kaže da je ukupna brzina promjene momenta količine gibanja jednaka ukupnom momentu sila koje djeluju na tu česticu, a što na kraju rezultira u činjenici da je tenzor naprezanja simetričan, tj.:

$$\sigma_{ij}=\sigma_{ji} \tag{5}$$

Direktna posljedica simetričnosti tenzora naprezanja je ta da se taj tenzor može rastaviti na sferni i devijatorski dio, kao u jed. (3).

2.1.4 Očuvanje energije

Specifična entalpija (kemijska + osjetna) se obično uzima kao varijabla energije u višekomponentnim sustavima. Transportna jednadžba specifične entalpije višekomponentnog sustava, kao što je izvedeno u [20], može se zapisati kao:

$$\frac{\partial(\rho h)}{\partial t}+\frac{\partial(\rho h u_j)}{\partial x_j}=\frac{\partial p}{\partial t}+u_j\frac{\partial p}{\partial x_j}-\frac{\partial q_j}{\partial x_j}+\tau_{ij}\frac{\partial u_i}{\partial x_j}+\rho\sum_{k=1}^{N_{spec}}Y_k f_{k,j}V_{k,j}+q_h \tag{6}$$

Prva dva člana na desnoj strani predstavljaju izvore specifične entalpije uslijed vremenskog i prostornih gradijenata tlaka. Četvrti član predstavlja viskozno zagrijavanje, dok posljednji (šesti) član predstavlja izvor/ponor specifične entalpije uslijed vanjskog djelovanja, npr. zračenja. Član sa sumom na desnoj strani jed. (6) je uslijed volumnih sila koje djeluju na kemijske vrste što se gibaju diferencijalnim brzinama $\vec{V}_k$. Treći član na desnoj strani je divergencija vektora toplinskog toka $\vec{q}$ te obuhvaća sve oblike difuznog prijenosa topline. Vektor toplinskog toka se računa kao:

$$q_j=-\lambda\frac{\partial T}{\partial x_j}+\rho\sum_{k=1}^{N_{spec}}Y_k h_k V_{k,j} \tag{7}$$

2.1.5 Transport skalarne veličine

Opća jednadžba očuvanja nekog specifičnog skalara φ [5], npr. masenog udjela smjese goriva, se može zapisati kao:

$$\frac{\partial(\rho\varphi)}{\partial t}+\frac{\partial(\rho\varphi u_j)}{\partial x_j}=\frac{\partial}{\partial x_j}\left(\Gamma_\varphi\frac{\partial\varphi}{\partial x_j}\right)+q_\varphi \tag{8}$$

Da bi se riješila jed. (8) potrebno je još dodatno modelirati koeficijent difuzije Γ_φ i izvorski član q_φ. Ako je izvorski član q_φ jednak nuli, kaže se da je skalar konzervativna veličina. Ako skalar ne utječe na sam tok fluida (preko gustoće, npr.), kaže se da je skalar pasivan.

2.2 Termo-kemijske relacije

Specifična entalpija (kemijska + osjetna) kemijske vrste k u višekomponentnom sustavu s N_{spec} kemijskih vrsta, gdje je $k = 1, 2, \ldots, N_{spec}$, je definirana kao:

$$h_k = \Delta h^0_{f,k} + \int_{T_0}^{T} c_{pk}(T)\, dT \tag{9}$$

Prvi član na desnoj strani predstavlja specifičnu entalpiju formacije kemijske vrste k na referentnoj temperaturi T_0 (obično $T_0 = 298.15\ K$), te sadrži kemijski vezanu energiju. Vrijednosti specifičnih entalpija formacije se tabeliraju za neku referentnu temperaturu te su dostupne u literaturi, npr. [20, 108], ili u računalnim bazama, npr. [98]. Drugi član na desnoj strani jed. (9) predstavlja osjetnu entalpiju kemijske vrste k. Kada su poznate specifične entalpije pojedinih kemijskih vrsta, specifična entalpija mješavine plinova se dobiva kao:

$$h = \sum_{k=1}^{N_{spec}} Y_k h_k \tag{10}$$

Na sličan način se dobiva i specifični toplinski kapacitet mješavine:

$$c_p = \sum_{k=1}^{N_{spec}} Y_k c_{pk} \tag{11}$$

Pod pretpostavkom idealnog plina, gustoća i tlak su povezani jednadžbom stanja kao:

$$\rho = \frac{p}{RT} \tag{12}$$

U jed. (12) R predstavlja plinsku konstantu mješavine. Ona se dobiva iz univerzalne plinske konstante $\boldsymbol{R}$ i molarne mase mješavine M kao:

$$R = \frac{\boldsymbol{R}}{M} \tag{13}$$

Molarna masa mješavine se dobiva iz molarnih masa pojedinih kemijskih vrsta M_k i njihovih masenih udjela Y_k kao:

$$M = \frac{1}{\sum_{k=1}^{N_{spec}} \frac{Y_k}{M_k}} \tag{14}$$

Molni udjeli kemijskih vrsta se dobivaju kao:

$$X_k = Y_k \frac{M}{M_k} \tag{15}$$

U problemima kemijske kinetike često se upotrebljava molna koncentracija kemijskih vrsta, a koja je definirana kao:

$$[X_k] = \rho \frac{Y_k}{M_k} \tag{16}$$

Konvencija sumacije po ponovljenim indeksima nije primijenjena u jed. (15) i (16).

U transportnim jednadžbama za kemijske vrste (npr. *flamelet* jednadžbe) pojavljuju se izvorski članovi $\dot{\omega}_k$. Kemijska kinetika daje odgovore na vrijednosti tih članova. Postojeći podaci o brzinama kemijskih reakcija, a sakupljeni iz različitih izvora, obično su dani u obliku kemijskih mehanizama. Kemijski mehanizmi se sastoje od mnoštva elementarnih reakcija i propisanih koeficijenata brzine za svaku reakcije, najčešće u formatu računalnog paketa CHEMKIN II [98].

Neki općeniti set elementarnih kemijskih reakcija se može prikazati kao:

$$\sum_{k=1}^{N_{spec}} \nu'_{k,l} \Upsilon_k \underset{k_{b,l}}{\overset{k_{f,l}}{\rightleftarrows}} \sum_{k=1}^{N_{spec}} \nu''_{k,l} \Upsilon_k \tag{17}$$

Simbol Υ_k predstavlja kemijsku vrstu uključenu u elementarnoj kemijskoj reakciji l, npr. $\Upsilon_k \equiv CO_2$, dok $\nu'_{k,l}$ i $\nu''_{k,l}$ predstavljaju stehiometrijske koeficijente te reakcije. Ukupan broj elementarnih reakcija je N_{reac} ($l = 1,...,N_{reac}$). Simboli $k_{f,l}$ i $k_{b,l}$ predstavljaju koeficijente reakcije l prema unaprijed, odnosno prema unatrag.

Brzina elementarne reakcije l se računa kao:

$$\Omega_l = k_{f,l} \prod_{k=1}^{N_{spec}} [X_k]^{\nu'_{k,l}} - k_{b,l} \prod_{k=1}^{N_{spec}} [X_k]^{\nu''_{k,l}} \tag{18}$$

Nakon što su poznate brzine svih elementarnih reakcije u kemijskom mehanizmu, izvorski član pojedine kemijske vrste se računa kao:

$$\dot{\omega}_k = M_k \sum_{l=1}^{N_{reac}} \left(\nu''_{k,l} - \nu'_{k,l} \right) \Omega_l \tag{19}$$

Zbog očuvanja mase, suma izvorskih članova za sve kemijske vrste je jednaka nuli, tj. $\sum_{k=1}^{N_{spec}} \dot{\omega}_k = 0$.

Koeficijenti reakcije prema unaprijed $k_{f,l}$ se dobivaju iz Arrheniusovih izraza:

$$k_{f,l} = \boldsymbol{A}_l T^{\beta_l} \exp\left(-\frac{E_l}{\boldsymbol{R} T} \right) \tag{20}$$

Koeficijenti $\boldsymbol{A}_l$, β_l i E_l su zadani za svaku od elementarnih reakcija u kemijskom mehanizmu. Koeficijenti reakcije prema unatrag $k_{b,l}$ povezani su s koeficijentima prema unaprijed $k_{f,l}$ preko ravnotežnih konstanti $K_{C,l} = \frac{k_{f,l}}{k_{b,l}}$, a koje se dobivaju kao:

$$K_{C,l} = \prod_{k=1}^{N_{spec}} \left[X_{k,e} \right]^{\left(\nu''_{k,l} - \nu'_{k,l} \right)} = \frac{k_{f,l}}{k_{b,l}} \tag{21}$$

U jed. (21) $\left[X_{k,e} \right]$ predstavlja molnu koncentraciju kemijske vrste k u slučaju ravnoteže [98, 108].

2.3 Modeliranje izgaranja

2.3.1 Fenomenološka perspektiva

Postoje dva osnovna režima izgaranja s obzirom na stupanj predmiješanosti goriva i oksidanta – predmiješano i nepredmiješano izgaranje.

U slučaju predmiješanog izgaranja reaktanti (gorivo i oksidant) su pomiješani na molekularnom nivou prije ulaska u ložište te se za vrijeme izgaranja dešava jednoznačna tranzicija od reaktanata do produkata. Kao takvi, predmiješani plamenovi propagiraju u smjeru reaktanata. Fronta plamena je tanki tranzicijski sloj (0.1-1 mm, [16]) između reaktanata i produkata, s velikim temperaturnim i koncentracijskim gradijentima. Kako se reaktanti troše prilikom izgaranja, plamen propagira u smjeru reaktanata laminarnom brzinom plamena S_L [20]. Laminarna brzina plamena, struktura i debljina fronte plamena ovise o početnom stanju smjese reaktanata, tj. o temperaturi i sastavu. Vrlo važan parametar u predmiješanom izgaranju je ekvivalentni omjer goriva i oksidanta ϕ, a koji je definiran kao:

$$\phi = \left(\frac{Y_F}{Y_O} \right) \Bigg/ \left(\frac{Y_F}{Y_O} \right)_{st} \tag{22}$$

U slučaju stehiometrijske mješavine je $\phi = 1$, za $\phi < 1$ se kaže da je mješavina siromašna gorivom, dok za $\phi > 1$ je mješavina bogata gorivom. U slučajevima previše oksidanta ili previše goriva u mješavini, plamen neće moći propagirati, tj. neće biti izgaranja. Postoji područje mješavina $\phi_{\min} \le \phi \le \phi_{\max}$ u kojem je moguće izgaranje (propagacija plamena), te mješavine $\phi_{\min}$ i $\phi_{\max}$ predstavljaju granice zapaljivosti smjese. Slika 1 prikazuje promjenu laminarne brzine plamena H_2/He-zrak za različite vrijednosti ekvivalentnog omjera unutar granica zapaljivosti – a kako je dobiveno upotrebom PREMIX programa [97].

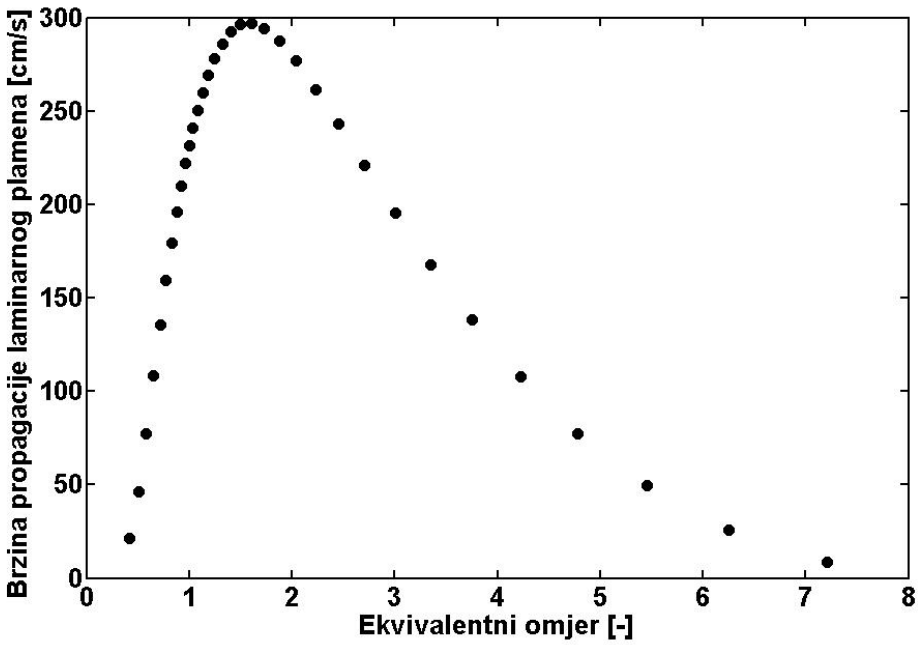

Slika 1 – Brzina propagacije laminarnog plamena H_2/He-zrak (gorivo: H_2 80%, He 20% – molni udjeli, 295 K; oksidant: zrak, 294 K)

U slučaju nepredmiješanog izgaranja gorivo i oksidant nisu predmiješani prije ulaska u ložište te oni odvojeno ulaze u ložište. Miješanje i izgaranje se istovremeno dešavaju tijekom izgaranja u ložištu kao dva kompetitivna procesa. Fronta plamena se stvara oko stehiometrijske iso-plohe miješanja goriva i oksidanta ($\phi = 1$). Kako se reaktanti (gorivo i oksidant) u ovom slučaju nalaze na različitim stranama od fronte plamena, mehanizmom difuzije se oni dovode do same fronte plamena gdje se održava izgaranje, te se zbog toga nepredmiješani plamenovi često nazivaju još i difuzijskim plamenovima.

Važna varijabla u nepredmiješanim plamenovima je udio smjese goriva Z. Ona predstavlja maseni udio svih kemijskih elemenata koji potječu od ulaza goriva. U konfiguraciji s po jednim ulazom goriva i oksidanta[3] udio smjese goriva je definiran kao:

$$Z = \frac{\dot{m}_F}{\dot{m}_F + \dot{m}_O} \tag{23}$$

Na ulazu goriva je $Z = 1$, dok je na ulazu oksidanta $Z = 0$. Plamen je lociran oko stehiometrijske iso-plohe udjela smjese goriva $Z = Z_{st}$ (Sl. 2).

[3] Može biti i više ulaza goriva/oksidanta u ložište, ali bitno je da svi ulazi goriva/oksidanta imaju jednak kemijski sastav.

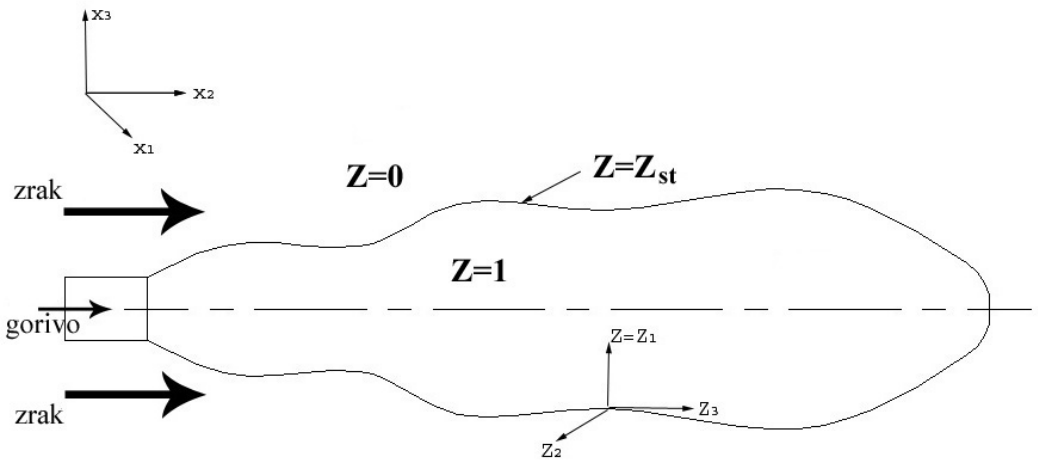

Slika 2 – Slobodni mlazni nepredmiješani plamen sa po jednim ulazom goriva i zraka

Maseni udio smjese goriva i ekvivalentni omjer povezani su sljedećom relacijom [15]:

$$\phi = \frac{Z\left(1-Z_{st}\right)}{\left(1-Z\right)Z_{st}} \tag{24}$$

U nepredmiješanom izgaranju ekvivalentni omjer ϕ treba sagledavati kao lokalnu mjeru pomiješanosti reaktanata koja se mijenja od točke do točke. Stehiometrijska iso-ploha $Z = Z_{st}$ se nalazi u točkama prostora gdje je $\phi = 1$. Neke druge definicije masenog udjela smjese goriva različite od jed. (23) se mogu pronaći u [15].

Za razliku od predmiješanih plamenova, nepredmiješani planovi ne propagiraju. Struktura i debljina fronte plamena jako ovise o lokalnom miješanju reaktanata. Zbog tog je dosta teže u slučaju nepredmiješanih plamenova konkretno odrediti relevantne prostorne i vremenske skale, a što nepredmiješane plamenove čini težim za modeliranje unutar statističkog okvira RANS-a od predmiješanih plamenova.

2.3.2 Pristup očuvanja skalara

Klasičan pristup u modeliranju izgaranja bi bio da se rješavaju transportne jednadžbe za svaku od kemijskih vrsta $k = 1, 2, \ldots, N_{spec}$ koje se pojavljuju:

$$\frac{\partial(\rho Y_k)}{\partial t} + \frac{\partial(\rho Y_k u_j)}{\partial x_j} = \frac{\partial}{\partial x_j}\left(\rho D_k \frac{\partial Y_k}{\partial x_j}\right) + \dot{\omega}_k \tag{25}$$

Fickov zakon se najčešće koriti za modeliranje molekularne difuzije, gdje su koeficijenti difuzivnosti D_k zadani za svaku od vrsta.

Međutim, kako je broj kemijskih vrsta koje sudjeluju u izgaranju, čak i kod najjednostavnijih goriva poput vodika ili metana, velik te se još povećava u slučaju primjene složenijih goriva, ovaj pristup rješavanja transportnih jednadžbi kemijskih vrsta ubrzo postaje računalno skup i neprihvatljiv. Dodatan problem u tom pristupu predstavlja i modeliranje usrednjenih izvorskih članova u turbulentnom slučaju te numerički problemi krutosti koji su povezani s procedurom zajedničkog rješavanja tih jednadžbi. Dakle, odvajanje proračuna kemijskih vrsta od proračuna toka fluida te tabeliranje kemijskih vrsta u pretprocesoru čine se kao nužni koraci da bi se dobila učinkovita numerička procedura modeliranja izgaranja.

U nepredmiješanom izgaranja najčešće se koristi konzervativni skalar masenog udjela smjese goriva. Njegova transportna jednadžba se može zapisati kao:

$$\frac{\partial(\rho Z)}{\partial t} + \frac{\partial(\rho Z u_j)}{\partial x_j} = \frac{\partial}{\partial x_j}\left(\rho D_Z \frac{\partial Z}{\partial x_j}\right) \tag{26}$$

Originalno je maseni udio smjese griva korišten još od vremena Burkea i Schumanna [110].

Prvi pokušaji da se sastavi kemijskih vrsta funkcijski vežu za varijablu masenog udjela smjese goriva su bili pod pretpostavkom beskonačno brzih kemijskih reakcija [15, 110]. U tom pogledu, Burke-Schumannovi i ravnotežni profili se mogu zapisati u formi:

$$T = T(Z) \qquad Y_k = Y_k(Z) \tag{27}$$

Međutim, kako se pod pretpostavkom beskonačno brzih kemijskih reakcija isključuju utjecaji toka fluida na lokalni kemijski sastav kod izgaranja, a gdje su vrste svugdje u

lokalnoj kemijskoj ravnoteži, složeniji fenomeni izgaranja, poput gašenja plamena, stabilizacije plamena, i dr., ne mogu se obuhvatiti ovim pristupom modeliranja izgaranja. U tom pogledu su potrebni modeli koji uzimaju u obzir lokalna odstupanja od ravnotežnog sastava.

2.3.3 Stacionarni laminarni *flamelet* model

Peters je razvio stacionarni laminarni *flamelet* model (SLFM) [15, 26, 67]. Postoje dva različita načina izvođenja *flamelet* jednadžbi – asimptotskom analizom ili lokalnom transformacijom koordinatnog sustava i primjenom argumentacije graničnog sloja. Ovdje će ukratko biti opisan ovaj drugi pristup (više detalja o izvodu se može pronaći u Prilogu A).

Osim jednadžbi kemijskih vrsta (jed. (25)), polazište prilikom izvoda *flamelet* jednadžbi je energijska jednadžba [15]:

$$\frac{\partial(\rho T)}{\partial t}+\frac{\partial(\rho T u_j)}{\partial x_j}=\frac{1}{c_p}\frac{\partial}{\partial x_j}\left(\rho c_p D\frac{\partial T}{\partial x_j}\right)+ \\ \frac{1}{c_p}\sum_{k=1}^{N_{spec}}\rho c_{pk} D_k\frac{\partial Y_k}{\partial x_j}\frac{\partial T}{\partial x_j}-\frac{1}{c_p}\sum_{k=1}^{N_{spec}}h_k\dot{\omega}_k+\frac{q_R}{c_p} \tag{28}$$

U jed. (28) D je toplinska difuzivnost, definirana kao $D=\dfrac{\lambda}{\rho c_p}$, dok je q_R izvorski član uslijed zračenja.

Lewisov broj kemijske vrste k je definiran kao omjer toplinske i masene difuzivnosti:

$$\mathrm{Le}_k=\frac{D}{D_k} \tag{29}$$

Uobičajena je pretpostavka u *flamelet* modelu da kemijske vrste i temperatura jednako difundiraju, tj. da su Lewisovi brojevi za sve vrste $\mathrm{Le}_k=1$. Ova pretpostavka je opravdana u turbulentnom strujanju, gdje je turbulentna difuzija za nekoliko redova veličine veća od molekularne te se molekularna difuzija može, u principu, zanemariti. Međutim, ukoliko je tok fluida laminaran, ili u područjima laminarnosti kod turbulentnog strujanja, efekti molekularne diferencijalne difuzije postaju izraženiji te ih je potrebno posebno modelirati [34, 35].

Uzimajući u obzir činjenicu da se kod nepredmiješanog izgaranja kemijske reakcije odvijaju u tankim slojevima gdje vladaju stehiometrijski uvjeti, te pod pretpostavkom da su gradijenti reaktivnih skalara u tangencijalnim smjerovima na iso-plohe udjela smjese goriva zanemarivi, mogu se dobiti *flamelet* jednadžbe s masenim udjelom smjese goriva kao nezavisnom prostornom koordinatom. To se postiže uvođenjem lokalnog koordinatnog sustava, kao što je pokazano na Sl. 2, te transformacijom jed. (25) i (28) za taj koordinatni sustav:

$$\begin{aligned} &Y_k\left(t,x_j\right)\rightarrow Y_k\left(\tau,Z_m\right) \\ &T\left(t,x_j\right)\rightarrow T\left(\tau,Z_m\right) \qquad\qquad m=1,2,3 \end{aligned} \tag{30}$$

Zbog prikladnosti, nova koordinata Z_1 je jednostavno označena kao Z jer se podudara sa smjerom gradijenta masenog udjela smjese goriva. U smjeru druge dvije koordinate Z_2 i Z_3 su promjene reaktivnih skalara pretpostavljene zanemarivim.

Pravila transformacije primijenjena na jed. (25) i (28) su:

$$\frac{\partial}{\partial t}=\frac{\partial}{\partial\tau}+\frac{\partial Z}{\partial t}\frac{\partial}{\partial Z} \qquad\qquad \frac{\partial}{\partial x_j}=\frac{\partial Z}{\partial x_j}\frac{\partial}{\partial Z} \tag{31}$$

Pod pretpostavkom jediničnih Lewisovih brojeva, te uzevši u obzir jed. (1) i (26), jednadžba kemijskih vrsta se dobiva kao:

$$\rho\frac{\partial Y_k}{\partial\tau}-\rho\frac{\chi}{2}\frac{\partial^2 Y_k}{\partial Z^2}-\dot{\omega}_k=0 \tag{32}$$

Bitna nova varijabla koja se pojavljuje u jed. (32) je brzina skalarne disipacije:

$$\chi=2D\left(\frac{\partial Z}{\partial x_j}\right)^2 \tag{33}$$

Brzina skalarne disipacije $\chi=\chi\left(Z\right)$ igra vrlo važnu ulogu u *flamelet* jednadžbama. Ona se može okarakterizirati kao inverzno vrijeme difuzije te kao takva ona određuje kako brzo reaktivni skalari difundiraju prema stehiometrijskim područjima. Povećanjem varijable brzine skalarne disipacije povećava se također i taj difuzni transport. Po definiciji (jed. (33)) brzina skalarne disipacije predstavlja funkcijsku vezu između toka

fluida i kemijskog opisa preko varijable masenog udjela smjese goriva. Da bi se riješila jed. (32), potrebno je poznavati funkcijsku ovisnost $\chi = \chi(Z)$. U [15] Peters izvodi tu ovisnost za dva različita slučaja nepredmiješanih plamenova – protustrujni nepredmiješani plamen, te 1D nestacionarni laminarni miješajući plamen. U oba slučaja dobila se ista funkcijska zavisnost brzine skalarne disipacije u obliku:

$$\chi(Z) = A \exp\left\{-2\left[\operatorname{erfc}^{-1}(2Z)\right]^2\right\} \tag{34}$$

Da bi se zaobišlo modeliranje koeficijenta A, a koji je zavisan od konfiguracije do konfiguracije, najčešće se upotrebljava parametrizirani oblik brzine skalarne disipacije prilikom proračuna kemijskih vrsta u pretprocesoru:

$$\chi(Z) = \chi_{st} \frac{\exp\left\{-2\left[\operatorname{erfc}^{-1}(2Z)\right]^2\right\}}{\exp\left\{-2\left[\operatorname{erfc}^{-1}(2Z_{st})\right]^2\right\}} \tag{35}$$

Vrijednost se brzine skalarne disipacije kod stehiometrijskih uvjeta χ_{st} mora zadati unaprijed[4] prilikom stvaranja *flamelet* tablica.

Na sličan način, te pod istim pretpostavkama kao i kod izvođenja jed. (32), dobiva se energijska jednadžba kao:

$$\rho\frac{\partial T}{\partial \tau} - \rho\frac{\chi}{2}\frac{\partial^2 T}{\partial Z^2} - \rho\frac{\chi}{2c_p}\frac{\partial T}{\partial Z}\frac{\partial c_p}{\partial Z} - \sum_{k=1}^{N_{spec}} \rho\frac{\chi}{2}\frac{c_{pk}}{c_p}\frac{\partial Y_k}{\partial Z}\frac{\partial T}{\partial Z} + \frac{1}{c_p}\sum_{k=1}^{N_{spec}} h_k\dot{\omega}_k - \frac{q_R}{c_p} = 0 \tag{36}$$

U SLFM konceptu se traže stacionarna rješenja jed. (32) i (36). Kao rezultat dobivaju se stacionarni laminarni *flamelet* profili u ovisnosti od masenog udjela smjese goriva i brzine skalarne disipacije kod stehiometrije:

$$T = T(Z, \chi_{st}) \qquad Y_k = Y_k(Z, \chi_{st}) \tag{37}$$

Za razliku od pretpostavke beskonačno brzih kemijskih reakcija, ovdje ta dodatna varijabla – brzina skalarne disipacije kod stehiometrije – mjeri utjecaj tok fluida na

[4] Obično χ_{st} varira od $\chi_{st} \to 0$ (blizu ravnoteže) do $\chi_{st} = \chi_{st,e}$ (blizu gašenja).

termo-kemijske profile te dopušta, do određene mjere, za odstupanjima od ravnotežnog kemijskog sastava.

Za $\chi \to 0$ se postižu *flamelet* profili vrlo slični ravnotežnim profilima. Povećanjem brzine skalarne disipacije povećava se i difuzija reaktivnih skalara prema stehiometrijskom području, te u određenom slučaju dovoljno velike vrzine skalarne disipacije dolazi do gašenja plamena zbog nemogućnosti održavanja kemijskih reakcija. Slika 3 prikazuje tri različita *flamelet* profila temperatura za različite vrijednosti brzine skalarne disipacije kod stehiometrijskih uvjeta χ_{st} (plamen H_2/He-zrak iz Poglavlja 4):

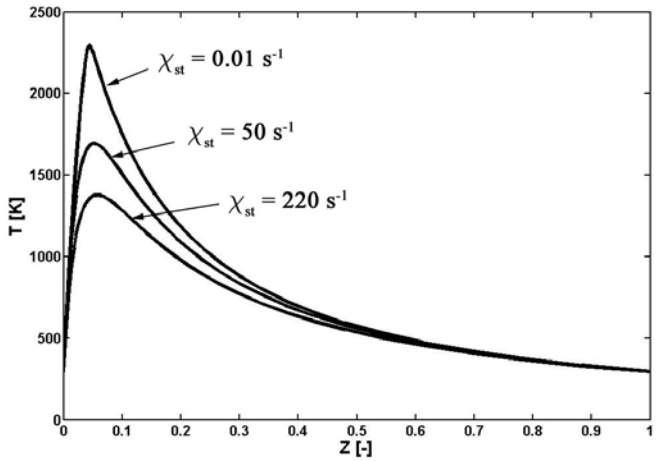

Slika 3 – Temperaturni flamelet profili plamena H_2/He-zrak (gorivo: H_2 80%, He 20% – molni udjeli, 295 K; zrak: 294 K)

Pitanje koje se postavlja kod *flamelet* modela je to da li je taj model sposoban obuhvatiti tranzijentne efekte poput lokalnog gašenja i ponovnog zapaljenja plamena? Generalno je stajalište da standardni *flamelet* model, a kako je prethodno opisan, nije za to sposoban. Također, sposobnost simulacije manjih vrsta, poput NO-a, pokazala se je slabom u [3, 71]. Zbog toga su naknadno predložena poboljšanja modela da bi se riješili spomenuti problemi. Nestacionarno *flamelet* modeliranje jedan je od mogućih načina, te su tim modelom u [71, 111] dobiveni poboljšani rezultati manjih vrsta. Proširenje modela koje uzima u obzir diferencijalnu molekularnu difuziju je dano u [34] (Prilog B). Izbor brzine skalarne disipacije kod stehiometrijskih uvjeta kao parametra tabeliranja kemijskih vrsta je najčešće okrivljavan za loše rezultate SLFM-a što se tiče sposobnosti simulacije manjih vrsta. U tom pogledu se trenutno razvijaju modeli koji, uz maseni udio smjese

goriva, uzimaju u obzir još jedan skalar, varijablu napretka reakcije, a koji bi trebao pomoći u uklanjanju spomenutih poteškoća [47, 73, 79].

2.3.4 Varijabla napretka reakcije

U svojoj doktorskoj disertaciji [79] Pierce uvodi varijablu napretka reakcije za parametrizaciju baze stacionarnih laminarnih *flamelet* profila. Transportna jednadžba varijable napretka reakcije glasi:

$$\frac{\partial\left(\rho Y_c\right)}{\partial t}+\frac{\partial\left(\rho Y_c u_j\right)}{\partial x_j}=\frac{\partial}{\partial x_j}\left(\rho D_c \frac{\partial Y_c}{\partial x_j}\right)+\dot{\omega}_c \tag{38}$$

Jed. (38) je formalno jednaka jed. (25). Obično se kao varijabla napretka reakcije odabire jedna ili linearna kombinacija više reprezentativnih kemijskih vrsta. Izvorski se član $\dot{\omega}_c$ računa prema jed. (19) za jednu ili linearnu kombinaciju više kemijskih vrsta, ovisno o odabiru varijable napretka reakcije.

Nadalje, uz postojeću bazu stacionarnih laminarnih *flamelet* profila u formi jed. (37), te odabirom varijable napretka reakcije tako da on monotono varira s brzinom skalarne disipacije kod stehiometrijskih uvjeta χ_{st}, Pierce predlaže ponovnu parametrizaciju postojeće baze novom varijablom $\chi_{st}^{*}=\chi_{st}^{*}\left(Z,Y_c\right)$, a koja je dobivena iz standardne *flamelet* baze, što dovodi do novog funkcijskog zapisa:

$$T=T\left(Z,Y_c\right) \qquad Y_k=Y_k\left(Z,Y_c\right) \tag{39}$$

Na ovaj se način, zapravo, parametar toka fluida χ_{st} zamjenjuje kemijskim parametrom Y_c, te se za ista *flamelet* rješenja dobiva nova funkcijska povezanost toka fluida i kemijskih vrsta. U općem slučaju je $\chi_{st}\neq\chi_{st}^{*}$, te kad se formalno izrazi [79], nova procedura parametriziranja podsjeća na dinamički odaziv termo-kemijskih profila na promjene u brzini skalarne disipacije, baš kao kod nestacionarnog *flamelet* modela.

Još uvijek je upitno hoće li ova nova procedura parametriziranja biti u stanju obuhvatiti složene fenomene gašenje/zapaljenja, ili pak mogućnost simulacije izgaranja u područjima s jakom deformacijom toka fluida, poput konfiguracije u [112], a gdje standardni SLFM daje loše rezultate?

2.3.5 Nisko-dimenzijski prostori

Zanimljive nove metode koje se baziraju na varijabli napretka reakcije te tabeliranju kemijskih vrsta u pretprocesoru su metoda *flamelet*-a (eng. *flamelet generated manifolds* – FGM) [74] te metoda produženja ILDM-a (eng. *flame prolongation of ILDM* – FPI) [73]. Obje te metode su bazirane na ideji intrinzičnih nisko-dimenzijskih prostora (eng. *intrinsic low-dimensional manifold – ILDM*) [113], ali s namjerom još veće uštede na računalnim troškovima. ILDM metoda je uvedena u [113] kao metoda redukcije kemijskog prikaza, a koja se bazira na ideji da su brzine nastajanja nekih kemijskih vrsta puno brže od brzina nastajanja nekih drugih vrsta, te na odvojenom tretiranju istih. U praksi se traži mali podskup tzv. 'sporih' kemijskih vrsta tako da se sve druge vrste i termodinamička svojstva mogu jednoznačno funkcijski prikazati u ovisnosti od prethodnih. Kemijske vrste iz tog malog podskupa čine koordinate nisko-dimenzijskog prostora u kojem se rasprostiru hiper-plohe po kojim su raspodijeljeni reaktivni skalari. Pitanje koje se postavlja je koji je to najmanji broj potrebnih koordinata u tom prostoru da bi se na pravilan način parametrizirali svi reaktivni skalari? Ukoliko je broj tih koordinata prevelik, računalni troškovi metode tabeliranja bi bili preveliki. Također se javlja problem ILDM-a sa malim brojem koordinata u područjima niskih temperatura s numerički krutom kemijskom kinetikom.

U FPI i FGM metodama se nisko-dimenzijski prostori stvaraju na osnovu rezultata 1D predmiješanih plamenova. U tom su pristupu čak dobro pokrivena i nisko-temperaturna područja [73], što čini ovaj pristup obećavajućim u pokušaju modeliranja fenomena gašenja/zapaljena u turbulentnom izgaranju. Nadalje, također su i transportni procesi uzeti u obzir kod tih metoda, za razliku od ILDM-a, preko rješenja 1D predmiješanih plamenova, a što omogućuje obuhvaćanje efekata diferencijalne molekularne difuzije prilikom tabeliranja [73].

Rješenja 1D predmiješanih plamenova mogu se dobiti proračunom slobodno propagirajućih predmiješanih plamenova uz pomoć PREMIX programa [97] (Prilog C) za različite vrijednosti ekvivalentnih omjera unutar granica zapaljivosti. Taj pristup je korišten u ovome radu. Slika 4 prikazuje adijabatske temperaturne profile slobodno propagirajućih plamenova metana i zraka (gorivo iz Sandia plamena D [40]). Maksimalne temperature su dobivene u blizini stehiometrijskih uvjeta ($\phi \approx 1$), kao što je i očekivano.

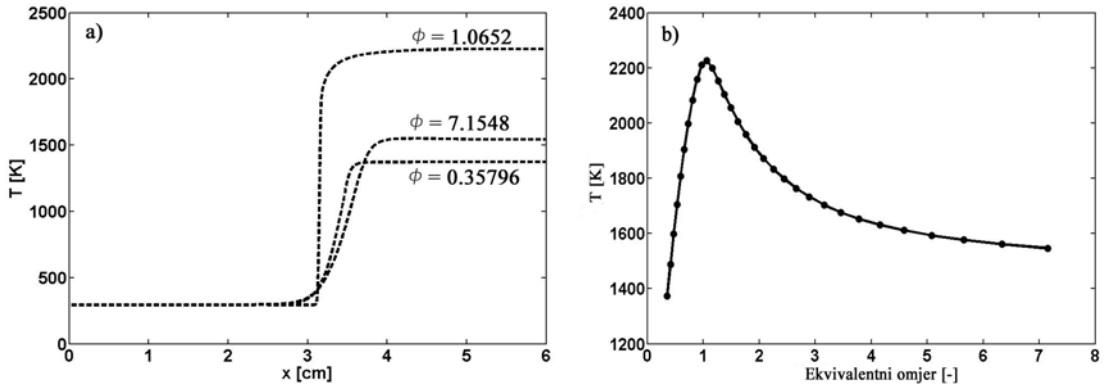

Slika 4 – Adijabatski temperaturni profili iz baze predmiješanih plamenova (razrijeđeni metan (25% CH_4, 75% zrak – molni udjeli)/zrak): a) T-x graf; b) T_{burnt}-Φ graf

Međutim, kad se predmiješani plamenovi dobiveni u pretprocesoru koriste u modeliranju nepredmiješanog izgaranja, s masenim udjelom smjese goriva kao varijablom, potrebno je proširiti bazu 1D predmiješanih plamenova izvan granica zapaljivosti. To se obično radi interpolacijom između siromašne/bogate granice zapaljivosti te čistog oksidanta/goriva [47, 75]. Nadalje, kod FPI metodologije [73] se nisko-dimenzijski prostori dobivaju za dvije nezavisne varijable: varijabla napretka reakcije te maseni udio smjese goriva (ekvivalentni omjer). Međutim, izbor varijable napretka reakcije nije proizvoljan već se varijabla napretka reakcije mora izabrati tako da uniformno raste između reaktanata i produkata, pokazujući stupanj do kojeg je došla kemijska reakcija [75, 79]. Kao parametar koji se koristi prilikom tabeliranja kemijskih vrsta potrebno je također da se kemijske vrste mogu jedinstveno funkcijski prikazati u ovisnosti varijable napretka reakcije. Obično se konačni produkti izgaranja, poput H_2O i CO_2, ili njihova linearna kombinacija, koriste kao varijabla napretka reakcije. Fiorina predlaže u [75] linearnu kombinaciju masenih udjela CO_2 i CO, tj. $Y_c \equiv Y_{CO_2} + Y_{CO}$, kao varijablu napretka reakcije u simulaciji laminarnog plamena metana i zraka.

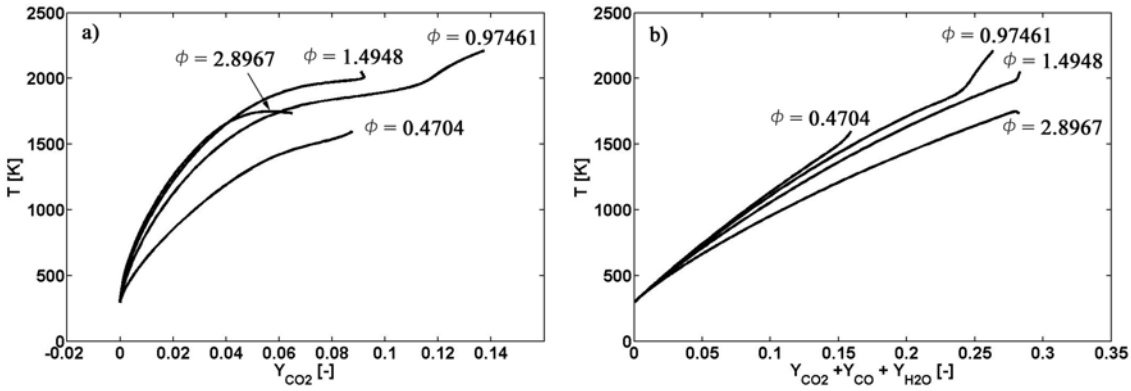

Slika 5 – Adijabatski temperaturni profili iz baze predmiješanih plamenova (razrijeđeni metan (25% CH_4, 75% zrak – molni udjeli)/zrak): a) T-Y_{CO2} graf; b) T-Y_{CO2}+Y_{CO}+Y_{H2O} graf

Kao što je spomenuto u [75], potrebno je da reaktivni skalari uniformno variraju s varijablom napretka reakcije te da nema preklapanja. Slika 5 prikazuje profile temperature u ovisnosti od varijable napretka reakcije za plamen metana i zraka (Sandia plamen D [40]) iz Poglavlja 5: a) Maseni udio CO_2 se koriti kao varijabla napretka reakcije, tj. $Y_c \equiv Y_{CO_2}$; b) Linearna kombinacija masenih udjela CO_2, CO i H_2O je korištena kao varijabla napretka reakcije, tj. $Y_c \equiv Y_{CO_2} + Y_{CO} + Y_{H_2O}$. Na Sl. 5a se može primijetiti problematičan profil $\phi = 1.4948$ kod kojeg se profil savija prema unatrag[5] te funkcijska veza temperature i varijable napretka reakcije nije jedinstvena u tom području. Slično se ponašaju i drugi profili blizu te vrijednosti, a koji nisu pokazani na Sl. 5a. Kod linearne kombinacije CO_2 i CO, tj. $Y_c \equiv Y_{CO_2} + Y_{CO}$, kao varijable napretka reakcije se javlja sličan problem (nije prikazano). Međutim, kod odabira linearne kombinacije $Y_c \equiv Y_{CO_2} + Y_{CO} + Y_{H_2O}$ kao varijable napretka reakcije, kao što je prikazano na Sl. 5b, taj problem se ne javlja te je linearna kombinacija CO_2, CO i H_2O odabrana za varijablu napretka reakcije prilikom simulacija u Poglavlju 5. Slično kao i kod temperature, jedinstvena se preslikavanja trebaju osigurati i za ostale reaktivne skalare koji se tabeliraju.

[5] To je zbog kemijske dekompozicije CO_2 u CO u bogatim smjesama metana i zraka kod ravnotežnih temperatura.

2.3.6 Nova procedura tabeliranja kemijskih vrsta

Normalizirana varijabla napretka reakcije je odabrana kao parametar tabeliranja kemijskih vrsta u pretprocesoru. Kao baza za tabeliranje mogu se koristiti predmiješani plamenovi [73] (FPI), nepredmiješani plamenovi [15, 79] (SLFM), ili njihova kombinacija, poput [47].

2.3.6.1 Predmiješani plamenovi

Za zadani maseni udio smjese goriva, varijabla napretka reakcije može poprimiti vrijednosti između hladnog miješanja $Y_c^{Mix}(Z)$ te ravnotežne vrijednosti $Y_c^{Eq}(Z)$, vidi Sl. 6. U slučaju predmiješanih plamenova normalizirana varijabla napretka reakcije može se definirati kao:

$$c(Z) = \frac{Y_c(Z) - Y_c^{Mix}(Z)}{Y_c^{Eq}(Z) - Y_c^{Mix}(Z)} \tag{40}$$

Kao takva, normalizirana varijabla napretka reakcije varira između nule (hladno miješanje, $Y_c(Z) = Y_c^{Mix}(Z)$) i jedinice (ravnotežno stanje izgaranja, $Y_c(Z) = Y_c^{Eq}(Z)$) – $0 \le c(Z) \le 1$, vidi Sl. 6.

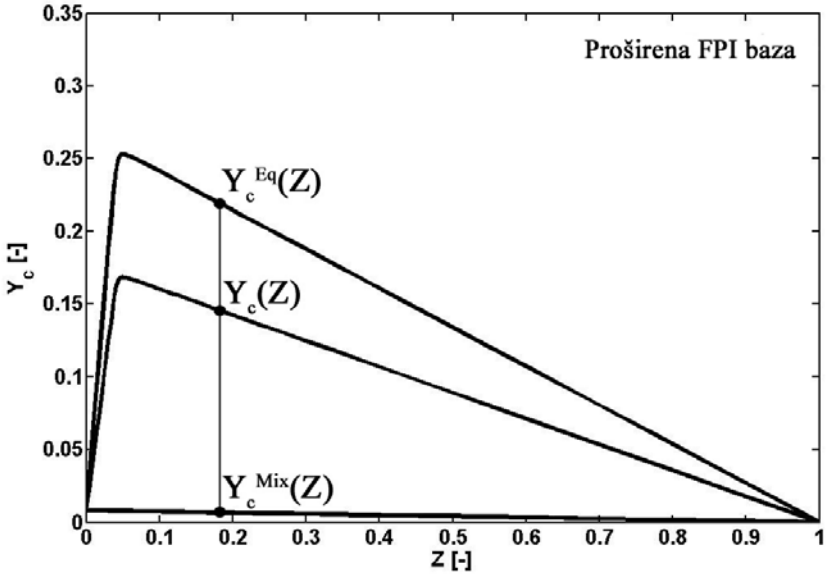

Slika 6 – Varijabla napretka reakcije (baza predmiješanih plamenova)

Predmiješani plamenovi dobiveni su u ovome radu upotrebom adaptiranom PREMIX programa [97]. Izvan granica zapaljivosti reaktivni skalari su linearno interpolirani između vrijednosti na gorivom siromašnoj/bogatoj granici zapaljivosti te vrijednosti oksidanta/goriva s druge strane. Dobiveno je strukturirano tabeliranje reaktivnih skalara u ovisnosti od dvije nezavisne koordinate – normalizirane varijable napretka reakcije, $0 \le c \le 1$; te masenog udjela smjese goriva, $0 \le Z \le 1$:

$$T = T(Z,c) \qquad Y_k = Y_k(Z,c) \tag{41}$$

Kompletno područje koje pokriva ova procedura tabeliranja je od hladnog miješanja pa do ravnotežnog izgaranja – vidi Sl. 7.

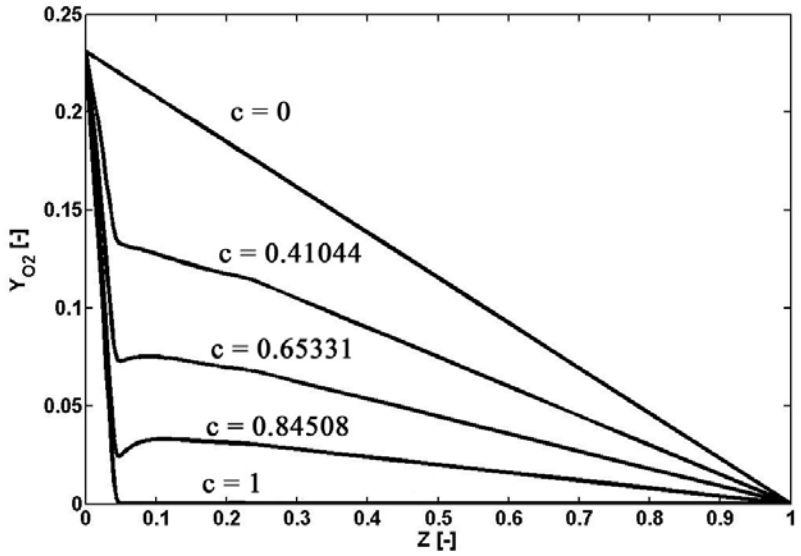

Slika 7 – O_2 profili (baza predmiješanih plamenova) za sustav H_2/He-zrak (gorivo: H_2 80%, He 20% – molni udjeli, 295 K; zrak: 294 K)

Pitanje koje se postavlja je da li su predmiješani plamenovi dobar odabir tabeliranja za slučaj simulacija nepredmiješanog izgaranja? U [47] se, naime, tvrdi da predmiješani plamenovi nisu dobar odabir za simulaciju nepredmiješanog izgaranja za više vrijednosti ekvivalentnih omjera, te ukoliko se žele postići točne vrijednosti međuprodukata izgaranja.

2.3.6.2 Nepredmiješani plamenovi

Situacija je drukčija ako se želi parametrizirati baza stacionarnih laminarnih *flamelet* profila, slično kao i u [79], ali upotrebom normalizirane varijable napretka reakcije. Naime, u standardnoj bazi nepredmiješanih plamenova (jed. (37)) varijabla napretka reakcije varira između donje vrijednosti koja je određena posljednjim *flamelet*-om u bazi prije gašenja ($\chi_{st} = \chi_{st,\max}$) te gornje vrijednosti ravnotežnog *flamelet*-a ($\chi_{st} \to 0$). Zbog različitog područja koje pokrivaju predmiješani, odnosno nepredmiješani plamenovi, potrebna je drukčija definicija normalizirane varijable napretka reakcije u slučaju nepredmiješanih plamenova. Da bi se zadržala ista struktura tabeliranih podataka kao i u slučaju predmiješanih plamenova, a prema jed. (41), normalizirana varijabla napretka reakcije u slučaju nepredmiješanih plamenova je definirana kao (vidi Sl. 8):

$$c\left(Z\right) = \frac{Y_c\left(Z\right) - Y_c^{Ext}\left(Z\right)}{Y_c^{Eq}\left(Z\right) - Y_c^{Ext}\left(Z\right)} \tag{42}$$

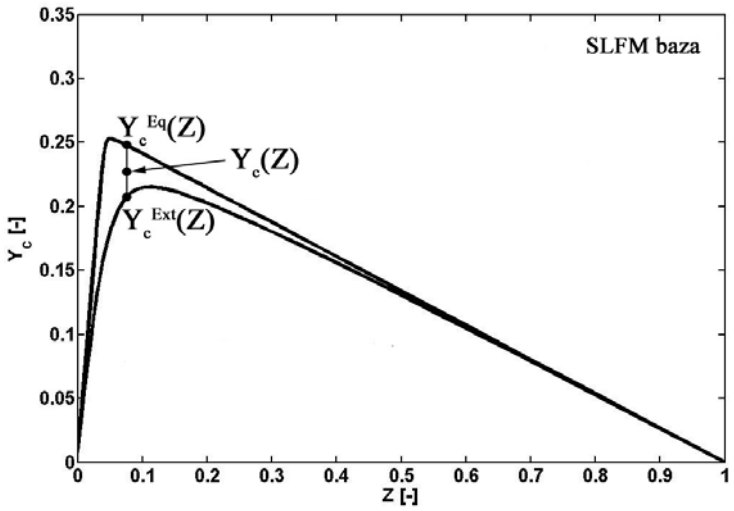

Slika 8 – Varijabla napretka reakcije (baza nepredmiješanih plamenova)

Dakle, obje normalizirane varijable napretka reakcije u jed. (40) i (42) variraju u području $0 \le c\left(Z\right) \le 1$, međutim, a kako je već spomenuto, donje granice varijable napretka reakcije Y_c se međusobno razlikuju.

Nova procedura tabeliranja prema jed. (41) u slučaju nepredmiješanih plamenova pokriva isto područje kao i standardna SLFM baza prema jed. (37), gdje profil kod $c = 0$ odgovara profilu $\chi_{st} = \chi_{st,\max}$, dok profil kod $c = 1$ odgovara profilu $\chi_{st} \to 0$.

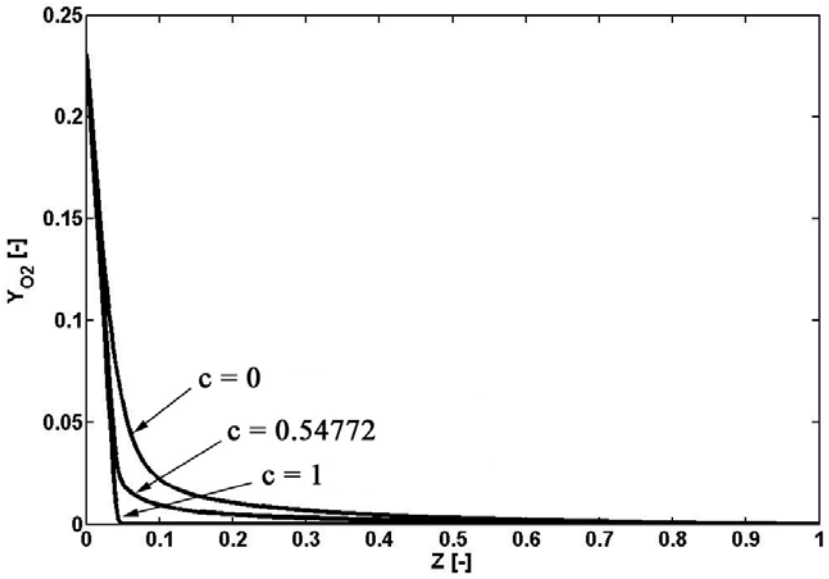

Slika 9 – O_2 profili (baza nepredmiješanih plamenova) za sustav H_2/He-zrak (gorivo: H_2 80%, He 20% – molni udjeli, 295 K; zrak: 294 K)

U slučaju nepredmiješanih plamenova, dakle, varijabla napretka reakcije ne pokriva cjelokupno područje od hladnog miješanja do ravnotežnog izgaranja, a kako je to bio slučaj kod predmiješanih plamenova. U [79] se tvrdi da baza nepredmiješanih plamenova, u stvari, pokriva cjelokupan set mogućih rješenja od ravnotežnog izgaranja do gašenja plamena, no tamo se brzina skalarne disipacije kod stehiometrijskih uvjeta optužuje kao loš odabran parametar za tabeliranje u standardnoj SLFM proceduri. Očekuje se da će se upotrebom varijable napretka reakcije dobiti bolji rezultati simulacije, posebice u slučajevima manjih vrsta i polutanata.

2.3.6.3 Mješovita formulacija

Da bi se pokrilo područje ispod granice gašenja u bazi nepredmiješanih plamenova, slično kao i u [47], predlaže se procedura tabeliranja gdje se predmiješani plamenovi koriste u područjima ispod granice gašenja, dok se iznad te granice zadržavaju profili iz baze nepredmiješanih plamenova. Dakle, ovom mješovitom procedurom bi se pokrilo cjelokupno područje od hladnog miješanja do ravnotežnog izgaranja, slično kao i kod predmiješanih plamenova, no s razlikom da se nepredmiješani plamenovi koriste kad god je to moguće. Očekuje se da bi ova procedura mogla dati bolju strukturu plamena u slučajevima nepredmiješanog izgaranja, pogotovo što se tiče među-vrsta u područjima bogatim gorivom [47]. Normalizirana varijabla napretka reakcije je definirana prema jed. (40) te je zadržano preslikavanje reaktivnih skalara prema jed. (41), kao kod predmiješanih plamenova. Dodatno, za svaku vrijednost masenog udjela smjese goriva se definira granična vrijednost normalizirane varijable napretka reakcije kao:

$$c_{thresh}\left(Z\right)=\frac{Y_c^{Ext}\left(Z\right)-Y_c^{Mix}\left(Z\right)}{Y_c^{Eq}\left(Z\right)-Y_c^{Mix}\left(Z\right)} \tag{43}$$

Za vrijednosti normalizirane varijable napretka reakcije $c\left(Z\right)\geq c_{thresh}\left(Z\right)$ koriste se nepredmiješani plamenovi, dok se za $c\left(Z\right)<c_{thresh}\left(Z\right)$ koriste predmiješani plamenovi tijekom tabeliranja. Slika 10 prikazuje, npr., maksimalne vrijednosti masenih udjela NO za slučaj plamena metana i zraka, a dobivene različitim procedurama tabeliranja.

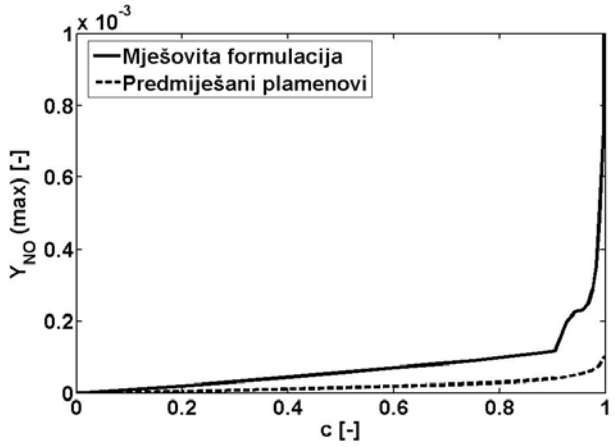

Slika 10 – Maksimalni maseni udjeli NO, razrijeđeni metan (25% CH_4, 75% zrak – molni udjeli)/zrak plamen: mješovita formulacija i predmiješani plamenovi

2.4 Modeliranje prijenosa topline zračenjem

Modeliranje prijenosa topline zračenjem samo po sebi je jedno složeno područje te je njegovo uključivanje u CFD proceduru rješavanja dosta problematično. Dosad su razvijeni različiti modeli sa željom postizanja što boljeg kompromisa između tri bitne stavke – prihvatljivi zahtjevi za računalnim resursima, što jednostavniji zapis matematičkog modela te primjenjivost u primjerima s proizvoljno kompliciranom geometrijom.

U narednim poglavljima će se opisati osnovni koncepti modela zračenja koji je implementiran u ovome radu, dok je za detaljniji opis prijenosa topline zračenjem potrebno konzultirati standardnu literaturu, poput [114, 115]. Praktični primjeri primjene modela zračenja se mogu pronaći, npr., u [30, 81, 83-88, 93, 100, 116, 117].

2.4.1 Jednadžba prijenosa topline zračenjem

Prilikom izgaranja medij sudjeluje u prijenosu topline zračenjem. Ovisno o apsorpcijskim svojstvima, medij može apsorbirati, emitirati i raspršivati zračenje [115]. Raspršivanje se pojavljuje kod interakcije toka zračenja sa česticama proizvoljne veličine koje preusmjeravaju dio tog zračenja u različitim pravcima. U simulacijama u ovome radu se raspršivanje zračenja zanemaruje. Također, kada se javlja tijekom izgaranja, čađa također značajno doprinosi zračenju [118].

Obično se varijabla spektralnog intenziteta zračenja i_λ koristi kao mjera energije zračenja koja prolazi kroz jediničnu površinu, u jedinici vremena, oko jedinične valne duljine λ, te kroz jedinični prostorni kut [115]. Energija se zračenja uzduž pravca S (vidi Sl. 11) prolaskom kroz participirajući medij djelomično apsorbira i raspršuje, dok istovremeno medij doprinosi energiji zračenja vlastitom emisijom i raspršivanjem u smjeru S.

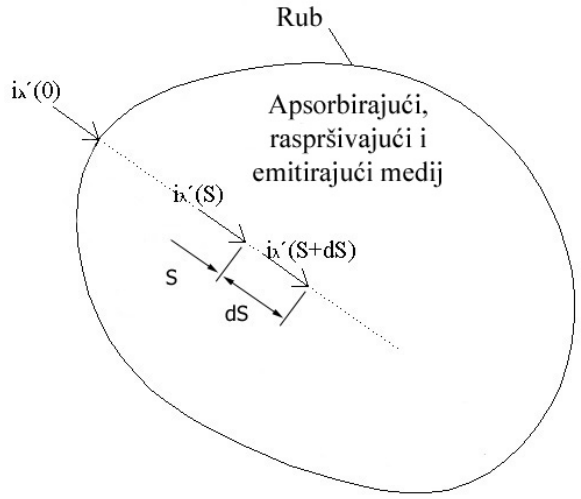

Slika 11 – Apsorbirajući, raspršivajući i emitirajući medij [115]

Intenzitet zračenja koji se emitira s rubne plohe te putuje kroz participirajući medij uzduž pravca S se mijenja prema jednadžbi prijenosa topline zračenjem (eng. *radiation transfer equation* – RTE) [115] kao:

$$\frac{di_\lambda^{\cdot}(S)}{dS} = -\left(a_\lambda + \sigma_{s\lambda}\right) i_\lambda^{\cdot}(S) + a_\lambda i_{\lambda b}^{\cdot}(S) + \frac{\sigma_{s\lambda}}{4\pi}\int_{4\pi} i_\lambda^{\cdot}(S,\vec{s}\,')\Phi(\lambda,\vec{s}\,',\vec{s})\,d\Omega' \qquad (44)$$

Prvi član na desnoj strani predstavlja smanjenje intenziteta zračenja uslijed apsorpcije i raspršivanja, dok drugi i treći član predstavljaju povećanje uslijed emisije participirajućeg medija, odnosno raspršivanja u pravcu S.

2.4.2 Metoda diskretnog prijenosa topline zračenjem

Pod pretpostavkom neraspršivajućeg i sivog medija, RTE se može zapisati kao:

$$\frac{di^{\cdot}(S)}{dS} = -ai^{\cdot}(S) + ai_b^{\cdot}(S) \qquad (45)$$

Budući je pretpostavljen sivi medij, njegova apsorpcijska svojstva ne ovise o valnoj dužini zračenja. Ukupni intenzitet zračenja crnog tijela se dobiva kao $i_b^{\cdot} = \frac{\sigma T^4}{\pi}$, dok σ predstavlja Stefan-Boltzmannovu konstantu.

Metoda diskretnog prijenosa topline zračenjem (eng. *discrete transfer radiation method* – DTRM) [85] pretpostavlja da je prostorna domena podijeljena u konačan broj

kontrolnih volumena te da se ukupno zračenje koje dolazi na neku rubnu plohu sastoji od zračenja koje dolazi na tu plohu u pravcima konačnog broja zraka koje su emitirane s te plohe – vidi Sl. 12.

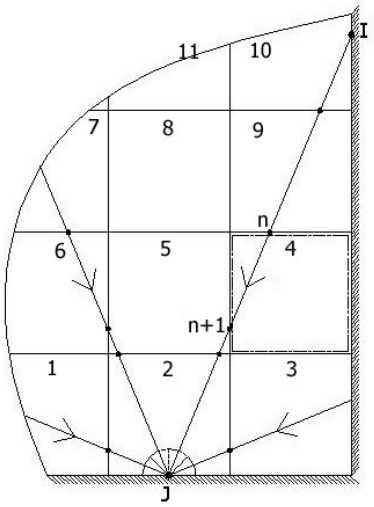

Slika 12 – Praćenje zraka (2D)

Zrake se odašilju s rubnih ploha kroz konačan broj prostornih kutova koji pokrivaju hemisferu oko te rubne plohe. Glavna pretpostavka DTRM-a je da se intenzitet toka zračenja kroz prostorni kut može aproksimirati intenzitetom toka zračenja uzduž zrake (linije) koja prolazi središtem tog prostornog kuta. Dakle, u slučaju upotrebe finije diskretizacije hemisfere oko rubne plohe (više zraka po rubnoj plohi) očekuju se bolji rezultati dobiveni DTRM metodom.

Temperatura i apsorpcijska svojstva medija su pretpostavljeni homogenim unutar jednog kontrolnog volumena, a čime se omogućuje analitičko rješavanje jed. (45) na bazi jednog kontrolnog volumena. Na primjer, ako promatramo zraku $\overrightarrow{IJ}$ koja presijeca kontrolni volumen 4 na Sl. 12, rješenje jed. (45) u kontrolnom volumenu 4 je:

$$i_{n+1}^{\cdot} = i_n^{\cdot}(1-\varepsilon) + \varepsilon \frac{\sigma T^4}{\pi} \tag{46}$$

Jed. (46) vrijedi za bilo koji kontrolni volumen u domeni kroz koji prolazi zraka zračenja poput one na Sl. 12. Ukupna intenzitet zračenja medija je definirana kao $\varepsilon = 1 - e^{-al}$ te ovisi o koeficijentu apsorpcije te duljini l koju čini zraka unutar kontrolnog volumena kojeg presijeca.

Unutar CFD procedure rješavanja, proračun prijenosa topline zračenjem po DTRM metodi se sastoji najprije od emitiranja zraka sa svih rubnih ploha računalne mreže. U tom dijelu se zrake emitiraju s rubnih ploha te se prati njihov put kroz medij te računaju presjecišta sa svim kontrolnim volumenima kroz koje one prolaze. Zrake se prate sve dok ne stignu do neke druge rubne plohe. Ovaj se dio proračuna radi samo jednom i to u pretprocesoru, dok se geometrijski podaci o zrakama i njihovim presjecištima s kontrolnim volumenima pohranjuju u datoteku. Kad su poznati svi ti geometrijski podaci, promjena intenziteta zračenja prema jed. (46) može se računati za svaku od zraka od kontrolnog volumena do kontrolnog volumena koji se nalaze na njenom putu. Na početku tog proračuna potrebno je poznavati intenzitet zračenja na početku tog inkrementalnog puta $i_0^{'}$ (npr., u točki I na Sl. 12). Ta vrijednost se dobiva iz rubnih uvjeta pod pretpostavkom da su rubne plohe sive te da se može primijeniti Lambertov zakon [115]:

$$i_0^{'} = \frac{q_{out}}{\pi} = \frac{q_{in}}{\pi}(1-\varepsilon_w) + \varepsilon_w \frac{\sigma T_w^4}{\pi} \tag{47}$$

Prema jed. (47), ukupni intenzitet zračenja koji se emitira s rubne plohe sastoji se od reflektirajućeg dijela (prvi član na desnoj strani jed. (47)) zračenja na tu plohu te onog dijela zračenja koje sama ta ploha emitira (drugi član na desnoj strani jed. (47)). U jed. (47) q_{in} predstavlja ukupnu snagu zračenja po jedinici površine koja dolazi na rubnu plohu, dok je ε_w emisijski faktor te rubne plohe. Temperatura rubne plohe je označena s T_w.

Ukupni tok zračenja koji dolazi na rubnu plohu dobiva se zbrajanjem zračenja uzduž svih zraka koje su emitirane s te rubne plohe:

$$q_{in} = \int_{\vec{s}\cdot\vec{n}<0} i^{'}\vec{s}\cdot\vec{n}d\Omega \approx \sum_{kk=1}^{N_{rays}} i_{kk}^{'} \cos\Theta_{kk}\Delta\Omega_{kk} \tag{48}$$

U jed. (48) Θ_{kk} je kut između jediničnog vektora $\vec{s}_{kk}$ *kk*-te zrake te jedinične normale $\vec{n}$ na rubnu plohu, dok $\Delta\Omega_{kk}$ predstavlja prostorni kut oko spomenute zrake [85] – vidi Sl. 13.

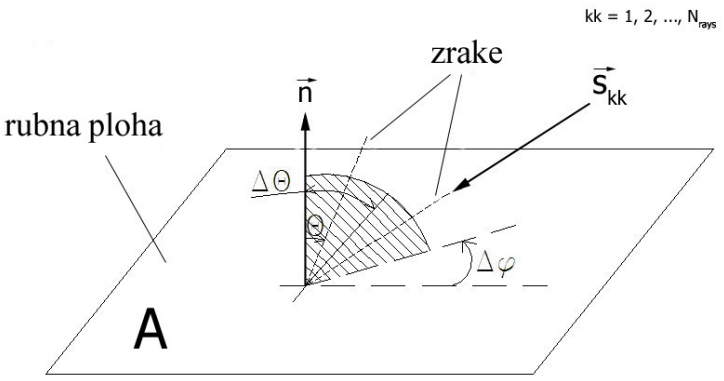

Slika 13 – Diskretizacija hemisfere oko rubne plohe

Zračenje uzduž zrake se mijenja dok prolazi kroz participirajući medij te se medij ili hladi ili zagrijava, ovisno o toj promjeni. Ta promjena zračenja unutar nekog kontrolnog volumena doprinosi izvorskom članu u transportnoj jednadžbi za entalpiju te se za jednu zraku koja presijeca kontrolni volumen izvorski član uslijed zračenja računa kao:

$$\overline{S}_{k_j} = (i_{n+1}^{'} - i_n^{'}) A_j \cos\Theta_j \Delta\Omega_j \tag{49}$$

A_j je površina rubne plohe s koje je emitirana zraka. Ukupni se izvorski član uslijed zračenja unutar nekog kontrolnog volumena dobije sumacijom jed. (49) za sve zrake koje prolaze kroz taj kontrolni volumen:

$$\overline{S}_k = \sum_{intersecting\_rays\_j} \overline{S}_{k_j} \tag{50}$$

U [100] je objavljeno da standardna DTRM procedura, a kako je opisana prema jed. (46)-(50), nije konzervativna što se tiče izmijenjene energije. Primijećeno je da ukupna razlika tokova zračenja na rubovima domene ne odgovara zračenju generiranom od strane participirajućeg medija, tj.:

$$\sum_{boundary\_faces\_j} A_j \left(q_{in,j} - q_{out,j} \right) \neq \sum_{\substack{internal \\ cells\_k}} \overline{S}_k \tag{51}$$

Zbog toga je u [100] predložena konzervativna formulacija DTRM-a, a gdje se definira korekcijski faktor C_R kao:

$$C_R = \frac{\sum_{boundary\_faces\_j} A_j q_{out,j}}{\sum_{\substack{starting \\ points\_j}} \left(q_{out,j} \left(\sum_{\substack{i=ending\_points \\ of\_ray\_j}} \cos\Theta_{i,j} \Delta\Omega_{i,j} A_i / \pi \right) \right)} \tag{52}$$

Intenzitet zračenja koje se emitira s rubne plohe (jed. (47)) se korigira prema:

$$i_0^{'} = C_R . \frac{q_{out}}{\pi} \tag{53}$$

Ostatak DTRM algoritma ostaje isti.

2.4.3 Svojstva participirajućeg medija

Prema metodi sivih plinova (eng. *weighted sum of grey gases model* – WSGGM) iz [101], ukupna emisivnost medija ε se dobiva kao:

$$\varepsilon = \sum_{ii=1}^{I+1} \alpha_{\varepsilon,ii}(T)(1 - e^{-a_{ii} Pl}) \tag{54}$$

U jed. (54) $\alpha_{\varepsilon,ii}(T)$ predstavlja težinski faktor emisivnosti *ii*-tog sivog plina te ovisi samo o temperaturi. Apsorpcijski koeficijent a_{ii} *ii*-tog sivog plina ne ovisi o temperaturi te je zadan, dok P predstavlja sumu parcijalnih tlakova apsorbirajućih kemijskih vrsta (CO_2, H_2O). Simbol l predstavlja duljinu zrake unutar kontrolnog volumena. Težinski faktori se računaju kao:

$$\alpha_{\varepsilon,I+1}(T) = 1 - \sum_{ii=1}^{I} \sum_{jj=1}^{J} b_{\varepsilon,ii,jj} T^{jj-1} \tag{55}$$

Za ukupan broj sivih plinova $I = 3$, te uz upotrebu polinoma trećeg reda ($J = 4$), polinomski koeficijenti $b_{\varepsilon,ii,jj}$ su zadani u [101].

2.5 Statistički opis

2.5.1 Turbulentne i kemijske skale

Turbulentne tokove karakteriziraju vremenske i prostorne skale različitih veličina te da bi se one direktno numerički simulirale (DNS) računalna prostorna domena bi trebala biti dovoljno velika da obuhvati najveće prostorne skale u turbulentnom toku fluida (vrtlozi čija je veličina usporediva s veličinom sustava koji se simulira, npr. promjer cijevi u slučaju simulacije protoka kroz cijev). No istovremeno bi gustoća numeričke mreže trebala biti dovoljno fina da uhvati i najmanje vrtloge (Kolmogorovljeve vrtloge) koji se javljaju. Kako razlika između najvećih i najmanjih vrtloga može biti nekoliko redova veličine, a koja se povećava s povećanjem Reynoldsovog broja, DNS postaje praktički neprimjenjiv u realnim konfiguracijama. Situacija se još dodatno komplicira uključivanjem modeliranja izgaranja, gdje mreža mora biti još finija da bi se obuhvatila i struktura samog plamena.

Kao što je opisano u [18], Richardson [119] i Kolmogorov [120] su prvi konceptualno i kvantitativno opisali fenomen transfera energije između turbulentnih vrtloga različitih veličina. Po njima se turbulentno polje sastoji od vrtloga različitih veličina te se većina turbulentne energije stvara kod najvećih vrtloga veličine l_0, a koja se postepeno transferira na sve manje i manje vrtloge sve do konačne disipacije zbog viskoznih sila kod najmanjih vrtloga veličine η. Ovaj se proces transfera energije još naziva i Kolmogorovljeva energijska kaskada, dok se najmanji vrtlozi još nazivaju i Kolmogorovljevi vrtlozi. Slika 14 (koristeći oznake iz [18]) shematski prikazuje kaskadu turbulentne energije.

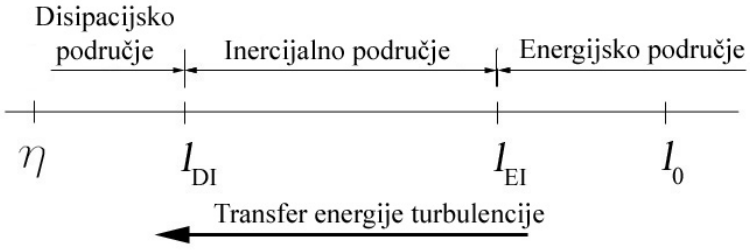

Slika 14 – Kaskada turbulentne energije (Kolmogorovljeva kaskada)

Prema Sl. 14, postroje tri različita područja u kaskadi turbulentne energije. Najveći energetski vrtlozi čine tzv. energijsko područje ($l > l_{EI} \approx \frac{1}{6} l_0$ [18]), te se ti vrtlozi mogu opisati kao anizotropni te njihov oblik ovisi o geometriji domene te rubnim uvjetima. Reynoldsov broj tih vrtloga je $\mathrm{Re}_0 = \frac{l_0 u_0}{\nu}$ te je po veličini usporediv s klasičnim Reynoldsovim brojem simuliranog sustava (npr. $\mathrm{Re}_0 \approx \mathrm{Re} = \frac{du}{\nu}$ u slučaju simulacije toka kroz cijev promjera d). Ispod energijskog područja ($l < l_{EI}$) turbulentni su vrtlozi univerzalniji i izotropniji [18] te ne ovise o geometrijskim karakteristikama domene ili rubnim uvjetima. Statistika tih univerzalnih po karakteru vrtloga ovisi samo o viskoznosti ν te brzini transfera energije ε. Unutar tzv. inercijskog područja ($60\eta \approx l_{DI} \ll l \ll l_{EI}$ [18], Sl. 14) vrtlozi su još dovoljno veliki da viskoznost ne igra značajnu ulogu te oni ovise samo o brzini transfera energije ε.

Najmanje turbulentne skale (Kolmogorovljeve skale) su definirane kao [15, 17, 18]:

$$\eta = \left(\frac{\nu^3}{\varepsilon}\right)^{\frac{1}{4}} \quad u_\eta = (\varepsilon\nu)^{\frac{1}{4}} \quad t_\eta = \left(\frac{\nu}{\varepsilon}\right)^{\frac{1}{2}} \tag{56}$$

Iz jed. (56) te iz zakona $\varepsilon \sim u^3/l$ [18] slijedi da je omjer veličina energijskih i Kolmogorovljevih vrtloga $l_0/\eta \sim \mathrm{Re}^{3/4}$, a što implicira da porastom turbulencije najmanji vrtlozi postaju još manjima. U tom se pogledu može pokazati da, ako je N broj računalnih točaka računalne mreže u pravcu jedne prostorne koordinate, bi gustoća mreže za obuhvaćanje najmanjih vrtloga trebala biti $N > \mathrm{Re}^{3/4}$ [20]. Dakle, za slučaj umjerenih Reynoldsovih brojeva, npr. $\mathrm{Re} = 2000$, gustoća 3D mreže bi trebala biti oko 27 milijuna točaka ($N \approx 300$, $N \times N \times N = 2.7 \cdot 10^7$). Očigledno je da bi upotreba DNS-a u praktičnim situacijama s puno većim Reynoldsovim brojevima [38] zahtijevala još finiju mrežu te je ova metoda još uvijek neprihvatljiva sa stajališta zahtjeva za računalnim resursima.

Vremenske i prostorne skale koje se javljaju kod izgaranja obično su još manje nego skale turbulentnog toka. Damköhlerov broj je definiran kao omjer vremenskih skala turbulencije i kemijskih reakcija [16]:

$$Da = \frac{\tau_t}{\tau_c} \tag{57}$$

U slučaju dovoljno velikih Damköhlerovih brojeva ($Da \gg 1$) kemijske reakcije se odvijaju jako brzo te turbulentni tok fluida ne može utjecati na strukturu same fronte plamena [20]. Ovaj se režim ($Da \gg 1$) najčešće pretpostavljao kod razvoja modela nepredmiješanog izgaranja baziranih na upotrebi masenog udjela smjese goriva, poput SLFM-a [15].Međutim, u praksi se javljaju situacije gdje su kemijske reakcije spore ($Da \approx 1$ ili manje), poput reakcija stvaranja NO-a, te primjena prethodno spomenutih modela nije pogodna za te slučajeve. To se potvrdilo lošim rezultatima koje ti modeli daju za spore kemijske vrste (pogledati TNF zbornike na [29]). Dakle, potrebno je imati u vidu pretpostavke pod kojima su modeli izgaranja razvijeni, te sukladno tome ih primjenjivati u praksi.

Kao što se može vidjeti iz prethodne analize, postoji široko područje vremenskih i prostornih skala u primjerima turbulentnog izgaranja te je primjena DNS-a u tim slučajevima isključena zbog nedovoljnih računalnih resursa [16, 20]. Zbog toga se još uvijek primjenjuje statistički pristup kod modeliranja turbulencije i izgaranja u praktičnim primjerima.

2.5.2 Reynoldsovo i Favreovo usrednjavanje

Budući da je DNS još uvijek računalno preskup, u praktičnim se slučajevima koristi pristup rješavanja usrednjenih jednadžbi. Neka se veličina može rastaviti na srednji i fluktuirajući dio kao (vidi Sl. 15):

$$\varphi = \overline{\varphi} + \varphi' \tag{58}$$

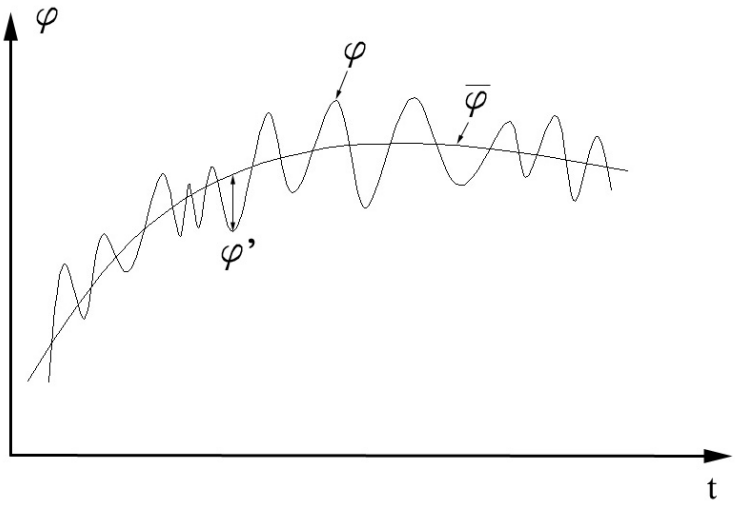

Slika 15 – Usrednjeni profil

Kao što se vidi sa Sl. 15, usrednjeni profil $\overline{\varphi}$ se blaže mijenja u vremenu nego stvarni trenutni profil φ, te ga je zbog toga lakše riješiti numerički. Po definiciji je usrednjena fluktuacija jednaka nuli, tj. $\overline{\varphi'} = 0$. U klasičnom RANS pristupu usrednjene se jednadžbe dobivaju ubacivanjem jed. (58) za zavisne varijable u odgovarajuće transportne jednadžbe te modeliranjem korelacija koje se javljaju zbog postupka usrednjavanja [17, 18, 23].

U slučajevima s velikim varijacijama u polju gustoće, prikladniji način usrednjavanja je onaj kako je predložio Favre [16, 121]. Favreova srednja vrijednost je definirana kao:

$$\tilde{\varphi} = \frac{\overline{\rho\varphi}}{\overline{\rho}} \tag{59}$$

Slično kao i u jed. (58), Favreova fluktuacija je definirana kao $\varphi'' = \varphi - \tilde{\varphi}$, gdje je $\widetilde{\varphi''} = 0$. Prednost Favreovog nad Reynoldsovim usrednjavanjem je u manjem broju

korelacija koje se javljaju prilikom usrednjavanja te koje je potrebno modelirati u slučajevima s varijabilnom gustoćom [16]. Također, Favreove jednadžbe u slučaju varijabilne gustoće su formalno jednake Reynoldsovim jednadžbama za slučaj konstantne gustoće, a što omogućava primjenu nekompresibilnih RANS rješavača razvijenih za hladan tok i u simulacijama izgaranja [16].

2.5.3 Usrednjene jednadžbe: održanje mase, momenta i energije

Jednadžbe toka fluida – jed. (1), (2) i (6) – se usrednjavaju tako da se trenutne vrijednosti zavisnih varijabli zamjenjuju usrednjenim i fluktuirajućim dijelovima prema:

$$\begin{aligned} \rho &= \overline{\rho} + \rho' \\ p &= \overline{p} + p' \\ u_i &= \tilde{u}_i + u_i'' \\ h &= \tilde{h} + h'' \end{aligned} \tag{60}$$

Nakon uvrštavanja jed. (60) u spomenute jednadžbe toka fluida te nakon primjene pravila usrednjavanja [16, 17] dobivaju se transportne jednadžbe za usrednjene vrijednosti. Usrednjena jednadžba kontinuiteta dobiva se kao:

$$\frac{\partial \overline{\rho}}{\partial t} + \frac{\partial \left(\overline{\rho} \tilde{u}_j \right)}{\partial x_j} = 0 \tag{61}$$

Na sličan način se dobivaju usrednjene jednadžbe (za $i = 1, 2, 3$) brzina:

$$\frac{\partial \left(\overline{\rho} \tilde{u}_i \right)}{\partial t} + \frac{\partial \left(\overline{\rho} \tilde{u}_i \tilde{u}_j \right)}{\partial x_j} = \overline{f}_i - \frac{\partial \overline{p}}{\partial x_i} + \frac{\partial \overline{\tau}_{ij}}{\partial x_j} - \frac{\partial \left(\widetilde{\overline{\rho} u_i'' u_j''} \right)}{\partial x_j} \tag{62}$$

Usrednjeni tenzor tangencijalnih naprezanja $\overline{\tau}_{ij}$ u jed. (62) dobiva se iz jed. (4), ali s uvrštenim vrijednostima usrednjenog tenzora brzine deformacije $\overline{D}_{ij} = \frac{1}{2}\left(\frac{\partial \tilde{u}_i}{\partial x_j} + \frac{\partial \tilde{u}_j}{\partial x_i} \right)$.

Posljednji član na desnoj strani jed. (62) pojavljuje se zbog postupka usrednjavanja te ga je potrebno modelirati, a kako će biti pokazano kasnije.

U turbulentnim su strujanjima molekularni tokovi za redove veličina manji od turbulentnih te se molekularni efekti obično zanemaruju prilikom rješavanja usrednjenih jednadžbi [15]. U tom slučaju se usrednjena energijska jednadžba može zapisati kao:

$$\frac{\partial\left(\overline{\rho}\tilde{h}\right)}{\partial t}+\frac{\partial\left(\overline{\rho}\tilde{h}\tilde{u}_j\right)}{\partial x_j}=\frac{\partial\overline{p}}{\partial t}+\tilde{u}_j\frac{\partial\overline{p}}{\partial x_j}+\overline{q}_h+\overline{u_j"\frac{\partial p}{\partial x_j}}-\frac{\partial\left(\overline{\rho}\widetilde{h"u_j"}\right)}{\partial x_j} \tag{63}$$

Posljednja dva člana na desnoj strani jed. (63) javljaju se zbog usrednjavanja. Dok se korelacija prostornog gradijenta tlaka i fluktuacije brzine obično zanemaruje, kao što je napravljeno i u ovome radu, posljednji se član na desnoj strani jed. (63) modelira.

2.5.4 Modeliranje turbulencije

Glavni problem kod modeliranja turbulencije je kako modelirati novonastale korelacije koje su nastale zbog usrednjavanja. To se posebice odnosi na modeliranje tzv. Reynoldsovih naprezanja $\overline{\rho}\widetilde{u_i"u_j"}$ (vidi jed. (62)) te se je u posljednjih nekoliko desetljeća dosta napora uložilo u tom pravcu te još uvijek nije pronađeno univerzalno rješenje, koje bi se s dovoljnom točnošću moglo upotrijebiti u simulacijama raznorodnih konfiguracija turbulentnog toka [18, 23-25]. Također, uglavnom se modelirala turbulencija u nereaktivnim tokovima, te su se pritom zanemarivali efekti Favreovog usrednjavanja i toplinske dilatacije prilikom modeliranja Reynoldsovih naprezanja [16]. Međutim, usprkos toga se tako razvijeni modeli turbulencije direktno primjenjuju u simulacijama izgaranja, a gdje su usrednjene jednadžbe formalno zapisane kao kod Favreovog usrednjavanja [20].

U ovome radu će se koristiti dva modela turbulencije, a kako su dostupni u FIRE CFD rješavaču [99] – to su $k-\varepsilon$ model [122] i hibridni model turbulencije (eng. *hybrid turbulence model* – HTM) [123]. Oba modela se temelje na Boussinesqovoj pretpostavci kod modeliranja Reynoldsovih naprezanja [17-19, 23]:

$$-\overline{\rho}\widetilde{u_i"u_j"}=2\mu_t\overline{D}_{ij}-\frac{2}{3}\overline{\rho}k\delta_{ij} \tag{64}$$

Dvije nove nepoznanice koje se javljaju u jed. (64) su turbulentna dinamička viskoznost μ_t te turbulentna kinetička energija k. To nisu molekularna svojstva fluida već

turbulentne veličine koje je potrebno modelirati. Turbulentna dinamička viskoznost se modelira kao:

$$\mu_t = \bar{\rho} C_\mu \frac{k^2}{\varepsilon} \tag{65}$$

U standardnom $k-\varepsilon$ modelu strukturni parametar C_μ ima konstantnu vrijednost $C_\mu = 0.09$, dok se brzina disipacije turbulentne kinetičke energije ε modelira preko transportne jednadžbe.

Dakle, u konceptu turbulentne viskoznosti (jed. (64) i (65)), dvije nepoznanice koje se modeliraju su turbulentna kinetička energija k i brzina disipacije turbulentne kinetičke energije ε, te se u standardnom $k-\varepsilon$ modelu one računaju preko sljedeće dvije transportne jednadžbe [18, 122]:

$$\frac{\partial\left(\bar{\rho}k\right)}{\partial t} + \frac{\partial\left(\bar{\rho}k\tilde{u}_j\right)}{\partial x_j} = \frac{\partial}{\partial x_j}\left(\frac{\mu_t}{\sigma_k}\frac{\partial k}{\partial x_j}\right) + P - \bar{\rho}\varepsilon \tag{66}$$

$$\frac{\partial\left(\bar{\rho}\varepsilon\right)}{\partial t} + \frac{\partial\left(\bar{\rho}\varepsilon\tilde{u}_j\right)}{\partial x_j} = \frac{\partial}{\partial x_j}\left(\frac{\mu_t}{\sigma_\varepsilon}\frac{\partial \varepsilon}{\partial x_j}\right) + C_{\varepsilon 1}\frac{\varepsilon}{k}P - C_{\varepsilon 2}\bar{\rho}\frac{\varepsilon^2}{k} \tag{67}$$

Izvorski član P u jed. (66) i (67) se računa kao:

$$P = 2\mu_t \bar{D}_{ij}\bar{D}_{ij} - \frac{2}{3}\bar{D}_{ii}\left(\bar{\rho}k + \mu_t \bar{D}_{ii}\right) \tag{68}$$

Standardne vrijednosti konstanti koje se pojavljuju su:

$$\begin{aligned} C_{\varepsilon 1} &= 1.44 \quad C_{\varepsilon 2} = 1.92 \\ \sigma_k &= 1.0 \qquad \sigma_\varepsilon = 1.3 \end{aligned} \tag{69}$$

U HTM konceptu [123] ne računa se transportna jednadžba za turbulentnu kinetičku energiju, već se ista dobiva iz Reynoldsovih naprezanja kao:

$$k = \frac{1}{2}\widetilde{u_i "u_i"} \tag{70}$$

Dakle, potrebno je dodatno računati transportne jednadžbe za Reynoldsova naprezanja da bi se dobio zatvoren skup jednadžbi:

$$\frac{d\left(\widetilde{u_i"u_j"}\right)}{dt}+\frac{\partial\left(\widetilde{u_i"u_j"}\tilde{u}_k\right)}{\partial x_k}=-\left(\widetilde{u_i"u_k"}\frac{\partial\tilde{u}_j}{\partial x_k}+\widetilde{u_j"u_k"}\frac{\partial\tilde{u}_i}{\partial x_k}\right)+$$
$$\frac{\partial}{\partial x_k}\left[\nu\frac{\partial\left(\widetilde{u_i"u_j"}\right)}{\partial x_k}+C_s\frac{k}{\varepsilon}\widetilde{u_k"u_l"}\frac{\partial\left(\widetilde{u_i"u_j"}\right)}{\partial x_l}\right]-\frac{2}{3}\varepsilon\delta_{ij}+\Phi_{ij} \tag{71}$$

U jed. (71) ν je kinematička viskoznost. Difuzija zbog turbulentnih fluktuacija je modelirana pod pretpostavkom da je u smjeru gradijenta usrednjenih vrijednosti (uz $C_s=0.22$), dok je viskozna disipacija pretpostavljena izotropnom. Član koji se odnosi na refleksiju tlaka u originalnom modelu Gibsona i Laundera [124] djelomično je zamijenjen uključivanjem nelinearnih članova u modeliranje člana deformacije zbog tlaka Φ_{ij} prema [125]. Više detalja o modeliranju Φ_{ij} može se pronaći u [123]. Također, zbog izračunatih i dostupnih Reynoldsovih naprezanja nešto je promijenjena i transportna jednadžba za disipaciju turbulentne kinetičke energije, a koja ima oblik kao kod modeliranja turbulencije na razini drugih momenata [123]. Dodatno se u HTM konceptu modelira strukturni parametar C_μ (umjesto konstantne vrijednosti $C_\mu=0.09$) kao [123]:

$$C_\mu=\left(-\widetilde{u_i"u_j"}\frac{\partial\tilde{u}_i}{\partial x_j}\right)\Bigg/\left(2\bar{D}_{ij}\bar{D}_{ij}\frac{k^2}{\varepsilon}\right) \tag{72}$$

Tokovi zbog turbulentnih fluktuacija u skalarnim jednadžbama, poput $\bar{\rho}\widetilde{h"u_j"}$ u jed. (63), modeliraju se pod klasičnom gradijentnom pretpostavkom:

$$\bar{\rho}\widetilde{h"u_j"}=-\frac{\mu_t}{\mathrm{Sc}_t}\frac{\partial\tilde{h}}{\partial x_j} \tag{73}$$

Na sličan se način računaju tokovi zbog turbulentnih fluktuacija i u ostalim skalarnim jednadžbama, poput jednadžbe za usrednjeni maseni udio smjese goriva, varijancu masenog udjela smjese goriva, usrednjenu varijablu napretka reakcije, i sl. Međutim, ovo modeliranje tokova uslijed turbulentnih fluktuacija je kritizirano u [18] te se pokazalo neprikladnim u nekim situacijama, te nije u stanju simulirati pojave protu-gradijentnog turbulentnog transporta, kao što je primijećeno u [16].

2.5.5 Statistički momenti praćenih skalara

U sklopu modeliranja izgaranja, u ovome radu, računaju se tri dodatne transportne jednadžbe, o to za usrednjeni maseni udio smjese goriva, varijancu smjese goriva te usrednjenu varijablu napretka reakcije. Gradijentna hipoteza je korištena kod modeliranja tokova zbog turbulentnih fluktuacija u sva tri slučaja, dok su molekularni efekti zanemareni.

U transportnoj jednadžbi za maseni udio smjese goriva (jed. (26)) ne pojavljuje se izvorski član, te je dodatni član koji se pojavljuje u jednadžbi za usrednjenu vrijednost masenog udjela smjese goriva onaj zbog turbulentnih fluktuacija [15, 20]:

$$\frac{\partial\left(\overline{\rho}\tilde{Z}\right)}{\partial t}+\frac{\partial\left(\overline{\rho}\tilde{Z}\tilde{u}_j\right)}{\partial x_j}=\frac{\partial}{\partial x_j}\left(\overline{\rho D_Z\frac{\partial Z}{\partial x_j}}\right)+\frac{\partial}{\partial x_j}\left(\frac{\mu_t}{\mathrm{Sc}_{t1}}\frac{\partial\tilde{Z}}{\partial x_j}\right) \tag{74}$$

Prvi član na desnoj strani je uslijed molekularne difuzije te je on zanemariv u usporedbi s ostalim članovima, pa se u ovome radu ne modelira. Zapisan je u jed. (74) samo zbog kompletnosti i referenciranja kod proširenog *flamelet* modela [34] (Prilog B). Drugi član na desnoj strani je zbog turbulentnih fluktuacija.

Transportna jednadžba za varijancu masenog udjela smjese goriva je [20]:

$$\frac{\partial\left(\overline{\rho}\widetilde{Z''^2}\right)}{\partial t}+\frac{\partial\left(\overline{\rho}\widetilde{Z''^2}\tilde{u}_j\right)}{\partial x_j}=\frac{\partial}{\partial x_j}\left(\frac{\mu_t}{\mathrm{Sc}_{t1}}\frac{\partial\widetilde{Z''^2}}{\partial x_j}\right)+2\frac{\mu_t}{\mathrm{Sc}_{t2}}\frac{\partial\tilde{Z}}{\partial x_j}\frac{\partial\tilde{Z}}{\partial x_j}-\overline{\rho}\widetilde{\chi} \tag{75}$$

Prvi član na desnoj strani jed. (75) je zbog turbulentnih fluktuacija, dok drugi član predstavlja izvor zbog gradijenata usrednjenog masnog udjela smjese goriva. Posljednji član predstavlja ponor zbog skalarne disipacije, te će njegovo modeliranje biti pokazano kasnije.

Varijabla napretka reakcije korištena je u ovome radu kao parametar prilikom tabeliranja kemijskih vrsta, a prema jed. (38), te je transportna jednadžba za usrednjenu varijablu napretka reakcije [47]:

$$\frac{\partial\left(\overline{\rho}\tilde{Y}_c\right)}{\partial t}+\frac{\partial\left(\overline{\rho}\tilde{Y}_c\tilde{u}_j\right)}{\partial x_j}=\frac{\partial}{\partial x_j}\left(\frac{\mu_t}{\mathrm{Sc}_{t1}}\frac{\partial\tilde{Y}_c}{\partial x_j}\right)+\widetilde{\dot{\omega}_c} \tag{76}$$

Turbulentni Schmidtovi brojevi u jed. (74)-(76) su odabrani $\mathrm{Sc}_{t1} = \mathrm{Sc}_{t2} = 0.7$, dok se usrednjeni izvorski član $\widetilde{\dot{\omega}_c}$ u jed. (76) dobiva iz baze predmiješanih ili nepredmiješanih plamenova, ovisno o modelu izgaranja.

2.5.6 Interakcija turbulencije i izgaranja

Interakcija između turbulentnog toka i izgaranja je obostrana [20]. Izgaranje utječe na turbulentni tok kroz oslobađanje topline, a čime se mijenjaju molekularna viskoznost i gustoća fluida. U tom pogledu izgaranje može ili povećati ili smanjiti nivo turbulencije (re-laminarizacija zbog povećane viskoznosti). Turbulencija, s druge strane, pospješuje procese izgaranja te je u praktičnim aplikacijama bitno da je tok fluida turbulentan zbog efikasnosti samog izgaranja. Međutim, u slučaju pojačane turbulencije i niskih Damköhlerovih brojeva turbulentni vrtlozi mogu utjecati na strukturu same fronte plamena, što u ekstremnim situacijama može dovesti do otpuhivanja ili čak i gašenja plamena [16].

Primjena funkcije gustoće vjerojatnosti (eng. *probability density function* – PDF) kod modeliranja nepredmiješanog izgaranja u RANS pristupu pogodno je zbog pojavljivanja statističkih momenata različitih varijabli. Ako se izrazi preko masenog udjela smjese goriva kao varijablom, PDF je definiran kao:

$$P(Z) = \frac{dF(Z)}{dZ} \tag{77}$$

U jed. (77) $F(Z)$ predstavlja vjerojatnost pronalaženja vrijednosti z u području $z < Z$. Sukladno tome, produkt $P(Z)dZ$ predstavlja vjerojatnost pronalaženja vrijednosti z u diferencijalnom intervalu $Z \le z < Z + dZ$ [15, 18, 108].

Budući da je vjerojatnost pronalaženja vrijednosti z (ili bilo koje druge varijable) u području $-\infty \le z \le +\infty$ sigurna, integral PDF-a u tom području je:

$$\int_{-\infty}^{+\infty} P(Z)\,dZ = 1 \tag{78}$$

Jed. (78) je svojstvo zajedničko svim PDF funkcijama. U slučaju masenog udjela smjese goriva kao varijable, a čije su granice $0 \le z \le 1$, jed. (78) postaje:

$$\int_0^1 P(Z)\,dZ = 1 \tag{79}$$

Usrednjena vrijednost (očekivanje) neke funkcije $\varphi = \varphi(Z)$ dobiva se kao:

$$\overline{\varphi} = \int_0^1 \varphi(Z) P(Z)\,dZ \tag{80}$$

Jed. (80) će se koristiti poslije kod izračuna usrednjenih vrijednosti reaktivnih skalara. Varijanca (drugi centralni moment) je definirana kao:

$$\overline{\varphi'^2} = \int_0^1 \left(\varphi(Z) - \overline{\varphi}\right)^2 P(Z)\,dZ \tag{81}$$

Kondicionalna usrednjena vrijednost neke varijable ψ, a za fiksnu vrijednost Z je definirana kao:

$$\overline{\psi|Z} = \int_0^1 \psi P(\psi|Z)\,d\psi \tag{82}$$

$P(\psi|Z)$ je kondicionalni PDF od ψ za fiksnu vrijednost Z.

Iz eksperimentalnih mjerenja je uočeno da je pretpostavljena β-PDF funkcija pogodna za dobar statistički prikaz reaktivnih skalara [108], te je ova funkcija primijenjena i u ovome radu. Dakle, statistički momenti reaktivnih skalara su povezani sa statističkim momentima masenog udjela smjese goriva preko pretpostavljene β-PDF funkcije:

$$P(Z) = \frac{Z^{\alpha-1}\left(1-Z^{\beta-1}\right)}{B(\alpha,\beta)} \tag{83}$$

U jed. (83) $B(\alpha,\beta)$ je beta funkcija koeficijenata α i β. Ti koeficijenti ne smiju poprimiti negativne vrijednosti te se dobivaju kao:

$$\alpha = \tilde{Z}\left[\frac{\tilde{Z}\left(1-\tilde{Z}\right)}{\widetilde{Z''^2}} - 1\right] \qquad \beta = \left(1-\tilde{Z}\right)\left[\frac{\tilde{Z}\left(1-\tilde{Z}\right)}{\widetilde{Z''^2}} - 1\right] \tag{84}$$

Beta funkcija se najčešće prikazuje u ovisnosti od gama funkcija Γ kao:

$$B(\alpha,\beta)=\frac{\Gamma(\alpha)\Gamma(\beta)}{\Gamma(\alpha+\beta)} \tag{85}$$

Gama funkcija je definirana kao:

$$\Gamma(x)=\int_0^\infty e^{-t}t^{x-1}dt \tag{86}$$

Neki β-PDF oblici, a za različite vrijednosti momenata masenog udjela smjese goriva $\tilde{Z}$ i $\widetilde{Z''^2}$, prikazani su na Sl. 16.

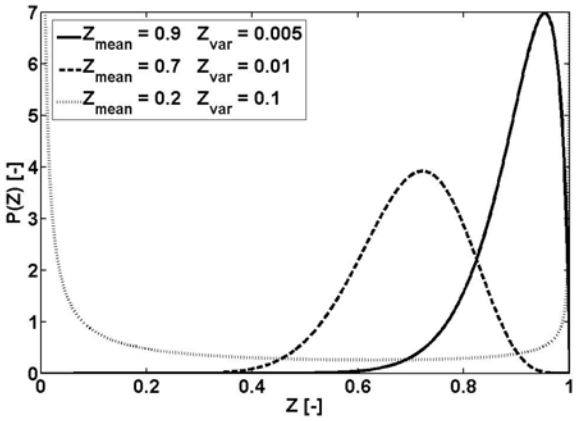

Slika 16 – Oblici β-PDF funkcije za različite vrijednosti parametara $\tilde{Z}$ i $\widetilde{Z''^2}$

Usrednjene vrijednosti masenih udjela kemijskih vrsta i temperature se, shodno prethodnom izlaganju, dobivaju kao [15]:

$$\tilde{Y}_i(\xi)=\int_0^1 Y_i(Z,\xi)P(Z)dZ \tag{87}$$

$$\tilde{T}(\xi)=\int_0^1 T(Z,\xi)P(Z)dZ \tag{88}$$

U jed. (87) i (88) $Y_i(Z,\xi)$ i $T(Z,\xi)$ su stvarne trenutne vrijednosti masenih udjela kemijskih vrsta i temperature, dobivene u pretprocesoru ili prema SLFM modelu (jed. (37)), gdje je $\xi\equiv\chi_{st}$, ili prema modelima baziranim na normaliziranoj varijabli napretka reakcije (jed. (41)), gdje je $\xi\equiv c$.

2.5.7 Usrednjena vrijednost brzine skalarne disipacije

Premda postoje modeli po kojima se računa dodatna transportna jednadžba za usrednjenu vrijednost brzine skalarne disipacije $\overline{\chi}$ [126], uglavnom se za izračun te varijable, a kako je to napravljeno i u ovome radu, koristi jednostavni linearni model:

$$\overline{\chi} = C_\chi \frac{\varepsilon}{k} \widetilde{Z''^2} \tag{89}$$

Kao što je predloženo u [15], konstanta C_χ poprima vrijednost $C_\chi = 2$. Usrednjavanjem jed. (35) dobiva se:

$$\overline{\chi} = \overline{\chi}_{st} \frac{\int_0^1 \exp\left\{-2\left[\mathrm{erfc}^{-1}(2Z)\right]^2\right\} P(Z)\,dZ}{\exp\left\{-2\left[\mathrm{erfc}^{-1}(2Z_{st})\right]^2\right\}} \tag{90}$$

Iz jed. (89) i (90) dobiva se usrednjena vrijednost brzine skalarne disipacije kod stehiometrijskih uvjeta $\overline{\chi}_{st}$ kao:

$$\overline{\chi}_{st} = \frac{C_\chi \frac{\varepsilon}{k} \widetilde{Z''^2} \exp\left\{-2\left[\mathrm{erfc}^{-1}(2Z_{st})\right]^2\right\}}{\int_0^1 \exp\left\{-2\left[\mathrm{erfc}^{-1}(2Z)\right]^2\right\} P(Z)\,dZ} \tag{91}$$

Pod pretpostavkom nepromjenjivosti u inercijalnom području energijske kaskade (vidi Sl. 14) [15, 71, 72], usrednjena vrijednost brzine skalarne disipacije kod stehiometrijskih uvjeta $\overline{\chi}_{st}$ koristi se kao parametar tabeliranja prema jed. (35), tj. $\chi_{st} \equiv \overline{\chi}_{st}$.

2.5.8 Pretpostavljeni kondicionalni momenti varijable napretka reakcije

U turbulentnom je slučaju potrebno aproksimirati normaliziranu varijablu napretka reakcije c (jed. (40) ili (42)), a da bi se dobio parametar za ulazak u tablicu kemijskih vrsta i temperature prema jed. (41). U ovome se radu koristi osnovna ideja pretpostavljenih kondicionalnih momenata za tu aproksimaciju, slično kao što je opisano u [47].

Prvi je kondicionalni moment varijable napretka reakcije Y_c, a prema definiciji iz jed. (82), definiran kao:

$$\overline{Y_c(Z)|Z} = \int_0^1 Y_c(Z)\,P\left(Y_c|Z\right)dY_c \tag{92}$$

$P\left(Y_c|Z\right)$ je kondicionalna PDF funkcija od Y_c za fiksnu vrijednost Z. Favreova usrednjena vrijednost varijable napretka reakcije je:

$$\tilde{Y}_c = \int_0^1 \overline{Y_c(Z)|Z}\;P(Z)\,dZ \tag{93}$$

Prvi kondicionalni moment varijable napretka reakcije Y_c također se može dobiti kondicionalnim usrednjavanjem jed. (40):

$$\overline{Y_c(Z)|Z} = \overline{c(Z)|Z}\left(Y_c^{Eq}(Z) - Y_c^{Mix}(Z)\right) + Y_c^{Mix}(Z) \tag{94}$$

$Y_c^{Eq}(Z)$ i $Y_c^{Mix}(Z)$ su konstantni za zadane vrijednosti masenog udjela smjese goriva, tj. $\overline{Y_c^{Eq}(Z)|Z} \equiv Y_c^{Eq}(Z)$ i $\overline{Y_c^{Mix}(Z)|Z} \equiv Y_c^{Mix}(Z)$. Kondicionalno usrednjena vrijednost normalizirane varijable napretka reakcije $\overline{c(Z)|Z}$ koristi se kao parametar u tabeliranju prema jed. (40).

U [47] se kaže da postoje uvjeti kada kondicionalna PDF funkcija $P\left(c|Z\right)$ slabo ovisi o masenom udjelu smjese goriva Z, a ako je dobro odabrana normalizirana varijabla napretka reakcije. U tom slučaju je $P\left(c|Z\right) \approx P(c)$ te se jed. (94) može aproksimirati kao:

$$\overline{Y_c(Z)|Z} = \overline{c}\left(Y_c^{Eq}(Z) - Y_c^{Mix}(Z)\right) + Y_c^{Mix}(Z) \tag{95}$$

Integriranjem jed. (95) po varijabli masenog udjela smjese goriva, a prema jed. (93), dobiva se Favreova usrednjena vrijednost varijable napretka reakcije kao:

$$\tilde{Y}_c = \overline{c}\left(\tilde{Y}_c^{Eq} - \tilde{Y}_c^{Mix}\right) + \tilde{Y}_c^{Mix} \tag{96}$$

U jed. (96) se vrijednosti za $\tilde{Y}_c^{Eq}$ i $\tilde{Y}_c^{Mix}$ dobivaju kao:

$$\tilde{Y}_c^{Eq} = \int_0^1 Y_c^{Eq}(Z)P(Z)dZ \tag{97}$$

$$\tilde{Y}_c^{Mix} = \int_0^1 Y_c^{Mix}(Z)P(Z)dZ \tag{98}$$

Slično je i u slučaju nepredmiješanih plamenova:

$$\tilde{Y}_c^{Ext} = \int_0^1 Y_c^{Ext}(Z)P(Z)dZ \tag{99}$$

Prema jed. (96) te uz pretpostavku da je $P(c|Z) \approx P(c)$, kondicionalna usrednjena vrijednost normalizirane varijable napretka reakcije $\overline{c(Z)|Z}$ može se aproksimirati kao:

$$\overline{c(Z)|Z} \approx \overline{c} = \frac{\tilde{Y}_c - \tilde{Y}_c^{Mix}}{\tilde{Y}_c^{Eq} - \tilde{Y}_c^{Mix}} \tag{100}$$

Vrijednosti $\tilde{Y}_c^{Eq}$ i $\tilde{Y}_c^{Mix}$ se tabeliraju u pretprocesoru zajedno s ostalim kemijskim vrstama, dok se usrednjena vrijednost varijable napretka reakcije $\tilde{Y}_c$ dobiva iz transportne jednadžbe prema jed. (76). U slučaju nepredmiješanih plamenova (Poglavlje 2.3.6.2) $\tilde{Y}_c^{Mix}$ u jed. (100) se zamjenjuje s $\tilde{Y}_c^{Ext}$ iz jed. (99).

Kondicionalna usrednjena vrijednost normalizirane varijable napretka reakcije $\overline{c(Z)|Z}$ prema jed. (100) koristi se kao parametar za ulazak u tablicu kemijskih vrsta prema jed. (40) ili (42). Još uvijek je potrebno modeliranje usrednjenog izvorskog člana

$\widetilde{\dot{\omega}_c}$ u jed. (76). Trenutna stvarna vrijednost tog izvorskog člana može se pretpostaviti ili iz FPI baze [47] ili iz SLFM baze, ovisno o modelu (vidi Poglavlje 2.3.6):

$$\widetilde{\dot{\omega}_c} = \int_0^1 \dot{\omega}_c\left(Z, \overline{c(Z)|Z}\right) P(Z)\, dZ \tag{101}$$

Konačno, Favreove usrednjene vrijednosti masenih udjela kemijskih vrsta i temperature, a prema jed. (87) i (88), dobivaju se iz tabeliranih podataka kao:

$$\tilde{Y}_i = \int_0^1 Y_i\left(Z, \overline{c(Z)|Z}\right) P(Z)\, dZ \tag{102}$$

$$\tilde{T} = \int_0^1 T\left(Z, \overline{c(Z)|Z}\right) P(Z)\, dZ \tag{103}$$

Prilikom modeliranja jed. (101)-(103) nisu uzete u obzir kondicionalne turbulentne fluktuacije normalizirane varijable napretka reakcije, te se ovaj pristup naziva još i modeliranje prvog reda [47]. Modeliranje drugog reda, a koje uzima u obzir kondicionalne turbulentne fluktuacije normalizirane varijable napretka reakcije, je opisano u [47].

3 Numerička procedura

Turbulentni tok fluida, prijenos topline zračenjem i nepredmiješano izgaranje simultano su simulirani tijekom cjelokupne procedure rješavanja u ovome radu. Međutim, da bi se smanjili računalni troškovi, neke su kalkulacije, a gdje je to bilo moguće, računate u pretprocesoru. Stacionarni laminarni *flamelet* profili, te naknadno PDF integracije, rađeni su u CSC rješavaču [96]. Prilikom tabeliranja kemijskih vrsta u pretprocesoru su pretpostavljeni adijabatski uvjeti, tj. $q_R = 0$ u jed. (36). Međutim, tijekom samog CFD proračuna temperature se nisu uzimale iz tih adijabatskih tablica dobivenih u pretprocesoru, već se je temperatura dobivala iterativno iz izračunate entalpije (a koja uzima u obzir i zračenje) te tabeliranih kemijskih vrsta iz pretprocesora. Dakle, izravan utjecaj prijenosa topline zračenja na stvaranje samih kemijskih vrsta nije u ovome radu uzet u obzir, te bi za to trebalo uvesti dodatnu treću koordinatu entalpijskog gubitka prilikom tabeliranja u pretprocesoru, a kako je predloženo, npr., u [75]. Kod DTRM-a proračuni praćenja zraka rađeni su u pretprocesoru te su svi geometrijski podaci pohranjeni u datoteku, a koja je korištena kasnije tijekom CFD proračuna [102]. Interakcija turbulencije i zračenja (eng. *turbulence/radiation interaction* – TRI) nije uzeta u obzir, te su usrednjene vrijednosti masenih udjela kemijskih vrsta i temperature korištene u proračunima prijenosa topline zračenjem (npr. u Jedn (46) te WSGGM-u [101]).

3.1 Kemijski pretprocesor

CSC rješavač [96] je razvijen za proračun kemijskih vrsta u pretprocesoru. Njegova funkcionalnost je dvostruka. Najprije se računaju proračuni kemijskih vrsta prema *flamelet* modelu (jed. (32) i (36)), dok se nakon toga vrše PDF integracije prema jed. (87) i (88). Rezultati PDF integracije (tzv. PDF tablice) pohranjuju se u datoteke koje se kasnije koriste prilikom CFD proračuna izgaranja za dobivanje kemijskih vrsta u ovisnosti od statističkih momenata izračunatih pratećih skalara (maseni udio smjese goriva ili varijabla napretka reakcije). Tabeliranje kemijskih vrsta pomoću normalizirane varijable napretka reakcije (predmiješani plamenovi i mješovita formulacija) djelomično se bazira na upotrebi PREMIX programa [97]. CHEMKIN II datoteke [98] korištene su za izračune termo-dinamičkih svojstava te za proračune kemijske kinetike. U daljnjem izlaganju će biti izneseni detalji implementacije CSC rješavača.

3.1.1 Modeli s pretpostavkom beskonačno brzih kemijskih reakcija

Zbog cjelovitosti prikaza te zbog korištenja kod inicijalizacije kod rješavanja *flamelet* jednadžbi, modeli bazirani na pretpostavci beskonačno brzih kemijskih reakcija – model 1-stupanjske ireverzibilne reakcije te ravnotežni model [20] – su implementirani u CSC rješavač te će ukratko biti spomenuti ovdje. Međutim, zbog svoje jednostavnosti ovi modeli nisu korišteni za modeliranje izgaranja u proračunima u ovome radu.

Prema modelu 1-stupanjske ireverzibilne reakcije, gorivo i oksidant ne mogu biti istovremeno prisutni na jednom mjestu te je pretpostavljena potpuna konverzija reaktanata u produkte izgaranja. Generalni zapis 1-stupanjske ireverzibilne reakcije je:

$$C_{a_1}H_{a_2}S_{a_3}O_{a_4}N_{a_5}+\left(a_1+\frac{a_2}{4}+a_3-\frac{a_4}{2}\right)O_2 \rightarrow a_1CO_2+\frac{a_2}{2}H_2O+a_3SO_2+\frac{a_5}{2}N_2 \qquad (104)$$

Gorivo je zadano u općenitoj formi kao $C_{a_1}H_{a_2}S_{a_3}O_{a_4}N_{a_5}$. Burke i Schumann prvi su koristili ovaj pristup kod modeliranja izgaranja još davne 1928 [110], pa se ovaj model još naziva i Burke-Schumannovim modelom. U ovom su modelu maseni udjeli kemijskih vrsta (reaktanata i produkata) jednoznačno povezani s masenim udjelom smjese goriva Z kao:

$$Y_j = Y_{j,O}\frac{Z_{st}-Z}{Z_{st}};\quad Z < Z_{st}$$
$$Y_j = Y_{j,F}\frac{Z-Z_{st}}{1-Z_{st}};\quad Z \geq Z_{st} \tag{105}$$

Jed. (105) opisuju linearne ili djelomično linearne distribucije reaktanata u području masenog udjela smjese goriva. Maseni sastavi produkata izgaranja dobivaju se tako da se od jedinice oduzme sastav reaktanata te upotrebom stehiometrijskih koeficijenata iz jed. (104). Kod ovog modela se ne računaju međuvrste koje se javljaju tijekom izgaranja.

Ravnotežni sastav kemijskih vrsta kod izgaranja može se dobiti ili upotrebom metode ravnotežnih konstanti ili minimizacijom slobodne energije – vidi [108]. Obje metode su ekvivalentne. U ovome radu su se za proračune kemijske ravnoteže koristile datoteke iz CHEMKIN II programa [98, 127].

Slika 17 prikazuje profile masenih udjela H_2O (uvećano blizu stehiometrijskog područja) dobivene 1-stupanjskim ireverzibilnim modelom te ravnotežnim modelom, a za slučaj plamena vodika i zraka iz Poglavlja 4. Maksimalne vrijednosti ravnotežnog H_2O profila manje su od 1-stupanjskog profila zbog disocijacije H_2O na višim temperaturama.

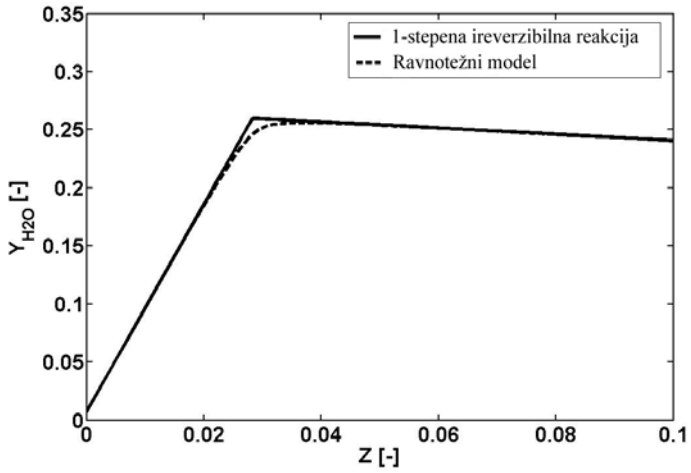

Slika 17 – H_2O profili (sustav H_2-zrak; povećano u blizini stehiometrije): Model 1-stupanjske ireverzibilne reakcije i ravnotežni model

Maseni se udio smjese goriva kod stehiometrijskih uvjeta Z_{st} može izračunati iz stehiometrijskih koeficijenata u jed. (104), a kako je pokazano u [15].

3.1.2 Numeričko rješenje *flamelet* jednadžbi

3.1.2.1 Diskretizacija konačnim razlikama

Korištena je metoda konačnih razlika [5, 106, 107, 128] prilikom dobivanja numeričkog rješenja *flamelet* jednadžbi (jed. (32) i (36)). Prostorna koordinata (maseni udio smjese goriva Z) podijeljena je u konačan broj točaka n_Z te su stacionarna rješenja *flamelet* jednadžbi tražena na toj mreži točaka. Diskretne točke su označene kao $Z^{(k)}$, gdje je $k = 1, 2, \ldots, n_Z$, dok su rubne točke uvijek $Z^{(1)} = 0$ i $Z^{(n_Z)} = 1$ (vidi Sl. 18).

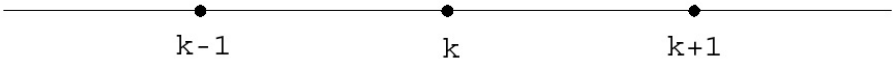

Slika 18 – Mreža za metodu konačnih razlika (1D)

Stacionarna rješenja *flamelet* jednadžbi označena su kao $T^{(k)} = T^{(k)}\left(Z^{(k)}, \chi_{st}\right)$ i $Y_i^{(k)} = Y_i^{(k)}\left(Z^{(k)}, \chi_{st}\right)$, gdje je $i = 1, 2, \ldots, N_{spec}$.

Da bi se dobio algebarski sustav jednadžbi, potrebno je aproksimirati derivacije koje se javljaju u jed. (32) i (36) odgovarajućim algebarskim izrazima. U ovome radu korištena je metoda središnjih derivacija (eng. *central differencing scheme* – CDS) [5] za aproksimaciju i prvih i drugih derivacija. Prema toj se metodi derivacije neke zavisne varijable ϕ u točki k (Sl. 18) na ne-ekvidistantnoj numeričkoj 1D mreži aproksimiraju kao:

$$\left(\frac{\partial \phi}{\partial Z}\right)_{(k)} = \frac{\phi^{(k+1)}\left(\Delta_{(k)}^{-}\right)^2 - \phi^{(k-1)}\left(\Delta_{(k)}^{+}\right)^2 + \phi^{(k)}\left[\left(\Delta_{(k)}^{+}\right)^2 - \left(\Delta_{(k)}^{-}\right)^2\right]}{\left(\Delta_{(k)}^{+} + \Delta_{(k)}^{-}\right)\Delta_{(k)}^{-}\Delta_{(k)}^{+}} \tag{106}$$

$$\left(\frac{\partial^2 \phi}{\partial Z^2}\right)_{(k)} = \frac{\phi^{(k+1)}\Delta_{(k)}^{-} + \phi^{(k-1)}\Delta_{(k)}^{+} - \phi^{(k)}\left(\Delta_{(k)}^{-} + \Delta_{(k)}^{+}\right)}{0.5\left(\Delta_{(k)}^{-} + \Delta_{(k)}^{+}\right)\Delta_{(k)}^{-}\Delta_{(k)}^{+}} \tag{107}$$

U gornjim su jednadžbama udaljenosti između susjednih točaka na numeričkoj mreži skraćeno označene kao:

$$\Delta_{(k)}^{-} = Z^{(k)} - Z^{(k-1)} \qquad \Delta_{(k)}^{+} = Z^{(k+1)} - Z^{(k)} \tag{108}$$

Osim prostornih derivacija, u *flamelet* jednadžbama također se javljaju i vremenske derivacije. Međutim, u ovome se radu nije koristio standardni način rješavanja jednadžbi marširanja u vremenu [5] sve do stacionarnosti. Naprotiv, zbog izrazite numeričke krutosti *flamelet* jednadžbi, korištena je Gearova metoda vremenske integracije, a koja je implementirana u DDASSL rješavaču [129] korištenom u ovome radu.

Nakon primjene diskretizacijskih pravila prema jed. (106) i (107) u *flamelet* jednadžbama, u prvom koraku se dobivaju sljedeće poludiskretizirane jednadžbe:

$$\left(\frac{\partial Y_i}{\partial \tau}\right)_{(k)} - \left(\frac{\chi}{2}\right)_{(k)} \frac{Y_i^{(k+1)}\Delta_{(k)}^{-} + Y_i^{(k-1)}\Delta_{(k)}^{+} - Y_i^{(k)}\left(\Delta_{(k)}^{-} + \Delta_{(k)}^{+}\right)}{0.5\left(\Delta_{(k)}^{-} + \Delta_{(k)}^{+}\right)\Delta_{(k)}^{-}\Delta_{(k)}^{+}} - \left(\frac{\dot{\omega}_i}{\rho}\right)_{(k)} = 0 \tag{109}$$

$$\begin{aligned}
&\left(\frac{\partial T}{\partial \tau}\right)_{(k)} - \left(\frac{\chi}{2}\right)_{(k)} \frac{T^{(k+1)}\Delta_{(k)}^{-} + T^{(k-1)}\Delta_{(k)}^{+} - T^{(k)}\left(\Delta_{(k)}^{-} + \Delta_{(k)}^{+}\right)}{0.5\left(\Delta_{(k)}^{-} + \Delta_{(k)}^{+}\right)\Delta_{(k)}^{-}\Delta_{(k)}^{+}} - \\
&\left(\frac{\chi}{2c_p}\frac{\partial c_p}{\partial Z}\right)_{(k)} \frac{T^{(k+1)}\left(\Delta_{(k)}^{-}\right)^2 - T^{(k-1)}\left(\Delta_{(k)}^{+}\right)^2 + T^{(k)}\left[\left(\Delta_{(k)}^{+}\right)^2 - \left(\Delta_{(k)}^{-}\right)^2\right]}{\left(\Delta_{(k)}^{+} + \Delta_{(k)}^{-}\right)\Delta_{(k)}^{-}\Delta_{(k)}^{+}} - \\
&\left(\frac{\chi}{2c_p}\right)_{(k)} \sum_{i=1}^{N_{spec}} \left\{ \left(c_{pi}\frac{\partial Y_i}{\partial Z}\right)_{(k)} \frac{T^{(k+1)}\left(\Delta_{(k)}^{-}\right)^2 - T^{(k-1)}\left(\Delta_{(k)}^{+}\right)^2 + T^{(k)}\left[\left(\Delta_{(k)}^{+}\right)^2 - \left(\Delta_{(k)}^{-}\right)^2\right]}{\left(\Delta_{(k)}^{+} + \Delta_{(k)}^{-}\right)\Delta_{(k)}^{-}\Delta_{(k)}^{+}} \right\} + \\
&\left[\frac{1}{\rho c_p}\left(\sum_{i=1}^{N_{spec}} h_i\dot{\omega}_i - q_R\right)\right]_{(k)} = 0
\end{aligned} \tag{110}$$

Preuređenjem jed. (109) i (110) dobiva se sustav diferencijalno-algebarskih jednadžbi kao:

$$\left(\frac{\partial Y_i}{\partial \tau}\right)_{(k)} = C_1^{(k)}Y_i^{(k-1)} + C_2^{(k)}Y_i^{(k)} + C_3^{(k)}Y_i^{(k+1)} + C_4^{(k)} \tag{111}$$

$$\left(\frac{\partial T}{\partial \tau}\right)_{(k)} = C_5^{(k)}T^{(k-1)} + C_6^{(k)}T^{(k)} + C_7^{(k)}T^{(k+1)} + C_8^{(k)} \tag{112}$$

Koeficijenti $C_1^{(k)} \ldots C_8^{(k)}$ su:

$$
\begin{aligned}
C_1^{(k)} &= \frac{\chi^{(k)}}{\left(\Delta_{(k)}^{-}+\Delta_{(k)}^{+}\right)\Delta_{(k)}^{-}} \\
C_2^{(k)} &= -\frac{\chi^{(k)}}{\Delta_{(k)}^{-}\Delta_{(k)}^{+}} \\
C_3^{(k)} &= \frac{\chi^{(k)}}{\left(\Delta_{(k)}^{-}+\Delta_{(k)}^{+}\right)\Delta_{(k)}^{+}} \\
C_4^{(k)} &= \left(\frac{\dot{\omega}_i}{\rho}\right)_{(k)}
\end{aligned}
\tag{113}
$$

$$
\begin{aligned}
C_5^{(k)} &= C_1^{(k)} - \left(\frac{\chi}{2c_p}\right)_{(k)}\left[\left(\frac{\partial c_p}{\partial Z}\right)_{(k)} + \sum_{i=1}^{N_{spec}}\left(c_{pi}\frac{\partial Y_i}{\partial Z}\right)_{(k)}\right]\frac{\Delta_{(k)}^{+}}{\left(\Delta_{(k)}^{-}+\Delta_{(k)}^{+}\right)\Delta_{(k)}^{-}} \\
C_6^{(k)} &= C_2^{(k)} + \left(\frac{\chi}{2c_p}\right)_{(k)}\left[\left(\frac{\partial c_p}{\partial Z}\right)_{(k)} + \sum_{i=1}^{N_{spec}}\left(c_{pi}\frac{\partial Y_i}{\partial Z}\right)_{(k)}\right] \\
C_7^{(k)} &= C_3^{(k)} + \left(\frac{\chi}{2c_p}\right)_{(k)}\left[\left(\frac{\partial c_p}{\partial Z}\right)_{(k)} + \sum_{i=1}^{N_{spec}}\left(c_{pi}\frac{\partial Y_i}{\partial Z}\right)_{(k)}\right]\frac{\Delta_{(k)}^{-}}{\left(\Delta_{(k)}^{-}+\Delta_{(k)}^{+}\right)\Delta_{(k)}^{+}} \\
C_8^{(k)} &= \left[\frac{1}{\rho c_p}\left(q_R - \sum_{i=1}^{N_{spec}} h_i\dot{\omega}_i\right)\right]_{(k)}
\end{aligned}
\tag{114}
$$

Prve derivacije, koje se javljaju u uglatim zagradama u jed. (114), aproksimiraju se kao:

$$
\left(\frac{\partial c_p}{\partial Z}\right)_{(k)} = \frac{c_p^{(k+1)}\left(\Delta_{(k)}^{-}\right)^2 - c_p^{(k-1)}\left(\Delta_{(k)}^{+}\right)^2 + c_p^{(k)}\left[\left(\Delta_{(k)}^{+}\right)^2 - \left(\Delta_{(k)}^{-}\right)^2\right]}{\left(\Delta_{(k)}^{+}+\Delta_{(k)}^{-}\right)\Delta_{(k)}^{-}\Delta_{(k)}^{+}} \tag{115}
$$

$$
\sum_{i=1}^{N_{spec}}\left(c_{pi}\frac{\partial Y_i}{\partial Z}\right)_{(k)} = \sum_{i=1}^{N_{spec}}\left\{c_{pi}^{(k)}\frac{Y_i^{(k+1)}\left(\Delta_{(k)}^{-}\right)^2 - Y_i^{(k-1)}\left(\Delta_{(k)}^{+}\right)^2 + Y_i^{(k)}\left[\left(\Delta_{(k)}^{+}\right)^2 - \left(\Delta_{(k)}^{-}\right)^2\right]}{\left(\Delta_{(k)}^{+}+\Delta_{(k)}^{-}\right)\Delta_{(k)}^{-}\Delta_{(k)}^{+}}\right\} \tag{116}
$$

Budući da su poznate vrijednosti masenih udjela kemijskih vrsta i temperature na rubovima, potrebno je rješavati diskretizirane *flamelet* jednadžbe samo za unutarnje točke, tj. za $k = 2,...,n_Z - 1$. Uz zadane početne profile (dobivene 1-stupanjskim ireverzibilnim modelom ili ravnotežnim modelom), diskretizirane *flamelet* jednadžbe (jed. (111) i (112)) se rješavaju upotrebom DDASSL rješavača [129] tako dugo u vremenu dok vremenske derivacije u jed. (111) i (112) ne postanu zanemarivima.

3.1.2.2 Rješenje sustava diferencijalno-algebarskih jednadžbi

U općenitom je slučaju kompletan set kemijskih reakcija složen, te se sastoji o puno elementarnih reakcija. Brzine stvaranja/nestajanja različitih kemijskih vrsta međusobno se razlikuju za više redova veličine, a što dovodi do nestacionarnog sustava s širokim područjem vremenskih konstanti. Ovakvi su sustavi označeni kao numerički krutim, te ih se teško rješava upotrebom standardnih numeričkih procedura vremenske diskretizacije. Članovi koji uzrokuju krutost *flamelet* jednadžbi su izvorski članovi kemijskih vrsta. U diskretiziranim *flamelet* jednadžbama ti se članovi pojavljuju u koeficijentima $C_4^{(k)}$ i $C_8^{(k)}$ (vidi jed. (113) i (114)). Međutim, problem rješavanja sustava krutih običnih diferencijalnih jednadžbi je matematičke prirode te su već razvijena efikasna rješenja. Gearova se metoda bazira na upotrebi konačnih razlika prema unatrag te je implementirana u DDASSL rješavaču [129] koji je korišten u ovome radu za postizanje stacionarnih rješenja diskretiziranih *flamelet* jednadžbi u obliku $G\left(t,\phi,\frac{d\phi}{dt}\right)=0$. Diskretizirane se *flamelet* jednadžbe računaju na unutarnjim točkama ($k=2,...,n_Z-1$) mreže. Budući da imamo ukupan broj od N_{spec} jednadžbi za kemijske vrste (jed. (32)) te jednu energijsku jednadžbu (jed. (36)), ukupan je broj diferencijalno-algebarskih *flamelet* jednadžbi koji se treba rješavati $\left(N_{spec}+1\right)\left(n_Z-2\right)$.

3.1.2.3 PDF integracije

Kao što je opisano u Poglavlju 2.5.6, u turbulentnom slučaju su trenutni stacionarni profili reaktivnih skalara povezani sa statističkim momentima masenog udjela smjese goriva preko jed. (87) i (88). Da bi se izbjegao proračun integracija u jed. (87) i (88) tijekom same CFD kalkulacije, a što bi bilo računalno skupo u slučaju velikog broja kemijskih vrsta, moguće je iste napraviti u pretprocesoru te rezultate spremiti u obliku PDF tablica. Da bi se to učinilo potrebno je identificirati područja mogućih realizacija momenata masenog udjela smjese goriva, a koji se koriste kao parametri u β-PDF funkciji, te je potrebno diskretizirati prostor obuhvaćen tim varijablama te izračunati PDF integracije za svaku točku iz tog prostora.

Usrednjena vrijednost masenog udjela smjese goriva $\tilde{Z}$ ima fiksno određene rubne vrijednosti, te poprima vrijednost $\tilde{Z}=1$ na ulazu goriva te $\tilde{Z}=0$ na ulazu oksidanta.

Kako se gorivo i oksidant miješaju tijekom nepredmiješanog izgaranja, usrednjena vrijednost masenog udjela smjese goriva $\tilde{Z}$ može poprimiti bilo koju vrijednost između rubnih vrijednosti, tj.:

$$0 \le \tilde{Z} \le 1 \tag{117}$$

Varijanca masenog udjela smjese goriva $\widetilde{Z''^2}$, s druge strane, nema jasno određenu gornju graničnu vrijednost. Kako je to pozitivan skalar, te iz zahtijeva da koeficijenti α i β u jed. (84) ne smiju biti negativni, slijedi sljedeća nejednakost:

$$0 \le \widetilde{Z''^2} \le \tilde{Z}\left(1-\tilde{Z}\right) \tag{118}$$

Iz jed. (118) se vidi da gornja vrijednost ovisi o usrednjenoj vrijednosti masenog udjela smjese goriva $\tilde{Z}$. Međutim, lako se može istražiti da je vrijednost usrednjenog masenog udjela smjese goriva, kod koje je gornja vrijednost varijance maksimalna ($\widetilde{Z''^2_{\max}} = 0.25$), $\tilde{Z} = 0.5$. U tom pogledu se uvodi skalirana varijanca $\widetilde{Z''^2_s}$ definirana kao:

$$\widetilde{Z''^2_s} = \widetilde{Z''^2_{\max}} \frac{\widetilde{Z''^2}}{\tilde{Z}\left(1-\tilde{Z}\right)} \tag{119}$$

Lako se može utvrditi da skalirana varijanca ima fiksno određene rubne vrijednosti:

$$0 \le \widetilde{Z''^2_s} \le 0.25 \tag{120}$$

Dakle, ukoliko se kao dvije koordinate kod konstrukcije PDF tablica koriste usrednjena vrijednost masenog udjela smjese goriva, te skalirana varijanca masenog udjela smjese goriva, može se dobiti strukturirano tabeliranje te se PDF integracije provode za svaku diskretnu točku u prostoru razapetom između te dvije koordinate. Varijanca masenog udjela smjese goriva dobiva se iz skalirane varijance prema jed. (119). Izračunate usrednjene vrijednosti reaktivnih skalara (jed. (87) i (88)) tabeliraju se u PDF tablicama. Tijekom same CFD kalkulacije računaju se transportne jednadžbe za momente masenog udjela smjese goriva, dok se usrednjeni maseni udjeli kemijskih vrsta dobivaju interpolacijom iz PDF tablica. Primjer PDF tablice za temperaturu (adijabatsku) prikazan je na Sl. 19.

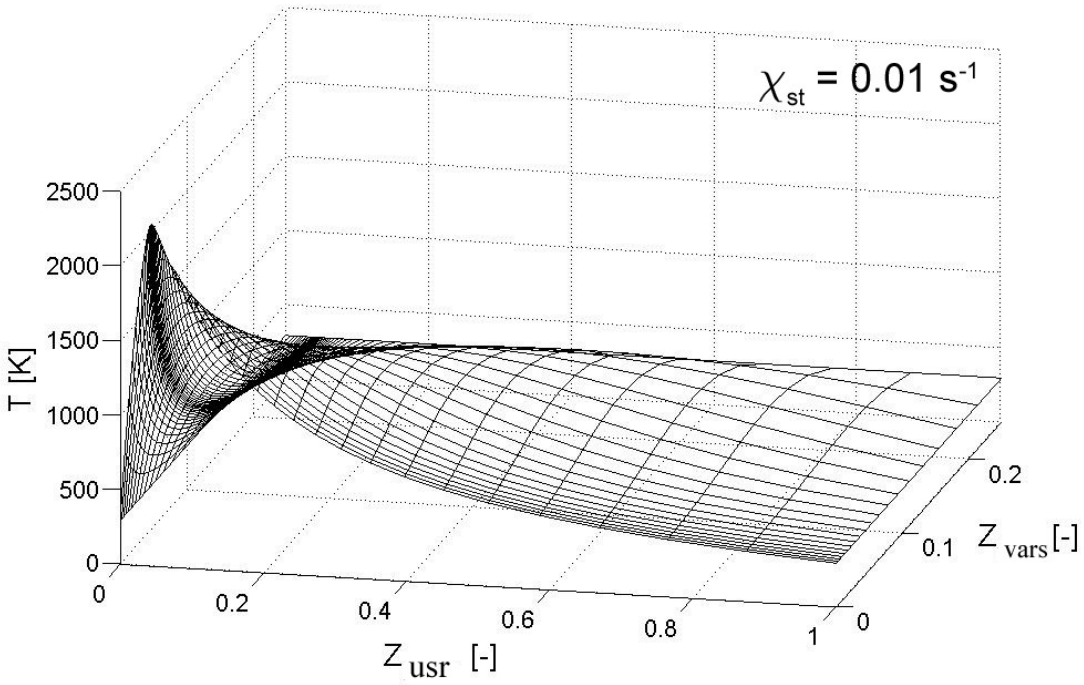

Slika 19 – Integrirani (pretpostavljeni β-PDF) adijabatski temperaturni profili ($\chi_{st} = 0.01$ s^{-1}) za plamen H_2/He-zrak (gorivo: H_2 80%, He 20% – molni udjeli, 295 K; zrak: 294 K) – vidi Sl. 3

Integracije prema jed. (87) i (88) riješene su numerički upotrebom trapeznog pravila integriranja [130] na unutarnjim točkama masenog udjela smjese goriva. Kod rubnih intervala, tj. $Z \in \left[Z^{(1)}, Z^{(2)} \right]$ i $Z \in \left[Z^{(n_Z-1)}, Z^{(n_Z)} \right]$, korištene su otvorene integracijske formule, poput Gaussovih integracijskih formula [130, 131], da bi se riješili problemi singulariteta koje β-PDF ima na rubovima za određene vrijednosti momenata masenog udjela smjese goriva (npr. $\tilde{Z} = 0.2$ i $\widetilde{Z''^2} = 0.1$, vidi Sl. 16). Više se detalja o metodama numeričke integracije može pronaći u literaturi [130, 132, 133].

3.1.3 Implementacija CSC rješavača

Razvijen je CSC rješavač [96] za potrebe proračuna kemijskih vrsta (1-stupanjski ireverzibilni model/ravnotežni model/stacionarni laminarni *flamelet* model) i PDF integracija u pretprocesoru. Cjelokupni se pretprocesor sastoji od dva glavna dijela – samog CSC rješavača te grafičkog korisničkog sučelja generiranog u MATLAB-u [134]. Sam CSC rješavač je programiran u FORTAN 90 programskom jeziku [135] te će njegova struktura biti iznesena u sljedećim poglavljima. Grafičko korisničko sučelje u MATLAB-u koristilo se samo za olakšanu upotrebu CSC rješavača te prikaz rezultata u postprocesoru, te se ono neće opisivati u ovome radu. Više se detalja može pronaći na [96].

3.1.3.1 Struktura rješavača

Ulazni podaci za CSC rješavač se zadaju preko ASCII ulazne datoteke. Prema odabiru CSC rješavač ili vrši proračun kemijskih vrsta prema odabranom modelu (1-stupanjski ireverzibilni model/ravnotežni model/stacionarni laminarni *flamelet* model) ili vrši PDF integracije. Rezultati se pohranjuju u datoteke. Slika 20 shematski prikazuje strukturu CSC rješavača.

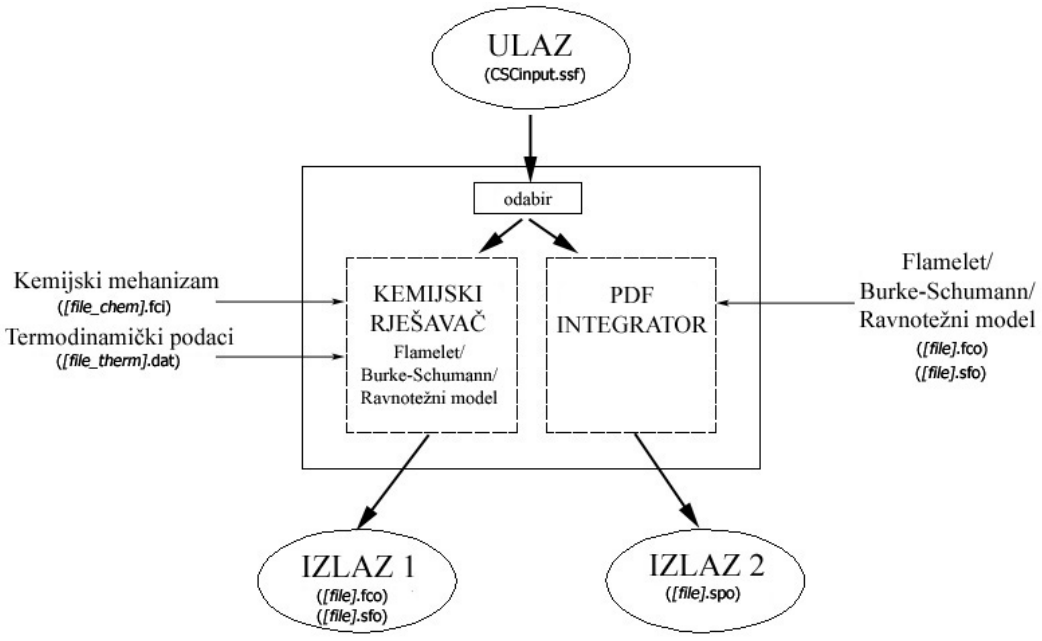

Slika 20 – Struktura CSC rješavača

3.1.3.2 Kemijski rješavač

Kemijski rješavač je dio CSC rješavača gdje se vrši proračun kemijskih vrsta ovisno o modelu – 1-stupanjski ireverzibilni model, ravnotežni model ili stacionarni laminarni *flamelet* model. Temperatura i maseni udjeli kemijskih vrsta računaju se na diskretnim točkama masenog udjela smjese goriva te se rezultati spremaju u datoteke (OUTPUT 1 na Sl. 20).

Ukratko, nakon svih potrebnih inicijalizacija, postavljanja rubnih uvjeta i stehiometrijskih proračuna, računa se 1D računalna mreža. Mreža može biti ekvidistantna ili ne-ekvidistantna. U slučaju ne-ekvidistantne mreže točke su gušće raspodijeljene u blizini stehiometrijskog područja, a gdje se očekuju veći gradijenti profila reaktivnih skalara. Nakon kreiranja mreže računaju se kemijske vrste za različite nivoe tlakova[6], a ovisno o odabranom modelu. U slučaju stacionarnih laminarnih *flamelet* profila, početni profili se inicijaliziraju primjenom rezultata modela 1-stupanjske ireverzibilne reakcije ili ravnotežnog modela. CHEMKIN II datoteke [98] su korištene za proračune termo-dinamičkih svojstava i kemijske kinetike. Slika 21 shematski prikazuje strukturu kemijskog rješavača.

[6] Burke-Schumann profili kemijskih vrsta ne ovise o tlaku.

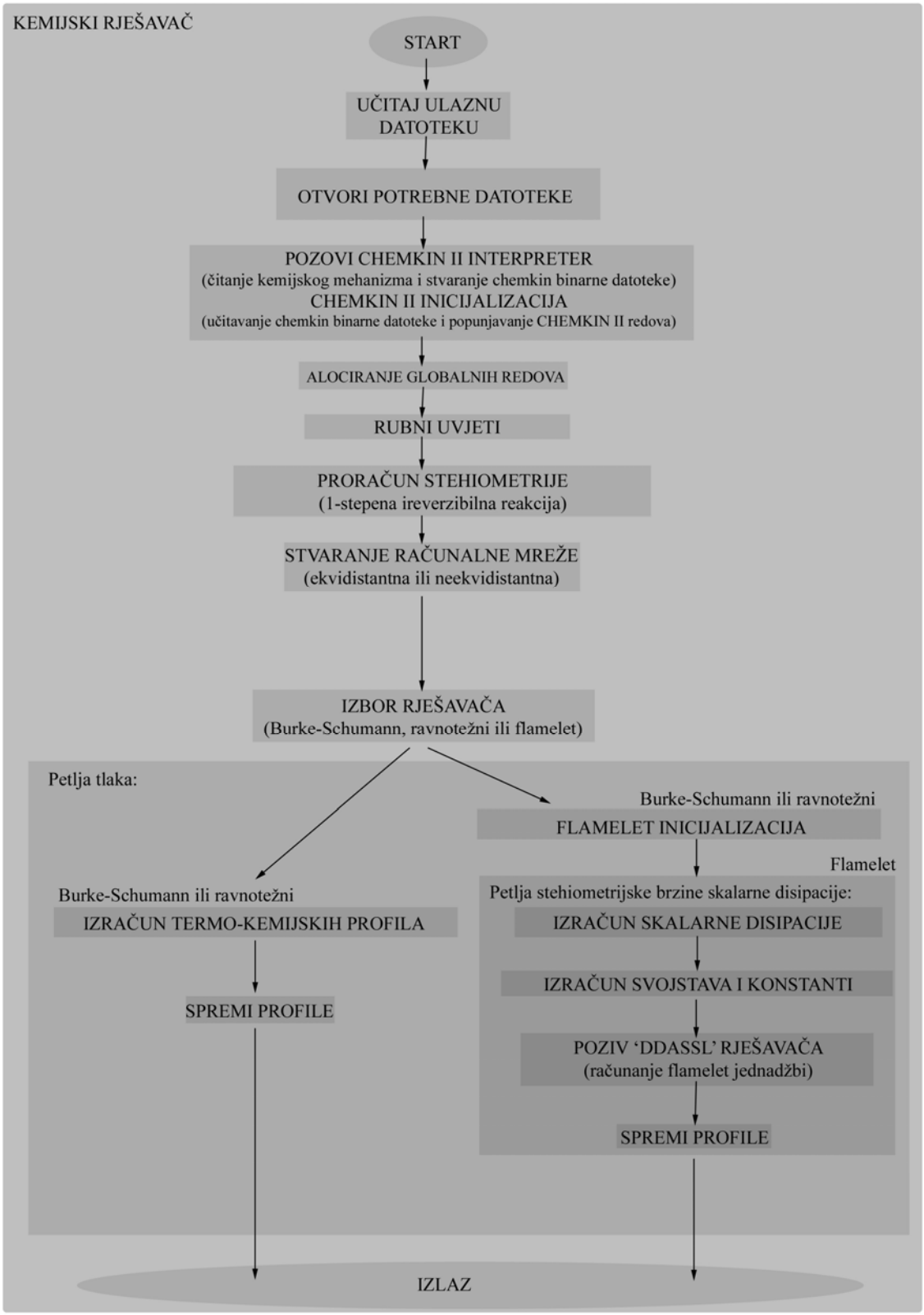

Slika 21 – Struktura CSC rješavača: kemijski rješavač

3.1.3.3 PDF rješavač

U PDF rješavaču (vidi Sl. 20) vrši se izračun PDF tablica, gdje se trenutni profili reaktivnih skalara integriraju za različite točke momenata masenog udjela smjese goriva. Trenutni profili mogu se dobiti ili primjenom kemijskog rješavača, a kako je opisano u prethodnom poglavlju, ili se mogu koristiti profili bazirani na normaliziranoj varijabli napretka reakcije (jed. (41)). Za potrebe numeričke integracije importirani se profili preslikavaju na posebnu mrežu. Potom se stvara mreža koja pokriva prostor razapet momentima masenog udjela smjese goriva, te se broj točaka raspodjele svake od koordinata zadaje u ulaznoj datoteci. Predlaže se upotreba ne-ekvidistantne mreže i veći broj točaka u stehiometrijskom području, gdje se očekuju veći gradijenti (vidi Sl. 19). Na kraju se vrše integracije, a kako je opisano u Poglavlju 3.1.2.3. Ovisno o importiranim profilima trenutnih vrijednosti reaktivnih skalara, usrednjene vrijednosti istih se dobivaju za različite nivoe tlaka te brzine skalarne disipacije kod stehiometrijskih uvjeta ili normalizirane varijable napretka reakcije, ovisno o modelu. Struktura PDF rješavača je shematski prikazana na Sl. 22. Rezultati PDF integracija se pohranjuju u PDF tablice (OUTPUT 2 na Sl. 20), a koje se poslije koriste tijekom CFD kalkulacija.

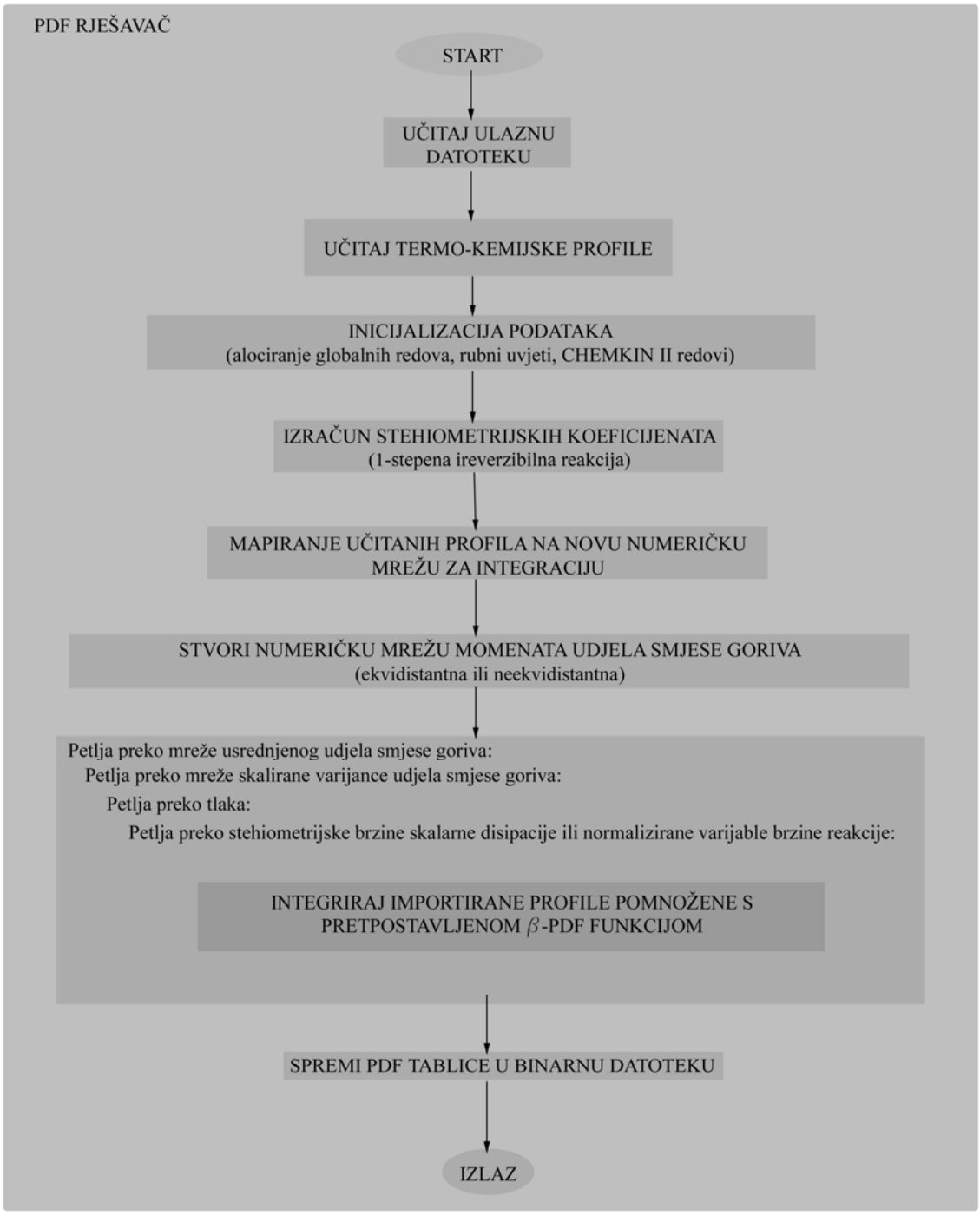

Slika 22 – Struktura CSC rješavača: PDF rješavač

3.2 Rješavač toka fluida

Usrednjene jednadžbe tok fluida, kao što su predstavljene u Poglavlju 2.5.3, moraju se riješiti zajedno s modelima turbulentnih korelacija, a da bi se dobile prostorne i vremenske raspodjele usrednjenih vrijednosti koje te jednadžbe opisuju. Međutim, spomenuti sustav parcijalnih diferencijalnih jednadžbi je nelinearan te analitička rješenja, u općem slučaju, nisu moguća. Da bi se stvorila generalna procedura rješavanja, a koja je primjenjiva u proizvoljno kompleksnim primjerima, potrebno je diskretizirati prostornu i vremensku domenu te sustav diferencijalnih jednadžbi, uz pomoć numeričkih metoda, transformirati u sustav algebarskih jednadžbi koji se lagano dade riješiti [5].

U ovome je radu za proračun toka fluida korišten CFD rješavač FIRE [99]. On se temelji na implicitnoj metodi rješavanja na nestrukturiranim mrežama sastavljenim od proizvoljnih polihedrona [99]. Transportne jednadžbe zbog modeliranja izgaranja relevantne za ovaj rad dodatno su implementirane u FIRE program preko korisnički definiranih funkcija.

U daljnjem će se izlaganju ukratko opisati procedura rješavanja i tehnike diskretizacije korištene u FIRE-u, dok je za detaljnije informacije o samom rješavaču potrebno konzultirati [99]. Također će se ovdje opisati način implementacije modela izgaranja.

3.2.1 Integralna forma transportnih jednadžbi

Transportne jednadžbe u integralnoj formi su polazna točka metode kontrolnih volumena. Dakle, potrebno je transportne jednadžbe koje su u Poglavlju 2 zadane u diferencijalnoj formi pretvoriti u sustav jednadžbi u integralnoj formi, a na način kako će biti opisano. Ovdje će se pokazati kako se transportna jednadžba, jed. (8), pretvara u integralnu formu, dok isti principi transformacije vrijede i za ostale jednadžbe, bez obzira da li je riječ o skalarnim, vektorskim ili tenzorskim komponentama [5, 99].

Ako se uzme integral jed. (8) po kontrolnom volumenu V_{CV}, a koji je obuhvaćen plohama S_{CV}, dobije se sljedeća integralna forma jed. (8):

$$\frac{\partial}{\partial t}\int_{V_{CV}} \rho\varphi dV + \int_{S_{CV}} \rho\varphi\, u_j n_j dS = \int_{S_{CV}} \Gamma_\varphi \frac{\partial \varphi}{\partial x_j} n_j dS + \int_{V_{CV}} q_\varphi dV \tag{121}$$

U narednom opisu se pretpostavlja da kontrolni volumeni miruju[7], a kao što je slučaj u konfiguracijama plamena koje su simulirane u ovome radu. Prvi član na lijevoj strani jed. (121) predstavlja brzinu promjenu specifičnog svojstva φ u kontrolnom volumenu. Ukupni neto tok tog svojstva kroz granice kontrolnog volumena, a zbog relativnog gibanja toka fluida naspram kontrolnog volumena, je opisan drugim članom na lijevoj strani. Prvi član na desnoj strani je uslijed neto difuzije specifičnog svojstva φ kroz granice kontrolnog volumena, dok je posljednji član izvor/ponor specifičnog svojstva φ. Kod izvoda jed. (121) je primijenjen Gaussov teorem divergencije [105], a da bi se volumenski integrali pretvorili u površinske integrale kod konvekcijskog i difuzijskog člana:

$$\int_{V_{CV}} \frac{\partial\left(\rho\varphi u_j\right)}{\partial x_j} dV = \int_{S_{CV}} \rho\varphi\, u_j n_j dS \tag{122}$$

$$\int_{V_{CV}} \frac{\partial}{\partial x_j}\left(\Gamma_\varphi \frac{\partial\varphi}{\partial x_j}\right) dV = \int_{S_{CV}} \Gamma_\varphi \frac{\partial\varphi}{\partial x_j} n_j dS \tag{123}$$

3.2.2 Diskretizacija kontrolnim volumenima

Prostorna domena se diskretizira u konačan broj kontrolnih volumena. Računalne točke su smještene u geometrijskim središtima tih kontrolnih volumena – vidi Sl. 23.

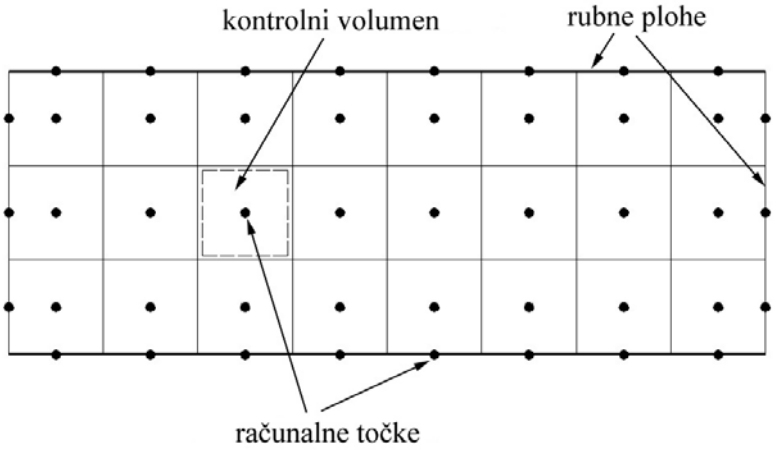

Slika 23 – Diskretizacija prostorne domene u kontrolne volumene (2D)

[7] FIRE CFD rješavač podržava pomične kontrolne volumene.

U općenitom slučaju kontrolni volumeni mogu biti polihedroni proizvoljnog oblika, sastavljeni od konačnog broja ravnih ploha. Kontrolni volumeni se ne smiju međusobno preklapati. Ukupan skup kontrolnih volumena koji pokrivaju prostornu domenu naziva se računalnom mrežom. Kontrolni volumeni na granicama prostorne domene mogu se smatrati beskonačno tankim te se podudaraju sa zajedničkim plohama susjednih unutarnjih kontrolnih volumena. Ti rubni kontrolni volumeni se zbog toga još često nazivaju i rubnim plohama, dok se rubni uvjeti po potrebi propisuju u njihovim računalnim točkama, vidi Sl. 23. Slika 24 prikazuje proizvoljni kontrolni volumen.

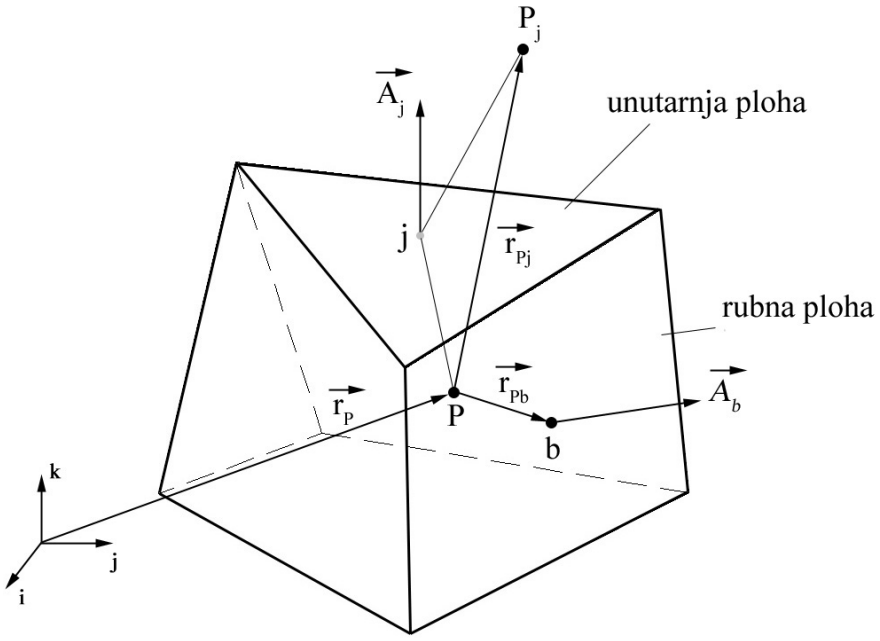

Slika 24 – Kontrolni volumen (proizvoljni polihedron)

Bilo se koja zavisna varijabla (komponenta brzine, entalpija, gustoća, tlak, i sl.) pretpostavlja homogenom unutar kontrolnog volumena te da ima vrijednost kao što je izračunata u računalnoj točki (točka P na Sl. 24). To je, tzv., kolocirani raspored varijabli [5]. Kada su potrebne vrijednosti zavisnih varijabli, ili njihovi gradijenti, na rubnim plohama kontrolnih volumena, kao kod površinskih integrala u jed. (122) i (123), ovisno o shemi diferenciranja i metodi aproksimacije gradijenata te se vrijednosti dobivaju interpolacijom između susjednih kontrolnih volumena. Pravilan izbor sheme diskretizacije je vrlo bitan što se tiče numeričkih svojstava kao što su točnost, konvergencija, stabilnost, konzervativnost, i sl. – vidi [5, 6]. Ovisno o svojstvu koje se

računa, mogu se upotrijebiti različite sheme diferencije [5]. Više informacija o shemama diferenciranja, metodama aproksimacije gradijenata, tehnikama interpolacije, i sl., a kako je implementirano u FIRE rješavaču, može se pronaći u [99].

Volumenski i površinski integrali u jed. (121) računaju se na bazi jednog kontrolnog volumena. Kako je kontrolni volumen obuhvaćen konačnim brojem rubnih ploha, tj. $S_{CV} = \sum_{k=1}^{N_{faces}} S_k$, površinski integrali u jed. (121) mogu se rastaviti kao:

$$\int_{S_{CV}} \rho\varphi\, u_j n_j dS = \sum_{k=1}^{N_{faces}} \int_{S_k} \rho\varphi\, u_j n_j dS \tag{124}$$

$$\int_{S_{CV}} \Gamma_\varphi \frac{\partial\varphi}{\partial x_j} n_j dS = \sum_{k=1}^{N_{faces}} \int_{S_k} \Gamma_\varphi \frac{\partial\varphi}{\partial x_j} n_j dS \tag{125}$$

Jed. (121) može se sada napisati kao:

$$\frac{\partial}{\partial t}\int_{V_{CV}} \rho\varphi dV + \sum_{k=1}^{N_{faces}} \int_{S_k} \rho\varphi\, u_j n_j dS = \sum_{k=1}^{N_{faces}} \int_{S_k} \Gamma_\varphi \frac{\partial\varphi}{\partial x_j} n_j dS + \int_{V_{CV}} q_\varphi dV \tag{126}$$

Aproksimacija se javlja kod približnog određivanja površinskih i volumenskih integrala u jed. (126). Kao što je već spomenuto, zavisne varijable su homogene unutar jednog kontrolnog volumena, pa isto to vrijedi i za podintegralne funkcije u volumenskim integralima. Dakle, volumenski integrali u jed. (126) mogu se izračunati kao:

$$\frac{\partial}{\partial t}\int_{V_{CV}} \rho\varphi dV = \frac{\partial}{\partial t}\left[\left(\rho\varphi\right)_c V_{CV}\right] \tag{127}$$

$$\int_{V_{CV}} q_\varphi dV = \left(q_\varphi\right)_c V_{CV} \tag{128}$$

Vrijednosti podintegralnih funkcija u računalnim točkama su $\left(\rho\varphi\right)_c$ i $\left(q_\varphi\right)_c$.

Pravilo središnje točke je upotrebljeno kod aproksimacije površinskih integrala [5]. Pretpostavlja se da vrijednost podintegralne funkcije u središtu rubne plohe prevladava preko cijele te plohe, te se površinski integrali, dakle, mogu aproksimirati kao:

$$\int_{S_k} \rho\varphi\, u_j n_j dS = \left(\rho\varphi\, u_j n_j\right)_c S_k \tag{129}$$

$$\int_{S_k} \Gamma_\varphi \frac{\partial \varphi}{\partial x_j} n_j dS = \left(\Gamma_\varphi \frac{\partial \varphi}{\partial x_j} n_j \right)_c S_k \tag{130}$$

Vrijednosti podintegralnih funkcija u središtima rubnih ploha su $\left(\rho\varphi u_j n_j\right)_c$ i $\left(\Gamma_\varphi \frac{\partial \varphi}{\partial x_j} n_j \right)_c$. Da bi se osigurala konzervativnost tokova kroz plohe kontrolnih volumena potrebno je osigurati da se površinski integrali na zajedničkim plohama između dva kontrolna volumena računaju na isti način [6].

3.2.3 Procedura rješavanja

Osim prostorne diskretizacije kontrolnim volumenima, a kako je opisano u prethodnom poglavlju, kod nestacionarnih problema je potrebno jed. (126) diskretizirati i u vremenu. Međutim, kako su u ovome radu simulirani samo stacionarni plamenovi, korišten je stacionarni FIRE rješavač te se detalji vremenske integracije neće prikazivati ovdje.

Kao rezultat diskretizacije transportne jednadžbe na bazi jednog kontrolnog volumena (Sl. 24) javlja se algebarska jednadžba u obliku:

$$a_P \varphi_P = \sum_{k=1}^{N_{faces}} a_k \varphi_{Pk} + S_\varphi \tag{131}$$

Sumacija u jed. (131) provodi se preko ploha kontrolnog volumena (uključujući i rubne plohe). Iz jed. (131) vidimo da vrijednost zavisne varijable u računalnoj točki P ovisi o vrijednostima iste u susjednim računalnim točkama te izvoru/ponoru unutar tog kontrolnog volumena. Ukupan broj algebarskih jednadžbi prema jed. (131) za jednu zavisnu varijablu je jednak ukupnom broju unutarnjih kontrolnih volumena N_{CV} korištenih kod diskretizacije prostorne domene. Dakle, ukupan broj svih algebarskih jednadžbi je jednak broju transportnih jednadžbi N_{eq} pomnoženom s ukupnim brojem unutarnjih kontrolnih volumena N_{CV}, dakle $N_{CV} \times N_{eq}$. Vrijednosti varijabli u računalnim točkama na rubnim plohama su ili zadane (preko Dirichletovih ili von Neumannovih rubnih uvjeta [5]) ili se aproksimiraju iz susjednih unutarnjih kontrolnih volumena.

Diskretizacijom neke transportne jednadžbe po cijeloj prostornoj domeni (tj. preko svih unutarnjih kontrolnih volumena) dobiva se sustav algebarskih jednadžbi u obliku:

$$A_\phi \phi = S_\phi \tag{132}$$

Matrica koeficijenata A_ϕ je rijetko popunjena i asimetrična te su potrebni efikasni rješavači linearnih sustava da bi se dobio vektor nepoznanica ϕ. Također, potrebno je osigurati dijagonalnu dominantnost ($a_P \geq \sum_{k=1}^{N_{faces}} a_k$, gdje je $sign(a_P) \equiv sign(a_k)$ [6]) spomenute matrice. U općem slučaju je sustav prema jed. (132) nelinearan te se rješenje postiže iteracijskim putem na način da se pretpostave rješenja te se izračuna linearan sustav, a postupak se ponavlja sve do konvergencije [5]. Također, zbog skupoće se ne koriste izravni linearni rješavači (poput Gaussove eliminacije, LR faktorizacije, i sl. [130, 132]), već se koriste iteracijski rješavači linearnih sustava. Među brojnim iteracijskim rješavačima koji su dostupni [5, 130], u CFD-u [5] najčešće se koriste oni bazirani na konjugiranim gradijentima (CGS, CGSTAB, i sl.) ili *multi-grid* rješavači (eng. *algebraic multi-grid* – AMG).

Osnovni problem kod rješavanja jednadžbi brzina kod nekompresibilnih strujanja (niski Machovi brojevi) je određivanje tlaka tako da bude zadovoljena jednadžba kontinuiteta. SIMPLE algoritam [6, 136] je korišten za povezivanje brzina i tlaka. Jednadžba korekcije tlaka je računata da bi se zadovoljio zakon očuvanja mase [99]. Također, kako se varijable koje se računaju često pojavljuju i u transportnim jednadžbama za druge varijable, cjelokupan sustav jednadžbi je spregnut te je potreban poseban tretman za njihovo rješavanje. Postoje, u principu, dva pristupa rješavanja te spregnutosti – spregnuto te odvojeno rješavanje. Kod spregnutog rješavanja se sve jednadžbe istovremeno rješavaju kao jedinstveni sustav. Međutim, ovaj način je računalno skup zbog velikog nelinearnog sustava te se obično ne upotrebljava u CFD rješavačima. Alternativni i češće upotrebljavani pristup je odvojeni pristup, a koji je implementiran i u FIRE-u, a gdje se posebno i odvojeno računaju transportne jednadžbe za svaku zavisnu varijablu, dok se drugi nelinearni članovi drže konstantni tijekom tog rješavanja. Konvergencija se ovdje postiže iteriranjem (vanjske iteracije) kroz sve jednadžbe i obnavljanjem nelinearnim članova nakon svake iteracije [5].

Konačno, dvije važne numeričke tehnike koje se koriste da bi se poboljšala dijagonalna dominantnost matrice koeficijenata A_ϕ će se ukratko opisati. To su

podrelaksacija te linearizacija izvorskih članova. Te dvije tehnike su upotrebljene u [6] da bi se poboljšala stabilnost kalkulacija i konvergencija.

Ako s $\phi^{(new)}$ označimo vektor rješenja sustava jednadžbi prema jed. (132), te ako je $\phi^{(i-1)}$ vektor rješenja iz prethodne iteracije, podrelaksirano rješenje u novoj iteraciji dobiva se kao:

$$\phi^{(i)} = \phi^{(i-1)} + \alpha_\phi \left(\phi^{(new)} - \phi^{(i-1)} \right) \tag{133}$$

Podrelaksacijski faktori α_ϕ poprimaju vrijednosti između 0 i 1 te njihov pravilan odabir ovisi o jednadžbi koja se računa te konfiguraciji koja se simulira [5, 6]. Općenito vrijedi pravilo da manje vrijednosti podrelaksacijskih faktora ($\alpha_\phi \to 0$) poboljšavaju stabilnost proračuna i konvergenciju, no potrebno je više iteracija da bi se postiglo konačno rješenje. Dakle, kod odabira podrelaksacijskih faktora potreban je kompromis takav da se dobije numerički stabilna procedura rješavanja, ali istovremeno i efikasna tako da ne treba previše iteracija da bi se dobilo konačno rješenje.

Izvorski članovi S_φ u jed. (131) se lineariziraju kao:

$$S_\varphi = S_{\varphi,S} - S_{\varphi,P}\varphi_P \qquad with \quad S_{\varphi,S} \geq 0,\ S_{\varphi,P} \geq 0 \tag{134}$$

Negativni doprinos izvorskom članu (drugi član na desnoj strani jed. (134)) implicitno se tretira na način da se $S_{\varphi,P}$ prebaci na stranu dijagonalnog koeficijenta a_P, čime se povećava dijagonalna dominantnost matrice koeficijenata A_ϕ.

3.2.4 Implementacija modela izgaranja

Modul izgaranja je implementiran u FIRE CFD rješavač preko korisnički definiranih funkcija. U inicijalnom dijelu učitava se datoteka s PDF tablicama te se postavljaju rubni uvjeti za dodatne transportne jednadžbe. Tijekom svake iteracije dodatno se računaju jednadžbe za usrednjenu entalpiju (jed. (63)), momente masenog udjela smjese goriva (jed. (74) i (75)) te usrednjenu varijablu napretka reakcije (jed. (76)), te se prema njima dobivaju usrednjene vrijednosti masenih udjela kemijskih vrsta iz PDF tablica i temperature. Usrednjena temperatura dobiva se iterativno iz poznatih usrednjenih vrijednosti masenih udjela kemijskih vrsta te izračunate usrednjene entalpije kao:

$$\tilde{h} = \sum_{k=1}^{N_{spec}} \tilde{Y}_k h_k \left(\tilde{T} \right) \tag{135}$$

Usrednjena gustoća te ostala svojstva obnavljaju se nakon svake iteracije. Shema implementacije modula izgaranja je prikazana na Sl. 25.

Implementirana su četiri modela izgaranja, a ovisno o parametru tabeliranja kemijskih vrsta u pretprocesoru te upotrebi predmiješanih ili nepredmiješanih plamenova tijekom tabeliranja. To su:

- Standardni stacionarni laminarni *flamelet* model – SLFM. Usrednjena brzina skalarne disipacije kod stehiometrijskih uvjeta $\overline{\chi}_{st}$ (jed. (91)) je korištena kao parametar tabeliranja. Jednadžba za usrednjenu varijablu napretka reakcije (jed. (76)) se ne računa.
- Parametrizacija normaliziranom varijablom napretka reakcije $\overline{c}$; korištenje baze predmiješanih plamenova (Poglavlje 2.3.6.1) – RPV (FPI).
- Parametrizacija normaliziranom varijablom napretka reakcije $\overline{c}$; korištenje baze nepredmiješanih plamenova (Poglavlje 2.3.6.2) – RPV (SLFM).
- Parametrizacija normaliziranom varijablom napretka reakcije $\overline{c}$; korištenje baze predmiješanih i nepredmiješanih plamenova (Poglavlje 2.3.6.3) – RPV (MIX).

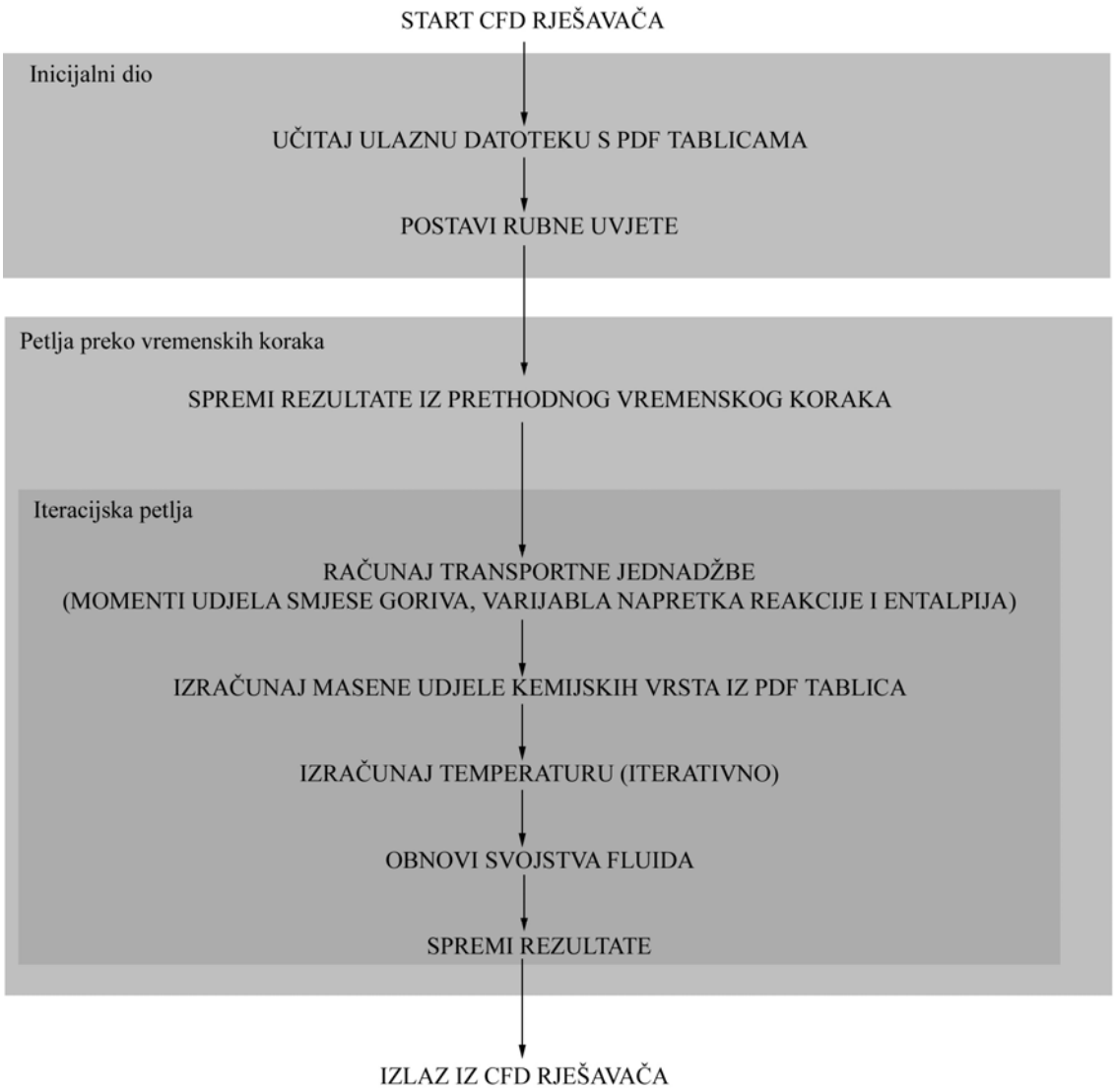

Slika 25 – Implementacija modela izgaranja (shema)

3.3 Implementacija DTRM-a

Metoda diskretnog prijenosa topline zračenjem (DTRM) je implementirana u FIRE CFD rješavač preko korisnički definiranih funkcija [102, 137].

U inicijalnom su dijelu (pretprocesoru) rađeni proračuni praćenja zraka emitiranih s rubnih ploha sve dok te zrake ne dođu do nasuprotnih rubnih ploha. Geometrijski podaci presijecanja zraka s unutarnjim kontrolnim volumenima su pohranjeni u datoteku. Tijekom iteracijskog ciklusa DTRM rješavač se poziva prije svake iteracije te se izvorski član za usrednjenu entalpiju $\overline{q}_h$ (jed. (63)) obnavlja doprinosom zbog zračenja prema jed. (50). Interakcija turbulencije i zračenja nije uzeta u obzor te su usrednjene vrijednosti temperature i masenih udjela kemijskih vrsta korištene u proračunima zračenja (jed. (46), WSGGM [101]).

Kao dio verifikacije implementacije DTRM modula simuliran je teoretski primjer cilindra [138], te su rezultati simulacije uspoređeni s egzaktnim rješenjem za taj slučaj. Geometrija cilindra je prikazana na Sl. 26.

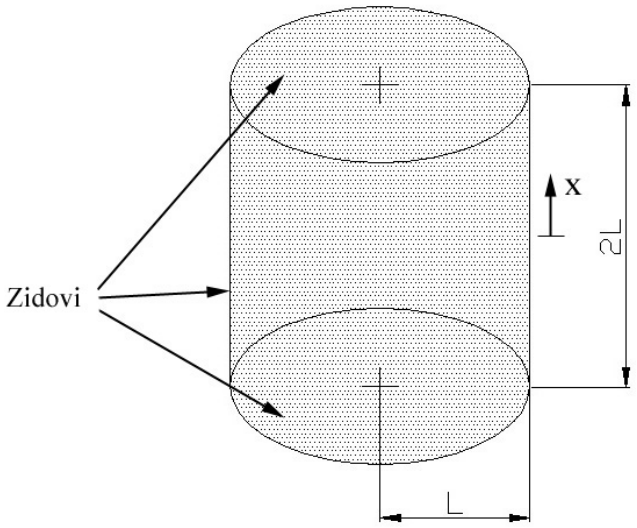

Slika 26 – Konačni cilindar

Ovo je hipotetski teoretski slučaj gdje su zidovi cilindra pretpostavljeni crnima ($\varepsilon_w = 1$) te da imaju konstantnu temperaturu $T_w = 0\,\mathrm{K}$. Medij unutar cilindra je na konstantnoj

temperaturi $T = 500\,\mathrm{K}$. U ovome slučaju rađeni su samo DTRM proračuni, bez uključivanja entalpije, te nema izmjene topline između zidova i medija. Varirani su broj zraka korištenih u DTRM-u te koeficijent apsorpcije medija, a da bi se istražio njihov utjecaj na rezultate simulacije.

Slika 27 prikazuje bezdimenzijski toplinski tok $Q = \frac{q_{net}}{\sigma T^4}$ u ovisnosti bezdimenzijske visine cilindra x/L, a gdje je optička debljina medija $aL = 1.0$. DTRM proračuni su rađeni za 4, 16 i 48 zraka po rubnoj plohi te na strukturiranoj računalnoj mreži s 6000 kontrolnih volumena. Kao što se i očekivalo, bolji rezultati simulacije dobiveni su upotrebom većeg broja zraka. Rezultati simulacije s 16 i 48 zraka su u zadovoljavajućem slaganju s egzaktnim rješenjem, dok rezultati simulacije s 4 zrake dosta odstupaju od egzaktnog rješenja.

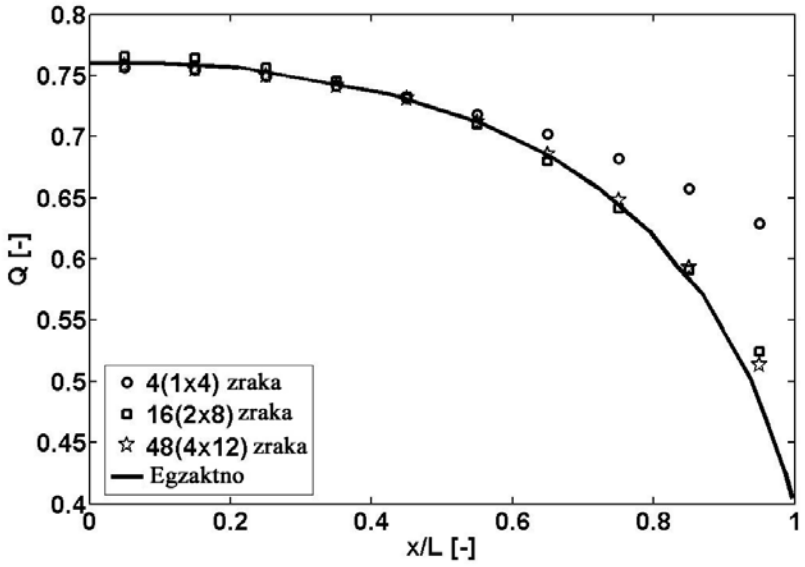

Slika 27 – Bezdimenzijski toplinski tok vs. bezdimenzijska pozicija na zidu za različiti broj zraka (optička debljina $aL = 1.0$)

Slika 28 prikazuje bezdimenzijske toplinske tokove za različite optičke debljine medija – $aL = 0.1$, $aL = 1.0$ i $aL = 5.0$, dok je korišteno 48 zraka po rubnoj plohi u svim DTRM proračunima. Rezultati simulacije dobro se slažu s egzaktnim rješenjima u svim slučajevima.

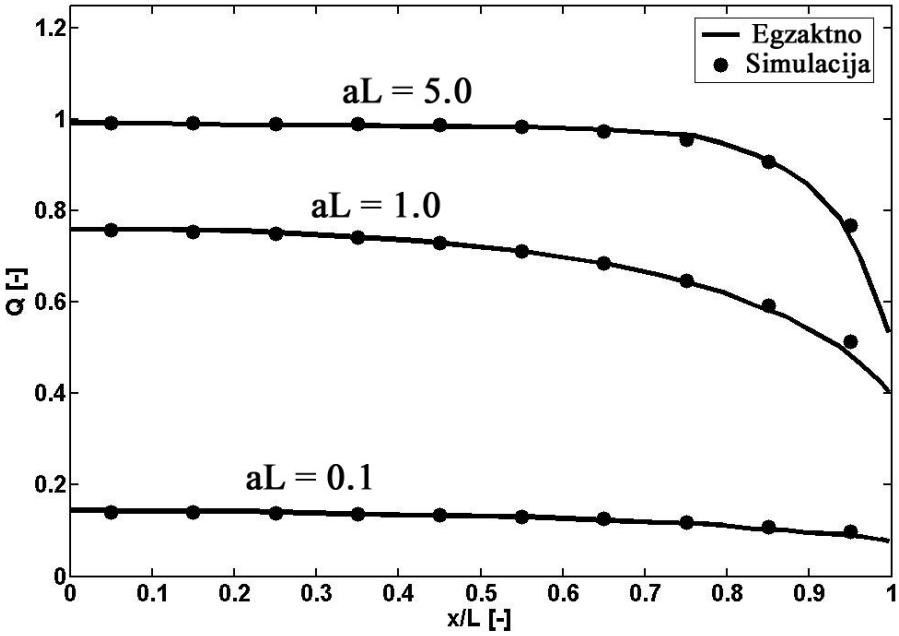

Slika 28 – Bezdimenzijski toplinski tok vs. bezdimenzijska pozicija na zidu za različite optičke debljine aL (48(4x12) zraka)

Prethodno prikazani rezultati simulacije primjera cilindra potvrđuju ispravnu implementaciju DTRM modula u FIRE CFD rješavač. Neke primjene DTRM modula na složenijim primjerima mogu se pronaći u [87, 139].

4 Vodikov mlazni plamen

4.1 Eksperimentalna konfiguracija

Serija laboratorijskih plamenova vodika i zraka je eksperimentalno istraživana i opisana u [103, 104, 140, 141]. Eksperimentalni se podaci mogu pronaći na [29].

Gorionik je bio ravna cijev unutarnjeg radijusa $d = 3.75$ mm (vanjski radijus $d_o = 4.84$ mm) centrirana u vertikalnom zračnom tunelu (kvadratni presjek, 30 cm). Brzina zraka je bila oko 1.0 m/s (± 0.06 m/s), dok je temperatura zraka bila 294 K (± 2 K). Molni sastav goriva u konfiguraciji simuliranoj u ovome radu je bio 80 % H_2 (vodik) i 20 % He (helij). Vodik je razrijeđen s helijem da bi se smanjio utjecaj prijenosa topline zračenjem na stvaranje termalnog NO-a [103]. Brzina goriva na izlazu iz cijevi je bila 294 m/s ($\mathrm{Re} = 9800$ [103]), dok je temperatura goriva bila 295 K (± 2 K). Zrak je bio vlažan, s prosječnim molnim udjelom H_2O 0.013. Plamen je bio slobodan. Vidljiva duljina plamena je bila oko $l_{vis} / d = 150$, dok je aksijalna duljina sa stehiometrijskim sastavom bila $l_{st} = 375$ mm. Slika 29 prikazuje izgled gorionika.

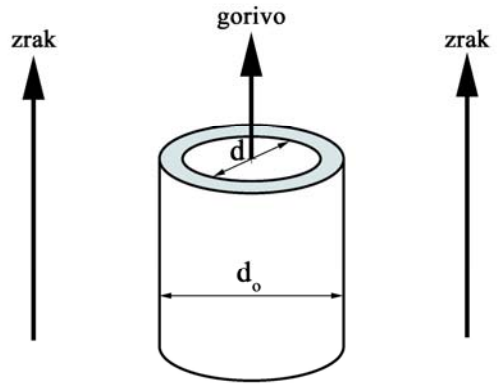

Slika 29 – Konfiguracija vodikovog plamena

Mjerenja skalara i komponenata brzina dostupna su kao aksijalni profili na centralnoj osi te kao radijalni profili na aksijalnim pozicijama $\frac{x}{l_{vis}} = \frac{1}{8}, \frac{1}{4}, \frac{3}{8}, \frac{1}{2}, \frac{5}{8}, \frac{3}{4}, \frac{1}{1}$. Mjerenja su dana u vidu usrednjenih (Reynoldsovih i Favreovih) vrijednosti, kondicionalno

usrednjenih vrijednosti te trenutnih mjerenih vrijednosti na različitim pozicijama. Za mjerenje brzine se je koristila laserska Dopplerova metoda mjerenja brzine (eng. *laser Doppler velocimetry* – LDV) [141], dok su se maseni udjeli glavnih kemijskih vrsta i temperatura mjerili kombinirano upotrebom Ramanovog raspršivanja, Rayleighovog raspršivanja te laserski inducirane fluorescencije (eng. *laser-induced fluorescence* – LIF) [103]. Više informacija o eksperimentalnom sastavu te upotrebljenim mjernim tehnikama može se pronaći u [103, 104, 140, 141].

4.2 Numerička konfiguracija

Numerička simulacija je provedena na strukturiranoj računalnoj mreži od 339000 kontrolnih volumena koji pokrivaju cilindričnu prostornu domenu od $x/d = 0$ do $x/d = 400$ u aksijalnom smjeru, te od $r/d = 0$ do $r/d = 75$ u radijalnom smjeru. Gustoća mreže je bila veća prema centralnoj osi te prema ulazima (vidi Sl. 30), slično kao i u simulacijama ovog plamena koje su objavljene u TNF zbornicima na [29], te se nije ispitivao utjecaj gustoće mreže na dobivene rezultate u ovome radu.

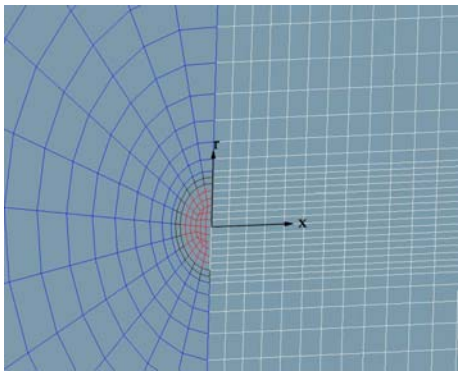

Slika 30 – Računalna mreža (vodikov plamen; vertikalni aksijalni presjek uzduž osi)

Profil brzine goriva na izlazu iz cijevi gorionika računao se je prema sljedećem izrazu, a koji je dobiven prema eksperimentalnim podacima:

$$u(r)_{x=0} = -4\cdot10^{10} r^3 + 6\cdot10^{7} r^2 - 37109 r + 306.39 \qquad 0 \le r \le 0.001875 \text{ m} \qquad (136)$$

Brzina zraka na ulazu je postavljena konstantnom i 1.0 m/s. Vrijednosti turbulentne kinetičke energije i brzine njene disipacije na ulazima su pretpostavljene prema empirijskim izrazima implementiranim u FIRE CFD rješavaču [99] kao:

$$k_b = \frac{3}{2}\left(I_\infty u_b\right)^2 \qquad \varepsilon_b = \frac{C_\mu^{3/4} k_b^{3/2}}{l} \tag{137}$$

Relativni intenzitet slobodne turbulencije je odabran $I_\infty = 7\,\%$.

Rađene su adijabatske i ne-adijabatske kalkulacije, ovisno o tome da li je bio uključen model zračenja ili nije. U neadijabatskom slučaju koristilo se 48 (4x12) zraka po rubnoj plohi u DTRM proračunima , dok su granice domene (ulazi i izlazi) smatrane kao crne površine ($\varepsilon_b = 1$). U svim slučajevima su se dobili maseni udjeli kemijskih vrsta u pretprocesoru pod pretpostavkom adijabatskih uvjeta. WSGGM [101] se je koristio za proračun koeficijenta apsorpcije participirajućeg medija.

Turbulencija se je modelirala standardnim k-ε modelom te HTM modelom [123]. Kao što je predloženo u TNF zbornicima (dostupnima na [29]), konstanta $C_{\varepsilon 2}$ (jed. (67)) je postavljena na vrijednost 1.83.

Izgaranje se modeliralo standardnim SLFM modelom te modelima baziranim na varijabli napretka reakcije (vidi Poglavlje 3.2.4). Baza stacionarnih laminarnih *flamelet* profila dobila se je u pretprocesoru upotrebom CSC rješavača [96] za 10 različitih vrijednosti parametara brzine skalarne disipacije kod stehiometrijskih uvjeta. Korišten je detaljni kemijskih mehanizam vodika koji se je sastojao od 13 kemijskih vrsta i 37 kemijskih reakcija (uključujući i NO reakcije). U svim slučajevima se je interakcija turbulencije i kemije obuhvatila preko pretpostavljene β-PDF funkcije (vidi Poglavlje 3.1.2.3).

Za proračun toka fluida korišten je stacionarni nekompresibilni (mali Machovi brojevi) rješavač. Konstantan statički tlak je nametnut na izlaznim rubnim površinama. Iteracijsko rješavanje se provodilo dok reziduali u svim jednadžbama nisu pali ispod vrijednosti 10^{-6}. Konvektivni član u jednadžbi kontinuiteta diskretiziran je shemom centralnih razlika (drugi red točnosti), dok su isti članovi u jednadžbama brzina diskretizirani hibridnom shemom između centralnih razlika i uzvodne sheme (težinski faktor 0.5). Konvektivni članovi u ostalim skalarnim jednadžbama diskretizirani su upotrebom uzvodne sheme diskretizacije (prvi red točnosti). Po običaju su se difuzijski članovi u svim transportnim jednadžbama diskretizirali centralnim razlikama. Ostali numerički postav je bio kao što je uobičajeno kod FIRE CFD rješavača [99].

4.3 Rezultati

4.3.1 Pretabulirani kemijski profili

4.3.1.1 SLFM baza

Stacionarni laminarni *flamelet* profili, a prema standardnom SLFM modelu (Poglavlje 2.3.3), dobiveni su u pretprocesoru upotrebom CSC rješavača [96] i to za sljedeće vrijednosti parametara brzine skalarne disipacije kod stehiometrijskih uvjeta:

$$\chi_{st} = 0.01, 0.1, 1, 5, 10, 20, 50, 100, 150, 220\ s^{-1} \tag{138}$$

Prvi *flamelet* ($\chi_{st} = 0.01\ s^{-1}$) ima približno ravnotežni sastav, dok je posljednji *flamelet* u bazi ($\chi_{st} = 220\ s^{-1}$) onaj neposredno prije gašenja. Rubni uvjeti masenog sastava kemijskih vrsta i temperature postavljene su prema eksperimentalnim postavkama. Kod računanja *flamelet* jednadžbi korištena je neekvidistantna mreža od 50 točaka, s gušćom raspodjelom oko stehiometrijskog područja ($Z_{st} \approx 0.042$).

Slika 31 prikazuje SLFM profile temperature (adijabatske) te masenih udjela različitih kemijskih vrsta. Dok se temperatura i glavne kemijske vrste jednoznačno mijenjaju u ovisnosti od parametara brzine skalarne disipacije kod stehiometrijskih uvjeta, manje vrste poput NO i OH pokazuju veće gradijente blizu ravnoteže. To se posebice odnosi na NO, gdje je prvih nekoliko profila u blizini ravnoteže dosta različitije od ostalih profila u bazi. Slično, premda u manjoj mjeri, vrijedi i za OH profile.

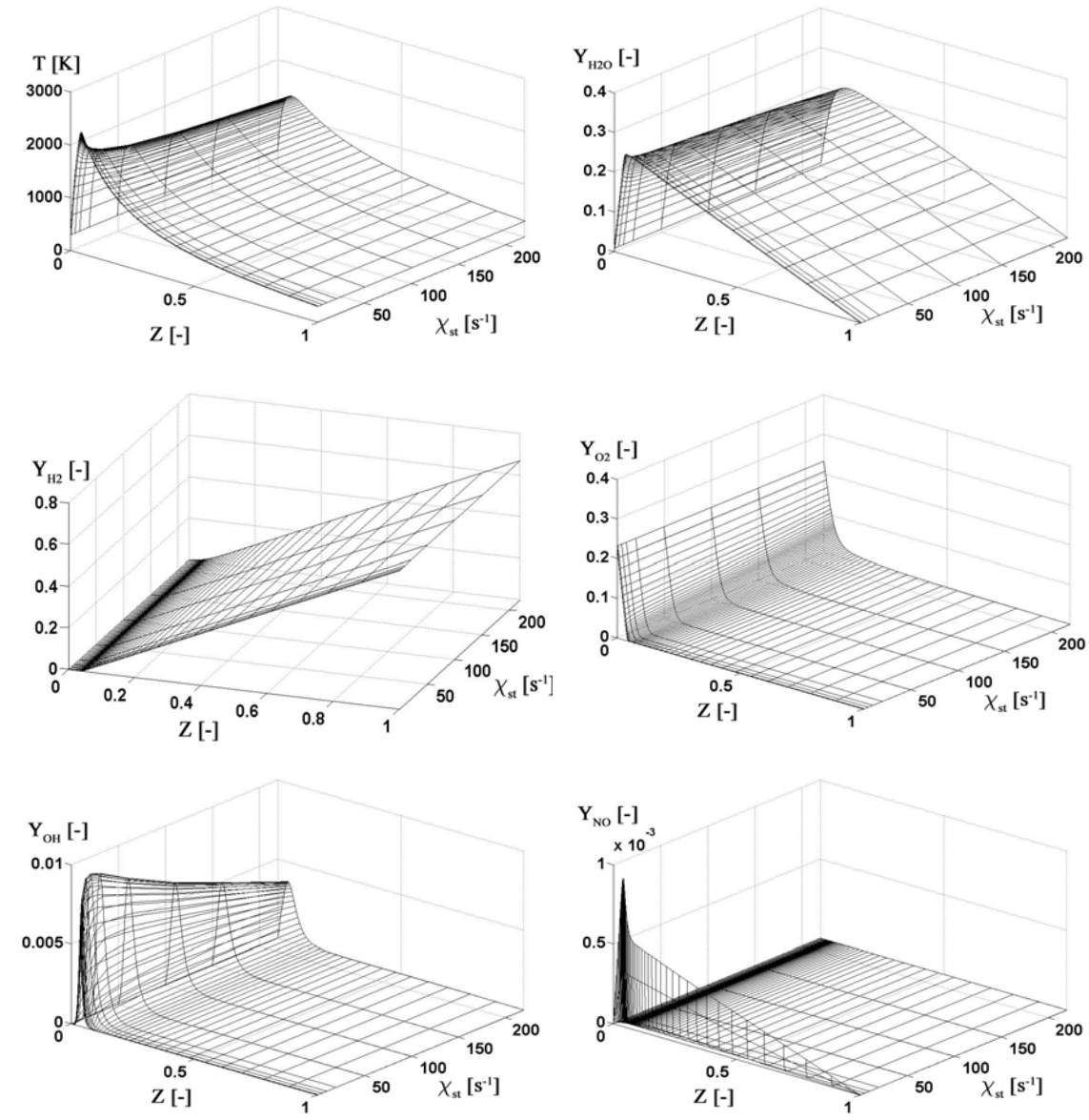

Slika 31 – SLFM (standardni) baza (vodikov plamen)

4.3.1.2 FPI baza

FPI baza predmiješanih plamenova je dobivena upotrebom PREMIX rješavača [97]. Adijabatski slobodno propagirajući 1D predmiješani plamenovi dobiveni su na istim točkama masenih udjela smjese goriva unutar granica zapaljivosti kao kod SLFM baze. Izvan granica zapaljivosti su profili interpolirani s graničnim vrijednostima. Granice zapaljivosti (siromašna i bogata) su približno određene računajući predmiješane plamenove sve dok je propagacija bila moguća (vidi Sl. 1, npr.). Ukupno su izračunata 34 predmiješana plamena unutar granica zapaljivosti ($0.42 \le \phi \le 7.208$[8]), dok su preostala 16 profila dobivena interpolacijom. Sastav reaktanata za zadane vrijednosti ekvivalentnog omjera (masenog udjela smjese goriva) dobiven je iz profila hladnog miješanja goriva i oksidanta.

Slika 32 prikazuje FPI bazu plamenova. Prikazane su iste kemijske vrste kao i na Sl. 31, dok su ovdje umjesto temperature prikazani profili izvorskih članova trenutne varijable napretka reakcije. Kao što je opisano u Poglavlju 2.3.6.1, normalizirana varijabla napretka reakcije c je korištena kao druga nezavisna koordinata (parametar). U ovom slučaju je kao varijabla napretka reakcije izabran maseni udio H_2O, tj. $Y_c \equiv Y_{H_2O}$. Za razliku od SLFM baze, kod FPI baze je pokriveno cjelokupno područje od hladnog miješanja reaktanata ($c = 0$) pa do ravnotežnog izgaranja ($c = 1$). Ukupno je bilo 21 profila u smjeru normalizirane varijable napretka reakcije, s većom gustoćom u blizini $c = 1$. Maksimalne vrijednosti masenih udjela kemijskih vrsta u FPI bazi i SLFM bazi su slične, osim u slučaju NO-a.

[8] Odnosno, $0.01796 \le Z \le 0.23894$ – prema jed. (24).

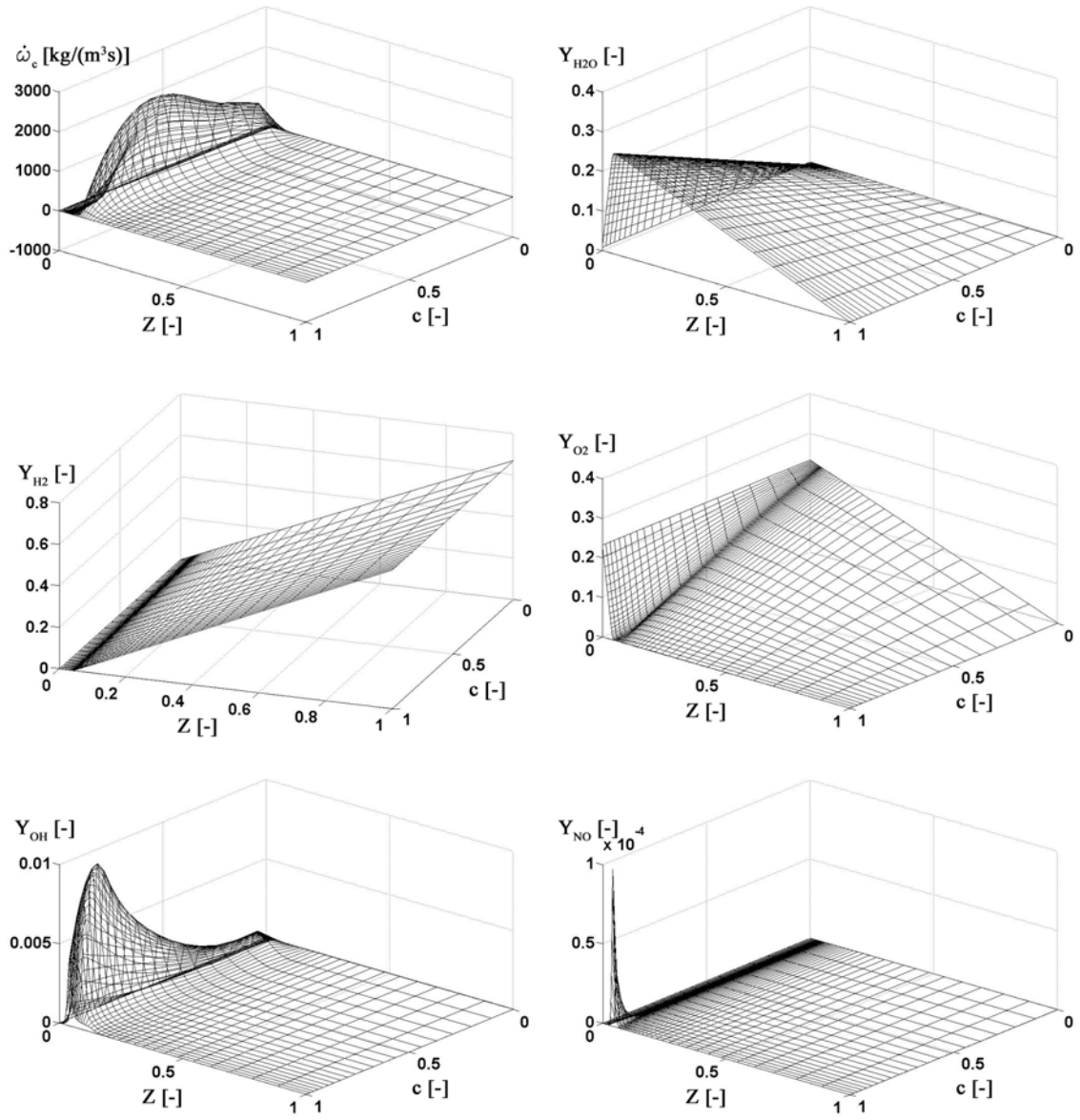

Slika 32 – FPI baza (vodikov plamen)

4.3.1.3 SLFM baza (varijabla napretka reakcije)

SLFM baza je reparametrizirana normaliziranom varijablom napretka reakcije prema jed. (42), a kako je opisano u Poglavlju 2.3.6.2. Međutim, zbog djelomično nemonotone promjene varijable napretka reakcije u SLFM bazi za određene vrijednosti masenog udjela smjese goriva, a u smjeru porasta parametra brzine skalarne disipacije kod stehiometrijskih uvjeta – $\chi_{st} \in [0.01, 220]$, nije bilo moguće provesti jedinstveno preslikavanje $Y_c(Z, \chi_{st}) \rightarrow Y_c(Z, c)$ za sve plamenove iz SLFM baze. Zbog toga su korišteni samo oni plamenovi kod kojih je bila osigurana uniformna varijacija varijable napretka reakcije ($\chi_{st} = 0.01, 150$ i $220\ s^{-1}$). Jasno je da je ova aproksimacija dosta velika, te, u biti, su profili u reparametriziranoj SLFM bazi zapravo uglavnom dobiveni interpolacijom između profile blizu ravnoteže ($\chi_{st} = 0.01\ s^{-1}$) te profila blizu gašenja ($\chi_{st} = 150\ s^{-1}$). Provjerom SLFM baze nije se mogla pronaći niti jedna druga varijabla napretka reakcije kod koje bi se mogao izbjeći spomenuti problem.

Slika 33 prikazuje reparametriziranu SLFM bazu dobivenu uz prethodno opisane aproksimacije. Prikazani su isti profili kao i kod FPI baze (Sl. 32). Međutim, bitna razlika ovdje je ta da je normalizirana varijabla napretka reakcije definirana prema jed. (42) te da je pokriveno područje plamenova dosta uže (od zadnjeg profila prije gašenja pa do ravnoteže) nego kod FPI baze. Dok je utjecaj spomenutih aproksimacija manje primjetan kod većih vrsta (H_2, O_2 i H_2O), kod NO i OH profila taj je utjecaj puno značajniji. Maksimalne vrijednosti OH nisu dobro reproducirane u reparametriziranoj SLFM bazi, dok je profil NO-a blizu ravnoteže ($\chi_{st} = 0.01\ s^{-1}$) umjetno proširen po re-parametriziranoj SLFM bazi zbog interpolacije. Dakle, može se zaključiti da je re-parametrizirana SLFM baza u ovom slučaju (Sl. 33) vrlo gruba aproksimacija originalne SLFM baze, te da je čak i kvalitativno pogrešna u slučaju OH i NO. Zbog toga je rezultate simulacije dobivene ovim modelom potrebno promatrati s rezervom, pogotovo u slučaju OH i NO.

Baza plamenova prema mješovitoj formulaciji, a kako je opisano u Poglavlju 2.3.6.3, nije prikazana ovdje niti je korištena tijekom simulacije, a zbog spomenutih problema kod reparametrizacije.

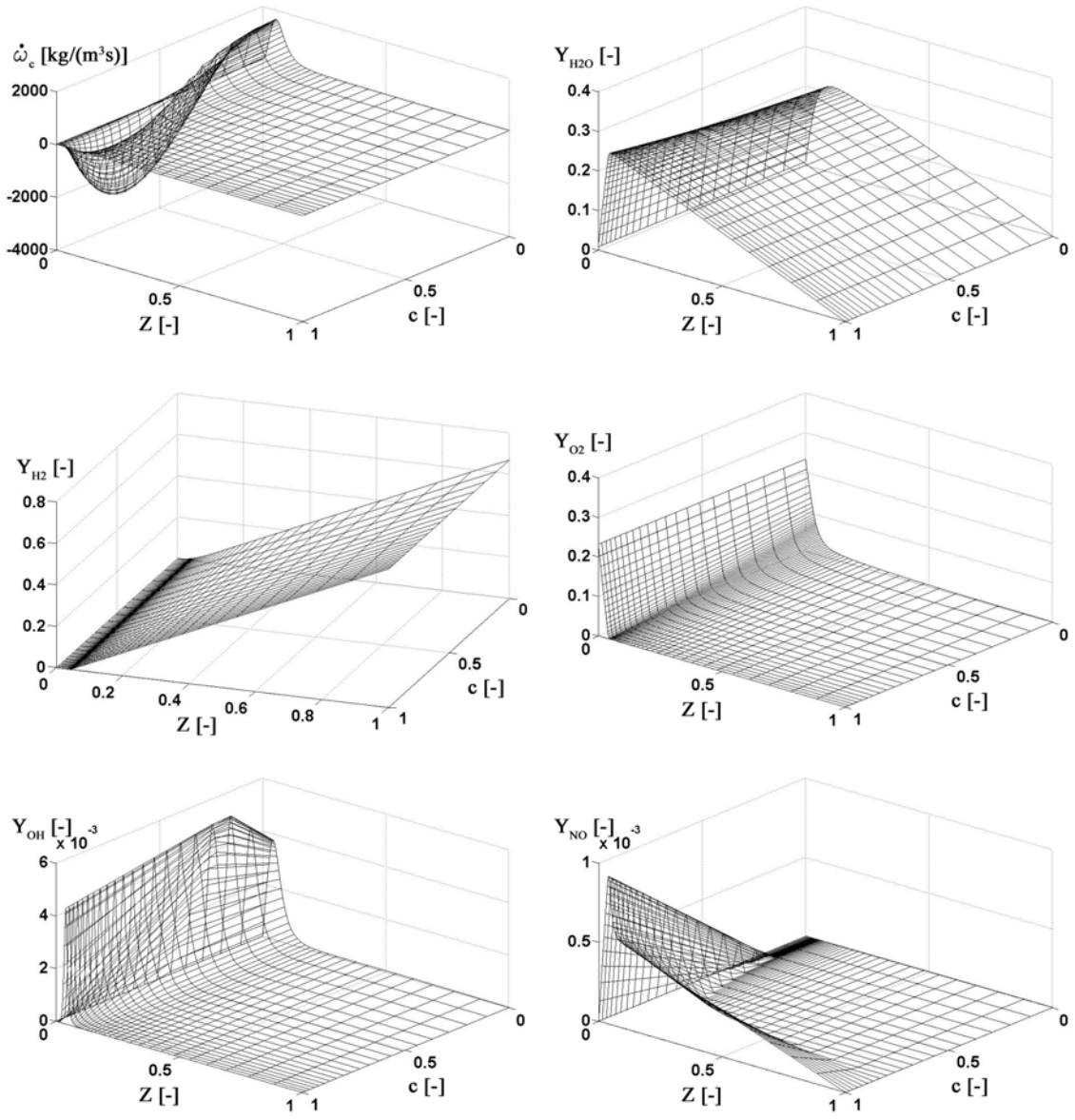

Slika 33 – SLFM (RPV) baza (vodikov plamen)

4.3.2 Širenje mlaza

Slika 34 prikazuje radijalne profile usrednjene aksijalne brzine na aksijalnim pozicijama $x/l_{vis}=1/8$ i $x/l_{vis}=3/8$. Korišten je standardni k-ε model turbulencije s različitim vrijednostima konstante $C_{\varepsilon 2}$ (vidi jed. (67)). Pretpostavljeni su adijabatski uvjeti, dok je standardni SLFM model korišten za proračun izgaranja. Bolji su rezultati širenja plamena dobiveni za vrijednost konstante $C_{\varepsilon 2}=1.83$. Rezultati simulacije na bližoj aksijalnoj poziciji ($x/l_{vis}=1/8$) su u slabijem slaganju s eksperimentalnim podacima nego rezultati na poziciji $x/l_{vis}=3/8$. Sličan je trend primijećen i na drugim aksijalnim pozicijama, s boljim rezultatima dalje od gorionika. Zbog boljih rezultata dobivenih uz $C_{\varepsilon 2}=1.83$, ova vrijednost konstante je zadržana i u ostalim simulacijama plamena vodika i zraka, a čiji će rezultati biti prikazani u sljedećim poglavljima.

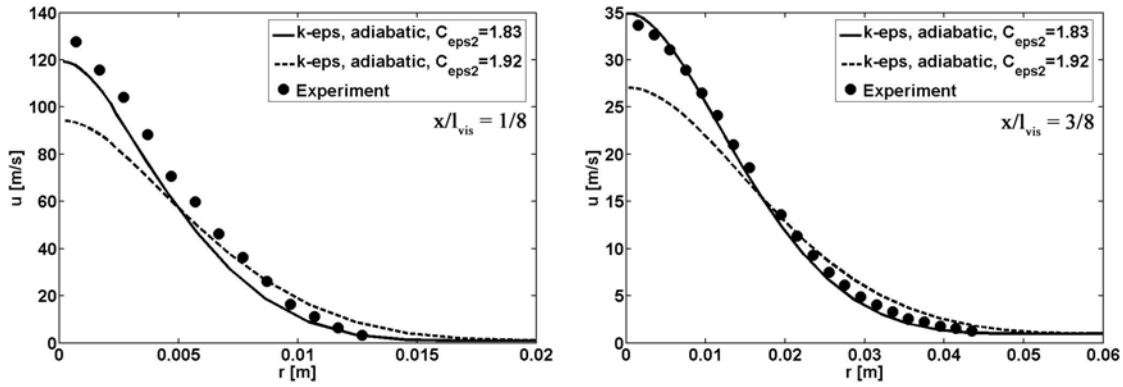

Slika 34 – Radijalni profili usrednjene aksijalne brzine na poziciji $x/l_{vis}=1/8$ i $x/l_{vis}=3/8$ (vodikov plamen; k-ε; adijabatski)

4.3.3 Adijabatski vs. neadijabatski profili

Ispitan je utjecaj uključivanja modeliranja prijenosa topline zračenjem na rezultate simulacije. Standardna SLFM baza plamenova korištena je kod modeliranja izgaranja, dok su uspoređena dva modela turbulencije – k-ε i HTM. Slika 35 prikazuje aksijalne profile uzduž centralne osi za usrednjene temperaturu te maseni udio H_2O[9].

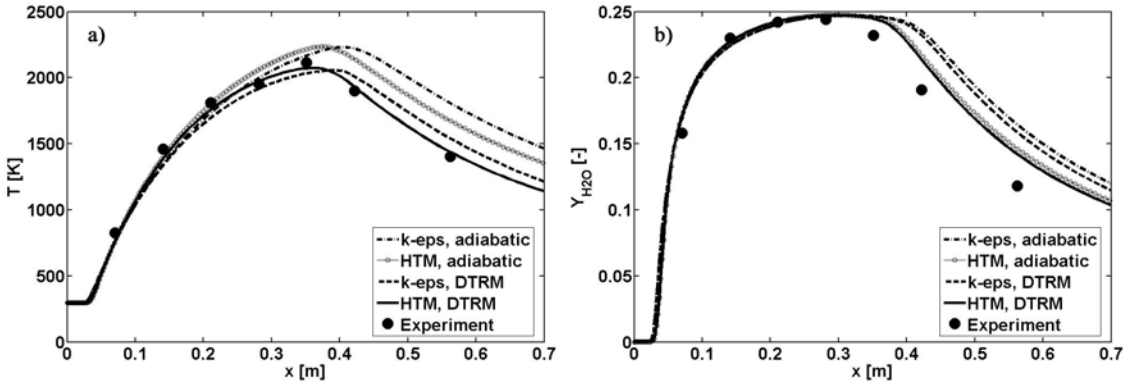

Slika 35 – Aksijalni profili uzduž osi (vodikov plamen; adijabatski vs. DTRM; k-ε vs. HTM): a) Usrednjena temperatura; b) Usrednjeni maseni udio H_2O

Neadijabatski (DTRM) aksijalni profili su u puno boljem slaganju s eksperimentalnim podacima nego adijabatski profili (zanemareno zračenje). Dakle, čak i u ovako jednostavnoj konfiguraciji slobodnog plamena se uključivanje modeliranja zračenja pokazalo bitnim za dobivanje boljih rezultata temperatura. Slika 35a također otkriva da HTM daje bolje rezultate od k- ε modela. To se posebno odnosi na iznos i aksijalnu poziciju maksimalne vrijednosti temperature.

Slika 36 prikazuje neadijabatske aksijalne profile momenata masenog udjela smjese goriva – usrednjene vrijednosti i RMS-a[10]. Rezultati simulacije se dobro slažu s mjerenjima, a što je važno zbog točnosti rezultata ostalih reaktivnih skalara koji ovise o masenom udjelu smjese goriva (vidi Sl. 19, npr.). HTM i k-ε rezultati su vrlo slični u ovom slučaju.

[9] Jedina kemijska vrsta koja sudjeluje u izmjeni topline zračenjem u ovom slučaju (WSGGM).

[10] $Z_{RMS} \equiv \sqrt{\widetilde{Z''^2}}$

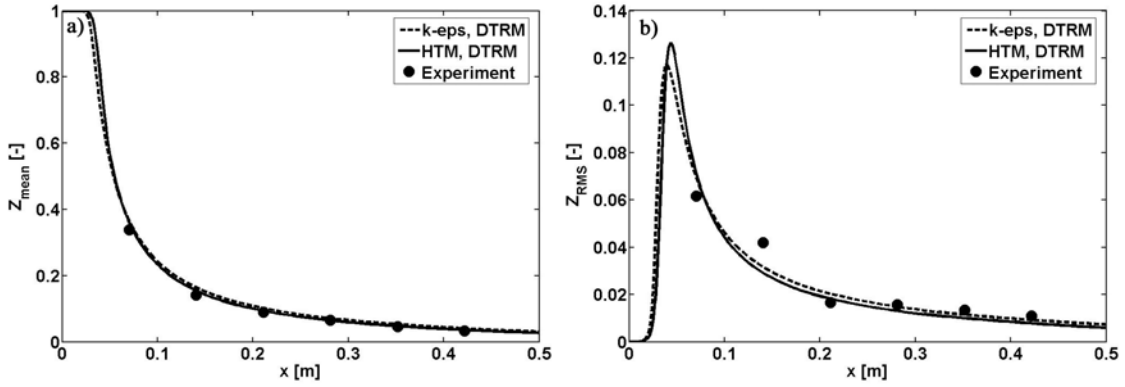

Slika 36 – Aksijalni profili uzduž osi (vodikov plamen; adijabatski vs. DTRM; k-ε vs. HTM): a) Usrednjeni maseni udio smjese goriva; b) RMS masenog udjela smjese goriva

Radijalni profili usrednjene temperature i masenog udjela H_2O na aksijalnoj poziciji $x/l_{vis} = 3/8$ prikazani su na Sl. 37. Utjecaj zračenja je značajniji u blizini centralne osi, a gdje su rezultati simulacije u dobrom slaganju s mjerenjima, dok su odstupanja značajnija dalje od osi. HTM daje bolje rezultate reaktivnih skalara u blizini osi, dok je k-ε bolji u udaljenijim područjima. Slično vrijedi i za radijalne profile na ostalim aksijalnim pozicijama.

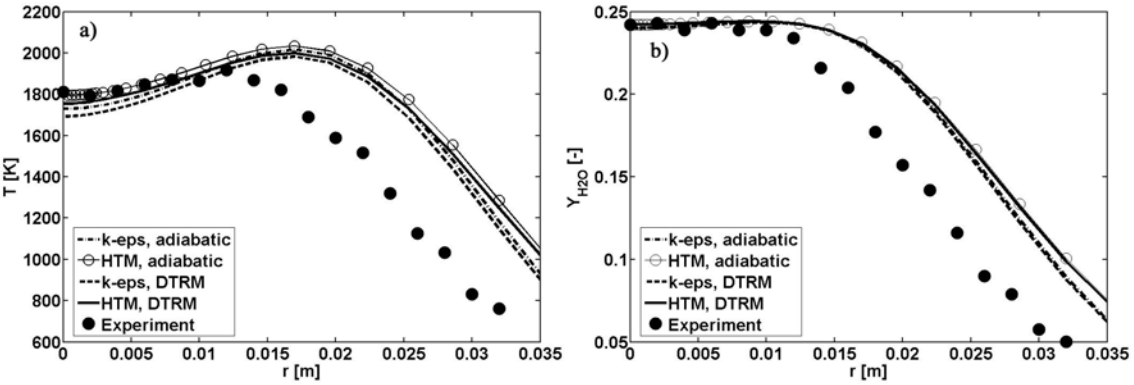

Slika 37 – Radijalni profili na poziciji x/l_{vis}=3/8 (vodikov plamen; adijabatski vs. DTRM; k-ε vs. HTM): a) Usrednjena temperatura; b) Usrednjeni maseni udio H_2O

Neadijabatski radijalni profili usrednjene aksijalne brzine na pozicijama $x/l_{vis} = 1/8$ i $x/l_{vis} = 3/8$ su prikazani na Sl. 38.

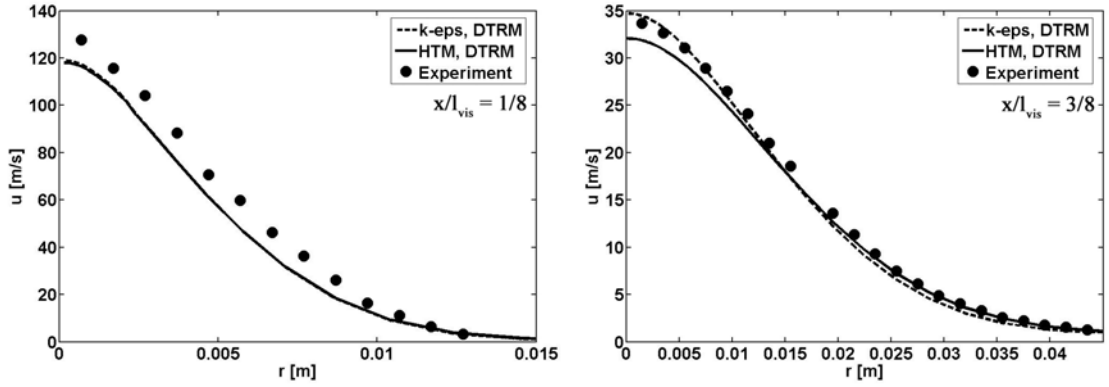

Slika 38 – Radijalni profili usrednjene aksijalne brzine na poziciji x/l_{vis}=1/8 i x/l_{vis}=3/8 (vodikov plamen; k-ε vs. HTM; neadijabatski)

Slično kao i u adijabatskom slučaju (Sl. 34), rezultati su bolji na pozicijama dalje od gorionika. k-ε model daje bolje rezultate aksijalne brzine na poziciji $x/l_{vis} = 3/8$ od HTM modela u blizini osi, dok je HTM nešto bolji dalje od osi.

Da bi se istražila odstupanja radijalnih profila na poziciji $x/l_{vis} = 3/8$ (Sl. 37), na Sl. 39 prikazani su radijalni profili momenata masenog udjela smjese goriva na istoj poziciji. Relativno neslaganje s mjerenjima ta dva skalara u područjima dalje od centralne osi ($r > 0.015$ m) objašnjava iste trendove primijećene kod reaktivnih skalara. Najvjerojatniji razlog za lošije rezultate u tom segmentu je jednostavna gradijentna pretpostavka korištena kod modeliranja turbulentnih fluktuacija, a kako je već spomenuto.

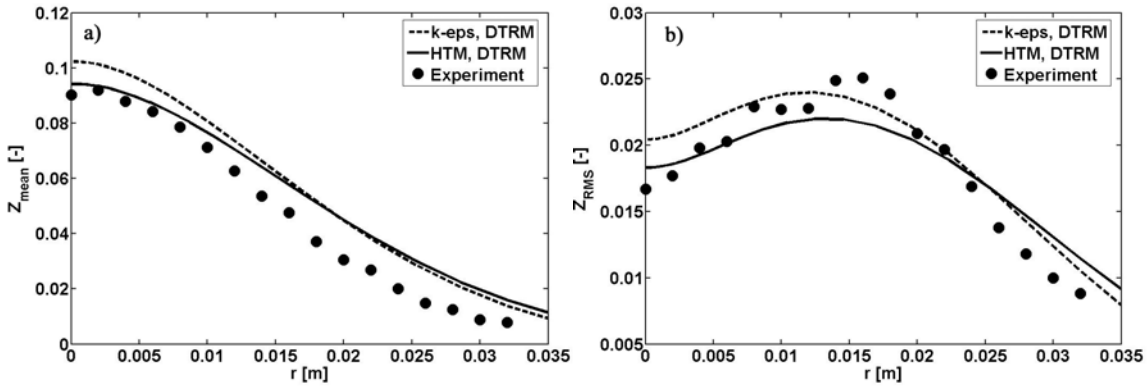

Slika 39 – Radijalni profili na poziciji x/l_{vis}=3/8 (vodikov plamen; neadijabatski; k-ε vs. HTM): a) Usrednjeni maseni udio smjese goriva; b) RMS masenog udjela smjese goriva

4.3.4 Usporedba modela izgaranja

Da bi se usporedili modeli izgaranja – SLFM, RPV (FPI) i RPV (SLFM) (Poglavlje 3.2.4) – procedura rješavanja bila je sljedeća. Najprije je dobiveno referentno stacionarno rješenje upotrebom HTM modela turbulencije, DTRM modela zračenja (48 zraka) te SLFM modela izgaranja. Usrednjene vrijednosti masenih udjela kemijskih vrsta prema RPV modelima su naknadno dobivene u postprocesoru. Na taj je način modeliranje izgaranja dobrim dijelom odvojeno od ostalih proračuna toka fluida, a što je omogućilo njihovo međusobno uspoređivanje. Znači, momenti masenog udjela smjese goriva, a koji čine koordinate tabeliranja kemijskih vrsta u pretprocesoru, bili su jednaki kod usporedbe modela izgaranja, dok se je u slučaju RPV modela dodatno u postprocesoru rješavala jednadžba za usrednjenu varijablu napretka reakcije (jed. (76)), a da bi se dobila usrednjena normalizirana varijabla napretka reakcije (vidi Poglavlje 2.5.8). Na osnovi rješenja usrednjene entalpije i masenih udjela kemijskih vrsta iteracijski se je dobilo polje usrednjene temperature, a kako je opisano u Poglavlju 3.2.4.

Radijalni profili momenata masenog udjela smjese goriva na različitim aksijalnim pozicijama su prikazani na Sl. 40. Simulirani profili usrednjenog masenog udjela smjese goriva na pozicijama $x/l_{vis} = 1/4$ i $x/l_{vis} = 3/4$ nešto su veći od mjerenih vrijednosti, dok su rezultati RMS-a nešto lošiji u blizini centralne osi. Općenito, slaganja s mjerenim vrijednostima su dobra.

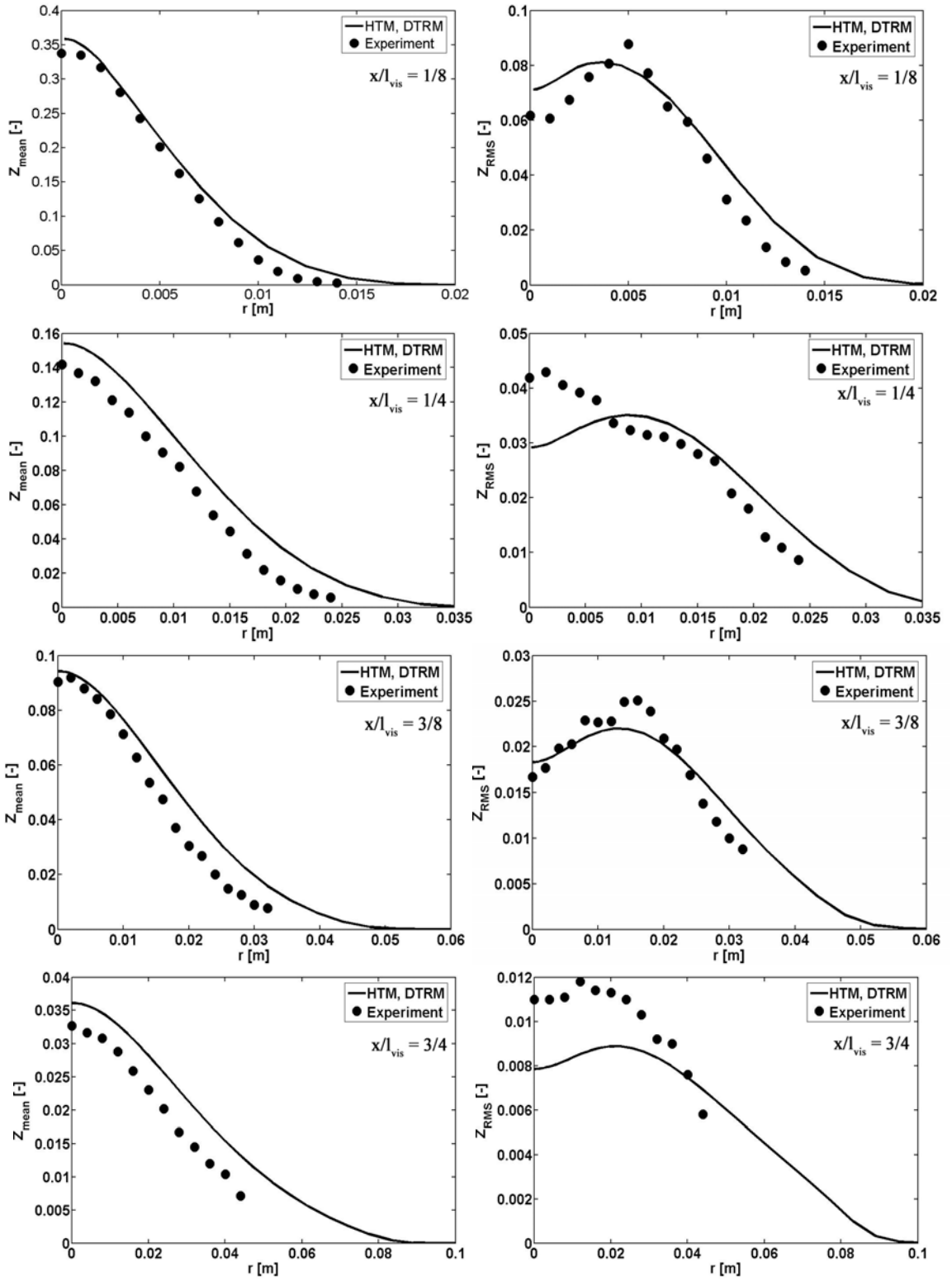

Slika 40 – Radijalni profili momenata masenog udjela smjese goriva (usrednjena vrijednost i RMS) na različitim aksijalnim pozicijama (vodikov plamen; neadijabatski; HTM)

Usrednjene temperature i maseni udjeli kemijskih vrsta (H_2O, H_2, O_2, OH i NO) uzduž centralne osi prikazani su na Sl. 41. Rezultati temperature su u dobrom slaganju s mjerenjima za sve modele izgaranja. RPV (FPI) model daje nešto niže vrijednosti temperature u području $0.1 \le x \le 0.2$ m, dok istovremeno taj model daje najbolje rezultate u područjima udaljenim od gorionika. Rezultati glavnih kemijskih vrsta (H_2O, H_2 i O_2) su vrlo slični među modelima izgaranja. U području iza fronte plamena ($x > l_{st} = 375$ mm) H_2O profili su nešto viši od mjerenja, a što ukazuje na pojačano izgaranje u tim područjima dobiveno simulacijama. O_2 rezultati su relativno loši u blizini gorionika. Manje vrste (OH i NO) su također prikazane, i dok su OH rezultati dobri i kod RPV (FPI) i kod SLFM modela, NO rezultati su slabiji kada ih se usporedi s mjerenjima. SLFM daje niže maksimalne OH vrijednosti, te je u tom pogledu vjerojatno u najboljem slaganju s mjerenjima. RPV (FPI) model, s druge strane, daje bolje OH rezultate u blizini gorionika. NO vrijednosti su značajno veće od mjerenih u slučaju korištenja nepredmiješanih plamenova kod tabeliranja u pretprocesoru (SLFM te RPV (SLFM)). Kako je Reynoldsov broj simulirane konfiguracije dosta nizak ($\mathrm{Re} \approx 10000$), utjecaj turbulencije na kemijske vrste nije tako značajan (Sl. 42), te prema tome, kemijski profili su vrlo slični ravnotežnim u većini domene. Međutim, u SLFM bazi (Sl. 31) se vidi da je vrijednost NO profila kod ravnoteže ($\chi_{st} \to 0$) puno veća od vrijednosti ostalih profila u bazi, te je to uzrok lošijih NO rezultata dobivenih simulacijom. FPI baza (Sl. 32), s druge strane, daje puno manje vrijednosti za NO u blizini ravnoteže ($c \to 1$) te su zbog toga RPV (FPI) modelom dobiveni bolji NO rezultati. Kao što je prethodno spomenuto, rezultate dobivene RPV (SLFM) modelom treba gledati kritički, a pogotovo se to odnosi na NO i OH (vidi Poglavlje 4.3.1.3).

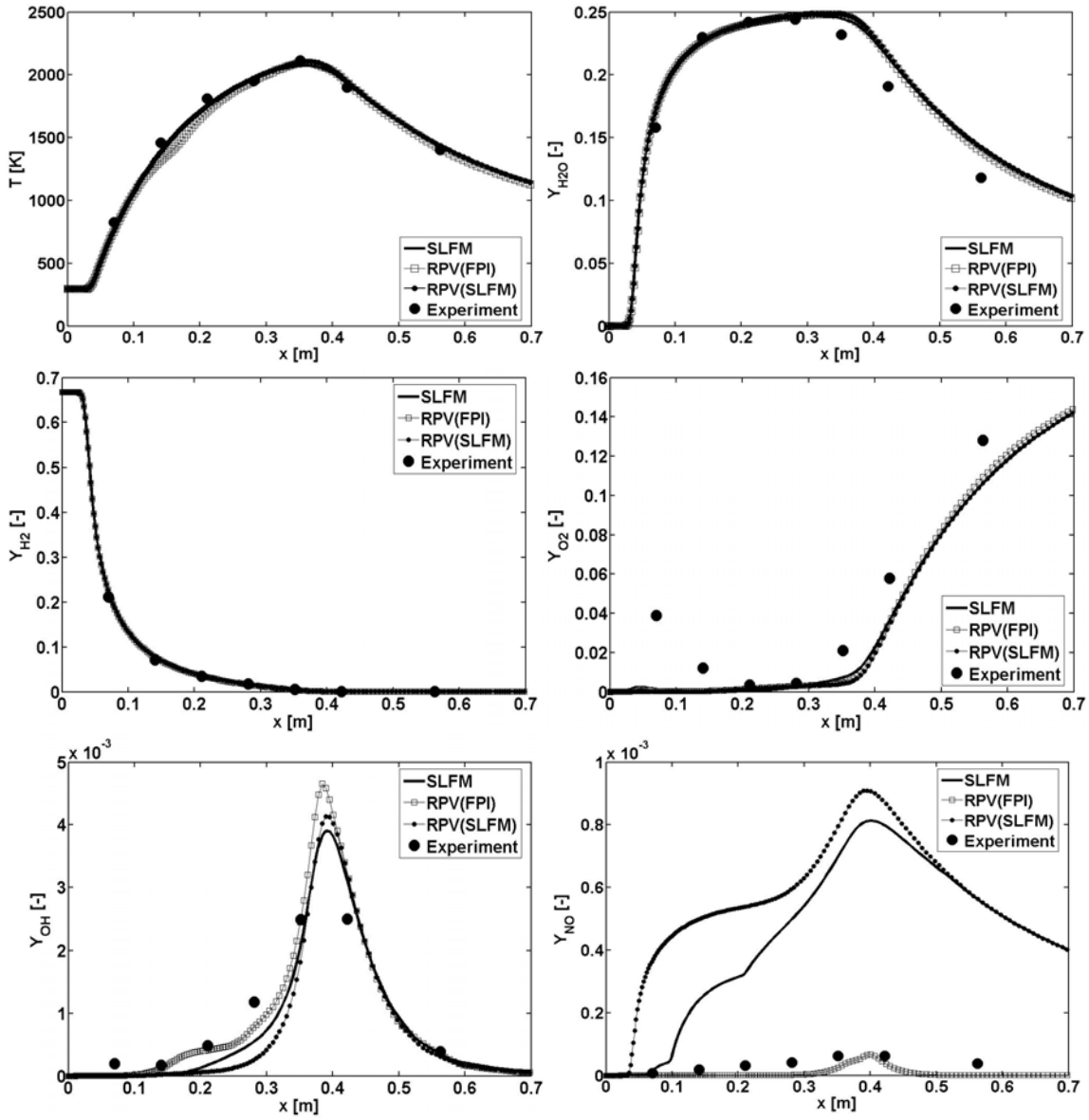

Slika 41 – Aksijalni profili usrednjenih vrijednosti temperature i masenih udjela različitih kemijskih vrsta (vodikov plamen; uzduž osi; neadijabatski; HTM)

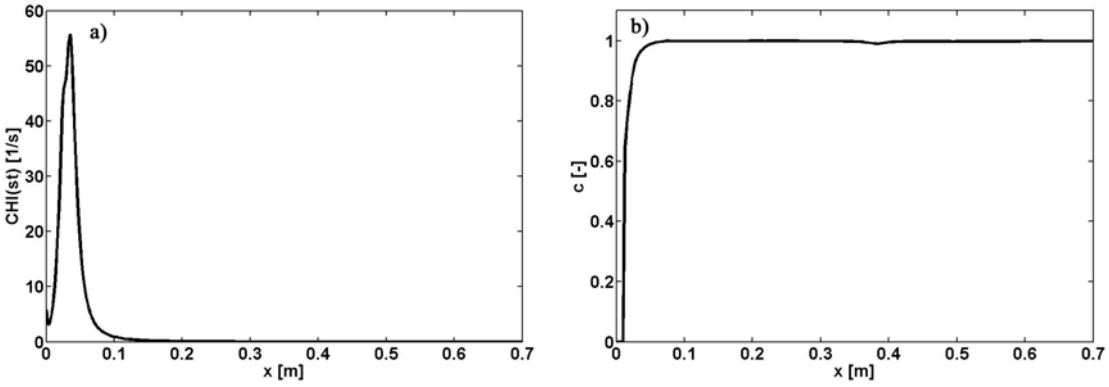

Slika 42 – Parametri tabulacije (vodikov plamen): a) $\overline{\chi}_{st}$ (jed. 91), SLFM baza; b) $\overline{c}$ (jed. 100), FPI baza

Radijalni profili usrednjene temperature i masenih udjela kemijskih vrsta (H_2O, H_2, O_2, OH i NO) na aksijalnim pozicijama $x/l_{vis} = 1/4$ i $x/l_{vis} = 3/4$ su prikazani na Sl. 43. i 44. Rezultati temperature i glavnih kemijskih vrsta su slični među modelima izgaranja, osim profila H_2 na poziciji $x/l_{vis} = 3/4$, a koji je loše simuliran RPV modelima. Rezultati temperature su lošiji dalje od centralne osi. Najveće razlike i ovdje su kod usporedbe OH i NO rezultata. Dok SLFM daje nešto bolje radijalne OH rezultate, RPV (FPI) model daje najbolje NO rezultate te se preporuča za upotrebu u situacijama gdje su bitni točni rezultati za NO. SLFM model daje NO rezultate koji su za red veličine veći od mjerenih. Slično kao i prije, rezultate RPV (SLFM) modela treba uzeti s rezervom i u ovome slučaju.

Radijalni profili na drugim aksijalnim pozicijama (nisu prikazani ovdje) se ponašaju slično.

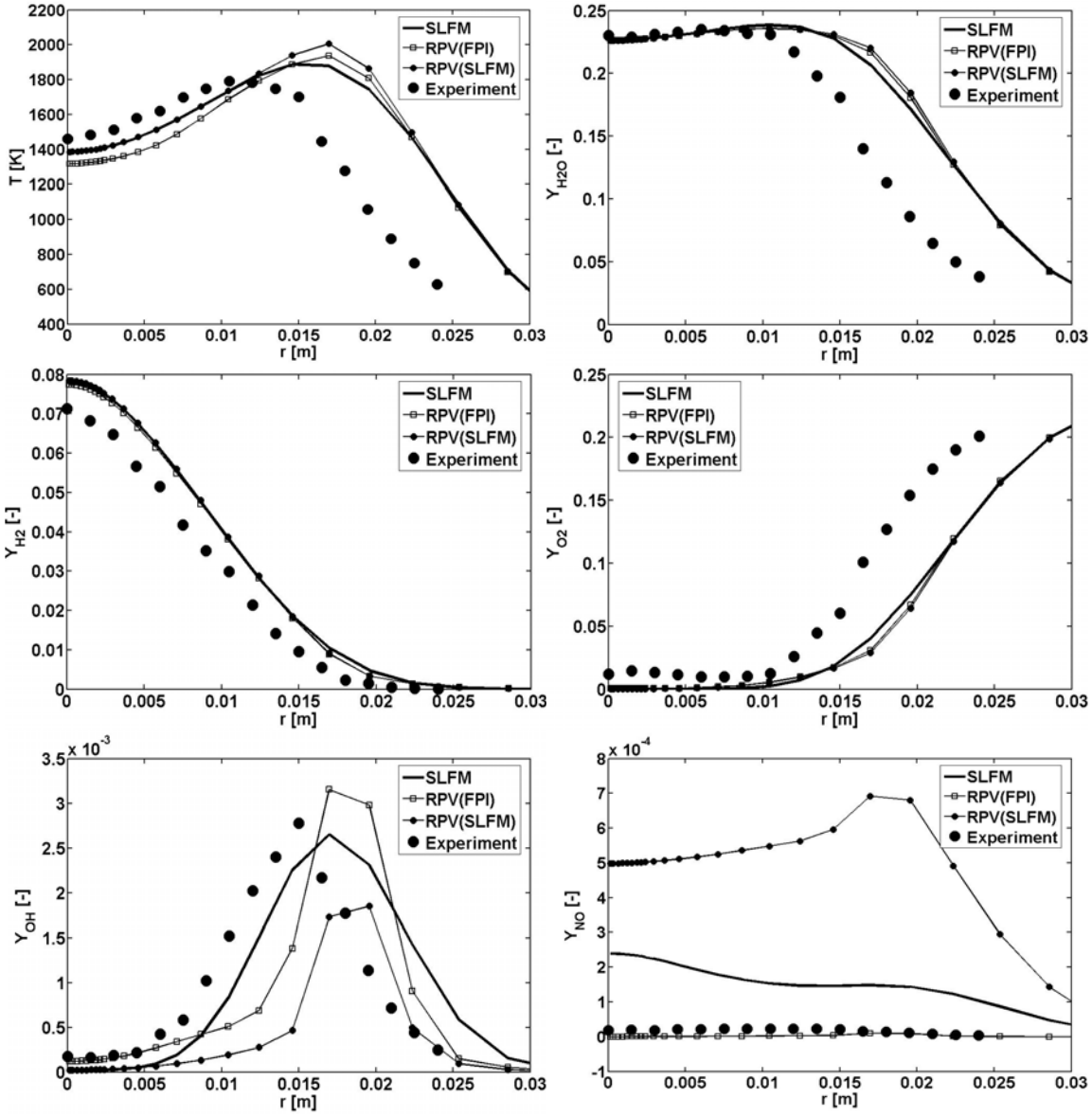

Slika 43 – Radijalni profili usrednjenih vrijednosti temperature i masenih udjela različitih kemijskih vrsta na poziciji x/l_{vis}=1/4 (vodikov plamen; neadijabatski; HTM)

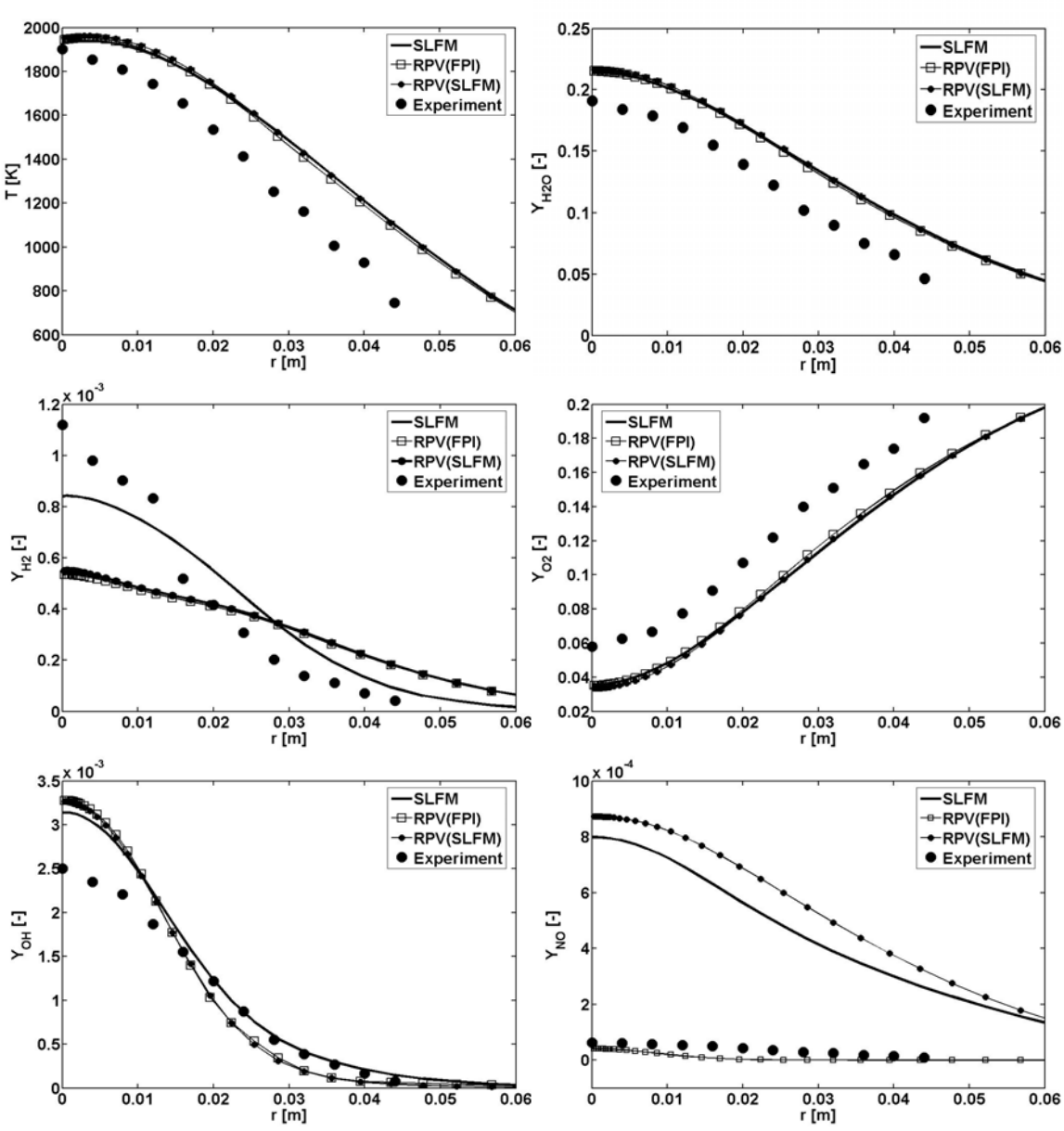

Slika 44 – Radijalni profili usrednjenih vrijednosti temperature i masenih udjela različitih kemijskih vrsta na poziciji x/l_{vis}=3/4 (vodikov plamen; neadijabatski; HTM)

5 Metanov mlazni plamen

5.1 Eksperimentalna konfiguracija

Gorionik se sastojao od koncentrično postavljenih struja goriva, pilota i zraka [29, 40, 142], a kako je prikazano na Sl. 45 .Gorivo se sastojalo od 25 % molnog udjela metana (CH_4) i 75 % molnog udjela zraka, te je imalo temperaturu 294 K. Pilot je imao kemijski sastav ekvivalentan ravnotežnom sastavu goriva i oksidanta kod $Z = 0.27$, a na temperaturi 1880 K. Temperatura zraka je bila 291 K. Plamen je radio kod $\mathrm{Re} = 22400$, sa malim stupnjem lokalnih gašenja (Sandia plamen D). Prosječne brzine na ulazu su bile 49.6 m/s za gorivo, 11.4 m/s za pilot te 0.9 m/s za zrak. Plamen je bio slobodan.

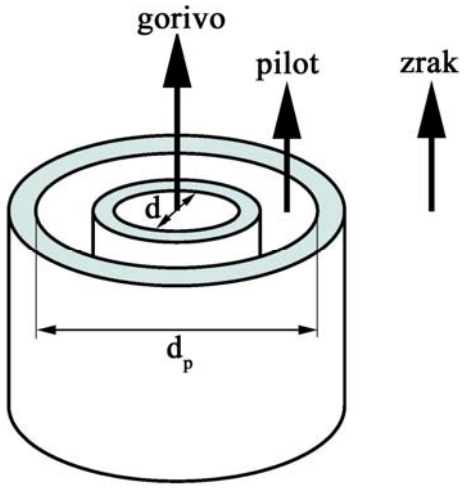

Slika 45 – Konfiguracija metanovog plamena

Dimenzije gorionika bile su sljedeće (Sl. 45):

Unutarnji promjer ulaza goriva:	$d = 7.2$ mm
Unutarnji promjer ulaza pilota:	7.7 mm (debljina cijevi 0.25 mm)
Vanjski promjer ulaza pilota:	$d_p = 18.2$ mm
Unutarnji promjer ulaza zraka:	18.9 mm (debljina cijevi 0.35 mm)
Vanjski promjer ulaza zraka:	300 mm

Dokumentacija o plamenu te eksperimentalna mjerenja mogu se pronaći na [29].

5.2 Numerička konfiguracija

Računalna mreža se sastojala od 338400 kontrolnih volumena koji pokrivaju cilindričnu prostornu domenu od $x/d = 0$ do $x/d = 150$ u aksijalnom smjeru te od $r/d = 0$ do $r/d = 40$ u radijalnom smjeru. Slično kao i kod plamena vodika i zraka, mreža je bila gušća prema centralnoj osi te ulazima goriva, pilota i zraka (vidi Sl. 46). Gustoća mreže u aksijalnim i radijalnim pravcima bila je slična kao i kod mreža korištenih u simulacijama ovog plamena objavljenim u TNF zbornicima [29], te se nije ispitivao utjecaj gustoće mreže na rezultate simulacije u ovome radu.

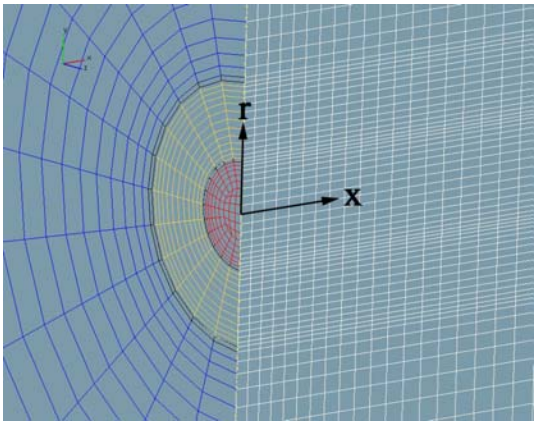

Slika 46 – Računalna mreža (metanov plamen; vertikalni aksijalni presjek uzduž osi)

GRI Mech 3.0 [65] kemijski mehanizam koristio se u proračunima kemijskih vrsta u pretprocesoru, a sastoji se od 53 kemijske vrste i 325 reakcija. Izgaranje se modeliralo standardnim SLFM modelom te modelima baziranim na varijabli napretka reakcije (Poglavlje 3.2.4). Interakcija turbulencije i izgaranja obuhvaćena je preko pretpostavljene β-PDF funkcije.

DTRM proračuni su rađeni sa 48 (4x12), 16 (2x8) i 4 (1x4) zraka emitiranih s rubnih ploha, a da bi se usput ispitao utjecaj broja zraka na točnost rezultata simulacije. WSGGM [101] je korišten za modeliranje koeficijenta apsorpcije participirajućeg medija. Rubne površine domene su pretpostavljene crnim površinama ($\varepsilon_b = 1$).

Konstanta $C_{\varepsilon 2}$ u jednadžbi za brzinu disipacije turbulentne kinetičke energije je postavljena $C_{\varepsilon 2} = 1.8$, a kao što je preporučeno u TNF zbornicima [29]. HTM i k-ε modeli su korišteni za turbulenciju.

Brzine na ulazu su postavljene prema eksperimentalnim podacima (Sl. 147) [143].

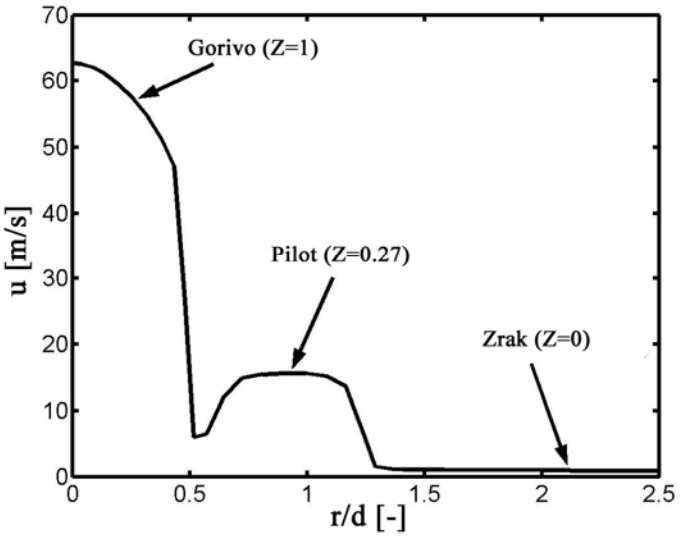

Slika 47 – Profili brzine na ulazu (metanov plamen)

Turbulentna kinetička energija na ulazima je procijenjena iz mjerenih podataka za Reynoldsova naprezanja. Brzina disipacije turbulentne kinetičke energije je propisana slično kao i u [55]:

$$\varepsilon = \sqrt{C_\mu} k \left| \frac{\partial u}{\partial r} \right| \tag{139}$$

Slično kao i kod plamena vodika i zraka, za proračun toka fluida je korišten stacionarni nekompresibilni (mali Machovi brojevi) rješavač. Konstantan statički tlak je nametnut na izlaznim rubnim površinama. Iteracijsko rješavanje se provodilo dok reziduali nisu pali ispod vrijednosti 10^{-6}, gdje god je to bilo moguće. Konvektivni član u jednadžbi kontinuiteta je diskretiziran shemom centralnih razlika (drugi red točnosti), dok su isti članovi u jednadžbama brzina diskretizirani hibridnom shemom između centralnih razlika i uzvodne sheme (težinski faktor 0.5). Konvektivni članovi u ostalim skalarnim jednadžbama su diskretizirani upotrebom uzvodne sheme diskretizacije (prvi red točnosti). Difuzijski članovi u svim transportnim jednadžbama diskretizirani su centralnim razlikama. Ostali numerički postav je bio kao što je uobičajeno kod FIRE CFD rješavača [99].

5.3 Rezultati

5.3.1 Pretabulirani kemijski profili

Slike 49-52 prikazuju profile kemijskih vrsta dobivene u pretprocesoru upotrebom različitih modela. Originalna SLFM baza (Sl. 49) dobila se je za 14 različitih parametara brzine skalarne disipacije kod stehiometrijskih uvjeta:

$$\chi_{st} = 0.01, 0.1, 1, 2, 5, 10, 20, 50, 100, 150, 200, 300, 450, 575\ s^{-1} \qquad (140)$$

Prvi profil ($\chi_{st} = 0.01\ s^{-1}$) ima sličan sastav ravnotežnom, dok je zadnji profil ($\chi_{st} = 575\ s^{-1}$) onaj neposredno prije gašenja. Kemijske vrste i temperature na rubovima postavljene su prema eksperimentalnim podacima. Varijabla masenog udjela smjese goriva diskretizirana je u 50 neekvidistantnih točaka, s gušćom raspodjelom oko stehiometrijske točke ($Z_{st} \approx 0.353$).

Linearna kombinacija masenih udjela CO_2, CO i H_2O koristila se kao varijabla napretka reakcije, tj. $Y_c \equiv Y_{CO_2} + Y_{CO} + Y_{H_2O}$. Granice zapaljivosti plamena bile su otprilike $0.369 \le \phi \le 7.193$[11] (Sl. 48). Ukupno je bilo 29 setova predmiješanih plamenova dobivenih upotrebom PREMIX rješavača [97] unutar granica zapaljivosti, dok se preostalih 21 dobilo linearnom interpolacijom s rubnim vrijednostima. Zadržana je diskretizacija masenog udjela smjese goriva (tj. ekvivalentnih omjera) iz originalne SLFM baze. FPI baza plamenova prikazana je na Sl. 50. Slično kao i kod vodikovog plamena, FPI profili za NO značajno se razlikuju od NO profila u bazi nepredmiješanih plamenova (SLFM). Ostale kemijske vrste imaju slične maksimalne vrijednosti kao i SLFM baza (Sl. 49) ili reparametrizirana SLFM baza (Sl. 51). Interpolirani profili između bogate granice zapaljivosti i granice goriva mogu se primijetiti u FPI bazi u području $Z > 0.8$, osobito u slučaju CO_2, CO, H_2O i H_2.

U ovom slučaju nije bilo problema kod reparametrizacije originalne SLFM baze, a kako je to bio slučaj s plamenom vodika i zraka. Reparametrizirana SLFM baza (Sl. 51) zadržala je sve bitne karakteristike originalne SLFM baze (Sl. 49) – maksimalne

[11] Odnosno, $0.16729 \le Z \le 0.79678$ – vidi jed. (24)

vrijednosti te početni i zadnji profili ($\chi_{st} = 0.01/575$ s^{-1} te $c = 1/0$) su jednaki u obje baze. Može se primijetiti da profili blaže variraju u reparametriziranoj bazi, naročito oni glavnih vrsta.

Mješovita baza plamenova, a kako je definirana u Poglavlju 2.3.6.3, prikazana je na Sl. 52. Ova baza je zadržala bite osobine obje baze od kojih se sastoji – FPI baze (predmiješani plamenovi) i SLFM baze (nepredmiješani plamenovi). No, mora se imati na umu da normalizirane varijable napretka reakcije u reparametriziranoj SLFM bazi, odnosno mješovitoj/FPI bazi, ne pokrivaju ista područja, a kako je opisano u Poglavlju 2.3.6. Može se uočiti prijelaz između predmiješanih (niže vrijednosti normalizirane varijable napretka reakcije) i nepredmiješanih (više vrijednosti normalizirane varijable napretka reakcije) plamenova u mješovitoj bazi kod graničnih vrijednosti c_{thresh} (jed. (43)).

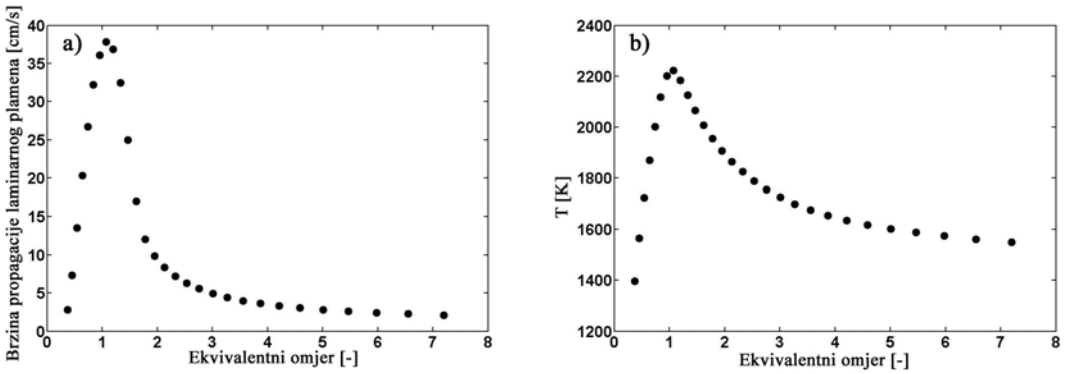

Slika 48 – Predmiješani plamen razrijeđenog metana (25% CH_4, 75% zrak – molni udjeli)/zraka: a) Brzina propagacije laminarnog plamena; b) Temperatura produkata izgaranja

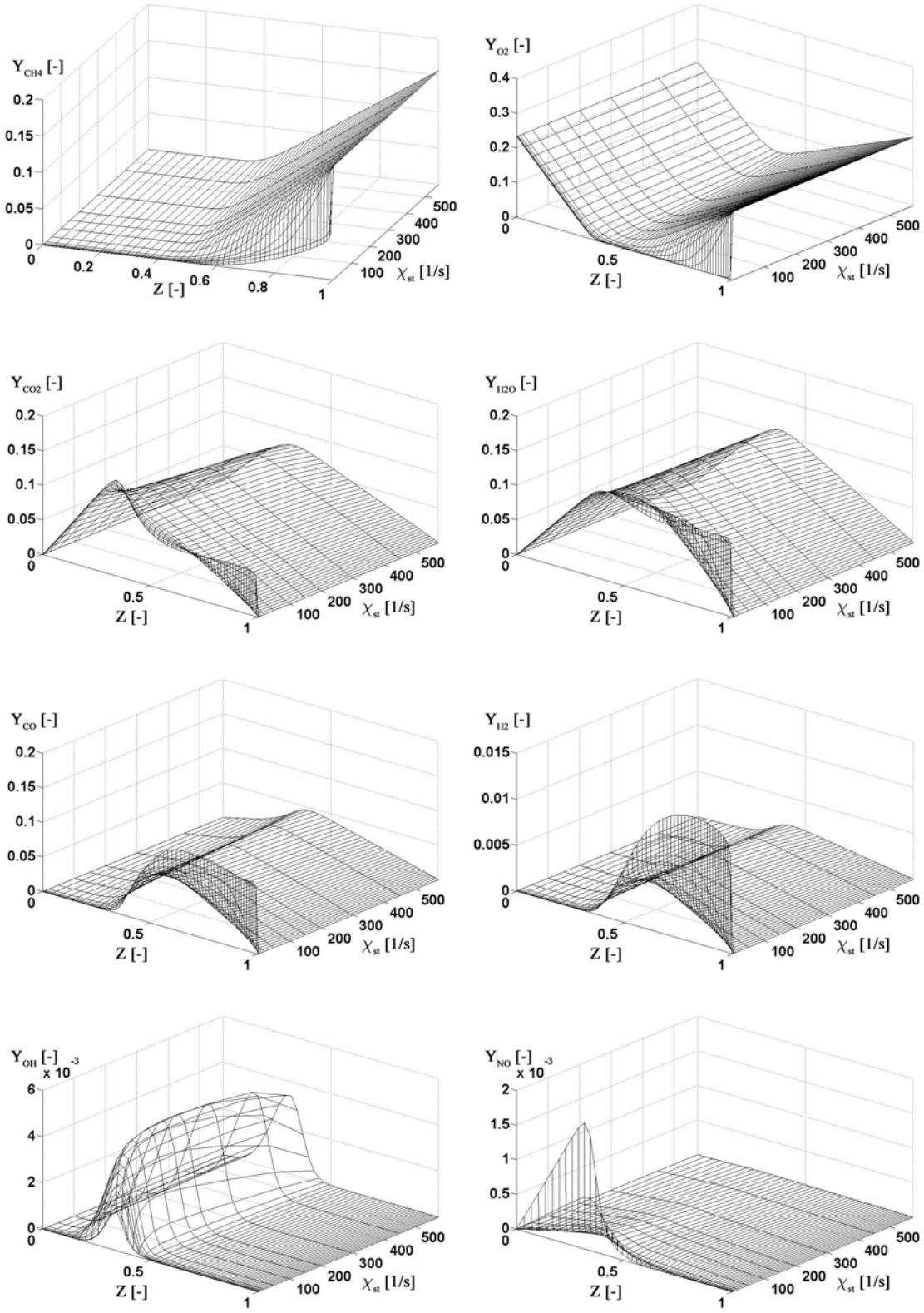

Slika 49 – SLFM (standardni) baza (metanov plamen)

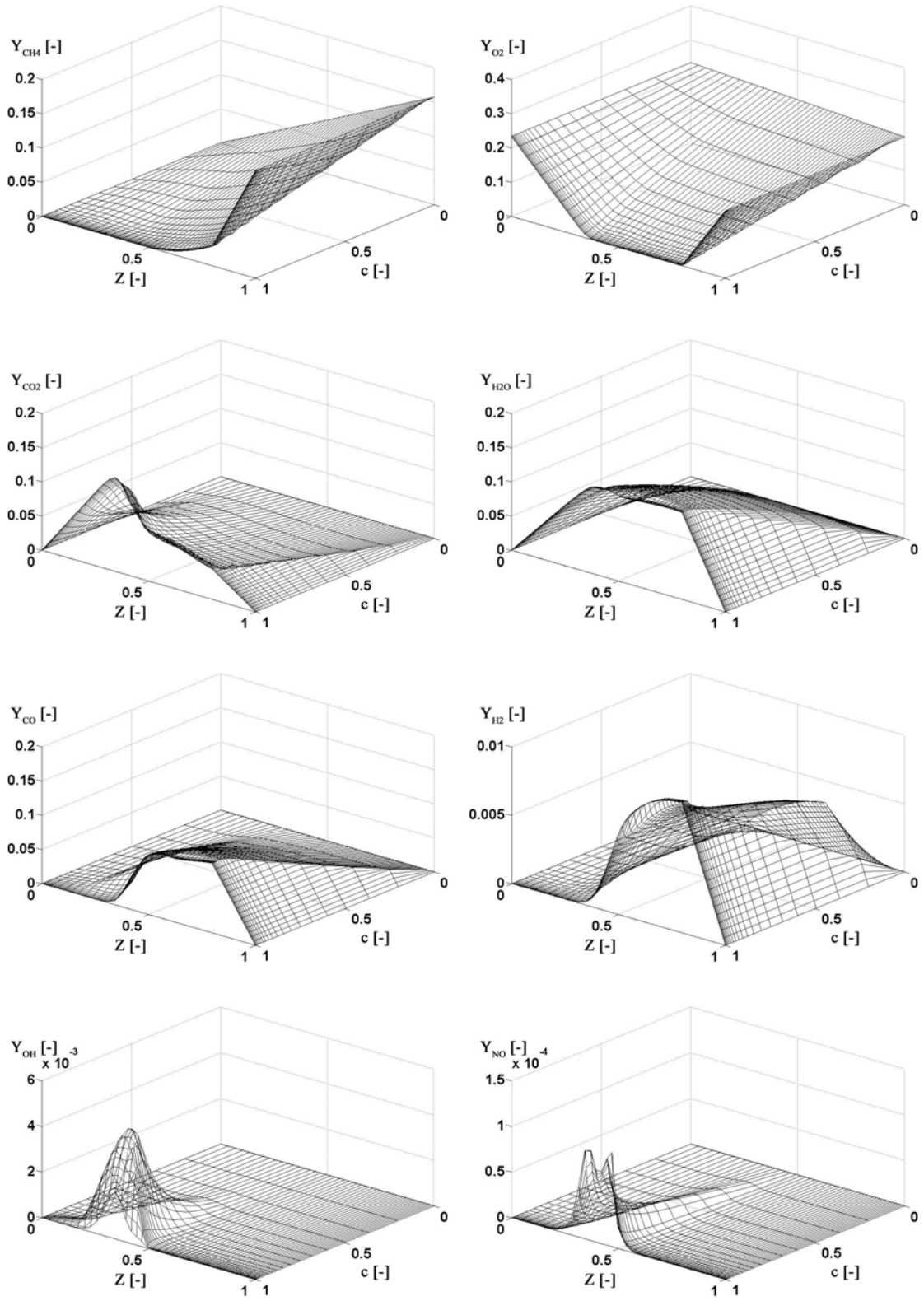

Slika 50 – FPI baza (metanov plamen)

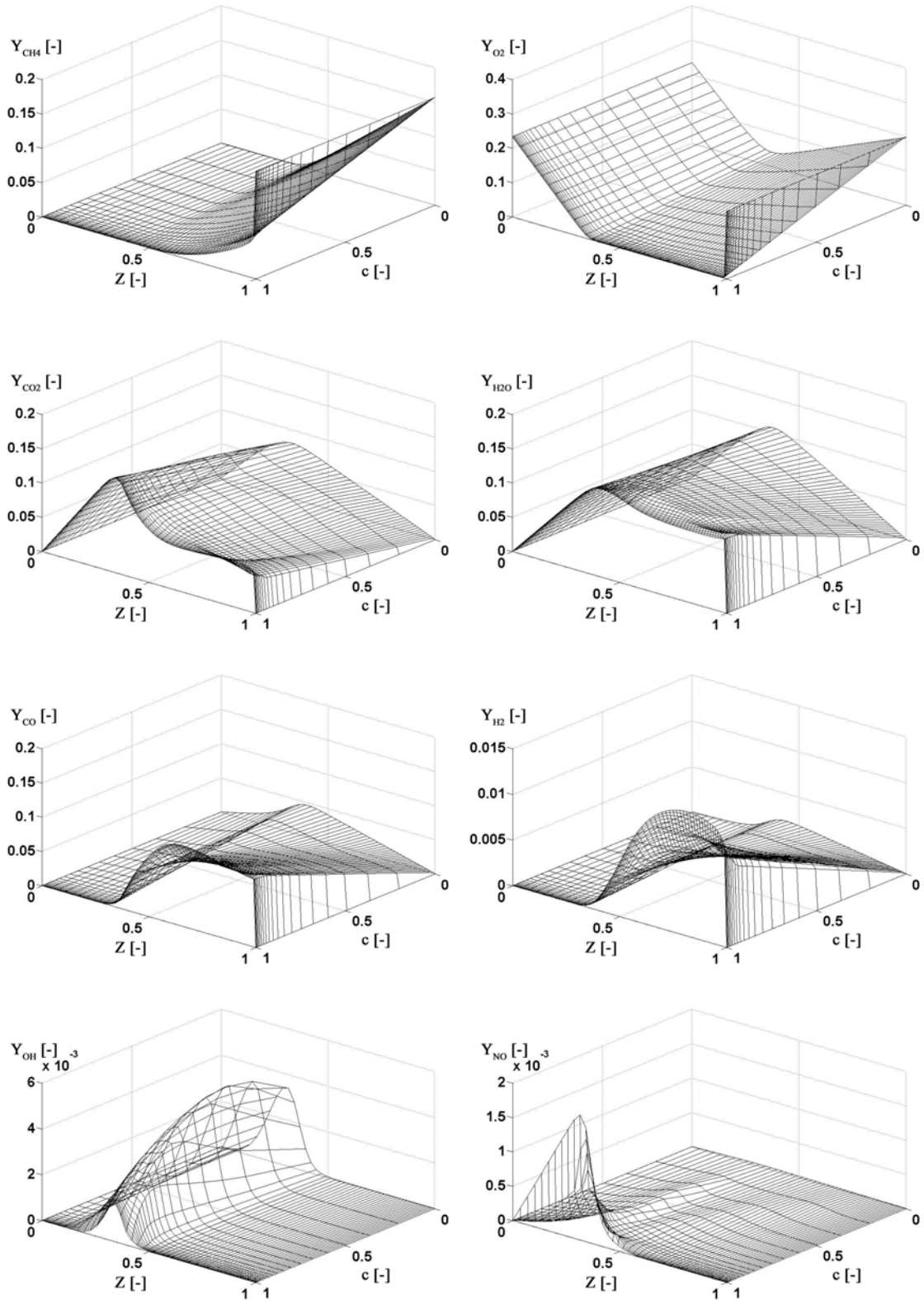

Slika 51 – SLFM (RPV) baza (metanov pamen)

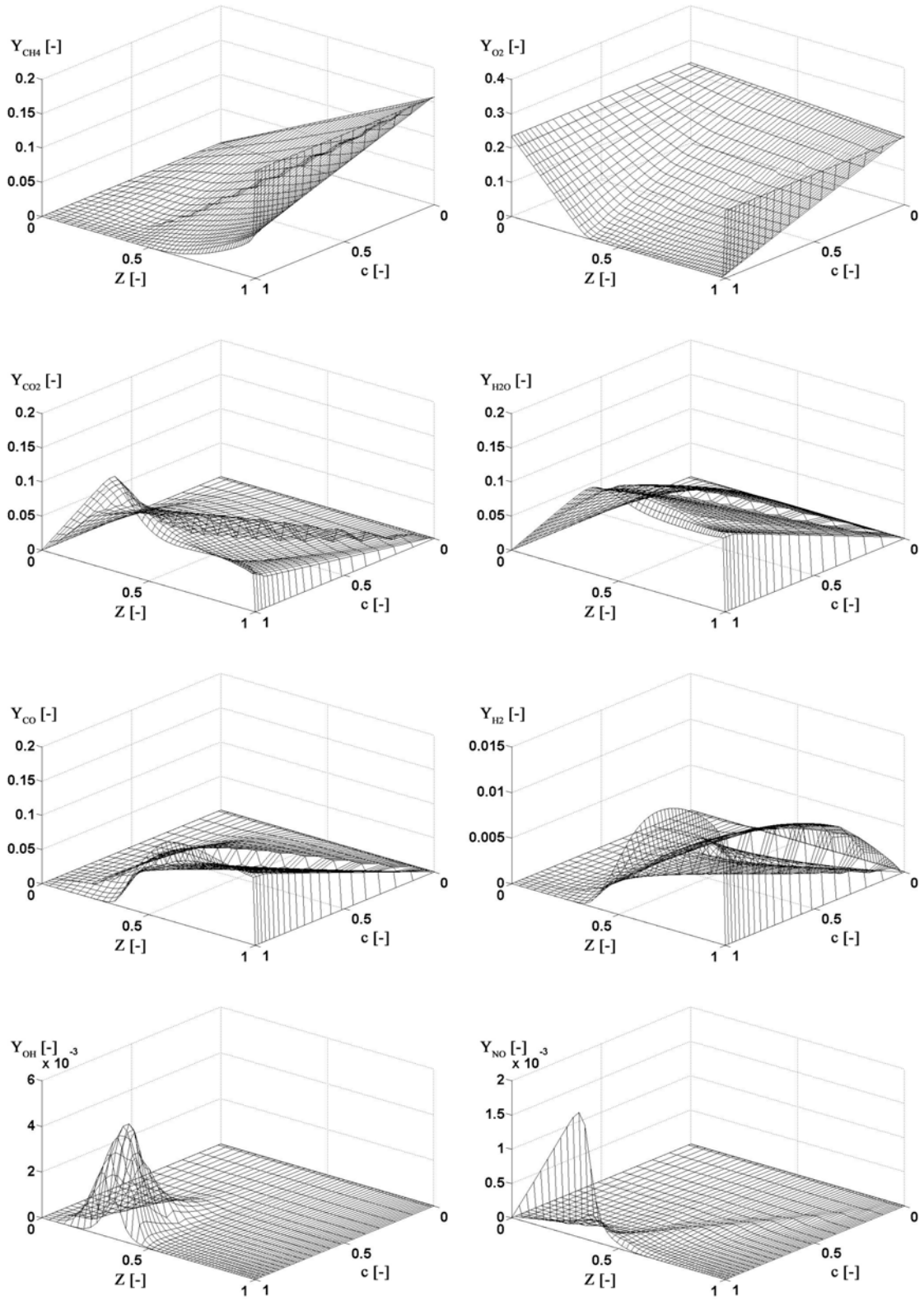

Slika 52 – Mješovita baza (metanov plamen)

5.3.2 Adijabatski vs. neadijabatski profili

Aksijalni profili usrednjene temperature na centralnoj osi sa i bez modeliranja zračenja prikazani su na Sl. 53. Standardni k-ε i HTM su korišteni kod modeliranja turbulencije, dok su DTRM (48 zraka) i WSGGM korišteni za modeliranje zračenja. Dobiveni su bolji profili temperature u slučaju modeliranja zračenja, kao što je i očekivano. Dok je razlika između adijabatskih i neadijabatskih profila mala u blizini gorionika ($x/d < 0.25$), značajnije razlike su vidljive na udaljenijim lokacijama, a gdje su značajniji udjeli participirajućih plinova CO_2 i H_2O (WSGGM [101]; Sl. 54). k-ε i HTM model daju slične rezultate u blizini gorionika, dok su razlike vidljive u području $x/d > 0.2$. Oba modela daju veće temperature od mjerenih u području $0.15 < x/d < 0.3$. k-ε model bolje simulira lokaciju maksimalne temperature te daje nešto više temperature od HTM modela u području $x/d > 0.325$. Adijabatske temperature su značajno veće od mjerenih na svim aksijalnim pozicijama.

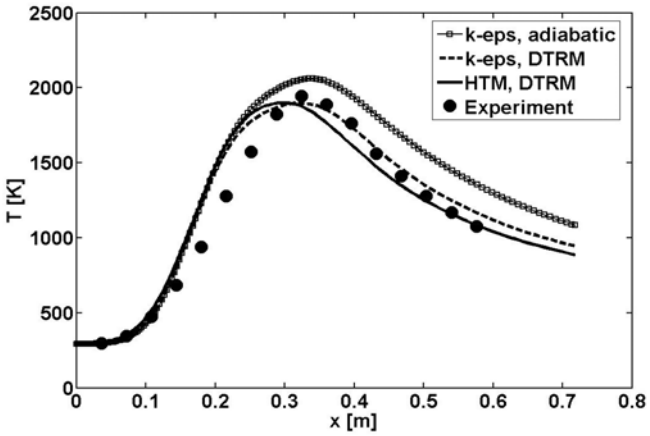

Slika 53 – Aksijalni profili usrednjene temperature uzduž osi (metanov plamen; adijabatski vs. DTRM; k-ε vs. HTM)

Usrednjeni maseni udjeli CO_2 i H_2O prikazani su na Sl. 54. Razlike zbog modeliranja turbulencije su izraženije nego razlike između adijabatskih i neadijabatskih profila. To se djelomično može objasniti činjenicom da se isključio utjecaj zračenja kod proračuna kemijskih vrsta u pretprocesoru. U tom pogledu je utjecaj zračenja na sastav kemijskih vrsta preko promjena u gustoći dosta manji nego utjecaj uslijed modela turbulencije. Slično kao i kod profila temperature, HTM daje CO_2 i H_2O profile koji su pomaknuti prema ulijevo u odnosu na k-ε model. Rezultati HTM-a za CO_2 i H_2O su bolji na

udaljenijim lokacijama od gorionika ($x/d > 0.35$), dok k-ε model daje bolje CO_2 rezultate u blizini gorionika.

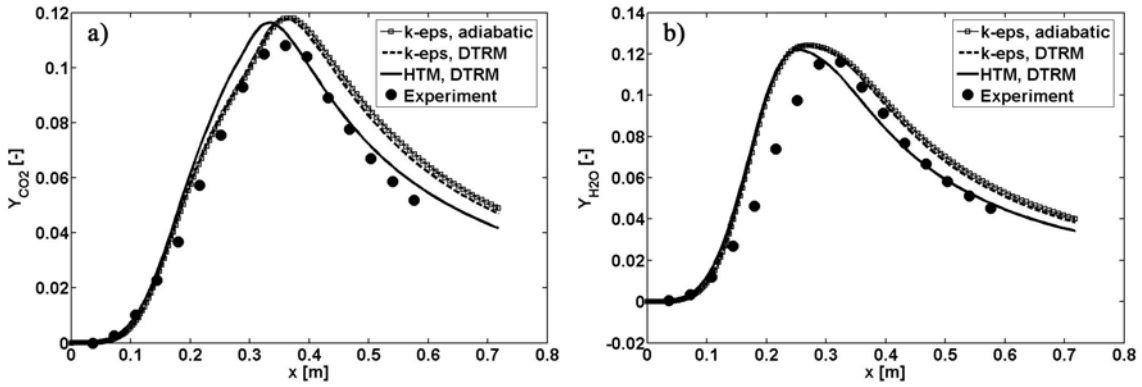

Slika 54 – Aksijalni profili uzduž osi (metanov plamen; adijabatski vs. DTRM; k-ε vs. HTM): a) Usrednjeni maseni udio CO_2; b) Usrednjeni maseni udio H_2O

Broj zraka po rubnoj plohi u DTRM proračunima je variran, a da bi se ispitao utjecaj broja zraka na točnost rezultata. Tablica 1 prikazuje ukupne toplinske gubitke zbog zračenja za različite brojeve zraka – 48, 16 i 4. Kao što se i očekivalo, bolji rezultati simulacija su dobiveni uz veći broj zraka. Međutim, u svim simulacijama su dobiveni rezultati toplinskih gubitaka koji su značajno veći od izmjerene vrijednosti. Slični rezultati su već objavljeni za ovaj plamen u [63], ali uz upotrebu modela zračenja za optički slabo apsorbirajući medij. WSGGM [101] se može djelomično optužiti za netočne rezultate toplinskih tokova zbog toga što nije u obzir uzeta spektralna ovisnost koeficijenta apsorpcije medija. Spektralni efekti su se pokazali bitnim za dobivanje točnih rezultata u [30].

Tablica 1 – Bilanca toplinskog toka zbog zračenja (metanov plamen)

	Toplinski tok uslijed zračenja [kW]
Mjereno	-0.8870
Simulacija, DTRM (48 zraka)	-2.1727
Simulacija, DTRM (16 zraka)	-3.1528
Simulacija, DTRM (4 zraka)	-6.8973

5.3.3 Usporedba modela izgaranja

Slično kao što je opisano u Poglavlju 4.3.4, različiti su modeli izgaranja – SLFM, RPV (FPI), RPV (MIX) i RPV (SLFM) (Poglavlje 3.2.4) – korišteni u postprocesoru (uz postojeće referentno rješenje) za dobivanje usrednjenog sastava kemijskih vrsta. Referentno se rješenje dobilo upotrebom standardnog SLFM modela izgaranja te upotrebom DTRM (48 zraka) i WSGGM modela za zračenje.

HTM se koristio kod modeliranja turbulencije zbog boljih rezultata brzina u usporedbi s k-ε modelom, vidi Sl. 55. Rezultati širenja plamena se dobro slažu s mjerenjima na svim aksijalnim pozicijama (Sl. 55), dok su razlike između modela turbulencije, a u prilog HTM-a, očite na lokacijama dalje od gorionika.

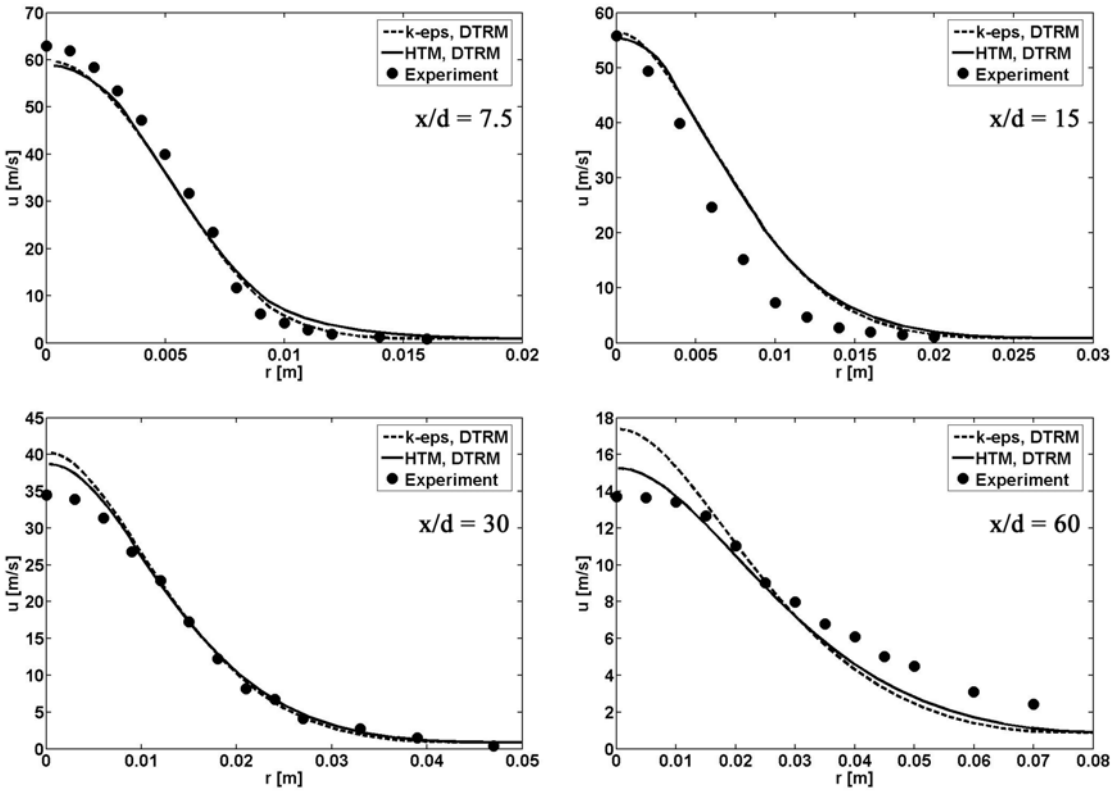

Slika 55 – Radijalni profili usrednjene aksijalne brzine (metanov plamen; DTRM; k-ε vs. HTM) na različitim aksijalnim pozicijama (metanov plamen)

Referentni aksijalni profili momenata masenog udjela smjese goriva prikazani su na Sl. 56. Radijalni profili istih na različitim aksijalnim pozicijama prikazani su na Sl. 57. općenito, usrednjena vrijednost masenog udjela goriva je u boljem slaganju s mjerenjima

nego RMS. Jednostavno modeliranje turbulentnih fluktuacija te usrednjene brzine skalarne disipacije najvjerojatniji je uzrok slabijeg slaganja RMS profila s mjerenim rezultatima. No generalno su slaganja rezultata simulacije i mjerenih rezultata zadovoljavajuća te u skladu s rezultatima objavljenih za ovaj plamen u TNF zbornicima [29].

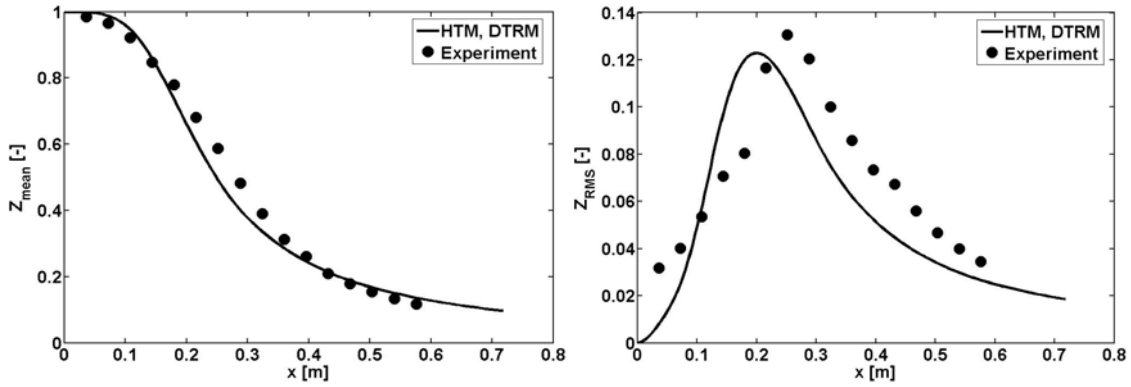

Slika 56 – Aksijalni profili (uzduž osi) momenata masenog udjela smjese goriva (usrednjena vrijednost i RMS) (metanov plamen)

Radijalni profili usrednjene temperature na različitim aksijalnim pozicijama, a dobiveni različitim modelima izgaranja, prikazani su na Sl. 58. Vidljive su razlike između modela izgaranja u područjima bogatim smjesom goriva u blizini gorionika ($x/d = 7.5$ i $x/d = 15$), dok su dalje od centralne osi te razlike manje. Općenito, slaganja s mjerenjima su lošija dalje od centralne osi.

Aksijalni profili usrednjenih masenih udjela različitih kemijskih vrsta na centralnoj osi prikazani su na Sl. 59. Modeli izgaranja bazirani na varijabli napretka reakcije pokazuju lošije rezultate od standardnog SLFM modela u područjima bogatim gorivom ($x < 0.325$ m). Profili su pomaknuti ulijevo u usporedbi s mjerenjima. Razlike su veće za H_2 i CO nego za glavne produkte izgaranja CO_2 i H_2O. Niže vrijednosti goriva (CH_4) i oksidanta (O_2) u područjima bogatim gorivom ukazuju na pojačano izgaranje dobiveno RPV modelima u tim područjima. Razlike između modela su male na udaljenijim lokacijama od gorionika. OH profili su slični između modela, s time da RPV (SLFM) daje najbolje OH rezultate u područjima iza fronte plamena ($x > 0.4$ m).

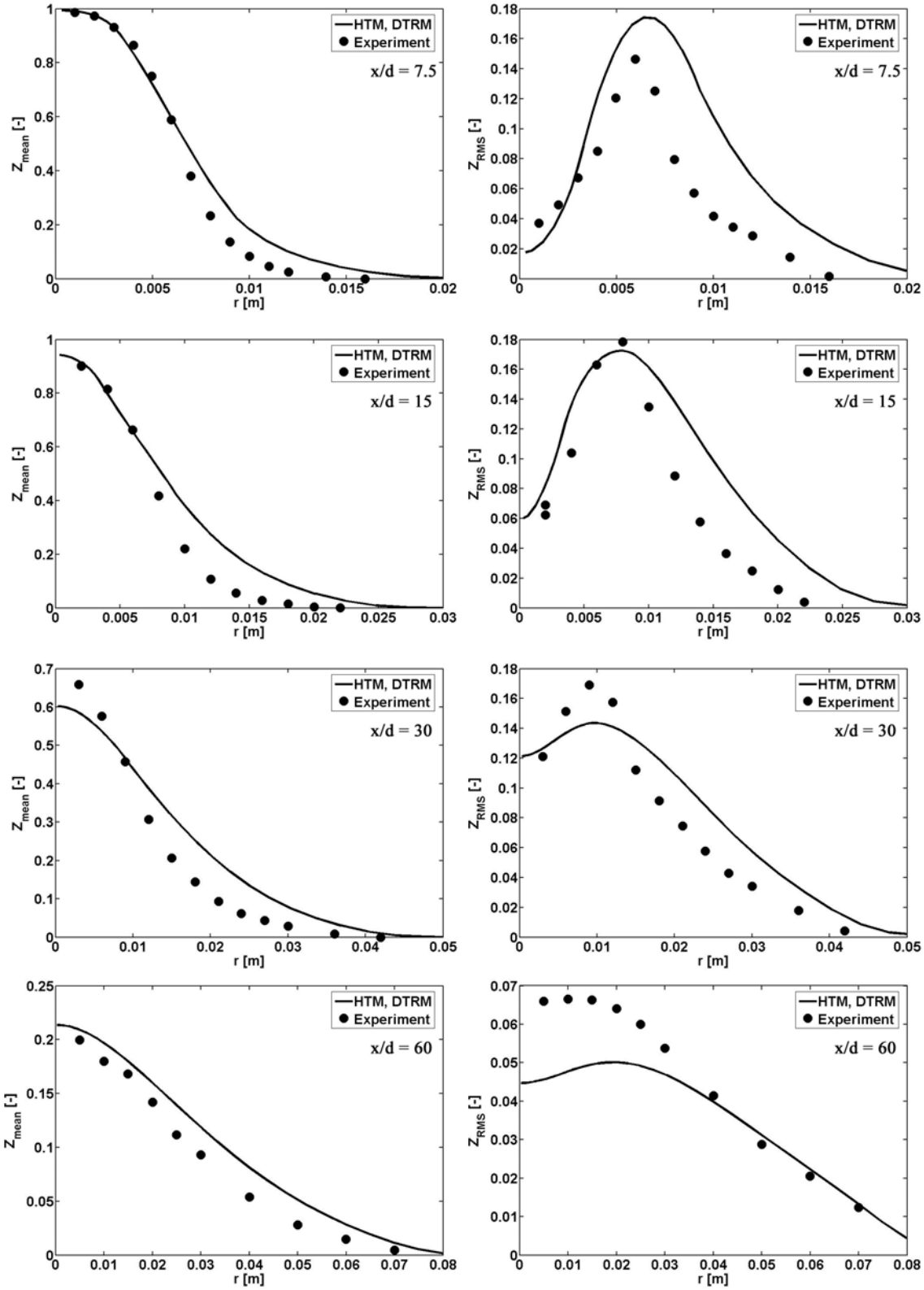

Slika 57 – Radijalni profili momenata masenog udjela smjese goriva (usrednjena vrijednost i RMS) na različitim aksijalnim pozicijama (metanov plamen)

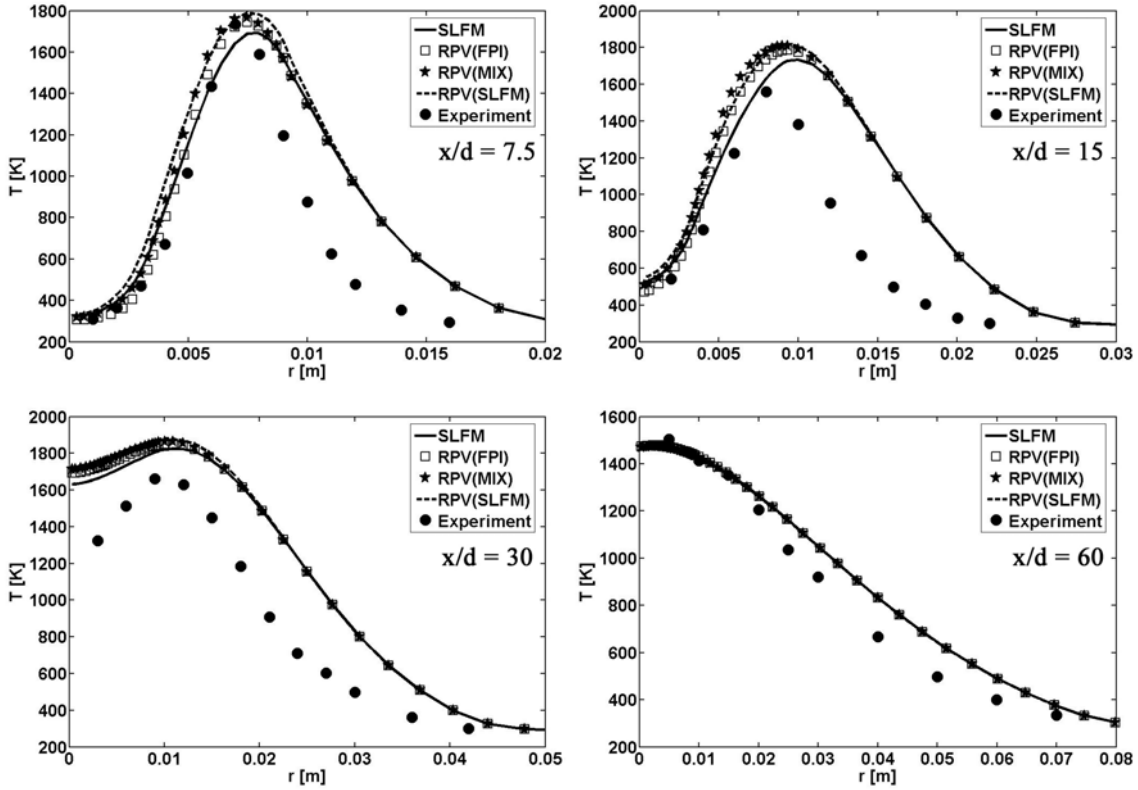

Slika 58 – Radijalni profili usrednjene temperature na različitim aksijalnim pozicijama (metanov plamen)

Najveća razlika među modelima izgaranja je ponovno vidljiva u rezultatima za NO. Ovdje se također dobivaju puno veće vrijednosti NO-a upotrebom modela izgaranja baziranih na nepredmiješanim plamenovima nego što je izmjereno, dok su najbolji rezultati dobiveni RPV (FPI) modelom. Nešto su bolji rezultati NO-a dobiveni upotrebom reparametrizirane SLFM baze (RPV (SLFM)) u usporedbi sa standardnim SLFM modelom. Mješovitom formulacijom (RPV (MIX)) dobiveni su najlošiji NO rezultati, posebice u zoni nakon fronte plamena.

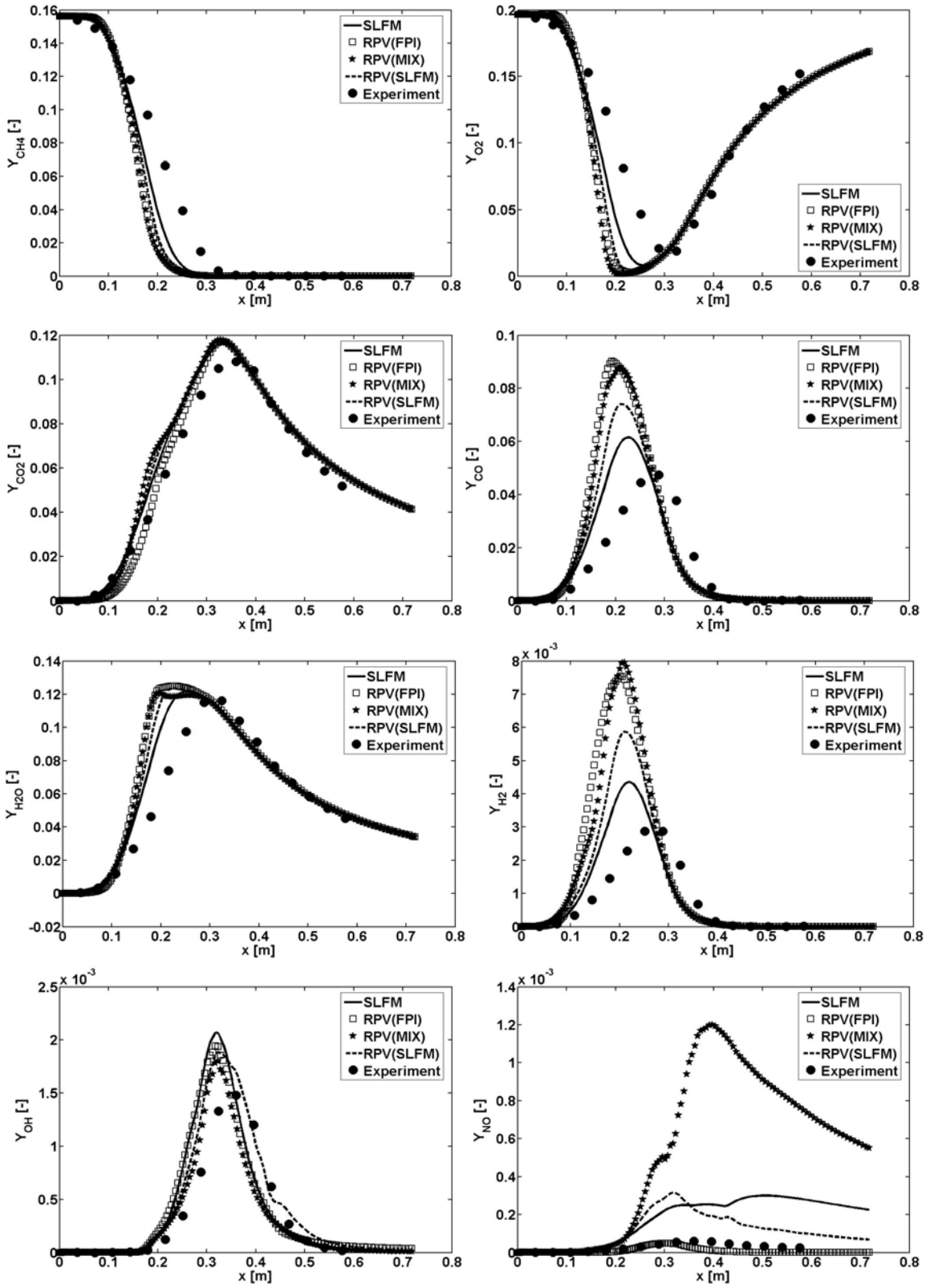

Slika 59 – Aksijalni profili (uzduž osi) usrednjenih vrijednosti masenih udjela različitih kemijskih vrsta (metanov plamen)

Radijalni profili usrednjenih masenih udjela različitih kemijskih vrsta na dvije aksijalne pozicije – $x/d = 30$ i $x/d = 60$ – prikazani su na Sl. 60 i 61.

Na bližoj aksijalnoj poziciji ($x/d = 30$) prevladava područje bogato gorivom oko centralne osi te je moguće primijetiti relativnu netočnost RPV modela u tom području. SLFM daje bolje rezultate od RPV modela u blizini osi za većinu glavnih vrsta (CH_4, O_2, H_2O, i dr.). Međutim, isto ne vrijedi i za CO_2 te manje vrste (OH i NO). CO_2 rezultati su najbolji kod RPV (FPI) i u blizini centralne osi, dok su rezultati dalje od osi slični među modelima te se slabije slažu s mjerenjima. Maksimalne vrijednosti OH su najbolje simulirane RPV (SLFM) modelom, dok ostali modeli daju maksimalne OH vrijednosti koje su veće od izmjerenih. I ovdje se vidi da RPV (FPI) model daje najbolje NO rezultate, dok modeli bazirani na nepredmiješanim plamenovima daju puno veće NO vrijednosti od mjerenih. Nepravilno ponašanje NO profila kod RPV (MIX) modela može se primijetiti dalje od centralne osi, a što je najvjerojatnije uzrokovano prijelazom između predmiješanih i nepredmiješanih plamenova u mješovitoj bazi (Sl. 52). CH_4 i O_2 vrijednosti su puno manje od mjerenih u blizini centralne osi kod svih modela izgaranja, a kao što je već i primijećeno kod aksijalnih profila (Sl. 59).

Radijalni profili na poziciji $x/d = 60$ pokazuju bolje rezultate RPV modela nego iste na poziciji $x/d = 30$. Glavni produkti izgaranja (CO_2 i H_2O) su dobro simulirani, te su razlike među modelima male što se tiče te dvije vrste. RPV (FPI) i SLFM modeli daju slične CO rezultate te su u boljem slaganju s mjerenjima od ostala dva modela izgaranja. Slično je i s rezultatima za H_2, premda su u ovome slučaju odstupanja od mjerenja nešto veća. RPV (SLFM) model opet daje najbolje OH rezultate, dok je RPV (FPI) najbolji za NO. RPV (MIX) model daje značajno veće rezultate za NO od mjerenih te se čini kao loš izbor u ovom slučaju.

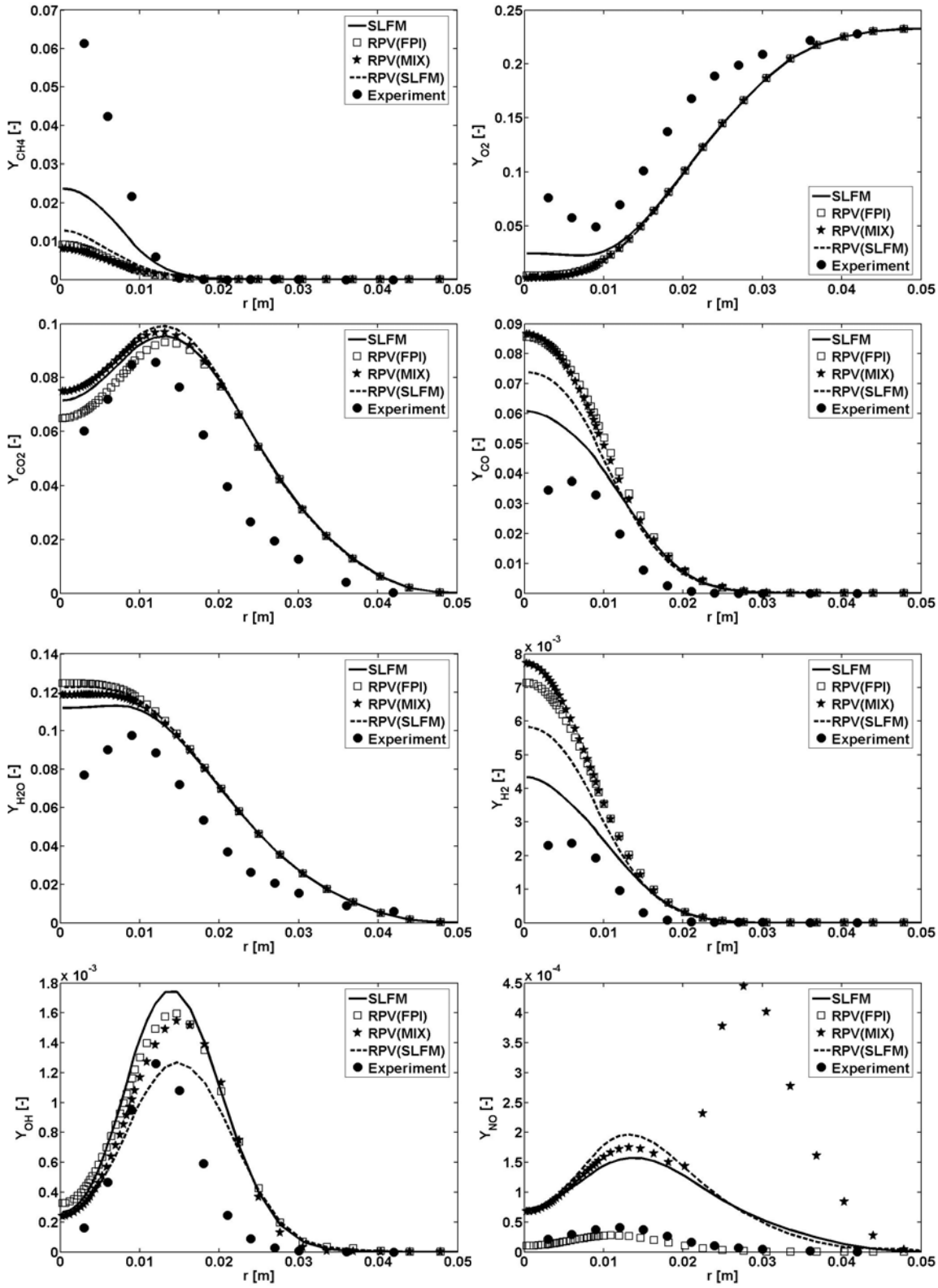

Slika 60 – Radijalni profili usrednjenih vrijednosti masenih udjela različitih kemijskih vrsta na poziciji x/d=30 (metanov plamen)

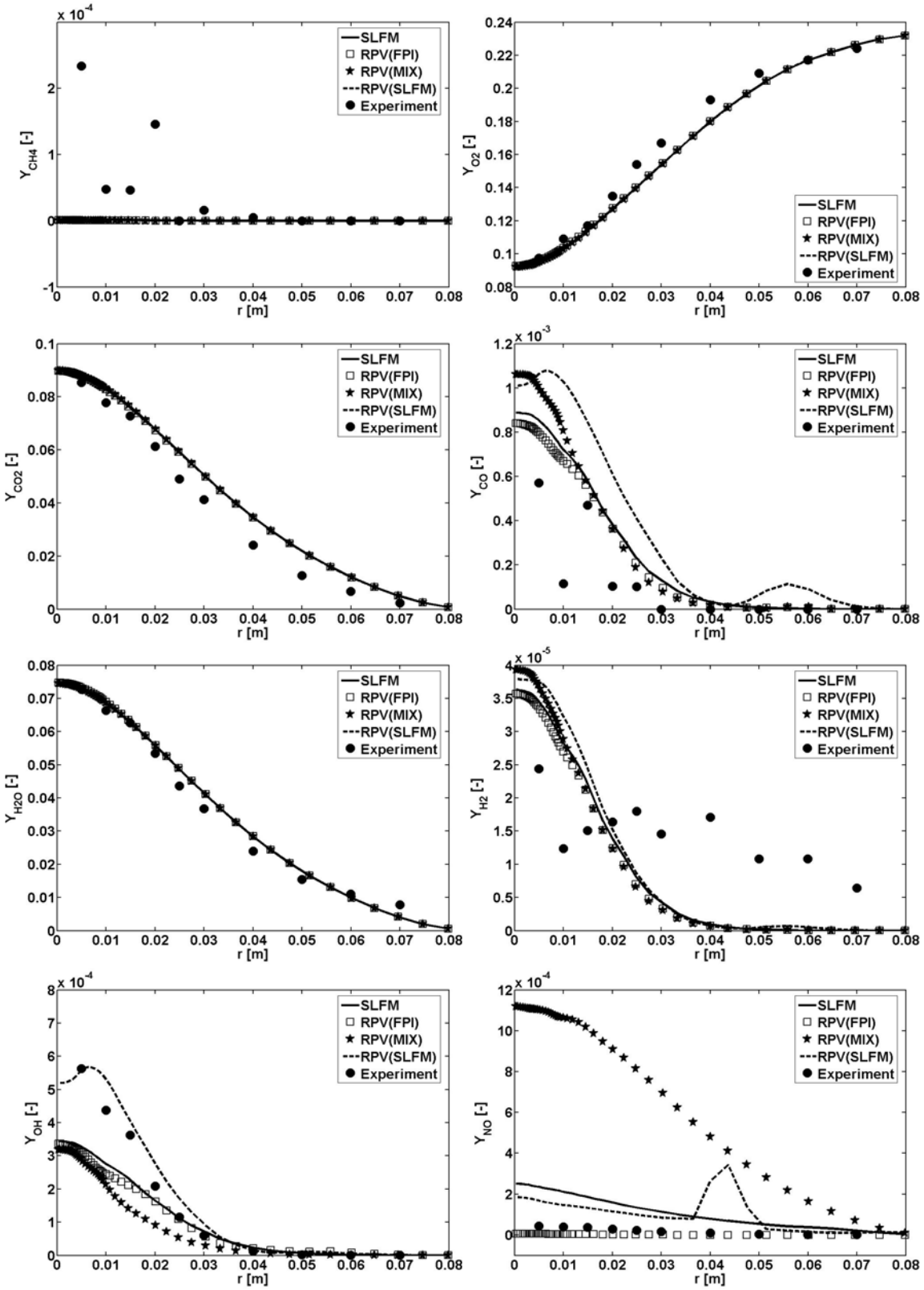

Slika 61 – Radijalni profili usrednjenih vrijednosti masenih udjela različitih kemijskih vrsta na poziciji x/d=60 (metanov plamen)

6 TECFLAM ložište

6.1 Eksperimentalna konfiguracija

TECFLAM ložište eksperimentalno je istraživano od više grupa znanstvenika. Iscrpna dokumentacija o ovom ložištu može se pronaći na [54]. Za simulaciju u ovome radu odabrana je konfiguracija S09c.

Prirodni plin korišten je kao gorivo u TECFLAM ložištu. Samo je ložište bilo vertikalni cilindar s gorionikom postavljenim na dnu u centru. Izlaz dimnih plinova je kroz prstenasti otvor na gornjem kraju. Izgled ložišta i dimenzije prikazani su na Sl. 62.

Gorionik se sastojao od ulaza goriva te vrtložnog ulaza zraka, a kako je shematski, zajedno s dimenzijama, prikazano na Sl. 63. Zrak je zavrtložen pokretnim lopaticama prije samog gorionika. Teoretski vrtložni broj zraka je bio $S = 0.9$. Ukupna toplinska moć goriva i zraka na ulazu u gorionik je bila oko 150 kW, dok je oko 80 kW odvedeno iz ložišta hlađenjem na zidove [55]. Ložište je radilo na okolišnjem tlaku, s ukupnim ekvivalentnim omjerom goriva i zraka 0.83. Prosječna brzina zraka na ulazu je bila 23 m/s ($\mathrm{Re} = 42900$), dok je prosječna brzina goriva (prirodni plin) bila 21 m/s ($\mathrm{Re} = 7900$).

Spontano Ramanovo raspršivanje je korišteno za simultano mjerenje temperature, masenog udjela smjese goriva te masenih udjela kemijskih vrsta (CH_4, N_2, O_2, H_2, CO, H_2O, CO_2) [144]. Svi su stadiji reakcije, od hladnog miješanja do ravnotežnog izgaranja, primijećeni u područjima miješanja goriva i zraka. Primijećene su dvije recirkulacijske zone (unutarnja i vanjska). LDV mjerenja brzine opisana su u [145].

Dodatne informacije o ovome ložištu te rezultati simulacija drugih grupa mogu se pronaći u TNF zbornicima na [29].

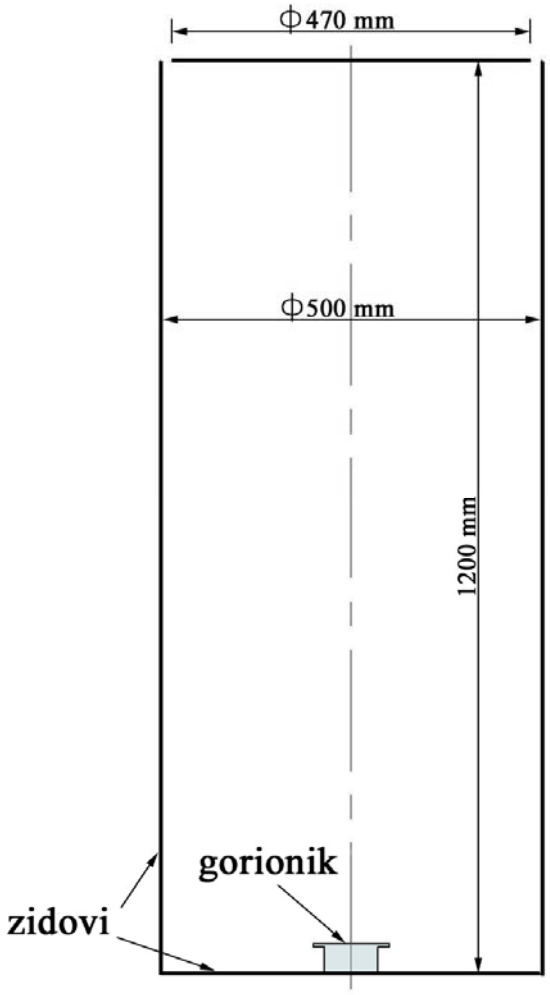

Slika 62 – Ložište (TECFLAM)

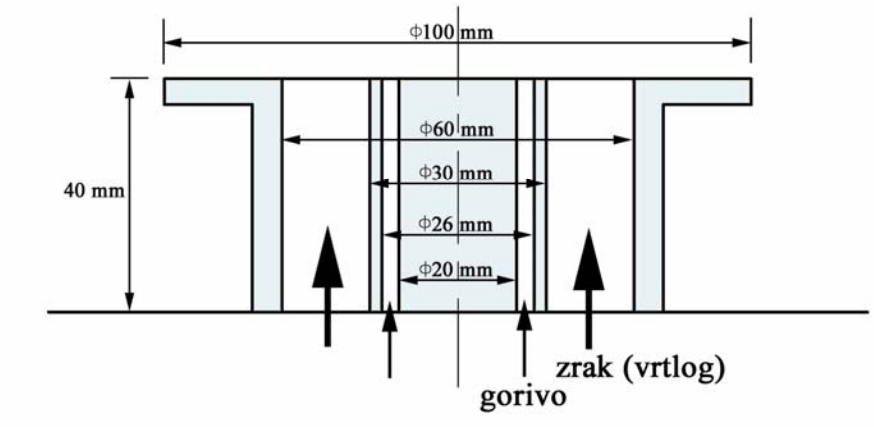

Slika 63 – Konfiguracija gorionika (TECFLAM)

6.2 Numerička konfiguracija

Za prostornu diskretizaciju korištena je mreža od 267864 kontrolnih volumena (heksahedroni). Mreža je bila gušća prema ulazima te na radijalnim pozicijama ulaza goriva i zraka (vidi Sl. 64). Dimenzije mreže su jednake dimenzijama domene na Sl. 62. Izlazni prsten je dodatno produžen, a da bi se izbjeglo natražno strujanje na toj rubnoj površini. Domena oko gorionika je prikazana na Sl. 64.

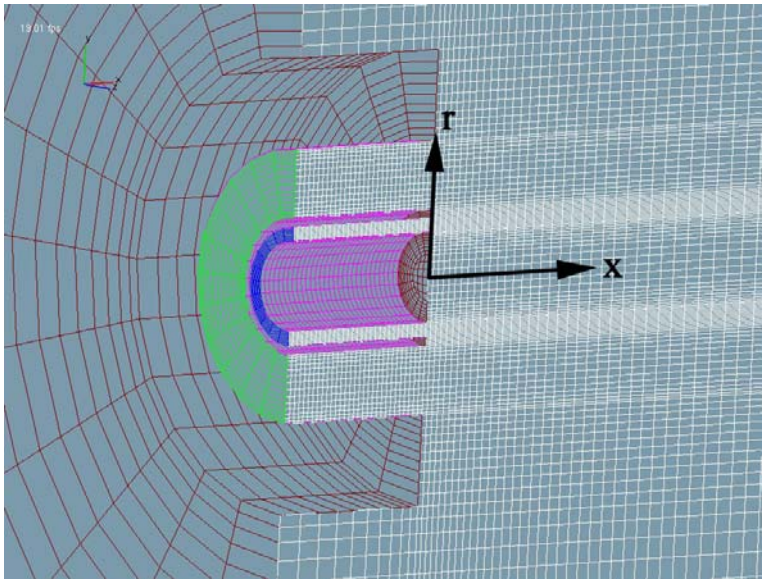

Slika 64 – Računalna mreža (TECFLAM; vertikalni aksijalni presjek uzduž osi)

Zadavanje rubnih uvjeta u ovom slučaju nije bilo jednostavno kao u slučajevima plamenova s vodikom ili metanom. Prstenovi ulaza goriva i zraka su dodatno izduženi (40 mm), a da bi se dobili razvijeni profili brzina na izlazu iz gorionika ($x = 0$ mm; Sl. 64). Ulazu zraka je dodatno zadana tangencijalna komponenta brzina na ulaznoj površini (označena zelenom bojom na Sl. 64) tako da se je na izlazu iz gorionika dobio nominalni vrtložni broj ($S = 0.9$). Prema definiciji vrtložnog broja prema jed. (141) (kao što je korišteno, npr., u [146-148]), te kada su se uzeli radijalni profili gustoće i brzina na aksijalnoj poziciji $x = 1$ mm, a uz $R = 0.03$ m, izračunat je vrtložni broj 0.9019. Slika 65 prikazuje profile komponenata brzina na izlazu iz gorionika ($x = -1$ mm).

$$S = \frac{\int_0^R \bar{\rho}\tilde{u}\tilde{w}r^2 dr}{R\int_0^R \bar{\rho}\tilde{u}^2 r dr} \tag{141}$$

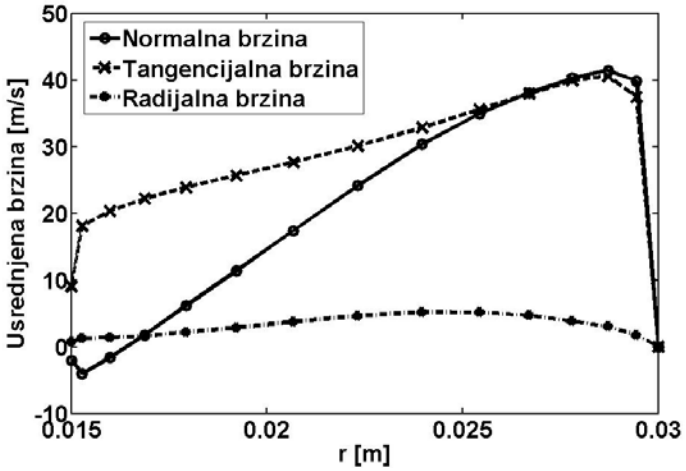

Slika 65 – Profili usrednjene brzine zraka na izlazu iz gorionika (TECFLAM)

Vrijednosti turbulentne kinetičke energije i njene disipacije na ulazu su zadane preko jed. (137). Intenzitet relativne slobodne turbulencije odabran je $I_\infty = 10\,\%$.

Kod neadijabatskih proračuna korišteni su DTRM s 48 zraka po rubnoj plohi te WSGGM [101] za modeliranje zračenja. Emisijski faktor zidova postavljen je na $\varepsilon_w = 0.7$, dok su temperature zidova odabrane tako da su toplinski gubici zbog zračenja otprilike iznosili 80 kW, a kako je izmjereno u eksperimentu [55]. Ulazne i izlazne površine su pretpostavljene kao crne površine.

Za modeliranje turbulencije koristili su se standardan k-ε model te HTM model [123]. Korištene su standardne vrijednosti konstanti u modelima turbulencije (vidi jed. (69)).

GRI Mech 3.0 [65] kemijski mehanizam korišten je kod proračuna kemijskih vrsta u pretprocesoru. Izgaranje je modelirano standardnim SLFM modelom te modelima RPV (FPI) i RPV (SLFM). Interakcija turbulencije i izgaranja postignuta je preko pretpostavljene β-PDF funkcije.

Ostali numerički postav je sličan postavu kod plamenova vodika ili metana.

6.3 Rezultati

6.3.1 Pretabulirani kemijski profili

Standardna SLFM baza, FPI baza te reparametrizirana SLFM baza plamenova prikazani su na Sl. 66-68. Originalna SLFM baza (Sl. 66) dobivena je za 10 parametara brzine skalarne disipacije kod stehiometrijskih uvjeta:

$$\chi_{st} = 0.01, 0.05, 0.1, 0.5, 1, 2, 5, 10, 20, 30\ s^{-1} \tag{142}$$

Prvi profil ($\chi_{st} = 0.01\ s^{-1}$) ima približno ravnotežni sastav, dok je posljednji profil ($\chi_{st} = 30\ s^{-1}$) onaj neposredno prije gašenja. Za prirodni plin odabran je sljedeći molni sastav: 95 % CH_4, 2.5 % C_2H_6, 1.5 % N_2 i 1 % CO_2. Temperature goriva i zraka su postavljene na 294 K. Varijabla masenog udjela smjese goriva je diskretizirana na 50 ne-ekvidistantnih točaka, s gušćom raspodjelom u blizini stehiometrijskog područja ($Z_{st} \approx 0.0581$).

Linearna kombinacija masenih udjela CO_2 i CO koristila se kao varijabla napretka reakcije, tj. $Y_c \equiv Y_{CO_2} + Y_{CO}$. Granice zapaljivosti približno su bile $0.385 \le \phi \le 2.949$[12]. Ukupno 30 setova predmiješanih plamenova je dobiveno upotrebom PREMIX rješavača [97] unutar granica zapaljivosti, dok se je preostalih 20 setova dobilo linearnom interpolacijom s rubnim vrijednostima. Zadržana je diskretizacija masenog udjela smjese goriva iz originalne SLFM baze.

Maksimalne vrijednosti masenih udjela kemijskih vrsta slične su između baza. Reparametrizirana SLFM baza (Sl. 68) konzistentna je s originalnom SLFM bazom (Sl. 66). Prikazane su samo one kemijske vrste za koje postoje eksperimentalna mjerenja.

[12] Odnosno, $0.02319 \le Z \le 0.15398$ – vidi jed. (24)

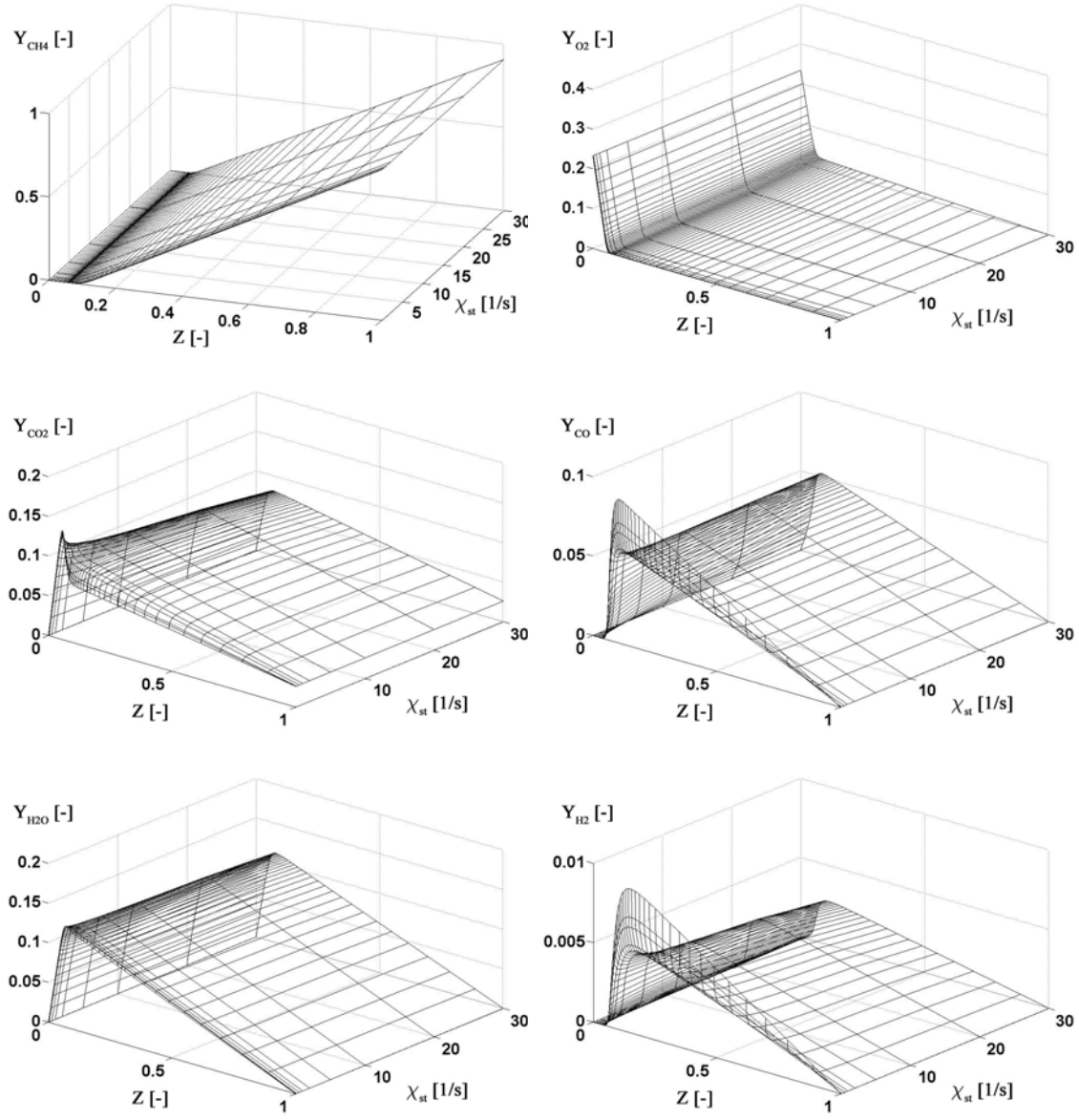

Slika 66 – SLFM (standardni) baza (TECFLAM)

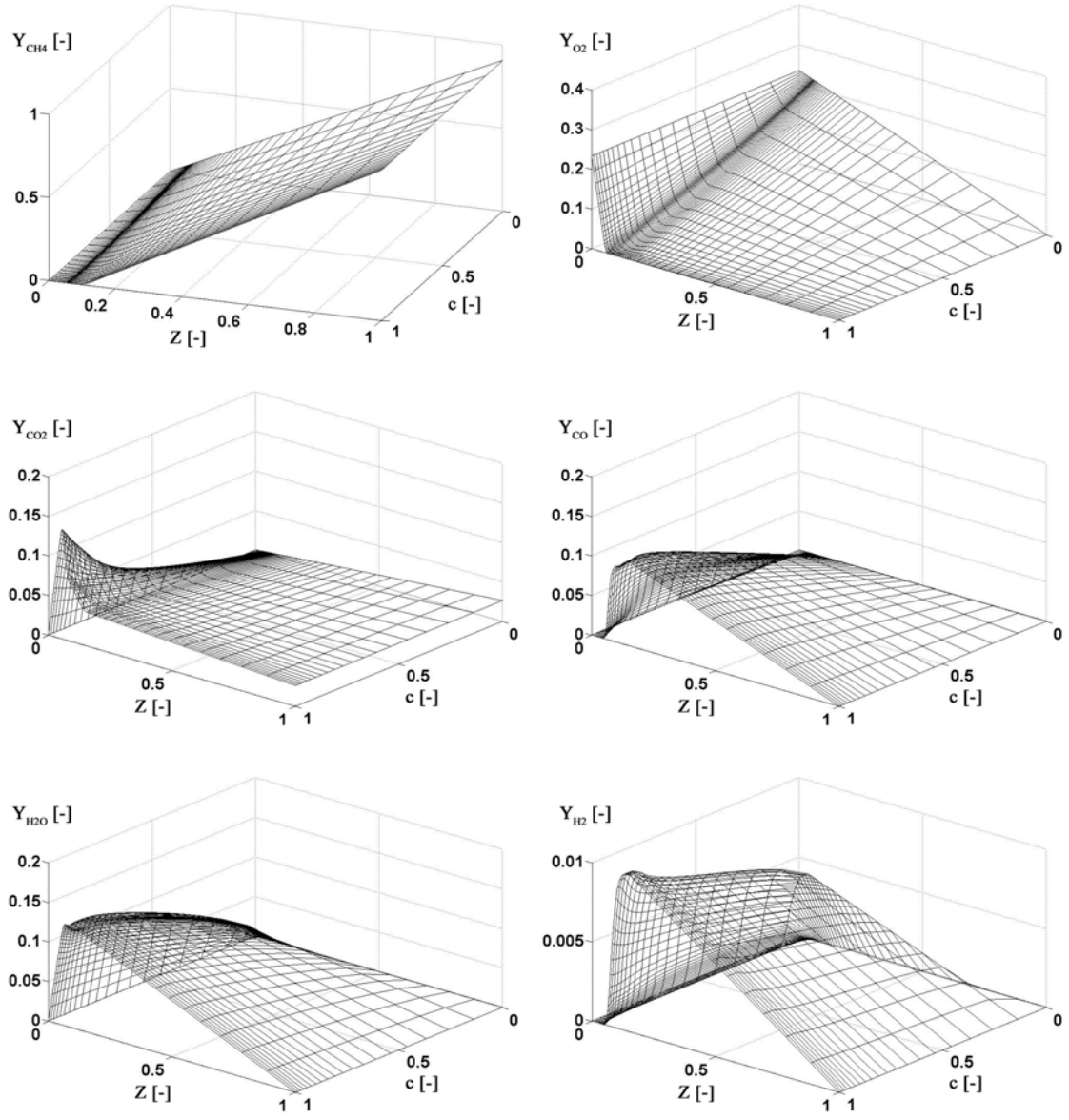

Slika 67 – FPI baza (TECFLAM)

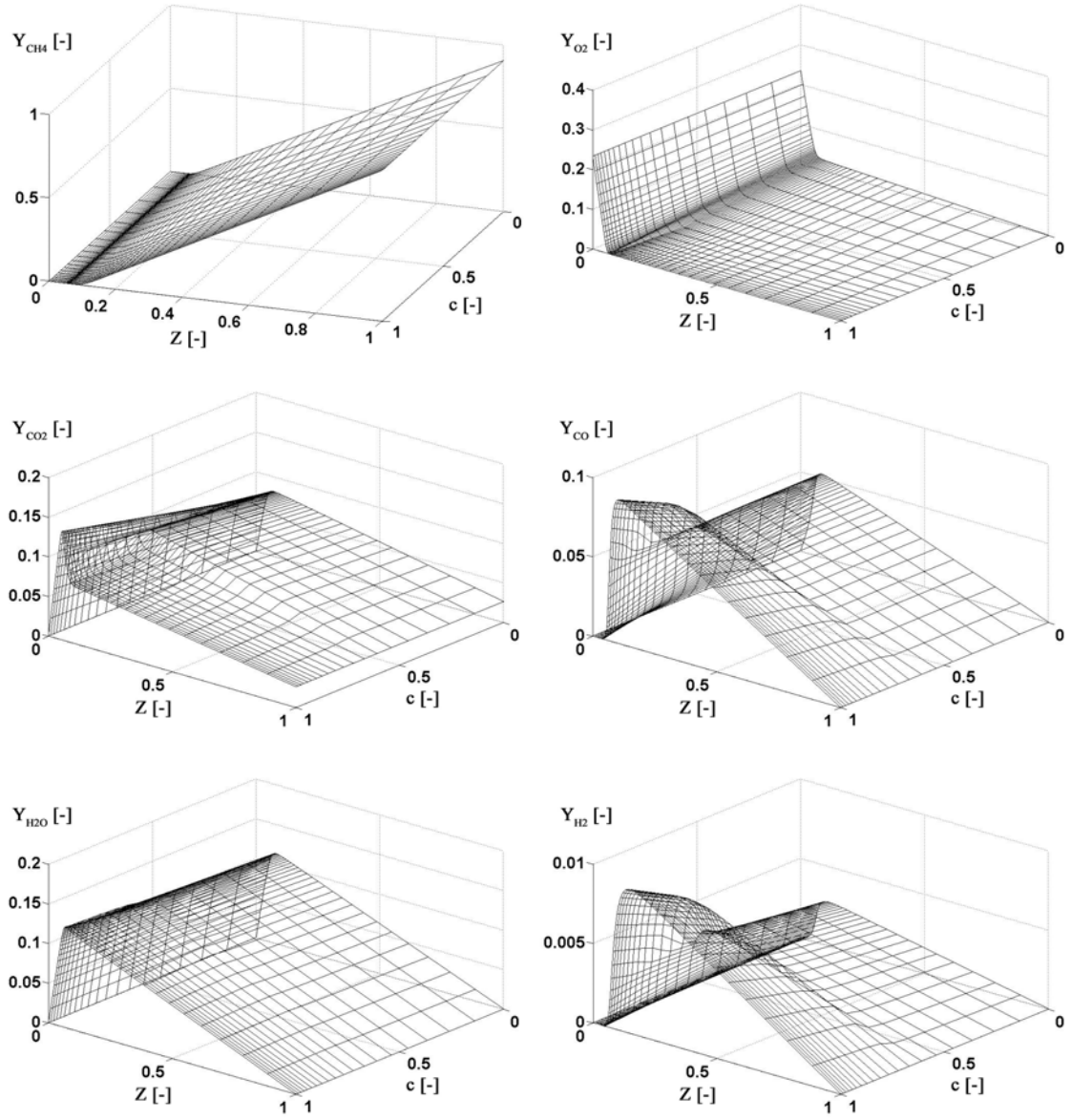

Slika 68 – SLFM (RPV) baza (TECFLAM)

6.3.2 Rezultati simulacije

Radijalni profili usrednjenih aksijalnih i tangencijalnih brzina na različitim aksijalnim pozicijama prikazani su na Sl. 69. Prikazani su rezultati dobiveni standardnim k-ε modelom te HTM modelom te su uspoređeni mjerenjima. Za izgaranje je korišten standardni SLFM model, dok je za zračenje korišten DTRM s 48 zraka po rubnoj plohi te WSGGM.

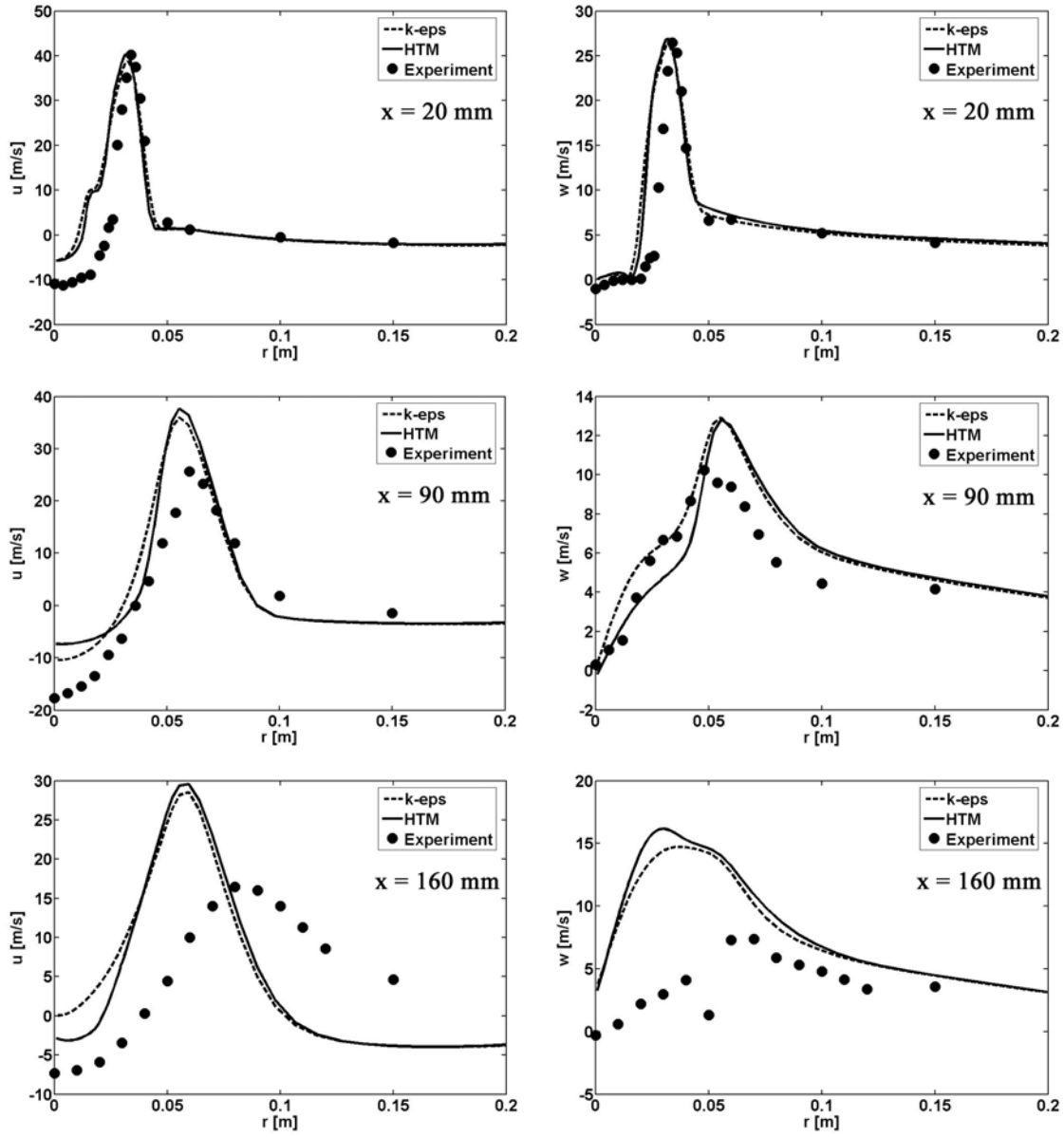

Slika 69 – Radijalni profili usrednjenih aksijalnih (u) i tangencijalnih (w) brzina na različitim aksijalnim pozicijama (TECFLAM)

Brzine se dobro slažu s mjerenjima, osobito u blizini gorionika ($x = 20$ mm), dok su slaganja lošija u udaljenijim pozicijama. Razlike između modela turbulencije su male na poziciji $x = 20$ mm, dok su razlike na druge dvije pozicije, $x = 90$ mm i $x = 160$ mm, veće, te bez naznake koji je od modela turbulencije bolji. Rezultati brzina su u skladu s ostalim rezultatima koji su objavljeni za TECFLAM ložište u TNF zbornicima na [29].

Radijalni profili momenata masenog udjela smjese goriva (usrednjena vrijednost i RMS) na aksijalnim pozicijama $x = 20$ mm i $x = 90$ mm prikazani su na Sl. 70. Dok su slaganja s mjerenjima prihvatljiva u područjima dalje od centralne osi, velika odstupanja su vidljiva u blizini centralne osi. HTM daje nešto bolje rezultate na poziciji $x = 20$ mm, dok k-ε model daje bolje rezultate na daljoj aksijalnoj poziciji ($x = 90$ mm). Slični trendovi su primijećeni kod aksijalnih profila usrednjenog masenog udjela smjese goriva, a kako je prikazano na Sl. 71. Razlike su manje na pozicijama dalje od gorionika.

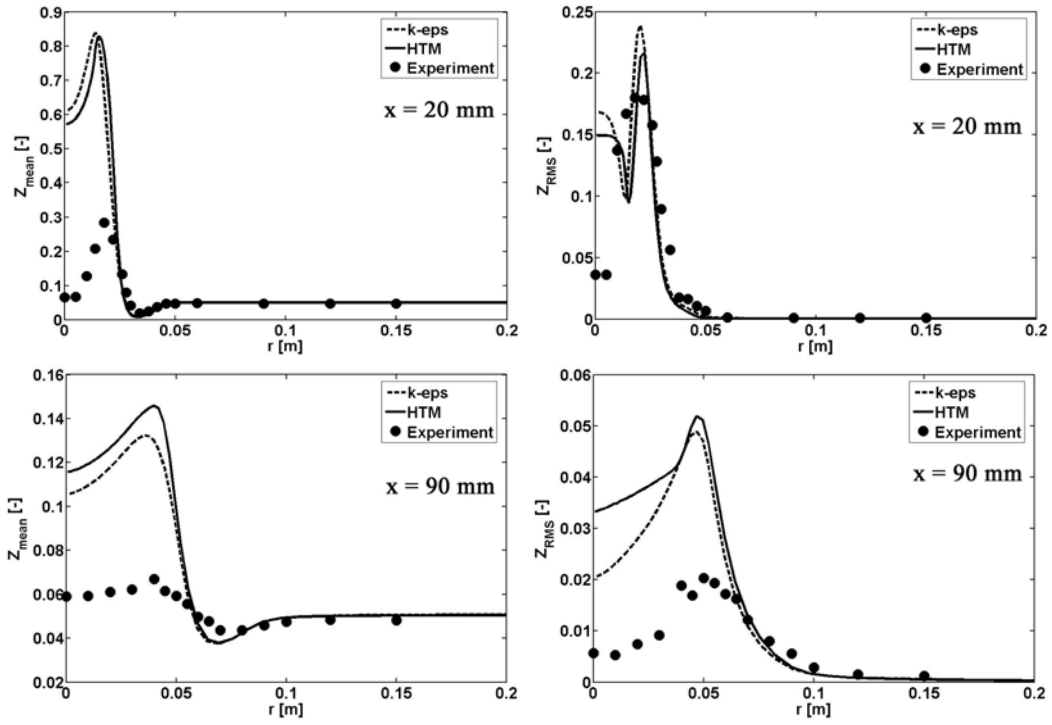

Slika 70 – Radijalni profili momenata masenog udjela smjese goriva na aksijalnim pozicijama x=20 mm i x=90 mm (TECFLAM)

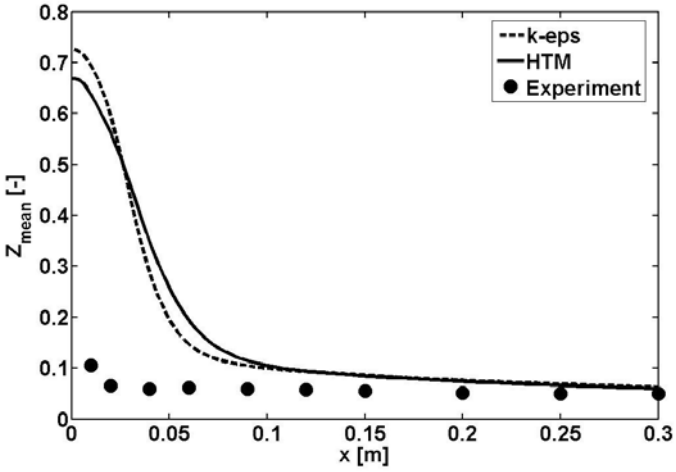

Slika 71 – Aksijalni profili (uzduž osi) usrednjenog masenog udjela goriva (TECFLAM)

Radijalni profili usrednjene temperature na aksijalnim pozicijama $x = 20$ mm i $x = 90$ mm prikazani su na Sl. 72. Slično kao i kod masenog udjela smjese goriva, rezultati u blizini centralne osi značajno odstupaju od mjerenja, dok su bolji rezultati postignuti dalje od osi. Rezultati temperature su bolje u blizini gorionika ($x = 20$ mm). HTM i k-ε modeli turbulencije daju slične rezultate.

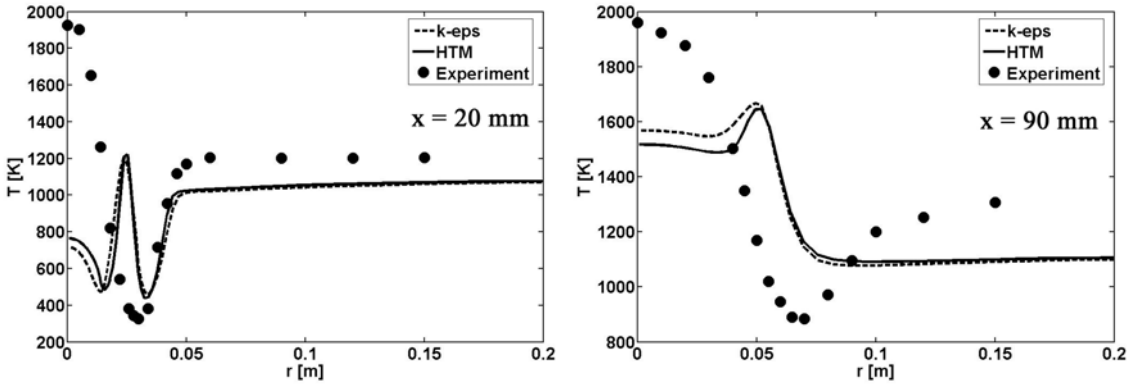

Slika 72 – Radijalni profili usrednjene temperature na aksijalnim pozicijama x=20 mm i x=90 mm (TECFLAM)

Bazirano na referentnom rješenju (k-ε, SLFM, DTRM, WSGGM), usrednjeni maseni udjeli kemijskih vrsta dobiveni su u postprocesoru, a prema modelima izgaranja RPV (FPI) i RPV (SLFM) (vidi Poglavlje 3.2.4). Slika 73 prikazuje radijalne profile normalizirane varijable napretka reakcije prema modelu RPV (FPI) (jed. (100)). Smjesa goriva i zraka je djelomično reagirala u području unutarnje recirkulacijske zone

($0 \le r \le 0.02$ m), a gdje manjak kisika nije dozvolio potpuno izgaranje. U području intenzivnog miješanja goriva i zraka ($0.02 \le r \le 0.04$ m) reakcija se odvija smanjenim intenzitetom, dok je smjesa potpuno kemijski reagirala u područjima dalje od centralne osi ($r > 0.05$ m).

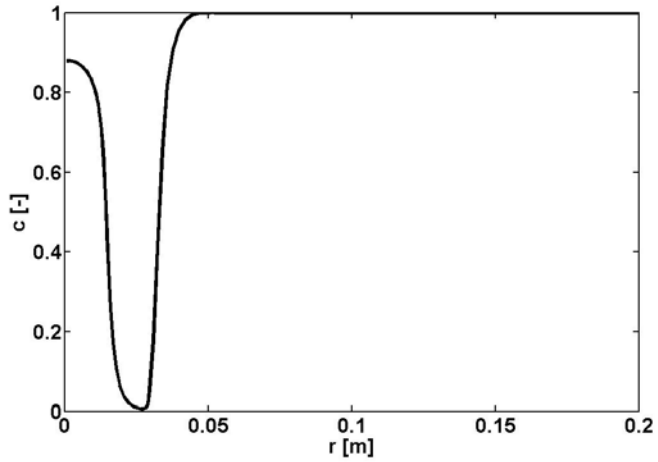

Slika 73 – Radijalni profil $\overline{c}$ (jed. (100); FPI) na aksijalnoj poziciji x=20 mm (TECFLAM)

Slike 74-76 prikazuju radijalne profile usrednjenih masnih udjela kemijskih vrsta na aksijalnim pozicijama $x = 20$ mm, $x = 60$ mm i $x = 120$ mm. Rezultati goriva (CH_4) su značajno veći od mjerenih vrijednosti na poziciji $x = 20$ mm u blizini centralne osi, dok su rezultati za O_2 dobri, pogotovo oni dobiveni modelom RPV (FPI). Međutim, rezultati pokazuju niže intenzitete reakcije u blizini osi, a kako se može zaključiti i iz niskih vrijednosti CO_2 i H_2O u tim područjima, nego što je to eksperimentalno potvrđeno. Sukladno tome, dobivene su veće vrijednosti CO i H_2 od mjerenih. Slično ponašanje, premda u manjoj mjeri, može se primijetiti i na drugim aksijalnim pozicijama – $x = 60$ mm i $x = 120$ mm. Dok su rezultati za O_2 svugdje dobri, vrijednosti CH_4, H_2 i CO su veće od mjerenih u blizini osi na svim aksijalnim pozicijama.

Općenito, rezultati simulacija se ne slažu tako dobro s mjerenjima, a kako je bio slučaj kod plamenova vodika i metana opisanih u prethodnim poglavljima. To je zbog složenijeg vrtložnog strujanja u slučaju TECFLAM ložišta. Također, zbog pojačane turbulencije do jačeg izražaja dolazi i modeliranje turbulentnih fluktuacija, a koje je dosta jednostavno u modelima primijenjenim u ovome radu te to djelomično utječe na lošije rezultate u slučaju TECFLAM ložišta. To se posebno može primijetiti kod loših radijalnih profila usrednjenog masenog udjela smjese goriva na poziciji $x = 20$ mm (Sl.

70), dok su rezultati brzina dobri na toj poziciji (Sl. 69). Dakle, relativno loši rezultati miješanja goriva i zraka u blizini centralne osi su razlog odstupanja i ostalih kemijskih vrsta u tim područjima. Također, čini se da RPV (FPI) model daje kvalitativno bolje radijalne profile u područjima bogatim smjesom goriva (u blizini osi) od SLFM ili RPV (SLFM) modela. To je najvjerojatnije zbog normalizirane varijable napretka reakcije u RPV (FPI) bazi, a koja pokriva cjelokupno područje od hladnog miješanja do ravnotežnog izgaranja.

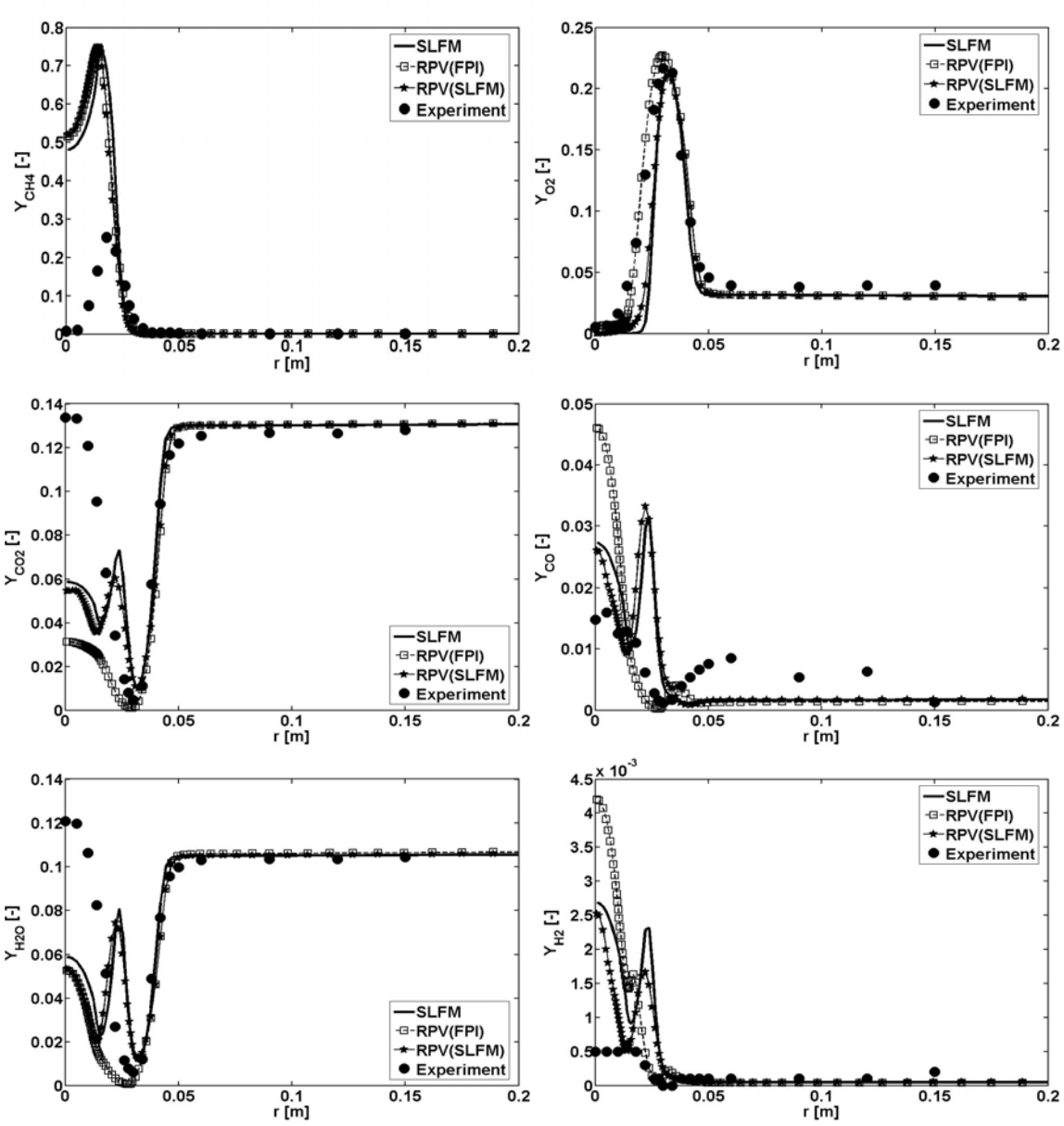

Slika 74 – Radijalni profili masenih udjela različitih kemijskih vrsta na aksijalnoj poziciji x=20 mm (TECFLAM)

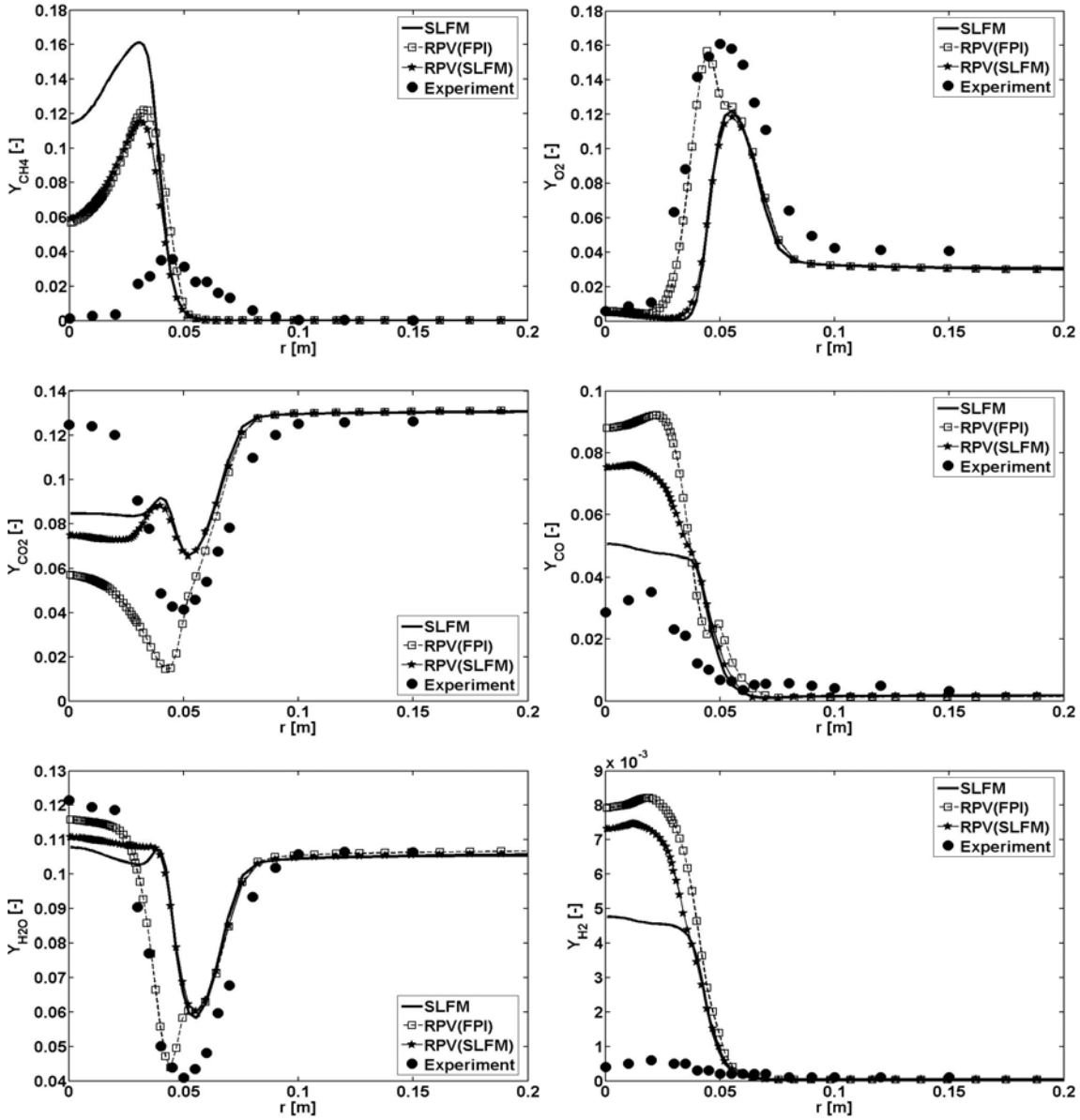

Slika 75 – Radijalni profili masenih udjela različitih kemijskih vrsta na aksijalnoj poziciji x=60 mm (TECFLAM)

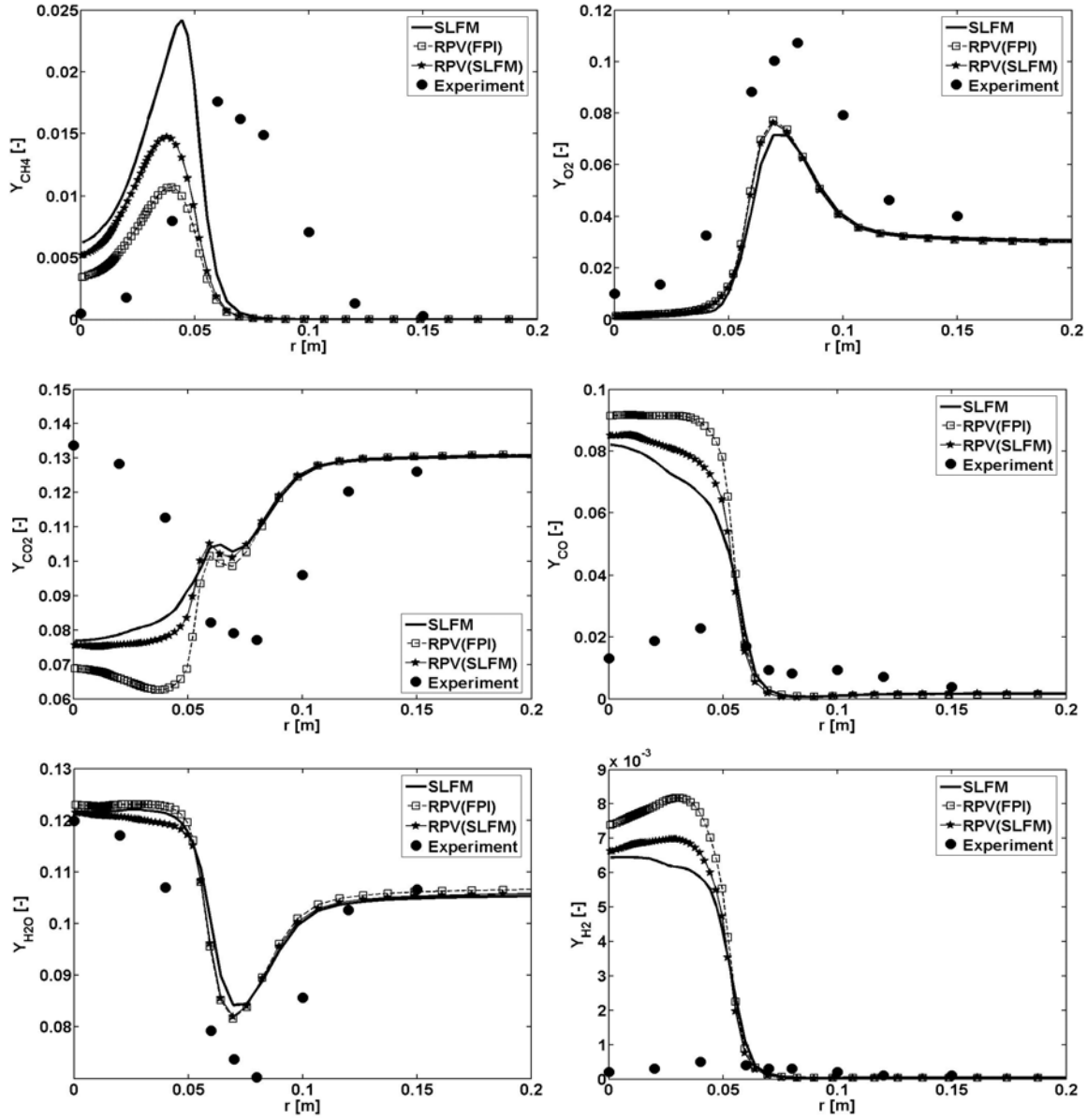

Slika 76 – Radijalni profili masenih udjela različitih kemijskih vrsta na aksijalnoj poziciji x=120 mm (TECFLAM)

7 Zaključak

Razvijen je i implementiran pristup tabeliranja kemijskih vrsta u pretprocesoru, a koji se bazira na upotrebi predmiješanih i nepredmiješanih plamenova. U tu svrhu je razvijen posebni računalni program (CSC rješavač). Modeliranje izgaranja tijekom CFD procedure se sastojalo od rješavanja transportnih jednadžbi za prateće skalare – maseni udio smjese goriva i varijablu napretka reakcije – dok su se maseni udjeli kemijskih vrsta funkcijski prikazali u zavisnosti od njih, ovisno o modelu. Razvijeni modeli izgaranja su se upotrijebili kod simulacija tri nepredmiješana plamena različitog stupnja složenosti. Rezultati simulacija su se usporedili s dostupnim eksperimentalnim mjerenjima te s rezultatima simulacije dobivenim upotrebom standardnog stacionarnog laminarnog *flamelet* modela. Simulirani su plamenovi bili sljedeći: slobodni mlazni plamen vodika i zraka (H_2/He-zrak plamen B), pilotirani slobodni mlazni plamen metana i zraka (Sandia plamen D) te zatvoreni vrtložni plamen prirodnog plina i zraka (TECFLAM ložište). U sva tri slučaja su upotrebljeni detaljni kemijski mehanizmi. Dodatno je implementirana metoda diskretnog prijenosa topline zračenjem u FIRE CFD program da bi se obuhvatili efekti zračenja. Hibridni model turbulencije (HTM) koristio se kod modeliranja turbulencije te su rezultati dobiveni tim modelom uspoređeni s rezultatima dobivenim standardnim k-ε modelom.

Plamen vodika i zraka uspješno je simuliran upotrebom modela izgaranja baziranih na tabeliranju kemijskih vrsta u pretprocesoru. Rezultati usrednjenih temperatura i glavnih kemijskih vrsta dobiveni različitim modelima međusobno su slični, te se dobro slažu s eksperimentalnim rezultatima. Značajnije razlike između modela izgaranja javljaju se kod simulacija manjih vrsta. U tom pogledu novi model izgaranja – RPV (FPI) – daje puno bolje NO rezultate od rezultata modela baziranih na upotrebi nepredmiješanih plamenova u pretprocesoru. Zbog problema se reparametrizacijom originalne SLFM baze plamenova, rezultate dobivene upotrebom RPV (SLFM) modela treba gledati s posebnim oprezom. Uključivanje modeliranja zračenja se pokazalo kao bitnim za dobivanje točnih rezultata usrednjenih temperatura. Poboljšanja zbog uključivanja modeliranja zračenja su posebno naglašena kod aksijalnih profila uzduž osi. Međutim, direktan utjecaj zračenja na stvaranje kemijskih vrsta u pretprocesoru je isključen te su maseni udjeli kemijskih

vrsta u pretprocesoru dobiveni pod pretpostavkom adijabatskih uvjeta. U tom pogledu je potrebno, a kao dio nekog budućeg rada, uključiti entalpijski gubitak kao dodatnu koordinatu prilikom tabeliranja kemijskih vrsta. HTM se je pokazao boljim od standardnog k-ε modela turbulencije u ovom slučaju. Premda se oba modela baziraju na jednostavnoj pretpostavci turbulentne viskoznosti, funkcijsko zadavanje strukturnog parametra C_μ te izračun turbulentne kinetičke energije iz izračunatih Reynoldsovih naprezanja kod HTM modela razlog je boljih rezultata turbulentnog miješanja dobivenih HTM modelom.

Zaključci za plamen metana i zraka (Sandia plamen D) su slični zaključcima plamena vodika i zraka. U ovome slučaju nije bilo poteškoća s odabirom varijable napretka reakcije, te je bila moguća konzistentna i potpuna reparametrizacija originalne SLFM baze plamenova. Uključivanje modeliranja prijenosa topline zračenjem rezultiralo je boljim rezultatima temperature i u ovom slučaju. Bolji rezultati toplinskih tokova zbog zračenja dobiveni su u slučaju korištenja većeg broja zraka po rubnoj plohi u modelu zračenja. Kao što je predloženo u drugim radovima, potrebno je uključiti i modeliranje spektralne ovisnosti faktora apsorpcije participirajućeg medija za postizanje još boljih rezultata prijenosa topline zračenjem. HTM se pokazao boljim od standardnog k-ε modela kod simulacije širenja plamena te je, sukladno tome, HTM model odabran za dobivanje referentnog rješenja kod usporedbe različitih modela izgaranja. Rezultati simulacije momenata masenog udjela smjese goriva su u dobrom slaganju s eksperimentalnim podacima, premda je slaganje manje dobro nego što je to bio slučaj kod plamena vodika i zraka. Složeniji prikaz kemijskih reakcija te povećani nivo turbulencije u slučaju plamena metana i zraka su najvjerojatniji razlog za relativno lošije rezultate simulacije nego u slučaju plamena vodika i zraka. Zbog povećanog nivoa turbulencije do većeg izražaja dolazi modeliranje turbulentnih fluktuacija, a koje ima veliki utjecaj na cjelokupnu točnost rezultata simulacije. Različiti modeli izgaranja – SLFM, RPV (FPI), RPV (SLFM) i RPV (MIX) – daju slične rezultate u slučaju velikih vrsta, poput CO_2 i H_2O. Veće razlike se pojavljuju kod simulacije manjih vrsta, poput CO i H_2, te u područjima bogatim smjesom goriva. Modeli bazirani na varijabli napretka reakcije daju veće vrijednosti masenih udjela CO i H_2 u područjima bogatim smjesom goriva te se slabije slažu s eksperimentalnim podacima nego standardni SLFM model.

Poboljšanja modela u tom pogledu ostaju kao prioritet nekog budućeg rada. Dok su rezultati simulacije za OH slični između modela, rezultati za NO su najbolji kod modela RPV (FPI), kao što je to bio slučaj i kod plamena vodika i zraka. U tom se pogledu čini da je model RPV (FPI) najpogodniji za simulaciju NO. Loši rezultati ravnotežnih NO profila nepredmiješanih plamenova su djelomično odgovorni za relativan uspjeh RPV (FPI) modela u slučaju NO-a.

TECFLAM ložište je simulirano posljednje. Ova je konfiguracija bila najsloženija te su dobiveni rezultati simulacije u najslabijem slaganju s eksperimentalnim podacima između simuliranih plamenova. Kompleksni prikaz kemijskih reakcija metana (GRI Mech 3.0), vrtložni ulaz zraka kod visokog Reynoldsovog broja te složena geometrija gorionika za to su glavni razlozi. Rezultati brzina u dobrom su slaganju s mjerenjima u blizini gorionika dok su odstupanja značajnija na područjima dalje od gorionika. HTM i k-ε rezultati su slični, bez evidentne prednosti jednog od modela turbulencije. Oba modela su bazirana na jednostavnoj pretpostavci turbulentne viskoznosti, a za koju je poznato da daje nedovoljno točne rezultate u simulacijama sa složenim tokovima, poput vrtloga, zakrivljenosti glavne strujnice, i sl. Očekuje se da bi upotreba modela turbulencije na razini drugih momenata donijela poboljšanje rezultata brzina. Rezultati simulacije momenata masenog udjela smjese goriva su relativno loši u blizini centralne osi, čak i u područjima gdje su rezultati brzine dobri. To navodi na zaključak da je gradijentna pretpostavka kod modeliranja tokova skalara zbog turbulentnih fluktuacija nedovoljno točna, što je osobito slučaj u tokovima s visokim Reynoldsovim brojevima, kao što je ovaj. Zbog netočnih rezultata simulacije momenata masenog udjela smjese goriva u blizini centralne osi, također su u tim područjima dobiveni i lošiji rezultati masenih udjela kemijskih vrsta. U tom se pogledu čini da bi se upotrebom LES-a u simulaciji ovog plamena dobio značajan napredak budući da bi se veći vrtlozi, a koji su odgovorni za miješanje goriva i oksidanta, direktno simulirali, dok bi pretpostavka β-PDF funkcije igrala manju ulogu. Različiti modeli izgaranja pokazali su se sličnima kod simulacije TECFLAM ložišta, premda se čini da RPV (FPI) model daje kvalitativno najbolje rezultate, barem što se tiče rezultata simulacije glavnih produkata izgaranja u blizini gorionika.

Općenito, nova procedura tabeliranja kemijskih vrsta u pretprocesoru, a bazirana na normaliziranoj varijabli napretka reakcije, pokazala se kao mogućom alternativom standardnom modelu stacionarnih laminarnih *flamelet*-a. U slučaju predmiješanih plamenova pokriveno je cjelokupno područje od hladnog miješanja do ravnotežnog izgaranja, a što čine modele izgaranja baziranim na tom konceptu univerzalnijima. NO je dobro simuliran u slučaju upotrebe predmiješanih plamenova, dok su se nepredmiješani plamenovi pokazali lošim izborom u ovom slučaju. Modeli bazirani na varijabli napretka reakcije pokazali su lošije rezultate u područjima bogatima smjesom goriva u slučaju plamena metana i zraka (Sandia plamen D), a što otvara prostor za daljnja unapređenja spomenutih modela. Uključivanje modeliranja prijenosa topline zračenjem pokazalo se važnim za točnost rezultata temperature, čak i u jednostavnim slučajevima slobodnih mlaznih plamenova. U tom pogledu dodatno se preporučuje upotreba entalpijskog gubitka kao dodatne koordinate kod tabeliranja kemijskih vrsta u pretprocesoru. HTM model turbulencije se, u generalnom slučaju, pokazao boljim od standardnog k-ε modela.

Prilog A – Korak-po-korak izvod *flamelet* jednadžbi

Početna točka u izvodu *flamelet* jednadžbi su transportne jednadžbe masenih udjela kemijskih vrsta i temperature u slabo konzervativnoj formi:

$$\rho\frac{\partial Y_k}{\partial t}+\rho u_j\frac{\partial Y_k}{\partial x_j}=\frac{\partial}{\partial x_j}\left(\rho D_k\frac{\partial Y_k}{\partial x_j}\right)+\dot{\omega}_k \tag{A.1}$$

$$\rho\frac{\partial T}{\partial t}+\rho u_j\frac{\partial T}{\partial x_j}=\frac{1}{c_p}\frac{\partial}{\partial x_j}\left(\rho c_p D\frac{\partial T}{\partial x_j}\right)+\frac{1}{c_p}\sum_{k=1}^{N_{spec}}\rho c_{pk}D_k\frac{\partial Y_k}{\partial x_j}\frac{\partial T}{\partial x_j}-\frac{1}{c_p}\sum_{k=1}^{N_{spec}}h_k\dot{\omega}_k+\frac{q_R}{c_p} \tag{A.2}$$

Slabo konzervativna forma transportne jednadžbe masenog udjela smjese goriva je:

$$\rho\frac{\partial Z}{\partial t}+\rho u_j\frac{\partial Z}{\partial x_j}=\frac{\partial}{\partial x_j}\left(\rho D_Z\frac{\partial Z}{\partial x_j}\right) \tag{A.3}$$

Pod pretpostavkom jediničnih Lewisovih brojeva, kemijske vrste i toplina jednako difundiraju, tj. $D_k=D_Z=D$. Ako se zanemare gradijenti reaktivnih skalara u tangencijalnim smjerovima na iso-plohe masenog udjela smjese goriva, pravila transformiranja za jed. (A.1) i (A.2) su:

$$\frac{\partial}{\partial t}=\frac{\partial}{\partial\tau}+\frac{\partial Z}{\partial t}\frac{\partial}{\partial Z}\qquad\qquad\frac{\partial}{\partial x_j}=\frac{\partial Z}{\partial x_j}\frac{\partial}{\partial Z} \tag{A.4}$$

Z je lokalna koordinata pozicionirana na fronti plamena koja gleda u smjeru gradijenta masenog udjela smjese goriva (vidi Sl. 2).

Maseni udjeli kemijskih vrsta

Nakon primjene pravila transformacije (jed. (A.4)) na jed. (A.1), u prvom koraku se dobiva:

$$\rho\left(\frac{\partial Y_k}{\partial \tau}+\frac{\partial Z}{\partial t}\frac{\partial Y_k}{\partial Z}\right)+\rho u_j\frac{\partial Z}{\partial x_j}\frac{\partial Y_k}{\partial Z}=\underbrace{\frac{\partial}{\partial x_j}\left(\rho D\frac{\partial Z}{\partial x_j}\frac{\partial Y_k}{\partial Z}\right)}_{\{1\}}+\dot{\omega}_k \tag{A.5}$$

$\{1\}$ se dalje razvija kao:

$$\begin{aligned}
&\frac{\partial}{\partial x_j}\left(\rho D\frac{\partial Z}{\partial x_j}\frac{\partial Y_k}{\partial Z}\right)=\frac{\partial(\rho D)}{\partial x_j}\frac{\partial Z}{\partial x_j}\frac{\partial Y_k}{\partial Z}+\rho D\frac{\partial}{\partial x_j}\left(\frac{\partial Z}{\partial x_j}\frac{\partial Y_k}{\partial Z}\right)\\
&=\frac{\partial(\rho D)}{\partial x_j}\frac{\partial Z}{\partial x_j}\frac{\partial Y_k}{\partial Z}+\rho D\left[\frac{\partial Y_k}{\partial Z}\frac{\partial^2 Z}{\partial x_j{}^2}+\frac{\partial Z}{\partial x_j}\frac{\partial^2 Y_k}{\partial Z^2}\frac{\partial Z}{\partial x_j}\right]\\
&=\frac{\partial(\rho D)}{\partial x_j}\frac{\partial Z}{\partial x_j}\frac{\partial Y_k}{\partial Z}+\underbrace{\rho D\frac{\partial Y_k}{\partial Z}\frac{\partial^2 Z}{\partial x_j{}^2}}_{\{1'\}}+\rho D\left(\frac{\partial Z}{\partial x_j}\right)^2\frac{\partial^2 Y_k}{\partial Z^2}
\end{aligned} \tag{A.6}$$

$\{1'\}$ se može zapisati kao:

$$\rho D\frac{\partial Y_k}{\partial Z}\frac{\partial^2 Z}{\partial x_j{}^2}=\frac{\partial Y_k}{\partial Z}\frac{\partial}{\partial x_j}\left(\rho D\frac{\partial Z}{\partial x_j}\right)-\frac{\partial Y_k}{\partial Z}\frac{\partial Z}{\partial x_j}\frac{\partial(\rho D)}{\partial x_j} \tag{A.7}$$

Nakon uvrštavanja jed. (A.7) u jed. (A.6) dobiva se:

$$\frac{\partial}{\partial x_j}\left(\rho D\frac{\partial Z}{\partial x_j}\frac{\partial Y_k}{\partial Z}\right)=\frac{\partial Y_k}{\partial Z}\frac{\partial}{\partial x_j}\left(\rho D\frac{\partial Z}{\partial x_j}\right)+\rho D\left(\frac{\partial Z}{\partial x_j}\right)^2\frac{\partial^2 Y_k}{\partial Z^2} \tag{A.8}$$

Konačno, nakon uvrštavanja jed. (A.8) nazad u jed. (A.5) dobiva se:

$$\rho\frac{\partial Y_k}{\partial \tau}+\frac{\partial Y_k}{\partial Z}\underbrace{\left[\rho\frac{\partial Z}{\partial t}+\rho u_j\frac{\partial Z}{\partial x_j}-\frac{\partial}{\partial x_j}\left(\rho D\frac{\partial Z}{\partial x_j}\right)\right]}_{\{2\}}=\rho D\left(\frac{\partial Z}{\partial x_j}\right)^2\frac{\partial^2 Y_k}{\partial Z^2}+\dot{\omega}_k \tag{A.9}$$

$\{2\}$ nestaje zbog jed. (A.3). Prvi član na desnoj strani jed. (A.9) može se napisati pomoću jed. (33). Konačna se forma *flamelet* jednadžbi za masene udjele kemijskih vrsta ($k = 1, \ldots, N_{spec}$) dobiva kao:

$$\rho \frac{\partial Y_k}{\partial \tau} = \rho \frac{\chi}{2} \frac{\partial^2 Y_k}{\partial Z^2} + \dot{\omega}_k \tag{A.10}$$

Temperatura

Ako se krene od jed. (A.2), te nakon upotrebe pravila transformacije prema jed. (A.4), dobiva se:

$$\begin{aligned}&\rho\left(\frac{\partial T}{\partial \tau}+\frac{\partial T}{\partial Z}\frac{\partial Z}{\partial t}\right)+\rho u_j\frac{\partial T}{\partial Z}\frac{\partial Z}{\partial x_j}\\&=\underbrace{\frac{1}{c_p}\frac{\partial}{\partial x_j}\left(\rho c_p D\frac{\partial T}{\partial Z}\frac{\partial Z}{\partial x_j}\right)}_{\{1\}}+\underbrace{\frac{1}{c_p}\sum_{i=1}^{N_{spec}}\rho c_{pi}D\frac{\partial Y_i}{\partial Z}\frac{\partial Z}{\partial x_j}\frac{\partial T}{\partial Z}\frac{\partial Z}{\partial x_j}}_{\{2\}}-\frac{1}{c_p}\sum_{i=1}^{N_{spec}}h_i\dot{\omega}_i+\frac{q_R}{c_p}\end{aligned}\tag{A.11}$$

Nakon uvrštavanja jed. (33) gdje je to potrebno, $\{1\}$ postaje:

$$\begin{aligned}&\frac{1}{c_p}\frac{\partial}{\partial x_j}\left(\rho c_p D\frac{\partial T}{\partial Z}\frac{\partial Z}{\partial x_j}\right)=\frac{1}{c_p}\frac{\partial T}{\partial Z}\frac{\partial Z}{\partial x_j}\frac{\partial\left(\rho c_p D\right)}{\partial x_j}+\rho D\frac{\partial}{\partial x_j}\left(\frac{\partial T}{\partial Z}\frac{\partial Z}{\partial x_j}\right)\\&=\frac{\partial T}{\partial Z}\frac{\partial Z}{\partial x_j}\frac{\partial\left(\rho D\right)}{\partial x_j}+\frac{\rho D}{c_p}\frac{\partial T}{\partial Z}\frac{\partial Z}{\partial x_j}\frac{\partial c_p}{\partial Z}\frac{\partial Z}{\partial x_j}+\rho D\frac{\partial T}{\partial Z}\frac{\partial^2 Z}{\partial x_j{}^2}+\rho D\frac{\partial Z}{\partial x_j}\frac{\partial^2 T}{\partial Z^2}\frac{\partial Z}{\partial x_j}\\&=\frac{\partial T}{\partial Z}\frac{\partial Z}{\partial x_j}\frac{\partial\left(\rho D\right)}{\partial x_j}+\frac{\rho D}{c_p}\frac{\partial T}{\partial Z}\left(\frac{\partial Z}{\partial x_j}\right)^2\frac{\partial c_p}{\partial Z}+\rho D\frac{\partial T}{\partial Z}\frac{\partial^2 Z}{\partial x_j{}^2}+\rho D\left(\frac{\partial Z}{\partial x_j}\right)^2\frac{\partial^2 T}{\partial Z^2}\\&=\frac{\partial T}{\partial Z}\frac{\partial Z}{\partial x_j}\frac{\partial\left(\rho D\right)}{\partial x_j}+\frac{\rho\chi}{2c_p}\frac{\partial T}{\partial Z}\frac{\partial c_p}{\partial Z}+\underbrace{\rho D\frac{\partial T}{\partial Z}\frac{\partial^2 Z}{\partial x_j{}^2}}_{\{1'\}}+\rho\frac{\chi}{2}\frac{\partial^2 T}{\partial Z^2}\end{aligned}\tag{A.12}$$

$\{1'\}$ se može zapisati:

$$\rho D\frac{\partial T}{\partial Z}\frac{\partial^2 Z}{\partial x_j{}^2}=\frac{\partial T}{\partial Z}\frac{\partial}{\partial x_j}\left(\rho D\frac{\partial Z}{\partial x_j}\right)-\frac{\partial T}{\partial Z}\frac{\partial Z}{\partial x_j}\frac{\partial\left(\rho D\right)}{\partial x_j}\tag{A.13}$$

$\{1\}$ konačno postaje:

$$\frac{1}{c_p}\frac{\partial}{\partial x_j}\left(\rho c_p D\frac{\partial T}{\partial Z}\frac{\partial Z}{\partial x_j}\right)=\frac{\rho\chi}{2c_p}\frac{\partial T}{\partial Z}\frac{\partial c_p}{\partial Z}+\frac{\partial T}{\partial Z}\frac{\partial}{\partial x_j}\left(\rho D\frac{\partial Z}{\partial x_j}\right)+\rho\frac{\chi}{2}\frac{\partial^2 T}{\partial Z^2}\tag{A.14}$$

Uvrštavanjem jed. (33) u $\{2\}$ dobivamo:

$$\frac{1}{c_p}\sum_{i=1}^{N_{spec}}\rho c_{pi}D\frac{\partial Y_i}{\partial Z}\frac{\partial Z}{\partial x_j}\frac{\partial T}{\partial Z}\frac{\partial Z}{\partial x_j}=\sum_{i=1}^{N_{spec}}\rho\frac{\chi}{2}\frac{c_{pi}}{c_p}\frac{\partial Y_i}{\partial Z}\frac{\partial T}{\partial Z}\tag{A.15}$$

Ubacivanjem jed. (A.14) i (A.15) nazad u jed. (A.11) dobiva se:

$$\rho\frac{\partial T}{\partial \tau}+\frac{\partial T}{\partial Z}\underbrace{\left[\rho\frac{\partial Z}{\partial t}+\rho u_j\frac{\partial Z}{\partial x_j}-\frac{\partial}{\partial x_j}\left(\rho D\frac{\partial Z}{\partial x_j}\right)\right]}_{\{3\}} = \frac{\rho\chi}{2c_p}\frac{\partial T}{\partial Z}\frac{\partial c_p}{\partial Z}+\rho\frac{\chi}{2}\frac{\partial^2 T}{\partial Z^2}+\sum_{i=1}^{N_{spec}}\rho\frac{\chi}{2}\frac{c_{pi}}{c_p}\frac{\partial Y_i}{\partial Z}\frac{\partial T}{\partial Z}-\frac{1}{c_p}\sum_{i=1}^{N_{spec}}h_i\dot{\omega}_i+\frac{q_R}{c_p} \tag{A.16}$$

Član $\{3\}$ nestaje zbog jed. (A.3). Konačni se oblik *flamelet* jednadžbe za temperaturu dobiva kao:

$$\rho\frac{\partial T}{\partial \tau}=\frac{\rho\chi}{2c_p}\frac{\partial T}{\partial Z}\frac{\partial c_p}{\partial Z}+\rho\frac{\chi}{2}\frac{\partial^2 T}{\partial Z^2}+\sum_{i=1}^{N_{spec}}\rho\frac{\chi}{2}\frac{c_{pi}}{c_p}\frac{\partial Y_i}{\partial Z}\frac{\partial T}{\partial Z}-\frac{1}{c_p}\sum_{i=1}^{N_{spec}}h_i\dot{\omega}_i+\frac{q_R}{c_p} \tag{A.17}$$

Prilog B – *Flamelet* model s diferencijalnom difuzijom

Formulacija laminarnog *flamelet* modela koja uzima u obzir diferencijalnu molekularnu difuziju, a prema [34], je implementirana kao dodatna opcija u CSC rješavaču [96]. Lewisovi brojevi su konstantni za svaku od kemijskih vrsta, no ne moraju imati jedinične vrijednosti te mogu biti proizvoljno odabrani. Sukladno tome, originalna formulacija prema [34] preoblikovana je tako da je pogodna za implementaciju u CSC rješavaču, a kao što će biti opisano. Više detalja o samom modelu može se pronaći u originalnoj referenci [34].

U skraćenom se obliku *flamelet* model može zapisati kao:

$$\frac{\partial \phi_i}{\partial \tau} + A_1^{(i)} \frac{\partial^2 \phi_i}{\partial Z^2} + A_2^{(i)} \frac{\partial \phi_i}{\partial Z} + A_3^{(i)} \phi_i + A_4^{(i)} = 0 \qquad i = 1, 2, \ldots, N_{spec} + 1 \tag{B.1}$$

U jed. (B.1) je $\phi_i \equiv Y_i$ ako je $i \le N_{spec}$ te je $\phi_i \equiv T$ ako je $i = N_{spec} + 1$. Koeficijenti $A_1^{(i)} \ldots A_4^{(i)}$ u slučaju jednadžbi kemijskih vrsta (tj. za $i \le N_{spec}$) su:

$$A_1^{(i)} = -\frac{\chi}{2} \frac{\mathrm{Le}_Z}{\mathrm{Le}_i} \tag{B.2}$$

$$A_2^{(i)} = \frac{\mathrm{Le}_Z \chi}{2} \sum_{k=1}^{N_{spec}} \left[\frac{1}{\mathrm{Le}_k} \left(\frac{Y_k}{M} \frac{\partial M}{\partial Z} + \frac{\partial Y_k}{\partial Z} \right) \right] - \frac{1}{2} \frac{\mathrm{Le}_Z}{\mathrm{Le}_i} \frac{\partial M}{\partial Z} \frac{\chi}{M} - \frac{1}{4\rho} \left\{ \left(\frac{\mathrm{Le}_Z}{\mathrm{Le}_i} - 1 \right) \left[\frac{\partial (\rho \chi)}{\partial Z} + \frac{\rho \chi c_p}{\lambda} \frac{\partial}{\partial Z} \left(\frac{\lambda}{c_p} \right) \right] \right\} \tag{B.3}$$

$$A_3^{(i)} = \frac{\mathrm{Le}_Z \chi}{2} \sum_{k=1}^{N_{spec}} \left[\frac{1}{\mathrm{Le}_k} \left(\frac{\partial^2 Y_k}{\partial Z^2} + \frac{Y_k}{M} \frac{\partial^2 M}{\partial Z^2} \right) \right] - \frac{\mathrm{Le}_Z}{\mathrm{Le}_i} \left\{ \frac{\chi}{2M} \frac{\partial^2 M}{\partial Z^2} + \frac{1}{4\rho} \frac{\partial M}{\partial Z} \left[\frac{\partial}{\partial Z} \left(\frac{\rho\chi}{M} \right) + \frac{\rho\chi c_p}{\lambda} \frac{\partial}{\partial Z} \left(\frac{\lambda}{c_p M} \right) \right] \right\} + \frac{\mathrm{Le}_Z}{4\rho} \sum_{k=1}^{N_{spec}} \left\{ \frac{1}{\mathrm{Le}_k} \left[\begin{array}{l} \dfrac{\partial Y_k}{\partial Z} \left(\dfrac{\partial (\rho\chi)}{\partial Z} + \dfrac{\rho\chi c_p}{\lambda} \dfrac{\partial}{\partial Z} \left(\dfrac{\lambda}{c_p} \right) \right) + \\ \dfrac{\partial M}{\partial Z} \left(\dfrac{\partial}{\partial Z} \left(\dfrac{\rho\chi Y_k}{M} \right) + \dfrac{\rho\chi c_p}{\lambda} \dfrac{\partial}{\partial Z} \left(\dfrac{\lambda}{c_p} \dfrac{Y_k}{M} \right) \right) \end{array} \right] \right\} \tag{B.4}$$

$$A_4^{(i)} = -\frac{\dot{\omega}_i}{\rho} \tag{B.5}$$

Koeficijenti $A_1^{(i)} \ldots A_4^{(i)}$ u slučaju jednadžbe temperature (tj. za $i = N_{spec} + 1$) su:

$$A_1^{(i)} = -\frac{\mathrm{Le}_Z \chi}{2} \tag{B.6}$$

$$A_2^{(i)} = \frac{\mathrm{Le}_Z \chi}{2} \sum_{k=1}^{N_{spec}} \left[\frac{1}{\mathrm{Le}_k} \left(\frac{Y_k}{M} \frac{\partial M}{\partial Z} + \frac{\partial Y_k}{\partial Z} \right) \left(1 - \frac{c_{pk}}{c_p} \right) \right] - \frac{1}{4\rho} \left\{ (\mathrm{Le}_Z - 1) \left[\frac{\partial (\rho\chi)}{\partial Z} + \frac{\rho\chi c_p}{\lambda} \frac{\partial}{\partial Z} \left(\frac{\lambda}{c_p} \right) \right] \right\} - \frac{\mathrm{Le}_Z \chi}{2c_p} \frac{\partial c_p}{\partial Z} \tag{B.7}$$

$$A_3^{(i)} = 0 \tag{B.8}$$

$$A_4^{(i)} = \frac{1}{\rho c_p} \left(\sum_{k=1}^{N_{spec}} h_k \dot{\omega}_k - q_R \right) \tag{B.9}$$

Lewisov broj za maseni udio smjese goriva Le_Z, a prema jed. (29), definiran je kao:

$$\mathrm{Le}_Z = \frac{\lambda}{\rho c_p D_Z} \tag{B.10}$$

Koeficijent provođenja topline λ računa se upotrebom datoteka iz programa [149].

Slično kao i u Poglavlju 3.1.2.1, metoda konačnih razlika prema jed. (106) i (107), te oznake udaljenosti među susjednim točkama mreže prema jed. (108), korištene su i kod

diskretizacije jed. (B.1). Nakon provedene diskretizacije dobiven je slijedeći sustav diferencijalno-algebarskih jednadžbi:

$$\left(\frac{\partial \phi_i}{\partial \tau}\right)_{(k)} = C_1^{(k)}(i)\,\phi_i^{(k-1)} + C_2^{(k)}(i)\,\phi_i^{(k)} + C_3^{(k)}(i)\,\phi_i^{(k+1)} + C_4^{(k)}(i) \tag{B.11}$$

Koeficijenti $C_1^{(k)} \ldots C_4^{(k)}$ su:

$$C_1^{(k)}(i) = \frac{A_2^{(i)}(k)\,\Delta_{(k)}^{+}}{\left(\Delta_{(k)}^{-} + \Delta_{(k)}^{+}\right)\Delta_{(k)}^{-}} - \frac{A_1^{(i)}(k)}{0.5\left(\Delta_{(k)}^{-} + \Delta_{(k)}^{+}\right)\Delta_{(k)}^{-}} \tag{B.12}$$

$$C_2^{(k)}(i) = \frac{A_1^{(i)}(k)}{0.5\Delta_{(k)}^{-}\Delta_{(k)}^{+}} - \frac{A_2^{(i)}(k)\left(\Delta_{(k)}^{+} - \Delta_{(k)}^{-}\right)}{\Delta_{(k)}^{-}\Delta_{(k)}^{+}} - A_3^{(i)}(k) \tag{B.13}$$

$$C_3^{(k)}(i) = -\frac{A_1^{(i)}(k)}{0.5\left(\Delta_{(k)}^{-} + \Delta_{(k)}^{+}\right)\Delta_{(k)}^{+}} - \frac{A_2^{(i)}(k)\,\Delta_{(k)}^{-}}{\left(\Delta_{(k)}^{-} + \Delta_{(k)}^{+}\right)\Delta_{(k)}^{+}} \tag{B.14}$$

$$C_4^{(k)}(i) = -A_4^{(i)}(k) \tag{B.15}$$

Diskretizirane jednadžbe prema jed. (B.11) su direktno primjenjive u DDASSL rješavaču [129]. Prve i druge derivacije koje se pojavljuju u koeficijentima $A_1^{(i)} \ldots A_4^{(i)}$ aproksimiraju se metodom središnjih razlika, slično kao i kod jed. (115) i (116).

Prilog C – Stacionarni laminarni 1D predmiješani plamen

PREMIX program [97] koristio se u ovome radu kod proračuna slobodno propagirajućih 1D predmiješanih plamenova (Poglavlje 2.3.6.1). Taj program se temelji na upotrebi metode konačnih razlika za dobivanje rješenja sljedećeg sustava jednadžbi:

$$\dot{m} = \rho u A \tag{C.1}$$

$$\dot{m}\frac{dY_k}{dx} + \frac{d}{dx}\left(\rho A Y_k V_k\right) - A\dot{\omega}_k = 0 \tag{C.2}$$

$$\dot{m}\frac{dT}{dx} - \frac{1}{c_p}\frac{d}{dx}\left(\lambda A\frac{dT}{dx}\right) + \frac{A}{c_p}\sum_{k=1}^{N_{spec}}\rho Y_k V_k c_{pk}\frac{dT}{dx} + \frac{A}{c_p}\sum_{k=1}^{N_{spec}} h_k\dot{\omega}_k = 0 \tag{C.3}$$

CHEMKIN II datoteke [98] korištene su za proračune termodinamičkih svojstava medija, dok su transportna svojstva medija (koeficijent provođenja topline) dobivene upotrebom datoteka iz [149]. Dakle, uz zadane rubne uvjete, stacionarna rješenja gornjeg sustava jednadžbi sadrže profile masenih udjela kemijskih vrsta i temperature od stanja reaktanata do potpuno izgorenog stanja, a u funkcijskoj zavisnosti od prostorne koordinate x te ekvivalentnog omjera reaktanata ϕ:

$$\begin{aligned} Y_k &= Y_k\left(x,\phi\right) \\ T &= T\left(x,\phi\right) \end{aligned} \tag{C.4}$$

Više informacija od numeričkim tehnikama, algoritmu rješavanja, i dr., korištenih u PREMIX programu može se pronaći u originalnoj referenci [97].

Popis literature

[1] L. D. Smoot, *A Decade of Combustion Research*, Prog. Energy Combust. Sci., 23 (1997), pp. 203-232.

[2] R. W. Bilger, *The future for energy from the combustion of fossil fuels*, Proc. 5th Intl. Conference on Technologies and Combustion for a Clean Environment, Lisbon, 1999.

[3] R. W. Bilger, *Future progress in turbulent combustion research*, Prog. Energy Combust. Sci., 26 (2000), pp. 367-380.

[4] J. M. Beér, *Combustion technology developments in power generation in response to environmental challenges*, Prog. Energy Combust. Sci., 26 (2000), pp. 301-327.

[5] J. Ferziger and M. Perić, *Computational Methods for Fluid Dynamics*, Springer Verlag, 1999.

[6] S. V. Patankar, *Numerical Heat Transfer and Fluid Flow*, Hemisphere Publishing Corporation, Washington, 1980.

[7] A. D. Gosman, *Development and current status of industrial thermofluids CFD analysis*, ICHMT International Symposium on Advances in Computational Heat Transfer, CHT-04-K2, 2004.

[8] N. Duić, *Contribution to the Mathematical Modelling of Gaseous Fuel Combustion in a Steam Generator Furnace*, PhD thesis (in Croatian), Power Engineering Department, University of Zagreb, Zagreb, 1998.

[9] N. Duić, *Trodimenzionalni matematički model procesa u ložištu generatora pare*, Master thesis (in Croatian), Power Engineering Department, University of Zagreb, Zagreb, 1993.

[10] Ž. Bogdan and N. Duić, *The mathematical model of the steam generator combustion chamber*, Proc. 24th Symposium KoREMA, Zagreb, 1992.

[11] Ž. Bogdan and N. Duić, *Three-dimensional simulation of the combustion process in an oil-fired furnace*, Proc. of the 15th International Conference Information Technology Interfaces '93, Pula, 1993.

[12] Ž. Bogdan, N. Duić and D. R. Schneider, *Three-dimensional simulation of the performance of an oil-fired combustion chamber*, Proc. 2nd European Thermal Sciences & 14th UIT National Heat Transfer Conference, Rome, 1996.

[13] K. N. C. Bray, *The challenge of turbulent combustion*, Proc. 26th Symposium (International) on Combustion, The Combustion Institute, 1996.

[14] S. B. Pope, *Computations of turbulent combustion: progress and challenges*, Proc. 23rd Symposium (International) on Combustion, The Combustion Institute, 1990.

[15] N. Peters, *Turbulent Combustion*, Cambridge University Press, Cambridge, 2000.

[16] D. Veynante and L. Vervisch, *Turbulent combustion modeling*, Prog. Energy Combust. Sci., 28 (2002), pp. 193-266.

[17] J. O. Hinze, *Turbulence*, McGraw-Hill, New York, 1975.

[18] S. B. Pope, *Turbulent Flows*, Cambridge University Press, Cambridge, 2000.

[19] H. Tennekes and J. L. Lumley, *A First Course in Turbulence*, MIT Press, Cambridge, MA, 1972.

[20] T. Poinsot and D. Veynante, *Theoretical and Numerical Combustion*, R.T. Edwards, Inc., Philadelphia, 2001.

[21] P. Givi, *Model free simulations of turbulent reactive flows*, Prog. Energy Combust. Sci., 15 (1989), pp. 1-107.

[22] O. Reynolds, *On the dynamical theory of incompressible viscous flows and the determination of the criterion*, Philos. Trans. R. Soc. London Ser. A, 186 (1894), pp. 123-161.

[23] D. C. Wilcox, *Turbulence modeling for CFD*, DCW Industries, Inc., La Cañada, California, 1993.

[24] P. Bradshaw, *Understanding and prediction of turbulent flow - 1996*, Int. J. Heat and Fluid Flow, 18 (1997), pp. 45-54.

[25] P. R. Spalart, *Strategies for turbulence modelling and simulations*, Int. J. Heat and Fluid Flow, 21 (2000), pp. 252-263.

[26] N. Peters, *Laminar diffusion flamelet models in non-premixed turbulent combustion*, Prog. Energy Combust. Sci., 10 (1984), pp. 319-339.

[27] A. Y. Klimenko and R. W. Bilger, *Conditional moment closure for turbulent combustion*, Prog. Energy Combust. Sci., 25 (1999), pp. 595-687.

[28] S. B. Pope, *Pdf method for turbulent reactive flows*, Prog. Energy Combust. Sci., 11 (1985), pp. 119-195.

[29] http://www.ca.sandia.gov/TNF/abstract.html.

[30] P. J. Coelho, O. J. Teerling and D. Roekaerts, *Spectral radiative effects and turbulence/radiation interaction in a non-luminous turbulent jet diffusion flame*, Combust. Flame, 133 (2003), pp. 75-91.

[31] R. Hilbert, F. Tap, H. El-Rabii and D. Thévenin, *Impact of detailed chemistry and transport models on turbulent combustion simulations*, Prog. Energy Combust. Sci., 30 (2004), pp. 61-117.

[32] V. Nilsen and G. Kosály, *Differential Diffusion in Turbulent Reacting Flows*, Combust. Flame, 117 (1999), pp. 493-513.

[33] R. Hilbert and D. Thévenin, *Influence of differential diffusion on maximum flame temperature in turbulent nonpremixed hydrogen/air flames*, Combust. Flame, 138 (2004), pp. 175-187.

[34] H. Pitsch and N. Peters, *A Consistent Flamelet Formulation for Non-Premixed Combustion Considering Differential Diffusion Effects*, Combust. Flame, 114 (1998), pp. 26-40.

[35] H. Pitsch, *Unsteady Flamelet Modeling of Differential Diffusion in Turbulent Jet Diffusion Flames*, Combust. Flame, 123 (2000), pp. 358-374.

[36] B. Wegner, A. Sadiki and J. Janicka, *Prediction of Flow and Combustion in Generic Gas Turbine Combustor Using Large Eddy Simulation*, Proc. 2nd International Workshop on TRENDS IN NUMERICAL AND PHYSICAL MODELLING OF TURBULENT PROCESSES IN GAS TURBINE COMBUSTORS (AND AUTOMOTIVE ENGINES), Heidelberg, Germany, 2004.

[37] L. Davidson and S. Dahlström, *Hybrid LES-RANS: An approach to make LES applicable at high Reynolds number*, ICHMT International Symposium on Advances in Computational Heat Transfer, CHT-04-K1, 2004.

[38] S. Menon, Modeling and Computational Constraints for LES of Turbulent Reacting Flows, CCL Report 2004-017, Computational Combustion Laboratory, School of Aerospace Engineering, Georgia Institute of Technology, 2004.

[39] A. Sadiki and J. Janicka, *Unsteady methods (URANS and LES) for simulation of combustion systems*, ICHMT International Symposium on Advances in Computational Heat Transfer, CHT-04-K3, 2004.

[40] R. S. Barlow and J. H. Frank, *Effects of turbulence on species mass fractions in methane/air jet flames*, Proc. 27th Symposium (International) on Combustion, The Combustion Institute, 1998.

[41] H. Pitsch, Extended flamelet model for LES of non-premixed combustion, Annual Research Briefs 2000, Center for Turbulence Research, 2000.

[42] H. Pitsch and H. Steiner, *Large-eddy simulation of a turbulent piloted methane/air diffusion flame (Sandia flame D)*, Phys. Fluids, 12 (2000), pp. 2541-2554.

[43] H. Pitsch and H. Steiner, Large-eddy simulation of a turbulent piloted methane/air flame (Sandia flame D), Annual Research Briefs 1999, Center for Turbulence Research, 1999.

[44] H. Pitsch and H. Steiner, *Scalar mixing and dissipation rate in large-eddy simulations of non-premixed turbulent combustion*, Proc. 28th Symposium (International) on Combustion, The Combustion Institute, 2000.

[45] S. Navarro-Martinez and A. Kronenburg, *Conditional Moment Closure Modelling in Large Eddy Simulation*, Proc. 2nd International Workshop on TRENDS IN NUMERICAL AND PHYSICAL MODELLING OF TURBULENT PROCESSES IN GAS TURBINE COMBUSTORS (AND AUTOMOTIVE ENGINES), Heidelberg, Germany, 2004.

[46] P. Domingo, L. Vervisch and K. N. C. Bray, *Partially premixed flamelets in LES of nonpremixed turbulent combustion*, Combust. Theory Modelling, 6 (2002), pp. 529-551.

[47] L. Vervisch, R. Hauguel, P. Domingo and M. Rullaud, *Three facets of turbulent combustion modelling: DNS of premixed V-flame, LES of lifted nonpremixed flame and RANS of jet-flame*, J. of Turbulence, 5 (2004), pp. 1-36.

[48] O. Colin, F. Ducros, D. Veynante and T. Poinsot, *A thickened flame model for large eddy simulations of turbulent premixed combustion*, Phys. Fluids, 12 (2000), pp. 1843-1863.

[49] R. Knikker, D. Veynante and C. Meneveau, *A priori testing of a similarity model for large eddy simulations of turbulent premixed combustion*, Proc. 29th Symposium (International) on Combustion, 2002.

[50] S. Subramaniam and S. B. Pope, *A Mixing Model for Turbulent Reactive Flows based on Euclidean Minimum Spanning Trees*, Combust. Flame, 115 (1998), pp. 487-514.

[51] Z. Ren and S. B. Pope, *An investigation of the performance of turbulent mixing models*, Combust. Flame, 136 (2004), pp. 208-216.

[52] S. Subramaniam and S. B. Pope, *Comparison of Mixing Model Performance for Nonpremixed Turbulent Reactive Flow*, Combust. Flame, 117 (1999), pp. 732-754.

[53] J. Xu and S. B. Pope, *PDF Calculations of Turbulent Nonpremixed Flames with Local Extinction*, Combust. Flame, 123 (2000), pp. 281-307.

[54] http://www.tu-darmstadt.de/fb/mb/ekt/tecflam/.

[55] A. Hinz, *Numerische Simulation turbulenter Methandiffusionsflammen mittels Monte Carlo PDF Methoden*, PhD thesis, Technische Universität Darmstadt, Darmstadt, 2000.

[56] S. B. Pope, *Computationally efficient implementation of combustion chemistry using in situ adaptive tabulation*, Combust. Theory Modelling, 1 (1997), pp. 41-63.

[57] M. A. Singer and S. B. Pope, *Exploiting ISAT to solve the reaction-diffusion equation*, Combust. Theory Modelling, 8 (2004), pp. 361-383.

[58] V. Saxena and S. B. Pope, *PDF Simulations of Turbulent Combustion Incorporating Detailed Chemistry*, Combust. Flame, 117 (1999), pp. 340-350.

[59] K. Liu, S. B. Pope and D. A. Caughey, *Calculations of bluff-body stabilized flames using a joint probability density function model with detailed chemistry*, Combust. Flame, Article in press (2005), pp. 1-29.

[60] A. Mura and R. Borghi, *Introducing a new partial PDF approach for turbulent combustion modeling*, Combust. Flame, 136 (2004), pp. 377-382.

[61] M. Fairweather and R. M. Woolley, *First-order conditional moment closure modeling of turbulent, nonpremixed hydrogen flames*, Combust. Flame, 133 (2003), pp. 393-405.

[62] M. Fairweather and R. M. Woolley, *First-order conditional moment closure modeling of turbulent, nonpremixed methane flames*, Combust. Flame, 138 (2004), pp. 3-19.

[63] M. R. Roomina and R. W. Bilger, *Conditional Moment Closure (CMC) Predictions of a Turbulent Methane-Air Jet Flame*, Combust. Flame, 125 (2001), pp. 1176-1195.

[64] C. B. Devaud and K. N. C. Bray, *Assessment of the applicability of conditional moment closure to a lifted turbulent flame: first order model*, Combust. Flame, 132 (2003), pp. 102-114.

[65] http://www.me.berkeley.edu/gri_mech/.

[66] S. H. Kim and K. Y. Huh, *Second-order conditional moment closure modeling of turbulent piloted jet diffusion flames*, Combust. Flame, 138 (2004), pp. 336-352.

[67] N. Peters, *Laminar flamelet concepts in turbulent combustion*, Proc. 21st Symposium (International) on Combustion, The Combustion Institute, Pittsburgh, 1986.

[68] N. Swaminathan and R. W. Bilger, *Assessment of Combustion Submodels for Turbulent Nonpremixed Hydrocarbon Flames*, Combust. Flame, 116 (1998), pp. 519-545.

[69] N. Peters, *Comment and Reply on the "Assessment of Combustion Submodels for Turbulent Nonpremixed Hydrocarbon Flames"*, Combust. Flame, 116 (1999), pp. 675-676.

[70] N. Swaminathan, *Flamelet Regime in Non-premixed Combustion*, Combust. Flame, 129 (2002), pp. 217-219.

[71] P. J. Coelho and N. Peters, *Unsteady Modelling of a Piloted Methane/Air Jet Flame Based on the Eulerian Particle Flamelet Model*, Combust. Flame, 124 (2001), pp. 444-465.

[72] P. J. Coelho and N. Peters, *Numerical Simulation of a Mild Combustion Burner*, Combust. Flame, 124 (2001), pp. 503-518.

[73] O. Gicquel, N. Darabiha and D. Thévenin, *Laminar premixed hydrogen/air counterflow flame simulations using flame prolongation of ILDM with differential diffusion*, Proc. 28th Symposium (International) on Combustion, The Combustion Institute, 2000.

[74] J. A. van Oijen, F. A. Lammers and L. P. H. de Goey, *Modeling of Complex Premixed Burner Systems by Using Flamelet-Generated Manifolds*, Combust. Flame, 127 (2001), pp. 2124-2134.

[75] B. Fiorina, R. Baron, O. Gicquel, D. Thévenin, S. Carpentier and N. Darabiha, *Modelling non-adiabatic partially premixed flames using flame-prolongation ILDM*, Combust. Theory Modelling, 7 (2003), pp. 449-470.

[76] B. Fiorina, O. Gicquel, L. Vervisch, S. Carpentier and N. Darabiha, *Approximating the chemical structure of partially premixed and diffusion counterflow flames using FPI flamelet tabulation*, Combust. Flame, 140 (2005), pp. 147-160.

[77] G. Ribert, M. Champion, O. Gicquel, N. Darabiha and D. Veynante, *Modeling nonadiabatic turbulent premixed reactive flows including tabulated chemistry*, Combust. Flame, Article in press (2005), pp. 1-10.

[78] G. Ribert, O. Gicquel and N. Darabiha, *Flame Prolongation of ILDM kinetics reduction technique applied to kerosene reaction mechanism*, Proc. European Combustion Meeting, 2003.

[79] C. D. Pierce, *Progress-variable approach for large-eddy simulation of turbulent combustion*, PhD thesis, Department of Mechanical Engineering, Stanford University, 2001.

[80] H. C. Hottel and A. F. Sarofim, *Radiative Transfer*, McGraw-Hill, New York, 1967.

[81] J. R. Howell, *Application of Monte Carlo to Heat Transfer Problems*, Advances in Heat Transfer, 5 (1968).

[82] B. G. Carlson and K. D. Lathrop, *Transport Theory - The Method of Discrete Ordinates*, Computing Methods in Reactor Physics (1968).

[83] W. A. Fiveland, *Discrete-Ordinates Solutions of the Radiative Transport Equation for Rectangular Enclosures*, J. Heat Transfer, 106 (1984), pp. 699-706.

[84] G. D. Raithby and E. H. Chui, *A Finite Volume Method for Predicting Radiant Heat Transfer in Enclosures with Participating Media*, J. Heat Transfer, 112 (1990), pp. 415-423.

[85] F. C. Lockwood and N. G. Shah, *A New Radiation Solution for Incorporation in General Combustion Prediction Procedures*, Proc. 18th Symposium (International) on Combustion, The Combustion Institute, 1981.

[86] B. R. Adams and P. J. Smith, *Three-dimensional Discrete-ordinates Modeling of Radiative Transfer in a Geometrically Complex Furnace*, Combust. Sci. and Tech., 88 (1993), pp. 293-308.

[87] M. Baburić, A. Raulot, P. J. Coelho and N. Duić, *Application of the Conservative Discrete Transfer Radiation Method to a Furnace With Complex Geometry*, ICHMT International Symposium on Advances in Computational Heat Transfer, CHT-04-168, 2004.

[88] M. Y. Kim, S. W. Baek and J. H. Park, *Unstructured Finite-Volume Method for Radiative Heat Transfer in a Complex Two-Dimensional Geometry with Obstacles*, Numerical Heat Transfer, Part B, 39 (2001), pp. 617-635.

[89] Ž. Bogdan, D. R. Schneider and N. Duić, *Prediction of the thermal radiation heat transfer in a furnace by Monte Carlo zone method*, Proc. of the 16th International Conference Information Technology Interfaces '94, Pula, 1994.

[90] D. R. Schneider, *Modeliranje prijenosa topline zračenjem u ložištu primjenom Monte Carlo metode*, Master thesis (in Croatian), Power Engineering Department, University of Zagreb, Zagreb, 1997.

[91] W. L. Grosshandler, RADCAL: A Narrow-Band Model for Radiation Calculations in a Combustion Environment, 1993.

[92] R. S. Barlow, A. N. Karpetis, J. H. Frank and J.-Y. Chen, *Scalar Profiles of NO Formation in Laminar Opposed-Flow Partially Premixed Methane/Air Flames*, Combust. Flame, 127 (2001), pp. 2102-2118.

[93] P. J. Coelho, *Detailed numerical simulation of radiative transfer in a nonluminous turbulent jet diffusion flame*, Combust. Flame, 136 (2004), pp. 481-492.

[94] L. Wang, D. C. Haworth, S. R. Turns and M. F. Modest, *Interactions among soot, thermal radiation, and NOx emissions in oxygen-enriched turbulent nonpremixed flames: a computational fluid dynamics modeling study*, Combust. Flame, Article in press (2005), pp. 1-10.

[95] X. L. Zhu and J. P. Gore, *Radiation effects on combustion and pollutant emissions of high-pressure opposed flow methane/air diffusion flames*, Combust. Flame, Article in press (2005), pp. 1-13.

[96] http://powerlab.fsb.hr/mbaburic/CSC.htm.

[97] R. J. Kee, J. F. Grcar, M. Smooke and J. A. Miller, PREMIX: A Fortran program for modelling steady laminar one-dimensional flames, SAND85-8240, Sandia National Laboratories, 1985.

[98] R. J. Kee, F. M. Rupley and J. A. Miller, Chemkin-II: A Fortran Chemical Kinetics Package for the Analysis of Gas-Phase Chemical Kinetics, SAND89-8009, Sandia National Laboratories, 1989.

[99] AVL AST, FIRE manual v8.1.1, AVL List GmbH, 2003.

[100] P. J. Coelho and M. G. Carvalho, *A Conservative Formulation of Discrete Transfer Method*, ASME Journal of Heat Transfer, 119 (1997), pp. 118-128.

[101] P. J. Smith, Z. F. Shen and J. N. Friedman, *Evaluation of Coefficients for the Weighted Sum of Gray Gases Model*, J. Heat Transfer, 104 (1982).

[102] M. Baburić, A. Raulot and N. Duić, *Implementation of discrete transfer radiation method into SWIFT computational fluid dynamics code*, Thermal Science, 8 (2004), pp. 19-28.

[103] R. S. Barlow, *Sandia H2/He Flame Data - Release 2.0, http://www.ca.sandia.gov/TNF*, Sandia National Laboratories, 2003.

[104] R. S. Barlow and C. D. Carter, *Raman/Rayleigh/LIF measurements of nitric oxide formation in turbulent hydrogen jet flames*, Combust. Flame, 97 (1994), pp. 261-280.

[105] I. Alfirević, *Uvod u tenzore i mehaniku kontinuuma*, Golden marketing, Zagreb, 2003.

[106] D. A. Anderson, J. C. Tannehill and R. H. Pletcher, *Computational Fluid Mechanics and Heat Transfer*, Hemisphere Publishing Corporation, 1984.

[107] C. Hirsch, *Numerical Computation of Internal and External Flows*, Volume 1: Fundamentals of Numerical Discretization, John Wiley & Sons, 1988.

[108] K. K. Kuo, *Principles of Combustion*, John Wiley & Sons, Inc., 1986.

[109] J. H. Heinbockel, Introduction to Tensor Calculus and Continuum Mechanics, Department of Mathematics and Statistics, Old Dominion University, 1996.

[110] S. P. Burke and T. E. W. Schumann, *Diffusion flames*, Proc. 1st Symposium (International) on Combustion, The Combustion Institute, Pittsburgh, 1928.

[111] H. Pitsch, M. Chen and N. Peters, *Unsteady Flamelet Modeling of Turbulent Hydrogen-Air Diffusion Flames*, Proc. 27th Symposium (International) on Combustion, The Combustion Institute, 1998.

[112] D. Bradley, P. H. Gaskell and X. J. Gu, *The Mathematical Modelling of Liftoff and Blowoff of Turbulent Non-Premixed Methane Jet Flames at High Strain Rates*, Proc. 27th Symposium (International) on Combustion, The Combustion Institute, 1998.

[113] U. Maas and S. B. Pope, *Simplifying chemical kinetics: Intrinsic low-dimensional manifolds in composition space*, Combust. Flame, 88 (1992), pp. 239-264.

[114] M. F. Modest, *Radiative Heat Transfer*, McGraw-Hill, Inc., 1993.

[115] R. Siegel and J. R. Howell, *Thermal Radiation Heat Transfer*, Hemisphere Publishing Corporation, McGraw-Hill Book Company, 1981.

[116] M. G. Carvalho, T. Farias and P. Fontes, *Predicting Radiative Heat Transfer In Absorbing, Emitting And Scattering Media Using Discrete Transfer Method*, Fundamentals of Radiation Heat Transfer, 160 (1991), pp. 17-26.

[117] T. R. Johnson, *Application of the Zone Method of Analysis to the Calculation of Heat Transfer from Luminous Flames*, PhD thesis, Department of Chemical Engineering and Fuel Technology, University of Sheffield, Sheffield, 1971.

[118] J. S. Truelove, A Mixed Grey Gas Model for Flame Radiation, AERE-R-8494, United Kingdom Atomic Energy Authority, 1976.

[119] L. F. Richardson, *Weather Prediction by Numerical Process*, Cambridge University Press, Cambridge, 1922.

[120] A. N. Kolmogorov, *The local structure of turbulence in incompressible viscous fluid for very large Reynolds numbers*, Dokl. Akad. Nauk SSSR 30 (1941), pp. 299-303.

[121] A. Favre, *Statistical equations of turbulent gases*, In: SIAM, editor. Problems of hydrodynamics and continuum mechanics. Philadelphia: SIAM (1969), pp. 231-266.

[122] W. P. Jones and B. E. Launder, *The prediction of laminarization with a two-equation model of turbulence*, Int. J. Heat Mass Transfer, 15 (1972), pp. 301-314.

[123] B. Basara and S. Jakirlic, *A new hybrid turbulence modelling strategy for industrial CFD*, Int. J. Numer. Meth. Fluids, 42 (2003), pp. 89-116.

[124] M. M. Gibson and B. E. Launder, *Ground Effects on Pressure Fluctuations in the Atmospheric Boundary Layer*, J. Fluid Mech., 86 (1978), pp. 491-511.

[125] C. G. Speziale, S. Sarkar and T. B. Gatski, *Modeling of Pressure-Strain Correlation of Turbulence: An Invariant Dynamical System Approach*, J. Fluid Mech., 227 (1991), pp. 245-272.

[126] W. P. Jones and P. Musonge, *Closure of the Reynolds stress and scalar flux equations*, Phys. Fluids, 31 (1988), pp. 3589-3604.

[127] MAE 504, Fluid Dynamics of Combustion I, Running EQUIL, 2002.

[128] J. D. Anderson, Jr., *Computational fluid dynamics: the basics with applications*, McGraw-Hill, Inc., 1995.

[129] http://www.kachinatech.com/~hjjou/slatec-doc/code/DDASSL.html.

[130] E. Kreyszig, *Advanced Engineering Mathematics*, John Wiley & Sons, Inc., 1993.

[131] M. Rogina, S. Singer and S. Singer, Numerička analiza, Prirodoslovno-matematički fakultet, Sveučilište u Zagrebu, 2002.

[132] J. W. Harris and H. Stocker, *Handbook of Mathematics and Computational Science*, Springer-Verlag, New York, Inc., New York, 1998.

[133] S. C. Chapra and R. P. Canale, *Numerical methods for engineers: with software and programming applications*, McGraw-Hill, New York, 2002.

[134] http://www.mathworks.com/.

[135] Intel, Intel® Fortran Programmer's Reference, FWL-710-02, Intel Corporation, 2003.

[136] S. V. Patankar and D. B. Spalding, *A calculation procedure for heat, mass and momentum transfer in three-dimensional parabolic flows*, Int. J. Heat Mass Transfer, 15 (1972).

[137] M. Baburić, D. R. Schneider, Ž. Bogdan and N. Duić, *User function approach in combustion and radiation modelling in commercial CFD environment*, Transactions of FAMENA, 26 (2002), pp. 1-12.

[138] S. S. Dua and P. Cheng, *Multi-dimensional Radiative Transfer in Non-isothermal Cylindrical Media with Non-isothermal Bounding Walls*, Int. J. Heat Mass Transfer, 18 (1975), pp. 246-259.

[139] M. Baburić, N. Duić, A. Raulot, R. Tatschl and B. Wiesler, *Accurate Discrete Transfer Radiation Modelling in Industrial Furnaces - a Validation Study*, Proc. Conference on MODELLING FLUID FLOW, Department of Fluid Mechanics, Budapest University of Technology and Economics, Budapest, 2003.

[140] R. S. Barlow and C. D. Carter, *Relationships among Nitric Oxide, Temperature, and Mixture Fraction in Hydrogen Jet Flames*, Combust. Flame, 104 (1996), pp. 288-299.

[141] M. Flury and M. Schlatter, *Laser Doppler Velocimetry Measurements in Turbulent Non Premixed Hydrogen/Helium Flames,* http://www.ca.sandia.gov/TNF, Institute of Energy Technology, ETH, Zuerich.

[142] R. S. Barlow and J. H. Frank, *Piloted CH4/Air Flames C, D, E, and F - Release 2.0,* http://www.ca.sandia.gov/TNF, Sandia National Laboratories, 2003.

[143] C. Schneider, A. Dreizler, J. Janicka and E. P. Hassel, *Flow field measurements of stable and locally extinguishing hydrocarbon-fuelled jet flames*, Combust. Flame, 135 (2003), pp. 185-190.

[144] W. Meier, O. Keck, V. Jörres and W. Stricker, Raman Measurements of Temperature and Major Species Concentrations in Confined Swirling Natural Gas Flames, http://www.tu-darmstadt.de/fb/mb/ekt/tecflam/Web-TECFLAM.html, EKT Data Archive, DLR Stuttgart.

[145] C. Schneider, A. Dreizler and J. Janicka, Velocity Measurements in Unconfined and Confined Strongly Swirling Natural Gas Flames, http://www.tu-darmstadt.de/fb/mb/ekt/tecflam/ekt.html, EKT Data Archive, Technische Universität Darmstadt.

[146] M. Garcia-Villalba, J. Fröhlich and W. Rodi, Large Eddy Simulation of oscillating flow in combustion chambers, SFB 606, Project A6, status report, University of Karlsruhe, 2003.

[147] J. U. Schlüter and H. Pitsch, Consistent boundary conditions for integrated LES/RANS simulations: LES outflow conditions, Annual Research Briefs 2001, Center for Turbulence Research, 2001.

[148] P. R. van Slooten and S. B. Pope, *Application of PDF Modeling to Swirling and Nonswirling Turbulent Jets*, Flow, Turbulence and Combustion, 62 (1999), pp. 295-333.

[149] R. J. Kee, J. Warnatz and J. A. Miller, A Fortran computer code package for the evaluation of gas phase viscosities, conductivities, and diffusion coefficients, SAND83-8209, Sandia National Laboratories, 1983.

Curriculum vitae

Osobni podaci:

Ime:	Mario
Prezime:	Baburić
Datum rođenja:	05.11.1977
Mjesto rođenja:	Karlovac
Državljanstvo:	Hrvatsko
E-mail:	Mario.Baburic@fsb.hr
URL:	http://powerlab.fsb.hr/mbaburic

Obrazovanje:

1983-1995	Osnovna škola 'Braća Ribar' u Skakavcu. Opća gimnazija u Karlovcu.
1995-2000	Fakultet strojarstva i brodogradnje (FSB), Sveučilište u Zagrebu
2001-2005	Doktorski poslijediplomski studij na FSB, Sveučilište u Zagrebu

Profesionalne aktivnosti:

2001-…	Stručni suradnik na Katedri za energetska postrojenja, FSB; Asistent u nastavi na dodiplomskom predmetu 'Numeričke metode u inženjerstvu' te 'Numeričke metode u zrakoplovstvu II' na FSB-u

Strani jezici:

Engleski, njemački – vrlo dobro (pisanje i govor)

Španjolski, francuski – komunikacijski nivo

Personal:

Name:	Mario
Family name:	Baburić
Date of birth:	05.11.1977
Place of birth:	Karlovac
Citizenship:	Croatian
E-mail:	Mario.Baburic@fsb.hr
URL:	http://powerlab.fsb.hr/mbaburic

Education:

1983-1995	Elementary and high school in Karlovac
1995-2000	Faculty of Mechanical Engineering and Naval Architecture (FMENA), University of Zagreb
2001-2005	PhD study at FMENA, University of Zagreb

Professional:

2001-…	Research assistant at the Power Engineering Department, FMENA; Teaching assistance in under-graduate courses 'Numerical Methods in Engineering' and 'Numerical Methods in Aerodynamics II' at FMENA

Foreign languages:

English, German – fluent (written and spoken)

Spanish, French – communication level